Towards a comprehensive framework for foam concrete mix design

by

Justin Forrest Breg

A thesis
presented to the University of Waterloo
in fulfilment of the
thesis requirement for the degree of
Doctor of Philosophy
in
Civil Engineering

Waterloo, Ontario, Canada, 2020

Examining Committee Membership

The following served on the Examining Committee for this thesis.
The decision of the Examining Committee is by majority vote.

External Examiner	Daman K. Panesar, Ph.D., P.Eng. Professor, University of Toronto
Supervisors	John F. Straube, Ph.D., P.Eng. Associate Professor
	Jeffrey S. West, Ph.D., P.Eng., FACI Adjunct Professor
Internal Members	Adil Al-Mayah, Ph.D., P.Eng. Associate Professor
	Hassan Baaj, Ph.D., P.Eng. Associate Professor
Internal-external Member	Maurice B. Dusseault, Ph.D., P.Eng. Professor

Author's Declaration

I hereby declare that I am the sole author of this thesis.
This is a true copy of the thesis, including any required
final revisions as accepted by my examiners.

I understand that my thesis may be made
electronically available to the public.

Abstract

Foam concrete is a low-density, highly workable cementitious material, created by blending a fine-aggregate paste with a foaming agent. Properties of foam concrete suggest potential for commercial exploitation of the material in a wide variety of applications and markets. However, reliably designing a foam concrete mix to a particular specification has proved a difficult challenge and a barrier to more widespread usage. This thesis builds a comprehensive framework for foam concrete mix design. A strategic set of mixes, across a broad range of densities, cementitious densities, and cementitious blends, is evaluated for an extensive array of properties: compressive strength, density, slump flow, segregation, modulus of elasticity, Poisson's ratio, crushing behaviour, creep, drying shrinkage, capillary water uptake, moisture storage, moisture movement, thermal conductivity, freeze-thaw resistance, and air-void distribution. Critical and previously neglected engineering properties are quantified and characterized. A proposed model assimilates interrelated trends, to explain observed behaviour of foam concrete in plastic, curing, and hardened phases at a micromechanical scale. Knowledge is summarized in a series of mix design guides, to assist in developing appropriate solutions for given applications, with less reliance on trial-and-error and speculation. Finally, this study lays a foundation for a systematic and methodologically consistent approach to future foam concrete research.

Acknowledgements

This research was financially supported by Rainbow Concrete Industries Ltd.; the Natural Sciences and Engineering Research Council of Canada (NSERC); and Mitacs, through an Accelerate Fellowship.

I am grateful to both of my supervisors, Drs. John Straube and Jeff West, for offering their profound expertise during the course of this project. Dr. Straube helped shape this research program from its earliest stages: recognizing the many factors at play in developing a product for industry, working through experimental design details, and recognizing interrelated implications of research results. Dr. West brought still greater depth to the research of mechanical properties, imparting keen insights in each conversation. I could not have asked for a more complimentary pairing of supervisors for this thesis.

My committee has further enriched my learning. Dr. Adil Al-Mayah first introduced me to re-entrant foams in an undergraduate class many years ago; during this research, his remarks concerning the complex behaviour of foamed materials alerted me to important patterns in crushing and creeping. Dr. Hassan Baaj encouraged me to clarify the relationship between my research and potential applications for foam concrete, inspiring important sections in Chapter 8. Among Dr. Maurice Dusseault's numerous and helpful suggestions, his recommendation to distill my research into a micromechanical model has been especially important for this work and for my own understanding.

I am thankful to Dr. Daman Panesar for her detailed and perceptive external review of this thesis.

Boris Naneff, P.Eng., provided the opportunity and industrial resources for this project. His experience in numerous markets enabled me to explore standard and niche applications for foam concrete, and allowed me to gain first-hand exposure to many aspects of the concrete industry, in building, mining, and infrastructure. I look forward to further collaboration as we extend the use of foam concrete in Northern Ontario.

Levi Alkoury, P.Eng., coordinated large-scale foam concrete testing, and procured a variety of projects. Don McPhee and Derek Edwards contributed their skills and time throughout the experimental program. Craig Tobodo patiently took me under his wing and mentored me as we worked alongside each other at the lab and on-site in Sudbury.

For training, coordination, and occasionally an extra set of hands, I would like to thank the staff of RDH Building Science Labs in Waterloo, including Aaron Grin, Jonathan Smegal, Trevor Trainer, Claire Lepine, and Michael Fox. I am especially thankful to Chris Schumacher for his major contributions to creep testing, and his ongoing feedback. His expertise is embedded throughout this document.

Peter Volcic was instrumental in my work at the Civil and Environmental Engineering Structures Lab. Richard Morrison and Chris Peace offered advice and training. Colin Van Niejenhuis provided technical skill and engaging conversation about concrete chemistry and microstructure.

Thanks to Carlo Luigi Pasini, the architect of early foam concrete experiments at the University of Waterloo, who motivated this research. I appreciate Jonathan Vander Hout's valuable work on the computer application described in Section 8.3. I have benefitted greatly from the assistance and encouragement I have received from my own family, as well as the Zwart and Alexander families.

Lastly, to my wife, Sadie Breg, for your sacrifices, steadfast support and much else, I am so very grateful.

FOR THE ONE TO COME

Table of Contents

List of Figures

Preliminary Graphic Reference for Mix Design

Detailed Protocol for Foam Concrete Mix Design

List of Tables

List of Abbreviations

Shorthand references to mixes:

100% PC	denotes mixes with 100% Portland cement binder (no SCMs)
6% SF	denotes mixes with 6% silica fume binder*
12% SF	denotes mixes with 12% silica fume binder*
30% GGBS	denotes mixes with 30% ground granulated blast furnace slag binder*
50% GGBS	denotes mixes with 50% ground granulated blast furnace slag binder*

0:1 silica fume	denotes mixes with 0:1 filler-binder ratio and 12% SF* in cementitious blend
2:1 slag	denotes mixes with 2:1 filler-binder ratio and 50% GGBS* in cementitious blend
etc.	

* primary binder is Portland cement

Technical abbreviations:

AA	alkaline activated
AAC	autoclaved aerated concrete
ASR	alkali-silica reactivity
C-S-H	calcium silicate hydrate
c.d.	cementitious density
cem. dens.	cementitious density
CTF	controlled thermal fill
CWU	capillary water uptake
DEF	delayed ettringite formation
DEMEC	demountable mechanical [strain gauge]
dia.	diameter
D.S.	drying shrinkage
EDL	electrical double layer
EMC	equilibrium moisture content
f'c	compressive strength
FC	foam concrete
f/b ratio	filler-binder ratio
f/c ratio	filler-cement ratio
FA	fly ash
FCA	foam concrete aggregate
FR	fibre reinforcing
GGBS	ground granulated blast furnace slag

HD	high density [concrete]
ITZ	interfacial transition zone
LWA	lightweight aggregate
LWAC	lightweight aggregate concrete
MC	moisture content
MOE	modulus of elasticity
MOR	modulus of rupture
n.d.	nominal density
nom. dens.	nominal density
PC	Portland cement
PET	Polyethylene terephthalate
PFA	pulverized fly ash; also pulverized fuel ash
PLA	polylactide [reinforcing fibres]
PMMA	poly(methyl methacrylate) , i.e. plexiglass
PP	polypropylene
PR	Poisson's ratio
PVC	polyvinyl chloride
QC	quality control
RH	relative humidity
SACON	shock absorbing concrete
SCM	supplementary cementitious material
SF	silica fume
SP	superplasticizer
UHPC	ultra high performance concrete
UPV	ultrasonic pulse velocity
V.S.	vacuum saturation
w/b ratio	water-binder ratio (SCMs included as binder)
w/c ratio	water-cement ratio
w/s ratio	water-solids ratio

A note on the citations—

As elaborated in Chapter 3, information on foam concrete is sometimes confusing or contradictory. Furthermore, properties of the material are frequently exaggerated, misinterpreted, communicated imprecisely, or extracted from outdated or unreliable sources, especially in promotional literature.

Given this context, it was considered important to reference all information presented in this work as rigorously as possible. Every attempt has been made to locate original articles, rather than relying on secondary sources. Footnote citations have been used throughout the text, which precisely define each reference, including page or section numbers, and which may be readily consulted without breaking the flow of the thesis.

1

Introduction

Foamed concrete is a highly workable, low-density material with a significant volume of deliberately produced air voids. The material is created by blending a fine-aggregate cement paste with a foaming agent. Foam air bubbles remain stable during the set-up of the concrete, resulting in fine, evenly distributed voids within the concrete matrix.

In addition to its low density and workability, properties of foam concrete include pumpability, and ease of leveling and form-filling without compaction as a fresh concrete mix; and porosity, sound absorption, and thermal resistance (relative to standard concrete) when cast. It may be placed *in situ* in immense quantities without the need for autoclaved curing or elevated temperatures. Through the use of mineral admixtures and appropriate aggregates (fillers), current research suggests that mechanical strengths acceptable for structural applications may be achieved.

These characteristics indicate possible commercial exploitation of the material in a wide variety of applications and markets. There may be opportunity for foam concrete in uses as diverse as interior acoustic demising walls or roadside sound barriers; precast applications from the scale of unit pavers or concrete masonry units, to wall or roof panels;

porous paving; low-density backfill in mining; or structural fill under roadways and building foundations.

The basis for foam concrete was first discovered in the 1920s. Valore described the state-of-the-art in 1954, and Neville provided a paragraph on the substance in "Properties of Concrete" in 1963. Applications of foam concrete, however, have been mainly limited to low-strength engineered fill for much of its history. In the past decade, a significant amount of research has propelled other uses for this lightweight material, attempting to push its performance envelope, incorporating new types of binders, and optimizing mixes for highly specific purposes. A number of manufacturers have developed equipment and surfactants for producing foam concrete, and the material has been used successfully in projects around the world, including Canada.

However, foam concrete remains a relatively unfamiliar engineering material for many practitioners. To improve this situation, attempts have been made to collect and categorize available research and provide a conspectus for researchers or industry.[1] Nevertheless, many acknowledged gaps in the literature remain; additionally, it is especially difficult to weave together diverse studies in foam concrete because its properties change radically according to many variables, especially density. Consequently, designing a foam concrete mix to a particular specification, or even to knowing where to begin, remains a difficult challenge and a barrier to more widespread usage.

This thesis develops a coherent and consistent framework for understanding how to control foam concrete properties.

The initial framework for foam concrete mix design will be based on a literature review, supplemented by a broad experimental program. Mixes with various cementitious blends, water-cement ratios, and dry densities between 600 and 2000 kg/m^3, will be evaluated for mechanical behaviour; density; workability; microstructural characteristics; transport properties; and durability. The consistency of cast samples, and allowable tolerances to the design criteria in production, will be important factors of interest. Due to

[1] Cf. Brady et al. (2001), Ramamurthy et al. (2009), Amran et al. (2015)

the uniformity of material sources, preparation technique, curing regime, and testing procedures among these samples, it will be possible to assess and compare mix designs and trends across a variety of properties. The resulting database will help to characterize foam concrete for important properties and mix parameters that have previously only been tested anecdotally.

Four major additional deliverables arise from the research. First, a proposed micromechanical model explains observed behaviour of foam concrete in plastic, curing, and hardened phases. Second, a mix design guide assists in developing appropriate solutions for given applications, with less reliance on trial-and-error and speculation, and provides insight on allowable tolerances and quality control measures. Third, the research clarifies the market niches in which foam concrete may be most commercially competitive, and identifies new opportunities for the exploitation of foam concrete. Finally, the research lays a foundation for a systematic and methodologically consistent approach to future foam concrete research.

2

Abbreviated Literature Review

The following chapter provides a brief overview of foam concrete literature, as a general introduction to the reader. The serious and committed researcher is advised to consult Appendix A, which includes an exhaustive literature review of hundreds of articles, papers and reports related to foam concrete.

2.1 Definition of Foam Concrete

Foam concrete is a low-density cementitious material, produced by entrapping significant volumes of air void within a mortar paste by means of a foaming agent. Bubbles remain stable during the stiffening and curing of the concrete, resulting in a relatively homogenous distribution of macroscopic pores throughout the hardened mass.

There is no universal agreement as to how dense or porous a mortar must be to qualify as foam concrete. The volume of air void is cited variously at 'up to 50 percent',[1] 'up to 75 percent',[2] '40 to 80 percent,'[3] 'more than 20 percent',[4] or '10 to 70 percent.'[5] Mixes

1 Mineral Products Association (2016)
2 Basiurski and Wells (2001) 66
3 Mydin et al. (2014)
4 Barnes (2009) 3, Van Deijk (1991) 49
5 Panesar (2013) 575

have also been attempted with greater than 90% porosity.[6] Most commonly, foam concrete has between 40 and 80% porosity, corresponding to a density of approximately 500 to 1500 kg/m^3.

The relationship between various cementitious materials with deliberately introduced air-voids in the mortar is shown graphically in Figure 2.**1a**. Strategies for introducing air void content in cementitious materials and products are shown schematically in Figure 2.**1b**. Varying scales of voids in concrete are indicated in Figure 2.**1c**, for reference. For further discussion, consult Appendix A.

2.2 Historical Background

Attempts to produce aerated, low density concrete are at least 125 years old. In 1889, a patent was registered for a lightweight concrete, with gas bubbles produced through the reaction of hydrochloric acid and limestone. Patents for other forms of cellular concrete were registered through the 1910s and 20s, using aluminum powder (1914), yeast (1917), or excess water (1923) to introduce significant volumes of air void into a mix.[7]

In 1923, foaming processes were introduced to produce 'foam concrete'. By 1926, moist-cured foam concrete had been produced commercially in Europe,[8] and within a short time was brought to North America.[9] Early foam concrete remained of low strength, due largely to the limitations of unstable and inadequate foam surfactants.[10] Research beginning in 1936 concerning air-foams for suppressing gasoline fires has been credited with improving foaming agents for foam concrete.[11]

In 1954, Valore[12] consolidated what was known about various types of cellular concrete in a comprehensive report based on literature from European sources, as well testing at the National Bureau of Standards in the United States. He commented on methods of production, use of pozzolans and accelerators, mixing speeds, and costs of gas and foamed concretes. He also compiled information on properties such as compressive

6 Akthar and Evans (2010)
7 Valore (1954a) 774
8 Christiani and Nielson (1925). Cited by Valore (1954a) 786.
9 *Christiani and Nielsen v. Rice*, Supreme Court of Canada (1930).
10 U.S. Patent 2089813 A
11 Valore (1954a) 774, Akroyd (1962) 302
12 Valore (1954a) and Valore (1954b)

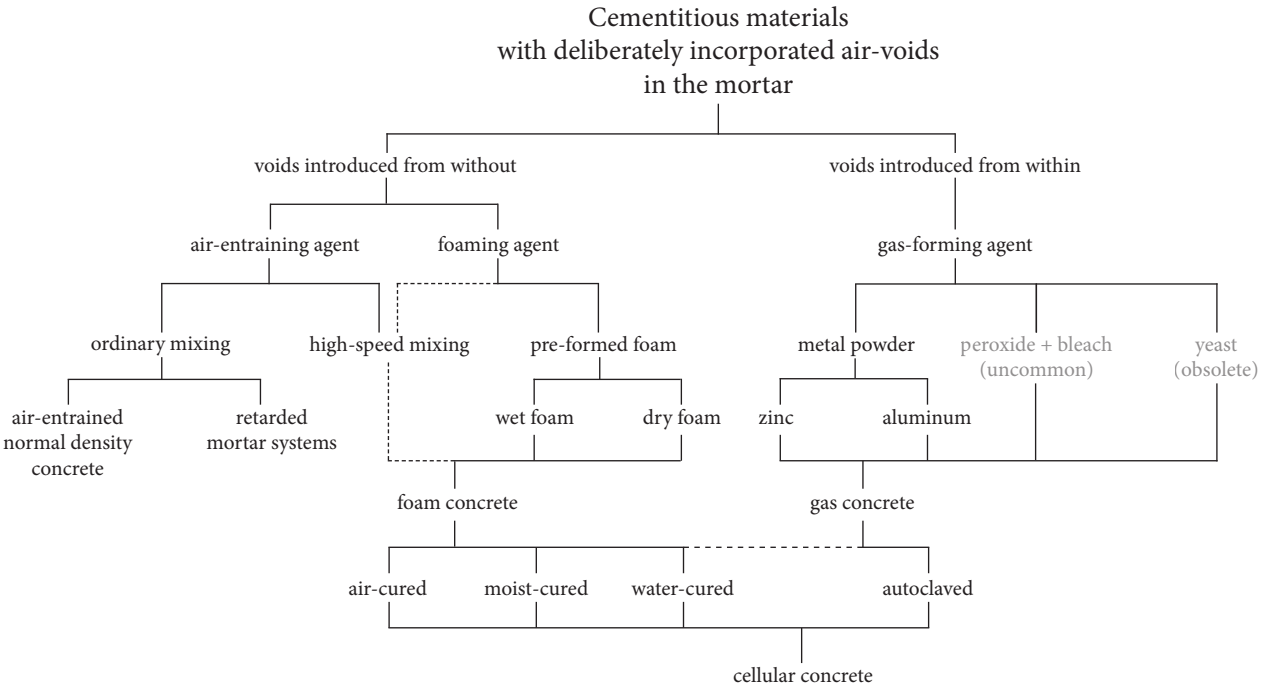

Figure 2.1a Relationship between cementitious materials with deliberately introduced air-voids in the mortar. Refer to Appendix A, Section 3.

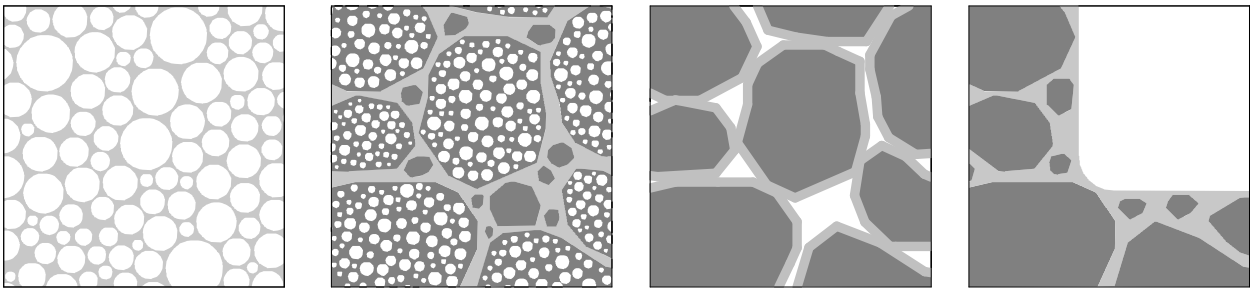

Figure 2.1b Strategies for introducing void in concrete. Refer to Appendix A, Section 7.1.

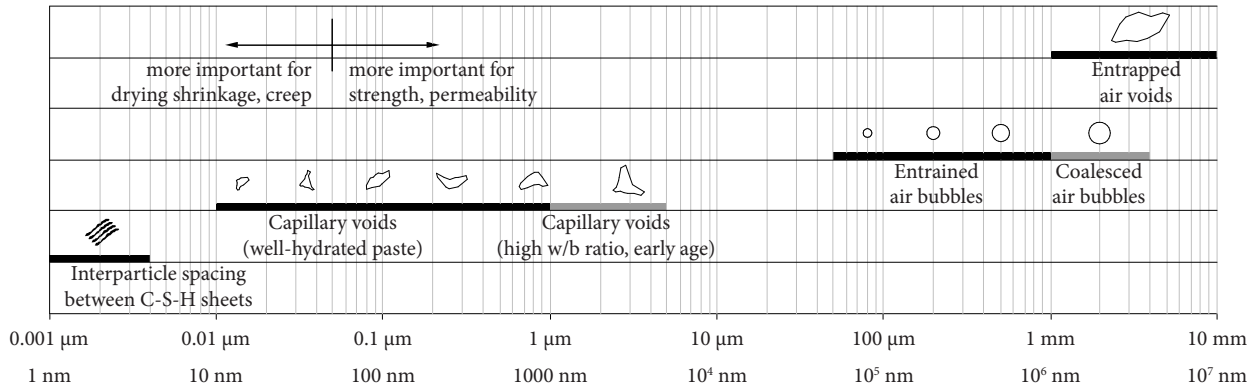

Figure 2.1c Scale of voids in concrete. Refer to Appendix A, Section 6.2.3. After Mehta (1986).

and flexural strength, elasticity, bond strength, adsorption and capillarity, freeze-thaw resistance, drying shrinkage, thermal expansion, and thermal conductivity. Valore noted that many trends were 'not well defined', and concluded that further research was needed, especially for moving from laboratory testing to commercial production.

In a 1960 publication on 'Foamed Materials,' Valore[13] noted that non-autoclaved foam concrete was still mostly used for non-structural applications, such as thermal insulation or fill. While precast planks had also been attempted, transportation and handling was difficult without excessive chipping and cracking.

During the late 1970s, an extensive research program was carried out in the Netherlands to develop foam concrete mixes for ground engineering applications.[14] By the 1980s and early 1990s, significant commercial projects had been undertaken based on this research, in the Netherlands and elsewhere. Foam concrete was used as soil replacement in areas of weak soils, as a form of soil stabilization on slopes, and as a void-filling material where low vertical or lateral load were required. Large volumes of foam concrete were sometimes demanded for these projects.[15]

Additionally, beginning in the early 1990s, foam concrete mixes were developed for raft foundations, low-slope roofs, precast sandwich panels, and for permeable landscaping surfaces (for example, under sports fields and athletic tracks).[16] Foam concrete was also used as an insulating fill for fire-resistance, thermal resistance, or sound-proofing. Numerous specialized applications for foam concrete were also researched, including projects as varied as decommissioning a nuclear facility,[17] retrofitting traditional dwellings,[18] and building extensions to runways to absorb energy and decelerate large planes.[19] Foam concrete continues to fulfill increasingly diverse roles as a commercially viable material, as its properties are recognized and refined.

---

13 Valore (1961) 6
14 Brady et al. (2001) 3
15 Van Diejk (1991), Cox (2005) 107
16 Van Deijk (1991)
17 Ashworth et al. (2013)
18 Shi et al. (2012)
19 Jones and Zheng (2013) Energy absorption

2.3 Contemporary Use of Foam Concrete

Foam concrete has been used in numerous building, geotechnical, industrial, transportation, mining, and military applications. A comprehensive list of existing and proposed applications for foam concrete is given in Appendix A, Section 8.1.

A selection of significant foam concrete projects in the past thirty years is given in Appendix A, Section 8.2; and available information on the annual regional use of foam concrete is given in Appendix A, Section 8.3.

2.4 Production of Foam Concrete

To produce foam concrete, a base mix is prepared from cementitious materials and water, as well as any fillers, coarse aggregate, reinforcing fibres, or chemical admixtures. This base mix is then aerated, and the bubbles stabilized with a surfactant. Aeration may be provided either through high-speed mixing, or through a pre-foaming method.

In the high speed mixing method, the liquid air entraining agent is added to a cementitious paste. The paste is then mixed at a high speed, drawing air into the mix through the shearing action of the mixer. The surfactant reduces the surface tension of the solution, stabilizing the bubbles. Concrete produced by high speed mixing tends to be used to produce heavier densities of aerated concrete. Controlled low-density fill may be produced in this way, for example.[20]

The composition of the base mix, mixing time, amount of foaming agent, and water temperature can affect the air void volume generated, making precise control of batch density difficult.[21] Paddles or screws that fold air into the mix are recommended, as these disperse air efficiently into the paste. If there is too little mixing, the paste will not be homogenous; but too much mixing will result in collapse of the foam.[22]

More commonly, however, a 'pre-foamed' method is employed. In this process, the surfactant is combined with water and aerated with compressed air to produce foam of

[20] Akroyd (1962) 302
[21] Fouad (2006) 561
[22] Brady et al. (2001) C7

shaving-gel-like consistency. The foam is then injected into the base mix slurry from a nozzle or via an inline mixer, and blended thoroughly. The bubbles remain suspended during the curing of the concrete. Pre-foaming is usually a more expensive method of production,[23] and is often a slower method for introducing air voids,[24] but it typically offers better control and consistency than the foam concrete produced by mechanical beating.[25]

2.5 Properties of Foam Concrete

Foam concrete mixes may be designed to cover a large range of specifications, with significant variation in physical properties. A brief introduction to important foam concrete properties is provided below.

2.5.1 Consistency

Foam concrete is a highly flowable material. Unlike most normal density concrete, its rheology is not measured according to its slump. Rather, its consistency is often evaluated according to its 'spreadability' (also referred to as 'spread rate') using a standard flow cone,[26] or its 'floawability' (also referred to as 'flow rate') using a modified Marsh cone test.[27]

The consistency of foam concrete in a plastic state is very important for producing good quality foam concrete. If the mix is too stiff, a large proportion of bubbles will break, increasing the density and the water-binder ratio. If the mix is too thin, bubbles will rise through the paste, causing segregation.

2.5.2 Drying Shrinkage

Foam concrete may experience significant drying shrinkage during curing, due in part to the absence of restraining coarse aggregate, and to the relatively high water-cement ratios used during mixing. Drying shrinkage of foam concrete may be an order of magnitude

[23] Panesar (2013) 576
[24] Brady et al. (2001) C7
[25] Fouad (2006) 561
[26] Cf. ASTM C230
[27] Cf. Jones et al. (2003), Nambiar and Ramamurthy (2008) 111

greater than that of normal density concrete.[28] Neat cement mixes may experience shrinkage as high as 3,300 to 4,400 microstrain,[29] while sanded foam concrete mixes may experience 700 or 1,200 microstrain.[30] By comparison, normal density concrete with a low w/c ratio may only experience 200 to 400 microstrain in drying shrinkage.[31]

2.5.3 Density

Density is a key property of foam concrete. Achieving low density is a critical consideration concern for many foam concrete applications; and density has a dominant effect on mechanical, thermal, transport, and durability properties, as well.

A remarkable range of densities is possible. With porosities in excess of 90 percent or as low as 10 percent of volume, dry density measurements of foam concrete may range from only 140 kg/m^3,[32] to more than 1900 kg/m^3.[33] In most foam concrete mixes, dry density measurements are between 400 and 1600 kg/m^3.[34]

Density is principally controlled by foam volume. Less significantly, the proportions and particle densities of fillers and binders will also influence the density of the hardened cement paste. The moisture content of a sample can have a strong influence on its measured density, as well.

2.3.4 Air-Void System

Characteristics of the air-void system vary strongly with density, as shown through the magnified images in Figure 3. The size and uniformity, shape, spacing, and interconnectivity of air voids are related parameters. Fine, uniform air voids are usually desirable in foam concrete mixes for mechanical properties,[35] and a high degree of closed porosity is advantages for suppressing gas and liquid transport. Foam concrete has a

[28] Valore (1954b) 830
[29] Neville (1963) 448
[30] Nambiar and Ramamurthy (2009) 632
[31] Neville (1963) 288
[32] Akthar and Evans (2010) 354
[33] Fouad (2006) 562, Gunawan and Busra (2014) 436
[34] Brady et al. (2001) 2
[35] Nambiar and Ramamurthy (2007) 228 Air-void

relatively high closed porosity in comparison with gas-aerated autoclaved concrete.[36] Open porosity increases markedly above 50% air content.[37]

Mixes of equivalent foam volume and density may vary in their properties due to other characteristics of their air-void systems, such as the water-binder ratio, the proportion of fillers, and the use of supplementary cementitious materials.

2.3.5 Mechanical Properties

The strength of foam concrete varies dramatically with porosity. Low density mixes of 160 kg/m^3 offer compressive strengths of only 0.04 MPa, while mixes of 1600 kg/m^3 may offer 25 MPa, as shown in Figure 4. Mixes of similar composition, with varying porosity, will generally conform to fundamental relationships between strength and porosity.

However, for a given density, widely diverse values of compression strength are reported for mixes of different compositions.[38] A 1600 kg/m^3 mix may have a compressive strength as low as 2 MPa, or as high as 60 MPa.[39] This variation may be attributed to differences in the intrinsic strength of the cement paste, as well as the presence of flaws in the matrix on account of the air-void system.

The ratio between splitting tensile strength and compressive strength of foam concrete mix may typically be between 0.06 and 0.10.[40] Tensile strength may be increased in the order of 50[41] to 100%[42] with the use of reinforcing fibres.

According to research by the British Cement Association,[43] the modulus of elasticity of foam concrete ranges from 1 to 12 GPa for conventional foam concrete with dry densities between 500 and 1600 kg/m^3, respectively. The addition of fibres can greatly increase foam concrete stiffness, in the order of 70% for a 1400 kg/m^3 sample.[44]

---

36 Nambiar and Ramamurthy (2007b) 1341
37 Jones et al. (2012) 521
38 Pan et al. (2007)
39 Wee (2005). Cited in Wee et al. (2011) 584
40 Amran et al. (2015) 997
41 Jones and McCarthy (2005b) 27, Gunawan and Busra (2014)
42 Byun et al. (1998)
43 British Cement Association (1994). Cited in Brady et al. (2001) C11, Table C5
44 Brady et al. (2001) Table C7

The Poisson's ratio of foam concrete is seldom reported in the literature. A value of 0.2 has been reported for mixes of less than 700 kg/m^3 density,[45] and a value of 0.327 has been reported for a sanded mix of 1300 kg/m^3 density.[46]

The shear strength of foam concrete is typically poor, due to the lack of coarse aggregate.[47]

2.3.6 Transport Properties

Capillary water uptake indices of foam concrete are relatively high, compared to normal density concrete. For sand-cement foam concrete mixes with between 10 and 50% air void, indices were reported to vary from 0.626 to 0.360 mm/min$^{0.5}$.[48] Capillary water uptake indices may be as low as 0.109 and 0.142 mm/min$^{0.5}$ for higher density mixes with less permeable matrices. The interconnectivity of voids has a strong influence on capillary water uptake.[49]

Likewise, absorption values for foam concrete are very high relative to normal density concrete. For example, in a test on conventional foam concrete mixes with between 10 and 50% foam volume, immersed in water for 7 days, the samples absorbed between 21 and 25% liquid by volume, respectively.[50] Other studies also indicate high absorption values, with variations in binders and fillers having a limited influence.[51]

The liquid permeability of foam concrete is typically low, relative to conventional fill materials.[52] However, foam concrete with a density of 600 to 650 kg/m^3 and a hydraulic conductivity of 300 mm/h has been used for outdoor tennis courts and soccer fields,[53] and foam concrete has been proposed for use in stormwater detention applications,[54] and for filtering wastewater.[55]

---

45 Cf. Byun et al. (1998), Wee et al. (2011) 591
46 Lim et al. (2013) 46
47 Brady et al. (2001) C12
48 Nambiar and Ramamurthy (2007b) 1345
49 Cf. Yang and Lee (2015)
50 Nambiar and Ramamurthy (2007b) 1344
51 Kearsley and Wainwright (2001) 810, Cong and Bing (2014) 65
52 Alobaidi et al. (2000) 151-159.
53 Van Deijk (1991) 51
54 U.S. Patent 8172937 B2
55 Doniec (2008) 264

Foam concrete also tends to be fairly permeable to gaseous diffusion. Values ranging from 2.53 to 3.20 g/mm/s x 10^{-13} have been reported for the water vapour diffusivity of conventional foam concrete with 1400 kg/m^3 plastic density.[56] These values are approximately twice as high as for normal density concrete with compressive strengths of 40 to 50 MPa.[57] However, the use of coarse fly ash as a replacement for sand filler appears to reduce the rate of vapour diffusivity in foam concrete, by as much as 50%.[58]

Oxygen permeability is typically very high in foam concrete, and increases with porosity. For foam concrete with a plastic density of 1800 kg/m^3 and 500 kg/m^3 cementitious density, oxygen permeability may be an order of magnitude higher than for normal density concrete.[59] However, the use of coarse fly ash filler as a complete replacement for sand filler is reported to reduce oxygen permeability dramatically, indicating that specially-designed foam concrete may be capable of providing adequate protection for carbon steel reinforcing bar.[60]

2.3.7 Thermal Properties

In general, the thermal conductivity of lightweight concrete increases logarithmically with oven dry density.[61] Foam concrete may have slightly better thermal resistance than other types of lightweight concrete, due to characteristics of the air-void system: a homogenous matrix of relatively thin cells walls produces a tortuous path for heat transfer by conduction, and low interconnectivity of air voids suppresses convection and radiative heat transfer.[62]

According to the American Concrete Institute,[63] neat cement foam concrete of 240, 480, 960, and 1920 kg/m^3 dry density will have thermal conductivity values of approximately 0.078, 0.125, 0.244, 0.629 W/m·K, respectively. By comparison, the thermal conductivity of normal density concrete is approximately 1.1 to 1.4 W/m·K.[64]

---

56 Brady et al. (2001) Table C1
57 Brady et al. (2001) C14
58 Dhir et al. (1989). Cited in Brady (2001) C14. Kearsley and Booyens (1998)
59 Dhir et al. (1989). Cited in Brady et al. (2001) C14.
60 Kearsley and Booyens (1998)
61 Valore (1980)
62 Petit et al. (2014) 37, Huang et al. (2015) 396
63 ACI 122R-02 Table 2.1
64 Brady et al. (2001) C16

Volumetric heat capacity of foam concrete increases with density, as well. For foam concrete of 350, 400, 800, and 1200 kg/m^3 dry density, values of 916, 967, 1479, and 1998 kJ/m^3·K have been calculated, respectively (that is, 2.62, 2.42, 1.85 and 1.67 kJ/kg·K).[65] By comparison, normal density concrete may have a specific heat of between 0.79 and 0.92 kJ/kg·K, corresponding approximately to between 1900 and 2200 kJ/m^3·K.[66]

Because foam concrete has a relatively low thermal conductivity and a relatively high heat capacity, the material changes temperature slowly, i.e. it has a low thermal diffusivity. This property is especially important for the resistance of extreme heat and fire.[67] For foam concrete of between 583 to 1370 kg/m^3, thermal diffusivity was reported to increase with density from 0.27 to 0.34 mm^2/s.[68] By comparison, the thermal diffusivity of fully hydrated, normal density, ordinary Portland cement concrete is approximately 1.1 mm^2/s.[69]

2.3.8 Durability Properties

The phenomenon of carbonation has important implications for the corrosion of reinforcing steel. Compared to normal density concrete, foam concrete is relatively permeable to water vapour and carbon dioxide, which promote carbonation.[70] Consequently, steel reinforcing is not typically recommended in foam concrete.[71] For conventional foam concrete with Portland cement contents of between 270 and 355 kg/m^3, and densities between 1330 and 1750 kg/m^3, the average rate of carbonation has been reported as approximately 5.7 mm/year$^{0.5}$, which is 50% higher than normal density concrete with similar cementitious density.[72]

Typically, the rate of carbonation in foam concrete may be expected to decrease with increasing density, and with increasing cementitious density. The relatively high permeability of foam concrete to water vapour and carbon dioxide gas increases

[65] Tarasov et al. (2010) 903
[66] ACI 122R-02 Section 5.1.4
[67] Mydin and Wang (2012b) 215, Zhang et al. (2014) 122
[68] Zhang et al. (2015) 100-101
[69] Schutter and Taerwe (1995). Cited in Zhang et al. (2015) 101
[70] Kosmatka et al. (2002) 266
[71] Brady et al. (2001) 10
[72] Brady (2000). Cited in Brady et al. (2001) C15

susceptibility to carbonation. The high cement content in many foam concrete mixes will help to reduce the rate of carbonation somewhat.[73]

Foam concrete performs well in many typical freeze-thaw tests.[74] The total large volume of air void typically provides ample space for the accumulation of water. However, non-standard tests may be necessary to accurately predict the freeze-thaw performance of foam concrete in real-world conditions.[75]

Resistance of foam concrete to fire and elevated temperatures is typically excellent.[76] Air voids provide insulation to protect inner zones from extreme heat. At high temperatures, heat transfer through a porous medium is strongly influenced by radiation. The closed cell structure of foam concrete provides many interruptions to the movement of heat by radiation, at each air-solid interface.[77] Furthermore, foam concrete has a relatively high heat capacity. Heat energy is absorbed into the material, suppressing temperature change.[78]

Comparisons of foam concrete and vermiculite lightweight aggregate concrete suggested that at lower densities of 500 kg/m^3, foam concrete had 30% better endurance, and 38% higher strength for the given testing parameters. Conversely, at higher densities of approximately 1250 kg/m^3, vermiculite lightweight aggregate concrete had somewhat better resistance to degradation under extreme heat.[79]

Fire endurance may be enhanced with a reduction in density.[80] There appears to be proportionally less strength loss in foam concrete compared to normal density concrete when exposed to extreme heat, especially at lower densities.[81]

---

73 Fabian et al. (2006) 189
74 Brady et al. (2001) 10, C12; Jones and McCarthy (2005a) 72
75 Tikalsky et al. (2004)
76 Cf. ACI 523.1R-06, Section 3.9, Fouad (2006) 566, Amran et al. (2015) 1001.
77 Valore (1954b) 834, Panesar (2013) 577
78 Mydin and Wang (2012b) 215, Zhang et al. (2014) 122
79 Aldridge (2005) 9-10
80 Ramamurthy et al. (2009) 394
81 Jones and McCarthy (2005b) 29

2.3.9 Acoustic Properties

Sound insulation is the capacity of a membrane or assembly to suppress the transmission of air-borne sound energy, typically measured as transmission loss, in decibels.[82] Transmission loss is approximately proportional to the mass of a wall.[83] Consequently, low-density foam concrete will perform poorly relative to normal density concrete, for the same thickness. Additionally, air tightness is necessary to ensure that sound will not 'leak' through an assembly.[84]

Sound absorption is a distinct property from sound insulation. While sound insulating materials reduce the sound energy transmitted through a membrane or assembly, sound absorbing material reduce the amount of sound energy reflected from the barrier.[85]

While the ability of foam concrete to isolate sound may be poor in comparison to normal density concrete, its ability to absorb sound may be relatively good. Instead of being reflected off of a stiff surface, sound energy is captured within small air voids at the surface of a wall and lost as heat.[86] Interconnectivity of bubbles allows for sound energy to travel deeper into the surface of a wall, improving absorption coefficients.[87] A greater pore size distribution may help attenuate sound at different frequencies.

Mean normal incidence absorption coefficients have been evaluated for foam concrete of different densities.[88] Mixes with dry densities of 250, 300, 400, and 500 kg/m^2 had mean absorption coefficients of 0.24,0.22, 0.15, and 0.12, respectively. Absorption coefficients will decrease if exposed surfaces are sealed, for example, with paint.[89]

82 London (1949)
83 Short and Kinniburgh (1978) 73
84 Short and Kinniburgh (1978) 73, Leitch (1980). Cited in Narayanan and Ramamurthy (2000b) 328
85 Short and Kinniburgh (1978) 73
86 Neville (1963) 446
87 Laukaitis and Fiks (2015) 291
88 Laukaitis and Fiks (2015) 291
89 Cf. RILEM Technical Committees 78-MCA and 51-ALC (1993) 40

2.3.10 Energy Absorption

The ability of foam concrete to absorb energy has been exploited in soft ground arrestor systems for aircraft,[90] as well as in military structures.[91] Capacity for energy absorption is related to several mechanical and physical properties. Compressive strength, flexural strength, elasticity modulus, and Poisson's ratio are significant parameters, as is the geometry of the air void system, which collapses during crushing.[92] For good energy absorption capacity, mixes require relatively strong bubble walls and sufficient void space into which crushed debris can be pushed, to avoid global fracturing of the specimen. 1000 kg/m^3 mixes performed better than other mixes of 500, 600, or 1400 kg/m^3 plastic density, in one study.[93]

[90] Zhang et al. (2013)
[91] Fabian et al. (2006) 187, Jones and Zheng (2013) 209
[92] Wee et al. (2011) 591
[93] Jones and Zheng (2013) 215

3

Research Needs

An exhaustive review of foam concrete literature has been compiled from English-language articles, papers, patents, data sheets, and reports published in the open literature since the 1920s. This review is presented Appendix A, and forms a basis for identifying critical research needs.

Among the hundreds of reports and articles on foam concrete written in the past twenty years, several attempts have already been made to collect and categorize available research and provide a conspectus for academic researchers or industry.[1] Nevertheless, many acknowledged gaps in the literature remain; and designing a foam concrete mix to a particular specification, or even knowing where to begin, remains a difficult challenge and a barrier to more widespread usage.

At present, foam concrete recipes are still usually produced on a 'trial-and-error' basis.[2] While there is a now a large amount of experimental data available for foam concrete, it may be difficult to translate this data into appropriate mix designs. Indeed,

1 Brady et al. (2001), Ramamurthy et al. (2009), Amran et al. (2015)
2 Ramamurthy et al. (2009) 389

Nambiar and Ramamurthy[3] acknowledge that limited work has been undertaken for predicting foam concrete properties based on known mix proportions.

The complications of deriving general mix design guidelines are two-fold. In the first place, many studies compare a relatively small number of mix designs. The range may not be extensive enough to adequately capture trends. For example, some previous studies on the influence of varying the water-cement ratio in foam concrete have offered inconclusive results.[4] More recently, Wee et al.[5] tested twenty-four foam concrete combinations with varying water-cement ratios and proportions of air volume. The resulting database is sufficiently detailed and wide-ranging to draw meaningful observations about optimizing the water-cement ratio of foam concrete for a given density. Even so, however, these conclusions are only valid for a limited set of operating conditions, i.e. for a particular binder blend with no fine or coarse aggregates.

In the second place, it is difficult to compile a more extensive database by relating the results of one study to another, especially due to the role of density. Density has a dominant effect on many foam concrete properties, thus two different mix designs with differing air-void volumes cannot be reasonably compared. Moreover, not only do researchers use differing density targets, but they may also choose to express density in ways that may not be readily or precisely correlated,[6] e.g. according to foam volume,[7] plastic density,[8] or dry density.[9]

To develop guidelines for the mix design of foam concrete, Nambiar and Ramamurthy[10] designed systematic experiments, and represented the results in the form of response surface plots, mapping the influence of three variables simultaneously. For example, a plot could show the relationship between foam volume, filler-to-cement ratio, and 28-day compressive strength. Such visualization of data is helpful for studying and optimizing trends, but is limited in the number of variable inputs.

---

3 Nambiar and Ramamurthy (2006b) 752
4 Brady et al. (2001) C9, Table C6
5 Wee et al. (2011)
6 Kearsley (1999b) 55
7 Panesar (2013), Nambiar and Ramamurthy (2007a)
8 Van Deijk (1991), Jones and McCarthy (2005b)
9 Akthar and Evans (2010) 354, Barnes (2009) 7
10 Nambiar and Ramamurthy (2006b)

Other researchers have proposed using artificial neural networks to predict foam concrete properties. Bayuaji and Nuruddin[11] used this approach to anticipate compressive strength based on inputs such as the sand-cement ratio, sand particle size distribution, and density; while Nehdi et al.[12] predicted production yield, foamed density, unfoamed density, and compressive strength. Artificial neural networks help reconcile differing parameters used in separate studies, accommodate many variables, and are relatively insensitive to incomplete information, as compared to traditional empirical models.[13]

Such techniques may assist mix designers in producing foam concrete to particular specifications in the future. A foundational task to this objective, however, is to develop a broad and consistent framework, confirming trends and filling in gaps to understand the effects of incremental variation in mix design on performance.

There are a number of significant mix design parameters and material properties that have not yet been thoroughly explored to date, and require further investigation.

For example, although the use of fly ash as a binder for foam concrete has been relatively well-researched, the study of other supplementary cementitious materials is less complete. In a review of articles on foam concrete published in the open literature since 1988, over fifty articles consider the influence of fly ash, either in the form of fine particles as a binder, or in a coarse form as a filler with some cementitious properties. Conversely, only nine articles include the influence of ground granulated blast furnace slag, and twelve address the use of silica fume. (Refer to Appendix B.)

Similarly, there appears to be strong potential for the use of fibre reinforcing and surface reinforcing with foam concrete, but the behaviour of reinforced cementitious foam has not been thoroughly characterized.[14] Research in the use of metal,[15] synthetic,[16] and natural[17] reinforcing fibres has been mostly anecdotal, typically conducted over a narrow range of mix designs.

---

11 Bayuaji and Nuruddin (2008)
12 Nehdi et al. (2001)
13 Bayuaji and Nuruddin (2008) 2
14 Bindiganavile and Hoseini (2008) 252
15 Gunawan and Busra (2014)
16 Awang and Ahmad (2014)
17 Jones and McCarthy (2005b)

The micromechanics of foam concrete during plastic and curing phases is an important area of research. Better understanding and control over the aging of foam through coarsening, drainage, and rupture is necessary to improve the stability and quality of mixes.[18] New models are necessary to predict core temperatures and resultant strains during curing, since heat of hydration in foam concrete occurs differently than in normal density concrete, due to the insulating effect of the air-voids.[19]

Among material properties of hardened foam concrete, long-term performance metrics are seldom reported in the open literature.[20] Creep is not well-characterized for foam concrete. Strain behaviour is not well understood for either static or dynamic loading. Limited testing has been conducted concerning chloride ingress of foam concrete. More research into long-term durability would be appropriate; especially as foam concrete is often used in ground engineering work, where later remediation may prove very difficult. Use of new binders requires additional durability testing.[21]

Other basic engineering properties, such as modulus of elasticity[22] and Poisson's ratio[23] must be confidently established to facilitate structural design, especially as higher strength mixes are developed for structural applications.

Advancement in the field of foam concrete research is hindered by the lack of a broad and consistent experimental framework. Most studies have insufficient scope for capturing large-scale, multivariate trends possible in foam concrete: in failing to vary a critical parameter, some studies may offer misleading conclusions. Moreover, compiling and correlating results from previous studies into larger datasets is problematic, due to differing experimental methodologies, incongruent density targets, and inconsistent approaches to expressing density.

---

18 Petit et al. (2014)
19 Tarasov et al. (2010) 905
20 Brady et al. (2001) 1
21 Cf. Yang et al. (2014) 232
22 Cf. Brady et al. (2001) C11, Van Deijk (1991) 50, Jones and McCarthy (2005b) 26
23 Cf. Wee et al. (2011) 591, Lim et al. (2013) 46, Byun et al. (1998), Tang et al. (2013) 347

4

Experimental Program: Objective and Scope

A systematic approach is necessary to confidently characterize foam concrete across a wide range of design parameters. The experimental program described in this chapter was designed to capture numerous material property trends for design parameters including density, cementitious density, binder composition, water-binder ratio, filler-binder ratio, and curing regime, in a tightly controlled study conducted by a single operator.

The resulting database has a number of uses. First, important properties and mix parameters that have only been tested anecdotally previously, can now be more thoroughly characterized and understood. A database incorporating many interrelated properties is a valuable resource for comprehending the behaviour of foam concrete at a micromechanical scale. Second, observed trends and relationships aid in developing appropriate mix designs for given applications, with less reliance on trial-and-error and speculation; the database can also serve as a fundamental resource in the development of prediction models. Finally, an extensive database may clarify in which market niches foam concrete can be most commercially competitive, and may help identify new opportunities for the exploitation of foam concrete.

Thus, the experimental program serves both academic and industry interests. Further research is facilitated, as data is added to the literature, and as test standards are established for conducting future studies. Concrete producers benefit from comprehensive, accessible, and impartial information for developing mix designs: in this experimental program, particular attention was given to the needs and resources of the concrete industry in Ontario.

The chapter below outlines the scope of the proposed research, and explains the strategy behind the selection of mix design parameters and tests. Detailed methodologies describing procedures and equipment used for the various tests are provided in Chapter 5.

4.1 Mix Design Parameters

Mix design parameters were varied in order to capture a relatively large range of the possible performance envelope of foam concrete. However, it was also intended that the mixes could be produced in a commercial setting at a reasonable level of effort and cost. For example, mixes with extremely low density (i.e. greater than 90% porosity) were excluded due to increased manufacturing challenges; and the cementitious densities of mixes were constrained by cost.

4.1.4 Water-Binder Ratio

Many foam concrete studies fail to optimize water-binder ratios, commonly applying a constant water-binder ratio across a range of mix designs. Such an approach may produce misleading conclusions. Mix water requirements for foam concrete can vary dramatically, in response to density (foam volume), cementitious density, surface area of solid ingredients, etc. Water-binder ratios should be optimized for each mix design, in order to fully capture the benefits of changes to mix ingredients.

To identify the optimum quantity of mix water for each mix, water-binder ratios were increased from 0.35 to as high as 0.85, in increments of 0.05. Foam volume was

adjusted to account for variations in the water-binder ratio, to maintain the appropriate proportion of solid ingredients in each mix.[1]

4.1.2 Cementitious Density

For the majority of mixes, the total cementitious density was held constant at 410 kg/m^3. This cementing factor is relatively generous, allowing for the production of a strong mix, but it is well below the cement 'strength ceiling' for foam concrete suggested by Jones.[2] Additionally, certain mixes were tested with varying cementitious densities, in order to chart the effect of increased cement content.

4.1.3 Binder Composition

Five cementitious blends were used throughout the proposed research. Initial mixes included only Portland cement as a binder. Binder replacements can improve performance and reduce ecological burden, thus subsequent mixes included 6% and 12% silica fume, and 30% and 50% slag, representing modest and high replacement proportions for these supplementary cementitious materials, based on the results of previous studies.[3]

Numerous studies have been conducted on the use of fly ash in foam concrete.[4] Canada, however, has relatively few domestic sources of fly ash,[5] and investigations based on the use of fly ash in foam concrete are not of interest to the industry sponsor of this research at this time.

4.1.4 Filler-Binder Ratio

The filler-binder ratio was varied to control density, from 0:1 to 3.5:1, corresponding to nominal mix densities ranging from 600 kg/m^3 to 2000 kg/m^3. Assuming that the mass of the cementitious materials multiplied by a factor of 1.2 gives the mass of the hydration

1 For more information on the chosen method of mix proportioning, refer to Appendix B.
2 Jones (2000). Cited in Brady et al. (2001) C1
3 Cf. Brady et al. (2001)
4 Refer to Appendix C.
5 Refer to Appendix D.

reaction products,[6] all samples with equal filler-cement ratios will theoretically have the same oven-dry density, allowing for consistent strength-to-density comparisons.

Mix combinations tested in the experimental program are indicated in grey in the Table below. Certain series of mix designs received particular emphasis: for example, mixes with Portland cement-only binders provide an experimental baseline; mixes with nominal densities of 600 kg/m^3 and 1400 kg/m^3 may fulfill important use cases (i.e. for geotechnical fill and insulating applications; and for structural applications, respectively); and silica fume mixes offer the possibility of relatively high strength.

For the stated Nominal Density, an asterisk (*) indicates that mixes were produced with cementitious densities of both 410 and 510 kg/m^3. A double-asterisk (**) indicates production of mixes with total cementitious densities from 410 to 710 kg/m^3. For all other mixes, total cementitious density was 410 kg/m^3.

	Filler-Binder Ratio (Nominal Density, kg/m^3)							
Cementitious Blend	0 : 1 (600)	0.5 : 1 (800)	1 : 1 (1000)	1.5 : 1 (1200)	2 : 1 (1400)	2.5 : 1 (1600)	3 : 1 (1800)	3.5 : 1 (2000)
12% Silica	*		*		*		*	
6% Silica								
100% Portland	**		*		*		*	
30% Slag								
50% Slag								

Table 4.1.4 Summary table of mix designs for testing.

[6] Cf. ASTM C567/C567M, Section 9.1

4.2 Scope of Testing: Conventional Foam Concrete Mixes

Among the properties of foam concrete described in Chapter 2, a selection of properties were identified as being significant for commercial applications in Canada:

- The relationship between **compressive strength** and **density** is fundamental to foam concrete mix design for almost all applications.
- **Slump flow** provides a convenient indication of the consistency and quality of fresh foam concrete during mixing and placing. Minimal **segregation** must be ensured.
- **Modulus of elasticity** and **Poisson's ratio** are essential engineering parameters for understanding the response of foam concrete to load.
- Data for **crushing behaviour** is important for impact absorbing applications, and for anticipating failure modes.
- **Creep** is not well-characterized for foam concrete, but merits closer study for any applications where foam concrete is to be used structurally long-term.
- **Drying shrinkage** is typically high in foam concrete, and affects the dimensional tolerances of a product. Furthermore, drying shrinkage can induce bulk cracking in a sample, affecting its mechanical and transport properties.
- **Capillary water uptake indices** and **sorption isotherms** help anticipate the moisture content of foam concrete for a given environment. The presence of moisture can have dramatic influences on durability, thermal properties, and **hygroscopic movement**.
- Low **thermal conductivity** of foam concrete is a desirable characteristic in fill applications and in building assemblies.
- **Freeze-thaw resistance** is important in any situation where foam concrete may be subject to moisture and freezing temperatures, which includes many outdoor applications in Canada.

Furthermore, the **microstructural properties** of foam concrete were evaluated through processes such as imaging and porosity testing, offering insights into each of the properties above.

Strategic sets of mixes combinations were tested to study each of these properties, as indicated in blue in the tables below.

4.2.1 Compressive Strength

A great number of samples were tested for compressive strength. The water-binder ratio for these mixes was varied from 0.35 to up to 0.80, in order to establish optimum values for each mix design, for use in subsequent tests.

Because compressive strength is almost always a critical parameter for mix design, compression testing was conducted for all mix combinations at 7- and 28-days.

56-day compression tests were also conducted on most mixes, including those with high concentrations of silica fume and slag, as well as all denser mixes of 1400 or 1800 kg/m^3 nominal density, to observe whether longer curing times could permit foam concrete to be used in higher-strength applications.

	Filler-Binder Ratio (Nominal Density, kg/m^3)							
Cementitious Blend	0 : 1 (600)	0.5 : 1 (800)	1 : 1 (1000)	1.5 : 1 (1200)	2 : 1 (1400)	2.5 : 1 (1600)	3 : 1 (1800)	3.5 : 1 (2000)
12% Silica	*		*		*		*	
6% Silica								
100% Portland	**		*		*		*	
30% Slag								
50% Slag								

Table 4.2.1a Mix designs tested for 7- and 28-day compressive strength.

	Filler-Binder Ratio (Nominal Density, kg/m^3)							
Cementitious Blend	0 : 1 (600)	0.5 : 1 (800)	1 : 1 (1000)	1.5 : 1 (1200)	2 : 1 (1400)	2.5 : 1 (1600)	3 : 1 (1800)	3.5 : 1 (2000)
12% Silica	*		*		*		*	
6% Silica								
100% Portland	**		*		*		*	
30% Slag								
50% Slag								

Table 4.2.1b Mix designs tested for 56-day compressive strength.

4.2.2 Slump Flow

Having established appropriate water-binder ratios for the mixes, slump flow tests were conducted on fresh mixes used for manufacturing specimens in subsequent tests. The slump flow tests captured the effects of varying density and cementitious density, and of introducing high proportions of silica fume and slag.

	Filler-Binder Ratio (Nominal Density, kg/m^3)							
Cementitious Blend	0 : 1 (600)	0.5 : 1 (800)	1 : 1 (1000)	1.5 : 1 (1200)	2 : 1 (1400)	2.5 : 1 (1600)	3 : 1 (1800)	3.5 : 1 (2000)
12% Silica	*				*			
6% Silica								
100% Portland	**		*		*		*	
30% Slag								
50% Slag								

Table 4.2.2 Mix designs tested for slump flow.

4.2.3 Segregation

Evaluations of segregation were conducted on mixes across a broad range of densities, cementitious densities, and cementitious blends, to confirm the viability of proposed mixes.

	Filler-Binder Ratio (Nominal Density, kg/m^3)							
Cementitious Blend	0 : 1 (600)	0.5 : 1 (800)	1 : 1 (1000)	1.5 : 1 (1200)	2 : 1 (1400)	2.5 : 1 (1600)	3 : 1 (1800)	3.5 : 1 (2000)
12% Silica	*				*			
6% Silica								
100% Portland	**		*		*		*	
30% Slag								
50% Slag								

Table 4.2.3 Mix designs tested for segregation.

4.2.4 Modulus of Elasticity, Poisson's Ratio

The modulus of elasticity and Poisson's ratio were evaluated on specimens at 28- and 56 days, over a range of densities. Mixes with only modest additions of SCM's were excluded, since measured differences between mixes were anticipated to be subtle.

Cementitious Blend		Filler-Binder Ratio (Nominal Density, kg/m³)							
		0 : 1 (600)	0.5 : 1 (800)	1 : 1 (1000)	1.5 : 1 (1200)	2 : 1 (1400)	2.5 : 1 (1600)	3 : 1 (1800)	3.5 : 1 (2000)
12% Silica		*		*		*		*	
6% Silica									
100% Portland		**		*		*		*	
30% Slag									
50% Slag									

Table 4.2.4 Mix designs tested for 28- and 56-day modulus of elasticity and Poisson's ratio.

4.2.5 Crushing Behaviour

Stress-strain curves were generated for specimens at 28- and 56 days, over a range of densities and with high proportions of silica fume and slag, to capture overall trends. Peak strengths from this large dataset were also compared to the compression testing results described above, to demonstrate repeatability.

Cementitious Blend		Filler-Binder Ratio (Nominal Density, kg/m³)							
		0 : 1 (600)	0.5 : 1 (800)	1 : 1 (1000)	1.5 : 1 (1200)	2 : 1 (1400)	2.5 : 1 (1600)	3 : 1 (1800)	3.5 : 1 (2000)
12% Silica		*		*		*		*	
6% Silica									
100% Portland		**		*		*		*	
30% Slag									
50% Slag									

Table 4.2.5 Mix designs tested for 28- and 56-day crushing behaviour.

4.2.6 Creep

Creep testing was conducted for a low-density Portland cement mix at 20 and 40% of its compressive strength, to observe how foam concrete may perform over the long term in fill applications. Higher density mixes were tested at 40% of their respective compressive strengths, for structural use: 12% silica fume and 50% slag mixes were included to detect whether SCM chemistry or particle-packing offered improvements.

Cementitious Blend		Filler-Binder Ratio (Nominal Density, kg/m³)							
		0 : 1 (600)	0.5 : 1 (800)	1 : 1 (1000)	1.5 : 1 (1200)	2 : 1 (1400)	2.5 : 1 (1600)	3 : 1 (1800)	3.5 : 1 (2000)
12% Silica									
6% Silica									
100% Portland									
30% Slag									
50% Slag									

Table 4.2.6a Mix designs tested for creep at 20% of compressive strength.

Cementitious Blend		Filler-Binder Ratio (Nominal Density, kg/m³)							
		0 : 1 (600)	0.5 : 1 (800)	1 : 1 (1000)	1.5 : 1 (1200)	2 : 1 (1400)	2.5 : 1 (1600)	3 : 1 (1800)	3.5 : 1 (2000)
12% Silica									
6% Silica									
100% Portland									
30% Slag									
50% Slag									

Table 4.2.6b Mix designs tested for creep at 40% of compressive strength.

4.2.7 Drying Shrinkage

Drying shrinkage was monitored for Portland cement, 12% silica fume, and 50% slag mixes, to determine the effects of density, cementitious density, and binder composition.

Cementitious Blend		Filler-Binder Ratio (Nominal Density, kg/m³)							
		0 : 1 (600)	0.5 : 1 (800)	1 : 1 (1000)	1.5 : 1 (1200)	2 : 1 (1400)	2.5 : 1 (1600)	3 : 1 (1800)	3.5 : 1 (2000)
12% Silica		*		*		*		*	
6% Silica									
100% Portland		**		*		*		*	
30% Slag									
50% Slag									

Table 4.2.7 Mix designs tested for drying shrinkage.

4.2.8 Capillary Water Uptake

A wide range of samples was tested for capillary water uptake indices, to observe how capillary water uptake varies with density and cementitious blend.

Cementitious Blend	Filler-Binder Ratio (Nominal Density, kg/m^3)							
	0 : 1 (600)	0.5 : 1 (800)	1 : 1 (1000)	1.5 : 1 (1200)	2 : 1 (1400)	2.5 : 1 (1600)	3 : 1 (1800)	3.5 : 1 (2000)
12% Silica								
6% Silica								
100% Portland								
30% Slag								
50% Slag								

Table 4.2.8 Mix designs tested for capillary water uptake.

4.2.9 Moisture Storage and Moisture Movement

Moisture storage and moisture movement were plotted for a range of mixes to capture trends for varying density, cementitious density and cementitious blend.

Cementitious Blend	Filler-Binder Ratio (Nominal Density, kg/m^3)							
	0 : 1 (600)	0.5 : 1 (800)	1 : 1 (1000)	1.5 : 1 (1200)	2 : 1 (1400)	2.5 : 1 (1600)	3 : 1 (1800)	3.5 : 1 (2000)
12% Silica								
6% Silica								
100% Portland	**							
30% Slag								
50% Slag								

Table 4.2.9 Mix designs tested for equilibrium moisture content and moisture movement.

4.2.10 Thermal Resistance

The thermal resistance of foam concrete was tested for a range of lower density Portland cement binder samples.

Thermal resistance is strongly dependent on density, and it was not anticipated that varying the binder composition would have a significant influence on thermal performance, for a given density. However, initial investigations revealed that 12% silica fume samples exhibited particularly fine air-voids. In response to this observation, samples with 12% silica fume binder were tested, to consider whether observable differences in microstructure have any discernable influence on the thermal resistance of mixes of similar density.

Cementitious Blend		Filler-Binder Ratio (Nominal Density, kg/m³)							
		0 : 1 (600)	0.5 : 1 (800)	1 : 1 (1000)	1.5 : 1 (1200)	2 : 1 (1400)	2.5 : 1 (1600)	3 : 1 (1800)	3.5 : 1 (2000)
12% Silica									
6% Silica									
100% Portland		*		*		*			
30% Slag									
50% Slag									

Table 4.2.10 Mix designs tested for thermal resistance.

4.2.11 Freeze-Thaw Resistance

Freeze-thaw resistance testing was conducted for Portland cement, 12% silica fume, and 50% slag mixes, to detect the effects of density and binder composition at varying degrees of saturation of distilled water.

Cementitious Blend		Filler-Binder Ratio (Nominal Density, kg/m³)							
		0 : 1 (600)	0.5 : 1 (800)	1 : 1 (1000)	1.5 : 1 (1200)	2 : 1 (1400)	2.5 : 1 (1600)	3 : 1 (1800)	3.5 : 1 (2000)
12% Silica									
6% Silica									
100% Portland									
30% Slag									
50% Slag									

Table 4.2.11a Mix designs tested for freeze-thaw resistance.

Saline freeze-thaw testing was used to indicate how foam concrete would perform in applications subject to de-icing salts and cold temperatures, such as roadways.

Accumulations of debris from relatively dense foam concrete mixes of 1400 and 1800 kg/m³, intended for structural applications, were compared to typical limits for normal density air-entrained concrete, to observe the influence of air-void volume on saline freeze-thaw resistance.

Cementitious Blend	Filler-Binder Ratio (Nominal Density, kg/m³)							
	0 : 1 (600)	0.5 : 1 (800)	1 : 1 (1000)	1.5 : 1 (1200)	2 : 1 (1400)	2.5 : 1 (1600)	3 : 1 (1800)	3.5 : 1 (2000)
12% Silica								
6% Silica								
100% Portland								
30% Slag								
50% Slag								

Table 4.2.11b Mix designs tested for saline freeze-thaw resistance.

4.2.12 Microstructural Analysis

Images were taken of the microstructure of each mix combination, and reproduced at various levels of magnification to assist in making general observations about the size and interconnectivity of air-voids for mixes of varying density and cementitious blends.

Cementitious Blend	Filler-Binder Ratio (Nominal Density, kg/m³)							
	0 : 1 (600)	0.5 : 1 (800)	1 : 1 (1000)	1.5 : 1 (1200)	2 : 1 (1400)	2.5 : 1 (1600)	3 : 1 (1800)	3.5 : 1 (2000)
12% Silica								
6% Silica								
100% Portland								
30% Slag								
50% Slag								

Table 4.2.12a Mix designs selected for qualitative air-void analysis.

Air-void analysis was used to quantify how air-void size distribution is influenced by the introduction of silica fume and slag as partial binder replacements, at two different densities.

Cementitious Blend	Filler-Binder Ratio (Nominal Density, kg/m³)							
	0 : 1 (600)	0.5 : 1 (800)	1 : 1 (1000)	1.5 : 1 (1200)	2 : 1 (1400)	2.5 : 1 (1600)	3 : 1 (1800)	3.5 : 1 (2000)
12% Silica								
6% Silica								
100% Portland								
30% Slag								
50% Slag								

Table 4.2.12b Mix designs selected for quantitative air-void analysis.

4.3 Scope of Testing: Foam Concrete Aggregate Mixes

The use of crushed and graded foam concrete as an inert, lightweight aggregate was an additional area of exploration within the Experimental Program. Implications and possibilities for the production of Foam Concrete Aggregate (FCA) material are discussed further in Appendix E.

Over fifty concrete mix designs incorporating foam concrete were evaluated during the course of this research. Two mix designs are included within the experimental results, for reference:

- Portland cement FCA with 600 kg/m^3 nominal density, in a Portland cement foam concrete matrix with 600 kg/m^3 nominal density
- Portland cement FCA with 1400 kg/m^3 nominal density, in a Portland cement foam concrete matrix with 1400 kg/m^3 nominal density

The FCA and matrix of both mix designs were produced with cementitious densities of 410 kg/m^3. FCA particle size was approximately 10mm. Limited testing results have been provided as part of this thesis. The remainder of the data related to FCA will be published at a later time, as part of ongoing research activities.

5

Experimental Program: Methodologies

5.1 General Parameters for Specimen Manufacture

5.1.1 Materials

Cementitious materials used for experimental testing were Type I Portland cement conforming to ASTM C150, ground granulated blast furnace slag conforming to ASTM C989, and silica fume conforming to ASTM C1240. The filler used was natural sand conforming to ASTM C33, Table 1. Grading data from a typical sample is shown in Appendix F. 'Dry,' prefoamed, protein-based foam was prepared using a commercial aerator machine, with a chemical admixture dilution ratio of 1:120, and an aerated density of between 68 and 70 g/L. Details of the surfactant and aerating equipment are supplied in Appendices G and H, respectively. Dilution and dosing water was potable, from a municipal source.

5.1.2 Mix Proportioning

The chosen methodology for mix proportioning is explained in Appendix D. Foam volume was regulated in response to desired mass of binder, mass of filler, and water-binder ratios. The quantity of sand and mixing water were corrected daily according to the moisture

content of the sand.

Note that water-binder ratios cited throughout the Experimental Program do not include the contribution of the surfactant dilution water. Rather, the dilution water is assumed to be necessary for the stability of the foam, and should not contribute immediately to the hydration water available to the cement particles. Furthermore, in an industrial setting, it is more expedient to state a water-binder ratio in relation to the cementitious content only, rather than having to subtract the contribution of dilution water in the foam volume, which is dependent upon density. However, some studies may choose to include the dilution water when reporting water-binder ratios. A method for determining Equivalent Water-Binder Ratios, including contribution of dilution water, is given in Appendix I. Further discussion is presented in Section 6.1.1.6.

5.1.3 Laboratory Mixing Process

Batches were produced in the laboratory unless otherwise noted, using a 700 L commercial barrel mixer. Before commencing each batch, the mixer was firstly wetted and drained. The required volume of water was then loaded, in accordance with ASTM C796, Section 8.5. The mixer was activated, and cementitious materials were added incrementally over a period of 30 seconds. Clumps of cement were broken up with a trowel until an even consistency was achieved. Any required sand was also added and mixed for 5 minutes to produce a homogenous paste.

Next, preformed dry foam was produced with a commercial aerator. A slightly conservative quantity of foam was added to the mix, based on calculated values. When the foam had been thoroughly blended into the cement paste (after approximately 3 minutes), a tared weighing container of known volume was filled with a representative sample of the foam concrete mix in conformance with ASTM C796, Section 8.7. The plastic density of the mix was calculated. Mixes within ±50 kg/m^3 of target density were accepted, as recommended by ASTM C796, Section 7.3.1. For mixes with a plastic density higher than the acceptable range, foam was added incrementally to the mixer, and blended thoroughly, until the target density was achieved. If the plastic density was found to be lower than the acceptable range, the mix was discarded.

Figure 5.1.3a Image of thoroughly blended, fresh foam concrete in a laboratory mixer.

Figure 5.1.3b Many foam concrete mixes tested in the experimental program were also produced in the field for real-world applications during the course of this research. Cf. Section 6.1.3.

5.1.4 Typical Casting Processes

Nominal 100 x 200 mm cylindrical specimens were produced with reference to ASTM C495. Fresh concrete was placed in non-reusable plastic moulds 100±2 mm in diameter and 200±3 mm in length, in two layers. After placing each layer, the outside of the mould was tapped lightly 10 to 15 times with an open hand to close voids. Each mould was overfilled, and the mortar surface struck-off. The samples were weighed, and the plastic density calculated and recorded to the nearest 10 kg/m^3. The specimens were covered to prevent evaporation.

Nominal 50 x 150 mm cylindrical specimens were cast in plastic moulds 50±2 mm in diameter and 150±2 mm in length. Fresh concrete was placed in three layers. After placing each layer, the fresh concrete was gently rodded 10 to 15 times with a 10 mm diameter steel rod, to close voids. Each mould was overfilled, and the mortar surface struck-off. The specimens were covered to prevent evaporation.

Other specimen formats were cast and placed as described in the methodologies below.

Demoulding was completed in accordance with ASTM C495, Section 6.5, with specimens removed after risk of damage was past, but always within 7 days after the date of creation.

5.1.5 Typical Moist-Curing Regimes

Unless noted otherwise, 28-day and 56-day moist-curing regimes were completed as outlined in the following tables. Moist-curing occurred in a commercial humidity room designed for curing concrete samples.

Period	Temperature	Humidity
Day 1	23±2°C	Seal-cured (contained in moulds)
Day 2* to Day 28	23±2°C	Moist-cured
Day 28	Removal from moist-curing environment for testing or for further conditioning	
** N.B. Where fragile specimens were at risk of damage during demoulding, removal from moulds was delayed in accordance with ASTM C495, Section 6.5.*		

Table 5.1.5a Typical 28-day curing regime.

Figure 5.1.4a Typical finished surface of fresh (left) and hardened (right) foam concrete in 100 x 200mm plastic moulds. The mix on the left is sanded, while the mix on the right contains no aggregate.

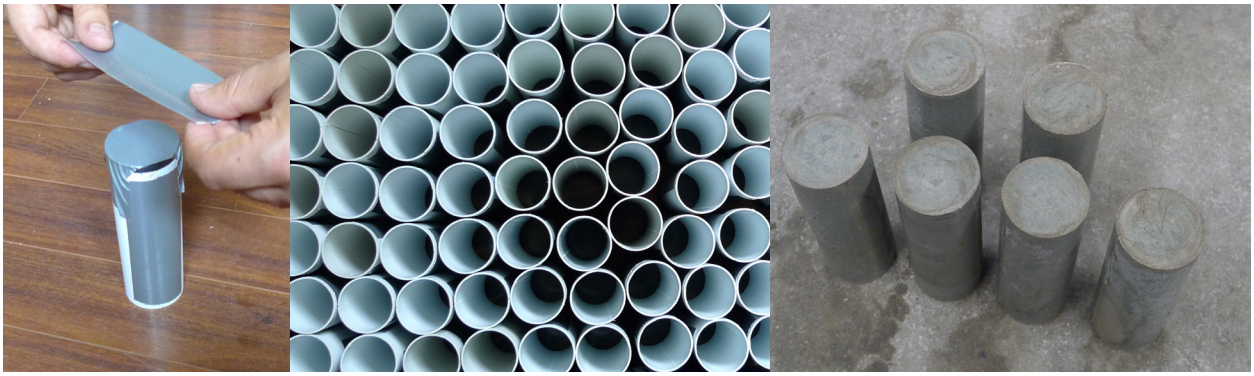

Figure 5.1.4b 50 x 150mm moulds, made from PVC (central vac) tubing and PP disc base. The PVC tubing was cut longitudintally and taped together again, for ease of demoulding. Castings were consistently circular, ±1mm.

Figure 5.1.4c Demoulding process for 50 x 300mm diameter specimens, used for drying shrinkage testing. Refer to Section 5.5.1.

Period	Temperature	Humidity
Day 1	23±2°C	Seal-cured (contained in moulds)
Day 2* to Day 56	23±2°C	Moist-cured
Day 56	Removal from moist-curing environment for testing or for further conditioning	
** N.B. Where fragile specimens were at risk of damage during demoulding, removal from moulds was delayed in accordance with ASTM C495, Section 6.5.*		

Table 5.1.5b Typical 56-day curing regime.

5.1.6 Typical Precision of Mass, Length Change Measurements

Masses were measured on a laboratory balance sensitive to within 0.1% of the weight of the specimen. Unless otherwise noted, specimens were deemed to have reached equilibrium (i.e., 'constant mass') in a given environment when change in mass was less than 0.1% per day.

Unless noted otherwise, changes in length were measured using a length comparator with a positive means of contact with the specimen via polished, heat-treated terminals, and a dial micrometer graduated to read in units of 0.002 mm or better.

5.2 Determining Porosities and Densities

5.2.1 Apparent Porosity and Density Values

Apparent porosity was determined through vacuum saturation.[1] For each mix tested, 50 x 150 mm cylindrical specimens were moist-cured for 28 days, and then exposed to 50±2% relative humidity and 25±2°C until constant mass (minimum one year).

The mature specimens were oven-dried for two days at 50±0.9°C, and then evacuated in dryness at 21±2°C for 24 hours at a pressure of 100 to 205 N/m^2.[2] The vacuum pump was turned on for no less than four 30-minute intervals during the 24-hour period, in order to exhaust gases from the chamber. Thereafter, distilled water at 21±2°C was let into the chamber as swiftly as possible, entirely covering the specimens. Vacuum pressure was maintained for 24 hours in the flooded chamber, allowing any remaining gases to migrate above the water surface. After the vacuum pressure was released,

1 Cf. Fagerlund (1977), ASTM C830-00. In Chapter 6, 'porosity' refers to apparent porosity by vacuum saturation.
2 This approach varies somewhat from ASTM C830. Refer to Appendix J.

Figure 5.2.1a Vaccum saturation chamber, resevoir, pump, and drying oven.

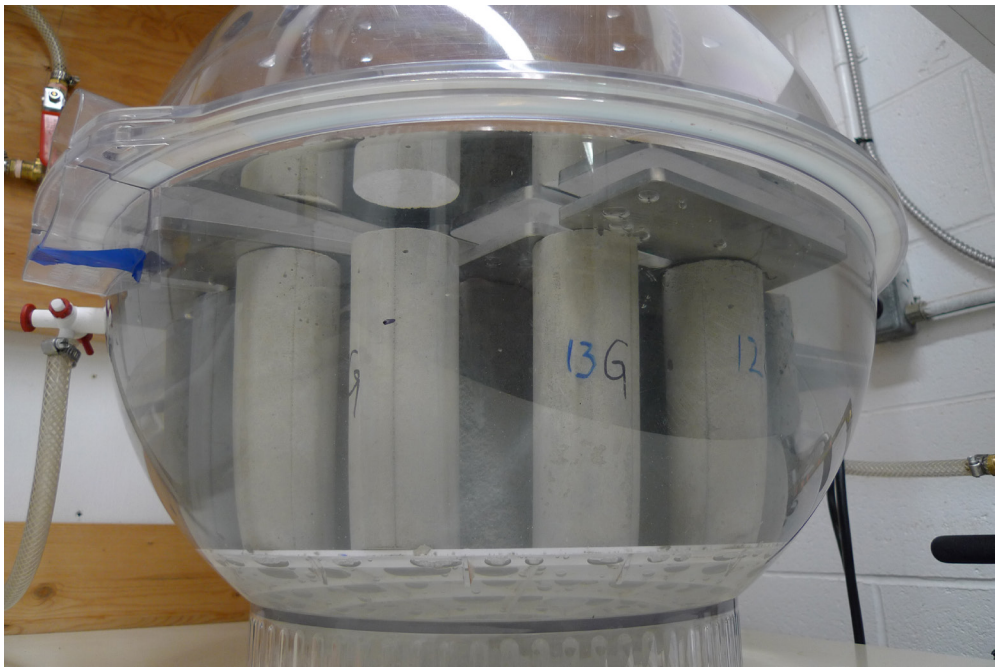

Figure 5.2.1b 50 x 150mm specimens tested for porosity, after a long period of evacuation. Stainless steel plates were used as weights to act against the bouyancy of low-density specimens with dry interiors, during the initial entry of water into the chamber.

specimens were removed from the vacuum chamber and quickly placed underwater for storage until volume and mass measurements could be determined.

Total sample volume, V, was determined by rapidly removing each specimen from underwater, briefly permitting excess water to drip from the specimen surface, totally immersing it in a water-filled container, and measuring the displacement of water gravimetrically.[2] Saturated weight in air, $Q_{s:a}$, was measured as the mass of the saturated sample, wiped with a moist cloth. Oven dry density, $Q_{d:105}$, was determined by drying the samples at 105±0.9°C in an oven with forced ventilation, until constant mass. Apparent porosity was calculated as $(Q_{s:a} - Q_{d:105})/(V \bullet \rho_{water})$, where ρ_{water} is the density of water.

Actual dry density values were determined by dividing the equilibrium mass of a specimen at 50% RH, by the volume of the saturated specimen. Actual oven-dry density values were taken as oven-dried mass, divided by the volume of the saturated specimen.

Actual plastic densities were determined by dividing the mass of fresh concrete in a tared container, by the volume of the container. The volume of the container was determined gravimetrically, using a balance sensitive to within 0.1% of the weight of the filled container.

5.2.2 Theoretical Porosity and Density Values

Where testing results refer to theoretical porosity, values have been calculated from known mix ingredients, as described in Appendix K.

Similarly, theoretical dry or oven-dry densities are calculated from known mix ingredients. Theoretical dry values assume that 40% of free mix water remain in the specimen in dry conditions, as capillary and adsorbed water. Refer to Appendix L.

5.3 Plastic Properties Testing

5.3.1 Slump Flow

The slump flow of various mixes was tested with reference ASTM C1611, Filling Procedure B (Inverted Mold, Section 8.3.3). This ASTM method is intended for measuring the slump

[2] This approach varies somewhat from ASTM C830. Refer to Appendix J.

Figure 5.3.1 Typical spread of fresh foam concrete.

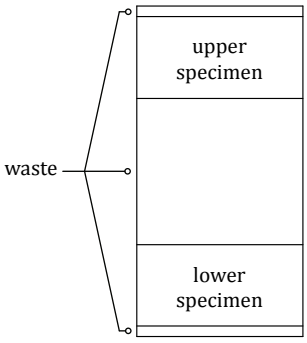

Figure 5.3.2 50mm high specimens were cut from the bottom and top of 100 x 200mm cylinders for segregation testing (left), and oven-dried (right). A 6mm thick layer was removed from the top and bottom surface of the cylinder, to eliminate local effects of particle packing and finishing on density.

flow of self-consolidated concrete, but is also commonly used to quantify the flow characteristics of foam concrete.[3]

A sample of freshly mixed concrete was placed in a metal mold conforming to ASTM C143, with a dampened interior and with the large opening of the mold facing downwards (i.e., 'inverted'). The concrete was placed in one lift without tamping or vibration. The surface of the concrete was struck off, excess concrete was removed from the base of the mold, and the mold was raised a distance of 225 ± 75 mm in 3±1 seconds with a steady upward lift. The entire test, from filling to removal of the mold, was completed within 2 minutes, 30 seconds.

After the concrete ceased spreading, the largest diameter of the concrete mass was measured to the nearest 5 mm. A second diameter was measured at an angle approximately perpendicular to the first measured diameter. Slump flow was taken as the average of the two diameters. If the two diameters differed by more than 50 mm, the test was deemed invalid, and was repeated.

The degree of circularity of the circumference of the concrete mass was observed qualitatively, and recorded. The presence of any 'halo' of bleedwater around the outside circumference of the concrete was also noted.

5.3.2 Segregation

Cylindrical test specimens, 100 x 200 mm, were cast and cured, as described in Sections 5.1.4 and 5.1.5. After 56 days of moist-curing, 6 mm thick slices were cut from both ends of the cylinder using a lapidary saw, to remove cast and finished surfaces. Subsequently, 50 mm high cylindrical sections were cut from both ends of the cylinder. The 50 mm high cylindrical sections were oven-dried at 50°C until constant mass, which was recorded as dry mass. Specimens were then immersed in limewater until constant mass. Total sample volume, V, was determined by rapidly removing each specimen from underwater, wiping it with a moist cloth, totally immersing it in a water-filled container, and measuring the displacement of water gravimetrically (refer to Appendix J). Dry density was taken to be

[3] Note that ASTM C143/C143M, "Standard Test Method for Slump of Hydraulic-Cement Concrete," is not suitable for foam concrete, since concretes having slumps greater than about 230 mm may not be adequately cohesive for the test to have significance. Refer to Note 2 in the Standard.

dry mass divided by volume of the saturated specimen, and the density of the two 50 mm high cylinders was compared.

Where segregation of mix ingredients was visibly apparent, the condition of the specimens was also documented with photographs.

5.4 Mechanical Testing

5.4.1 Compressive Strength

Proportioning, Mixing, and Casting

Proportioning and mixing was completed in accordance with Section 5.1.2 and 5.1.3. Water-binder ratio was varied from 0.35 to as high as 0.85, in increments of 0.05. Foam volume was adjusted to compensate for variations in the water-binder ratio. Cylindrical test specimens, 100 x 200 mm, were cast as described in Sections 5.1.4.

Curing

Specimens were moist-cured in a commercial humidity room designed for curing concrete samples. The curing regime was designed with reference to ASTM C495, Section 6.6, as outlined in the following tables.

Period	Temperature	Humidity
Day 1	23±2°C	Seal-cured (contained in moulds)
Day 2* to Day 6	23±2°C	Moist-cured
Day 7	23±2°C	Air-cured @ 45 ± 10 % RH
Day 7	7-Day Compression Testing	
** N.B. Where fragile specimens were at risk of damage during demoulding, removal from moulds was delayed in accordance with ASTM C495, Section 6.5.*		

Table 5.4.1a Curing regime for 7-day compression testing.

Period	Temperature	Humidity
Day 1	23±2°C	Seal-cured (contained in moulds)
Day 2* to Day 25	23±2°C	Moist-cured
Day 26 to Day 28	23±2°C	Air-cured @ 45 ± 10 % RH
Day 28	28-Day Compression Testing	
** N.B. Where fragile specimens were at risk of damage during demoulding, removal from moulds was delayed in accordance with ASTM C495, Section 6.5.*		

Table 5.4.1b Curing regime for 28-day compression testing.

Period	Temperature	Humidity
Day 1	23±2°C	Seal-cured (contained in moulds)
Day 2* to Day 53	23±2°C	Moist-cured
Day 54 to Day 56	23±2°C	Air-cured @ 45 ± 10 % RH
Day 56	56-Day Compression Testing	
** N.B. Where fragile specimens were at risk of damage during demoulding, removal from moulds was delayed in accordance with ASTM C495, Section 6.5.*		

Table 5.4.1c Curing regime for 56-day compression testing

Measurements

Upon removal from moulds, the height of the specimen was measured to the nearest 0.5 mm. The diameter of the specimen was measured to the nearest 0.5 mm, calculated as the average of two diameters measured at right angles to each other at about midheight of the specimen. The cylinder was weighed. Its density was calculated from the measured dimensions, and recorded to the nearest 10 kg/m^3.

Testing

Compression testing was conducted with reference to ASTM C495, Section 7. Four cylinders of 100 x 200 mm were used for 28-day compressive strength. Two cylinders of 100 x 200 mm were used for 7-day compressive strength, to provide an indication of strength development. Three additional cylinders were cast for 56-day compressive strength testing, to provide an indication of longer-term strength gain. These 56-day cylinders were tested, if 28-day compressive strength results were favourable.

Figure 5.4.1a Specimens were capped with sulphur and tested for compressive strength.

Figure 5.4.1b Additional compression tests were performed on unbonded specimens, in a different testing frame. (Refer to Section 5.4.4.) Results are compared in Figures 6.6.1.1a to 6.6.1.3b.

Bearing faces of the test specimen were capped in accordance with ASTM C617, using molten sulfur. Capped surfaces were made plane within 0.05 mm. (Additional tests were conducted with specimen ends ground plane to within 0.05 mm, for comparison. Refer to Section 5.4.4.)

After the sulfur caps had hardened sufficiently, bearing faces of the test specimen and compression machine were wiped clean. The specimen was seated centrally between the upper and lower bearing blocks. The applied load was increased continuously at a constant rate, such that the maximum load was reached in 65 ± 15 seconds, in conformance with ASTM C495, Section 7.2. The maximum load, type of failure, and appearance of the concrete were recorded. Unit compressive strength was found by dividing the maximum load by the average cross-sectional area.

5.4.2 Static Modulus of Elasticity

Specimen Preparation

Proportioning and mixing was completed in accordance with Section 5.1.2 and 5.1.3. For each mix design and hydration time, three 100 x 200 mm cylindrical test specimens were cast as described in Section 5.1.4. The water-binder ratio for each mix design was based on optimal values previously determined during the course of the compression testing described in Sections 5.4.1, above.

Curing

Specimens were moist-cured in in a commercial humidity room designed for curing concrete samples. Specimens were briefly removed from the humidity room one day prior to testing, for end-grinding of bearing faces in conformance with ASTM C617. Specimens were removed from the humidity room again just prior to testing, as described in the following tables.

Period	Temperature	Humidity
Day 1	23±2°C	Seal-cured (contained in moulds)
Day 2* to Day 27	23±2°C	Moist-cured
Day 27	23±2°C	Exposed to lab air and running water during end-grinding of cylinders
Day 27 to Day 28	23±2°C	Moist-cured
Day 28 (less than 1 hour prior to testing)	23±2°C	Air-cured @ 45 ± 10 % RH
Day 28	28-Day Modulus of Elasticity Testing	
** N.B. Where fragile specimens were at risk of damage during demoulding, removal from moulds was delayed in accordance with ASTM C495, Section 6.5.*		

Table 5.4.2a Curing regime for 28-day modulus of elasticity testing.

Period	Temperature	Humidity
Day 1	23±2°C	Seal-cured (contained in moulds)
Day 2* to Day 55	23±2°C	Moist-cured
Day 55	23±2°C	Exposed to lab air and running water during end-grinding of cylinders
Day 55 to Day 56	23±2°C	Moist-cured
Day 56 (less than 1 hour prior to testing)	23±2°C	Air-cured @ 45 ± 10 % RH
Day 56	56-Day Modulus of Elasticity Testing	
** N.B. Where fragile specimens were at risk of damage during demoulding, removal from moulds was delayed in accordance with ASTM C495, Section 6.5.*		

Table 5.4.2b Curing regime for 56-day modulus of elasticity testing.

Companion specimens

Prior to modulus of elasticity testing, three 100 x 200 mm companion cylinders with the same mix design and curing regime were compression tested in conformance with Section 5.4.1. The maximum applied load used for modulus of elasticity testing was equal to 40% of the average ultimate load of the companion specimens.

Measurements

Just prior to testing, the height of each specimen was measured to the nearest 0.1 mm. The diameter of the specimen was measured to the nearest 0.1 mm, calculated as the average of two diameters measured at right angles to each other at about midheight of the specimen.

Testing

Testing was conducted with reference to ASTM C469. An unbonded compressometer sensing device was used, consisting of two yokes. One yoke was rigidly attached to the specimen, and the other was attached at two diametrically opposite points so that it was free to rotate. At one point on the circumference of the rotating yoke, midway between two diametrically opposite support points, was a pivot rod, used to maintain a constant distance of 100 mm between the two yokes at that location. At the opposite point on the circumference of the rotating yoke, the change in distance between the yokes was continuously measured using a string potentiometer, capable of measuring to the nearest 1.27 μm.

Bearing faces of the test specimen and compression machine were wiped clean. The specimen was seated centrally between the upper and lower bearing blocks. The lower bearing block was elevated at a constant rate of 1 mm per minute in conformance with ASTM C499, Section 6.4. When the applied load reached 40% of the average ultimate load of the companion specimens, the actuator direction reversed, travelling at a rate of 1 mm per minute. When the actuator returned to its origin, another compression cycle began. The specimen was loaded six times. Data from the first cycle was excluded due to seating effects, and calculations were based only on subsequent loadings.

Longitudinal deformation of the cylinder under load was calculated according to the following formula:

$$d = \frac{g\ e_r}{(e_r + e_g)}$$

where

d is the total deformation of the specimen throughout the effective gauge length [μm],

g is the gauge reading [μm],

e_r is the perpendicular distance, measured to the nearest 0.2 mm from the pivot rod to the vertical plane passing through the two support points of the rotating yoke, and

e_g is the perpendicular distance, measured to the nearest 0.2 mm from the gauge to the vertical plane passing through the two support points of the rotating yoke.

Figure 5.4.2a Set-up for testing of modulus of elasticity and Poisson's ratio. An unbonded compressometer is attached to the specimen; the specimen is seated centrally in the testing frame. As load is applied, changes in specimen height and diameter are recorded continuously.

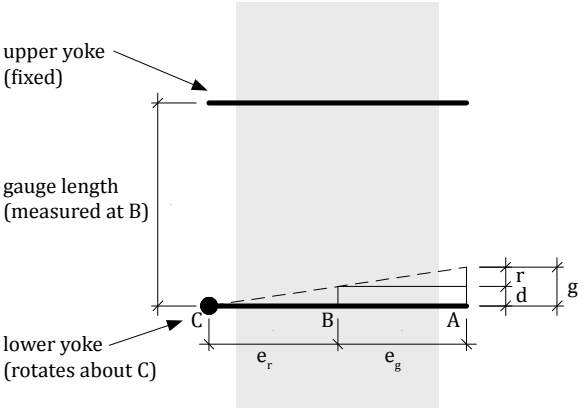

A location of gauge
B support point of the rotating yoke
C location of pivot rod

d displacement due to specimen deformation
r displacement due to rotation of the yoke about the pivot rod
g gauge reading
e_r perpendicular distance from the pivot rod to the vertical plane passing through the two support points of the rotating yoke
e_g perpendicular distance from the gauge to the vertical plane passing through the two support points of the rotating yoke

Figure 5.4.2b Diagram of displacements for modulus of elasticity testing. Elevation view.

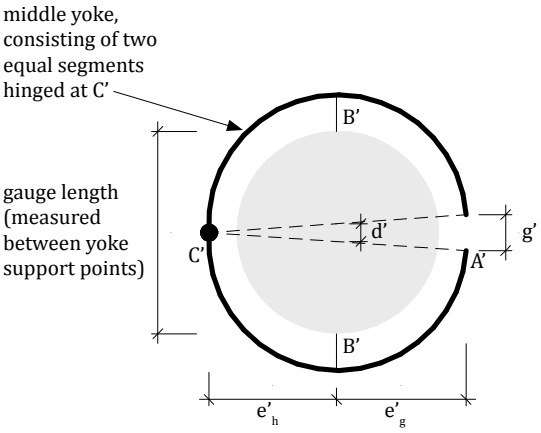

A' location of transverse gauge
B' support point of the yoke segments
C' location of hinge between yoke segments

d' transverse deformation of the specimen diameter
g' transverse gauge reading
e'_h perpendicular distance from the hinge to the vertical plane passing through the two support points of the middle yoke
e'_g perpendicular distance from the gauge to the vertical plane passing through the two support points of the middle yoke

Figure 5.4.3 Diagram of displacements for Poisson's ratio testing. Plan view. Refer to Section 5.4.3.

A stress-strain curve was plotted for each cycle. Strain was determined as the total deformation of the specimen throughout the effective gauge length, d, divided by the effective gauge length, 100 mm. Stress was calculated as applied force divided by the average cross-sectional area of each specimen.

The modulus of elasticity, E, was calculated as

$$E = \frac{S_2 - S_1}{(\varepsilon_2 - 0.00050)}$$

where

S_2 is the stress corresponding to 40% of ultimate load,

S_1 is the stress corresponding a longitudinal strain of 50 x 10^{-6}, and

ε_2 is the longitudinal strain produced by stress S_2.

An average modulus of elasticity, E_{avg}, was found from the data for cycles 2 to 6.

5.4.3 Poisson's Ratio

Specimen Preparation, Curing, and Measurements

The same specimens used for modulus of elasticity testing were simultaneously evaluated for Poisson's ratio. The maximum applied load used for Poisson's ratio testing was equal to 40% of the average ultimate load of three companion specimens.

Testing

Testing was conducted with reference to ASTM C469-14, using an unbonded extensometer sensing device. Halfway between the two compressometer yokes used for modulus of elasticity testing, a third yoke, consisting of two equal segments, was attached to the specimen at two diametrically opposite points. The yoke was hinged at one point on its circumference, midway between two diametrically opposite points, allowing the two segments of the yoke to rotate in the horizontal plane. At the opposite point on the circumference of the yoke, the change in distance between the yokes segments was

continuously measured using a string potentiometer, capable of measuring to the nearest 1.27 μm.

Bearing faces of the test specimen and compression machine were wiped clean. The specimen was seated centrally between the upper and lower bearing blocks. The lower bearing block was elevated at a constant rate of 1 mm per minute in conformance with ASTM C499, Section 6.4. When the applied load reached 40% of the average ultimate load of the companion specimens, the actuator direction reversed, travelling at a rate of 1 mm per minute. When the actuator returned to its origin, another compression cycle began. The specimen was loaded six times. Data from the first cycle was excluded due to seating effects, and calculations were based only on subsequent loadings.

Transverse deformation of the cylinder under load was calculated according to the following formula:

$$d' = \frac{g'\, e'_h}{\left(e'_h + e'_g\right)}$$

where

d' is the total transverse deformation of the specimen diameter [μm],

g' is the transverse gauge reading [μm],

e'_h is the perpendicular distance, measured to the nearest 0.2 mm, from the hinge to the vertical plane passing through the two support points of the middle yoke, and

e'_g is the perpendicular distance, measured to the nearest 0.2 mm from the gauge to the vertical plane passing through the two support points of the middle yoke.

Longitudinal strain, determined for the evaluation of modulus elasticity, was plotted against transverse strain, for each cycle. Transverse strain was taken as the measured change in specimen diameter, d', divided by the original diameter.

Poisson's ratio, μ, was calculated from the modulus of elasticity data, as well as the transverse strain, according to the formula

$$\mu = \frac{\varepsilon_{t2} - \varepsilon_{t1}}{(\varepsilon_2 - 0.00050)}$$

where

ε_{t2} is the transverse strain at midheight of the specimen produced by stress S_2, and

ε_{t1} is the transverse strain at midheight of the specimen produced by stress S_1.

The calculated Poisson's ratio was drawn on the plot of longitudinal strain against transverse strain, in order to confirm linearity of the relationship. An average Poisson's ratio, μ_{avg}, was found from the data for cycles 2 to 6.

5.4.4 Crushing Behaviour

Specimen Preparation, Curing, and Measurements

The same specimens used for modulus of elasticity testing and Poisson's ratio were subsequently evaluated for crushing behaviour.

Testing

Immediately after the testing cycles were completed for determining modulus of elasticity and Poisson's ratio, the yoke apparatus used to measure displacements was removed.

The specimen was re-seated centrally between the upper and lower bearing blocks of the compression machine. The lower bearing block was elevated at a constant rate of 1 mm per minute, applying load to the specimen, such that the maximum load was reached in 65 ± 15 seconds, in conformance with ASTM C495, Section 7.2.

During crushing, the compression machine continuously recorded the displacement of the actuator and the force applied to the specimen. Strain was determined as actuator displacement after contact with the specimen, divided by the height of the specimen. Stress was found by dividing the applied force by the average cross-sectional area of the specimen. Stress-strain curves were plotted from the data.[4]

The test was stopped after a total actuator displacement of 4 mm. The maximum load, type of failure, and appearance of the concrete were recorded. Unit compressive

[4] The initial portion of each plot (i.e., where the applied load were less than 20% of the maximum load) was permitted to be adjusted to eliminate seating effects, based on the linearity of data collected during Modulus of Elasticity testing in Section 5.4.2.

strength was found by dividing the maximum applied force by the average cross-sectional area of the specimen.

5.4.5 Creep

Specimen Preparation

Eight 100 x 200 mm cylindrical specimens were proportioned, mixed, and cast in accordance with Sections 5.1.2 to 5.1.4.

Companion specimens

Just prior to modulus of elasticity testing, three of the 100 x 200 mm cylinders were compression tested in conformance with Section 5.4.1, except that ends were ground plane, rather than being capped with molten sulphur. The maximum applied load used for the first creep test was equal to 20% of the average ultimate load of the companion specimens. The maximum applied load used for the remainder of the creep tests was equal to 40% of the average ultimate load of the companion specimens.

Testing

Evaluation of creep was based on a modified form of ASTM C512.[5]

Specimens were moist-cured for a total of 56 days. After 55 days of curing, specimens were temporarily removed from the humidity room. Bearing faces were end-ground in conformance with ASTM C617, and exposed surfaces were then permitted to desorb to laboratory air for up to 2 hours. Two pairs of stainless steel locating discs, suitable for receiving a demountable mechanical (DEMEC) strain gauge, were epoxied on diametrically opposite sides along the length of each specimen, at gauge lengths of 100 mm. After the epoxy had hardened for 1 hour, specimens were returned to the fog room for the final day of curing.

At 56 days, the gauge distance between pairs of locating discs were recorded to the nearest 0.002 mm, as initial gauge length measurements. The height of each specimen was measured to the nearest 0.1 mm. The diameter of the specimen was measured to the

[5] ASTM C512/C512M-15

nearest 0.1 mm, calculated as the average of two diameters measured at right angles to each other at about midheight of the specimen.

All five cylinders were then removed from the humidity room, and brought to an environment maintained at a temperature of 25±2°C, and relative humidity of 50±2%. Specimens were maintained in a moist environment until just prior to being stacked in the loading frame.

Three cylinders were stacked in a steel loading frame, as shown in Figure 5.**4.5a**. The cylinders were separated by 3.2 mm thick steel plates, acting as transfer plates to avoid transmitting differential strain between specimens. The top and bottom of the loading frame were connected with two threaded rod assemblies. 12 mm thick upper and lower steel platens were located midway between the two threaded rods, separated from the steel frame by 19 mm diameter spherical steel spheres centred in conical depressions, to reduce eccentric loading on the cylinder stack. A load cell was placed above the uppermost cylinder, between the upper platen and a 3.2 mm thick steel plate. Compression was applied to the specimens by tightening nuts at the top of the threaded rods against stacks of disc springs, designed for the intended loads. The stiff disc springs reduced variation in applied loading due to displacement resulting from deformation of the cylinders. The desired compression was achieved within 5 minutes of applying load.

The two remaining cylinders for each mix were used as control specimens, placed in the same environment as the loaded samples, to observe the length change due to drying shrinkage. The ends of the two control specimens were capped with microcrystalline wax, so that moisture loss would match the drying patterns of the loaded specimens, where moisture loss through the ends was prevented by the steel plates.

Following the initial loading, measurements of loaded and control specimens were taken according to the following schedule:

- immediately
- daily until the end of the first week
- weekly until the end of the first month
- monthly thereafter until the end of six months
- bi-monthly thereafter until the end of one year

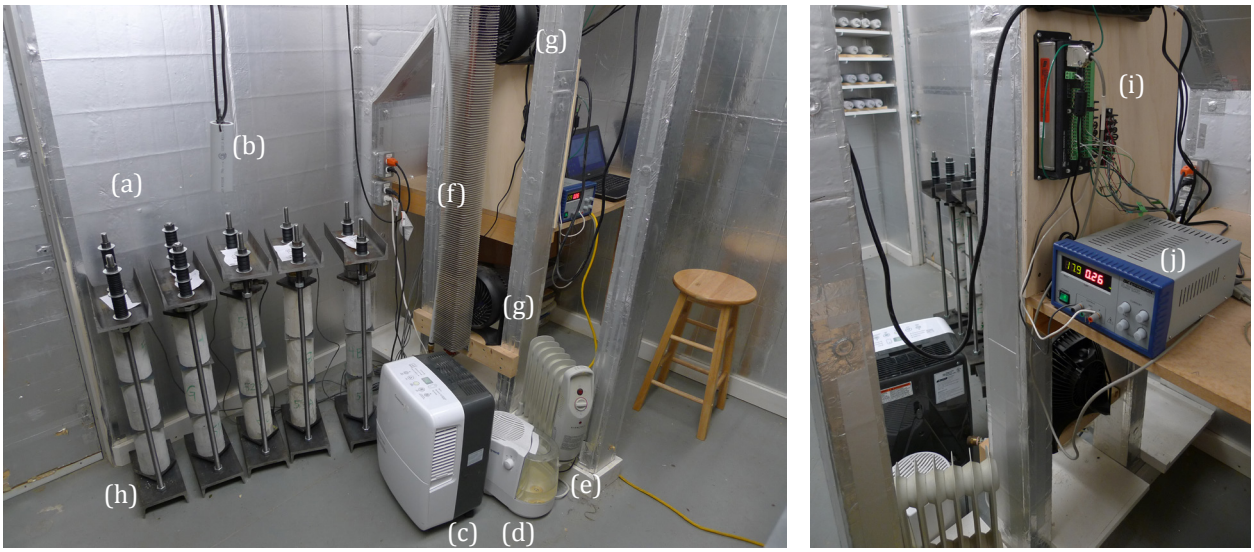

Figure 5.4.5a Unsealed creep specimens in controlled climate chamber: (a) insulated, low emissivity walls; (b) temerature and RH sensor; (c) dehumidifier; (d) humidifier; (e) electric resistance heater; (f) cooling coil; (g) fans; (h) creep frames with specimens; (i) data logger; (j) power supply.

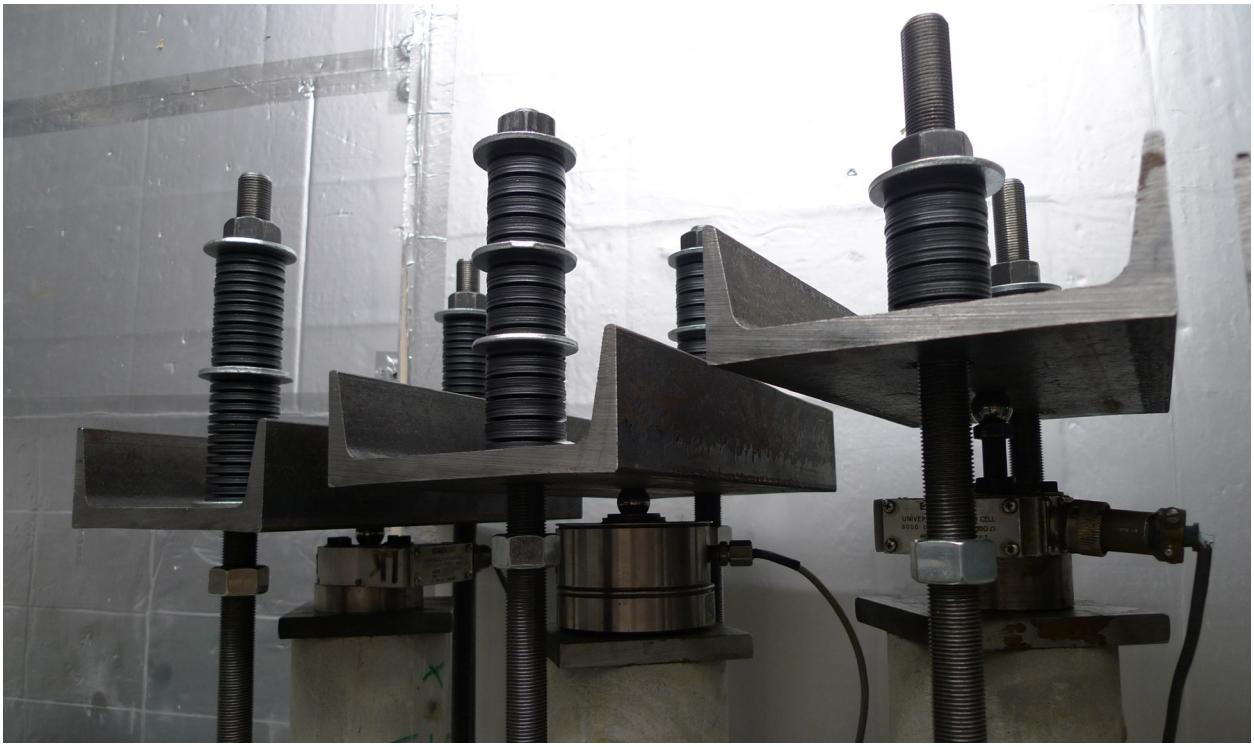

Figure 5.4.5b Detail of creep frames. Specimens bear against thick steel platens. Load cells bear against spherical steel spheres, centred in conical depressions in the steel frame, to reduce eccentric loading on the cylinder stack. Varying combinations of disc springs, tuned for each intended load, reduce variation in applied loading as the specimens deform. Nuts on the threaded rods are tightened regularly to accomodate displacement.

Loaded specimens were evaluated for changes in length, and control specimens were evaluated for changes in length as well as changes in mass, to register the loss of moisture from the specimens. The nuts at the top of the assembly were routinely tightened, to keep applied loads close to target loads, accounting for creep of the specimens. Actual applied loads are available in Appendix R.

The total load-induced strain per unit stress at any time was calculated as the difference between the average strain values of the loaded and control specimens, divided by the average stress. To determine creep strain per unit stress at a given age, the strain per unit stress immediately after loading was subtracted from the total load-induced strain per unit stress at that age.

The total strain per unit stress was plotted against a logarithmic axis of time, to determine the constants 1/E and F(K) for the following equation:

$$\varepsilon = \left(\frac{1}{E}\right) + F(K)\ln(t+1)$$

where ε is the total strain per unit stress, MPa;

E is the instantaneous elastic modulus, MPa;

$F(K)$ is the creep rate, calculated as the slope of a straight line representing the creep curve on a semilog plot; and

t is the time after loading, days.

1/E is the initial elastic strain per unit stress, and was determined from the strain readings taken immediately before and after loading of the specimen.

An alternative methodology for evaluating creep was also developed, as described in Appendix M. This methodology proposed applying force using a gravity load and a lever arm, to minimize the possibility of variation in the applied force, due to the changing length of the specimens during the course of the experiment. However, the smaller scale of the creep apparatus proved to be more convenient during this experimental program. The smaller testing apparatus allowed testing to be conducted in a climate control chamber with more tightly controlled conditions. The variation in loading experienced during testing was managed through routine tightening of the nuts against the disc spring stacks.

5.5 Hygroscopic Testing

5.5.1 Drying Shrinkage

Evaluation of drying shrinkage was conducted with reference to ASTM C157,[6] and MTO Test Method LS-435.[7] Alterations to the standard, especially in the manner of specimen preparation, helped facilitate the rapid manufacture of a large number of specimens.

Specimen Preparation

Mixes were proportioned in conformance with Section 5.1.2. Ingredients were brought to a temperature of between 18 and 24°C prior to mixing.

Three cylindrical specimens were cast for each mix design, in vertical plastic moulds of 50±2 mm diameter and 300 mm height. Moulds were lightly coated with concrete form release oil. Fresh foam concrete was placed in approximately 6 layers. After placing each layer, the outside of the mould was tapped lightly 5 to 10 times with an open hand to close voids. When the concrete was within 15±3 mm of the top of the mould, a 7.9 mm diameter x 57 mm long (5/16" dia. x 2 ¼") stainless steel bolt was suspended into the mix, with the head of the bolt directed downwards. The head and plain shank were embedded to a depth of approximately 35 mm, such that the distance from the bottom of the concrete to the lower surface of the bolt head was 250±2 mm. The plain shank was coated with concrete form release oil prior to placement, so that drying shrinkage in the concrete above the bolt head would have minimal influence on length change occurring below the bolt head. During set-up of the concrete, the bolt was threaded into a tee-nut, which was supported on a 6 mm thick piece of open cell foam, adhered to a plastic cap. The foam permitted initial shrinkage of the concrete, without inducing additional stresses at the bolt head. (Refer to Figure 5.**1.4c**.)

All specimens were demoulded at 23 hours, 30 minutes ± 15 minutes after initial hydration of the cement. A stainless steel domed cap nut, with a 0.5 mm diameter central conical drilled depression, was turned onto the threaded end of the bolt and jammed against a stainless steel nut. A DEMEC stainless steel locating disc was epoxied to the

[6] ASTM C157/C157M-08
[7] MTO Test Method LS-435 (2001)

centre of the bottom face of the cylindrical specimen. Specimens were placed in their respective curing environments at 24 hours ± 15 minutes after initial hydration of the cement.

Curing

The influence of curing regime on drying shrinkage was matter of interest in this study. Three distinct curing regimes were used, for comparison.

The first curing regime included moist-curing in a commercial humidity room designed for curing concrete samples, and lasted for 28 days.

Period	Temperature	Humidity
Day 1	23±2°C	Seal-cured (contained in moulds)
Day 2* to Day 28	23±2°C	Moist-cured
End of Day 28	Removal from moist-curing environment	
** N.B. Day 2 began at 24 hours ± 15 minutes after initial hydration of the cement, for all specimens.*		

Table 5.5.1a 28-day moist-curing regime for drying shrinkage specimens.

The second curing regime included water-curing in limewater, saturated with high-calcium hydrated lime in conformance with ASTM C511, Section 7.2, and lasted for 28 days.

Period	Temperature	Humidity
Day 1	25±2°C	Seal-cured (contained in moulds)
Day 2* to Day 28	25±2°C	Water-cured
End of Day 28	Removal from moist-curing environment	
** N.B. Day 2 began at 24 hours ± 15 minutes after initial hydration of the cement, for all specimens.*		

Table 5.5.1b 28-day water-curing regime for drying shrinkage specimens.

The third curing regime included water-curing in limewater, saturated with high-calcium hydrated lime in conformance with ASTM C511, Section 7.2. Specimens were seal-cured for 24 hours, followed by 24 hours of water-curing.

Figure 5.5.1a Drying shrinkage specimens in controlled climate chamber.

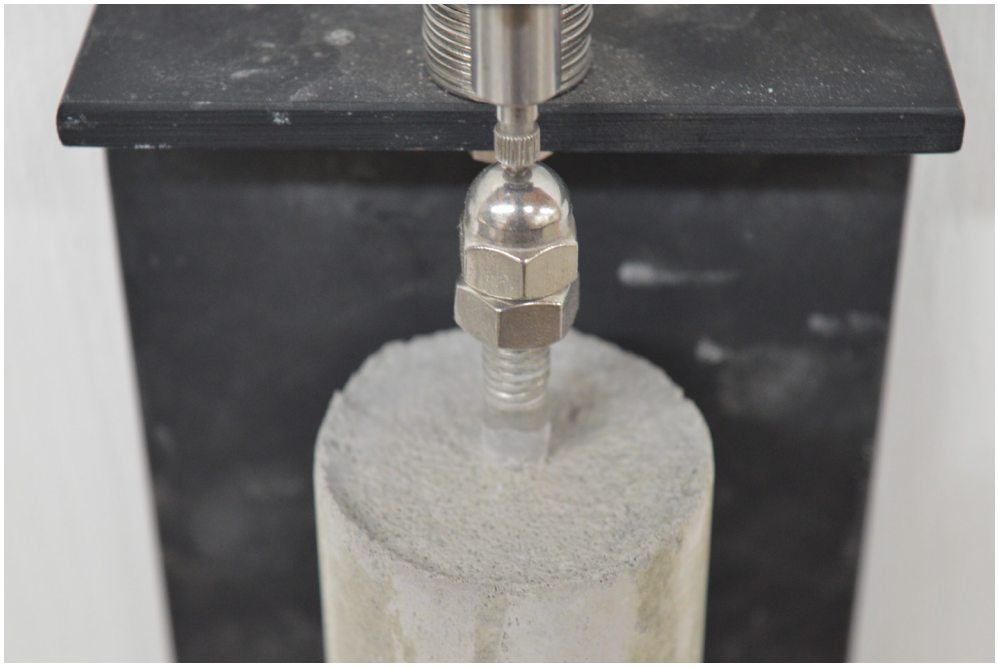

Figure 5.5.1b Detail of stainless steel domed cap nut, mounted on stainless steel bolt. A central conical drilled depression in the cap nut provided a reliable, positive means of contact with the the terminals of the dial gauge. The plain shank of the embedded bolt was coated with form release oil prior to placement, to reduce influence on length change below the bolt head.

Period	Temperature	Humidity
Day 1	25±2°C	Seal-cured (contained in moulds)
Day 2*	25±2°C	Water-cured
End of Day 2**	Removal from water-curing environment	
** N.B. Day 2 began at 24 hours ± 15 minutes after initial hydration of the cement, for all specimens.* *** N.B. Day 2 ended at 48 hours ± 15 minutes after initial hydration of the cement.*		

Table 5.5.1c 1-day water-curing regime for drying shrinkage specimens.

Testing

Upon completion of the curing regime, the length and mass of each specimen was recorded in conformance with Section 5.1.6. Thereafter, specimens were stored in a curing environment of 25±2°C and 50±2% relative humidity. A minimum 25 mm gap was maintained between specimens for the first four months; thereafter, specimens were permitted to be stored within 10 mm of each other, to reduce space requirements. Regular measurements were taken according the following schedule:

- daily until the end of the first week
- weekly until the end of the first month
- at 28 days, and at 56 day
- bimonthly thereafter until the end of one year

The actual time at which measurements were taken was recorded within a five-minute accuracy. The change in length due to drying shrinkage of each specimen was plotted against time, on a semi-log graph.

The mass of specimens was adjusted to account for the stainless steel studs and locating discs, and change was plotted against time, on a semi-log graph.

Measurements from 7 days, 28 days, 56 days, 112 days, and 12 months after the end of the curing regime, were taken at the prescribed time interval ± 1%. This level of precision was deemed sufficient to facilitate numeric comparison of specimen results at these time intervals.

Shrinkage testing results were also compared to the movement of unloaded companion cylinders used in the creep testing described in Section 5.4.5.

Companion specimens

For several of the mix designs and curing regimes tested, 50 x 150 mm cylindrical specimens were cast from the same fresh batch, in conformance with the process described in Section 5.1.4. These companion specimens were subject to the same curing regimes and drying environments as the drying shrinkage specimens. By measuring their masses during drying, and evaluating the specimens in conformance with Section 5.2.1, the loss of moisture content over time could be expressed as a percentage of dry mass or volume, for the 50 mm diameter cylindrical specimens.[8]

5.5.2 Moisture Storage

Drying shrinkage specimens described in Section 5.5.1 were also used to produce moisture storage functions for the mixes. Specimens were water-cured for 28 days, and then conditioned for one year at 50±2% RH, as noted above.

Equilibrium moisture contents (EMCs) at 25±2°C and 50±2% were established for each mix. 50 x 150 mm companion specimens were oven-dried at 105±2°C until constant mass, to drive free water out of the specimens. The specimens were then vacuum-saturated, and volumes determined as described in Appendix J. EMC was taken to be the change in mass from 50% RH to oven dry conditions, divided by volume.

A second set of 50 x 150 mm companion specimens, conditioned at 50% RH, was immersed in water until constant mass, facilitating liquid water absorption (saturation). Volumes were determined gravimetrically; specimens were then oven-dried at 105±2°C. Water absorption at saturation was taken to be the change in mass from saturated to oven-dry conditions, divided by volume.

Concurrently, specimens were stored at 50±2, 80±2, and 90±2% RH, respectively. Temperature was maintained at 25±2°C in these three environments. The mass of the steel studs and locating discs was subtracted from the measured masses. Accumulated moisture content relative to oven dry mass was calculated based on EMCs determined at 50% RH,

[8] The rate of drying of both the 50 x 150 mm and 50 x 250 mm specimens is assumed to be similar, since the surface area of the curved cylinder wall will have a dominant influence on the drying potential for both specimen formats.

and the proportional increase in the mass of the foam concrete. EMCs for humid environments were determined after specimens had reached constant mass.

Moisture storage functions at 25°C were produced by plotting equilibrium moisture content against relative humidity.

5.5.3 Moisture Movement

Cylindrical specimens, 50 x 150 mm, were conditioned in 50±2 % RH for one year. Stainless steel locating discs were epoxied to the centre of cylinder ends. Length and mass, with and without locating discs, were recorded. One set of specimens were immersed in water at 25°C, facilitating liquid water absorption (saturation). A second set of specimens were oven-dried at 50±0.9°C until constant mass.

The change in length of the specimens subjected to immersion and drying, respectively, were plotted as a percentage of the initial length of the specimen at 50% RH.

Drying shrinkage specimens described in Section 5.5.1 were re-used for an additional investigation. Specimens stored in 50% RH were immersed in distilled water for 14 days. Length and mass measurements were recorded periodically. The saturated specimens were subsequently returned to storage in 50±2% RH. Length and mass measurements were recorded periodically, until specimens reached constant mass. Initial specimen length in 50% RH was compared to the length after one wetting and drying cycle.

5.5.4 Capillary Water Uptake

Capillary water uptake was determined through the method of assessing the capillary degree of saturation proposed by Fagerlund,[9] and with reference to the recommendations of ISO 15148[10] and ASTM C1585.[11] Cylindrical specimens, 200 x 100 mm, were cast and moist-cured for 56 days. Two 50±2 mm high samples were cut from the center of cured cylinders for each mix design. The cylindrical sections were stored in 50±10% RH for more than three months, until constant mass. Specimens were then placed on a plastic lattice in a tray of water such that one flat surface was immersed in 1 to 3 mm of water. Water and

[9] Fagerlund (1977).
[10] ISO 15148 (2002)
[11] ASTM C1585-13

Figure 5.5.4a 50 x 150mm specimens immersed fully in water, for water absorption and moisture movement testing.

Figure 5.5.4b 100 x 50mm specimens, with lower surface immersed in 1 to 3mm of water, for capillary water uptake testing.

air temperature were maintained at 23±2°C. Water was added to the tray to maintain immersion of the surface, as required. Samples were taken from the lattice and weighed at intervals of 2, 5, 10, 30 minutes; 1 2, 4, 6, 24 hours; and 2, 4, 7, 14 days, from the start of the test. The accumulation of water mass in the sample per unit area of immersed surface was plotted against the square root of time, and interpreted in accordance with ISO 15148 and ASTM C1585. (A discussion of differing methodologies is presented in Appendix M.)

The degree of capillary saturation for each specimen, S_{CAP}, was defined as the degree of saturation for water uptake times longer than the 'nick-point time'; that is, the time at which water uptake sharply decelerates, as indicated on a plot against the square root of time. The calculated degrees of saturation for shorter times cannot be used since an upper part of the specimen is still dry and, consequently, the values are not representative of the lower, wet part. The degree of capillary saturation is used for establishing the freeze-thaw resistance of various mixes, as explained in Section 5.8.1 below.

In order to consider the influence of specimen conditioning on capillary water uptake, a variation of the test was conducted. All aspects of the testing remained the same, including the specimens used, except that prior to wetting, specimens were placed in a ventilated drying oven at 50±0.9°C until constant mass to drive free water out of the specimens. Results of the two testing protocols were compared. Specimens were oven-dried at 105±0.9°C, in conformance with the methodology described in Section 5.2.1, in order to determine the initial degrees of saturation of the specimens for both tests.

5.6 Thermal Testing

5.6.1 Thermal Conductivity

Steady state thermal conductivity was performed with reference to ASTM C518 using a LaserComp heat flow meter instrument, manufacturered by LaserComp Inc. Selected mixes were proportioned, mixed and placed stiff, non-absorbent moulds to produce foam concrete panels with approximate dimensions of 200 x 200 x 75 mm. After 28 days of moist-curing, the panels were conditioned in an environment of 23±2°C and 50±10% RH for six months prior to the start of the test. The mass of each specimen was recorded to the

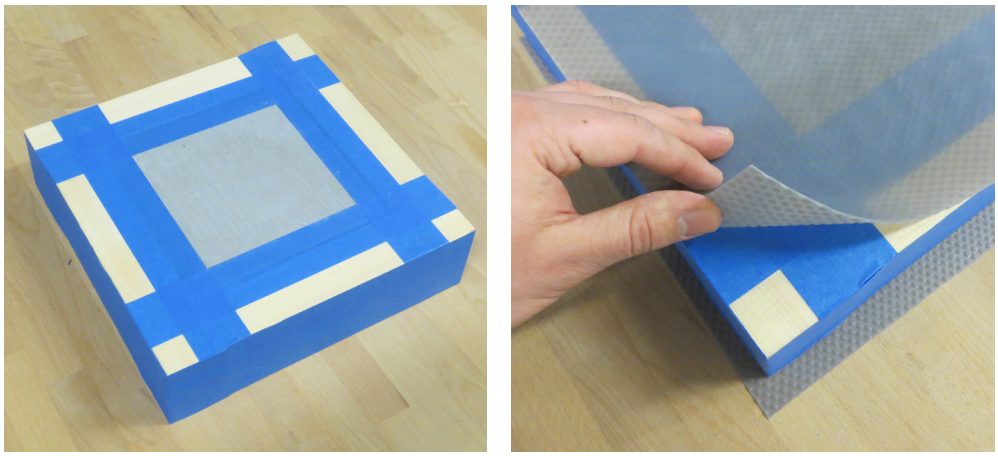

Figure 5.6.1a Foam concrete panel for thermal thermal conductivity testing, taped tightly to pine guard (left). Flexible, dimpled plastic facers mats (right) were used to ensure consistent conductivity between the specimens and the hot and cold plates of the guarded hot plate apparatus.

Figure 5.6.1b Set-up for thermal conductivity testing. Specimen is loaded in the guarded hot plate apparatus on right. Heat transfer between the hot plate, panel, and cold plate is automatically recorded every minute until steady state conditions are achieved.

nearest 0.1g, and the dimensions of each panel were recorded to the nearest 0.5 mm. Density was calculated as the quotient of mass and volume and reported to the nearest 10 kg/m^3.

Each panel was then prepared for testing in a guarded hot plate apparatus. A thermal guard of clear white pine was affixed to the perimeter of each foam concrete panel, producing a panel with overall dimensions of 300 x 300 x 75 mm, suitable for the dimensions of the apparatus. The guard was assumed to have a sufficiently similar thermal conductivity as the foam concrete panels, to facilitate steady-state conditions. Furthermore, a flexible, dimpled plastic mat approximately 1 mm thick was placed as a facer on the top and bottom of the sample, to ensure consistent conductivity between the specimen and the hot and cold plates of the guarded hot plate apparatus, despite any roughness or unevenness in the casting surface.

A hot plate with a temperature was placed on top of the panel, while a cold plate was placed at the base of the panel, for mean temperatures of −4, 4, 10, and 24°C. (Hot plate setpoint temperatures were 10, 18, 24, and 38°C, while cold plate setpoint temperatures were −18, −10, −8 and 10°C, respectively.) Heat transfer between the hot plate, panel, and cold plate was automatically recorded every minute until steady state conditions were achieved. Data was analyzed using software to determine an average thermal conductivity value for the assembly. The thermal resistance for the foam concrete panel was determined by subtracting the contribution of the flexible, dimpled plastic mat, as described in Appendix N.

The thermal resistance value for each specimen was plotted against its density, and compared to other values published in the open literature.

5.7 Freeze-Thaw Testing

5.7.1 Freeze-Thaw Susceptibility: Degree of Saturation

Freeze-thaw susceptibility was determined with reference to the method proposed by Fagerlund.[12] For each mix design, 7 cylindrical specimens of 50 mm diameter and 150 mm

[12] Fagerlund (1977)

length were cast, moist-cured for 28 days, and then stored at 50±2% RH and 25±2°C until constant mass. Stainless steel locating discs were epoxied on either end of each specimen. The mass of the specimens plus locating discs was recorded, and length was determined to the nearest 0.002 mm.

Preliminary benchmarks for 0% and 100% saturation were established based on dry densities at 50% RH and long-term immersion, respectively, of companion specimens.

Freeze-thaw specimens were then wetted. Specimens were not vacuum-saturated, since this process might distribute moisture throughout the pore structure of the foam concrete in a way that was not representative of actual moisture ingress in foam concrete. Large quantities of water would be drawn by vacuum into air voids, producing high apparent moisture content values. However, water in partially filled air voids can freeze and thaw without inducing damage, causing the foam concrete specimens to appear unrealistically freeze-thaw resistant for a given moisture content.[13] Instead, foam concrete specimens were permitted to soak in distilled water,[14] fully saturating the capillary pore structure, since accumulation of ice in filled capillary voids is typically responsible for mechanical damage.[15]

The length of each saturated sample was recorded to the nearest 0.002 mm. The volume of each saturated specimen was determined via displacement in water. (Refer to Appendix J.) The first three specimens were then permitted to dry in air, such that they were conditioned to degrees of saturation of 60, 80 and 100%, based on their densities. Upon reaching a desired degree of saturation, the length and mass of each specimen was recorded. Each specimen was wrapped in a continuous vapour barrier in such a way that locating disc were exposed (Figure 5.**7.1a**). Length could thus be measured without removing the vapour barrier and exposing the specimen to dry air, reducing the risk of moisture movement (refer to Section 6.13).

---

[13] Conversely, small, insolated voids of the freeze-thaw specimens that would not normally fill with liquid water might be saturated by vacuum pressure, and might not readily release moisture during drying, affecting results.

[14] Immersing the specimens in distilled water will have some effect on the chemistry of the hardened cement paste, as calcium hydroxide is leached from the specimens. Nevertheless, use of distilled water was deemed preferable to limewater, to reduce osmotic effects during freezing.

[15] Refer to Appendix A, Section 6.3.5c for further discussion. Refer also to Appendix M for a discussion of methodologies.

The wrapped specimens were sealed in polyethylene bags and suspended in a freeze-thaw bath of 30% propylene glycol in aqueous solution. The following freeze-thaw regime was repeated for 12 cycles:

- bath temperature of 10°C maintained for a 1-hour period
- bath temperature decreased from 10°C to −15°C over a 2-hour period
- bath temperature of −15°C maintained for a 2-hour period
- bath temperature increased from −15°C to 10°C over a 2-hour period
- bath temperature of 10°C maintained for a 1-hour period

After 12 cycles, the specimens were allowed to acclimatize to an ambient temperature of 23±2°C. They were removed from their seals, and the length and mass of each sample was immediately measured. Any evident length change (dilation) in the sample was deemed to have been caused by freeze-thaw damage.

Length change was plotted against degree of saturation. The critical degree of saturation, S_{CR}, was defined as the nick-point value indicated by the figure. The critical degree of saturation represents the highest degree of saturation that may be permitted for the mix design, without significant risk of freeze-thaw damage.

Based on the critical degree of saturation indicated by the figure, additional degrees of saturation were established to provide greater resolution around the apparent critical degree of saturation. Untested and undamaged specimens were conditioned to these new benchmarks, and subjected to the freeze-thaw regime described above. New data was added to the plot, and the value for S_{CR} was refined. Damaged specimens were oven-dried to precisely determine their moisture content at the time of freeze-thaw testing; plots of dilation against moisture content were updated accordingly.

The critical degree of saturation was compared to actual degrees of saturation for mixes in various states of wetting, such as for various times of capillary water uptake.

5.7.2 Freeze-Thaw Susceptibility: Saline Scaling

This test method was developed with reference to Test Method LS-412 from the Ministry of Transportation, Ontario,[16] and ASTM C1262. The methodology described below is an

[16] MTO LS-412 (1997). Cf. OPSS 1352 (1989).

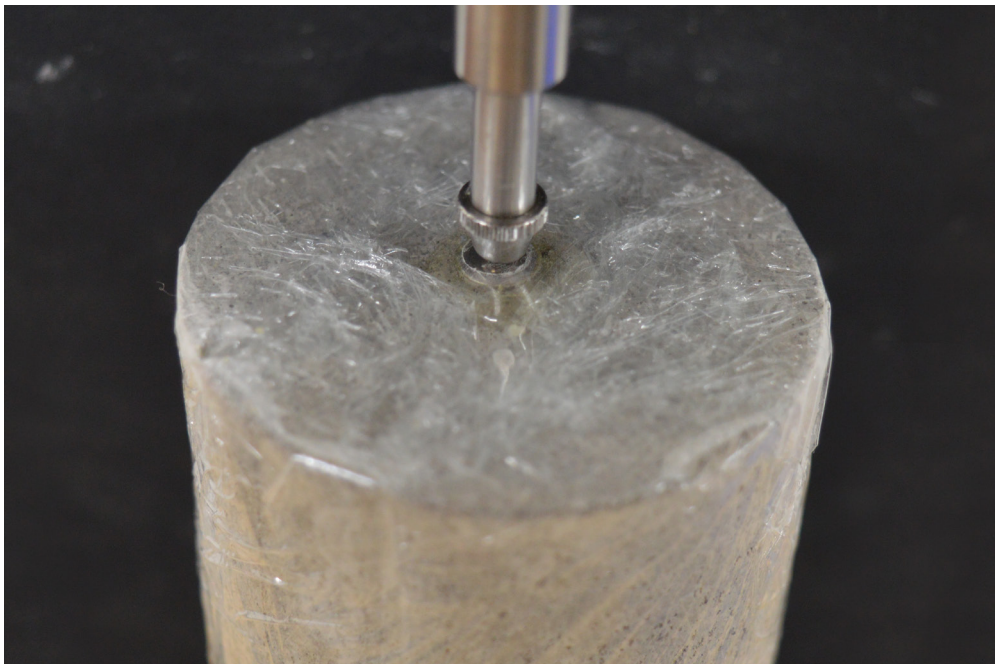

Figure 5.7.1a 50 x 150mm specimen sealed to prevent moisture loss. A 4mm diameter apeture in the taped ends, centred on the stainless steel locating discs, facilicated a positive connection to the terminals of the length comparator.

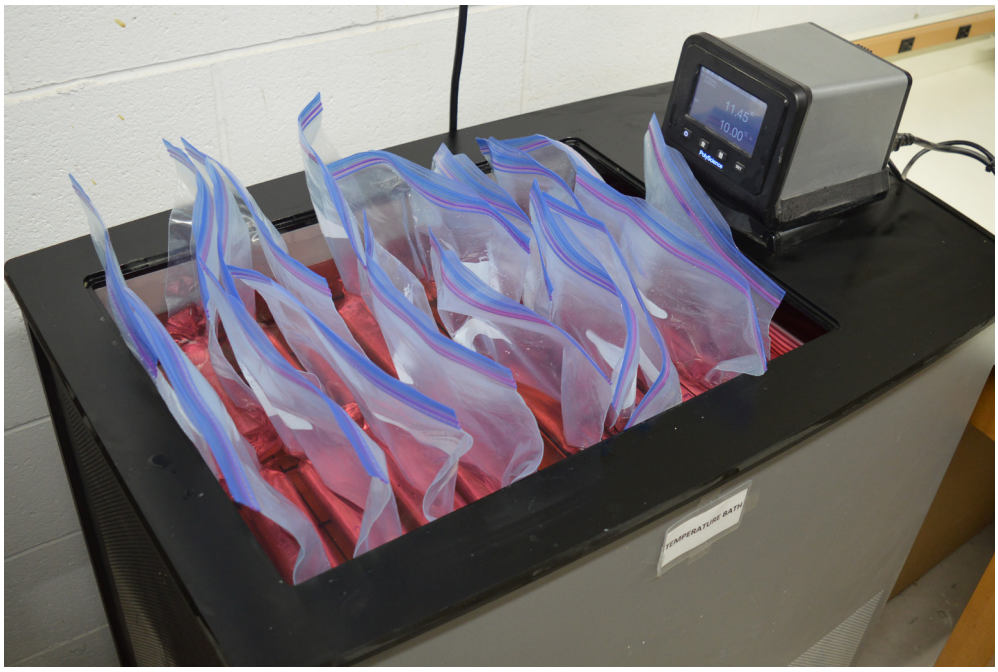

Figure 5.7.1b Specimens were suspended in a freeze-thaw bath of 30% propylene glycol, and subjected to 12 freeze-thaw cycles. Evident length change (dilation) in the sample was deemed to have been caused by freeze-thaw damage.

adaptation of these standard for foam concrete testing. Note that an initial trial was attempted which adhered more strictly to the MTO standard, but this methodology was abandoned as unsuitable for use with foam concrete, as explained in Appendix M.

For each mix design, three foam concrete panels were cast in rigid, non-absorptive, prismatic moulds, with dimensions of 300 x 200 x 75 mm. Specimens were moist-cured for 56 days.

At 56 days, each specimen was placed in a pan, elevated above the bottom of the pan using two 2 mm thick by 10 mm wide by 250 mm long strips of polymethylmacrlite. The strips were located along the short edges of the specimens, such that the contact area of the foam concrete and PMMA was 10 mm by 200 mm. The finished face of the specimen was oriented downwards. Pans were tapered, to accommodate expansion of water during freezing.

A solution of 3% sodium chloride was poured into two of the pans to a depth of 4±1 mm, such that one surface of the specimen was submerged to a depth of 2±1 mm. The remaining pan was filled to the same depth with distilled water. The specimens were stored at room temperature for 24 hours, to permit capillary water uptake. Liquid in the pans was replenished as required.

The panels were then stored in a freezing environment of −18±2°C, supported on wooden strips to permit free circulation of cold air, for between 16 and 18 hours. After this time, the samples were permitted to thaw for 6 to 8 hours in a condition of 23±2°C and a relative humidity of 50±5%. Aqueous solution was added as required to maintain an immersed depth of 2±1 mm, before returning the samples to the freezing environment for the next cycle.[17] The order of the panels in the freezing chamber was rotated with each freezing cycle.

After five freeze-thaw cycles, any loose flakes and particles of concrete were washed from the surface of each panel and collected in a funnel of filter paper. The particles were oven-dried at 50±0.9°C until constant mass, and the loss of mass from each panel was recorded.

[17] In general, the immersed face of the specimens remained saturated, while the top surface of the panels were dry, due to sublimation of capillary water exposed to freezing air. Approximately 6 hours after the start of each thawing cycle, any condensation that had collected on the cold concrete was wiped once with a dry clean cloth.

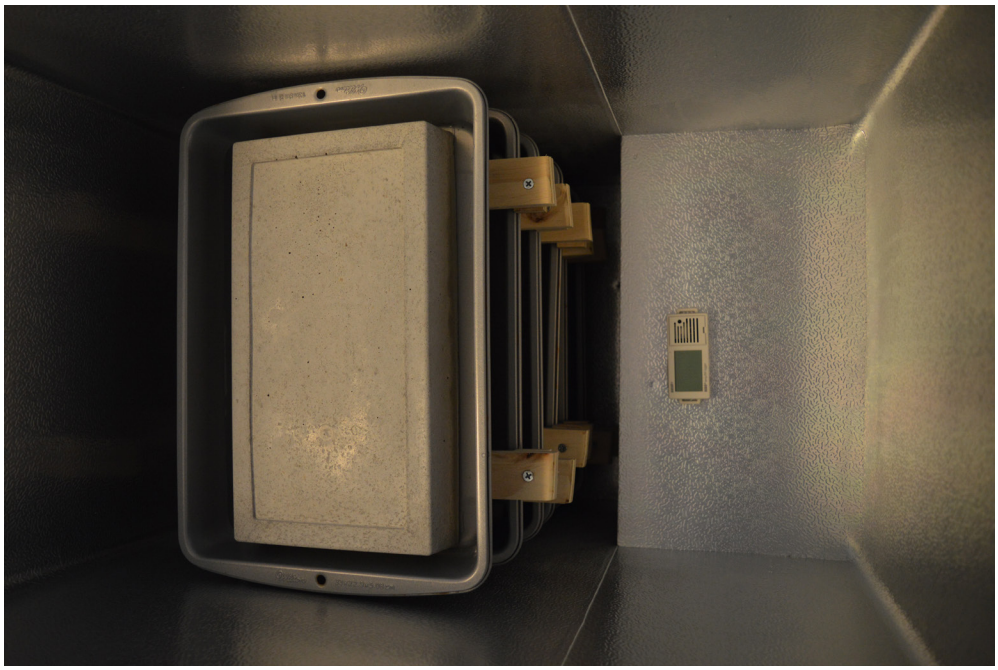

Figure 5.7.2a Storage of saline scaling specimens in freezing chamber. The order of the containers was rotated with each freezing cycle.

Figure 5.7.2b Typical accumulation of loose flakes and particles of concrete (scale) from foam concrete panel surface after 5 freeze-thaw cycles in 3% sodium chloride solution. Images of scaled surfaces are shown in Section 6.16.2.

The damaged surface of the specimens was photographed. Specimens were returned to their pans, and either 3% sodium chloride solution or distilled water was replenished to provide an immersed depth of 2±1 mm, before recommencing the next series of freeze-thaw cycles. Note that specimens were kept frozen in the event of any interruption to the daily cycling.

Testing was terminated after 50 cycles. Cumulative loss of mass from each panel was plotted against the number of freeze-thaw cycles.

5.8 Microstructural Analysis

5.8.1 Qualitative Air-Void Analysis

Physical microstructural differences were revealed by cutting specimens with a lapidary saw to expose their internal pore structures. Photographs were taken of the specimens' sections with a high-resolution camera, arranged in a matrix according to cementitious blend and density, and reproduced at four levels of magnification, to facilitate general observation of pore size, uniformity, and interconnectivity.

5.8.2 Quantitative Air-void Analysis

Evaluation of air-voids was conducted with reference to ASTM C457[18] and EN 480-11[19] standards. Testing was conducted using a flatbed scanner.[20]

Cylinders, 100 x 200 mm, were cast and cured in accordance per Section 5.1.4. After 28 days, each cylinder was cut using a lapidiary saw, and a 90 x 90 x 25 mm thick sample was removed for processing.

One face of the sample was ground and lapped with successively finer grits of 80, 100, and 120. A thin layer of lacquer and acetone was applied to the sample surface before each step, to strength the paste. Swarf was flushed away from the specimen surface during grinding with a continuous stream of water. Flatness was confirmed using a straight-edge,

[18] ASTM C457/C457M-12
[19] EN 480-11 (2001)
[20] Jakobsen et al. (2006)

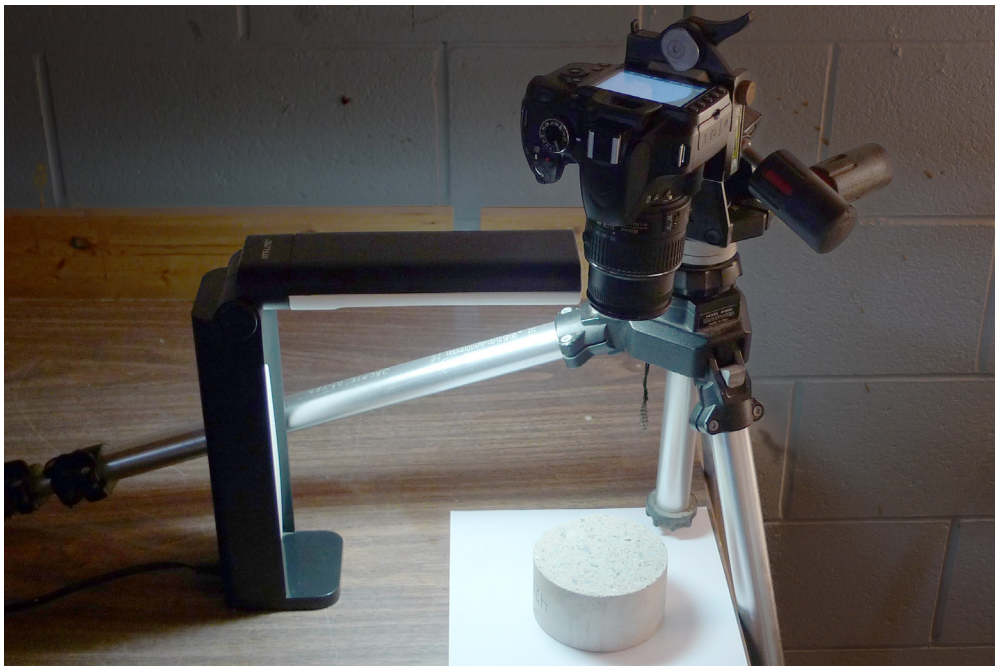

Figure 5.8.1a Set-up for photographing air-void structure of foam concrete specimens.

Figure 5.8.2a Surface of specimen coloured in black for air-void analysis.

and by periodically applying crayon marks in the low spots of the specimen and ensuring that the marks were fully ground away.

After achieving suitable flatness, grits of 320, 600, 800, and 1200 were used successively to further improve the resolution of the sample surface. The quality of the concrete was evaluated visually, until the concrete paste was observed to be smooth, without ripping or tearing of the air void edges.

After the final grinding, accumulated lacquer in the sample surface was removed with acetone. The specimen surfaces were scanned with a flatbed scanner having an optical resolution of 6400 dpi (5.1 μm per pixel).

The surface of the sample was coloured black using a broad tipped marker pen. Slightly overlapping lines were drawn over the entire surface of the sample; the samples was turned 90°, and the process repeated. The ink was allowed to dry completely.

White $BaSO_4$ powder with an average grain size of 2 μm was tamped into the voids using a hard rubber stopper. The surface was cleaned by gently dragging the edge of a rubber plate across the sample surface, and then by rubbing the surface smooth with the palm of the hand, taking care not to disturb the white powder in the air voids.

After preparation, the samples were scanned one more time on the flatbed scanner. All automatic software adjustments were turned off. Images were then opened in ImageJ software, and converted to binary using a threshold of 108. The "Watershed" command was applied to segment touching objects. The progression of applied filters is shown in Section 6.17.2. Note that calibration against a known reference[21] was not completed, so results should be taken as preliminary. The average area of each air void was determined using the "Analyze particles" command: voids at edges were excluded. Data was imported into Excel, and air void diameter was plotted against the cumulative area of the air-void system.

[21] For example, the RapidAir 457 automated air void analysis system manufactured by Concrete Experts International. Cf. Jakobsen et al. (2006)

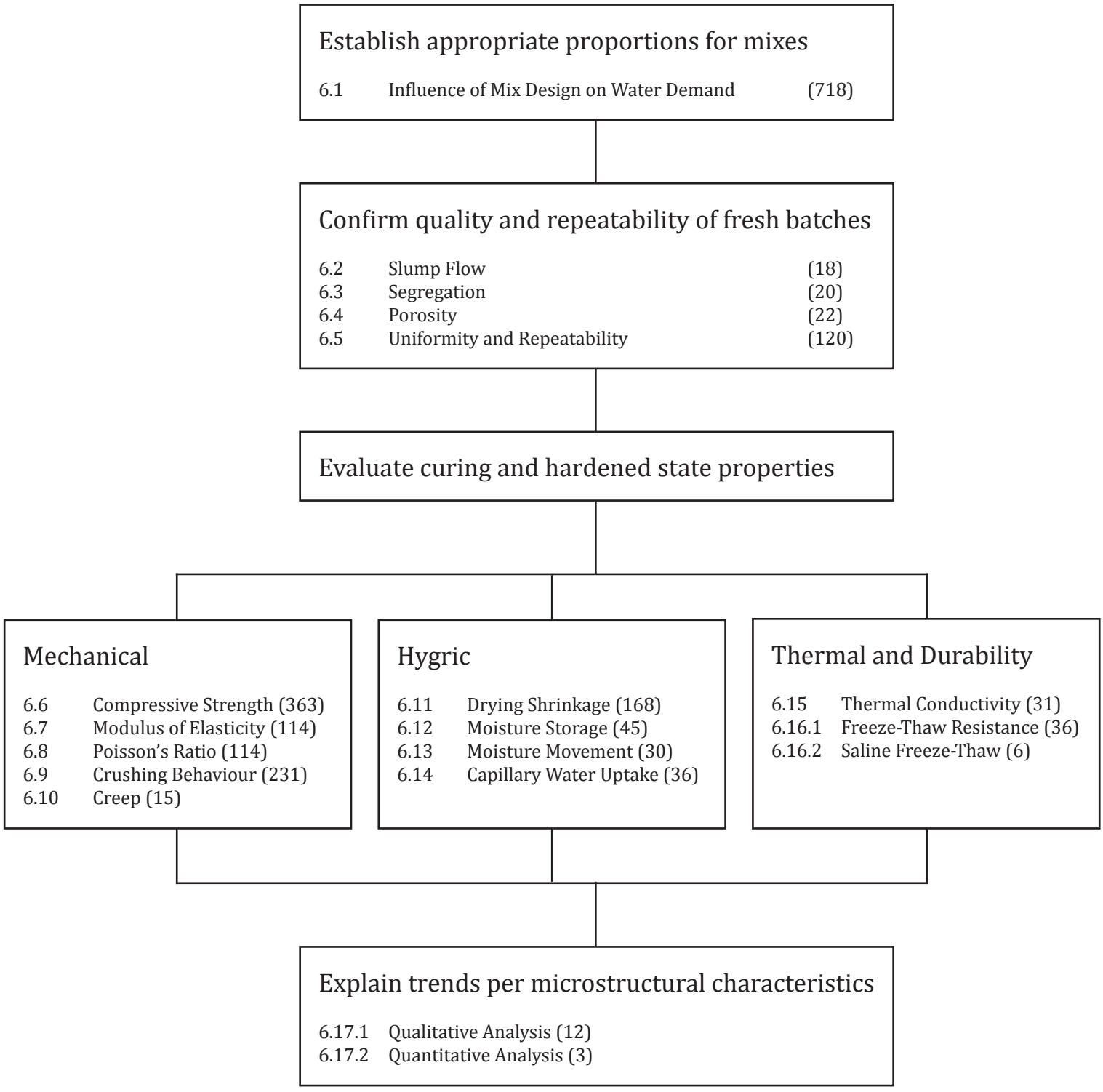

Figure 6a 'Graphic roadmap' to the experimental program. The total number of specimens tested is noted in parentheses for each Section.

6

Experimental Program: Results and Discussion

A graphic roadmap to the experimental program is provided on the opposite page.

In Section 6.1, appropriate water-binder ratios are established for each mix by examining the influence of water-binder ratio on compressive strength and visible segregation. In Sections 6.2 to 6.5, mixes with suitable water-binder ratios are tested further, to confirm foam concrete quality and consistency of results. Viable mixes are then evaluated for additional mechanical, hygric, and thermal properties, as reported in Sections 6.6 to 6.16. Microstructural analyses, in Section 6.17, help to explain observed trends.

6.1 Influence of Mix Design on Water Demand

In Section 6.1.1, water-binder ratios are varied for a series of mixes with varying cementitious blends. Cementitious densities were maintained at 410 kg/m^3 for these mixes. In Section 6.1.2, water-binder ratios are varied for Portland cement mixes with varying cementitious densities. Note that reported water-binder ratios cited throughout the experimental program do not account for the contribution of the dilution water from the foam. Refer to Section 6.1.6 for further discussion.

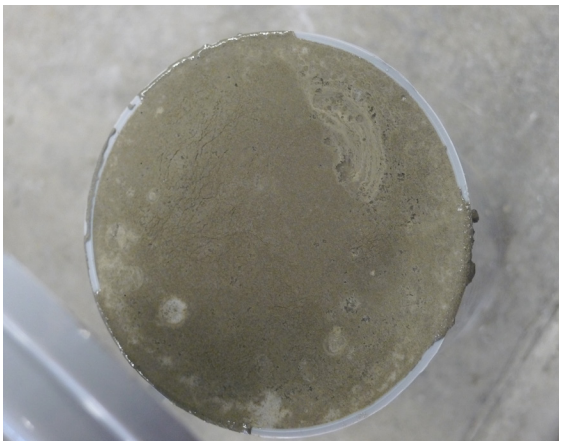

Figure 6.1.1a
Bleedwater evident on surface of a freshly-cast cylinder.

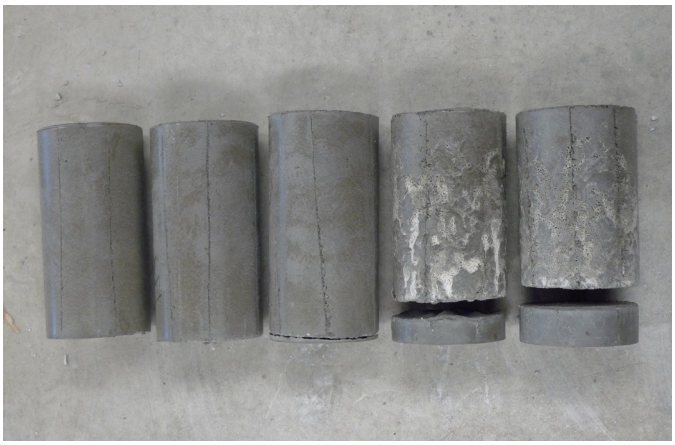

Figure 6.1.1b
From left to right, water-binder ratios of 0.6, 0.65, 0.7, 0.75, and 0.8. Segregation is evident in mixes with high w/b ratios. Note the whitish veins running through specimens on the right, where cement has dropped from the mix.

6.1.1 Varying Cementitious Blend, Constant Cementitious Density

Compression strength is plotted against water-binder ratio, in Figures 6.**1.1.1a** to **4f**. The plots indicate optimal values, and record mix tolerance to over- or under-watering.

Where the water supplied was insufficient, collapse of the foam was observed. Water was drawn from the aqueous foam to hydrate the cement, and bubbles ruptured during mixing due to the stiffness of the paste. Furthermore, reduced workability in mixes with a low water-binder ratio made it somewhat more difficult to blend the foam thoroughly within the mix in order to produce a homogenous paste. Compression results for water-binder ratios below certain thresholds were discounted, as indicated on the figures, due to observed foam collapse.

Where the supplied water-binder ratio was too high, the paste was not thick enough to avoid segregation, and bleed water was evident on the surface of freshly cast cylinders (Figure 6.**1.1a**). Foam bubbles rose and concentrated near the top surface of the cylinder, producing a weak zone that collapsed readily during compression testing, resulting in failure types similar to 'Type 6'. In mixes with extremely high water-binder ratios, cement particles sank to the bottom of the mix, forming a dense, bubble-free layer, while a low-density mass of foam and cement particles floated on top of a layer of water (Figure 6.**1.1b**). Compression results for water-binder ratios above certain thresholds were omitted, as indicated on the figures, due to due to evident bleeding and segregation.

0:1 Filler-Binder Ratio

Compressive Strength vs. w/b Ratio

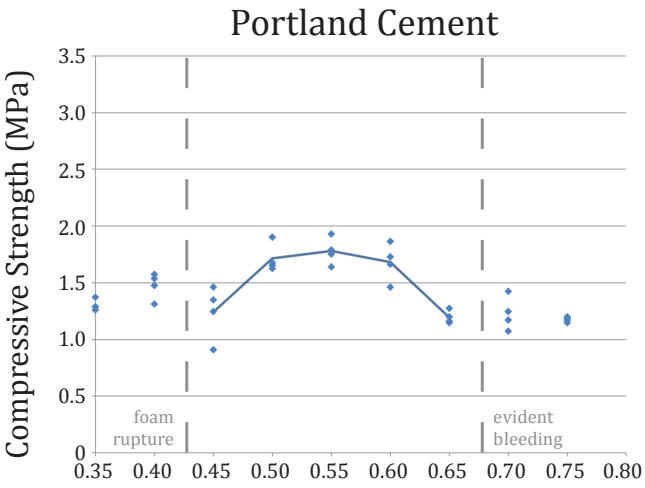

Figure 6.1.1.1a

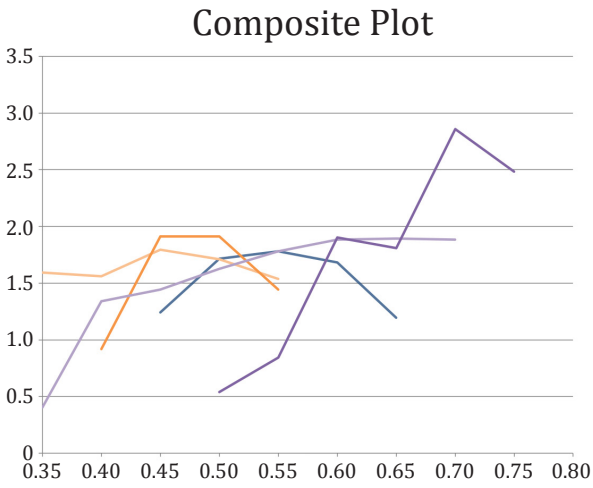

Figure 6.1.1.1d

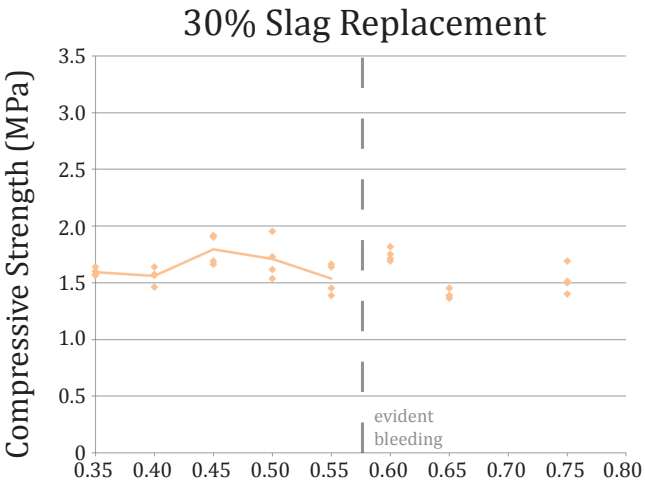

Figure 6.1.1.1b

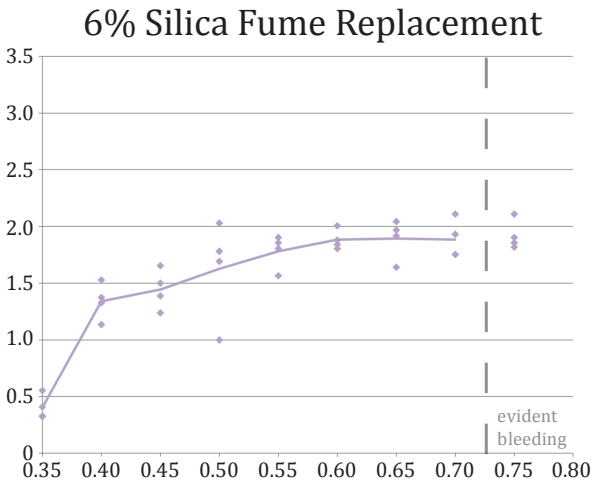

Figure 6.1.1.1e

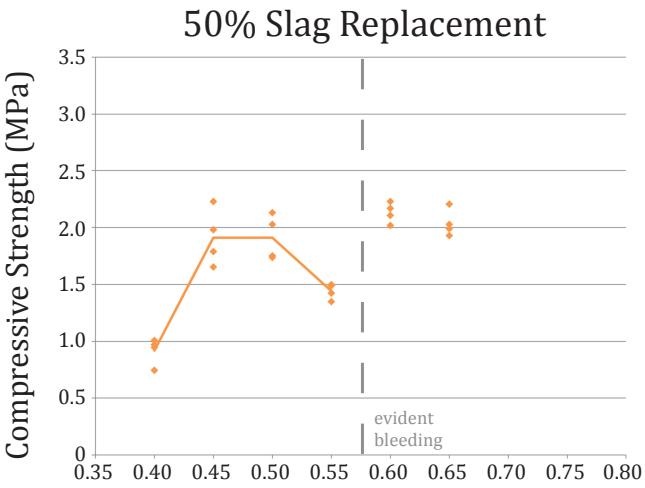

Figure 6.1.1.1c

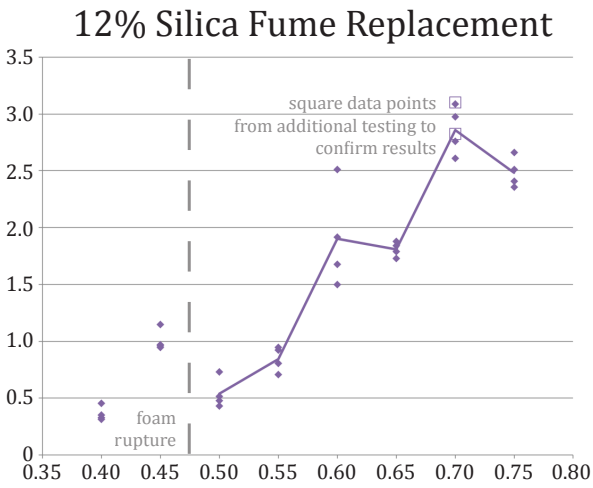

Figure 6.1.1.1f

6.1.1.1 *Filler-Binder Ratio of 0:1*

Data for mixes with no filler are shown in Figures 6.**1.1.1a** to **1f**.

Water demand varied widely according to cementitious blend. The optimal water-binder ratio of a Portland binder mix was found to be approximately 0.55. The mix showed reasonable tolerance to over- or under-hydration: where the water-binder ratio was 0.50 or 0.60, the reduction in strength was only 6%.

Mixes with 30% and 50% slag replacement required less water than for 100% Portland binder mixes. Bleedwater was also evident at much lower w/b ratios. Lower optimal w/b ratios may be expected, for two reasons: first, the glassy surface of slag accommodates less adhered water than the rough surface of Portland cement particles; and second, the reaction of slag is mostly pozzolanic, rather than hydraulic, therefore less water is initially chemically required and incorporated into the mix. Mixes also appeared to become less tolerant to non-optimal w/c ratios as the proportion of slag was increased, due to the inability of slag to store additional water on the flat, glassy surfaces its particles.

The addition of silica fume, conversely, increased water demand. Silica fume is extremely fine, and a large amount of water is required to completely cover its surface area and provide suitable workability.

Silica fume mixes exhibited somewhat unusual results. The performance of the mix with 6% SF appeared very tolerant to variations of w/b ratio, while the mix with 12% SF exhibited a relatively high peak at a w/b ratio of 0.70. In order to confirm that these results were repeatable, two additional cylinders were created according to the same mix recipe and prepared in the same manner as the original set. Compression results from these additional tests are depicted as hollow, square data points in Figure 6.**1.1.1f**. Break results from the second set of cylinders showed good conformity with the original data.

6.1.1.2 *Filler-Binder Ratio of 1:1*

A filler-binder ratio of 1:1 was used for the mixes shown in Figures 6.**1.1.2a** to **2f**. In general, the optimal water demand appeared to be higher with the addition of the fine aggregate. This phenomenon may be attributed to the increased surface area of solids within the mix, which had to be wetted for adequate workability.

1:1 Filler-Binder Ratio

Compressive Strength vs. w/b Ratio

Portland Cement

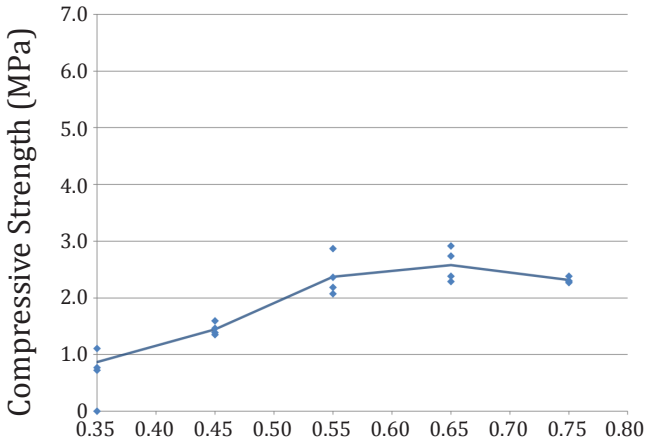

Figure 6.1.1.2a

30% Slag Replacement

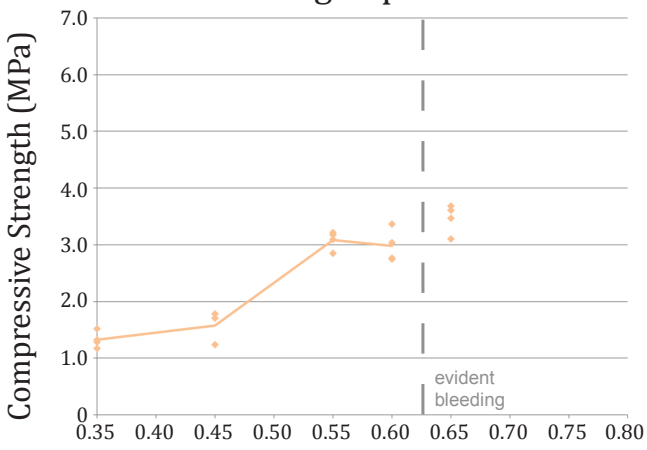

Figure 6.1.1.2b

50% Slag Replacement

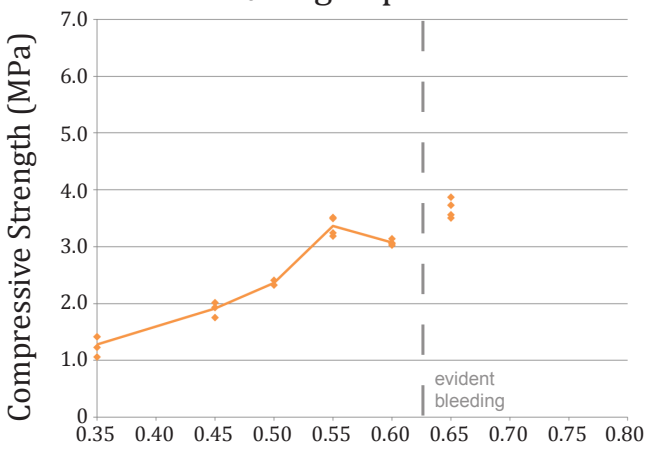

Figure 6.1.1.2c

Composite Plot

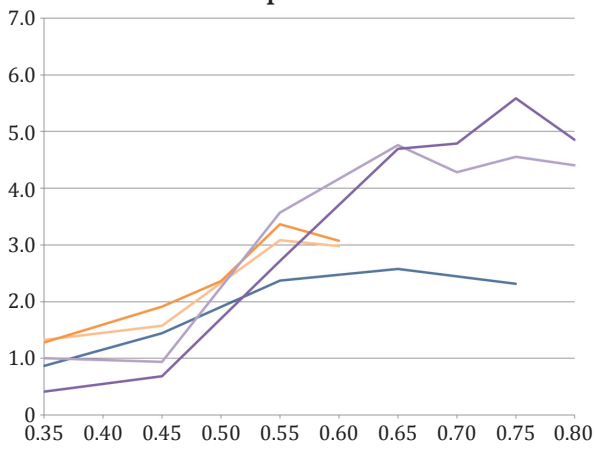

Figure 6.1.1.2d

6% Silica Fume Replacement

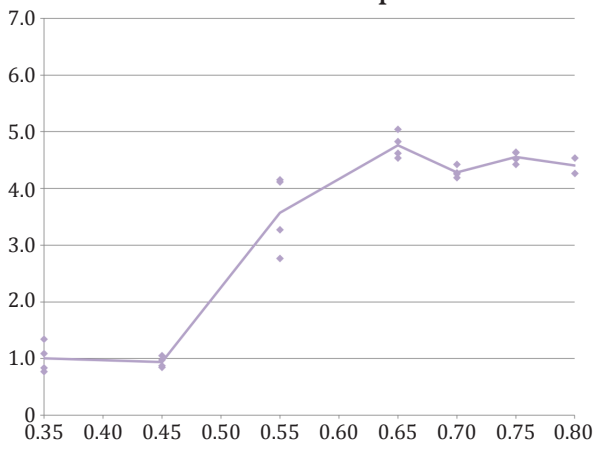

Figure 6.1.1.2e

12% Silica Fume Replacement

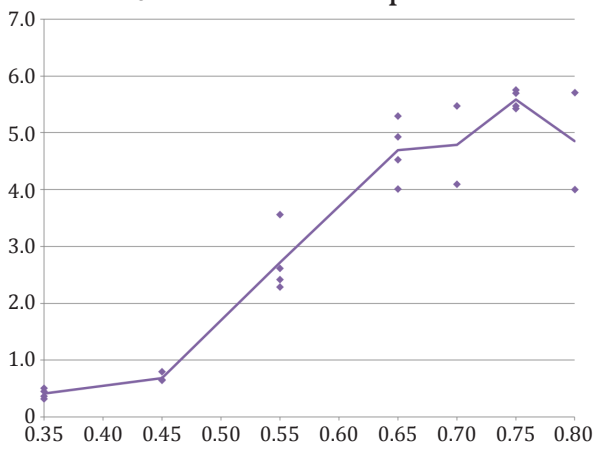

Figure 6.1.1.2f

A water-binder ratio of 0.65 was appropriate for the Portland cement mix. The optimal water-binder ratio for both of the slag mixes appeared to be approximately 0.55. As observed in the previous section, slag mixes showed limited tolerance for non-optimal water-binder ratios.

The optimal water-binder ratio for the 6% silica fume replacement appeared to be 0.65. However, mixes with water-binder ratios of 0.70 and 0.75 did not show evidence of bleeding or segregation, and also offered reasonably good performance.

The 12% silica fume replacement mix showed a noticeable peak in compressive strength, with a w/b ratio of 0.75. As in the previous Section, precision in the water-cement ratio was necessary in order to achieve optimal strength. Break results were highly consistent at this water-binder ratio, with a variation among four samples of less than 0.3 MPa. This uniformity indicates a highly homogenous air-void system, and a good distribution of sand, Portland cement, and silica fume particles throughout the mix, with no segregation. By comparison, the variation among specimens with water-binder ratios of 0.7 and 0.8 was relatively high, indicating inconsistency among specimens due to foam collapse and segregation, respectively.

The 12% silica fume replacement mix offered the highest average 28-day compressive strength, at 5.6 MPa. The Portland cement mix provided the lowest average 28-day compressive strength, at 2.7 MPa.

6.1.1.3 Filler-Binder Ratio of 2:1

A filler-binder ratio of 2:1 was used for the mixes shown in Figures 6.**1.1.3a** to **3f**. For all cementitious blends, the optimal water-binder ratio increased or stayed constant with the addition of the fine aggregate, as the wetted surface area of solids within the mix increased.

Smooth optimization curves were evident in the data at this filler-binder ratio, for all cementitious blends. Notably, slag mixes were more tolerant to variations in water-binder ratio at this density than in previous Sections, and no sharp peak was evident in the data for 12% silica fume mixes. These developments are likely due to the influence of increased density. As porosity decreases, strength development is less dependent on precise conditions required for the creation of thin-walled skeletal structures surrounding the foam bubbles. The severity and frequency of flaws is reduced as the addition of solid

2:1 Filler-Binder Ratio

Compressive strength vs. w/b Ratio

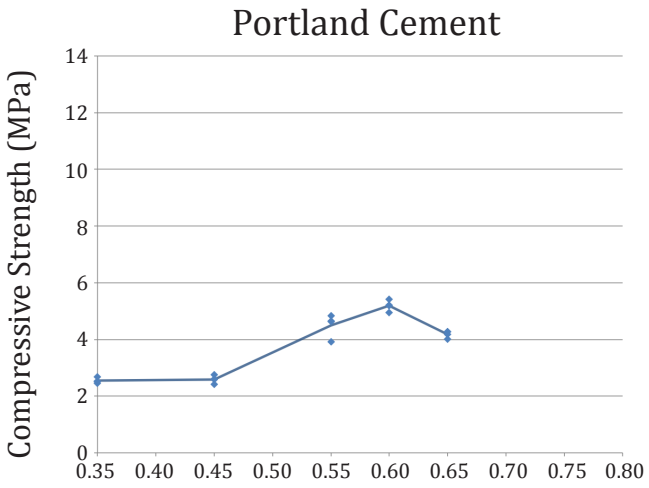

Figure 6.1.1.3a

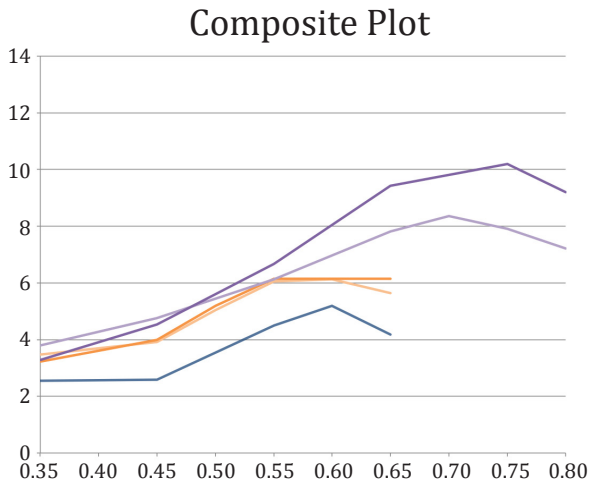

Figure 6.1.1.3d

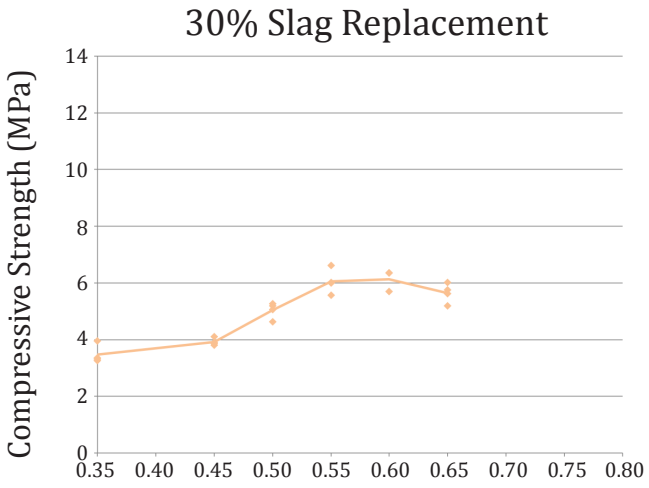

Figure 6.1.1.3b

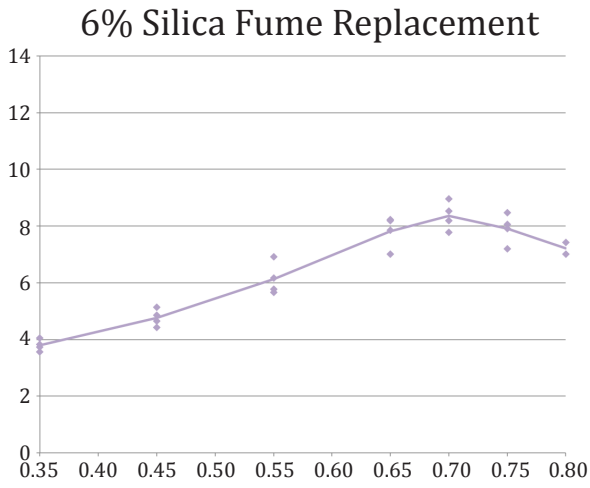

Figure 6.1.1.3e

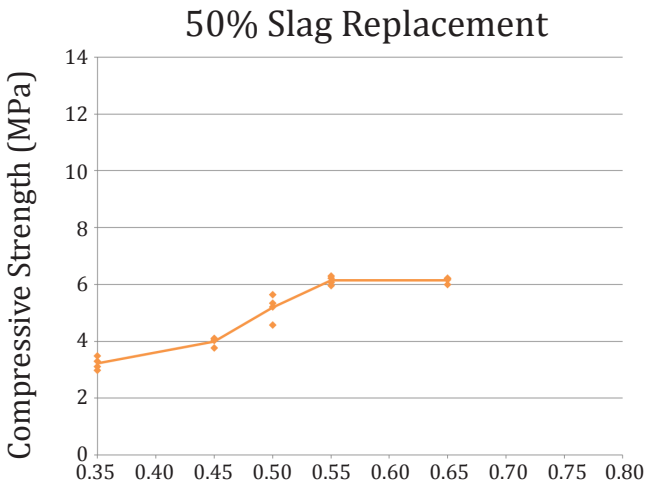

Figure 6.1.1.3c

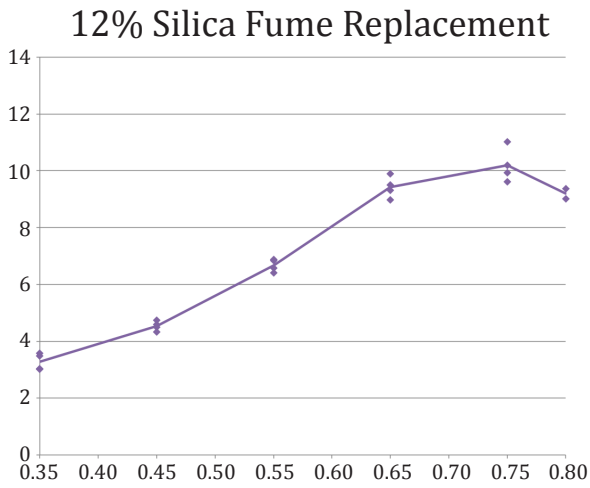

Figure 6.1.1.3f

material increases the average wall thickness surrounding each cell, reducing the probability of collapse or coalescence.

The Portland cement mix provided a maximum average compressive strength of 5.2 MPa at a water-binder ratio of 0.6. Where the ratio was varied to 0.55 or 0.65, strength decreased by 13 and 19%, respectively. The maximum average compressive strength achieved by both slag mixes was just over 6 MPa.

A 6% silica fume mix with a water-binder ratio of 0.7 achieved an average compressive strength of 8.4 MPa. Strength decreased by 6 and 8%, respectively, where the water-binder ratio was 0.65 or 0.75. It was observed that a minor amount of bleeding occurred where the w/b ratio was greater than 0.75.

A 12% silica fume mix with a water-binder ratio of 0.75 achieved an average compressive strength of 10.2 MPa. A modest loss of strength of 8 or 10% was observed where the water-binder ratio was 0.7 or 0.8, respectively.

The variation in break results at an appropriate water-binder was lowest for the Portland binder mix, on the order of 0.3 MPa. A variation of up to 1.0 MPa was observed in the break results for the slag mixes. The variation in results for 6 and 12% silica fume mixes was 1.2 and and 1.4 MPa, respectively.

6.1.1.4 *Filler-Binder Ratio of 3:1*

A filler-binder ratio of 3:1 was used for the mixes shown in Figures 6.**1.1.4a** to **4f**. In general, the water demand of mixes did not change significantly as the filler cement ratio was increased from 2:1 to 3:1. During mixing, it was observed that the momentum of the saturated sand in the mixer helped to produce a homogenous base mix relatively swiftly. Additionally, with the use of an appropriate water-binder ratio, there was little difficulty incorporating the low-density foam into the dense base mix to produce a homogenous paste.

Portland cement binder mixes were fairly tolerant to variations in water-binder ratio from 0.45 to 0.65. However, a peak in compressive strength was evident at a ratio of 0.60. The average compressive strength was 14.1 MPa. Where the water-binder ratio was 0.55 or 0.65, a loss in strength of 7 and 13%, respectively, was observed.

3:1 Filler-Binder Ratio

Compressive Strength vs. w/b Ratio

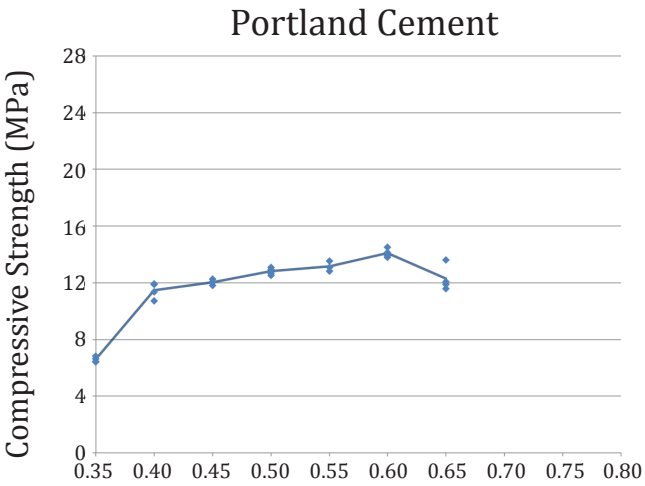

Figure 6.1.1.4a

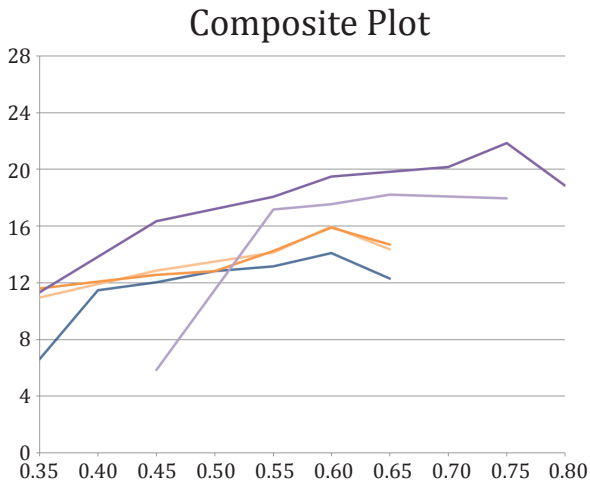

Figure 6.1.1.4d

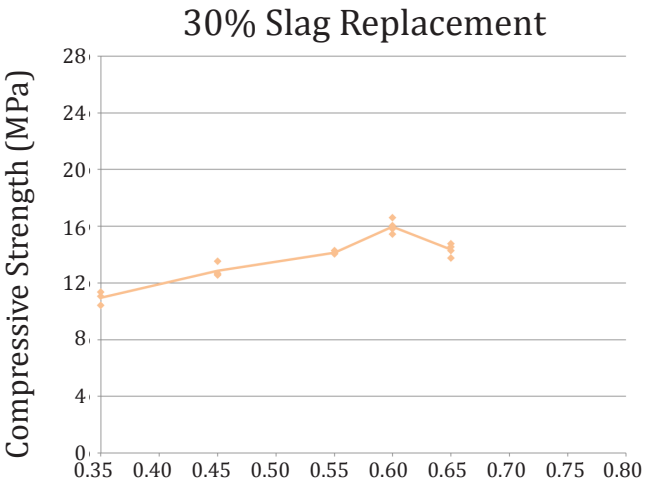

Figure 6.1.1.4b

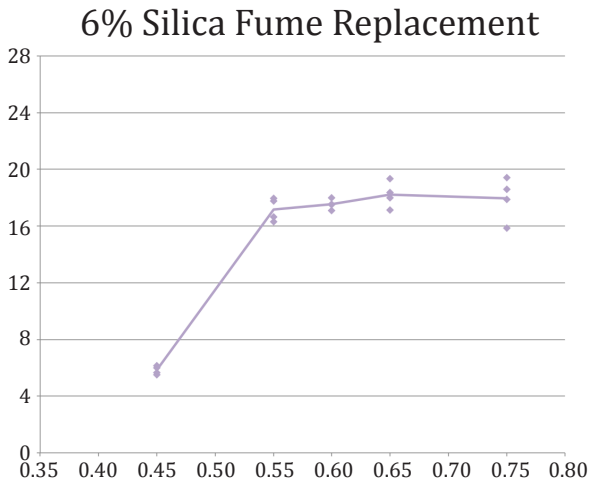

Figure 6.1.1.4e

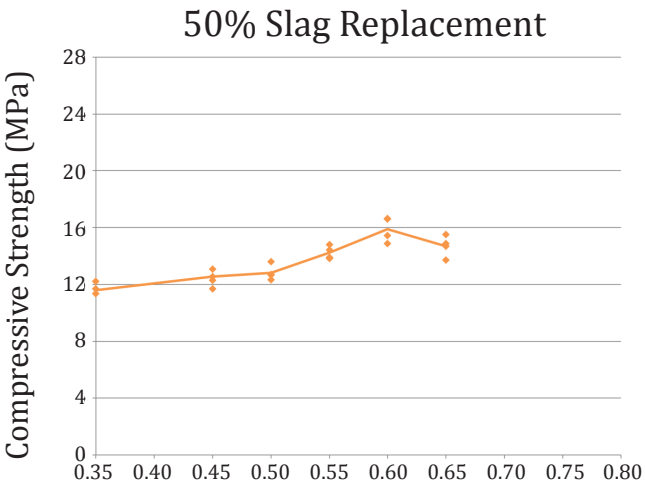

Figure 6.1.1.4c

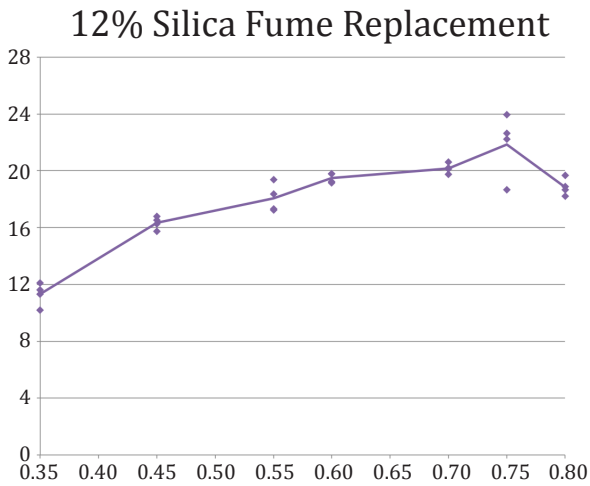

Figure 6.1.1.4f

Water requirements for the slag mixes were very similar to the Portland binder mix, peaking at a water-binder ratio of 0.6. The slag mixes provided a marginally higher strength, in the order of 16 MPa.

For the 6% silica fume mix, the maximum average compressive strength observed was 18.2 MPa. Notably, satisfactory strengths were achieved with a considerable range of water-binder ratios: for example, a water-binder ratio of 0.55 provided an average strength of 17.2 MPa, and a water binder ratio of 0.75 resulted in an average strength of 17.9 MPa. Bleeding was not observed in the 0.75 water-binder ratio mix. A water-binder ratio of 0.7 may be appropriate for this cementitious blend, consistent with the value observed for a filler-binder ratio of 2:1.

The maximum average compressive strength of the 12% silica fume mix was 21.9 MPa. The optimal water-binder ratio was 0.75, consistent with the value observed for a filler-binder ratio of 2:1.

Variation in break results was lowest for Portland binder mixes, at 0.7 MPa for a water-binder ratio of 0.6. Variation was highest for the 50% slag mix, at 5.5 MPa with a water-binder ratio of 0.75. This latter result was influenced by one especially poor break result.

6.1.1.5 *Optimal w/b Ratio vs. Filler-Binder Ratio*

Based on the data above, optimal water-binder ratios were estimated for each mix, which achieved high compressive strengths for a given density and cementitious blend. Water-binder ratios are plotted against filler-binder ratios for each cementitious blend in Figures 6.**1.1.5a** to **5f.** The coloured lines represent optimal ratios, while the grey lines represent upper and lower bounds within which satisfactory strengths may still be achieved.

The composite plot in Figure 6.**1.1.6a** provides a helpful reference. Water-binder ratios are highest for 12% silica fume mixes, and 6% silica fume mixes also have significant water demand. Silica fume particles are very fine; consequently, these mixes have a large surface area that must be wetted for adequate workability.

The optimal water-binder ratio of Portland binder mixes varied from 0.55 to 0.6. Water demand was consistent for filler-binder ratios of 1:1, 2:1, and 3:1. Additional testing,

Water Demand

Optimal w/b Ratio vs. Filler-Binder Ratio

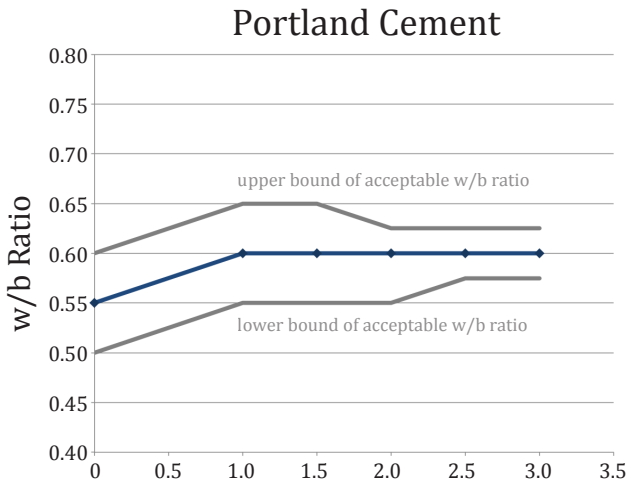

Figure 6.1.1.5a

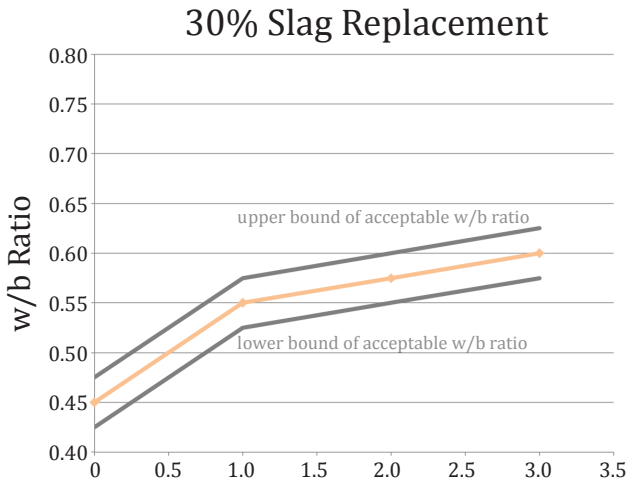

Figure 6.1.1.5b

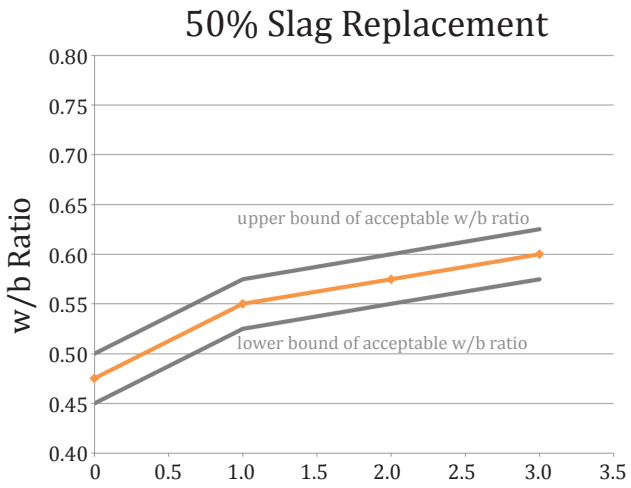

Figure 6.1.1.5c

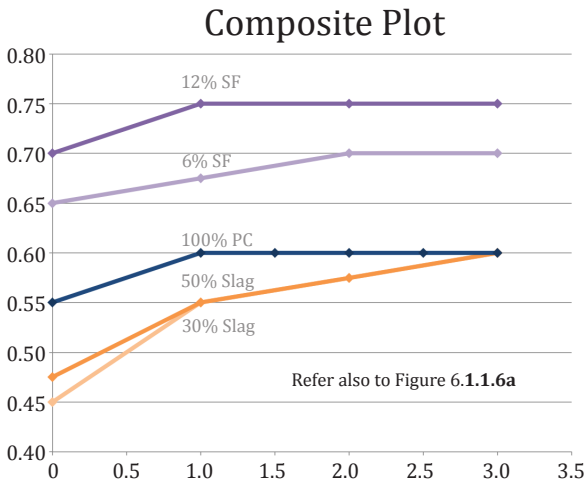

Figure 6.1.1.5d

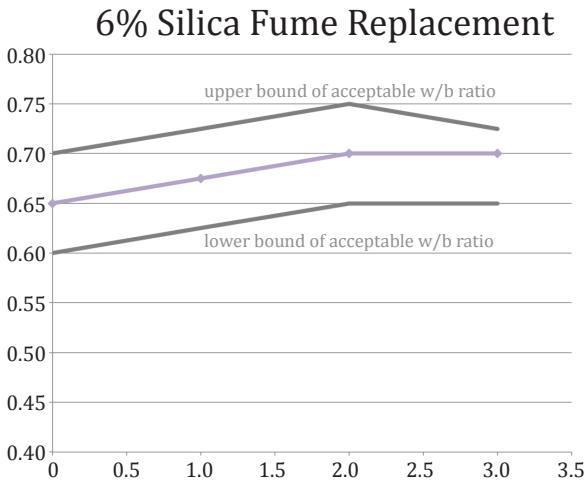

Figure 6.1.1.5e

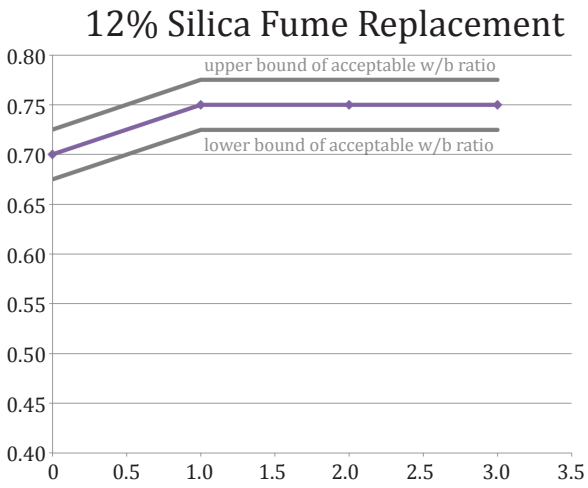

Figure 6.1.1.5f

conducted for filler-binder ratios of 1.5:1 and 2.5:1, offered further corroboration for this consistent water demand. (Data from these tests may be reviewed in Appendix R.)

The water demand of slag mixes was generally lower than for Portland binder mixes, varying from 0.45 to 0.6. At filler-binder ratios of 0:1 and 3:1, the 30% slag mix required marginally less water than the 50% slag mix, but otherwise the mixes followed the same trend, with water-binder ratio increasing in relation to the filler-binder ratio.

For all cementitious blends, water-binder ratios were lowest for mixes with no filler. In general, when filler was added to a mix, the water demand increased relatively sharply. Subsequent additions of filler were not as consequential for the water-binder ratio.

Mixes with 6% silica fume were especially tolerant to variations in water-binder ratio, as indicated by the grey lines in the plots. Mixes with high proportions of pozzolans required relatively precise water-binder ratios at all filler-binder ratios, in order to achieve good strength results.

Optimal water-binder ratios are plotted against cementitious blend in Appendix R.

6.1.1.6 *Water-Binder Ratios and Dilution Water*

As noted in Section 6.1, water-binder ratios cited throughout this experimental program do not include the contribution of the dilution water from the foam. Dilution water is assumed to be necessary for the stability of the foam, and thus does not contribute directly to the wetting and workability of the mix, and does not contribute immediately to the hydration water available to the cement particles. Water-binder ratios that depend only upon total cementitious content are also expedient in a commercial setting.

However, some studies may choose to include the dilution water when reporting water-binder ratios. For example, ASTM Standard C796[1] proposes that a water-cement ratio of 0.58 may be used as a starting point for mixes with Type I cement, and includes the weight of the foam in this value.

For convenient comparisons with other studies, optimized water-binder ratios, modified to include dilution water, are in Figure 6.**1.1.6b**. Further discussion is presented in Appendix I.

[1] ASTM C796/C796M-12, Section 8.4.3.1

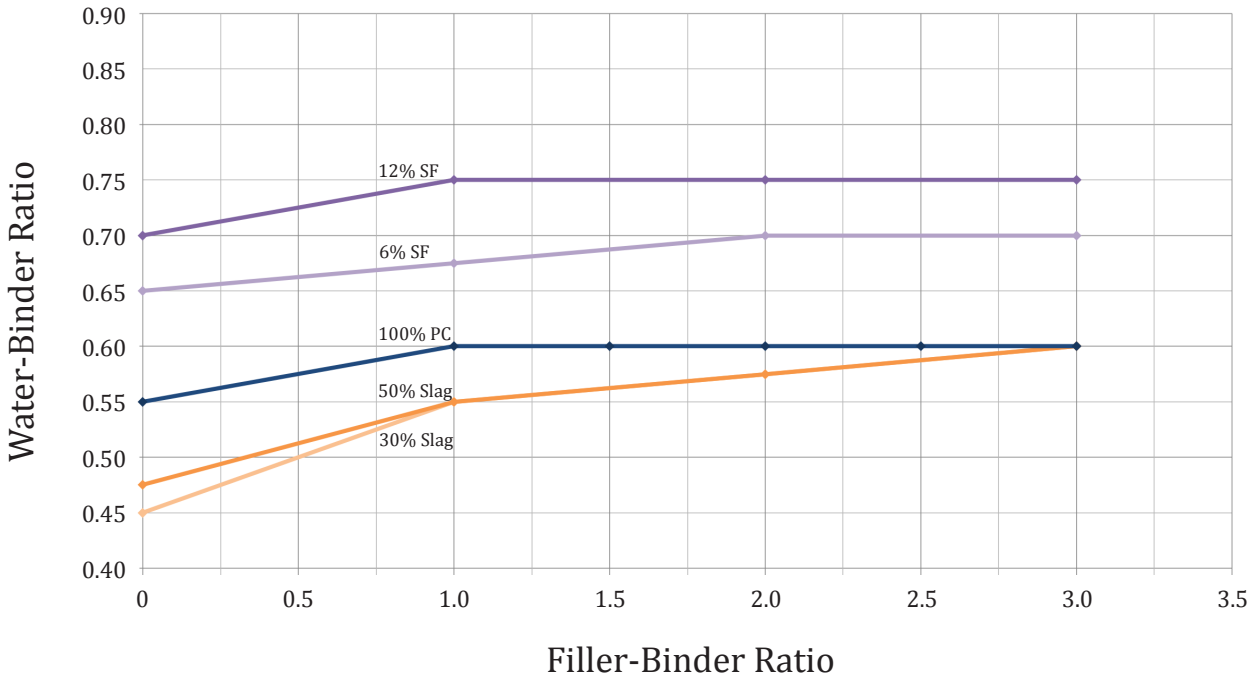

Figure 6.1.1.6a Optimal water-binder ratios, not including dilution water from foam.

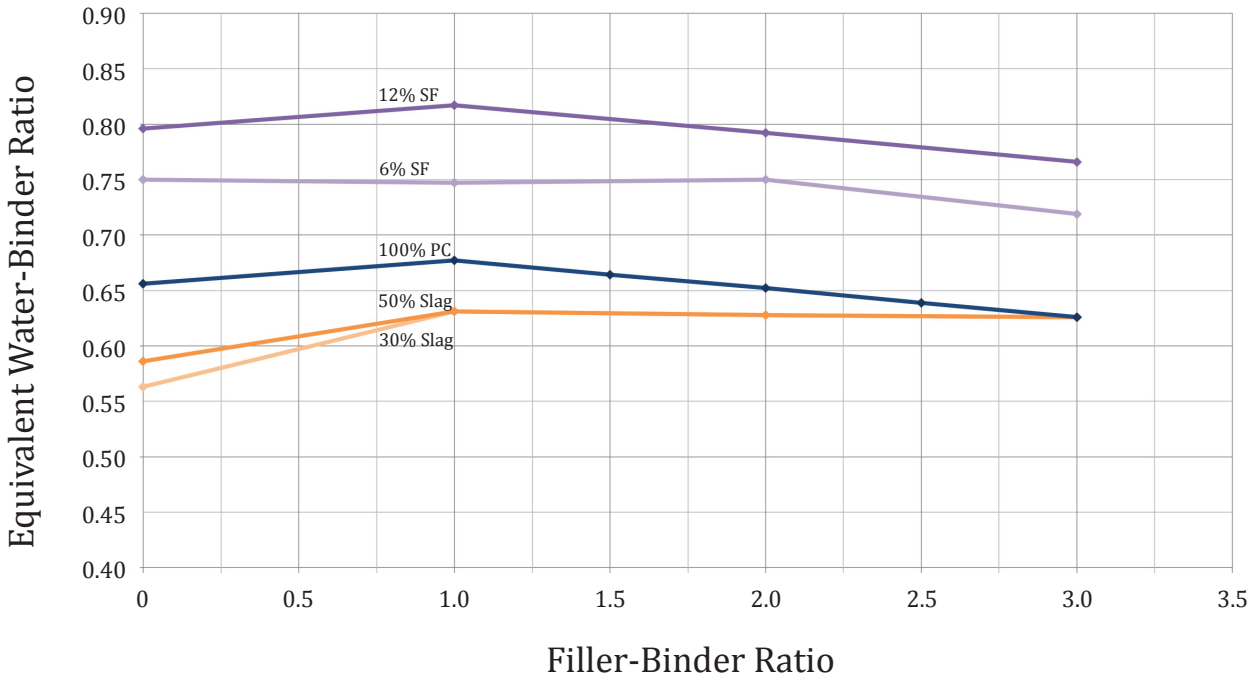

Figure 6.1.1.6b Optimal equivalent water-binder ratios, including dilution water from foam.

6.1.2 Varying Cementitious Density

6.1.2.1 Mixes with No Filler

A series of 100% Portland binder mixes were produced at cementitious densities varying from 410 kg/m^3 to 760 kg/m^3. The mixes contained no filler. Compressive strength is plotted against the water-binder ratio of each mix, in Figure 6.**1.2.1a**.

The overall trend of the graph may indicate that water demand increases very slightly with increasing cementitious density. For example, the optimal water-cement ratio appears to be between 0.5 and 0.55 for all mixes with between 410 and 560 kg/m^3 of cementitious content; mixes with 610 to 660 kg/m^3 of cement appear to require a water-binder ratio of 0.55 kg/m^3; and mixes with 710 to 760 kg/m^3 of cement may require slightly more than 0.55 kg/m^3 for optimal performance. However, more testing would be needed to substantiate this pattern.

Tolerance to variations in water-binder ratio appeared to diminish with increasing cementitious content. For example, the average compressive strength of a mix with 760 kg/m^3 of cement and a water-binder ratio of 0.55 was 7.5 MPa; however, strength was reduced by 15 and 11%, or 1.1 and 0.8 MPa, when the water-binder ratio was varied to 0.5 or 0.6, respectively. By comparison, the average compressive strength of a mix with 610 kg/m^3 of cement and a water-binder ratio of 0.55 was 3.9 MPa; strength was reduced by 10 and 5%, or 0.4 and 0.2 MPa, when the water-binder ratio was varied to 0.5 or 0.6, respectively.

The variability of break results also became more significant with increasing density. For mixes with between 410 and 560 kg/m^3 of cementitious content and appropriate water-binder ratios, variation among break results was in the order of 0.3 MPa. For mixes with 710 and 760 kg/m^3 of cement, variations of 1.5 and 0.8 MPa, respectively, were observed. However, break results for the mix with 710 kg/m^3 of cement and a water-binder ratio of 0.6 were extremely close, within approximately 0.1 MPa. This outcome may indicate that with excellent consistency of the plastic mix, and thorough blending of the foam within the base mix, highly uniform results are achievable. Nevertheless, greater care may be necessary in producing these mixes with higher cementitious densities, for optimal performance.

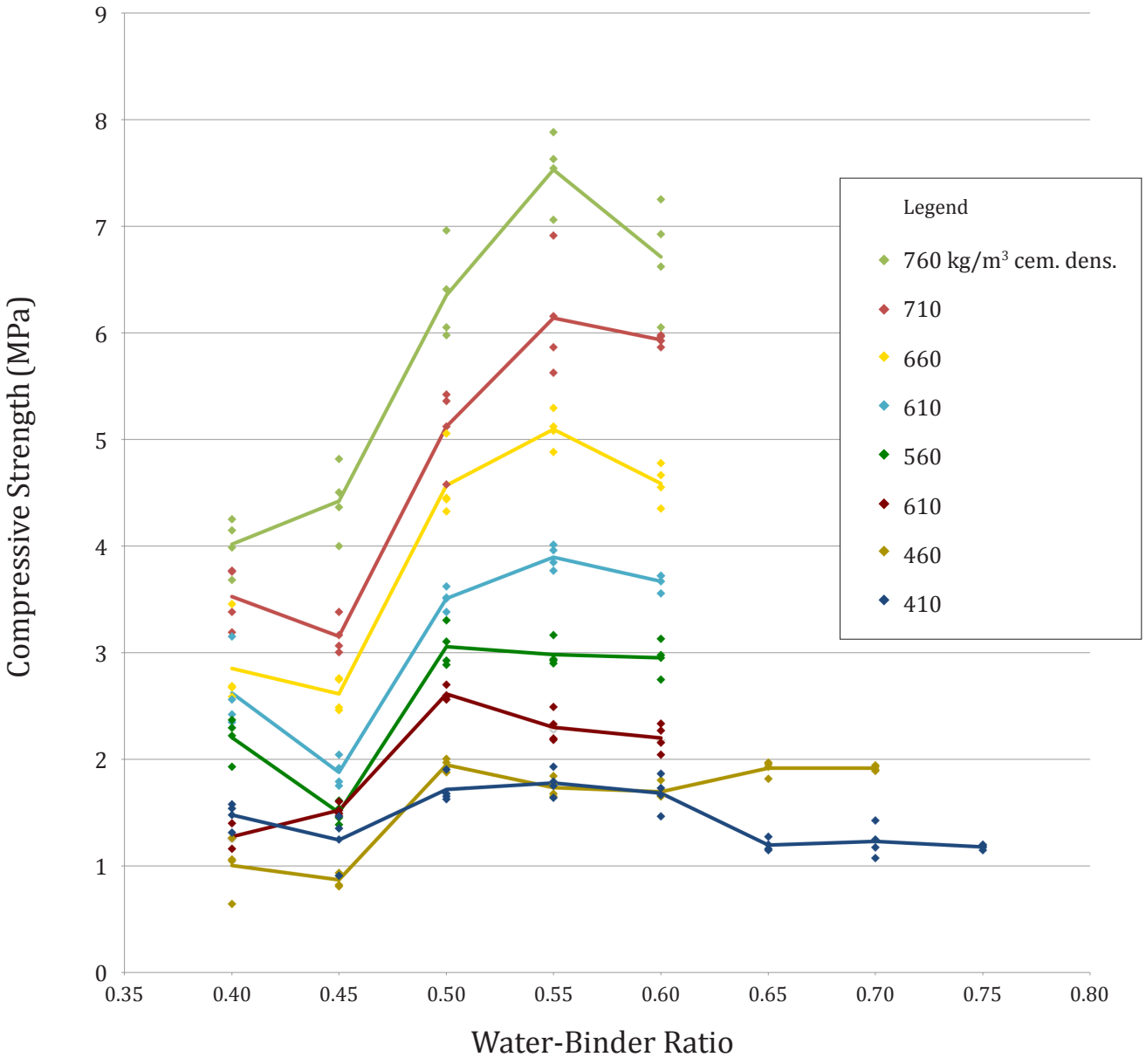

Figure 6.1.2.1a Water demand for low density (neat cement) mixes, varying cementitious density.

6.1.2.2 *Mixes with Filler*

The influence of varying cementitious density contents was tested for Portland binder mixes that contained filler. Base mixes contained 410 kg/m^3 of cement, with filler-binder ratios of 2:1 and 3:1. Subsequent mixes increased cementitious density by 100 kg/m^3 or 200 kg/m^3, while reducing the amount of filler to maintain nominal densities of 1400 kg/m^3 or 1800 kg/m^3.

Appropriate water-binder ratios for mixes with 410 kg/m^3 of cement were determined in Sections 6.1.1.3 and 6.1.1.4. Similar tests were conducted for mixes with cementitious densities of 510 and 610 kg/m^3. The influence of varying water-binder ratio on compressive strength is shown in Figures 6.**1.2.2a** and 6.**1.2.2c**. It was assumed that the water-binder ratio would remain constant or decrease with cementitious density. Mixes with 610 kg/m^3 density and water-binder ratios of 0.6 exhibited minor bleeding, and were not compression tested.

For the 1400 kg/m^3 nominal density mixes in 6.**1.2.2a**, strength increased from 5.2 to 8.1 to 10.0 MPa, with cementitious densities of 410, 510, and 610 kg/m^3, respectively. For the 1800 kg/m^3 nominal density mixes in Figure 6.**1.2.2c**, strength increased from 14.1 to 19.4 to 21.7 MPa. Strength improvement was more significant in the 1400 kg/m^3 nominal density mix, with strength improvements of 56 and 92% for 510 kg/m^3 and 610 kg/m^3 of cementitious density, respectively, compared to 38 and 54% for the higher density mix.

Figures 6.**1.2.2b** and 6.**1.2.2d** indicate that total water demand increases significantly with increasing cementitious content.

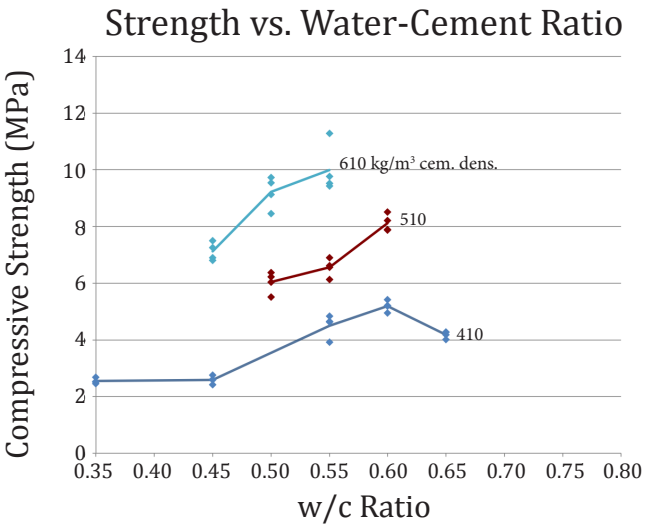

Figure 6.1.2.2a Water demand for 1400 kg/m³ nominal density mixes. Influence of cementitious density on optimal w/c ratio.

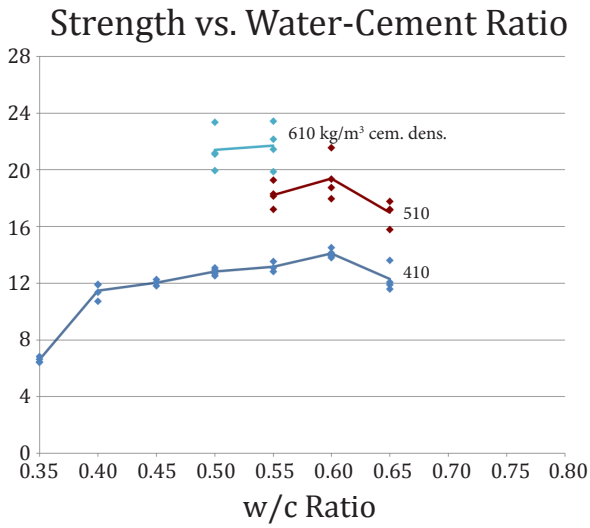

Figure 6.1.2.2c Water demand for 1800 kg/m³ nominal density mixes. Influence of cementitious density on optimal w/c ratio.

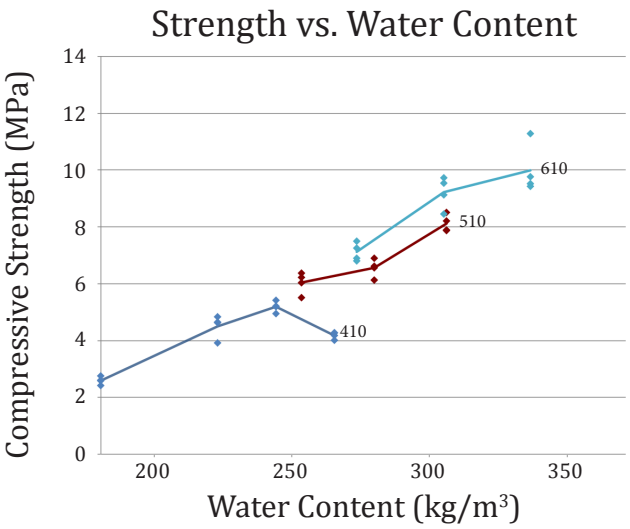

Figure 6.1.2.2b Water demand for 1400 kg/m³ nominal density mixes. Influence of cementitious density on optimal water content (kg/m³).

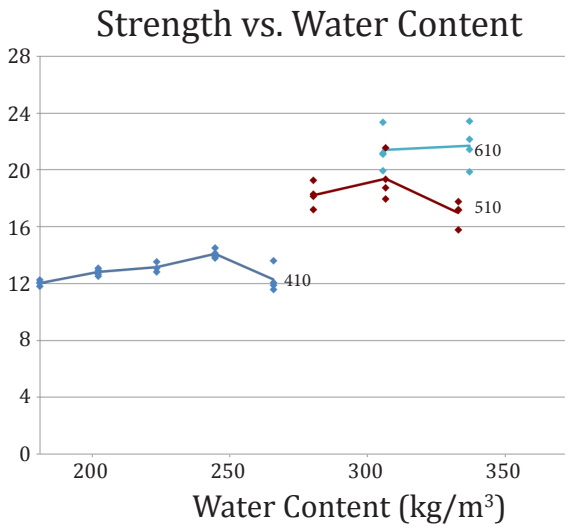

Figure 6.1.2.2d Water demand for 1800 kg/m³ nominal density mixes. Influence of cementitious density on optimal water content (kg/m³).

6.1.3 Further Refinements

The laboratory findings reported in Sections 6.1.1 and 6.1.2 provided initial guidance in selecting appropriate water-binder ratios for various mixes.

Water-binder ratios were further refined as mixes were batched and cast at production scales during the course of the research program. For example, slight reductions in water-binder ratio reduced the risk of segregation, especially for mixes in the range of 1000 to 1400kg/m^3: increased paste stiffness helped reduce the mobility of dense sand particles, as they were accelerated in large mixing drums.[2] Moreover, a slight increase in the water-binder ratio of a 50% slag mix with no filler improved consistency, reducing the tendency for stiff paste to adhere to the interior of the mixing drum.

Figure 6.**1.3a** shows initial and refined water-binder ratios used during testing. Refined water-binder ratio values were used for specimen manufacture in the majority of the experimental program, as indicated in the table below.

Section	Test	Original	Refined	Notes
Section 6.1	Water-Binder	X	X	Comparable compressive strengths
Section 6.2	Slump Flow		X	
Section 6.3	Segregation		X	
Section 6.4	Porosity		X	
Section 6.5	Repeatability	X	X	Comparable compressive strengths
Section 6.6	Compression	X	X	Comparable compressive strengths
Section 6.7	MOE		X	
Section 6.8	Poisson's Ratio		X	
Section 6.9	Crushing		X	
Section 6.10	Creep		X	
Section 6.11	Drying Shrinkage		X	
Section 6.12	Moisture Storage		X	
Section 6.13	Moisture Movement		X	
Section 6.14	Water Uptake		X	
Section 6.15	Thermal Conduct.		X	
Section 6.16	Freeze-Thaw		X	
Section 6.17	Microstructure	X		Photographs of microstructure
			X	Air-void analysis

Table 6.1 Table clarifying whether test specimens were prepared with original water-binder ratios (Sections 6.1.1 and 6.1.2), or refined water-binder ratios (Section 6.1.3).

[2] For further discussion on the influence of scale of batching on segregation, refer to Appendix O.

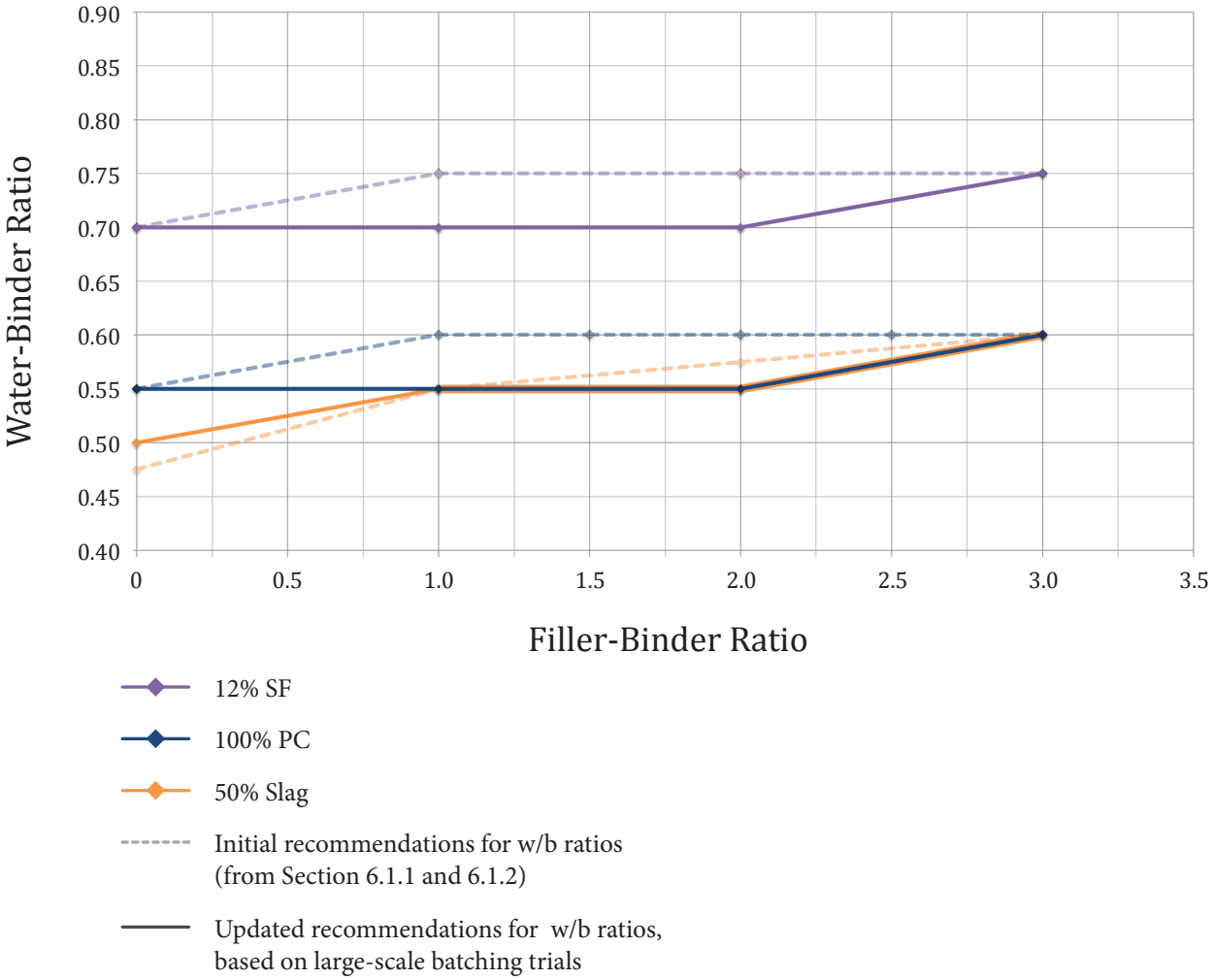

Figure 6.1.3a Refined water-binder ratios, based on large-scale batching trials.

6.2 Slump Flow

Slump flow values are shown in Figure 6.**2b**. Equivalent water-binder ratios, which include dilution water from the foam, are shown in Figure 6.**2a**, for reference.

The slump flow, or spread, of foam concrete is relatively high. Foam concrete mixes with 410 kg/m^3 cementitious density had slump flow between approximately 500 and 700 mm, which is comparable to self-consolidating concrete.

For mixes with a constant 410 kg/m^3 cementitious density, 1000 kg/m^3 sanded mixes had a higher spread than 600 kg/m^3 mixes with no filler. It appeared that increased self-weight propelled the concrete to flow a greater distance. However, additional increases in aggregate content tended to reduce slump flow, due to the increased wetted surface area of solids in the mix, and due to increased density of interlocking sand aggregate particles.

Slump flow tended to increase with cementitious density, which may be attributed to the presence of higher total water content in the mix.

Reductions in foam volume tended to increase slump flow. This effect may be attributed largely to increased self-weight. Additionally, the hydrophilic properties of the foam may have a role in absorbing some portion of the mix water, causing mixes with high foam volume to be more cohesive.

Notably, despite the high water-binder ratio used for the 12% silica fume mix, slump flow was comparable to that of the 100% Portland cement and 50% slag mixes, across densities. This effect is likely due to the high surface area of silica fume particles, which adsorb significant quantities of mix water.

For the densest mixes, the slump flow of the silica fume mix was greatest. The fineness and roundness of silica fume particles may improve the smoothness and workability of the mix somewhat. By contrast, the angular particles of ground granulated blast furnace slag may tend to produce relatively harsh mixes, corresponding to slightly reduced slump flow measurements.

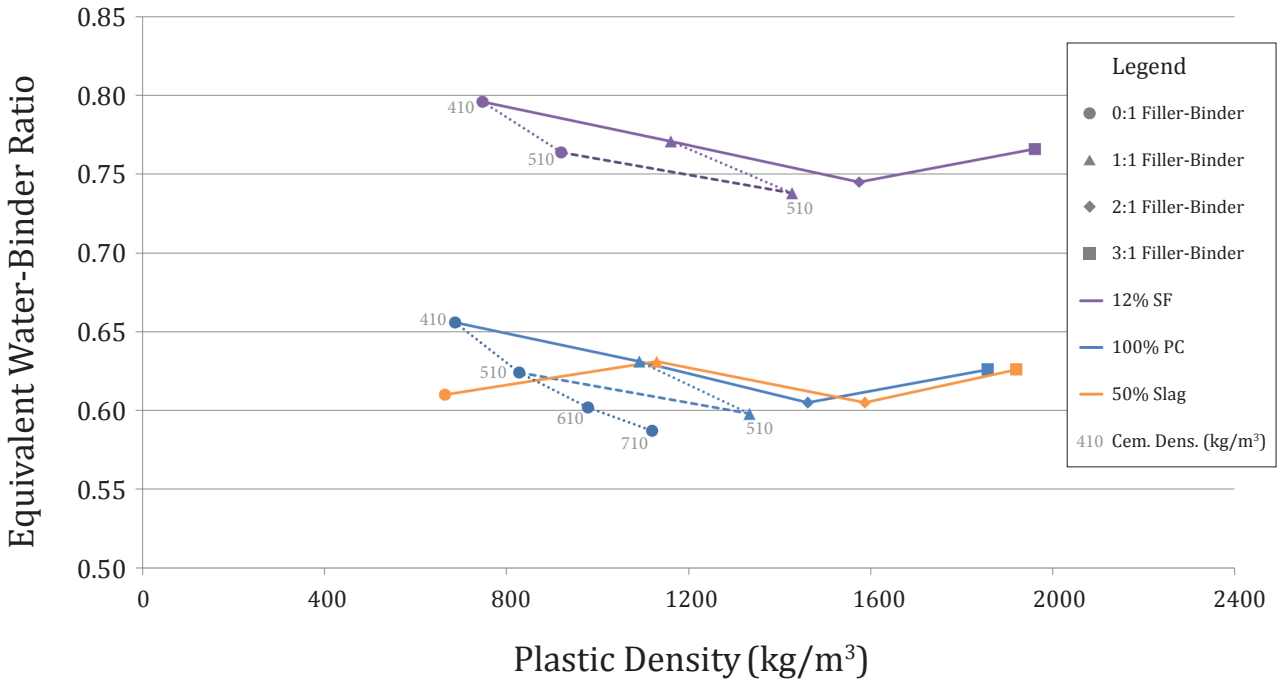

Figure 6.2a Equivalent water-binder ratios (incl. dilution water) vs. plastic density.

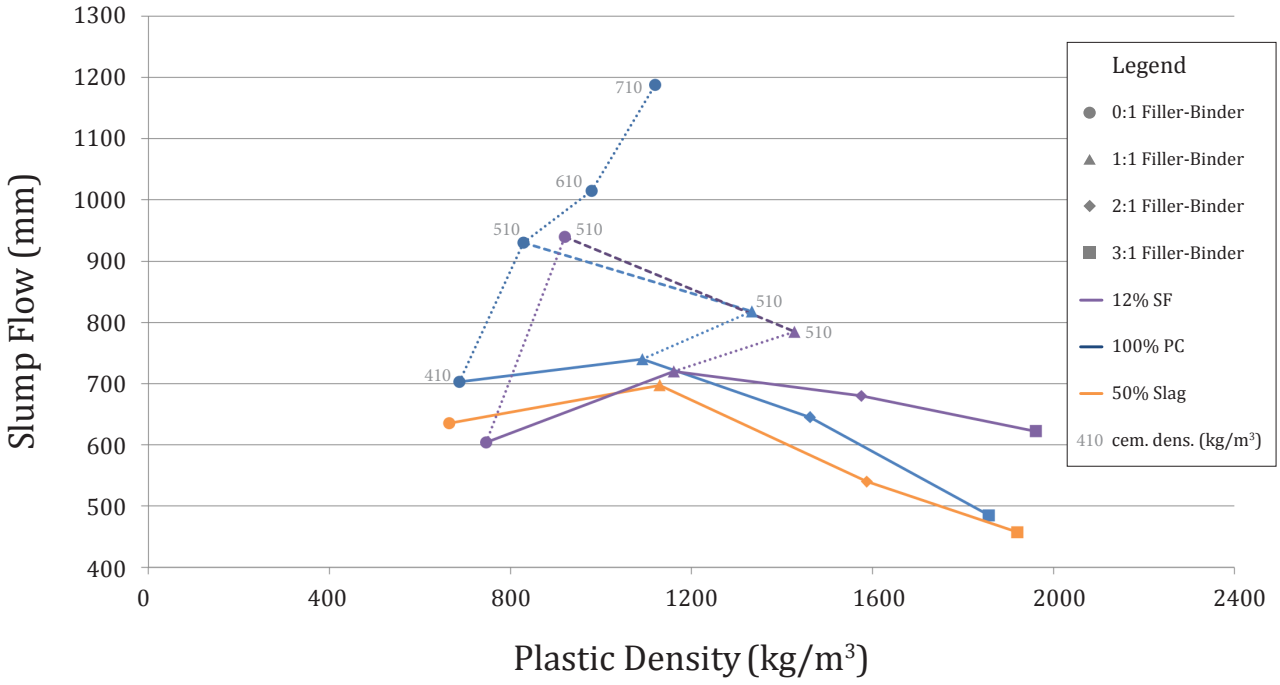

Figure 6.2b Slump flow vs. plastic density.

6.3 Segregation

Segregation was evaluated by comparing the densities of the top and bottom portions of specimens. Percent differences in density are plotted against dry density in Figure 6.**3a**. Despite the high workability of the mixes, segregation was generally low, with segregation values of less than 2.5% for most mixes. These results indicate a high degree of foam stability, and minimal migration of buoyant air bubbles or dense sand particles.

Two types of mixes exhibited relatively high segregation. For foam concrete aggregate (FCA) mixes, density measurements varied by as much as 7.1%. On inspection, it appeared that smaller aggregate particles, with high surface area to volume ratios, become impregnated with cement paste and mix water, and tended to sink. Conversely, larger aggregates, with isolated air voids and relatively dry interiors, tended to rise during set up. It may be possible to manage this phenomenon by wetting the FCA to be equal in density to the mix matrix, or by increasing the stiffness of the mix.

Segregation was also high for a dense, 1800 kg/m^3 specimen with a filler-binder ratio of 2:1 and cementitious density of 510 kg/m^3. This effect may be due to the high water content of the mix. Suppressing the water-binder ratio slightly for cement-rich mixes may be necessary to achieve suitable paste stiffness.

6.4 Porosity

Porosity measurements provide a means of quality assurance. For a given plastic density, measured porosity may exceed the porosity predicted from a mix design if the foam has collapsed and dispersed as additional liquid in the mix, rather than remaining stable as bubbles. Measured porosity may otherwise vary from predicted values due to segregation, or inaccurate proportions of foam volume or other ingredients.

Measured porosity slightly exceeded predicted values for most mixes, which may be due to increased capillarity from collapsed foam dilution water. Conversely, FCA specimens were somewhat denser than intended, due to the tendency for the porous outer 'crust' of FCA to become impregnated with hydrated cement paste. FCA mixes increased in density after placement, as mix water and fluid paste were drawn into the porous aggregate by capillarity. Pre-wetting of aggregates may reduce this effect.

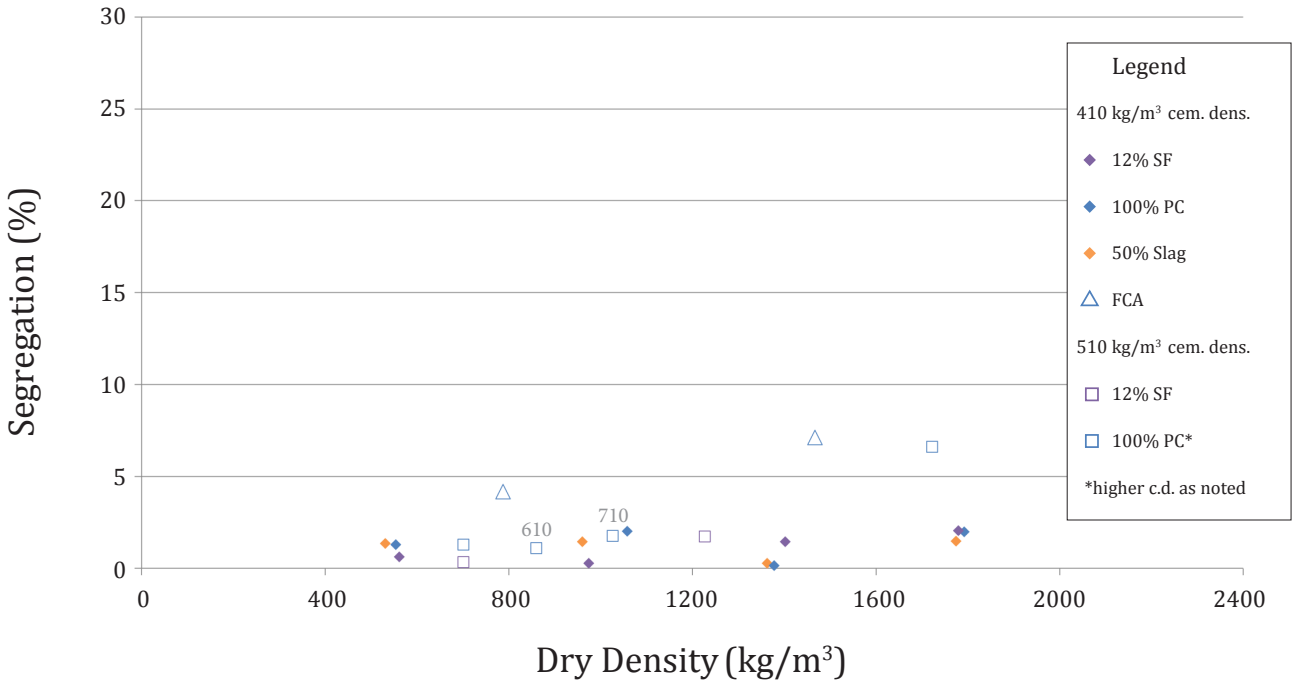

Figure 6.3a Segregation vs. dry density. Comparison of dry density at top and bottom of cast cylinder.

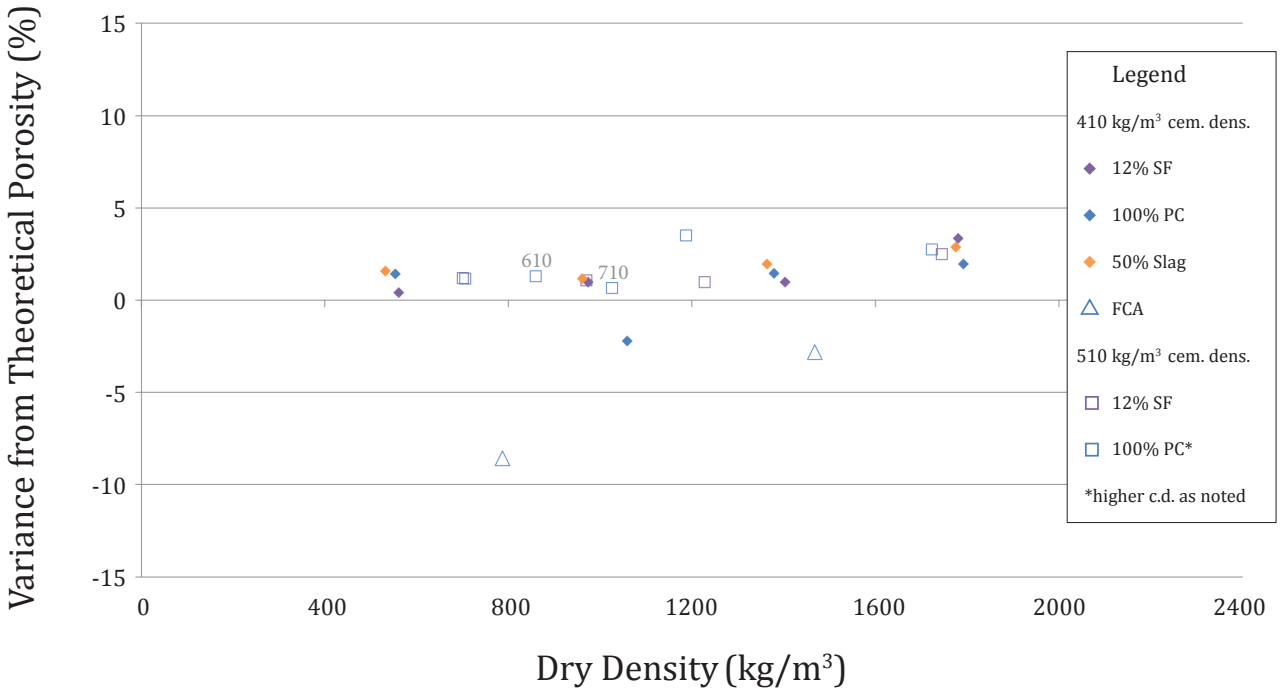

Figure 6.4a Variance of measured and predicted porosity vs. dry density.

6.5 Uniformity and Repeatability

The viability of a given mix design is substantiated by uniformity and repeatability of test results. The ability to reliably produce foam concrete to a specification is an important aspect of foam concrete mix design.

Variability in compressive strength data is assessed here briefly. Three datasets were compared for various cementitious blends across a range of densities, after 56 days of curing. Minor differences in the manufacture and preparation of the specimens are delineated in the table below.

Parameter	Dataset 1	Dataset 2	Dataset 3
Water-Binder Ratio	Initially proposed values (Sections 6.1.1 and 6.1.2)	Refined values (Section 6.1.3)	Refined values (Section 6.1.3)
Capping	Sulphur caps	End-ground	End-ground
Number of Specimens	4	3	3

Table 6.5 Differences in manufacture and preparation of specimens from Datasets 1, 2 and 3.

Relative to normal density concrete, foam concrete exhibits high variability in compressive strength. This effect can be attributed to variability in the air-void system, as coalesced air-voids or other large Griffith flaws govern failure. For a given batch, the coefficient of variation among three or four specimens was typically less than 15%. The CoV was lower for very dense batches, and for silica fume mixes, which typically have relatively small voids with minimal coalescence.

The coefficient of variation among ten specimens from three different batches was also typically less than 15%. However, for 1400 kg/m^3 mixes, compressive strengths from Dataset 3 were unusually low. These Dataset 3 specimens were each cast on the same day, sequentially. There may have been a shared error in the manufacture of the specimens (e.g. unaccounted moisture in the sand). These outlier values have been included on the CoV plot as indicated, but have otherwise been excluded from average values. Foam concrete in the 1400 kg/m^3 density range contains large proportions of dense sand and foam bubbles, which can make it difficult to avoid segregation as described in Section 6.1.3.

Further statistical analyses are presented in Appendix R. Note that variability for certain other properties, such as drying shrinkage, was very low. (Refer to Section 6.11.)

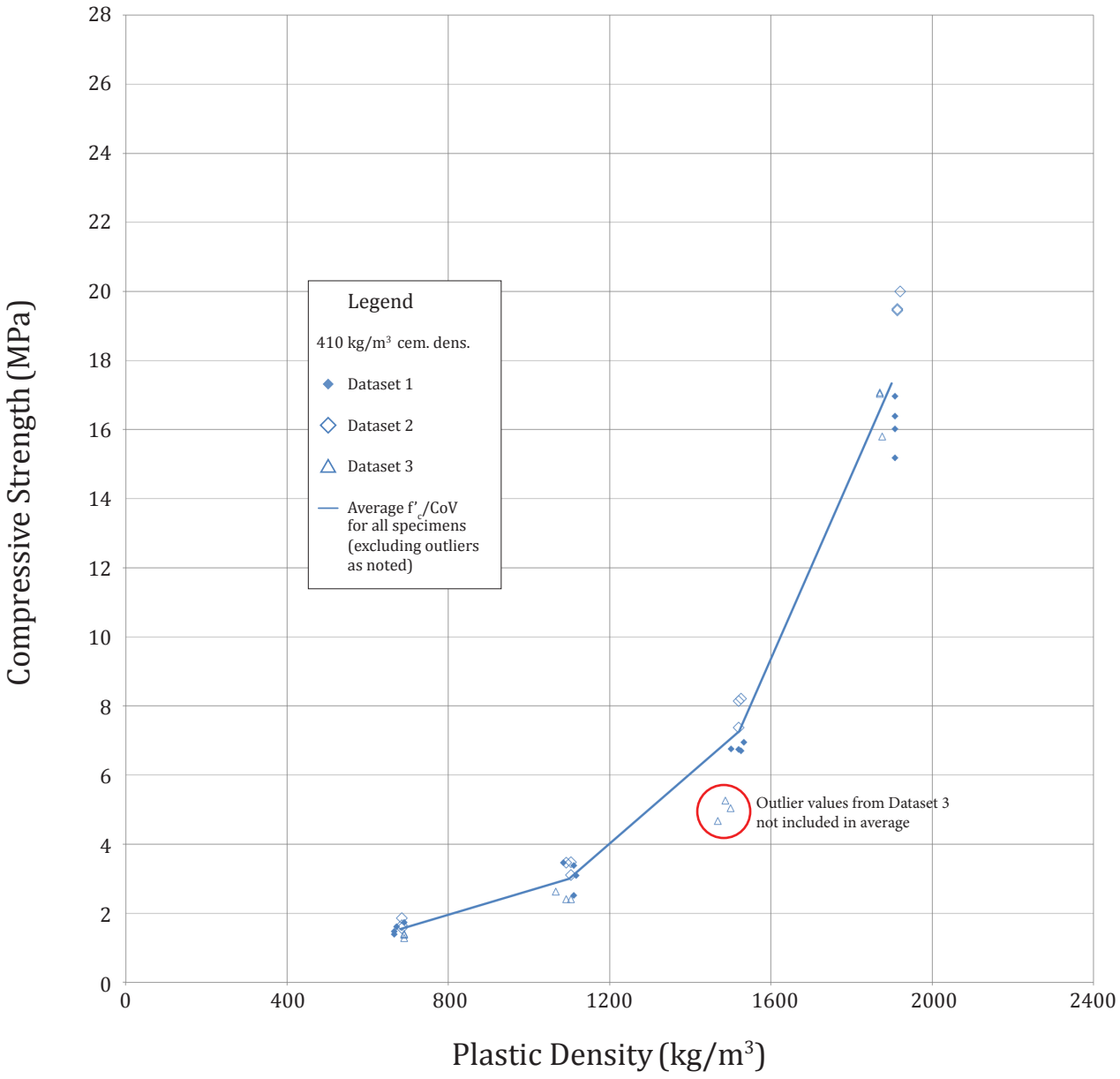

Figure 6.5a Uniformity and repeatability among 100% Portland cement binder trials, 56-days moist-cured.

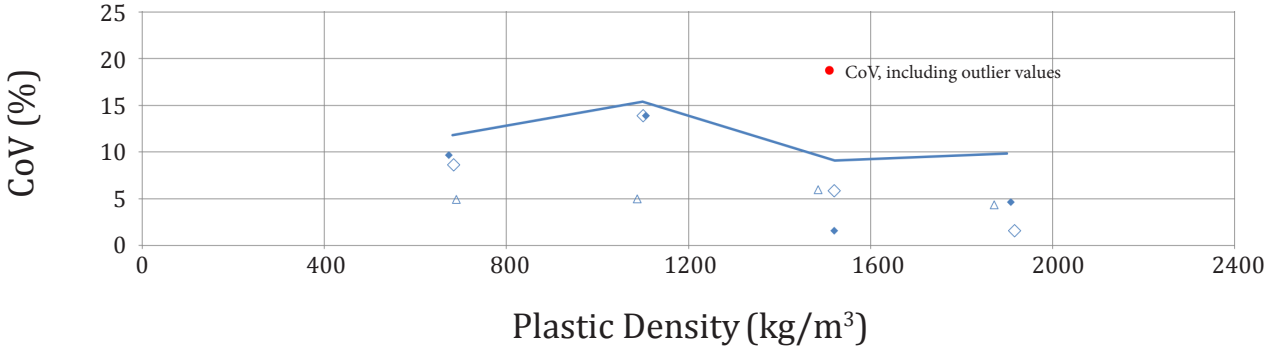

Figure 6.5b Coefficient of variation among 100% Portland cement binder trials, 56-days moist-cured.

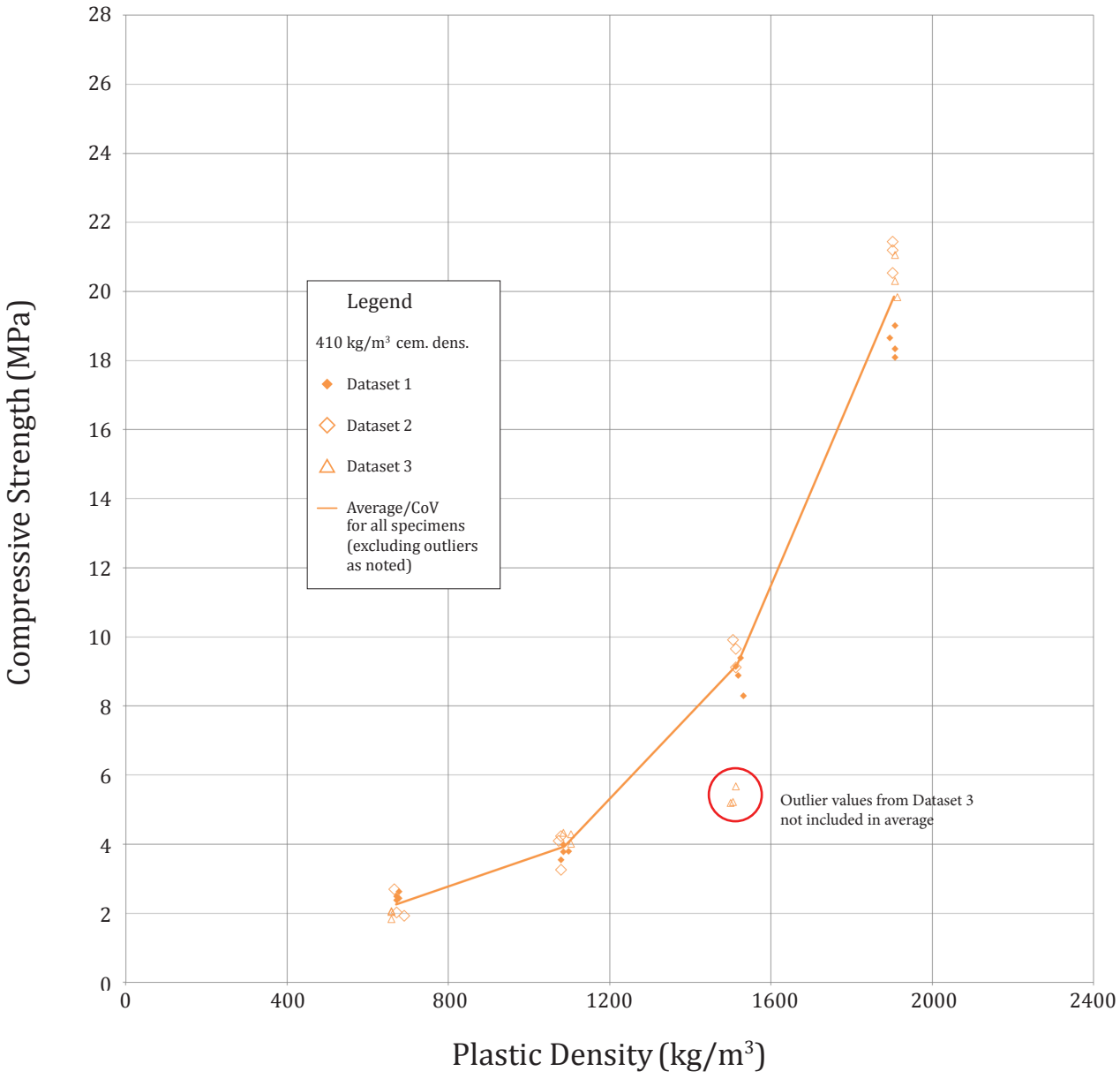

Figure 6.5c Uniformity and repeatability among 50% slag trials, 56-days moist-cured.

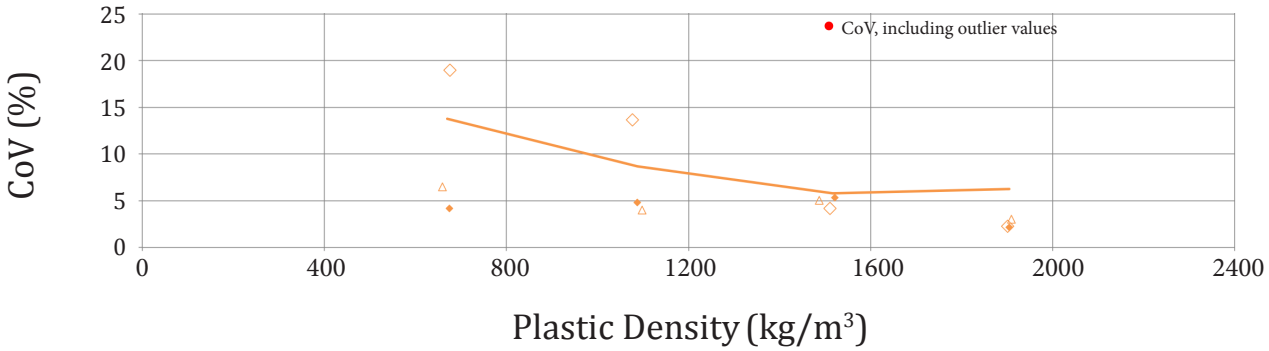

Figure 6.5d Coefficient of variation among 50% slag trials, 56-days moist-cured.

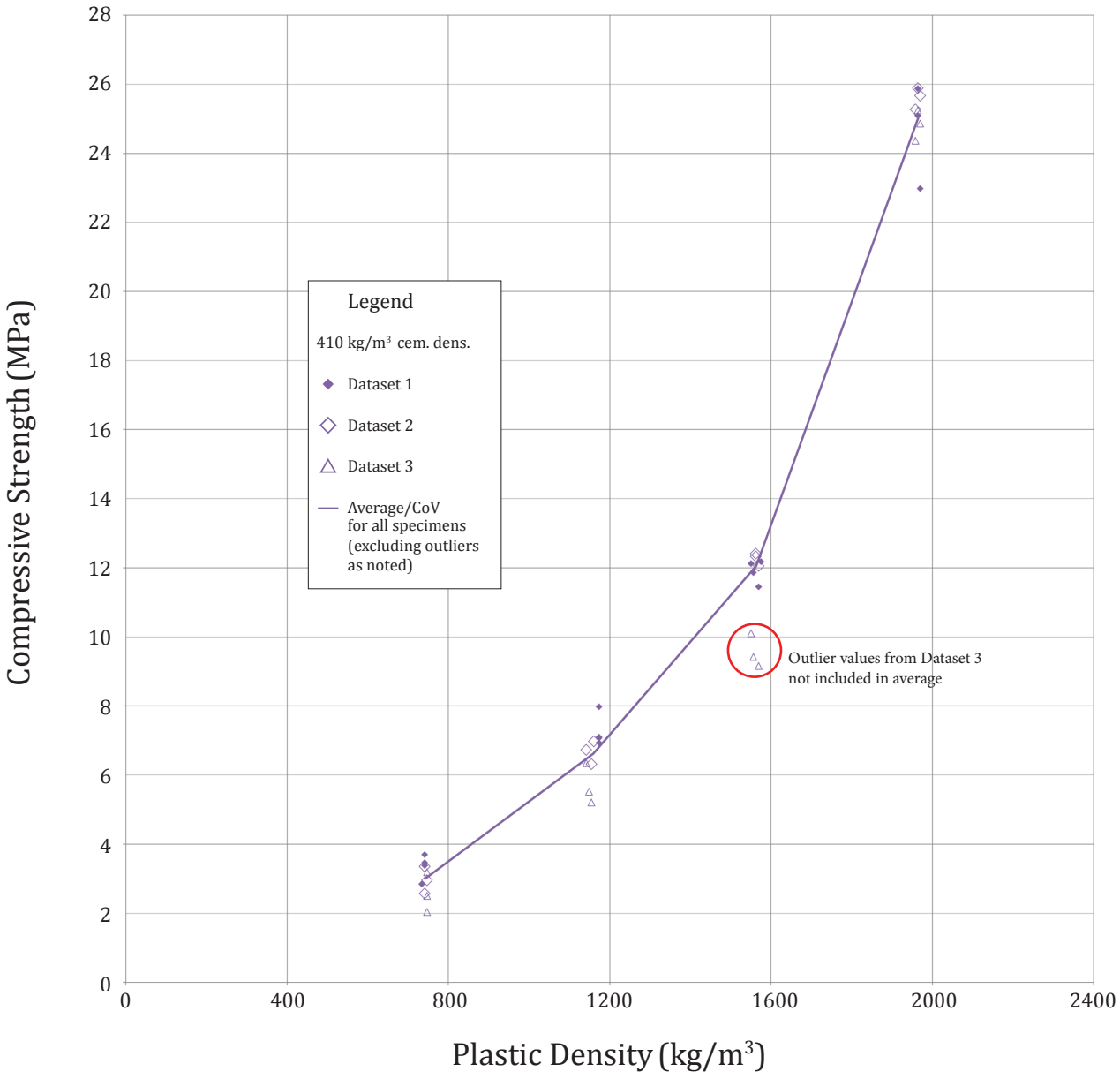

Figure 6.5e Uniformity and repeatability among 12% silica fume trials, 56-days moist-cured.

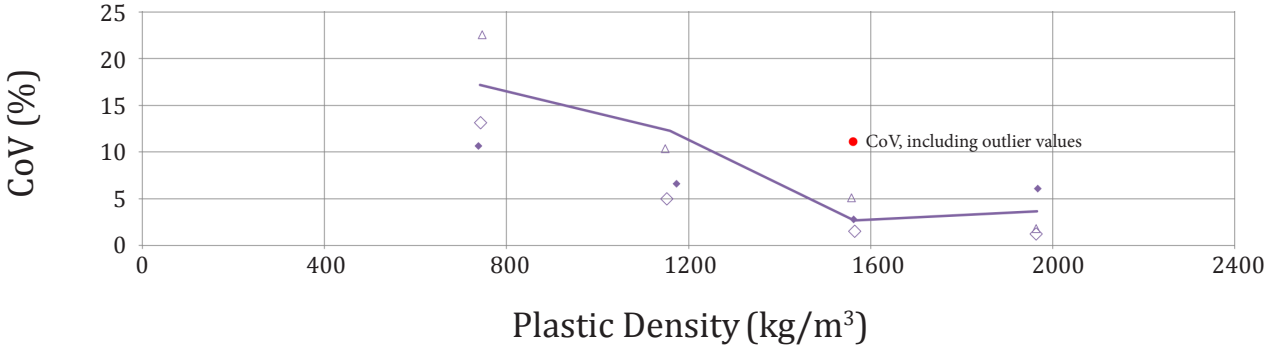

Figure 6.5f Coefficient of variation among 12% silica fume trials, 56-days moist-cured.

6.6 Influences on Compressive Strength

Compressive strength data is plotted against plastic, dry, and oven dry density in various figures throughout this Section, to examine the influences of density, cementitious density, cementitious blend, and curing age on compressive strength.

Results from Datasets 1 and 2 are included in the discussion, as noted. Refer to Table 6.5 for differences in specimen manufacture and preparation.

6.6.1 Influence of Density and Porosity on Compressive Strength

The influence of density was studied first by altering the filler-binder ratio while maintaining constant cementitious density (i.e. foam volume is replaced by fine aggregate); and second by maintaining a constant filler-binder ratio, while varying foam volume.

6.6.1.1 Plastic Density vs. Compressive Strength

The compressive strength of mixes were plotted against actual plastic density, in Figures 6.**6.1.1a** and **1b**. Strength increased with density, at a powerfully increasing rate.

Silica fume mixes tended to have a greater plastic density than Portland binder mixes, due to their increased water demand. Conversely, slag mixes tended to be slightly less dense than Portland binder mixes, as they have a greater proportion of air bubbles, and less water volume.

Notably, among the least dense mixes, with a filler-cement ratio of 0:1, the plastic densities of the slag mixes are approximately 100 kg/m^3 less than the plastic density of the Portland cement mixes, or approximately 14% lighter. It may be possible to exploit mixes with a reduced plastic density in applications where restrictions on construction loads or hydrostatic pressures are critical.

6.6.1.2 Dry Density vs. Compressive Strength

Strength is plotted against theoretical dry density in Figure 6.**6.1.2a**, determined as per Appendix K. Figure 6.**6.1.2b** plots results against measured dry density values from companion specimens, stored in 50% RH. These graphs may be used to estimate the density of foam concrete in-service.

Dry densities were approximately 90, 112, 135, and 160 kg/m^3 less than plastic densities, for water-binder ratios of 0.45, 0.55, 0.65, and 0.75, respectively. Significant reductions in density were calculated and measured for the silica fume mixes upon curing and drying, in particular, due to their high water-binder ratios.

6.6.1.3 *Oven-Dry Density vs. Compressive Strength*

Strength is plotted against theoretical and actual oven-dry density values in Figures 6.**6.1.3a** and 6.**6.1.3b**, respectively. In general, plastic mixes may be expected to lose approximately 149, 187, 225, or 264 kg/m^3 of density during oven drying, for water-binder ratios of 0.45, 0.55, 0.65, and 0.75, respectively.

6.6.1.4 *Porosity vs. Compressive Strength*

Compressive strength was plotted against actual porosity values from companion specimens, in Figure 6.**6.1.4a**. Strength increases powerfully with decreasing porosity, with mixes exhibiting similar trends to those described above.

Strength-porosity relationships for mixes with constant filler-binder ratios are shown in Figure 6.**6.1.4b**. The intrinsic strength of the cement paste for each batch was assumed to be constant. The data was fitted according to a power model, following Balshin,[1] and to an exponential model, following Ryshkewitch.[2] Formulae and coefficients of determination are given in Table 6.6.1.4. Given the scarcity of the data, these formulae should be taken as preliminary. A logarithmic model, following Schiller,[3] did not fit the data well. (See Appendix R.)

Observations during the experimental program, as well as data from high porosity mixes developed by other researchers (included on Figure 6.**6.1.4b**), indicate that foam concrete strength decreases rapidly at very high porosities. The power model, following Balshin, captures this phenomenon well. For an extensive discussion on strength-porosity relationships for foam concrete, refer to Appendix A, Section 6.3.2a.

---

1 Balshin (1949)
2 Ryshkevitch (1953)
3 Schiller (1971)

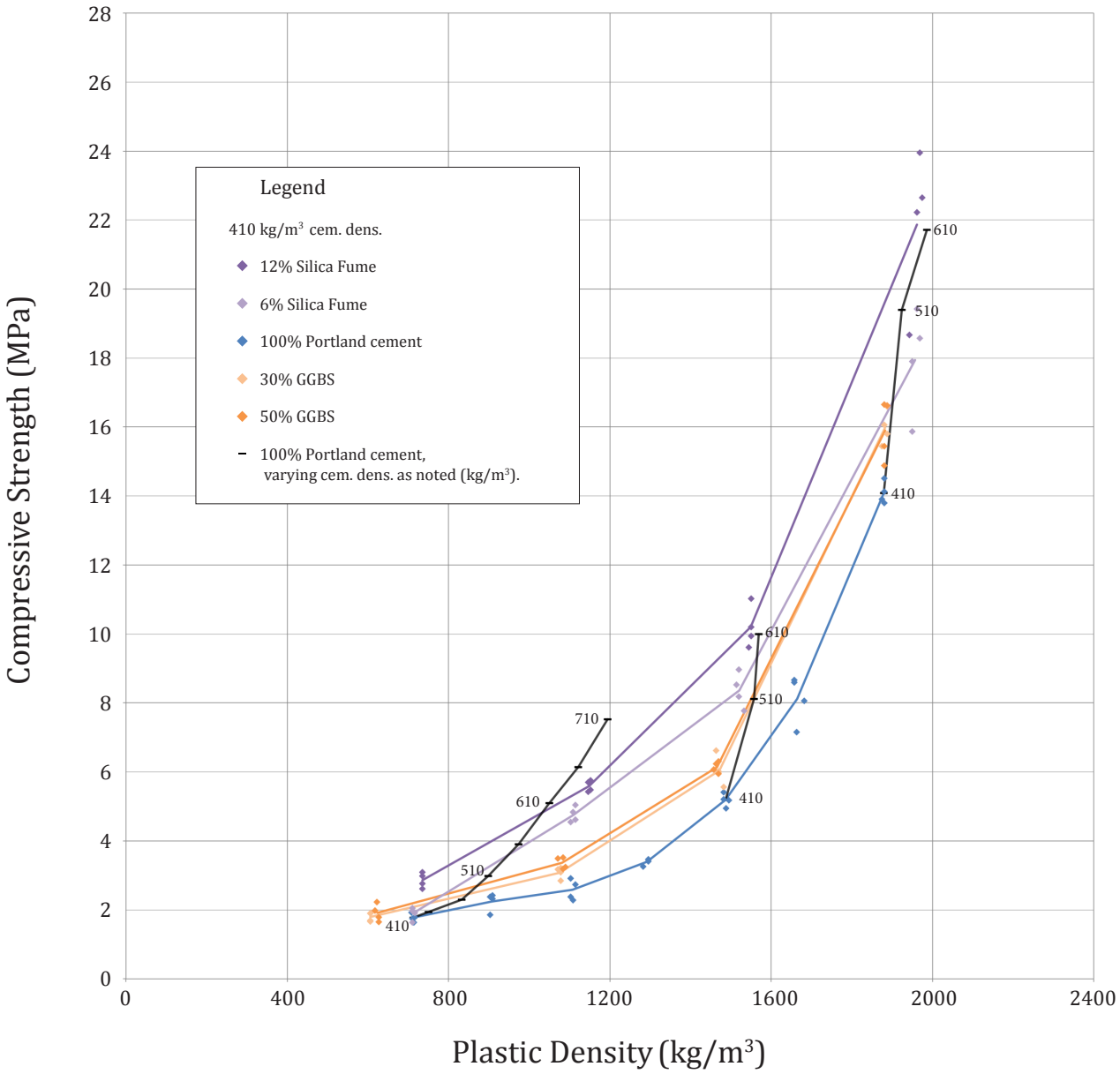

Figure 6.6.1.1a Compressive strength vs. plastic density, 28 days moist-cured, Dataset 1 (sulphur caps).

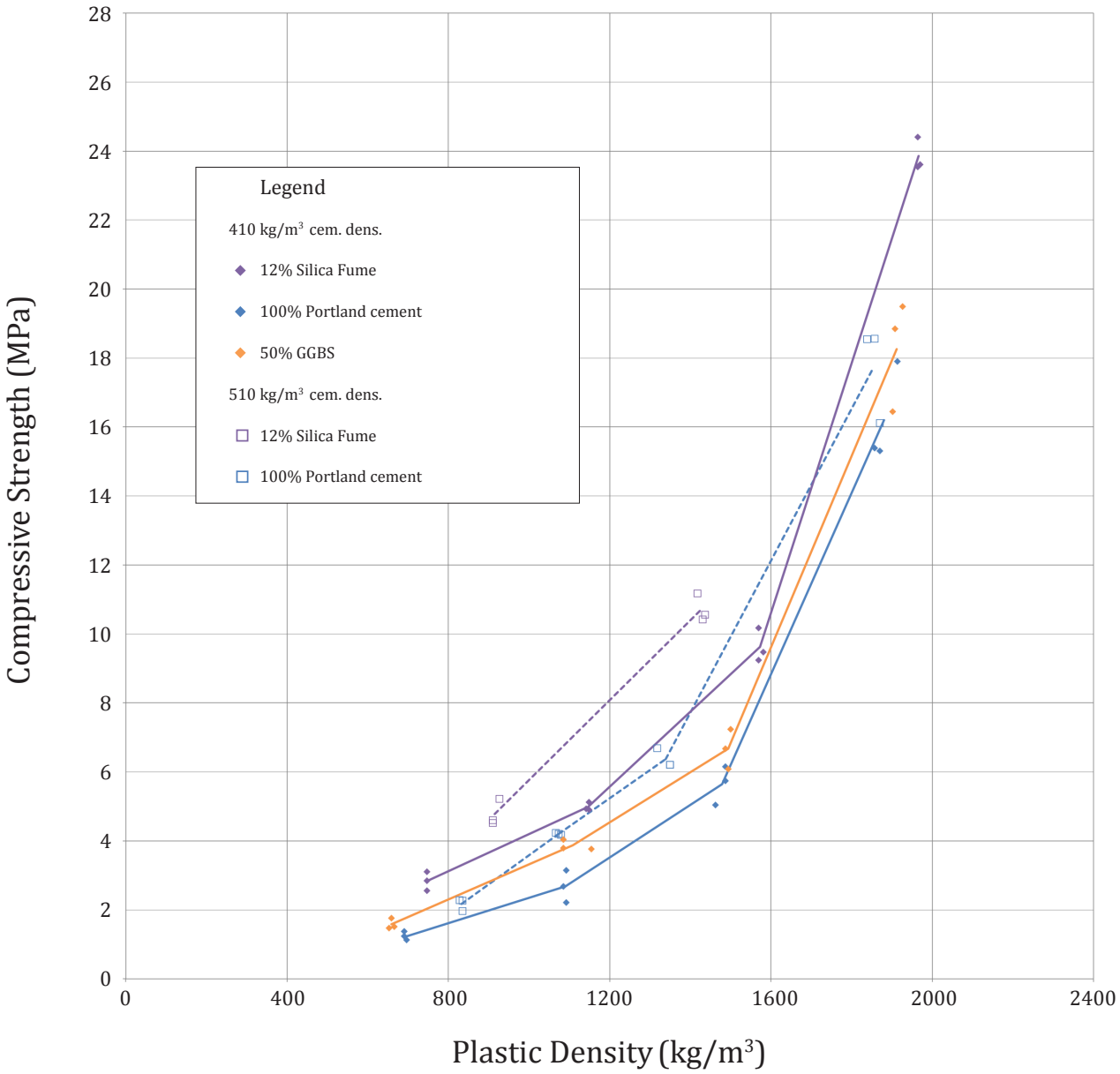

Figure 6.6.1.1b Compressive strength vs. plastic density, 28 days moist-cured, Dataset 2 (unbonded).

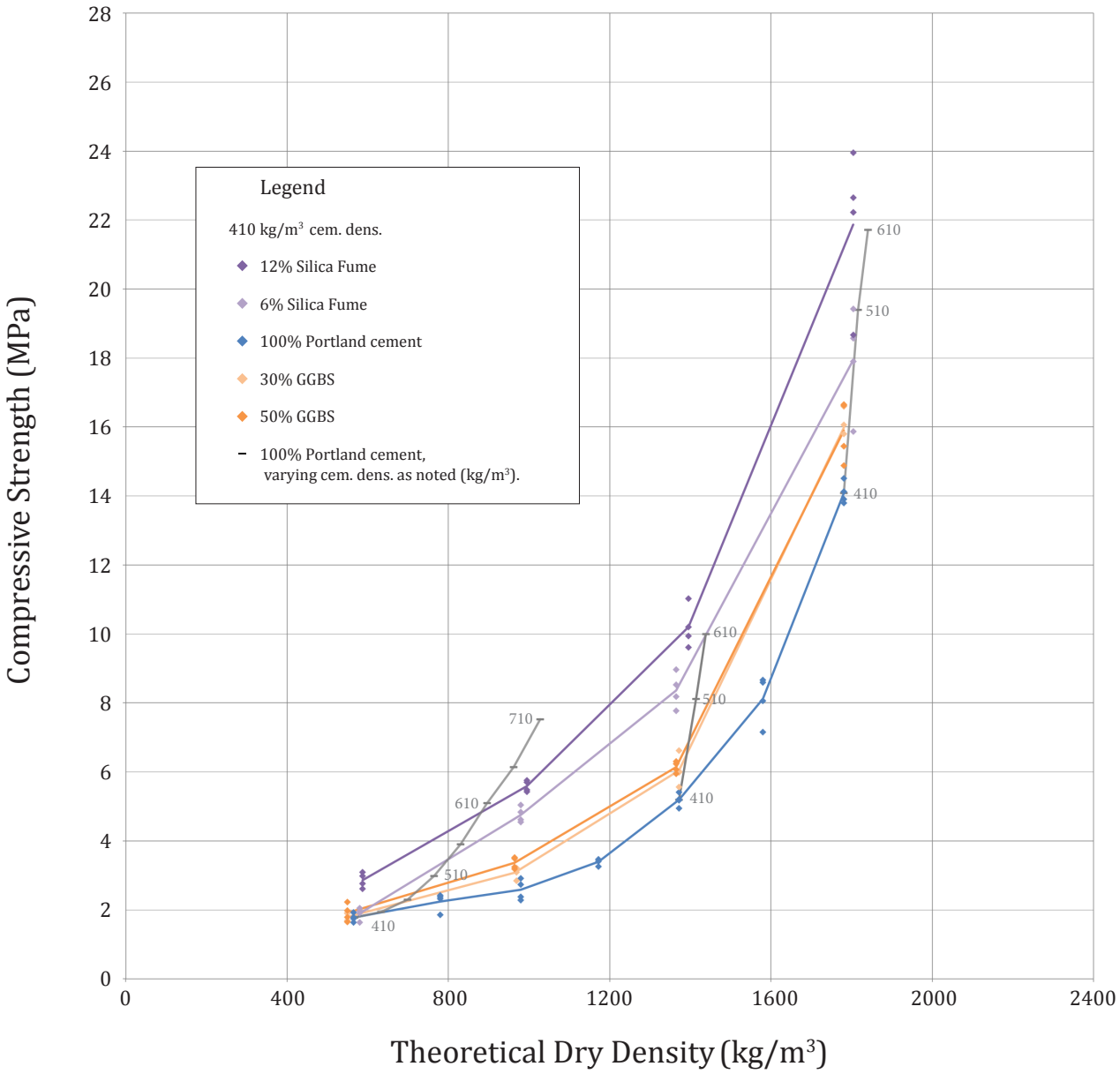

Figure 6.6.1.2a Compressive strength vs. theoretical dry density, 28 days moist-cured, Dataset 1 (sulphur caps).

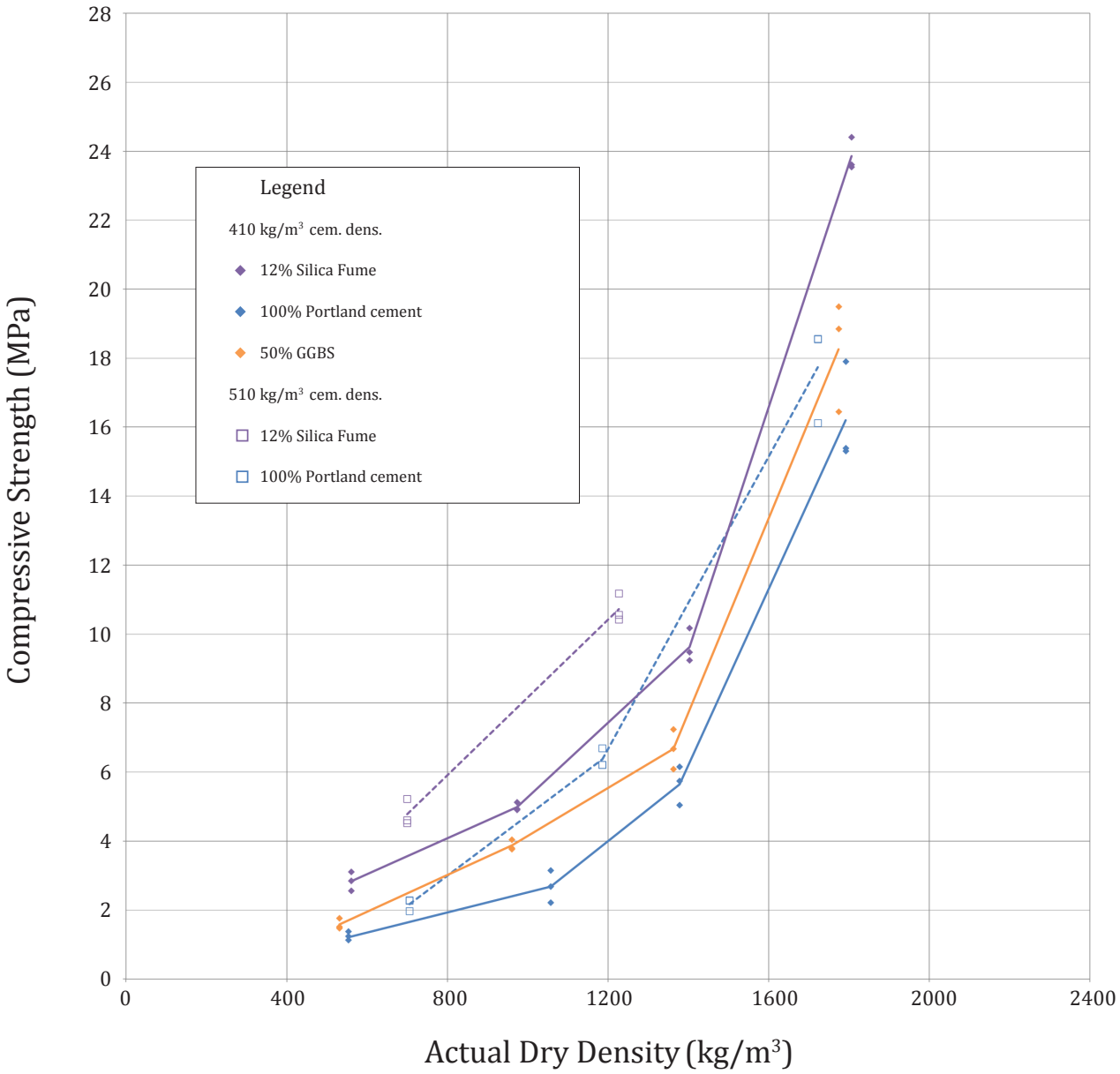

Figure 6.6.1.2b Compressive strength vs. actual dry density, 28 days moist-cured, Dataset 2 (unbonded).

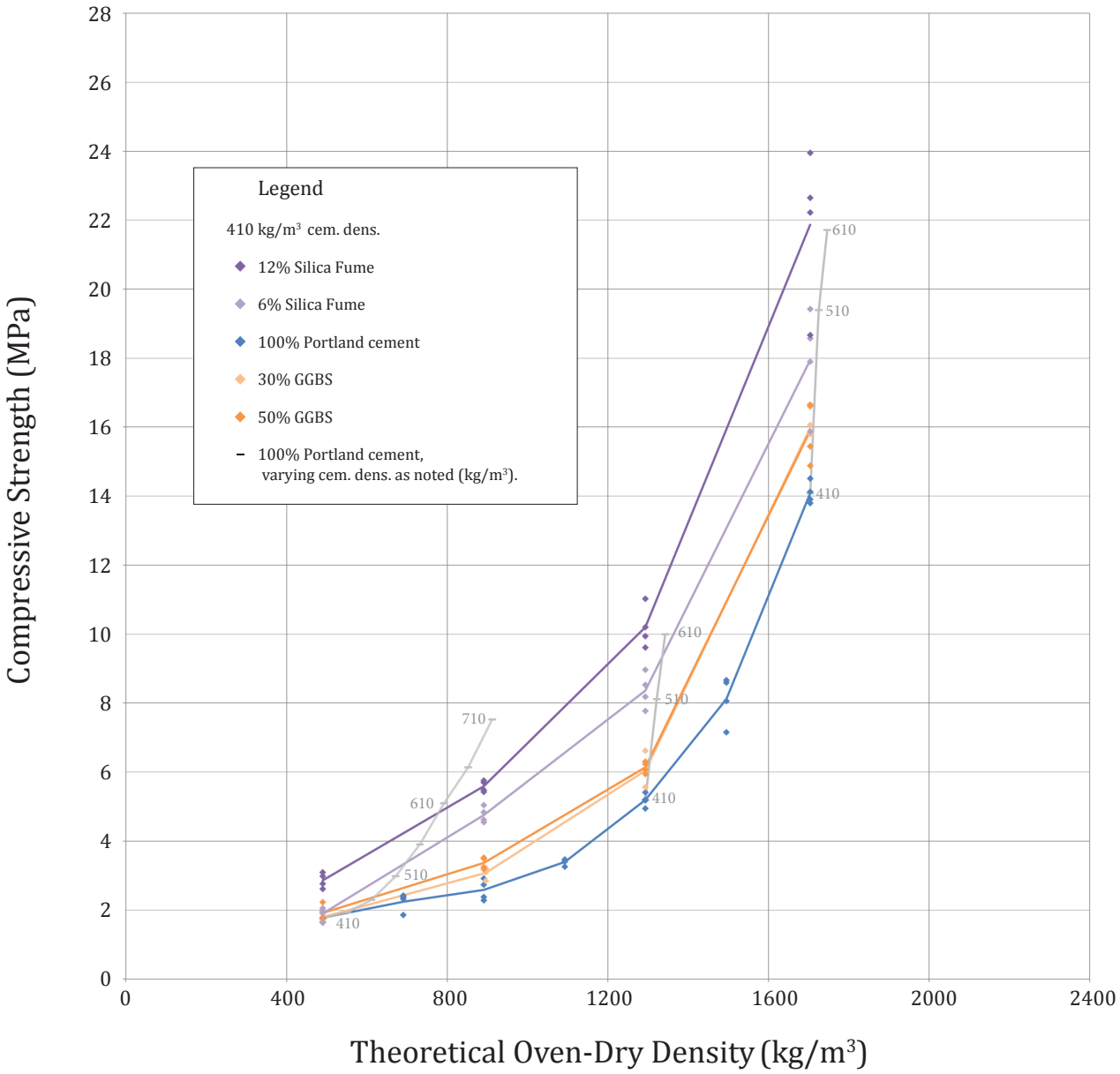

Figure 6.6.1.3a Compressive strength vs. theoretical oven-dry density, 28 days moist-cured, Dataset 1 (capped).

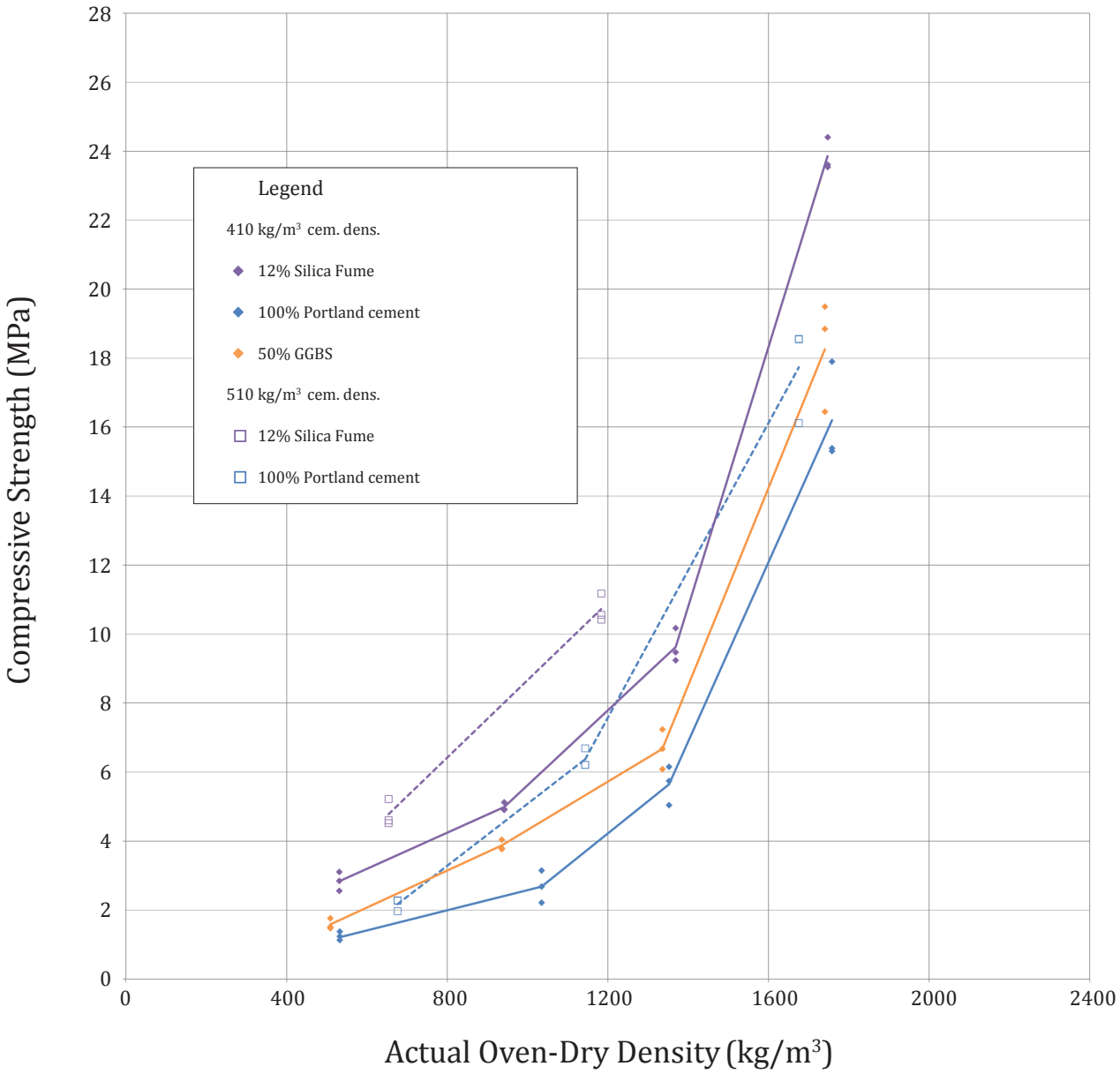

Figure 6.6.1.3b Compressive strength vs. actual oven-dry density, 28 days moist-cured, Dataset 2 (unbonded).

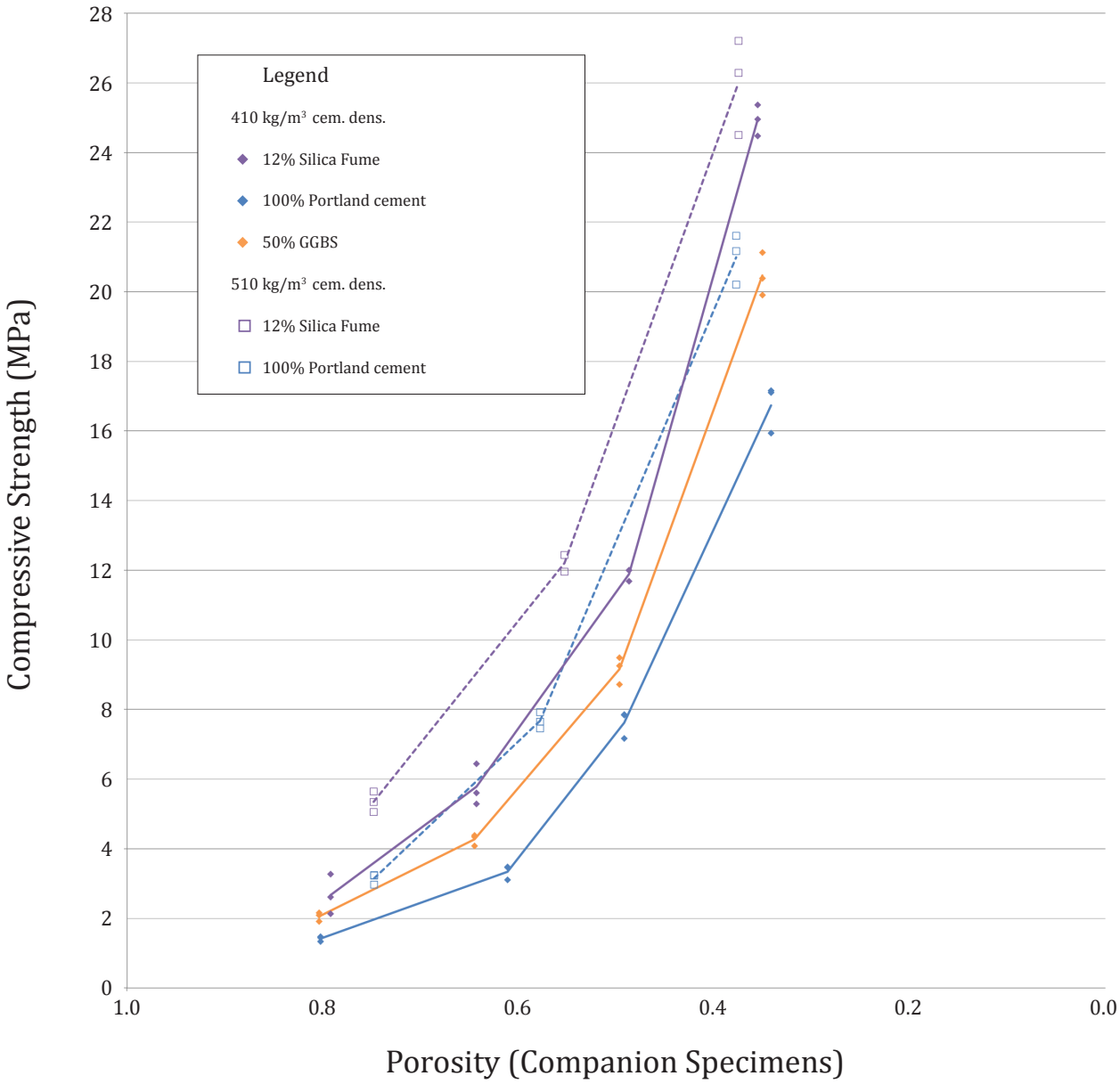

Figure 6.6.1.4a Compressive strength vs. porosity, 56 days moist-cured, Dataset 2 (unbonded).

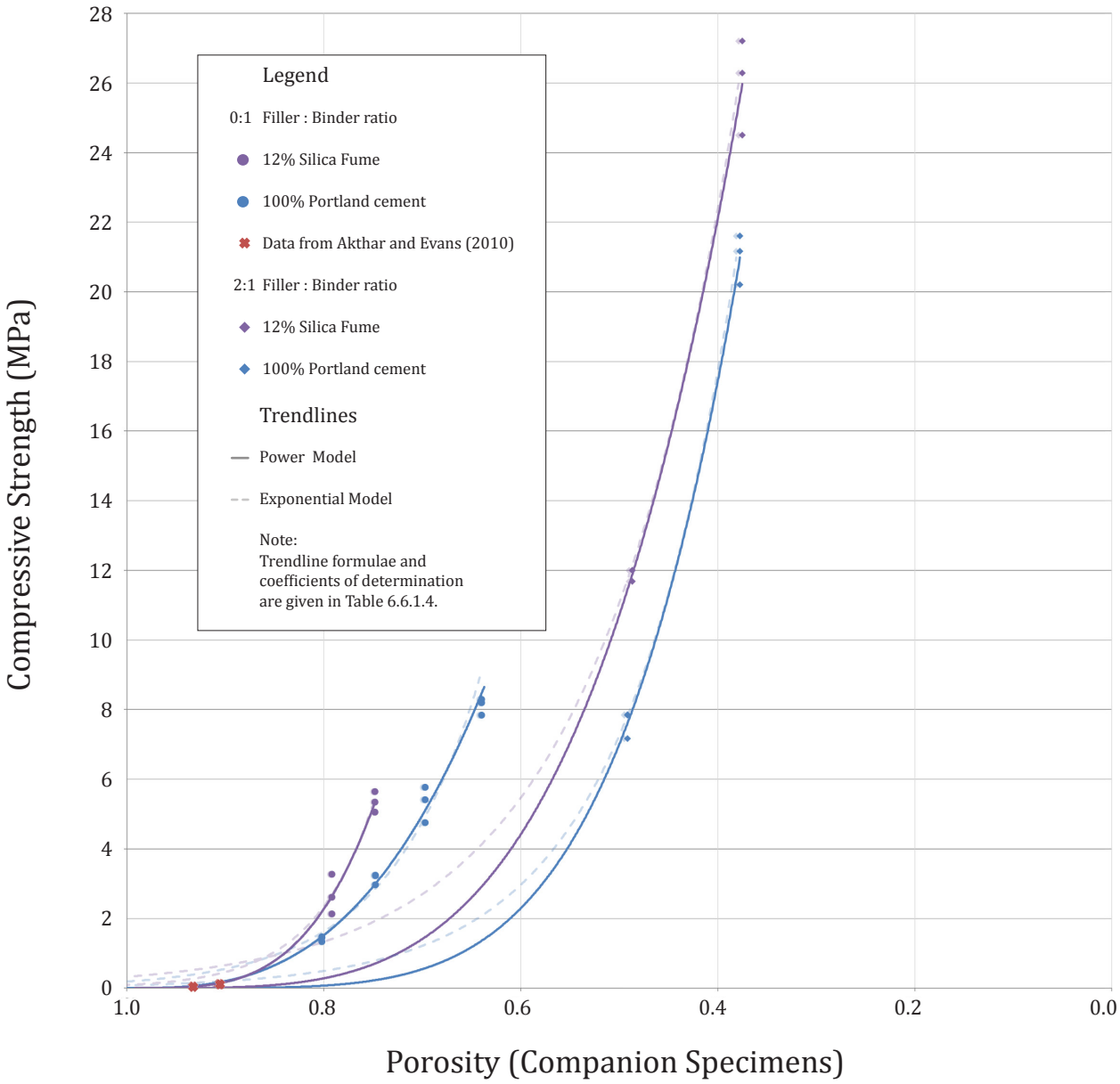

Figure 6.6.1.4b Compressive strength vs. porosity, 56 days moist-cured, Dataset 2 (unbonded). Trendlines shown for constant base mixes with varying foam volume.

Cem. Blend	Filler : Binder	Power Model (Balshin) $S = S_0(1-p)^{k_B}$	CoD	Exponential Model (Ryshkewitch) $S = S_0 e^{-k_R p}$	CoD
100% PC	0:1	$S = 167(1-p)^{2.92}$	0.990	$S = 11311e^{-11.22p}$	0.963
	2:1	$S = 225(1-p)^{5.00}$	0.993*	$S = 597.9e^{-8.88p}$	0.995*
12% SF	0:1	$S = 872(1-p)^{3.70}$	0.884*	$S = 924353e^{-16.12p}$	0.884*
	2:1	$S = 168(1-p)^{3.97}$	0.995*	$S = 358.5e^{-7.00p}$	0.993*

Table 6.6.1.4 Strength-porosity relationships for foam concrete, based on the data in Figure 6.6.1.4 *Note that the coefficient of determination is of little significance for most formulae, as indicated, due to scarcity of data. Refer to Appendix A, Section 6.3.2a for more information on strength-porosity relationships.

6.6.2 Influence of Cementitious Blend on Compressive Strength

Use of slag and silica fume binder replacements improved the 28-day compressive strength of every mix tested, compared to 100% Portland binder mixes (refer to Figures 6.**6.1.4a** to 6.**6.1.4b**). This strength improvement may be attributed in part to the pozzolanic process, by which structural discontinuities in the porous matrix, such as large calcium hydroxide crystals, are eliminated and replaced with strong C-S-H gel. Additionally, the fineness of mineral admixtures may improve the particle packing of the cementitious ingredients, and enhance the microstructure of the foam matrix. However, in Dataset 1, it was observed that that while Portland binder mixes produced very consistent break results at 28 days, the addition of supplementary cementitious materials increased variability, especially in denser mixes. This effect may be due to greater heterogeneity in paste strength.

In general, strength improved substantially and along a reasonably linear trend with the addition of silica fume, as observed in Figure 6.**6.2a**. Conversely, strength improvement with the addition of slag was less significant. There appeared to be very little effect on compressive strength, as the slag binder replacement was increased from 30 to 50%.

The additional strength achieved by slag and silica fume mixes relative to Portland binder mixes is shown in Figure 6.**6.2b**, expressed as a percentage. Average values from Datasets 1 and 2 were used for the comparison. Binder replacements had the strongest influence on compressive strength for mixes with a filler-binder ratio of 1:1 (nominal density of 1000 kg/m^3), with relative strength improvements of approximately 40 and 100% for the slag and silica fume mixes, respectively. Relative strength improvements were reduced at lower densities.

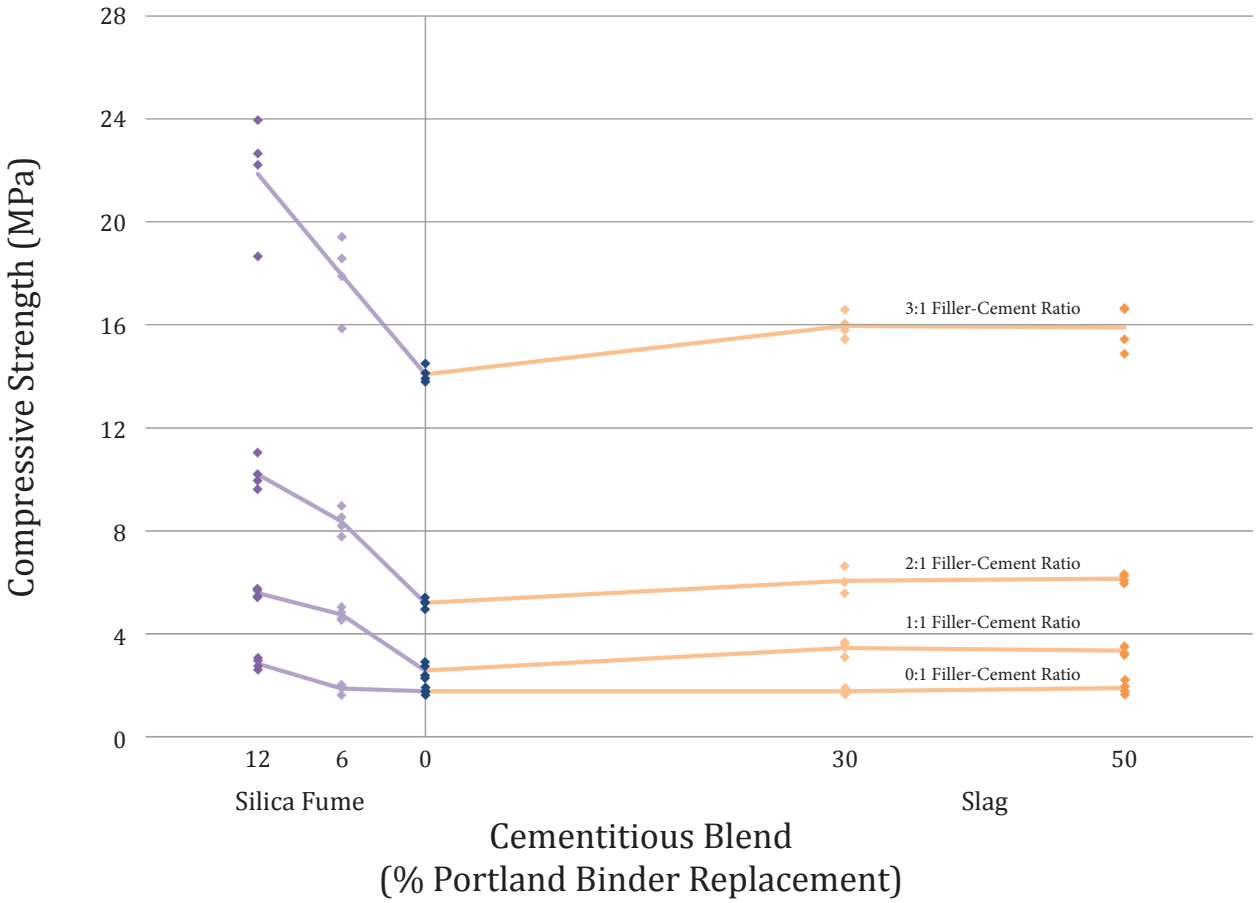

Figure 6.6.2a Compressive strength vs. cementitious blend. 28 days moist-cured, Dataset 1 (sulphur caps).

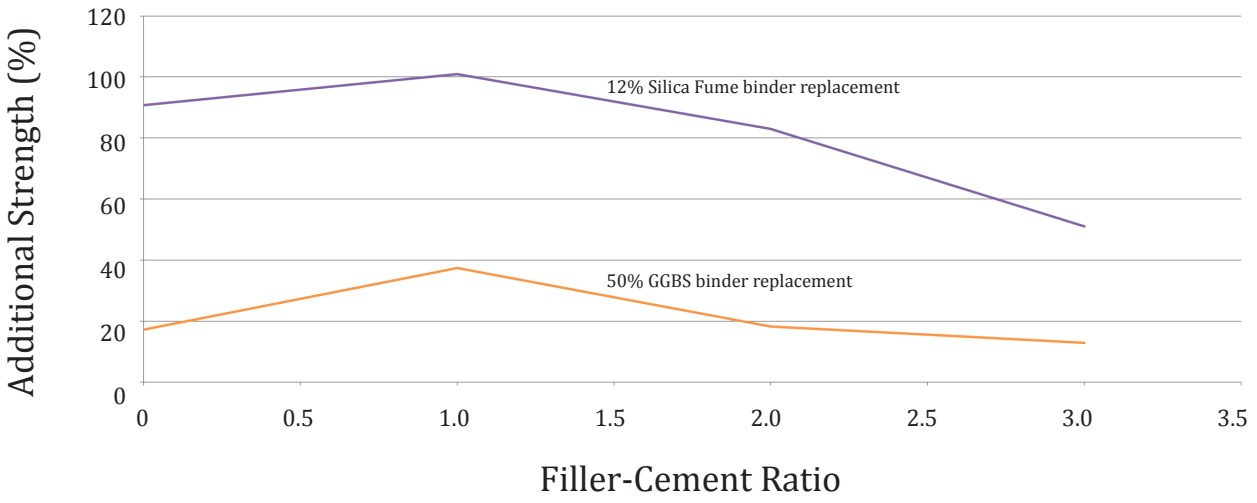

Figure 6.6.2b Strength gain relative to 100% Portland cement binder mixes.
28 days moist-cured, average of Datasets 1 and 2.

Importantly, for mixes with a filler-binder ratio of 0:1, 12% silica fume binder replacement offered 91% strength improvement over neat Portland cement foam concrete. Previous research has suggested that silica fume is not an effective SCM for low density foam concrete;[4] however, these results indicate that silica fume can be very effective in low-density mixes, if supplied in sufficient quantities and with sufficient mix water.

6.6.3 Influence of Cementitious Density on Compressive Strength

The influence of varying cementitious density may be reviewed in Figures 6.**6.1.4a** to 6.**6.1.4b**.

In general, mixes with cementitious densities of 510 kg/m^3 offered compressive strengths comparable with or better than the slag mixes, for a given density or porosity. Mixes with cementitious densities of 610 kg/m^3 offered compressive strengths comparable to 12% silica fume mixes (Figure 6.**6.1.2a**).

Based on this data, in many cases it may be more efficient to provide supplementary cementitious materials as a partial replacement for Portland cement as a strategy for strength gain, rather than increasing cementitious density. Where especially high compressive strengths are required, high cementitious densities may be used in combination with supplementary cementitious materials. 12% silica fume mixes with 510 kg/m^3 cementitious density offered strength improvement in excess of 250%, compared to Portland binder mixes with 410 kg/m^3 cementitious density, for the same dry densities (refer to Figure 6.**6.1.2b**, based on interpolated density values).

For sanded mixes in Dataset 1, strength improvement was more significant when the cementitious density was increased from 410 kg/m^3 to 510 kg/m^3, than when the cementitious density was increased from 510 kg/m^3 to 610 kg/m^3. Percent improvement for the lower density sanded mix was 56% and 23%, respectively, while percent improvement for the higher density sanded mix was 38 and 12%, respectively. Adding cement to a mix with a high cementitious density increases strength at a slower rate than adding cement to a mix with a lower cementitious density. Previous foam concrete literature has suggested that cementitious densities in excess of 500 kg/m^3 offer minimal

[4] cf. Brady et al. (2001), Zulkarnain and Ramli (2011)

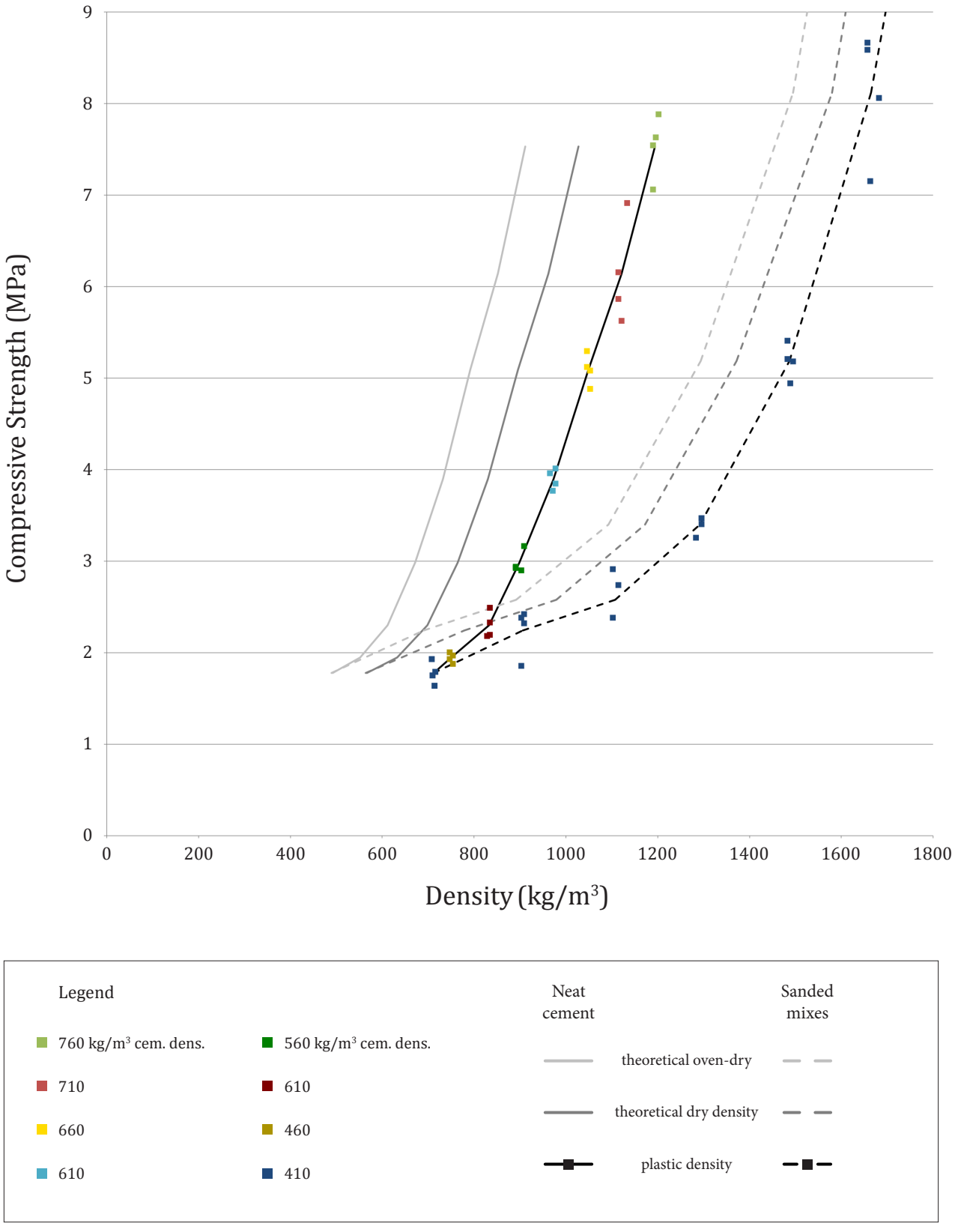

Figure 6.6.3a Compressive strength of neat cement and sanded mixes, varying density. 28 days moist-cured, Dataset 1 (sulphur caps).

strength gain.[5] However, the data from this experimental program indicates that increasing cementitious density up to 610 kg/m^3 has a meaningful influence on compressive strength.[6]

Data for neat cement mixes are emphasized in Figure 6.**6.3a**. Strength gain increased swiftly with increasing cement content. This accelerating strength gain may be attributed to reduced porosity, reduced coalescence of air-voids (i.e. smaller air-voids), and increased continuity of C-S-H within the mix.

Significantly higher strengths may be achieved in neat cement foam concrete mixes, compared to sanded cement mixes, for a given density. For example, a Portland cement binder mix with a filler cement ratio of 1:1 and a plastic density of 1110 kg/m^3 offered an average compressive strength of 2.6 MPa, while a Portland cement mix with no filler and a similar plastic density of 1120 kg/m^3 produced an average compressive strength of 6.1 MPa, representing improvement of over 230%. The highest average compressive strength of the neat cement mixes tested was 7.5 MPa, achieved where cementitious density was 760 kg/m^3.

6.6.4 Influence of Curing Age on Compressive Strength

Figures 6.**6.4a** to 6.**6.4d** indicate strength gain development patterns for Portland binder, slag, and silica fume mixes with cementitious densities of 410 kg/m^3

In the first seven days of hydration, silica fume mixes gained the greatest strength. Slag mixes were as strong or less strong than Portland-only mixes. Between 7 and 28 days, the rate of strength gain of Portland cement mixes was slow in comparison to slag and silica fume mixes, and by 28 days, slag mixes surpassed Portland cement mixes in strength. From 28 days to 56 days, the slag mixes continued to grow in strength, while the Portland and silica fume mixes grew relatively slowly.

The excellent performance of silica fume mixes may be attributed to the small average grain size of silica fume. Calcium hydroxide crystals that form in the mixes are likely to be within close proximity to silica fume particles, facilitating a pozzolanic reaction

---

5 Cf. Brady et al. (2001) B1, C1.

6 Note that issues of thermal stresses and other issues related to heat of hydration must be considered for cement-rich foam concrete mixes. Refer to Appendix A, Section 6.2.2.

Dataset 1, Strength Development

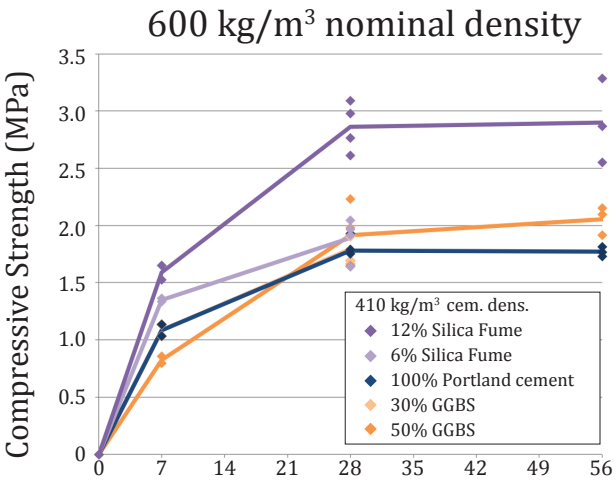

Figure 6.6.4a

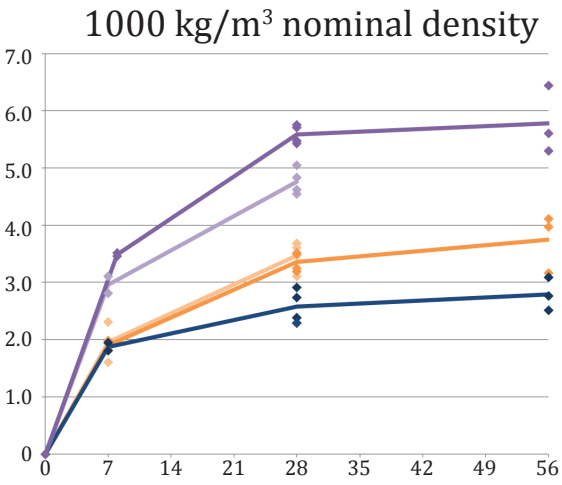

Figure 6.6.4b

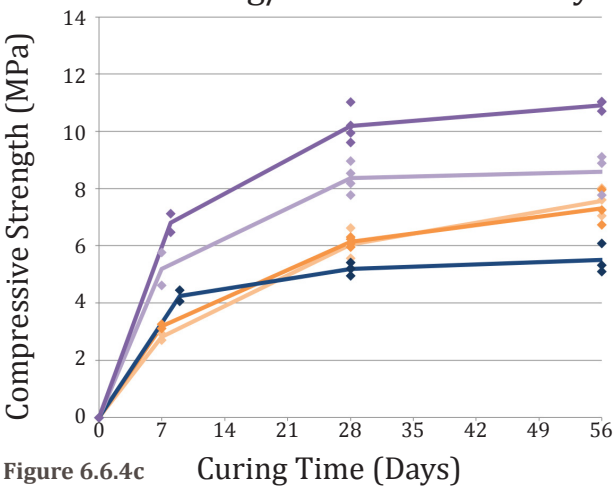

Figure 6.6.4c

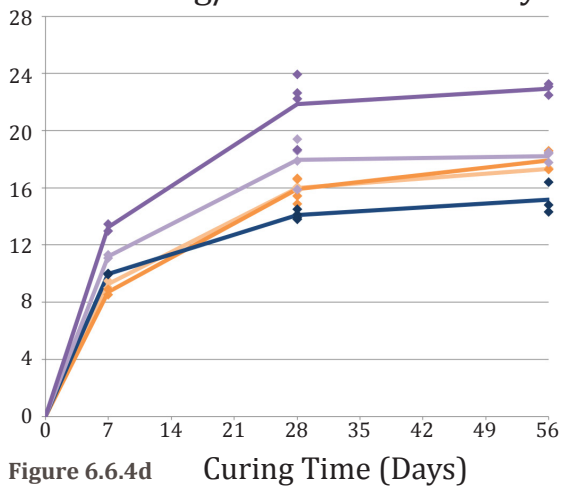

Figure 6.6.4d

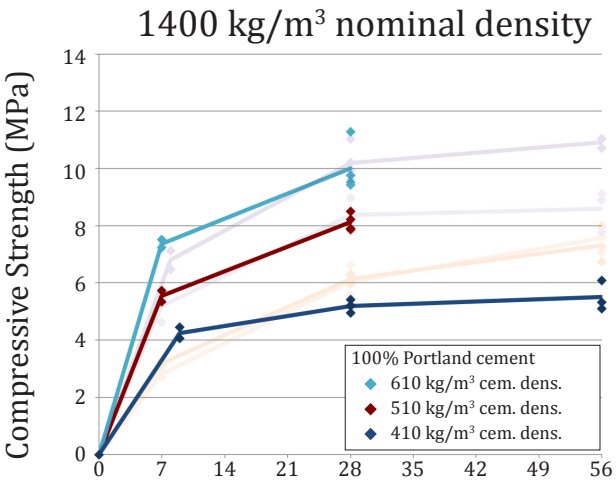

Figure 6.6.4e

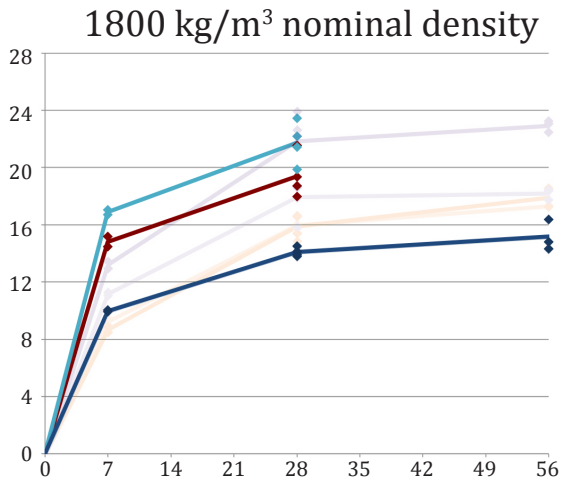

Figure 6.6.4f

for the production of C-S-H gel. Furthermore, the small grain size may improve particle packing around the foam bubbles.

Notably, however, the 6% silica fume mix with no filler did not perform especially well at 28 days. In order to help ensure that this was not due to a testing error in the 28-day break results, the results of strength gain development for slightly underhydrated and slightly overhydrated mixes (refer to Appendix R). Similar patterns of strength development at 7 and 28 were observed, suggesting that sufficient amounts of silica fume are necessary for continued strength gain in mixes with no filler.

Patterns of strength development for sanded mixes with varying cementitious contents are shown in Figures 6.**6.4e** to 6.**6.4f**. Data for mixes with supplementary cementitious materials and similar densities, taken from Figures 6.**6.4c** to 6.**6.4d**, respectively, are shown on the same plot, for reference.

For both the lighter and denser sanded mixes, additional cementitious density increased the rate of strength gain, from creation until 7 days. However, the rate of strength gain was higher for mixes with supplementary cementitious materials, between 7 and 28 days. By 28 days, the 12% silica fume mixes surpassed the mixes with cementitious densities of 610 kg/m^3 in average compressive strength.

56-day compressive results from Dataset 2 have been included in Figure 6.**6.1.4b**, for reference.

6.6.5 Comparison to Extant Mixes

The compressive strengths and theoretical equilibrium densities of foam concrete mixes tested in this Experimental Program are plotted in Figure 6.**6.5a**, marked with large X's. Data from foam concrete mixes by other authors is plotted with small X's; details of these other studies are given in Appendix A, Figure 7.**1.4a**. Data for other lightweight mineral-bound materials is presented in grey, in the background of the plot. Details for these materials may be found in Appendix A, Section 7.1.4.

Mixes tested in this Experimental Program lie within the general performance envelope of foam concrete mixes reported in the open literature. Mixes with 410 kg/m^3 of

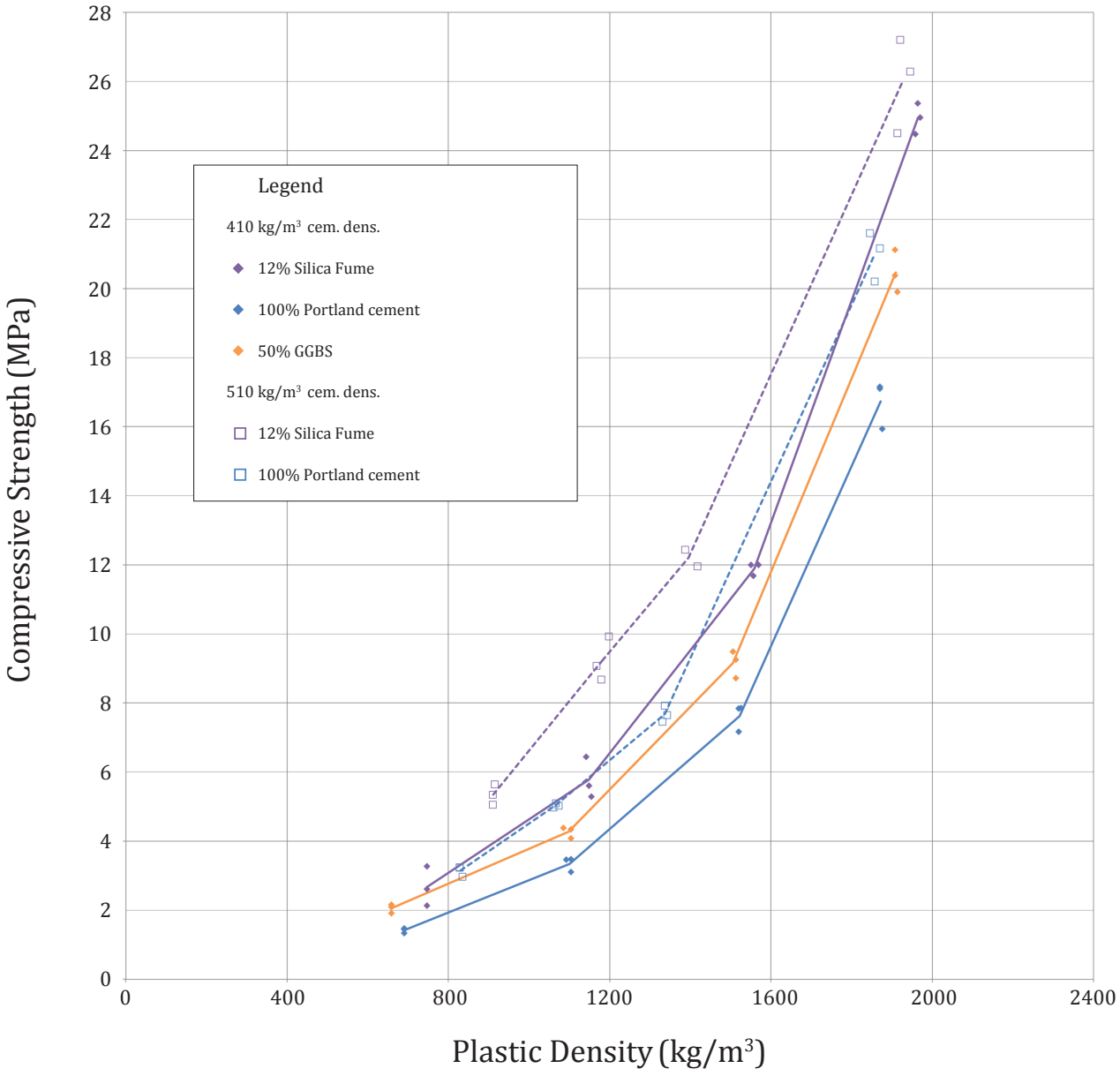

Figure 6.6.4g Compressive strength vs. plastic density, 56 days moist-cured, Dataset 2 (unbonded).

Portland binder are among the lower strength recipes, while mixes with 12% silica fume binder perform well compared to most mixes.

A number of mixes from other studies have exceptionally high strengths for densities between approximately 1000 and 1600 kg/m^3; however, these mixes utilize very high cementitious densities or specialized curing regimes for strength development. (Refer to Appendix A, Section 7.1.4 for details.) Additionally, other researchers have developed mixes with dry densities of less than 500 kg/m^3, which were not attempted in this experimental program.

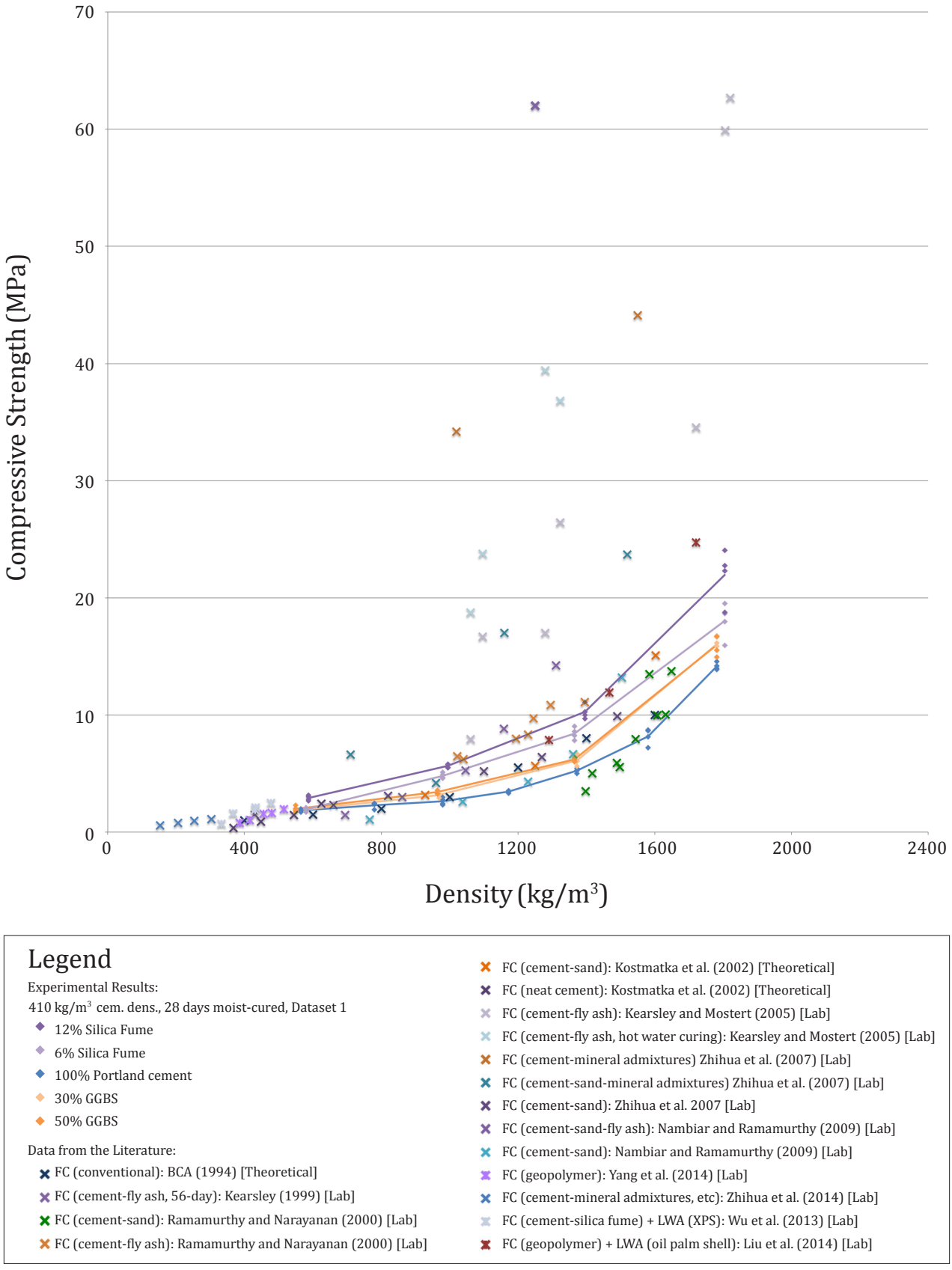

Figure 6.6.5a Comparison of experimental results and data from the literature.

6.7 Static Modulus of Elasticity

Figure 6.**7a** shows typical stress-strain relationships for foam concrete across a range of densities and cementitious blends, for stresses of up to 0.4 f'c. Trends were highly linear. Table 6.7 shows typical data for multiple loading cycles and specimens. In general, there was no clear trend of stiffening or softening of specimens with multiple loading cycles. Variation among specimens was greater than variation among cycles.

	Modulus of Elasticity 100% PC binder, 410 kg/m³ cem. dens., 28 days					
	600 kg/m³ nom. dens.			1400 kg/m³ nom. dens.		
	Specimen 1	Specimen 2	Specimen 3	Specimen 1	Specimen 2	Specimen 3
Cycle 1	1.74	1.22	1.59	5.92	6.32	5.66
Cycle 2	1.74	1.29	1.57	5.81	6.31	5.76
Cycle 3	1.69	1.31	1.59	5.93	6.27	5.81
Cycle 4	1.66	1.32	1.57	5.75	6.28	5.75
Cycle 5	1.64	1.33	1.57	5.71	6.28	5.76
Cycle 6	1.62	1.32	1.57	5.81	6.27	5.71
Avg. 2-6	**1.67**	**1.31**	**1.57**	**5.80**	**6.28**	**5.76**

Table 6.7 Typical variation in MOE values, across specimens and loading cycles. Note that values from loading Cycle 1 were not included in the average, to avoid capturing seating effects. See also Figure 7.3.**2e**.

Figures 6.**7b** and 6.**7c** plot the modulus of elasticity (MOE) of specimens against dry density of companion specimens, for a variety of mixes. The strong dependence of elastic modulus on density is clearly evident. With increasing density, there is more paste available to transmit load, reducing total strain.

For a given density, use of silica fume and slag improved the modulus of elasticity. Silica-rich SCMs may improve the stiffness of the paste by promoting the creation of long silica chains, as discussed in Section 7.3.2. The fineness of SCM particles, especially silica fume, may contribute to stiffness by promoting dense particle-packing.

The presence of load-bearing water may also contribute to stiffness. Moist densities at the time of testing were similar to specimen plastic densities, since the vapour drive between curing specimens and humidity room was low (refer to Section 5.4.2). When MOE is plotted against plastic density, as in in Figures 6.**7d** and 6.**7e**, the data is tightly correlated to density, independent of mix design. The liquid mass of water in capillaries

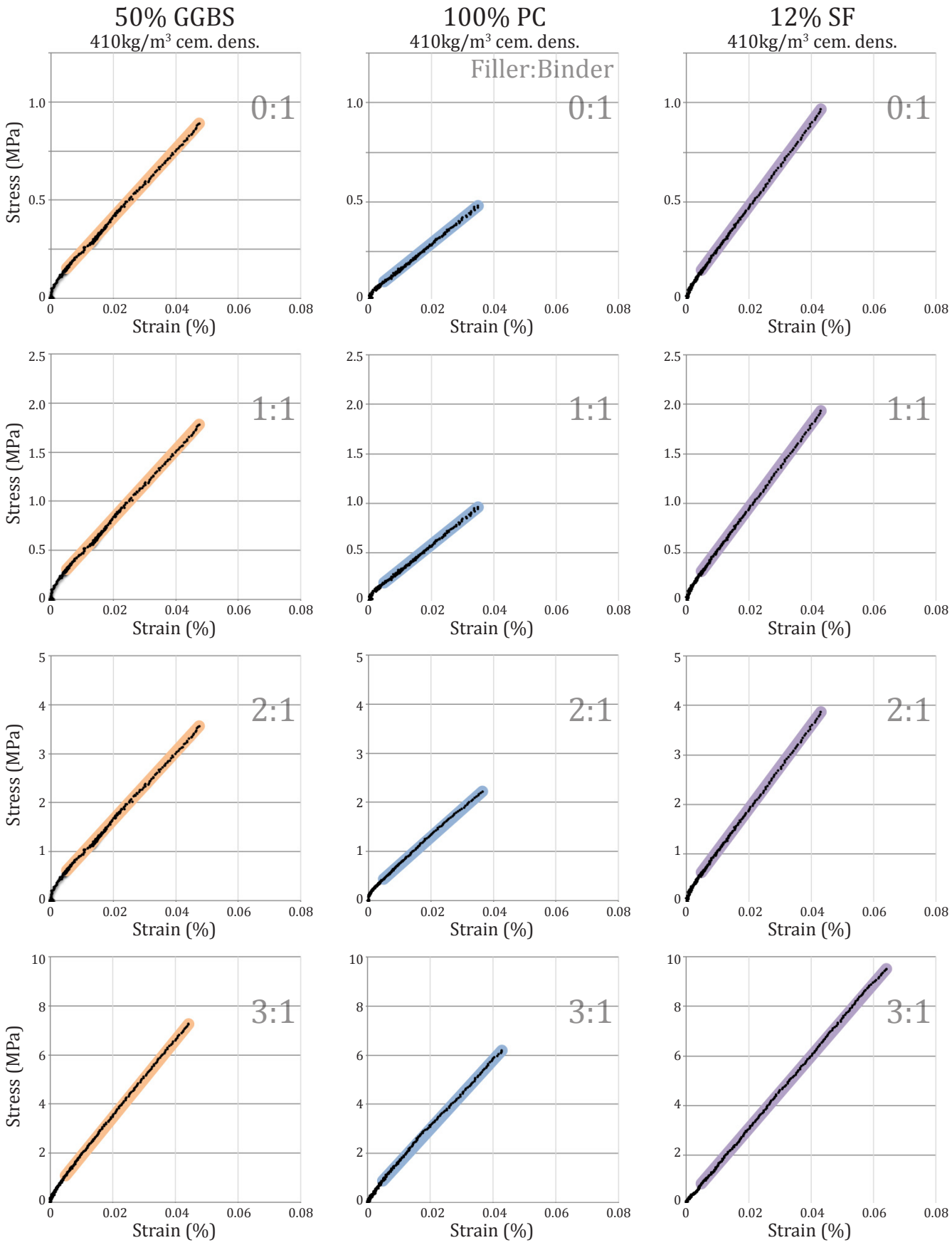

Figure 6.7a Linearity of stress-strain relationships.

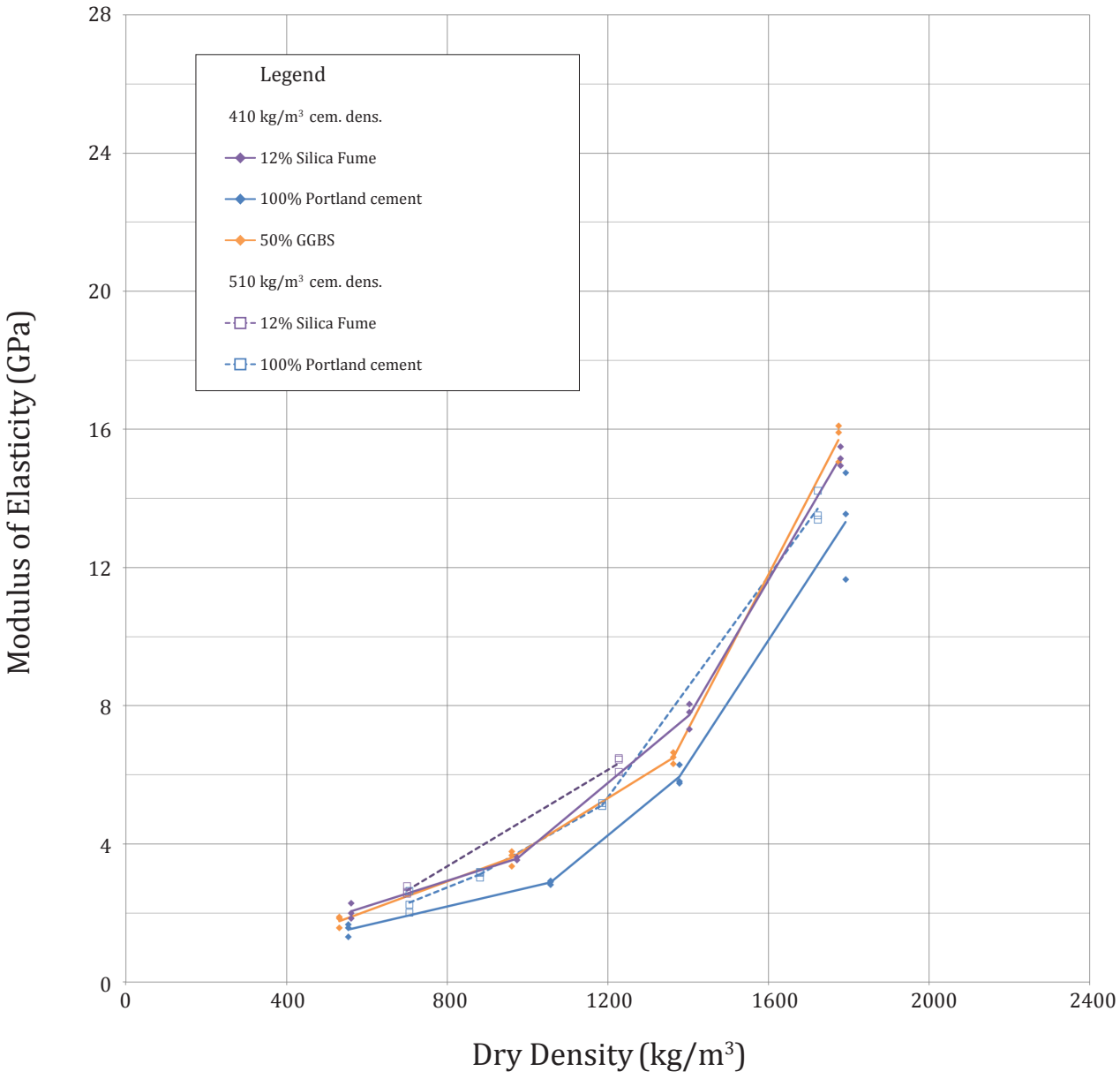

Figure 6.7b Modulus of elasticity vs. dry density, 28 days moist-cured.

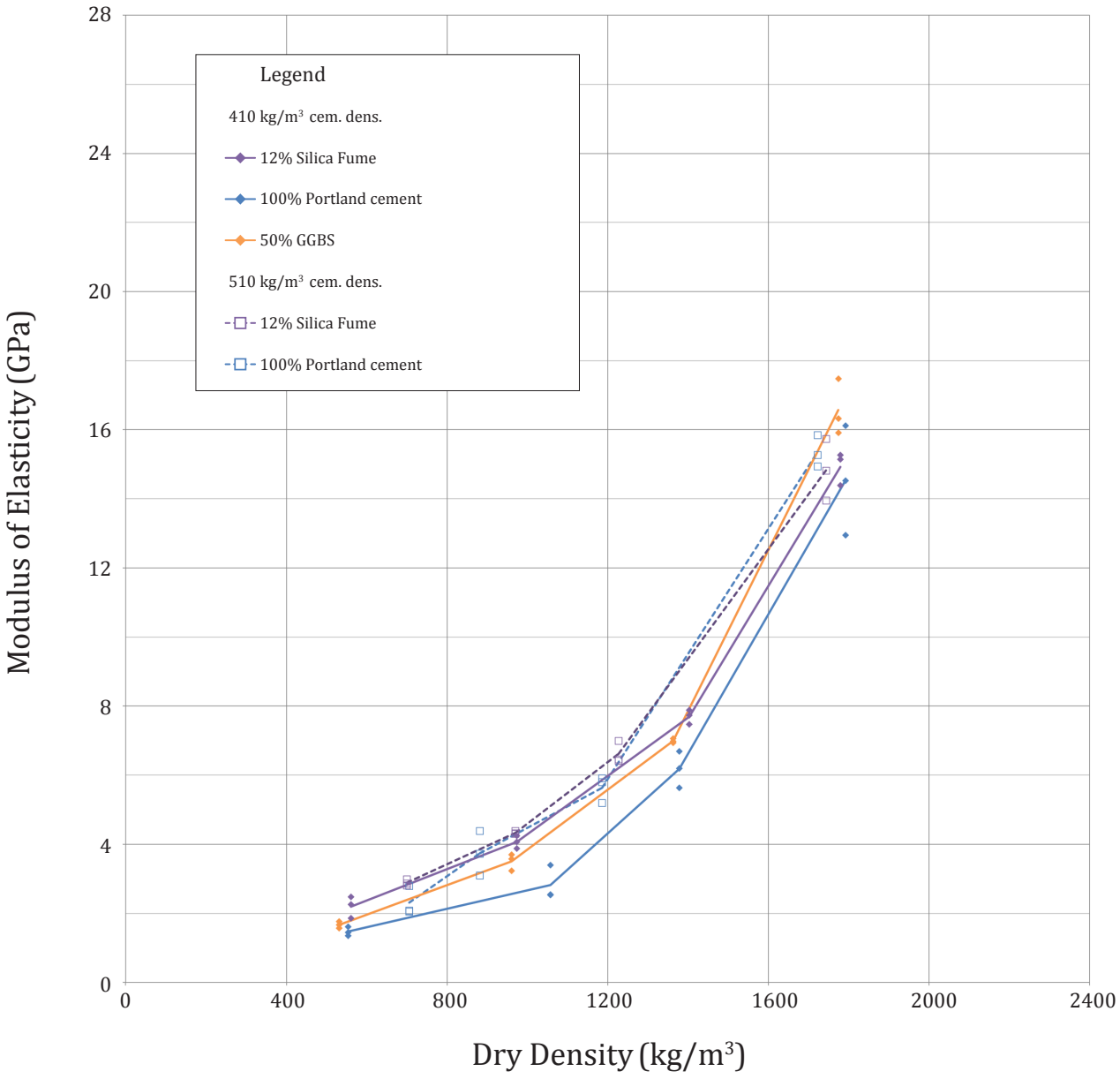

Figure 6.7c Modulus of elasticity vs. dry density, 56 days moist-cured.

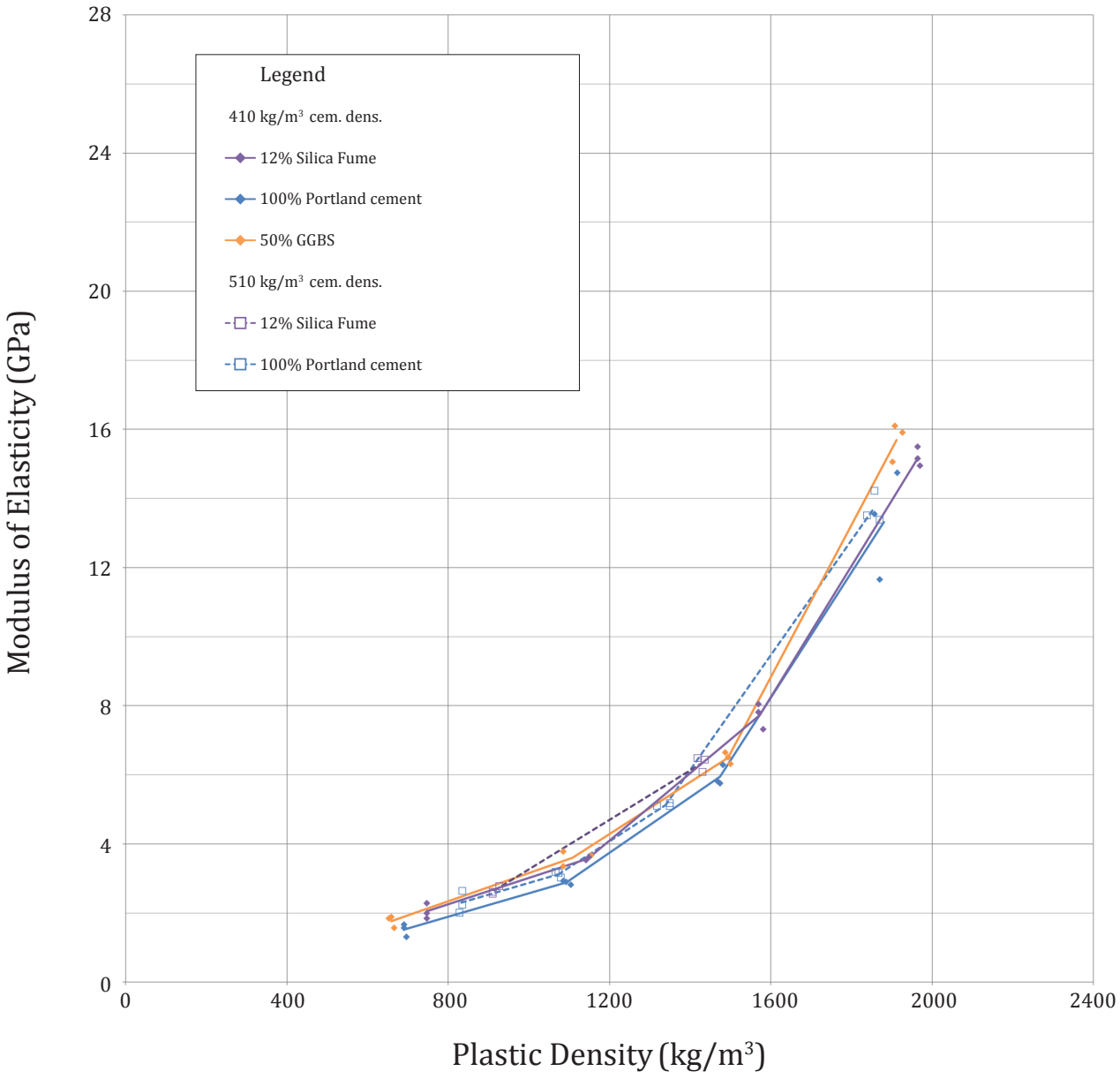

Figure 6.7d Modulus of elasticity vs. plastic density, 28 days moist-cured.

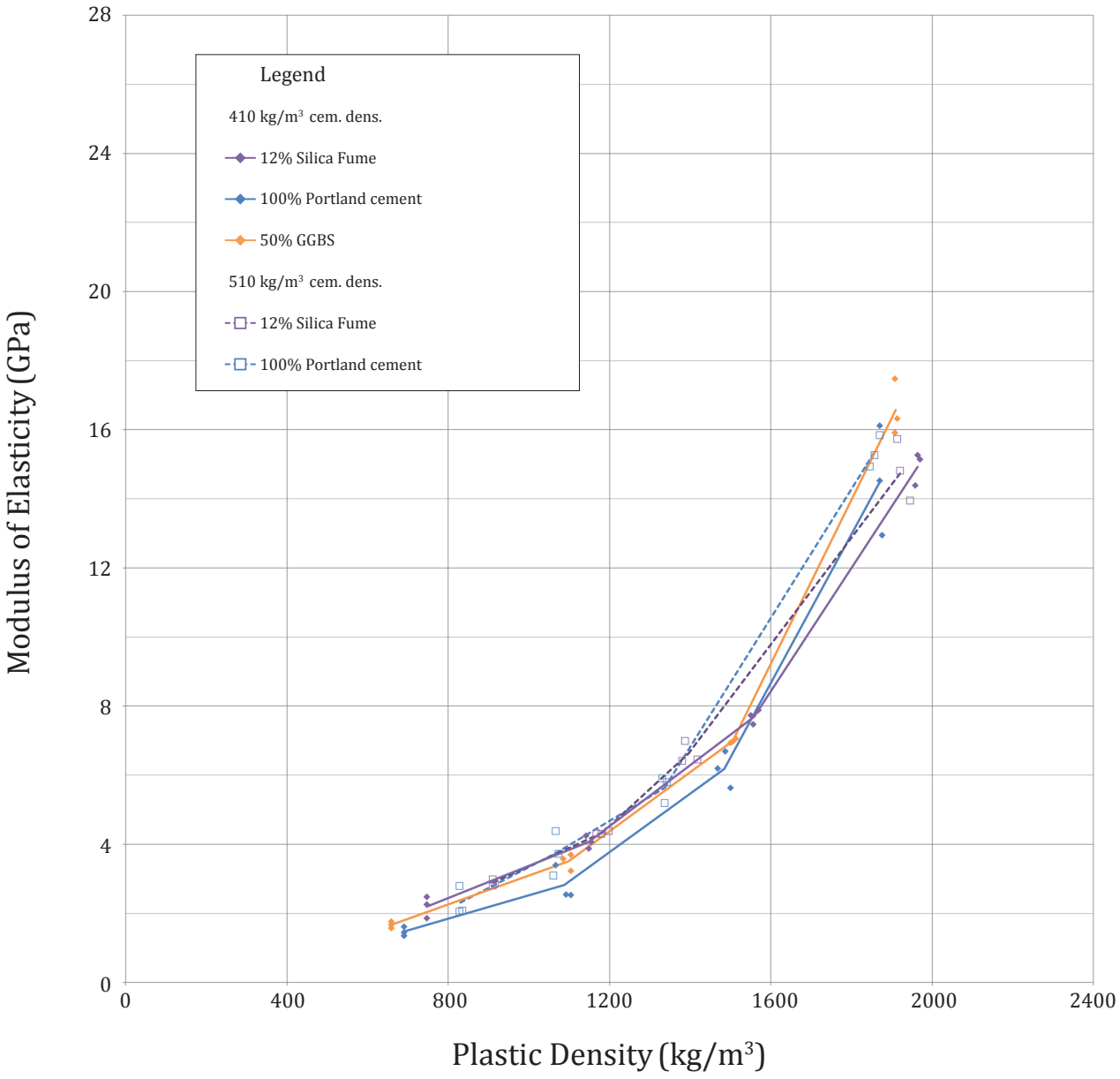

Figure 6.7e Modulus of elasticity vs. plastic density, 56 days moist-cured.

adds density and may also increase stiffness, especially for mixes with high water-binder ratios, such as silica fume mixes.

SCMs offered less significant improvement to elastic modulus than to compressive strength, for a given density. Improvements over 100% Portland cement mixes were are given in Figure 6.**7f**, and range between 9 and 35%. By comparison, improvements in compressive strength were between 51 and 101% for silica fume mixes, as shown in Figure 6.6.**2b**.

As observed in Section 6.4.4, compressive strength improved with increasing curing time, presumably due to the conversion of calcium hydroxide into strong C-S-H via pozzolanic reactions. However, increased curing time did not significantly improve modulus of elasticity, as shown in Figure 6.**7g**. In fact, some 56-day specimens were slightly less stiff than 28-day specimens produced from the same batch. These results indicate that pozzolanic reactions do not offer meaningful improvement in stiffness past 28 days of curing. Factors such as cracking due to autogenous or drying shrinkage may explain minor loss of stiffness with increased curing age.

CSA A-23.3-14, Section 8.6.2.2 gives the following formula to estimate modulus of elasticity, E_c, for concrete with density between 1500 and 2500 kg/m^3, based on compressive strength, f_c', and density, γ_c:

$$E_c = \left(3300\sqrt{f_c'} + 6900\right)\left(\frac{\gamma_c}{2300}\right)^{1.5}$$

Calculated values are compared to measured values for specimens at 28 days, in Figure 6.**7h**. The portion of the plot outside of the prescribed density range is shaded grey.

Within the prescribed density range of the formula, calculated values were between 80 and 120% of measured values, as suggested in CSA A-23.3-14. For lower density specimens, the formula over-estimated the stiffness of a low-density sanded Portland cement mix by 33%, and generally underestimated the MOE of mixes with no filler. For slag, silica fume, and Portland cement mixes with no fillers, measured stiffness was 53, 37, and 22% higher, respectively, than calculated values based on compressive strength and density. Relationships between measured and calculated MOE values were similar for specimens tested at 56 days (refer to Appendix R).

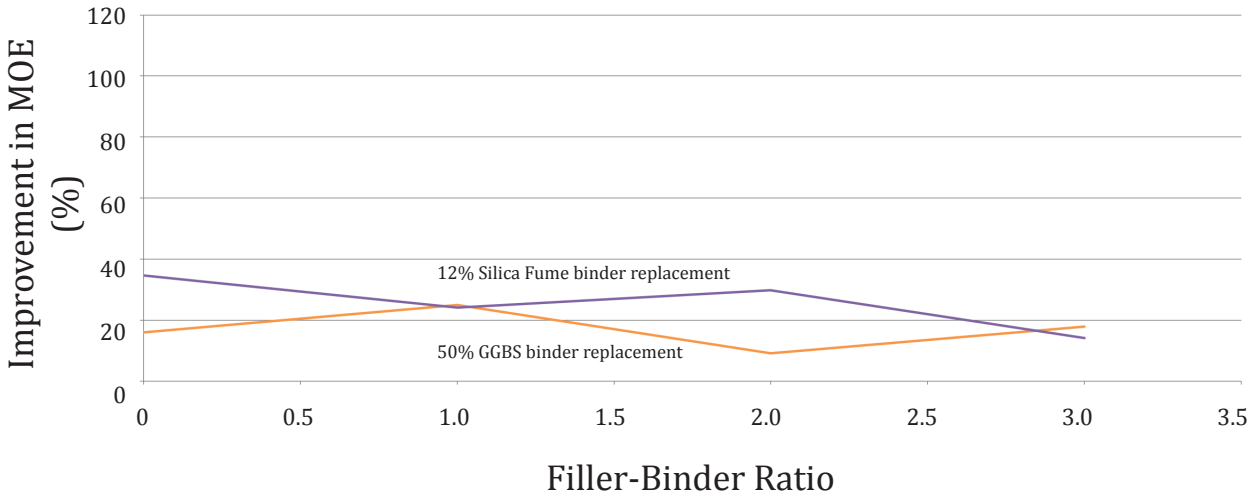

Figure 6.7f Influence of SCMs on Modulus of Elasticity (% improvement relative to 100% PC binder mixes).

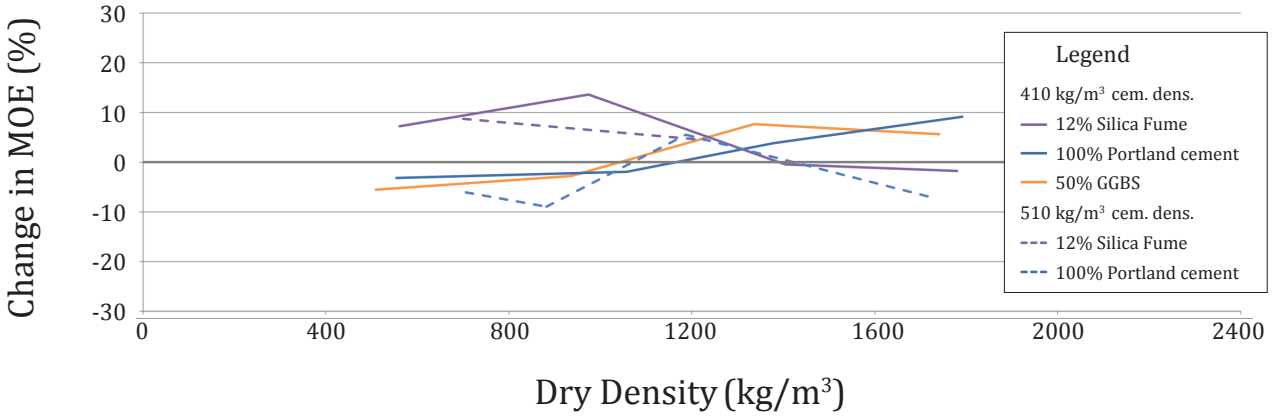

Figure 6.7g Change in MOE from 28 to 56 days (%). Values based on average of three specimens.

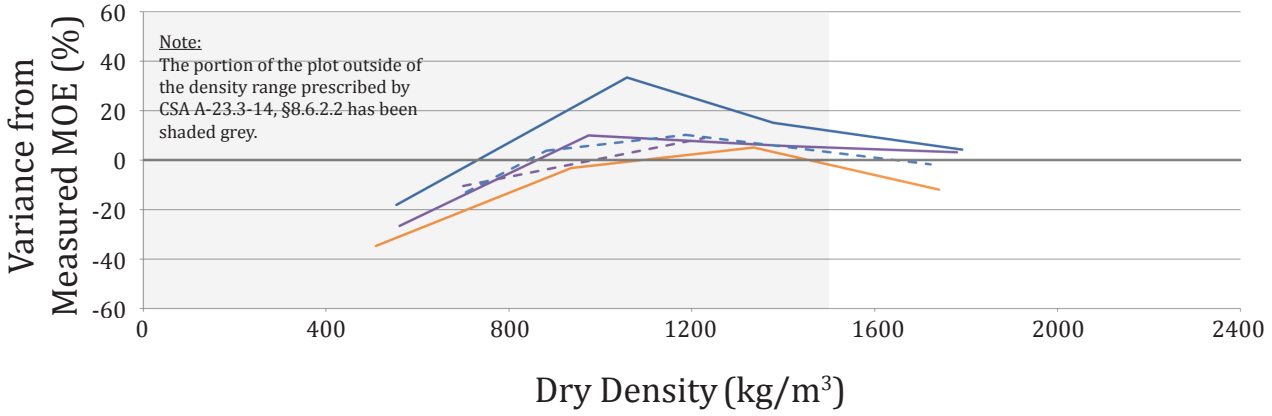

Figure 6.7h Accuracy of calculated MOE values (per CSA A-23.3-14, §8.6.2.2) for specimens at 28 days.

Further insight into the effects of SCMs may be derived from Figures 6.**7i** and 6.**7j**, which plot stiffness relative to compressive strength.

Notably, slag mixes offered high stiffness-to-strength. This trend may be related in part to the crystalline properties of C-A-S-H, produced in slag mixes because of the large proportion of aluminates present in the SCM. Refer to further discussion in Section 7.3.6.

By contrast, silica fume mixes offered relatively low stiffness-to-strength. High homogeneity brought about by improved particle packing and conversion of calcium hydroxide into C-S-H reduces initiation sites for microcracking, delaying fracture until high rates of loading; some sources of restraint, such as calcium hydroxide crystals and unhydrated cement grains, are also reduced in the high water-binder ratio, high silica mix. The low Ca/Si ratio in C-S-H produced with partial silica fume consists of highly polymerized silicate chains,[1] which may be more efficient in resisting fracture than in resisting flexure or slip:[2] due to the geometry of the air-void system, any flexure of cell walls can translate into meaningful strains, especially in low-density mixes. The compression and migration of load-bearing water from capillary pores in high water-binder ratio silica fume mixes may also contribute to specimen softness.

The strength-to-stiffness ratio of Portland cement and silica fume mixes diminished with increasing cementitious density. This result is reasonable, given the higher proportion of viscoelastic C-S-H and the reduction in volume of inert, restraining aggregate.

Strength-stiffness relationships from the experimental program are consistent with the findings of other researchers for mixes with sand filler.[3] In the literature, dense foam concrete mixes with no sand filler typically have much lower stiffness for a given strength, which is broadly consistent with the present findings on the effects of varying cementitious density.

1 Hou et al. (2013) 10
2 Refer to Section 7.3.6.
3 Refer to Appendix A, Figure 6.3.2.

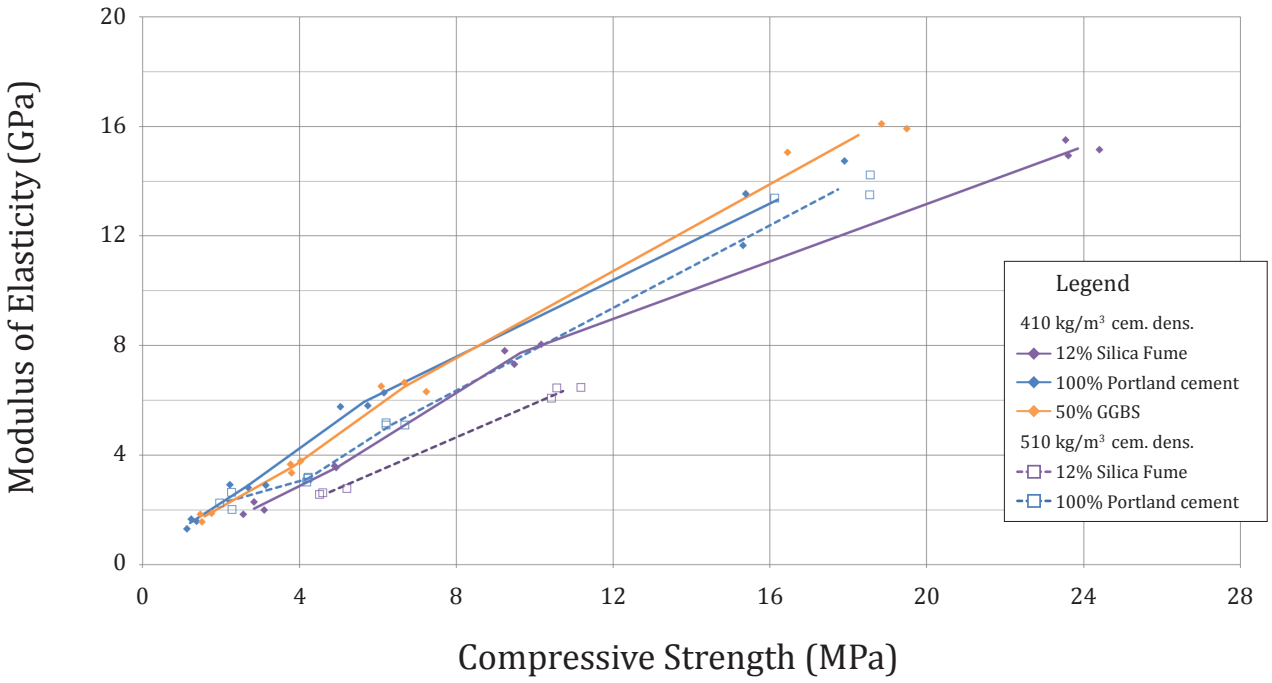

Figure 6.7i Modulus of elasticity vs. compressive strength, 28 days moist-cured.

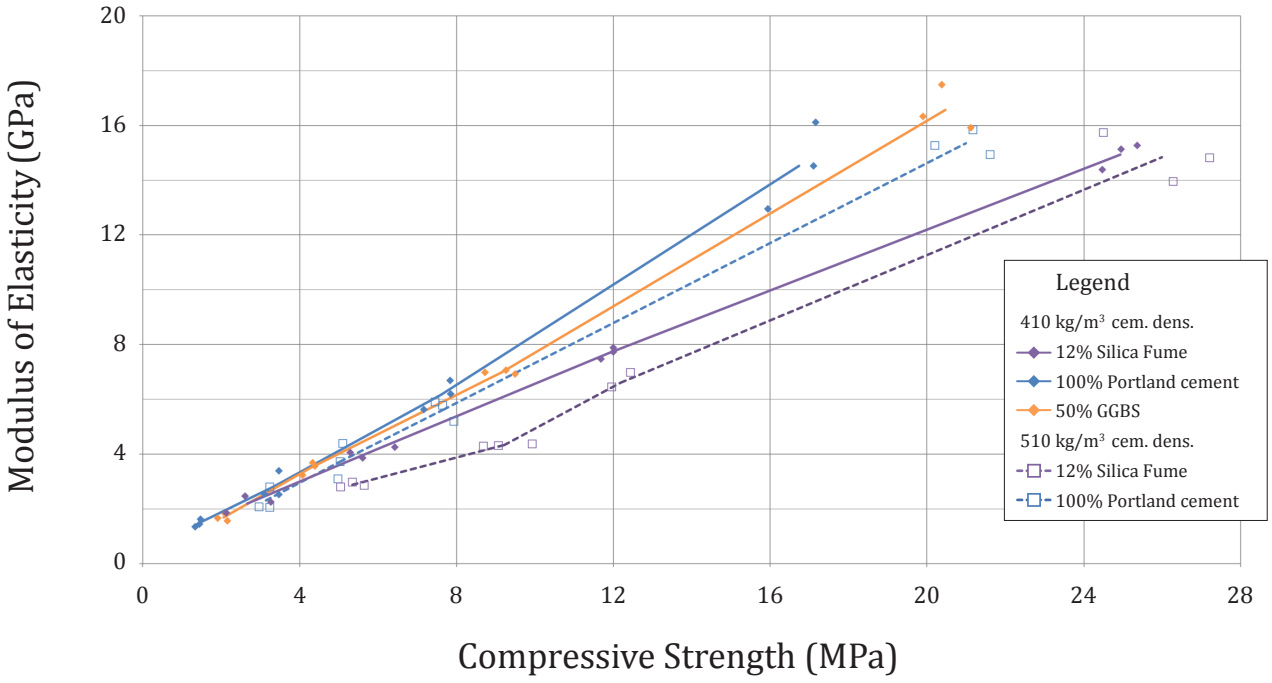

Figure 6.7j Modulus of elasticity vs. compressive strength, 56 days moist-cured.

6.8 Poisson's Ratio

Figure 6.**8a** shows relationships between axial and transverse strain for foam concrete specimens under uniaxial compression across a range of densities and cementitious blends, for stresses of up to 0.4 f'c. Reasonably linear trends were observed.

Figures 6.**8b** and 6.**8c** plot the Poisson's ratio (PR) of specimens against plastic density, for a variety of mixes. There is considerable scatter in the data. Variability may be due in part to the difficulty of accurate measurement, but it may also be due to the nature of the material itself, both in its pore structure, and as a heterogeneous composite of fine aggregate and hardened cement paste. Further discussion is presented in Section 7.3.5.

Observed PR values for foam concrete range from 0.33 to 0.15. Average PR values were lowest in dense, sanded mixes. Sand aggregate is stiffer than the C-S-H, and restrains lateral expansion of the matrix (refer to Section 7.3.5). The air-void system of dense mixes includes small, consistently sized pores (refer to Section 6.17), which may contribute to reduced variability among specimens.

PR was highest for neat cement foam concrete. The compliant C-S-H is not restrained by aggregate inclusions. Furthermore, flexure of the fine microstructure may contribute to lateral expansion. The geometry of the air-void system is more variable with decreasing density, due to coalescence of air voids during plastic state (refer to Section 6.17); variability of the microstructure may help explain some of the variability in PR, as the shape and orientation of interconnected voids can influence lateral response.[1]

PR appeared to be highest in low-density mixes with silica fume. This pattern may be related to the chemistry of the paste, the geometry of the air-void system, or both. Chemically, pozzolanic activity eliminates stiff calcium hydroxide crystal. With fewer stiff restraining inclusions, the C-S-H paste can expand laterally more easily. Geometrically, a fine and consistent air-void system minimizes local microcracking in regions of high stress, which helps ensure that applied axial stress is translated into lateral deformation.

Poisson's ratio is typically slightly higher in 28-day specimens than in 56 days, which could be due to decreasing porosity with age (i.e., a higher gel-space ratio from continued hydration). However, further study would be necessary to confirm this trend.

[1] Cf. Dunn and Ledbetter (1995)

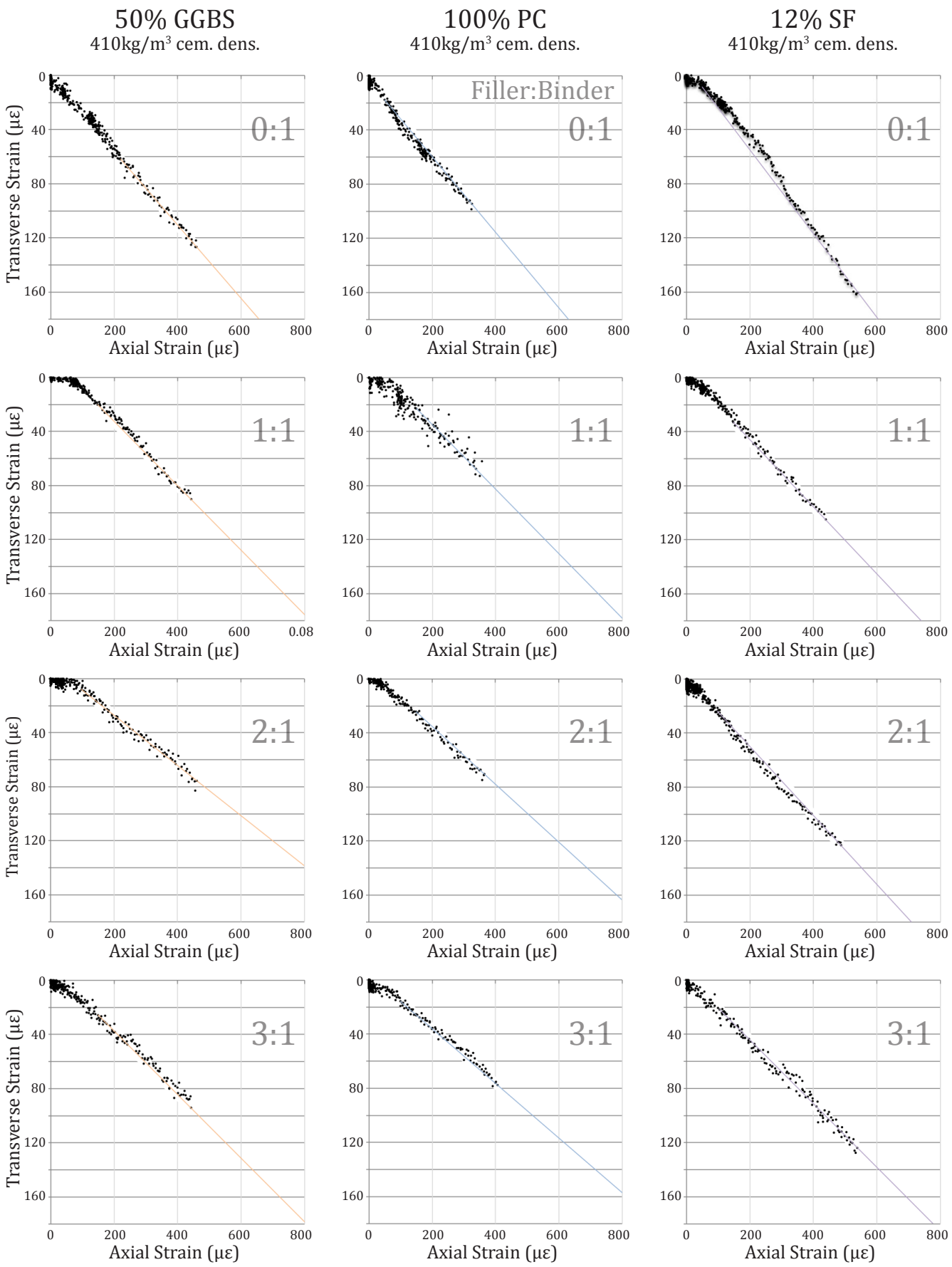

Figure 6.8a Linearity of relationship between transverse and axial strains.

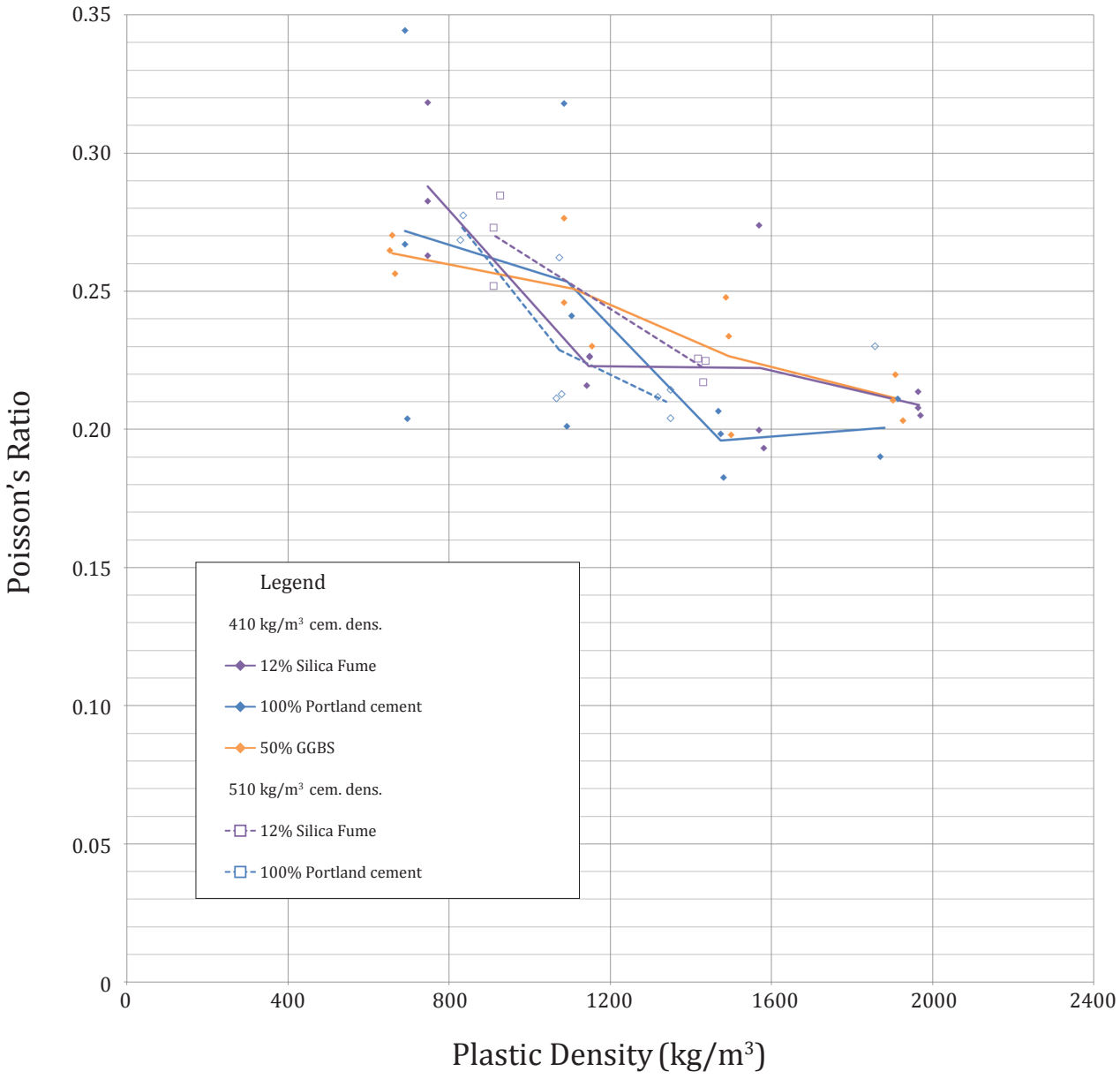

Figure 6.8b Poisson's ratio vs. plastic density, 28 days moist-cured.

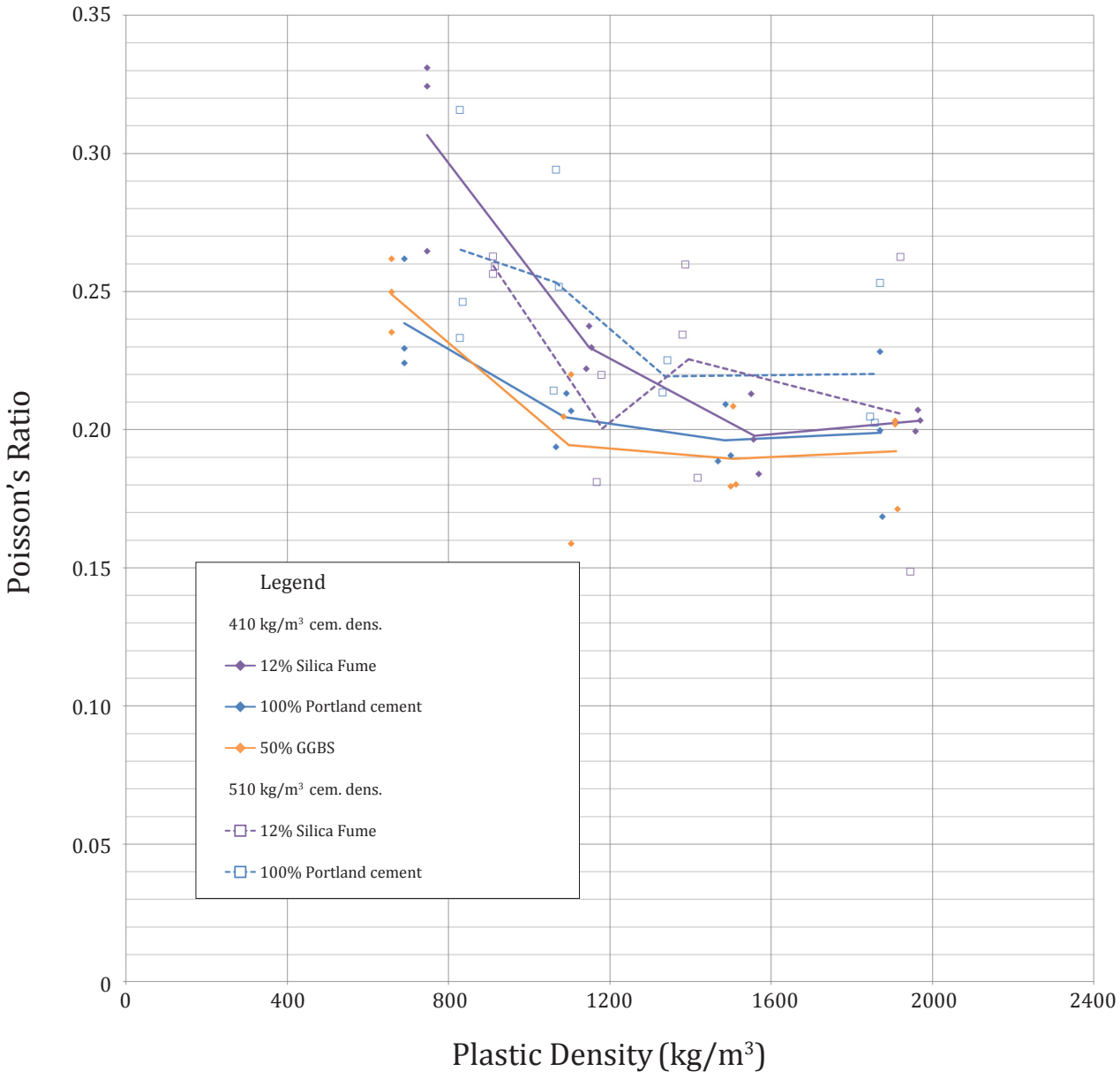

Figure 6.8c Poisson's ratio vs. plastic density, 28 days moist-cured.

6.9 Crushing Behaviour

The type of failure was recorded for every foam concrete specimen crushed, as described in Section 5.4.1. Compiled results for specimens with unbonded caps are presented in Figure 6.**9b**. Note that results for specimens cured for 28 days and 56 days are included together.

A number of trends are evident. Type 6 failure tends to dominate for the weakest of mixes. The strata near the top of the casting may be slightly weaker than the remainder of the specimen, due to upward migration of bubbles, and side fractures near the top of the cylinder result in a pointed form. In some cases, failure can occur as collapse of horizontal strata near the top of the cast. In such cases, failure of the specimen may not be visibly obvious upon inspection, even though the specimen has experienced peak load.

For stiffer, neat cement foam concrete, columnar Type 3 cracking tends to dominate. Vertical splitting cracks nucleate at air-voids as Mode I fracture, and propagate parallel to the compressive stress field, with no stiff aggregate present to arrest or divert the cracks. The resulting slender columns fracture laterally by buckling.

By contrast, the final cracking pattern of sanded foam concrete includes random and steep triangular and conical fragments, resulting from a combination of vertical splitting cracks and inclined shear cracks. Where cracks have been arrested by the presence of aggregate or dense paste, there may be spreading patterns. Type 2 fractures are common. Very dense mixes, and sanded silica fume mixes, include especially small air-voids (refer to Section 6.17). Type 4 failure, common among these specimens, may be related to the greater homogeneity of the paste, with fewer weak sites, resulting in more concentrated localization along the shear plane.

Dominant failure types are related to mix characteristics in Figure 6.**9a**, below.

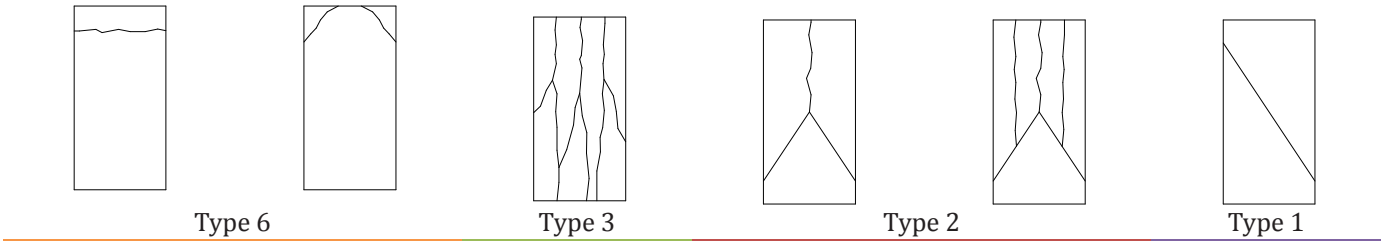

Figure 6.9a Dominant failure types in relation to mix characteristics.

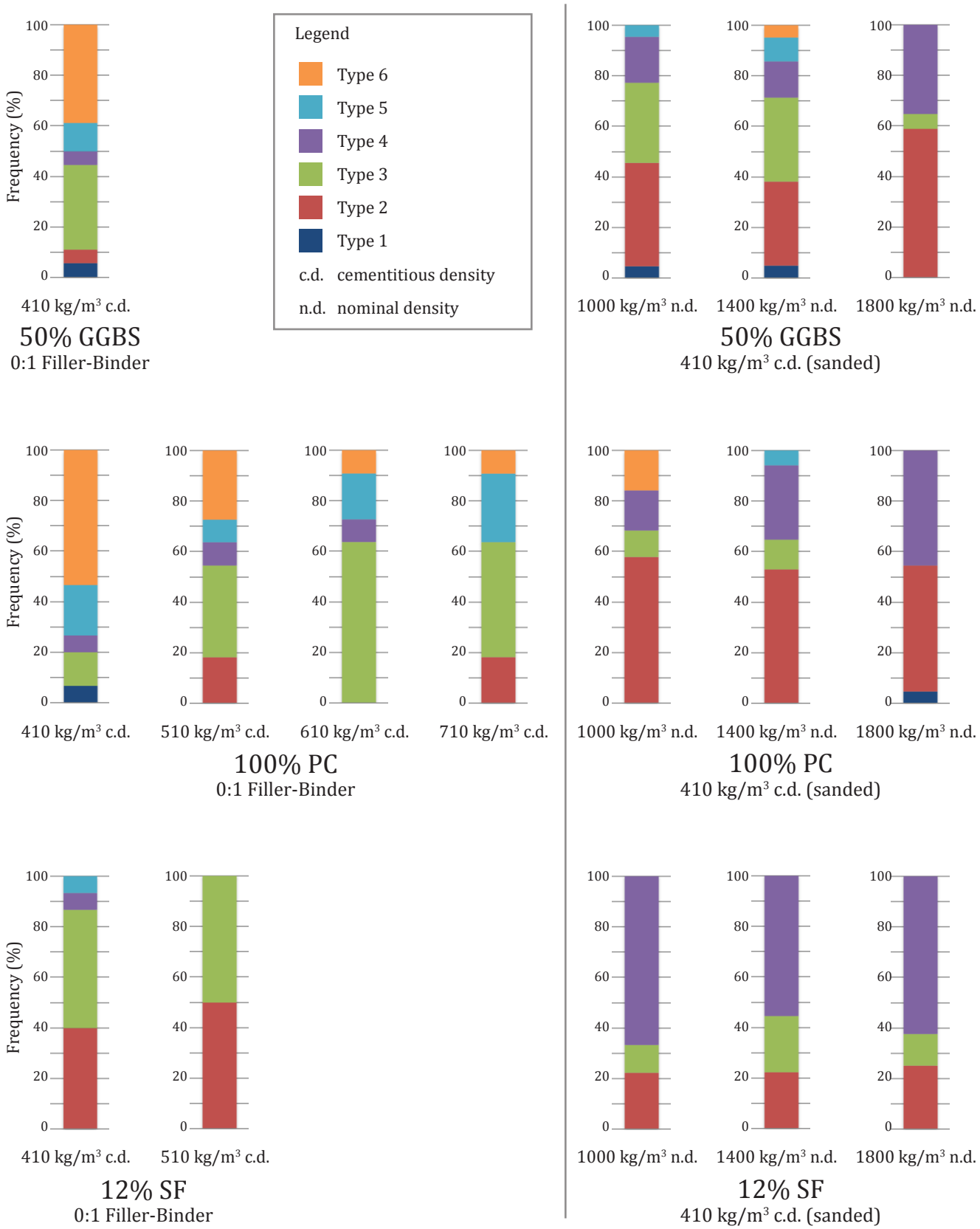

Figure 6.9b Frequency of compressive failure types. 28 and 56 day moist-cured, unbonded caps.

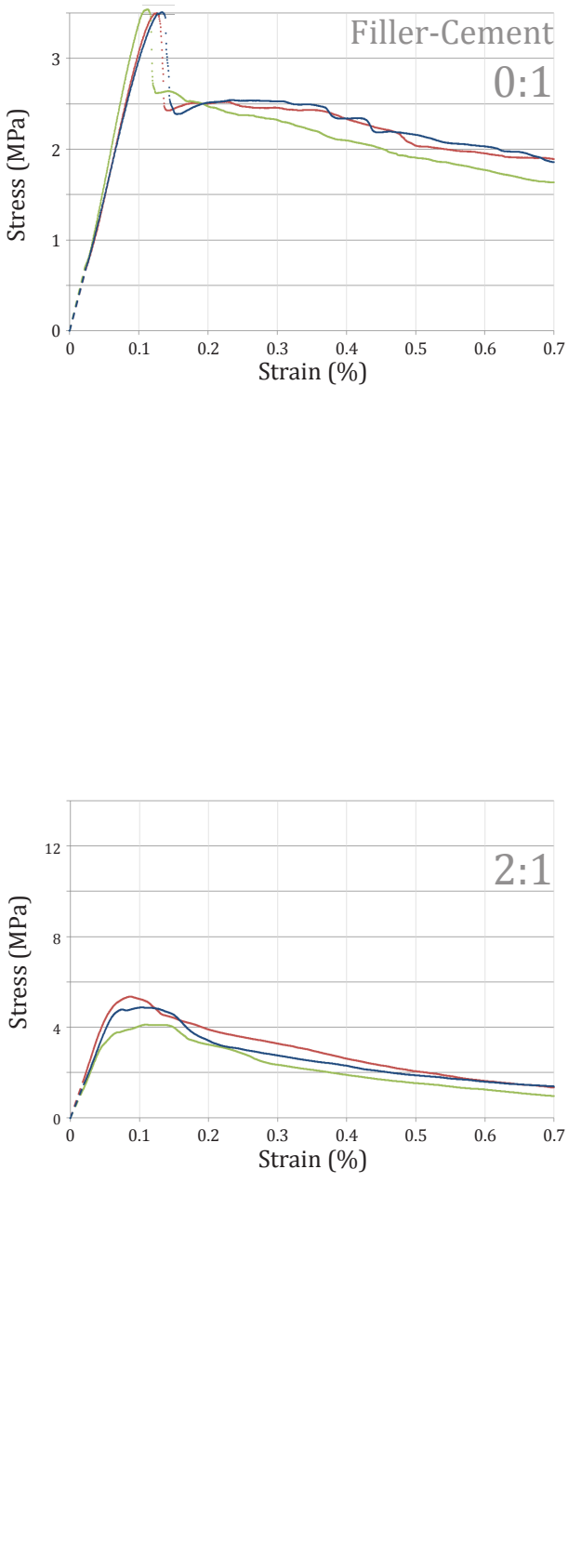

Figure 6.9c Crushing behaviour of FCA mixes.

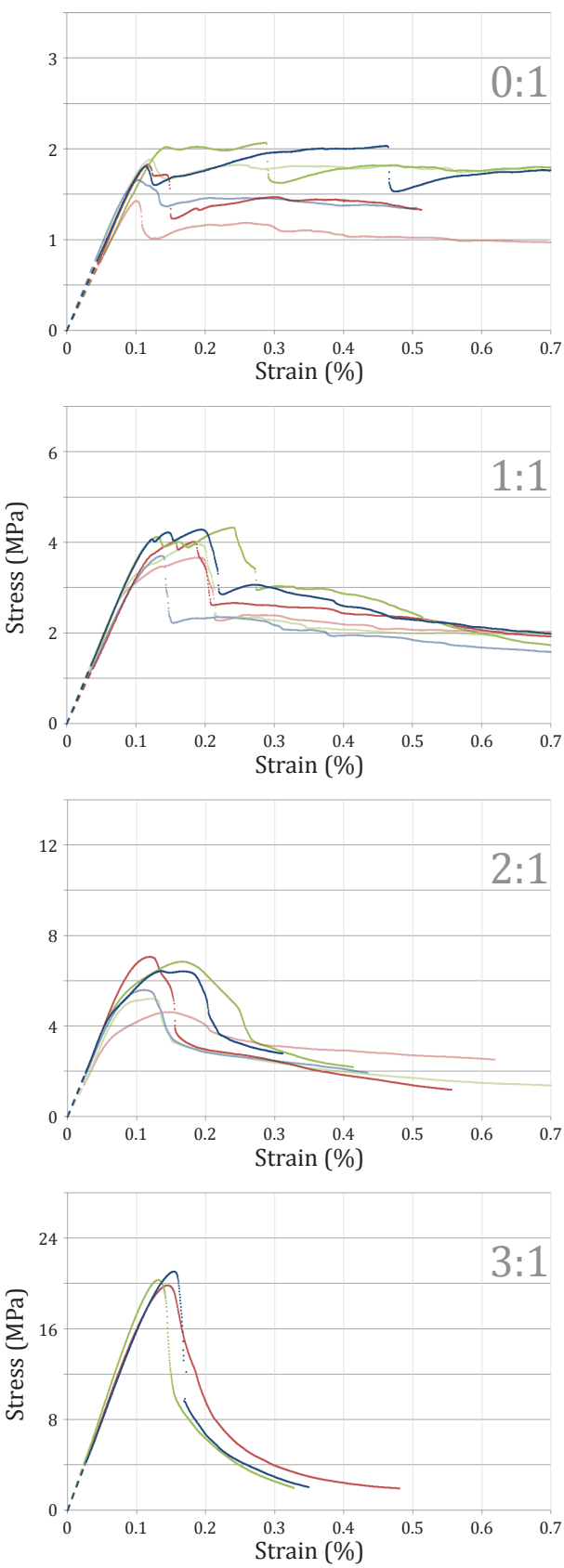

Figure 6.9d Crushing behaviour of 50% slag mixes.

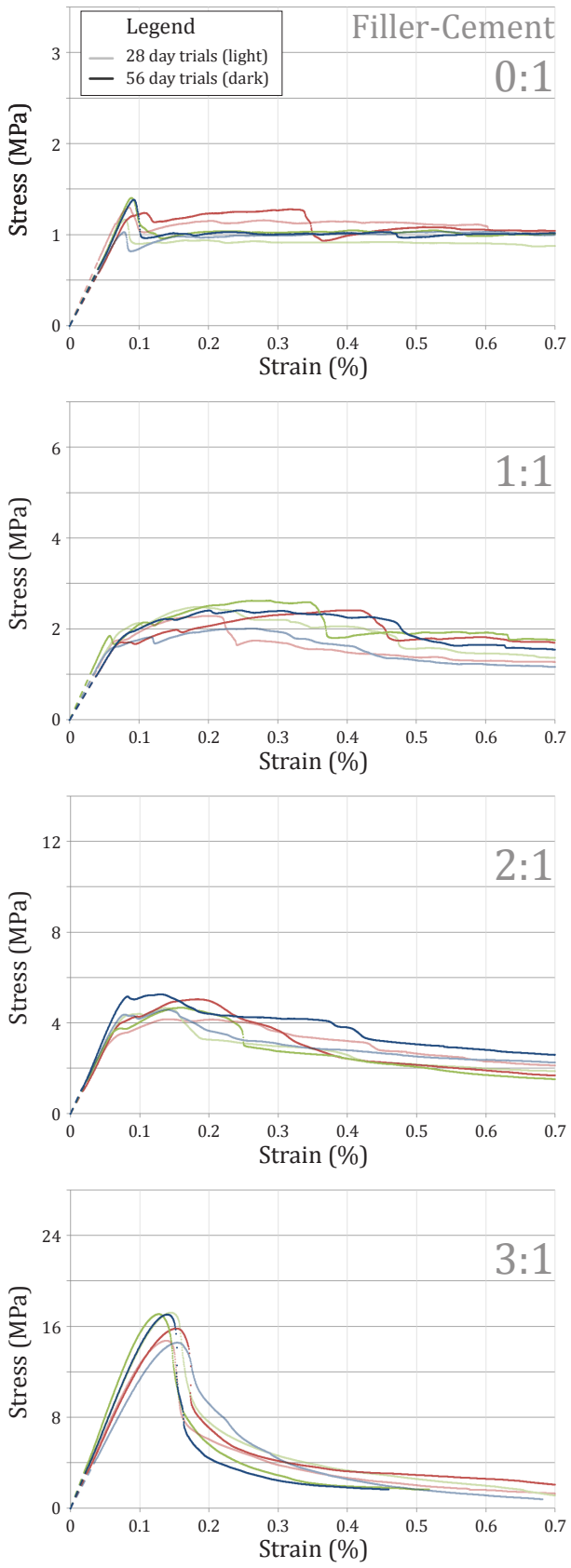

Figure 6.9e Crushing behaviour of PC mixes.

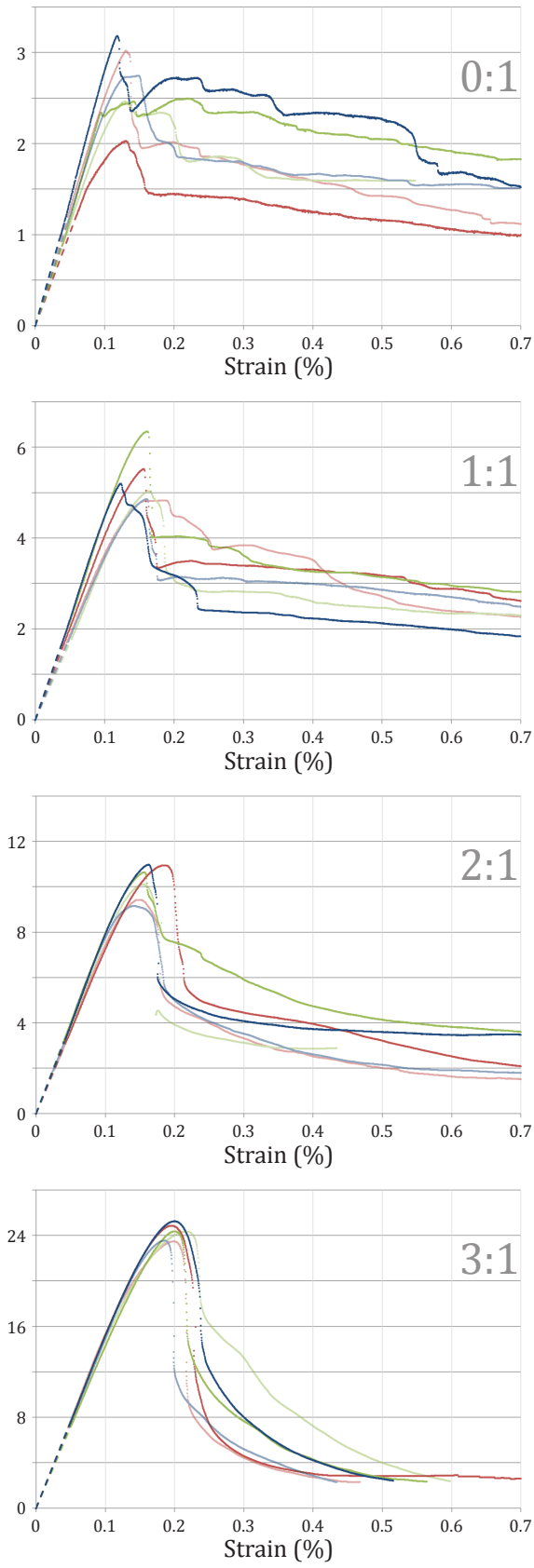

Figure 6.9f Crushing behaviour of 12% SF mixes.

Stress-strain curves for foam concrete are shown in Figures 6.**9c** to 6.**9e**, across a range of densities, filler-binder ratios, cementitious densities, and cementitious blends. Results for specimens cured for 28 and 56 days are shown in light and dark tones, respectively. Data in the early part of each graph has been modified to eliminate seating effects, as indicated with dashed lines, based on the linearity of stress-strain relationship observed in Section 9.6.

The stress-strain relationship of foam concrete specimens was typically linear to 0.6 f'c or more. For low-density mixes, the plastic regime was especially short, suggesting that once initiated, damage quickly propagated (localized) through the entire specimen.

For higher density specimens, the plastic regime was more obvious. With a greater volume of material available to be fractured and rearranged, strain energy could be relieved through microcracking of the paste during loading, without inducing large-scale failure of the air-void system. The plastic regime is most evident in mixes with a high cementitious content (refer to specimens with filler-binder ratios of 1:1 and 2:1 in Figure 6.**9d** and specimens with cementitious densities of 610 kg/m^3 and 710 kg/m^3 in Figure 6.**9e**). The high cementitious content provides a higher volume of compliant C-S-H, which may accommodate plastic deformation.

The influence of mix design on compressive strength is discussed in Section 6.6. Curing age did not appear to significantly influence crushing behaviour around peak loading.

Various phenomena were observed following peak loading. For low-density Portland binder mixes, stress dropped slightly; thereafter, fracture energy was released continually and reasonably consistently, as the debris material crushed through soft paste into adjacent void spaces. This characteristic may make neat Portland cement foam concrete a good choice for impact absorbing applications. For many low-density slag mixes, the reduction in stress after failure was more significant. For low-density silica fume mixes, stress dropped sharply after peak loading and continued to decline.

In some low-density specimens, stress continued to rise post-failure. For example, higher stresses were observed post-failure in 1:0 slag specimens, in one 0:1 Portland specimen, and in 1:1 Portland cement specimens (Figure 6.**9c**). This phenomenon is due to the densification and elimination of weak strata.

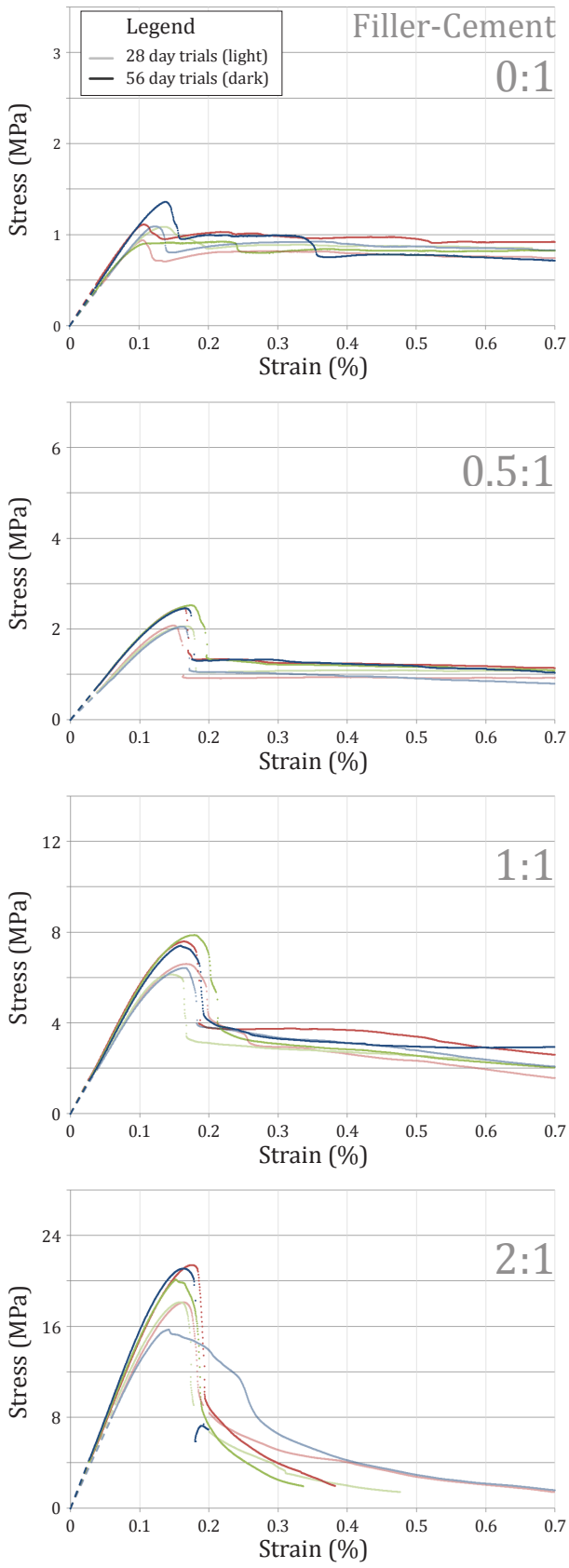

Figure 6.9g Crushing behaviour of PC mixes.

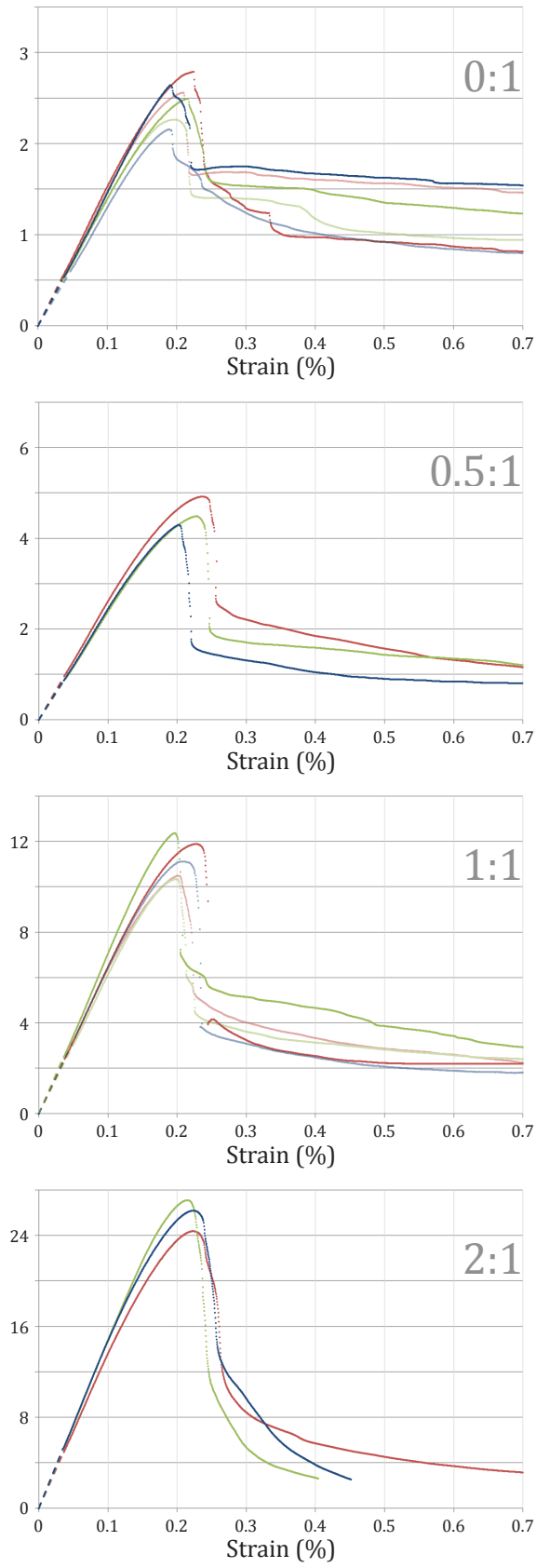

Figure 6.9h Crushing behaviour of 12% SF mixes.

For most specimens, stress declined beyond peak loading, indicating that the initial condition of the unfractured specimen was most stable. Irregularity was observed in the descending branch of the stress-strain curve for many mixes, for example the silica fume specimens with filler-binder ratio of 1:1 in Figure 6.**9d**. This pattern may be attributed to a non-uniform cracking process, as macrocracks are arrested and elongated in different regions of the specimen.

An irregular pattern of softening tended to occur in specimens with soft paste and high air-void volumes, as fractured surface geometries contacted and interlocked, conforming readily to each other by local crushing of exposed cell walls. With many points of contact, the damage zone was enlarged, and ductility was increased.

Conversely, brittleness is signified by a steep slope in the stress-strain curve, post-peak. Brittleness was high in denser mixes. These mixes had less air-void space available for debris, causing fractured surfaces to be pushed apart at points of contact, rather than conforming to each other.

Brittleness was also high for dense or especially strong neat cement mixes. As observed in Figure 6.**9a**, these mixes often fracture cleanly into discrete columnar fragments. Frictional restraint was minimized, as damage was concentrated along vertical splitting cracks. (Refer to the figure in Section 7.3.4.)

For a 2:1 Portland cement specimen and a 1:1 silica fume specimen with 510 kg/m^3 cementitious density (Figure 6.**9d**), explosive brittle failure caused a 'bounce' in applied stress. These mixes are strong enough to resist load, and also have compliant fractured surfaces, which can contact and transfer shear, offering residual strength.

In the final stages of crushing, the crushing stress of low-density mixes undulated as weak strata were densified and eliminated, or as fractured surfaces transferred shear via interlocking surfaces. In denser foam concrete mixes, the softening curve became relatively smooth after global facture. Crack growth was no longer significant; instead, friction at contacts provided residual mechanical resistance. The load-bearing capacity of the remaining material continued to decrease as the crack patterns opened with increasing deformation, reducing the number of contact regions between fragments.

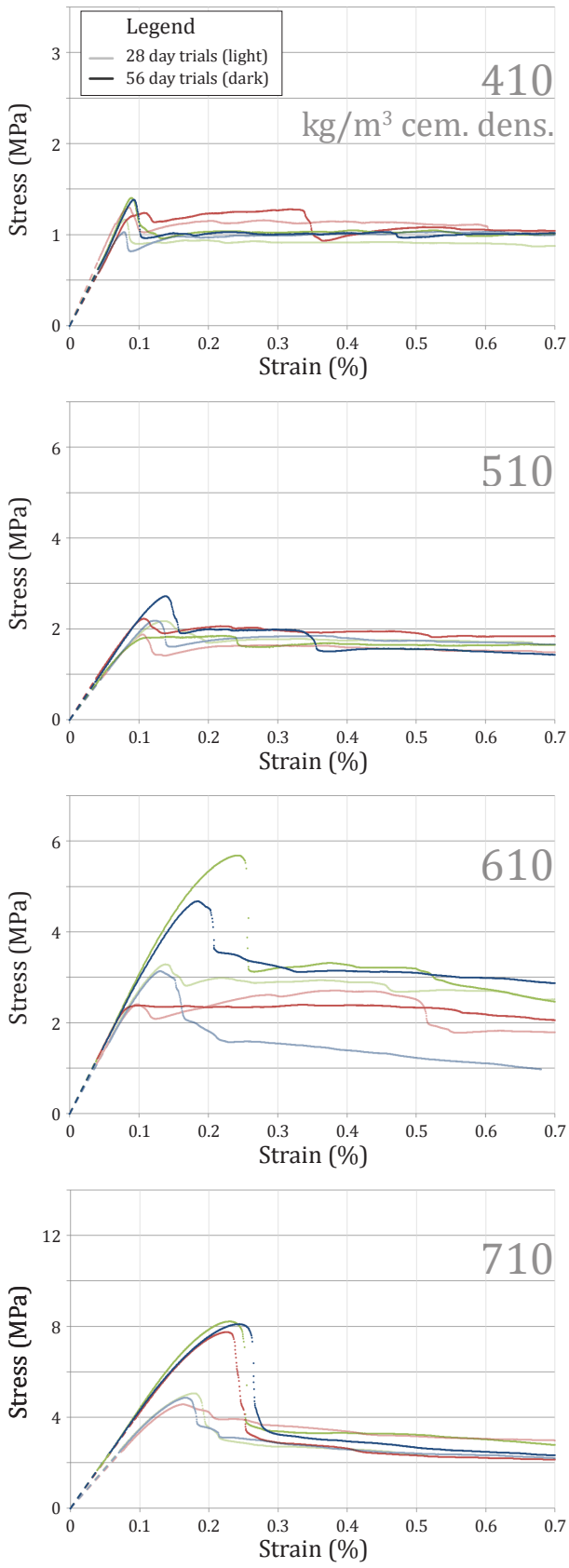

Figure 6.9i Crushing behaviour of PC mixes.

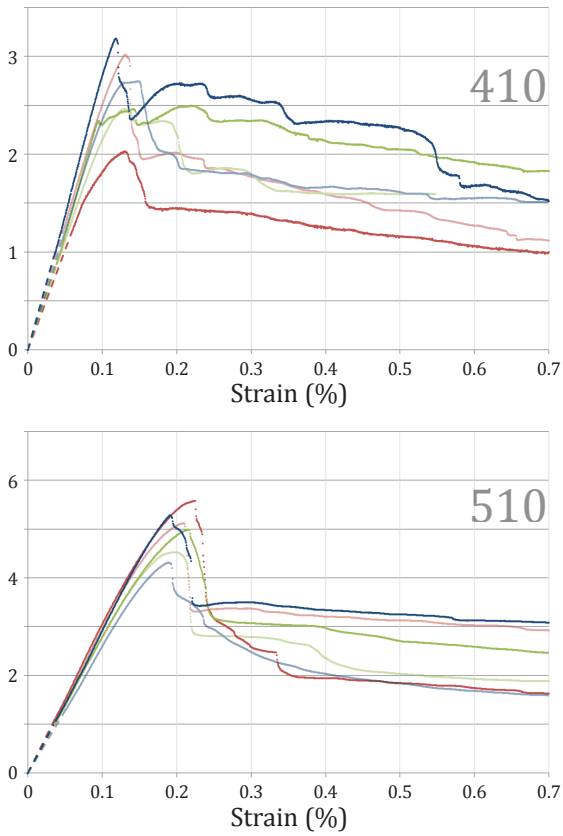

Figure 6.9j Crushing behaviour of 12% SF mixes.

6.10 Creep

Specific creep strain is plotted in Figures 6.**10a**, for 600 and 1400 kg/m^3 nominal density specimens, with applied loads of 0.2 and 0.4 f'c, as indicated.

The specific creep of foam concrete is very high, relative to normal density concrete. Specific creep after one year was approximately 12,000 μstrain/MPa (1.2%/MPa) for 600 kg/m^3 foam concrete, and between 1000 and 2000 μstrain/MPa (0.1 to 0.2%/MPa) for 1400 kg/m^3 foam concrete. In comparison, specific creep values for normal density concrete typically lie between 100 and 200 μstrain/MPa.[1]

Basic creep values for the unsealed specimens were higher than values determined previously by other researchers using sealed specimens of similar density.[2] It is probable that exposure to drying conditions has a strong effect on creep rate. Further studies with consistent mix designs and methodologies would be needed to quantify this Pickett effect.[3]

Results for low-density foam concrete indicate that creep is not linearly dependent on stress. Interestingly, a lower load produced a higher specific strain. This phenomenon is discussed at length in Section 7.3.6.

The addition of aggregate reduces specific creep rates considerably, as the non-viscous aggregate phase elastically restrains creep deformations in the surrounding viscous C-S-H matrix. Among 1400 kg/m^3 mixes, partial replacement of Portland binder with silica fume had a minor influence on specific creep strain, while partial replacement of Portland binder with slag increased specific creep by more than 30%.

For PC and SF mixes, there appeared to be strong correlations in patterns of specific creep, drying shrinkage, and mass loss (i.e. change in moisture content), as shown in Figures 6.**10e**, 6.**10f**, and 6.**10g**, respectively. Initial rates of change were highest for the Portland cement binder mix, but long-term values were highest for the SF mix. Such correlation of humidity levels, drying shrinkage and creep is to be expected where drying shrinkage introduces residual stresses in the C-S-H, creating overstressed sites that facilitate creep. Patterns of mass loss, drying shrinkage, and creep are less obvious for the slag specimens. For example, while the initial loss of mass upon drying was relatively rapid,

[1] Mehta (1986) 93
[2] Kearsley (1999b) 153-156, Brady et al. (2001) C12. Refer to Appendix A, 6.3.2g.
[3] Cf. Pickett (1942), refer also to Section 7.3.6.

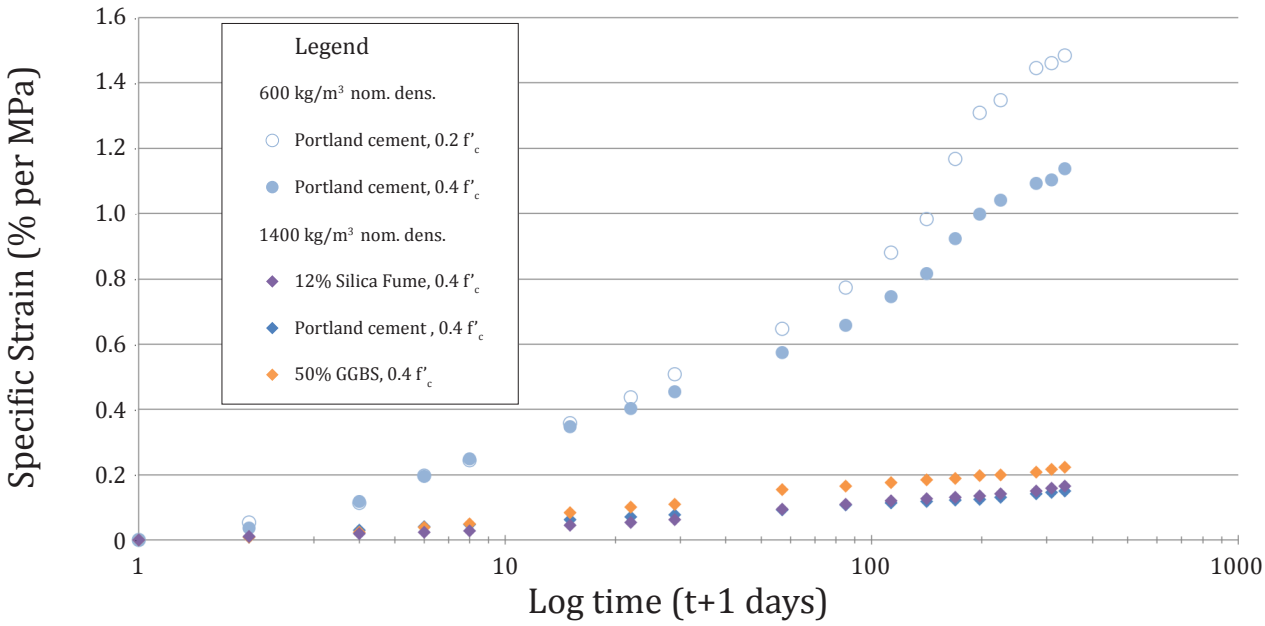

Figure 6.10a Specific creep strain. Does not include strain induced immediately after loading.

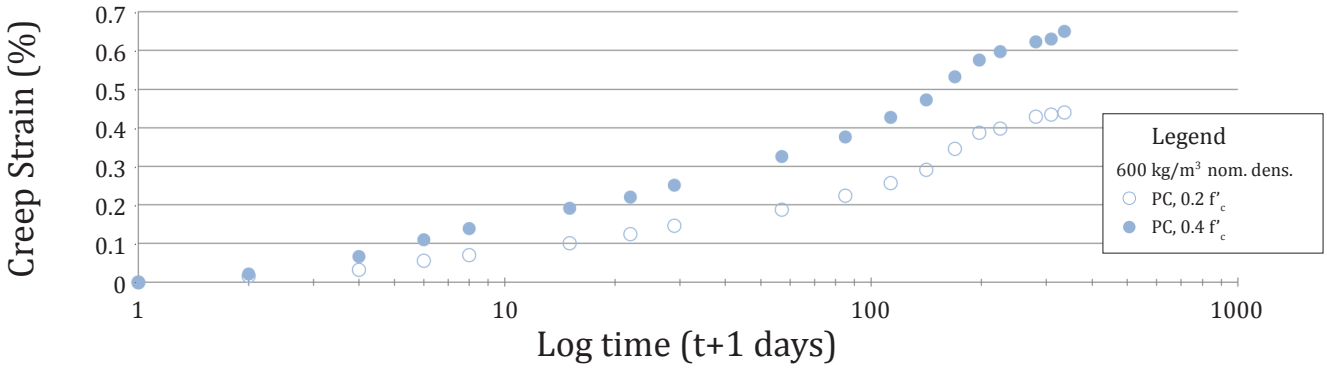

Figure 6.10b Creep strain. 600 kg/m^3 nominal density specimens, subjected to 0.2 and 0.4 f'$_c$.

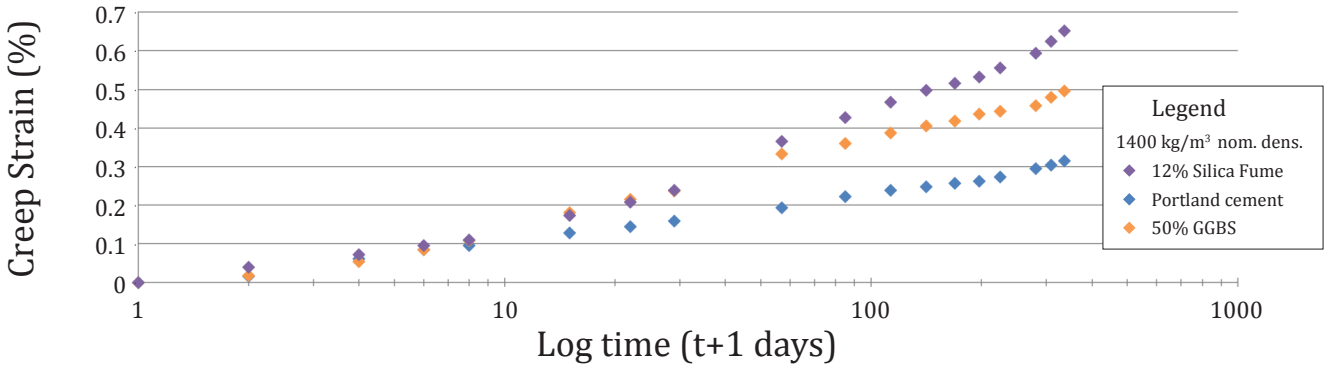

Figure 6.10c Creep strain. 1400 kg/m^3 nominal density specimens, subjected to 0.4 f'$_c$.

slag specimens experienced minimal shrinkage prior to Day 7. Possible explanations for these observations are reviewed in Section 7.3.6.

Actual creep strain values are plotted in Figures 6.**10b** and 6.**10c**. After 1 year, creep strain of up to 6,000 μstrain could be expected for specimens loaded to 0.4 f'c.

By the end of the testing period, the cast surface of low-density foam concrete specimens had visibly buckled in many locations (Figure 6.**10d**). The cast surface was less porous and therefore stiffer than the specimen interior, which likely have caused it to take slightly more stress, proportionally. Since the cast surface could not relieve stress by crushing of its microstructure, it buckled as flakes, instead.

This buckling may have had some influence on deformation measurements, since Demec locating discs were epoxied to the cast surfaces. However, damage did not occur in the region of the epoxy, and it appeared that that the skin was generally relieving stress by buckling, while the core was relieving stress by crushing, with the result that the cylinders deformed fairly uniformly across their cross-sections. The buckling of the outer skin may have slightly reduced the effective cross-sectional area of the specimens.

Increasing density, evident in Figures 6.**10e** and 6.**10g**, indicated that specimens experienced ongoing hydration or carbonation in the 50% RH environment.

Figure 6.10d Buckling along cast surface of 600kg/m^3 foam concrete after 12 months of exposure to 50% RH, for loadings of 0.2 and 0.4 f'c (above and below, respectively).

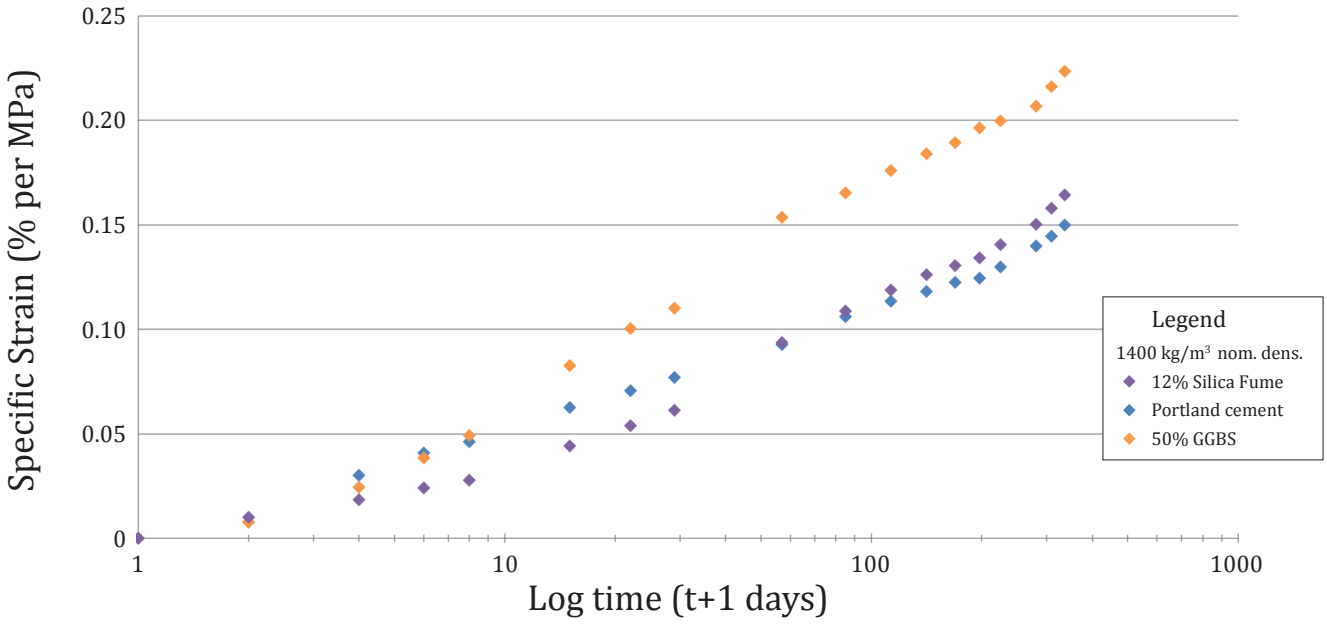

Figure 6.10e Specific creep strain. 1400 kg/m³ nominal density specimens.

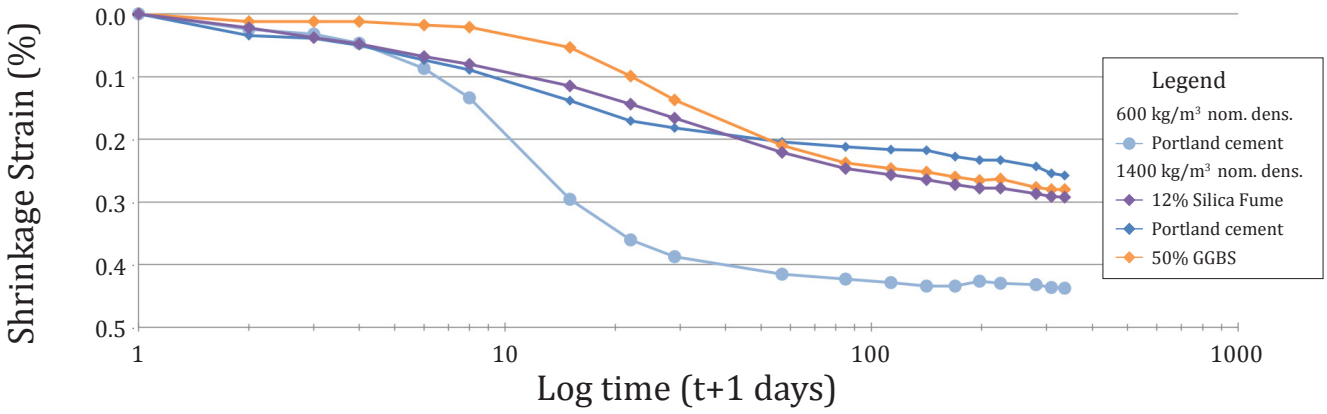

Figure 6.10f Drying shrinkage of creep companion specimens.

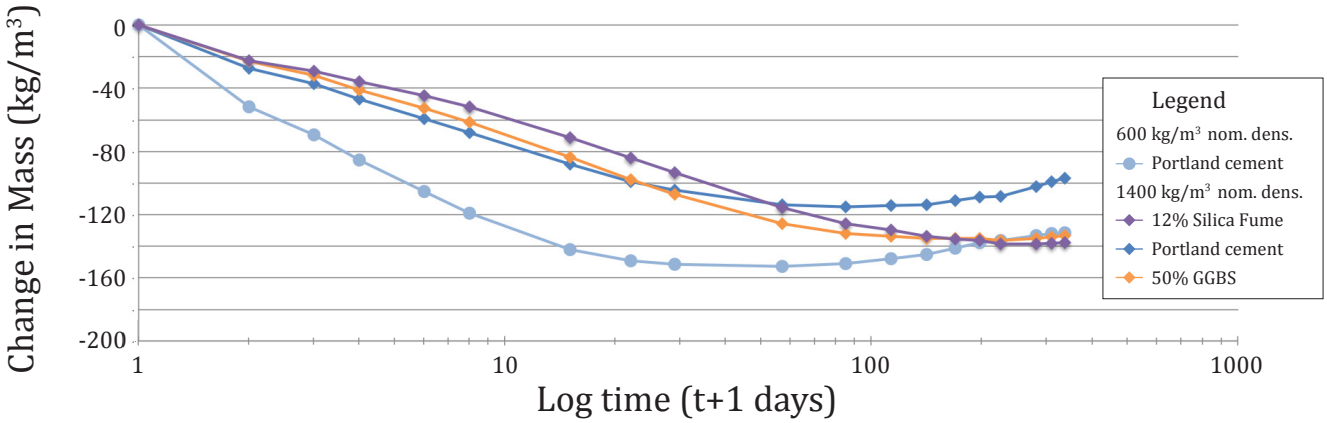

Figure 6.10g Change in mass of 600 and 1400 kg/m³ Portland cement foam concrete specimens during drying in 50% RH.

6.11 Drying Shrinkage

Drying shrinkage is high for conventional foam concrete relative to normal density concrete. Various influences on drying shrinkage were tested in the experimental program, including density, filler-binder ratio, cementitious density, cementitious blend, and curing regime.

In order to compare results, it was important to understand how much variability in drying shrinkage could be expected among specimens. Shrinkage patterns are plotted in Figures 6.**11a** and 6.**11b**, for 28-day water-cured specimens with filler-binder ratios of 0:1 and 2:1, respectively, having varying cementitious blends. For each mix design, three specimens were cast from the same batch, and at least one additional specimen was cast from a different batch of the same mix design.

Specimens from the same batch had closely similar results. Coefficients of variation for one year drying shrinkage values were 0.85, 1.95, and 2.95%, for neat 0:1 slag, Portland cement, and silica fume mixes, respectively. Coefficients of variation were 0.50, 0.71, and 1.48%, for sanded 2:1 slag, Portland cement, and silica fume mixes, respectively.

For slag and Portland cement mixes, drying shrinkage patterns of specimens from two different batches were closely similar. Drying shrinkage patterns diverged slightly for 0:1 silica fume batches, and diverged more significantly for 2:1 silica fume batches, although ultimate average shrinkage strain values after one year were similar, i.e. within 15.9% for 0:1 silica fume mixes, and within 8.1% for 2:1 silica fume mixes.

A selection of further comparisons is given in Figures 6.**11c** and 6.**11d**. For the 28-day water cured specimens in Figures 6.**11c**, drying shrinkage decreased with increasing density. Stiff fine aggregate restrained the shrinking C-S-H matrix.

Figure 6.**11d** provides evidence for expansive cracking in some low-density mixes. Surprisingly, among neat Portland cement mixes, the lowest density mixes experienced less shrinkage than higher density mixes. The reduced shrinkage of these very low-density specimens may perhaps be attributed to increased cracking, introducing expansive strains. Similarly, for 1-day water cured specimens, 0:1 silica fume specimens experienced expansion between 14 and 28 days, which may indicate expansive cracking.

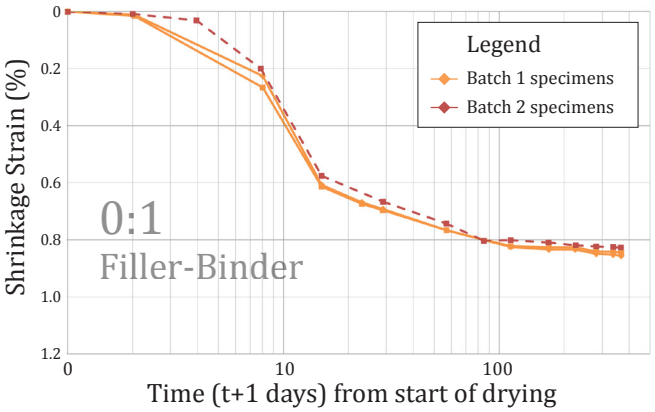

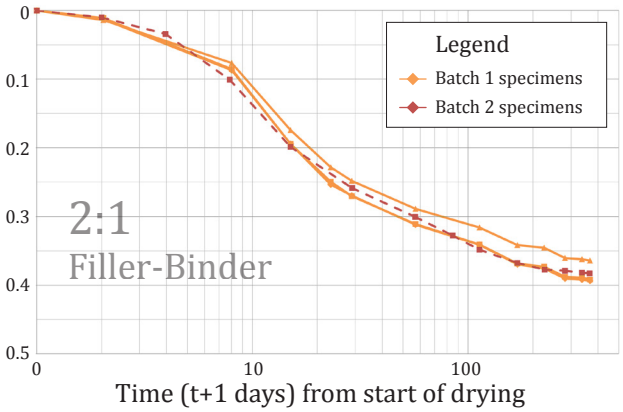

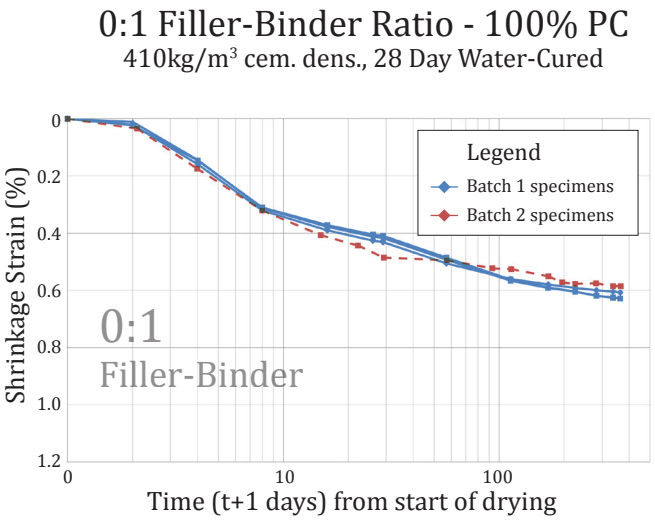

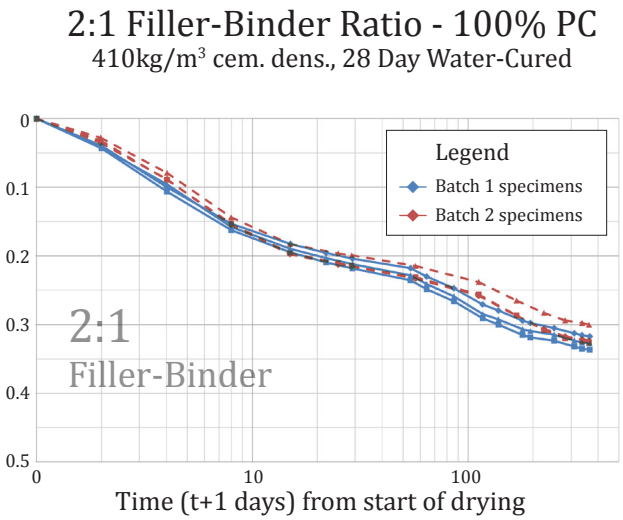

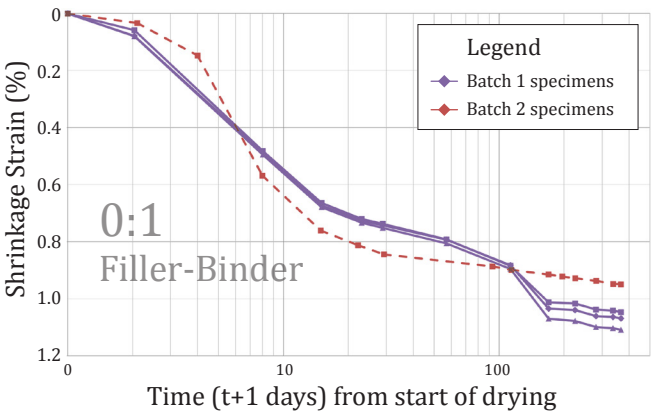

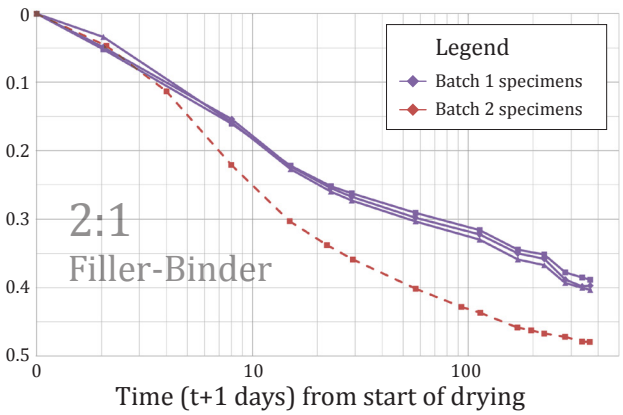

Figure 6.11a Repeatability of results, neat mixes.

Figure 6.11b Repeatability of results, sanded mixes.

The influence of curing regime is shown in Figures 6.**11e** to 6.**11h**. Curing regimes included water curing for 1 day (dark lines), water curing for 28 days (light lines), and moist-curing for 28 days (broken light lines). Each line represents the average shrinkage of up to three specimens. (Refer to Appendix R.) Note that specimens from two separate batches were water-cured for 28 days, as shown in the Figure.

Longer periods of curing in water tended to reduce short-term drying shrinkage. This pattern is especially evident for low density mixes, and for slag mixes.

This phenomenon may be partially due to greater saturation of specimens with increased curing time. Free water drawn into large voids by capillarity during long curing periods maintains a high internal RH for longer, and must be removed before the effects of capillary tension, surface tension, and disjoining pressures can induce volumetric change. Furthermore, water that entered small voids during long curing periods would be held more rigidly upon exposure to 50% RH, reducing the initial rate of shrinkage.

Ultimately, however, drying shrinkage increased with increased curing time. Long curing periods may have introduced significant disjoining pressures in the C-S-H. During hydration in a high RH environment, thick layers of adsorbed water would tend to induce swelling of the C-S-H at many areas of hindered absorption, where solid surfaces come close together. Later, when the specimen is dried, disjoining pressures decrease in these locations, the surfaces draw close, and the volume of the specimen is significantly reduced. (Refer to Appendix A, Section 6.2.3.) It is also possible that unhydrated cement grains in 1-day cured specimens contributed to restraint of drying shrinkage. (Refer to Section 7.2.)

The effect of curing time on long-term drying shrinkage was especially pronounced for slag and silica fume mixes. Given the low Ca/Si ratio for these cementitious blends, comparisons between 28-day water-curing and 28-day moist-curing offered insight into whether free calcium in the limewater had an appreciable influence on drying shrinkage, e.g. through densification of the microstructure during curing.

Drying shrinkage patterns for 28 day moist-cured specimens are shown for silica fume mixes and a 2:1 Portland cement mix. In all cases, the drying shrinkage patterns for 28-day moist-cured specimens were very similar to patterns for 28-day water-cured specimens. While high humidity had a significant influence on drying shrinkage patterns, the introduction of calcium from the limewater did not have an obvious effect.

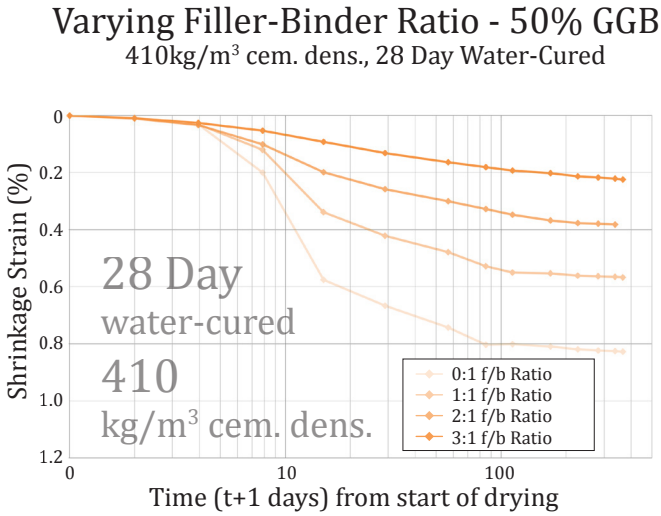

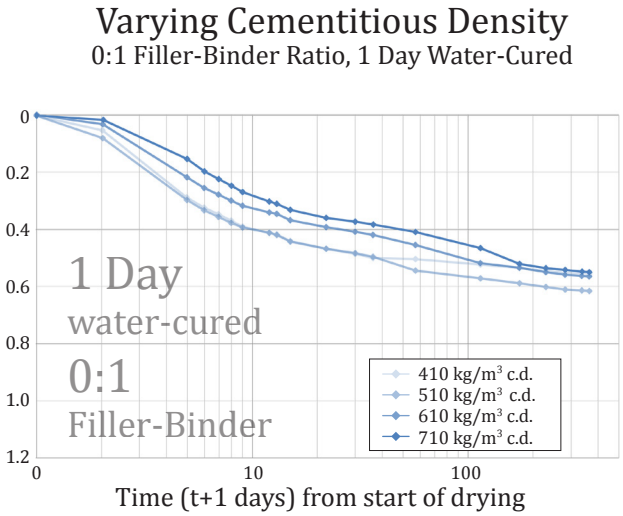

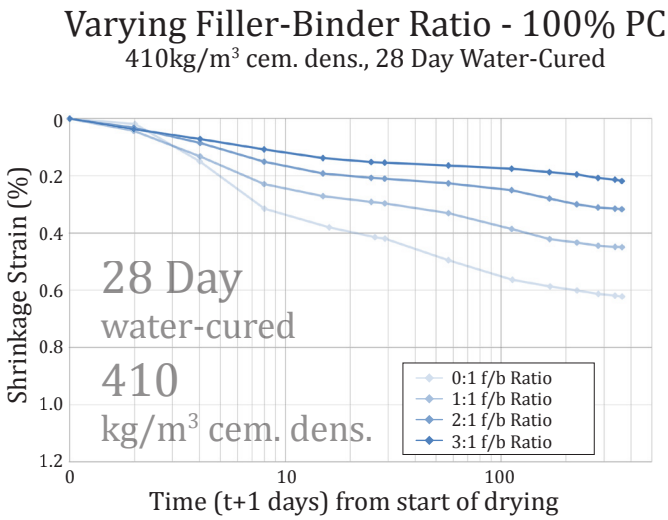

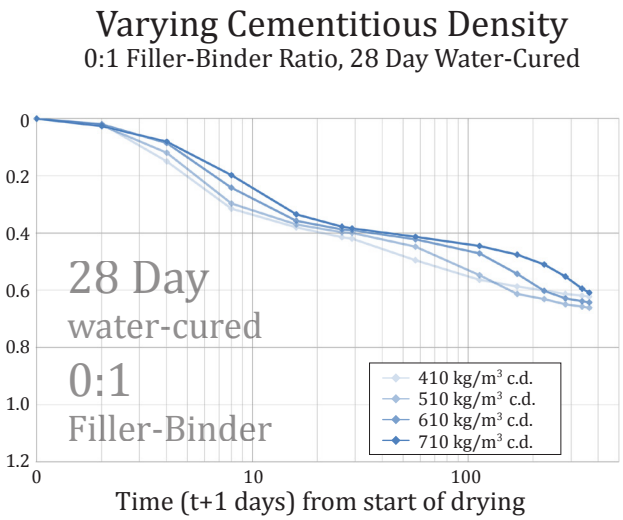

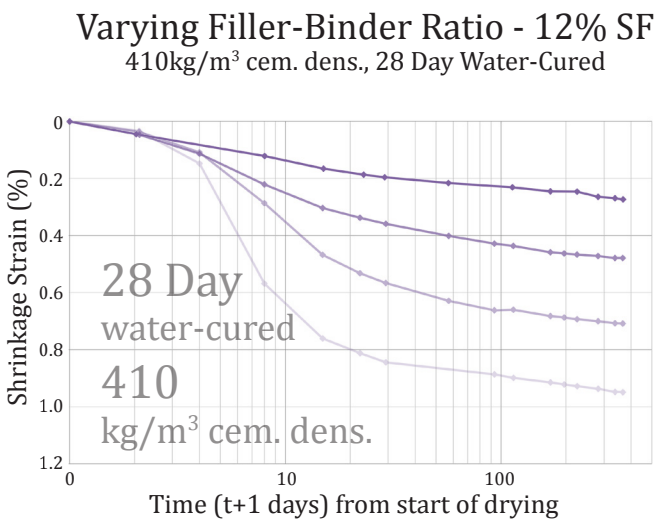

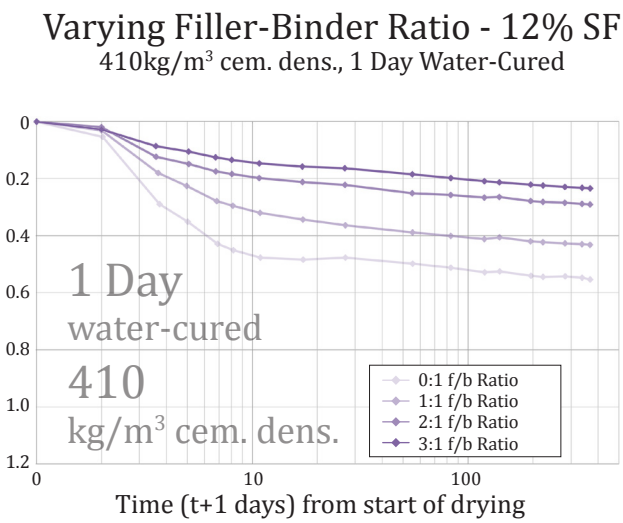

Figure 6.11c D.S. of specimens with varying f/b ratios. **Figure 6.11d** Evidence of expansive strains.

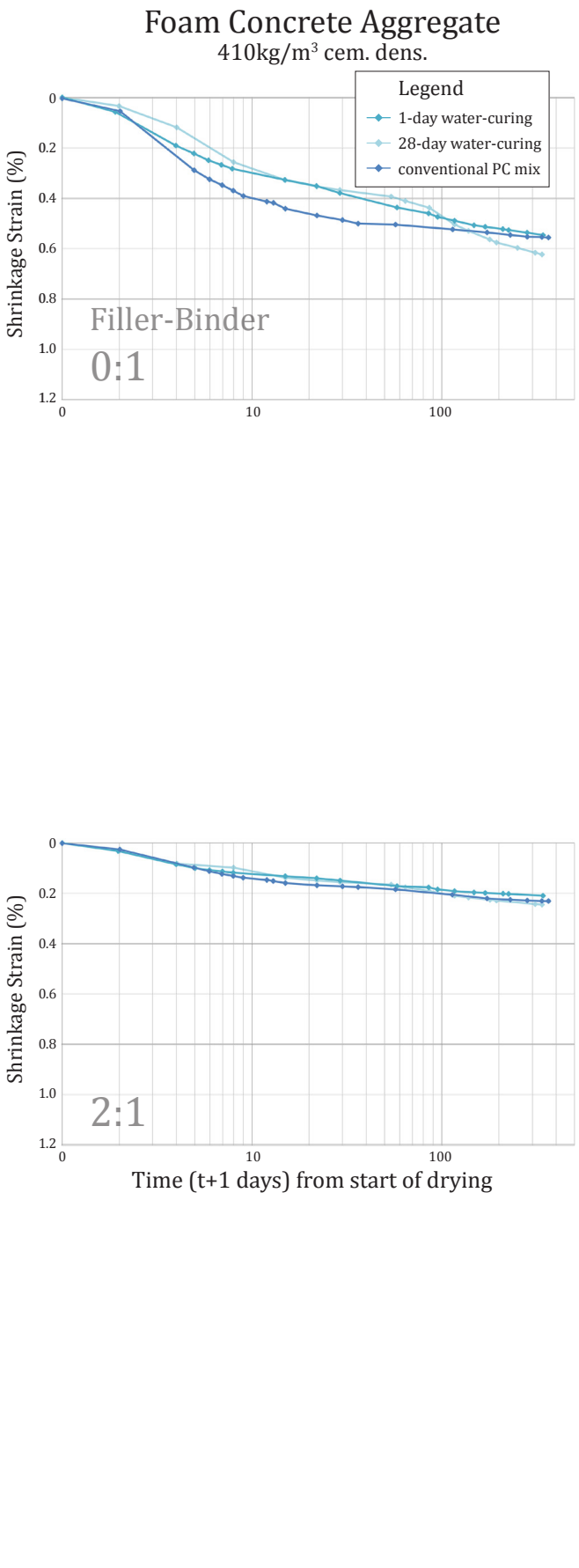

Figure 6.11e D.S. of FCA specimens.

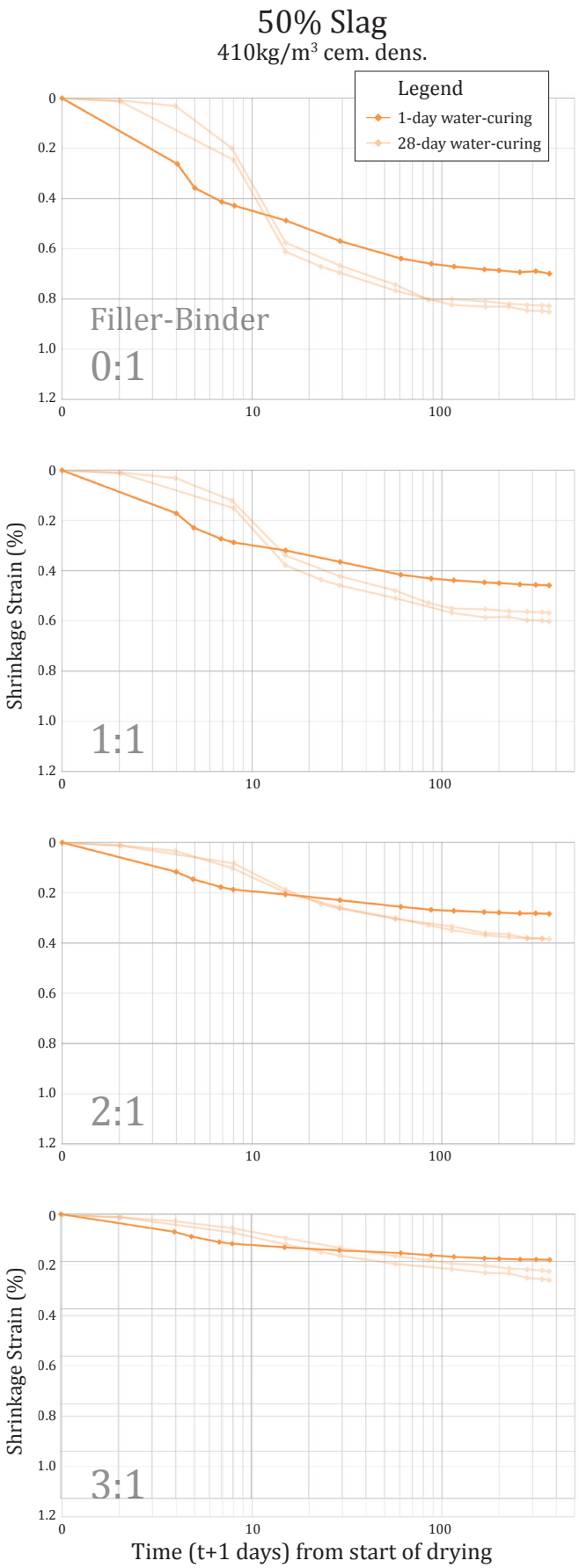

Figure 6.11f D.S. of slag specimens.

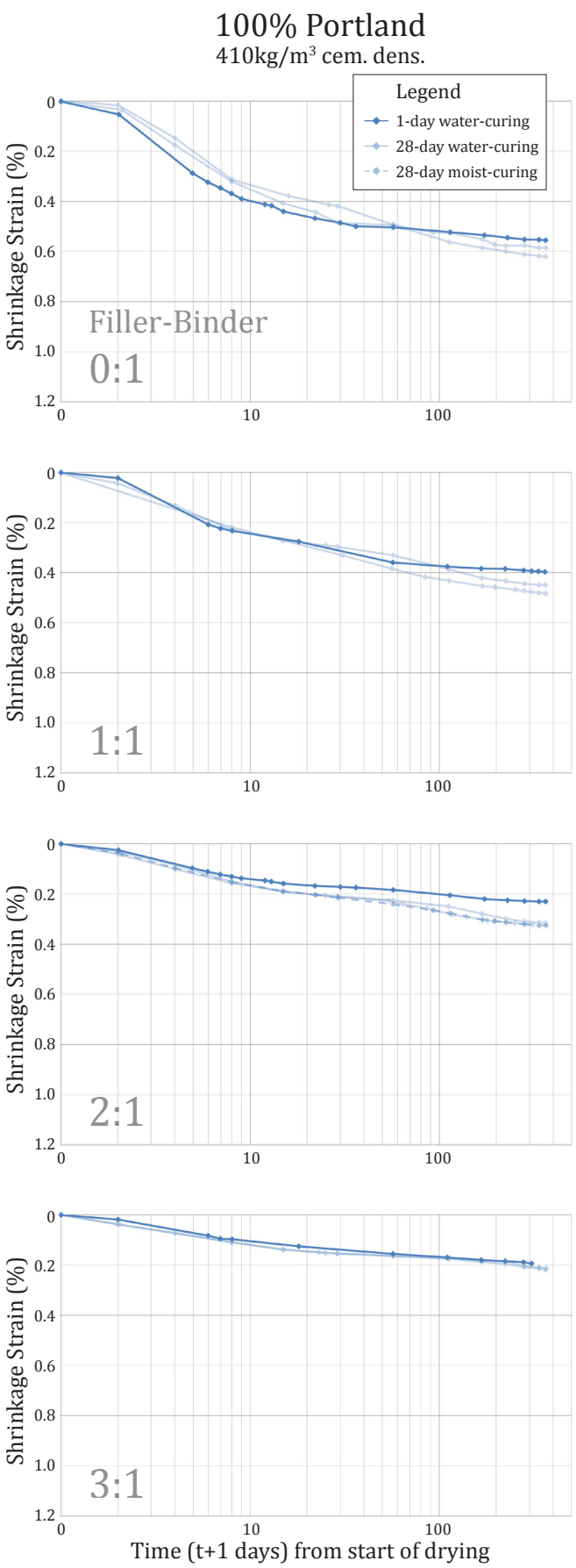

Figure 6.11g D.S. of PC specimens.

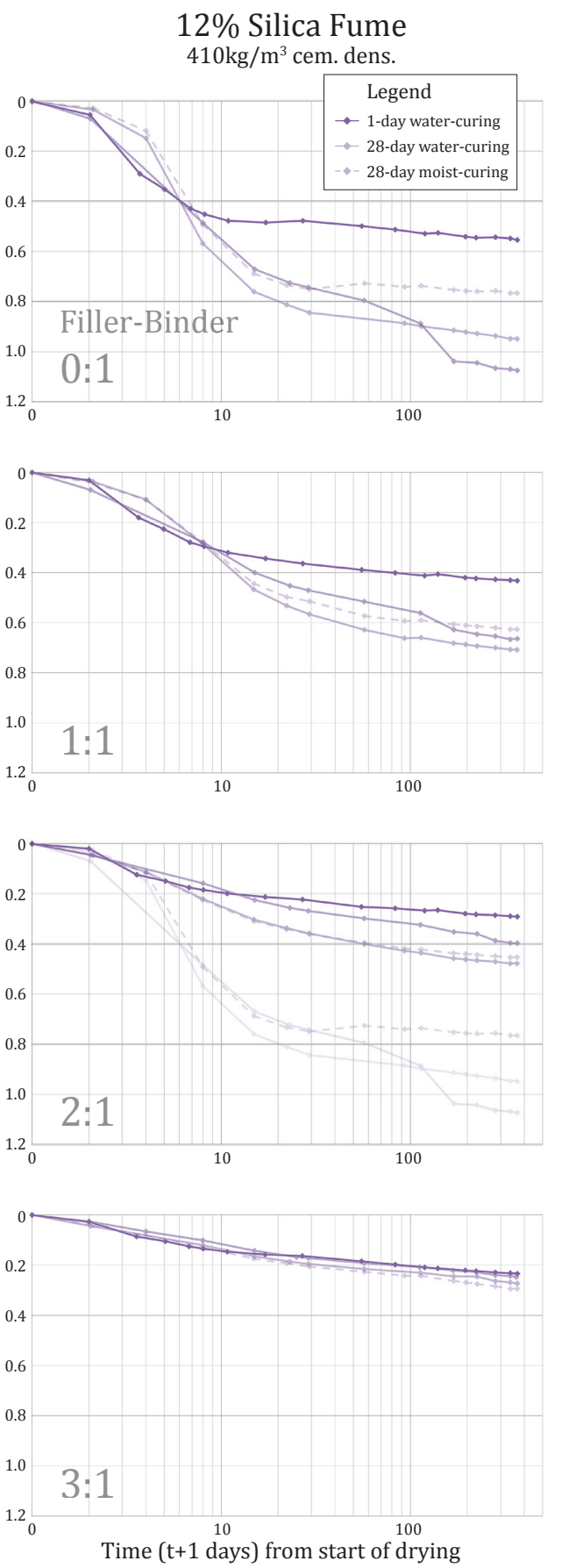

Figure 6.11h D.S. of SF specimens.

The use of FCA modestly improved drying shrinkage in the short term. At 56 days, drying shrinkage was reduced by 20 and 27% for nominal 600 and 1400 kg/m^3 mixes, respectively, compared to conventional Portland binder foam concrete mixes. The crushed material had already undergone volumetric contraction during previous curing, and restrained movement in the newer surrounding matrix.

At longer ages, however, shrinkage strain of FCA specimens was similar to that of conventional foam concrete of the same density and cementitious density. Continued drying resulted in lower internal RH, eventually removing water from small capillaries present in the FCA and inducing capillary tension. (Refer to Appendix A, Section 6.2.3.)

Figures 6.**11i** and 6.**11j** show the changing mass of specimens upon exposure to 50% RH drying conditions, providing further insight into shrinkage behaviour. Note that each data series is based on measurements from a single specimen, and therefore results should be interpreted with caution. Nevertheless, a number of patterns are evident.

Trends are most clear among silica fume mixes. The rate of moisture loss decreased with longer curing times. After 1 year, the equilibrium densities of the specimens with a long curing regime were between 39 and 45 kg/m^3 higher than the equilibrium density of specimens with a 1-day curing regime. The data supports the conclusion that a longer curing time produced a higher degree of hydration, which would be associated with increased density, higher closed porosity and slower moisture loss. It is also possible that a longer exposure to high RH during curing increased the proportion of fine capillary pores. These finer capillary pores would retain water for longer during drying, and would store more water at 50% RH, resulting in higher equilibrium density.

For specimens cured for 28 days, moist-cured and water-cured exhibited similar patterns of mass loss. Among the specimens tested, 28-day moist-cured specimens took on more mass during curing than 28-day water-cured specimens. It is possible that moisture ingress in water-cured specimens was limited by greater closed porosity, due to enhanced hydration or the availability of calcium in the limewater for densifying cell walls. Submersion in liquid water may have reduced cracking due to differential strain, or may have limited carbonation, preserving closed porosity by reducing damage to cell walls at plateau boundaries. Alternatively, submersion in liquid water may have 'sealed' the outer

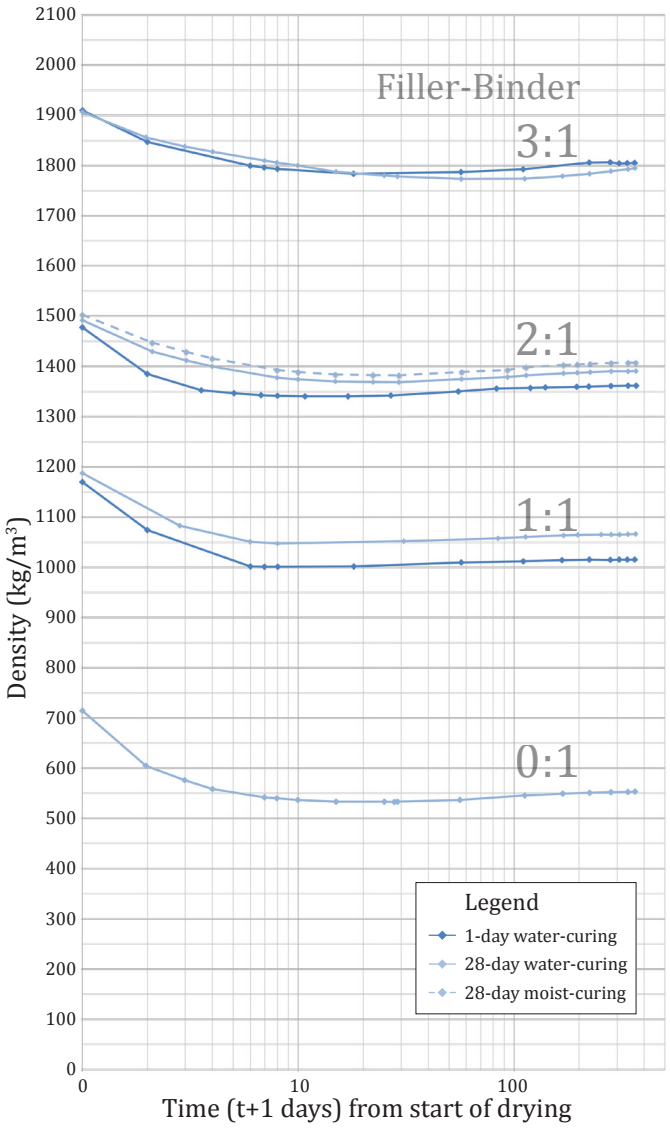

Figure 6.11i Change in mass of PC specimens.

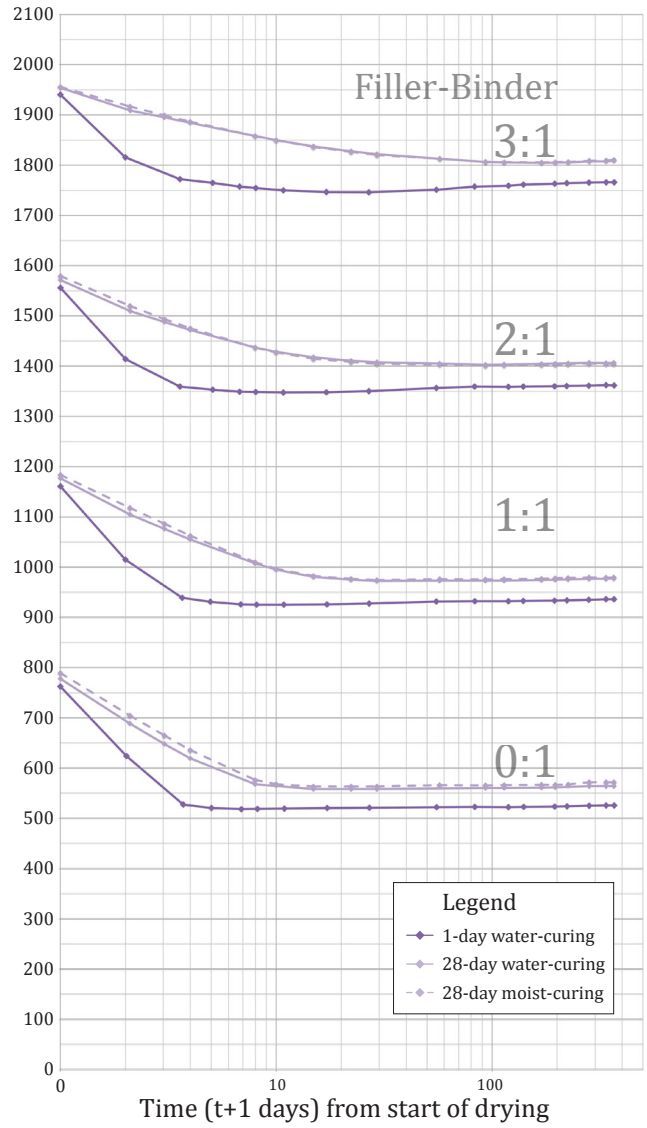

Figure 6.11j Change in mass of SF specimens.

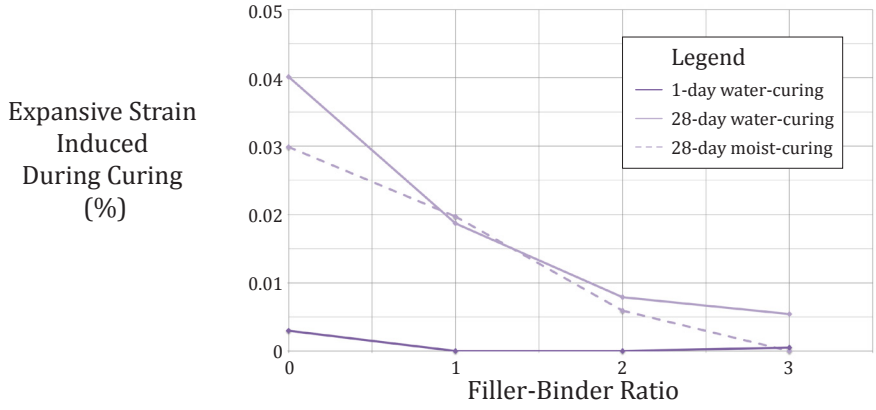

Figure 6.11k Expansive strains during curing.

surface of the specimens, limiting the potential for moisture to enter and displace trapped air. (Refer to Section 6.12 for comparison with a similar phenomenon of reduced moisture ingress in a high RH environment.)

Equilibrium densities for 28-day moist-cured specimens were similar to, or slightly higher than, those for 28-day water-cured specimens. These results suggest that calcium in the limewater did not contribute significantly to the mass of water-cured specimens. The higher density of moist-cured specimens may be due to a higher degree of hydration, produced because of a higher initial degree of saturation. Alternatively, the moist-curing regime may have produced a greater proportion of fine capillary pores which store more water at 50% RH, resulting in higher apparent density, as discussed above.

Notably, at long times of exposure to 50% RH, specimens continued to gain mass due to ongoing hydration or carbonation, as discussed later in this section.

Figure 6.**11k** shows the expansive strain induced during curing for silica fume mixes. Note that each data point is based on measurements from a single specimen, so results should be interpreted with caution; however, general patterns and magnitude of strain are indicated.

Expansive strain was negligible for specimens cured in water for 1 day. Given the high water-binder ratios, specimens were already saturated, with a high internal RH. The availability of liquid water did not significantly affect volume. With longer curing times, very small expansive strains were induced, which increased with porosity. Elongation was between 0 and 54 μstrain for the densest specimens, and between 299 and 401 μstrain for the most porous specimens.

These data confirm that differences in shrinkage strain due to curing regime is not simply a consequence of global swelling that is reversed upon drying. Rather, variations in shrinkage behaviour are related to internal microstructural changes that have relatively negligible effects on volume during curing.

Drying shrinkage data for specimens with higher cementitious densities are given in Figures 6.**11l** and 6.**11m**. Data is consistent with previously observed trends. With longer curing times, initial rates of drying shrinkage were lower, but drying shrinkage after one year was higher. Additionally, Figure 6.**11m** reveals that for a 28-day water-curing regime,

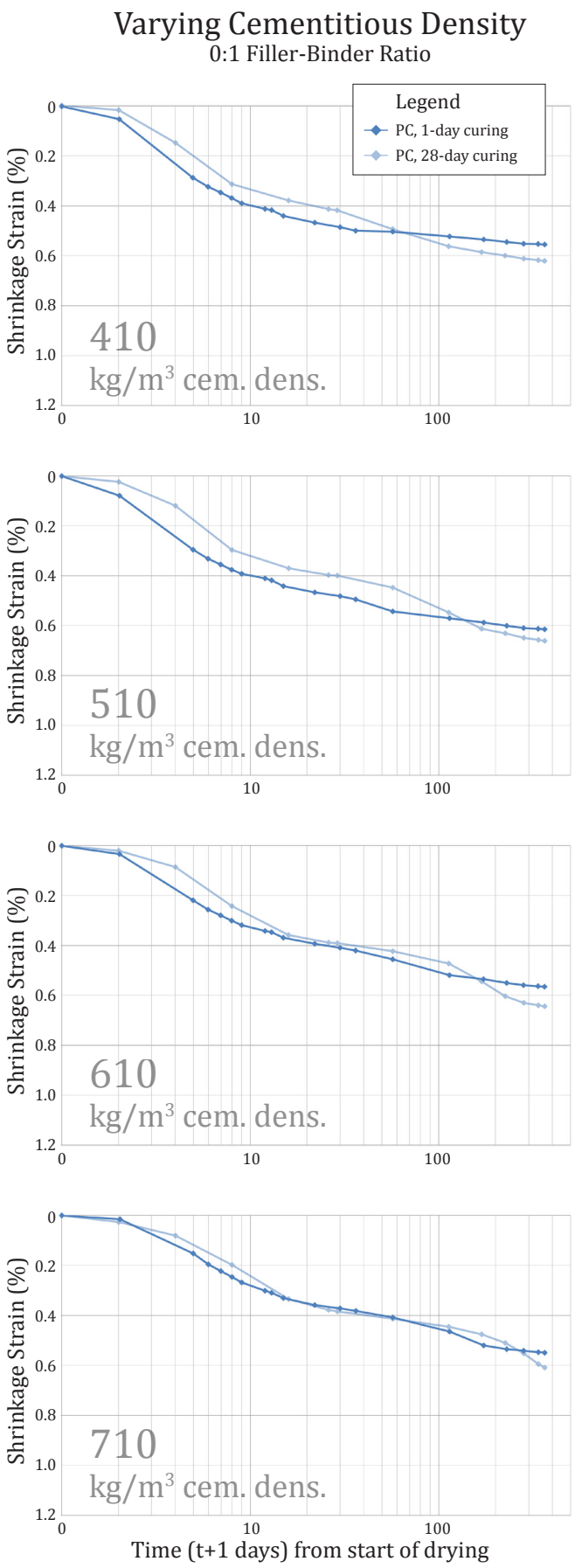

Figure 6.11l D.S. of neat cement specimens.

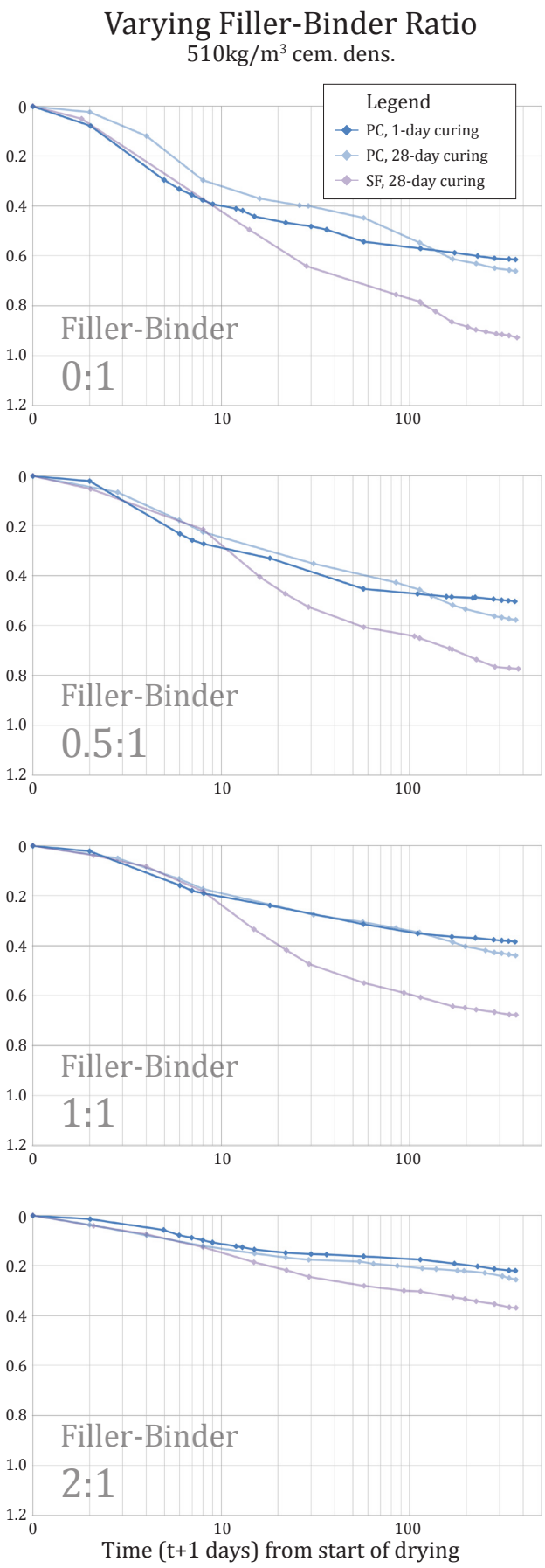

Figure 6.11m D.S. of 510 kg/m^3 c.d. specimens.

drying shrinkage was higher for silica fume mixes than for equivalent Portland mixes.

Figures 6.**11n** to 6.**11p** show shrinkage strain for various cementitious blends, grouped according to curing regime.

Among 1-day water-cured specimens, patterns of shrinkage varied slightly with changes in cementitious blend. Use of SCMs typically increased drying shrinkage, except that in mixes with no filler, the silica fume blend experienced the least total strain. Rates of moisture loss increased with higher water-binder ratios, per Figure 6.**11q**, and cracking due to differential shrinkage may have introduced expansive strain in the silica fume blend.

For 28-day water-cured specimens, variations in shrinkage among cementitious blends were more pronounced. Patterns were likely dominated by capillary porosity. For example, minimal early movement in slag mixes may be attributed to a low proportion of large capillary voids, due to relatively low water-binder ratios. At high RH (i.e. early drying times), smaller voids remain fully filled, and there would be few partially filled voids present to

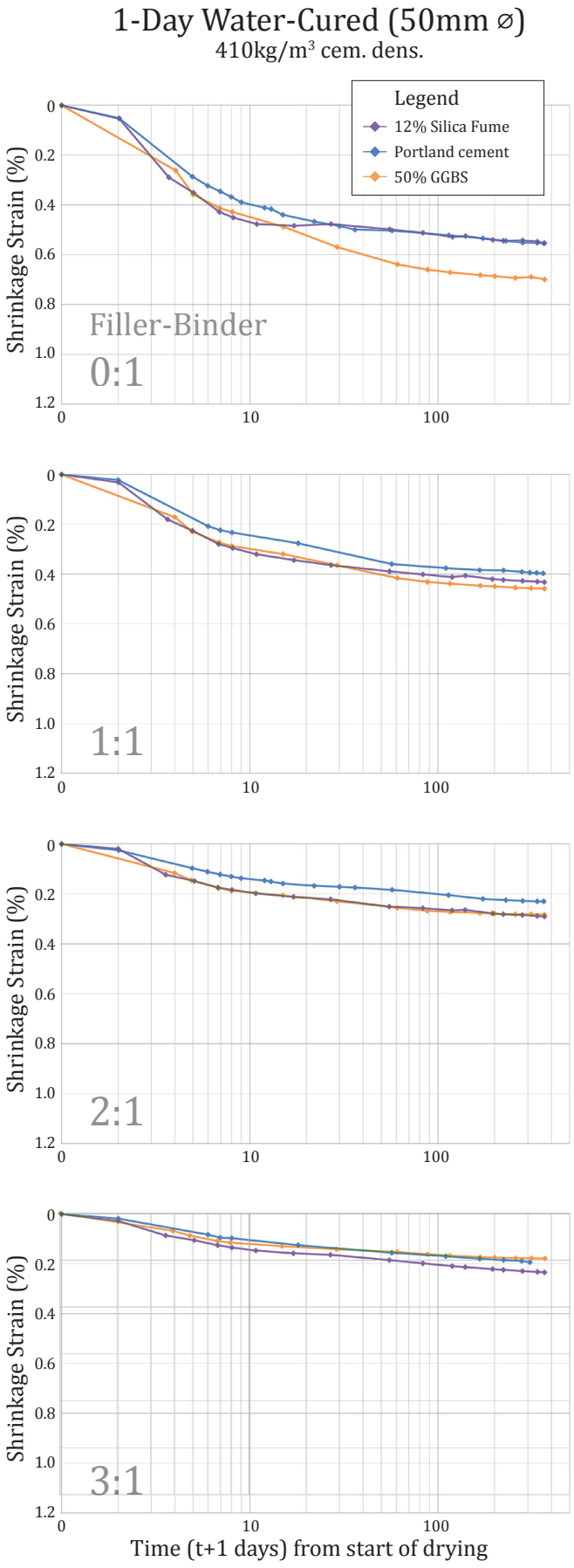

Figure 6.11n D.S. of 1-day water-cured specimens.

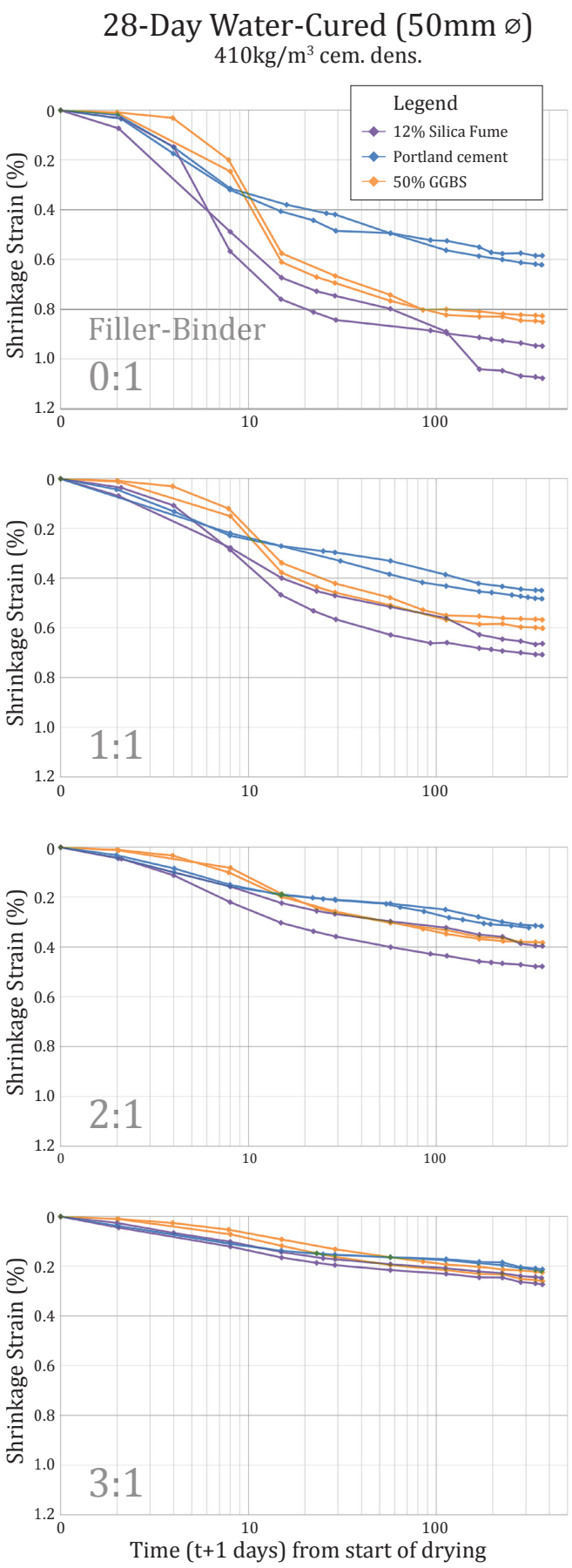

Figure 6.11o D.S. of 28-day water-cured specimens.

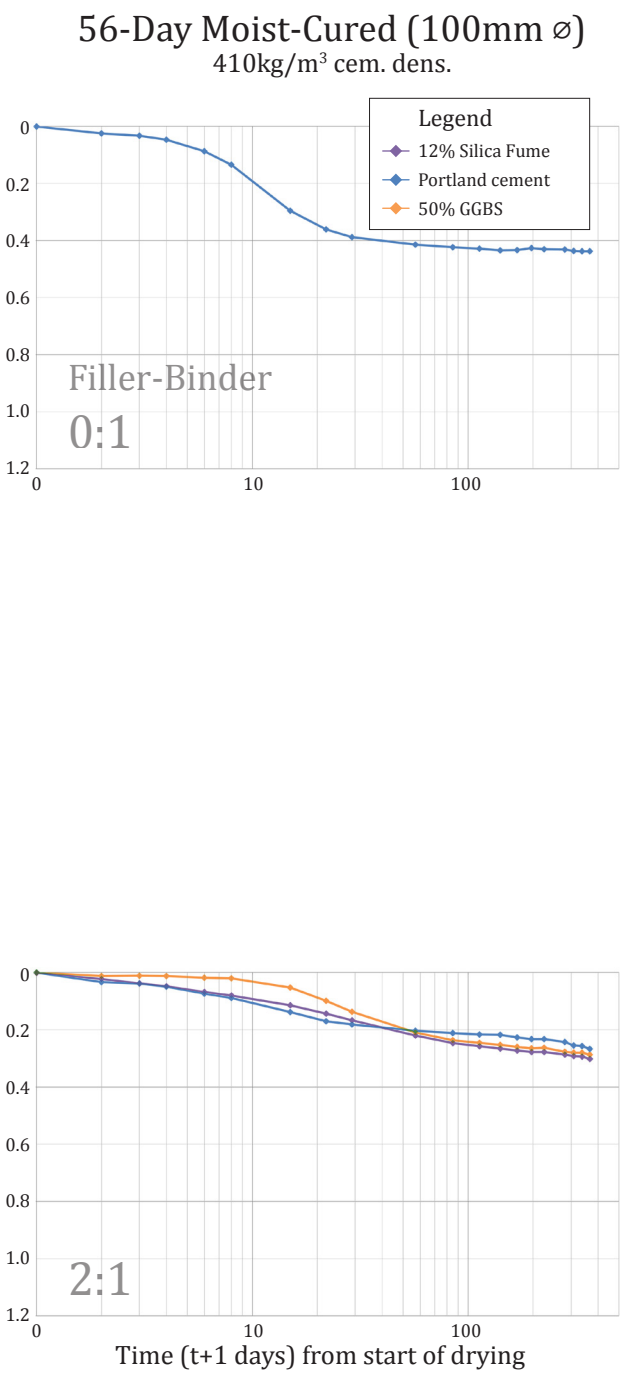

Figure 6.11p D.S. of 56-day moist-cured specimens.

contribute to capillary tension via capillary menisci (refer to Appendix A, 6.2.3). Similarly, the significant drying strain of silica fume mixes may be due to a large total volume of capillary pores.

56-day moist-cured specimens showed similar shrinkage patterns to 28-day water-cured specimens, although strain rates were slower and strains after one year were less extreme. Size effects may contribute to these differences. Figure 6.**11s** shows a reduced rate of moisture loss through the larger specimens, which would slow shrinkage and simultaneously promote a higher degree of hydration, reducing the volume of capillary pores available to participate in capillary tension.

In Figures 6.**11q** to 6.**11s**, long-term mass gain is evident, especially in Portland cement specimens. Ongoing hydration may account for the increasing density. As internal water chemically bonds and forms C-S-H, interior RH decreases, and additional moisture is drawn from the controlled 50% RH environment to maintain equilibrium. Density would also increase with ongoing carbonation, as atmospheric carbon dioxide is chemically bound.

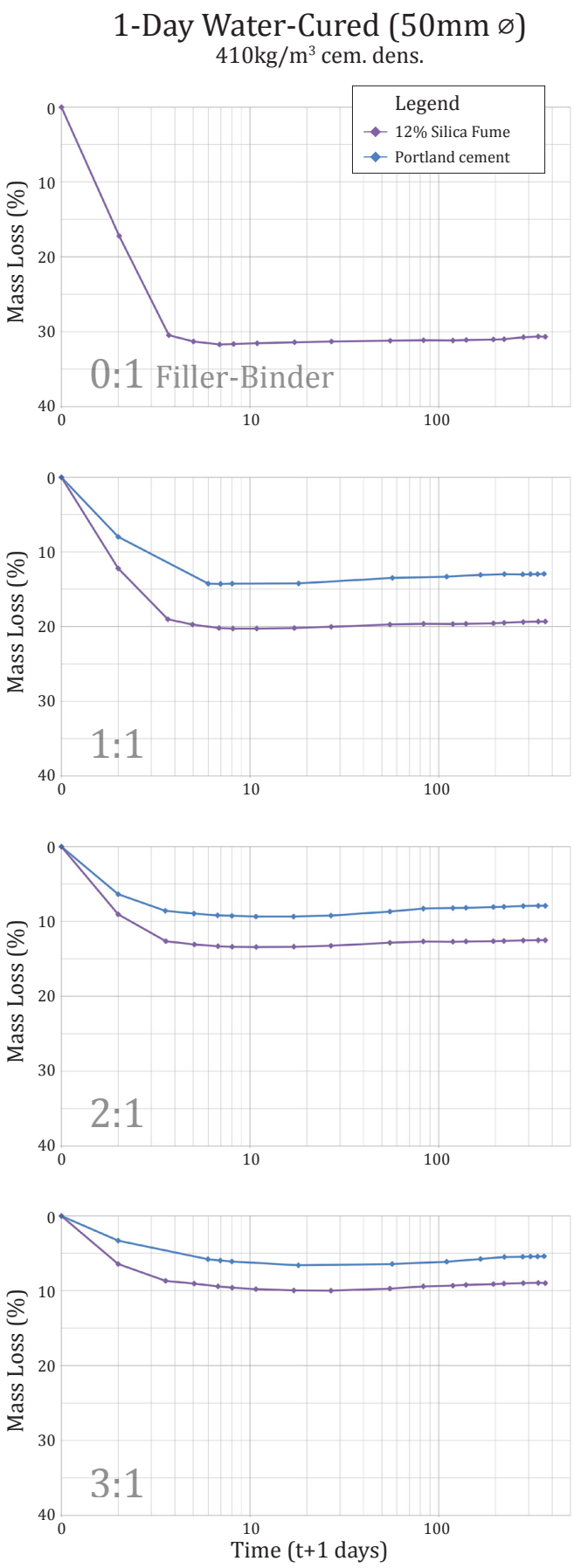

Figure 6.11q Change in mass, 1-day water-cured.

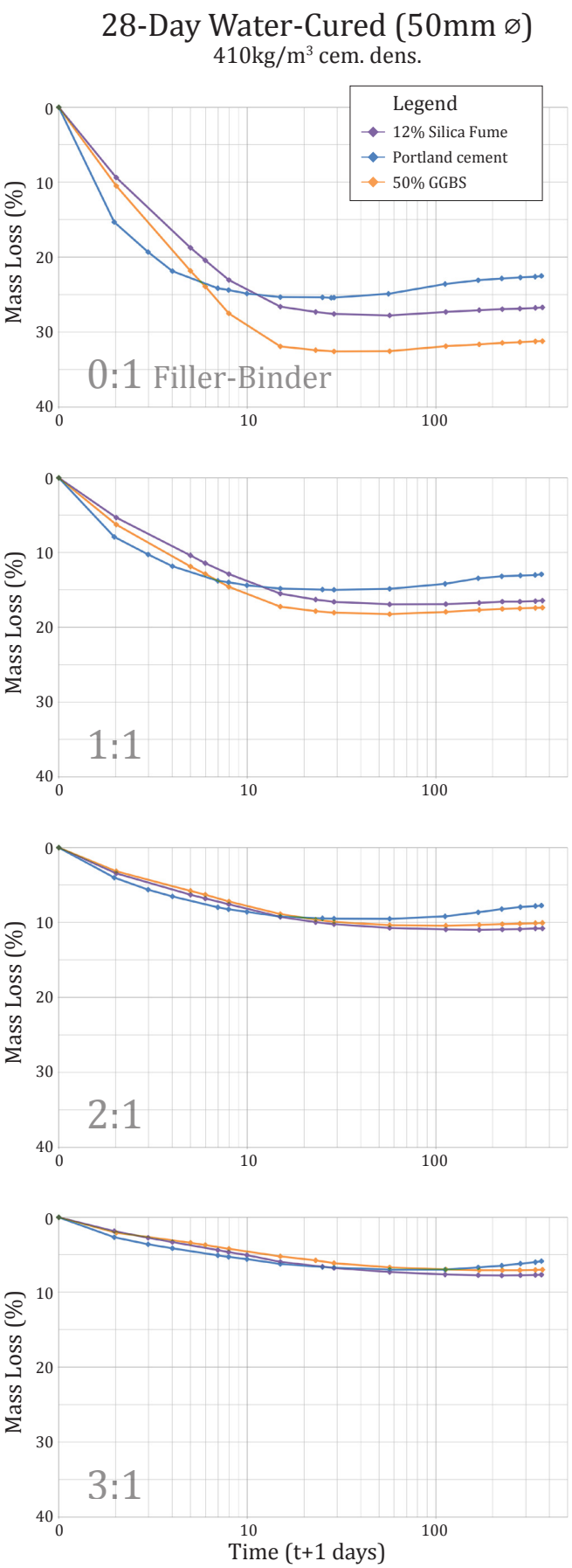

Figure 6.11r Change in mass, 28-day water-cured.

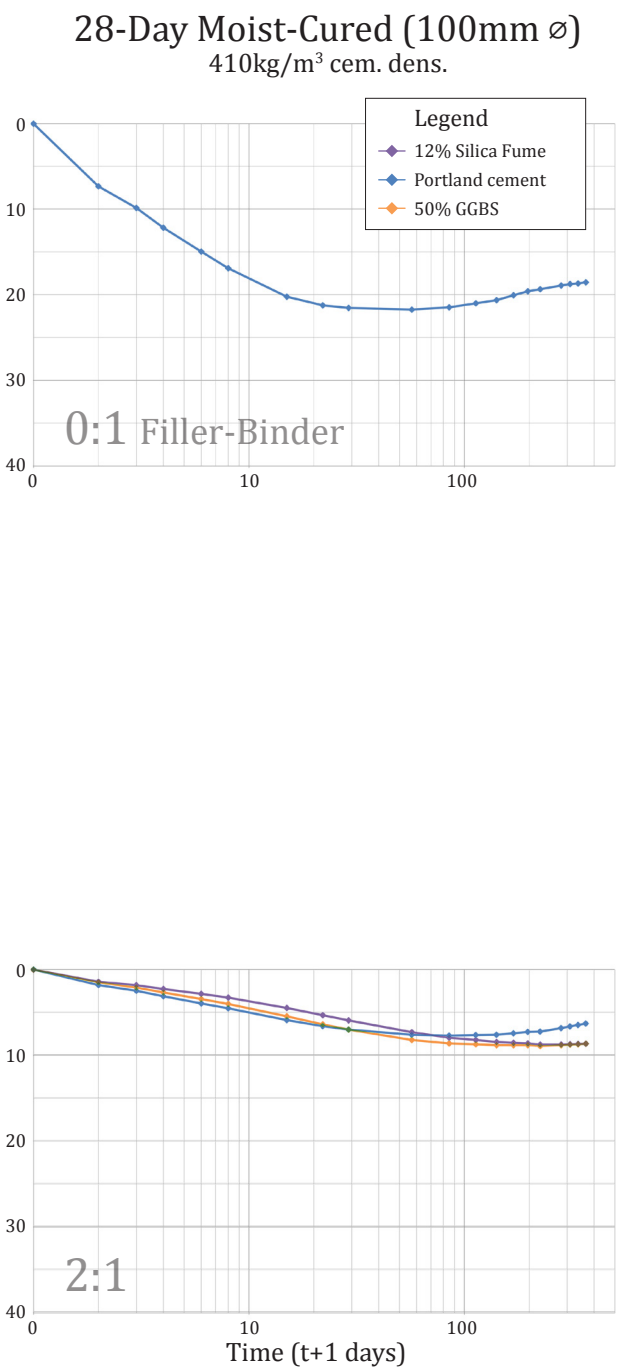

Figure 6.11s Change in mass, 56-day moist-cured.

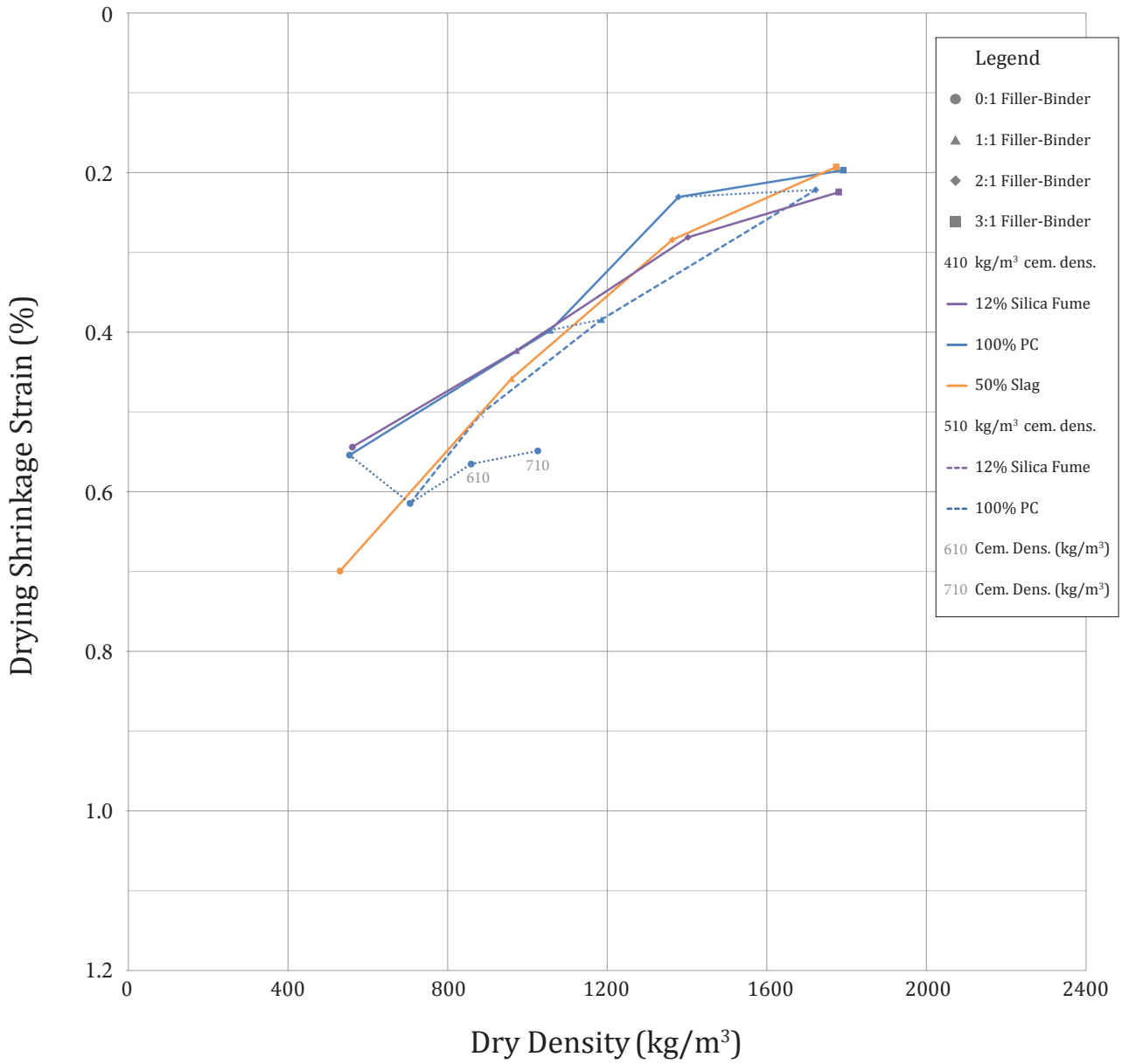

Figure 6.11t Drying shrinkage strain vs. dry density, 1-day water-cured specimens.

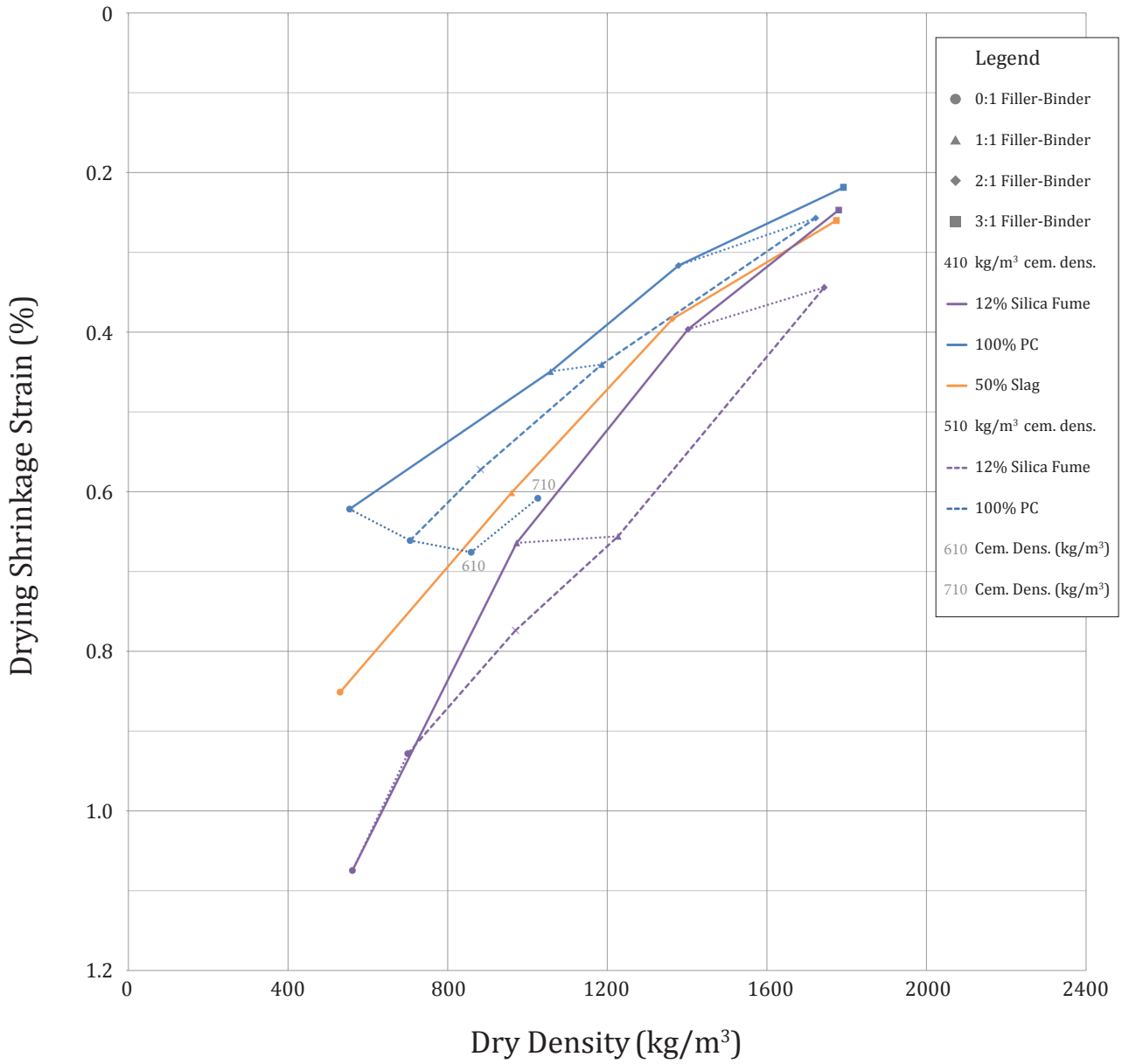

Figure 6.11u Drying shrinkage strain vs. dry density, 28-day water-cured specimens.

6.12 Moisture Storage

Figure 6.**12c** shows the moisture content of foam concrete specimens exposed to 50, 80, and 90% RH, respectively. Specimens were water-cured for 28 days, and conditioned in 50% RH for one year, prior to the start of the test, as described in Section 5.5.2. Initial MC values were determined from companion specimens at the start of the test. Subsequent MC values were based on accumulated mass gain in the specimens.

Specimens maintained in 50% RH provided a reference for ongoing processes of hydration or carbonation. Accumulated mass gain at 50% RH was relatively low, indicating that change in mass in 80 and 90% RH environments was mainly due to water adsorption.

Specimens in 80% RH gained mass at a decreasing rate until approximately four months. Mass gain was typically lowest for slag mixes. This trend may be due in part to the low water-binder ratios used, resulting in low capillary porosity and thus low internal surface area for water absorption. Higher mass gain for Portland cement and silica fume mixes reflects higher internal surface areas, resulting from many fine capillary voids.

Surprisingly, specimens in 90% RH gained mass at a slower rate than specimens in 80% RH. It is possible that initial wetting of the exterior surface of the specimens 'sealed' the specimens via capillary condensation, creating a barrier to diffusion of air and slowing the ingress of moisture (refer to Figure 6.**12b**). Due to circumstances beyond the author's control, the sorptivity tests were terminated at 5 months, prior to specimens reaching equilibrium, therefore 90% RH equilibrium moisture content values remain undetermined.

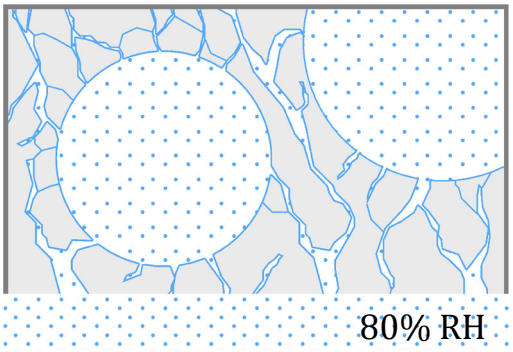

Figure 6.12a
Exposure to 80% RH, proposed model.
Specimen initially conditioned to 50% RH.
High RH air progresses through open capillaries in the highly permeable material. Water adsorbs on available internal surface area throughout the specimen.

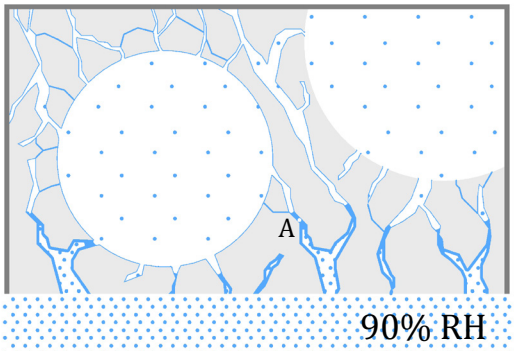

Figure 6.12b
Exposure to 90% RH, proposed model.
Specimen initially conditioned to 50% RH.
Vapour condenses in small diameter capillaries near the exposed surface of the material. Interior air is 'trapped'. Interior air can only evacuate the specimen via diffision through capillary condensation water (A).

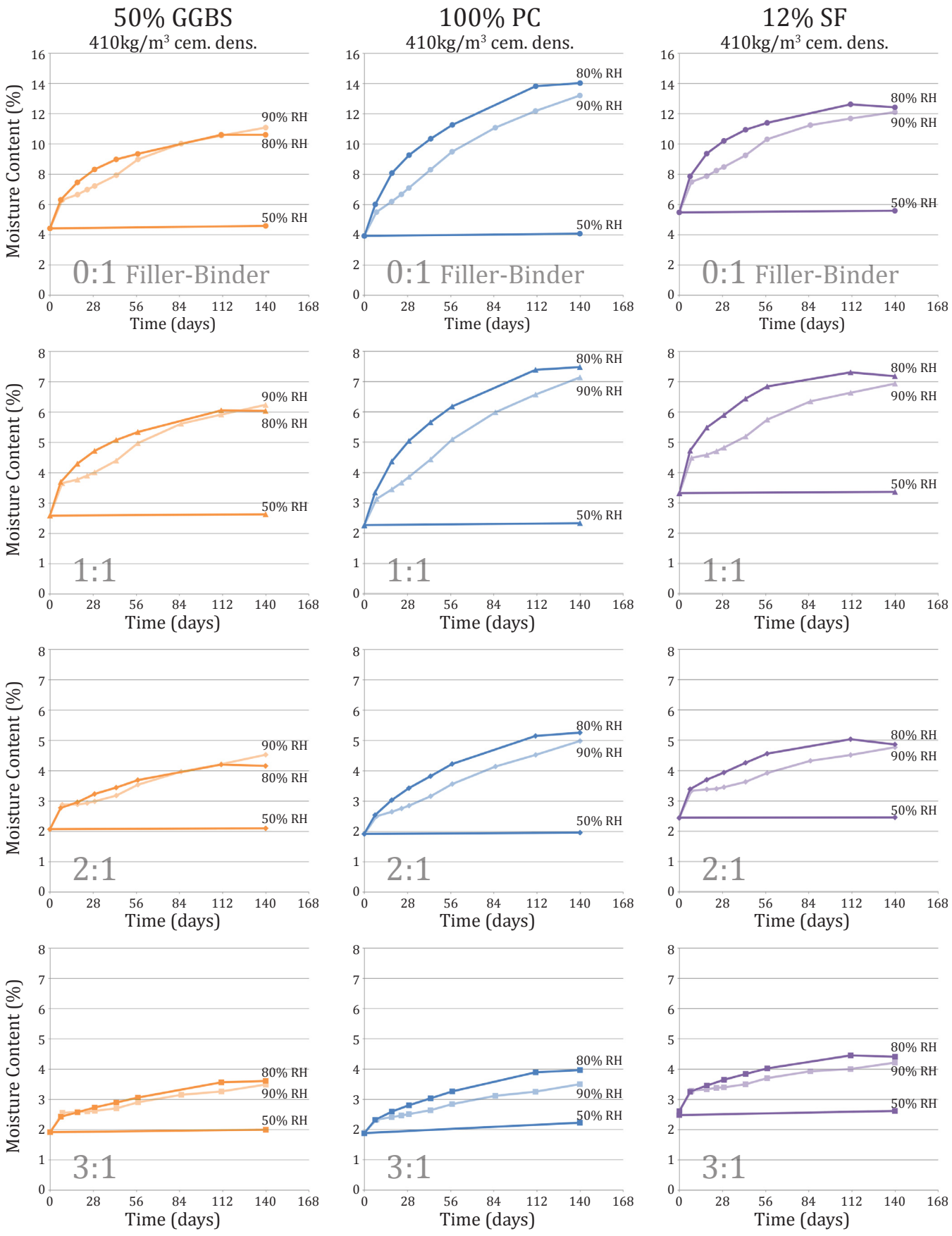

Figure 6.12c Patterns of moisture accumulation in 50, 80, and 90% RH environments.

Equilibrium moisture contents (EMC) in environments of varying relative humidity are expressed as a percentage of oven dry mass in Figure 6.**12e**. For specimens of varying dry densities, trends may be more easily detected by comparing moisture content per unit volume, as referenced in Figure 6.**12f** and in the discussion below.

For specimens in 50% RH, there appeared to be a correlation between moisture storage and water-binder ratios (Figure 6.**12d**). Capillary porosity (and internal surface area) increased with water-binder ratio, resulting in especially high ECMs for silica fume mixes. Decreasing moisture storage with increasing porosity may be partially attributed to reductions in water-binder ratio, and the addition of solid aggregate surface area in the mix. Additionally, at higher densities, there may be more fine capillary pores, for example due to high local water-binder ratios and high capillary pore concentration adjacent to aggregate (refer to Appendix A, Section 6.3.1b). While large capillaries and air voids adsorb thin layers of water, smaller capillary pores can store proportionally greater concentrations of water via capillary tension.

For specimens in 80% RH, moisture storage was relatively constant across porosities. At this higher humidity, very fine capillary pores may be saturated. A greater proportion of capillary pores, with a greater range of pore diameters, are likely engaged in storing water via capillary tension. Among cementitious blends, it appeared that slag mixes stored the least moisture, likely due to a low accumulated volume of capillary pores capable of participating in capillary tension at 80% RH, in addition to having a low internal surface area for water adsorption. An increase in moisture storage for the highest density mixes reflects an increase in capillary porosity with water-binder ratio, as discussed above.

For specimens immersed in water, moisture storage did not vary significantly with porosity, which suggests that both solid aggregate and discrete air-voids were similarly competent at resisting liquid water ingress during the 14 days of immersion. The slight increase in moisture storage with porosity may be attributed to increased interconnectivity and capillarity of air voids, resulting from shrinkage cracks (Section 6.11) or damage to thin cells walls during curing or aging (Appendix A, Section 6.3.1b). Among low-density mixes, the resistance of SF mixes to water ingress may be due to fine, closed air-voids.

For specimens with constant cementitious density, at 50 and 80% RH, the inclusion of aggregate had a relatively small influence on moisture storage, as shown in Figure 6.**12g**.

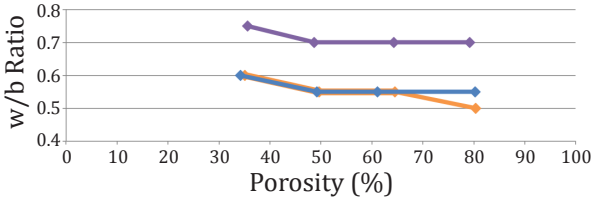

Figure 6.12d Water-binder ratios used for mixes.

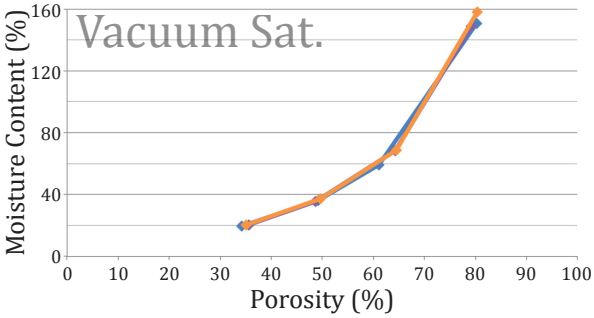

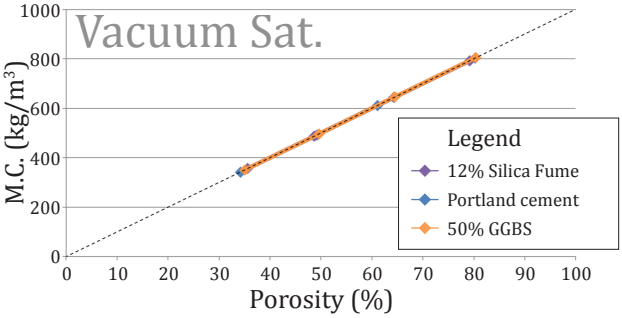

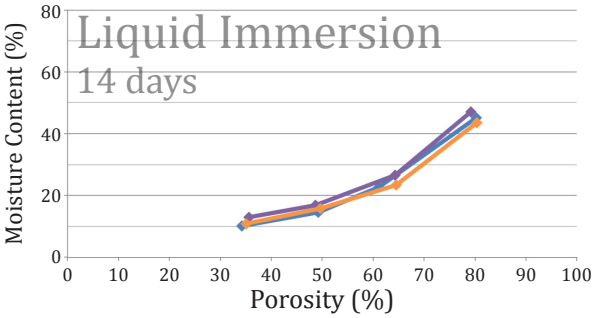

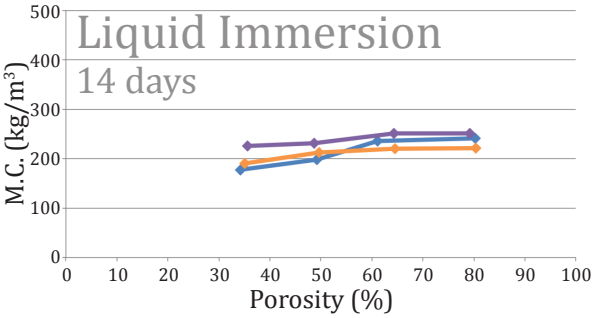

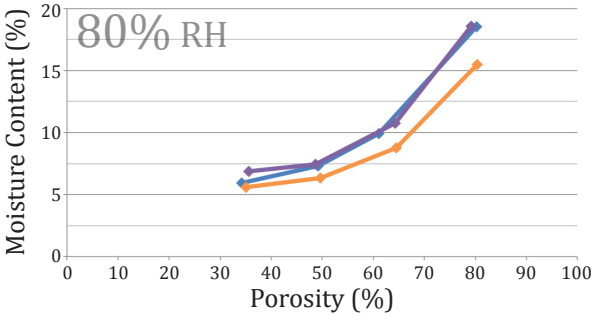

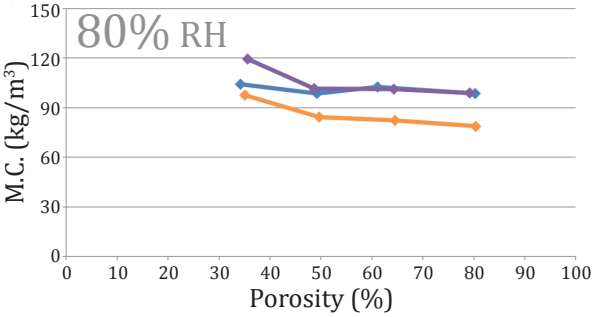

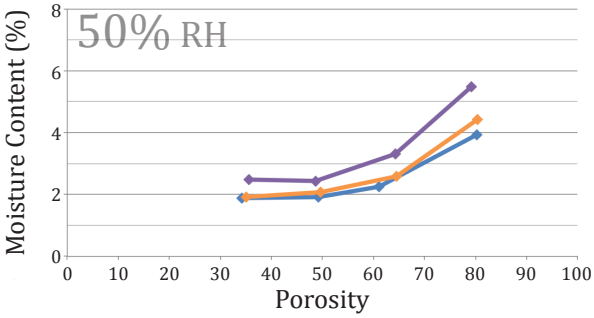

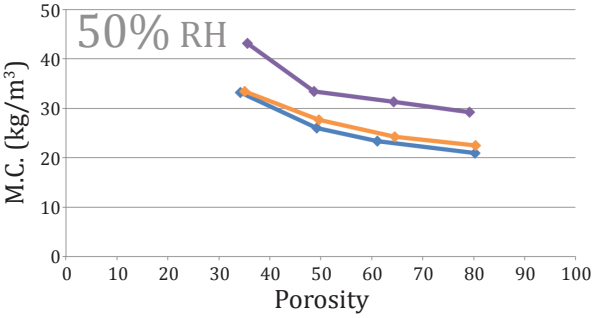

Figure 6.12e Moisture content (% mass).

Figure 6.12f Volumetric moisture content.

By contrast, moisture storage increased significantly with paste volume (Figure 6.**12h**), due to increased capillary void volume and internal surface area. At 100% RH, increasing density by adding filler reduced moisture storage during immersion, due to reduced permeability, while increasing density by adding cementitious content tended to increase moisture storage during immersion, due to increased available capillary void volume.

Moisture storage functions for slag, Portland cement, and silica fume mixes of varying densities are given in Figures 6.**12i**, 6.**12j**, and 6.**12k**, respectively, for reference.

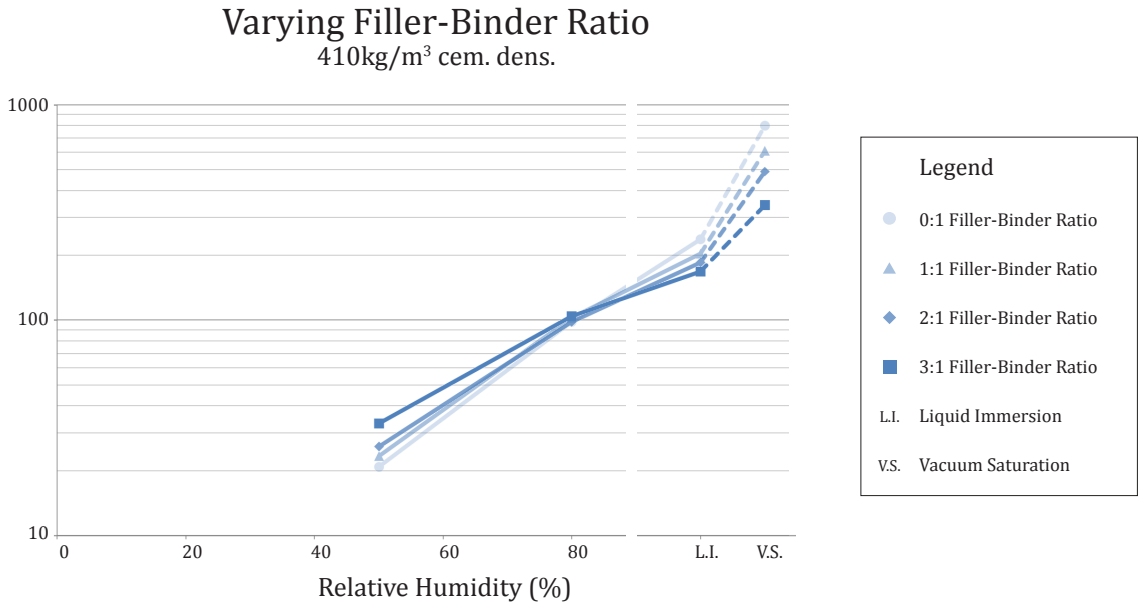

Figure 6.12g Moisture storage functions for Portland cement specimens (log scale).

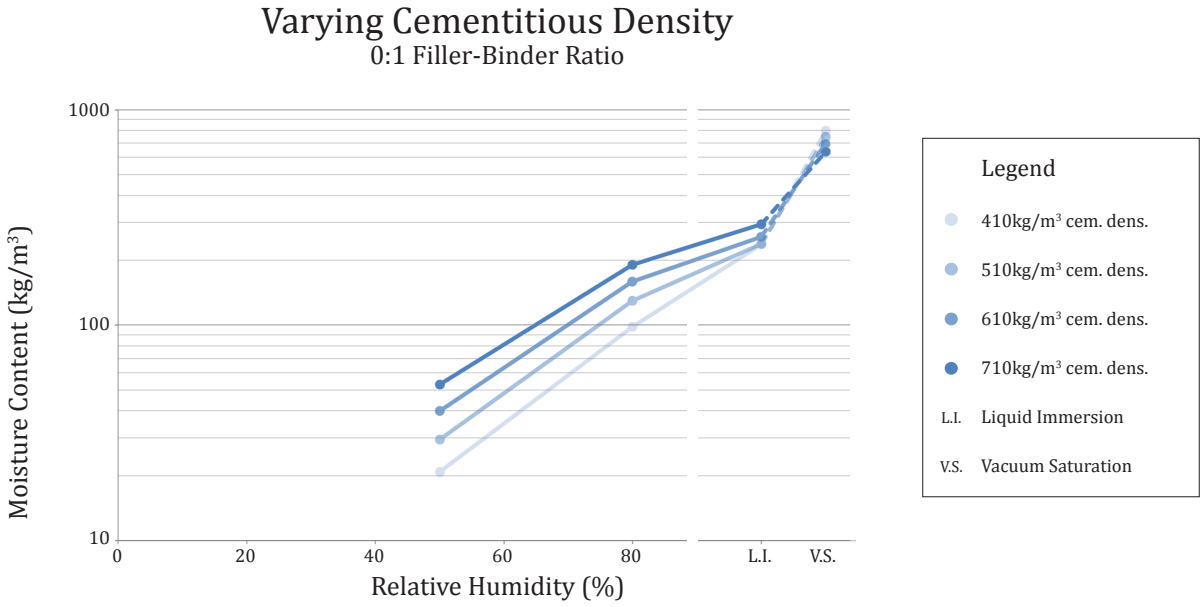

Figure 6.12h Moisture storage functions for neat cement specimens (log scale).

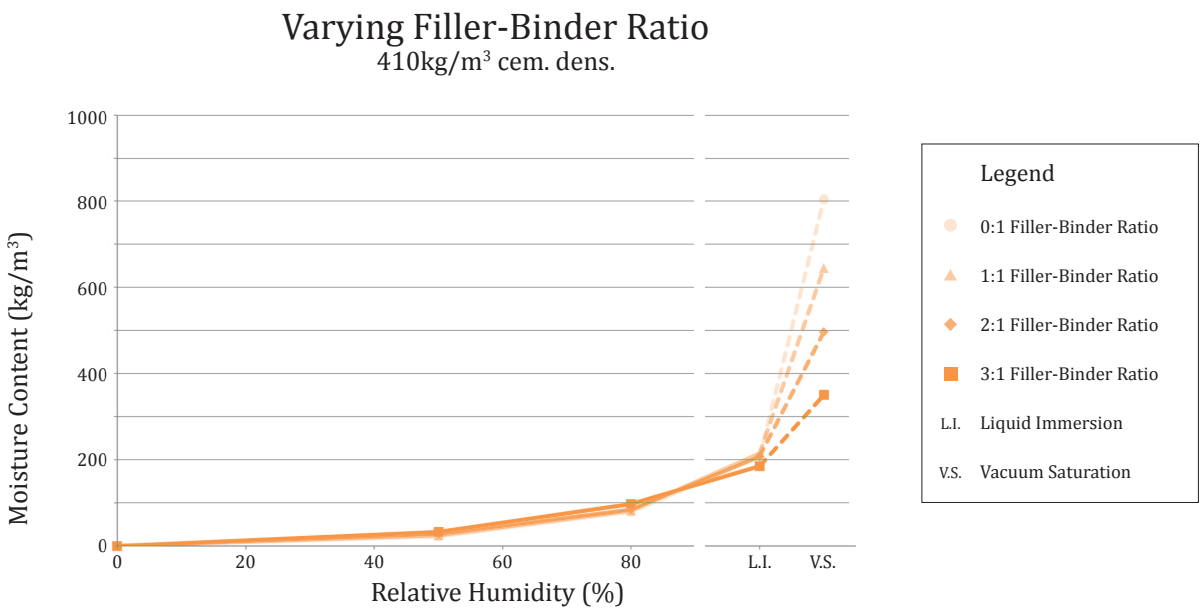

Figure 6.12i Moisture storage functions for 50% slag specimens.

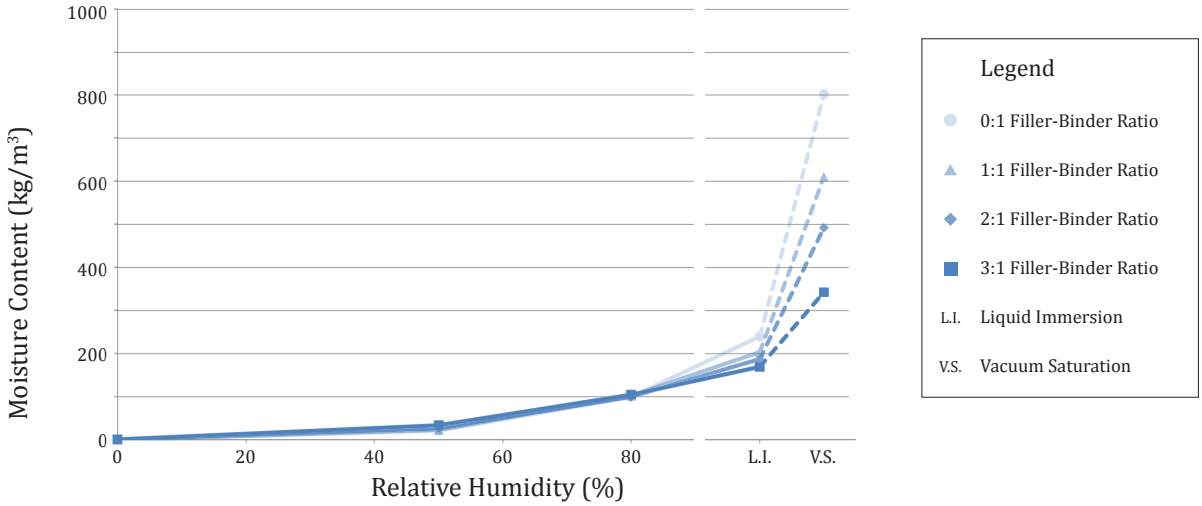

Figure 6.12j Moisture storage functions for Portland cement specimens.

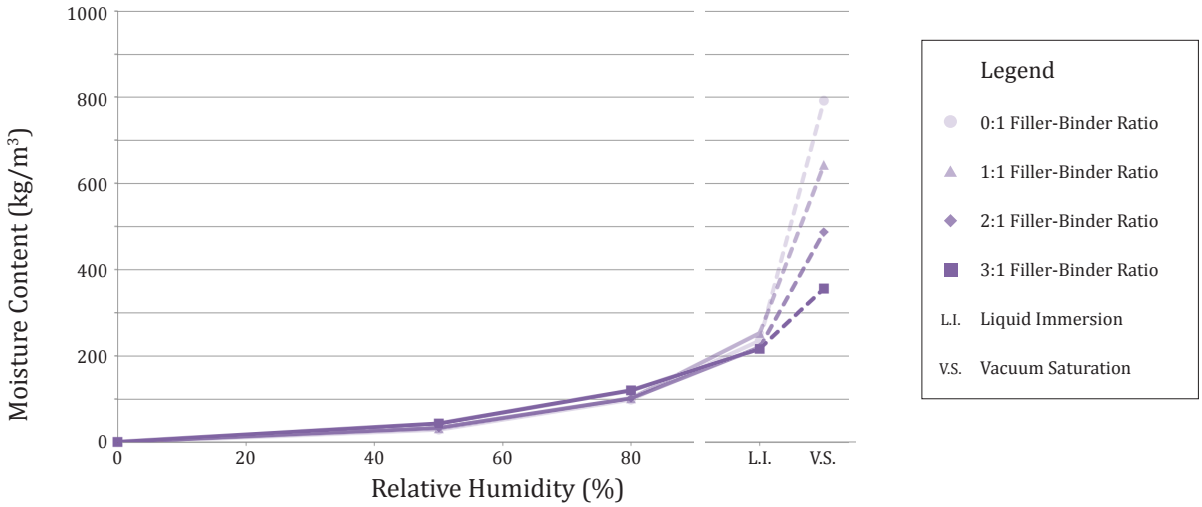

Figure 6.12k Moisture storage functions for 12% silica fume specimens.

6.13 Moisture Movement

Figure 6.**13a** shows the change in length of specimens after immersion in water for 1 and 28 days, respectively, and after exposure to strong drying at 50°C. Change in length is referenced relative to equilibrium conditions after more than 1 year at 50% RH and 25°C.

Approximately 50 to 70% of the total elongation experienced upon immersion occurred within the first 24 hours of wetting. While filler and air voids were similarly competent at resisting ingress of water for a long period (refer to Figure 6.**12e**), capillary pores readily absorbed liquid water, promoting expansion in accordance with the mechanisms described in Section 6.11 and Appendix A, Section 6.2.3.

Moisture movement decreased with increasing volume of aggregate filler. Expansion upon 28-day immersion was between 1000 and 1200 μstrain (0.10 to 0.12%) for mixes with no filler, compared to approximately 500 μstrain (0.05%) for mixes with filler-binder ratios of 3:1. Inert filler restrained movement of the C-S-H phase.

The effects of cementitious blend on moisture movement were relatively minor. Expansion increased slightly with cementitious density, for the neat cement mixes tested. This trend may be attributed to an increase in the total volume of capillary pores available to participate in effects of capillary tension, etc. (refer to Appendix A, Section 6.2.3).

Contraction induced by oven drying was less than 150 μstrain for mixes with filler-binder ratios of 3:1. Inert aggregate restrained movement of the C-S-H, with relatively thin layers of shrinkable C-S-H separating filler particles at points of contact. Conversely, for mixes with filler-binder ratios of 0:1, shrinkage upon oven-drying was 1000, 1200 and 1500 μstrain for slag, Portland cement, and silica fume binders, respectively. Change in cementitious density did not significantly affect shrinkage strain of neat cement mixes.

In general, moisture movement was significantly lower than strain observed during initial drying (Section 6.11). Drying shrinkage was 6200 μstrain (0.62%) for a neat Portland cement mix, and 2100 μstrain (0.21%) for a Portland mix with a 3:1 filler-binder ratio. Drying shrinkage strain was still higher for mixes using SCMs (refer to Figure 6.**11o**).

Figure 6.**13b** offers a preliminary indication of the potential stress that might be exerted by dry, rigidly constrained foam concrete, when exposed to liquid water. Stress has been calculated as strain upon immersion, multiplied by the elastic moduli determined

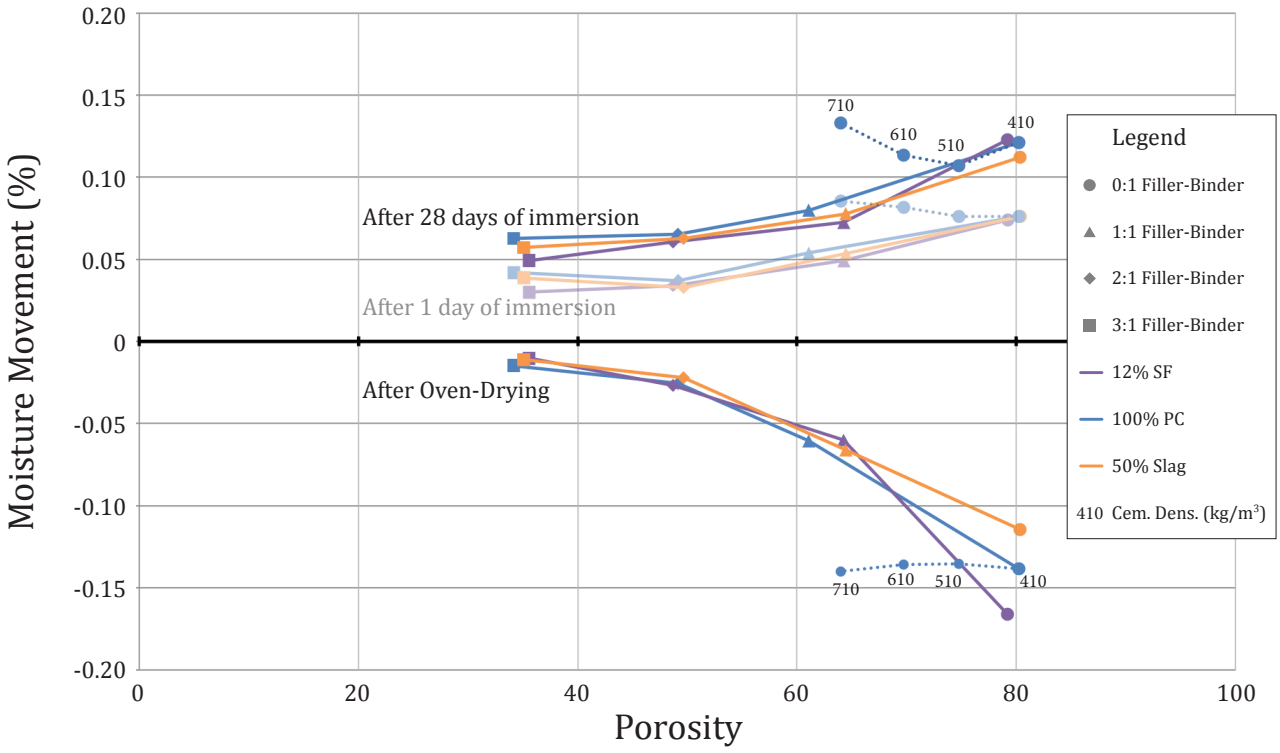

Figure 6.13a Moisture movement of specimens initially conditioned in 50% RH.

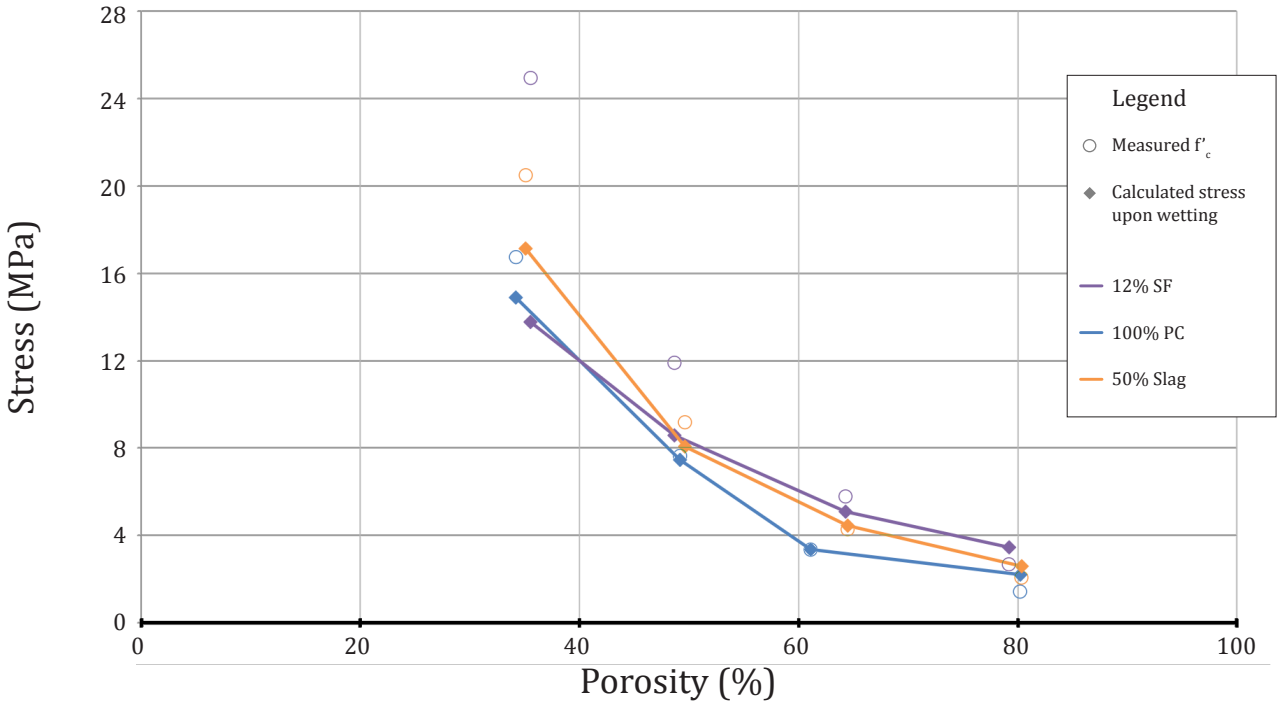

Figure 6.13b Calculated stress exerted upon wetting, for specimens conditioned in 50% RH.

in Section 6.7. Note that the elastic modulus has been assumed to be constant: in actuality, the elastic modulus for a given mix design may vary with moisture content due to the introduction of load-bearing water, disjoining pressures, etc.

The compressive strength of mixes is shown with open markers. Importantly, the calculated stress due to wetting exceeds the compressive strength for some mixes, particularly those with filler-binder ratios of 0:1. This result suggests that dry, rigidly constrained foam concrete could expand with sufficient force to induce crushing of the material, when soaked with water. The compressive strength of the concrete may be diminished after initial crushing, as indicated by the crushing behaviors recorded in Section 6.9. If moisture movement is cyclical, debris may accumulate at cracks or at boundaries, causing a 'ratcheting' increase in crushing deformation.

This preliminary study indicates that this damage mechanism may be non-negligible. Further research should measure actual stresses induced by liquid uptake of foam concrete, rather than deriving the stress from the strain, and should consider creep.

Figure 6.**13c** shows images of 710 kg/m^3 neat cement foam concrete specimen, after varying conditioning regimes, as noted. Visible drying shrinkage cracking shown in the Figure under 100°C oven-drying conditions was typical across experimental program mix designs. A 50°C oven drying benchmark may be more appropriate for some tests, to minimize physical change to the air-void system. Even under gentler drying conditions, an increase in microcracking may need to be accounted for. (Refer to Section 6.14.)

Results of a preliminary test of damage due to wetting and drying are shown in Figures 6.**13d** and 6.**13e**. Specimens were conditioned for over one year at 50% RH and 25°C, immersed in water for 14 days, and then permitted to dry in air at 50% RH and 25°C. All specimens included 410kg/m^3 cementitious density.

After one wetting and drying cycle, residual mass gain and elongation were highest for SCM mixes. Microstructural changes and damage may be most significant for foam concrete mixes that incorporate SCMs. Further study is recommended to better understand how mature foam concrete is affected by moisture-related damage mechanisms such as microcracking (due to differential strain upon partial wetting); hydration; carbonation; dissolution and precipitation; and creep from wetting strain.

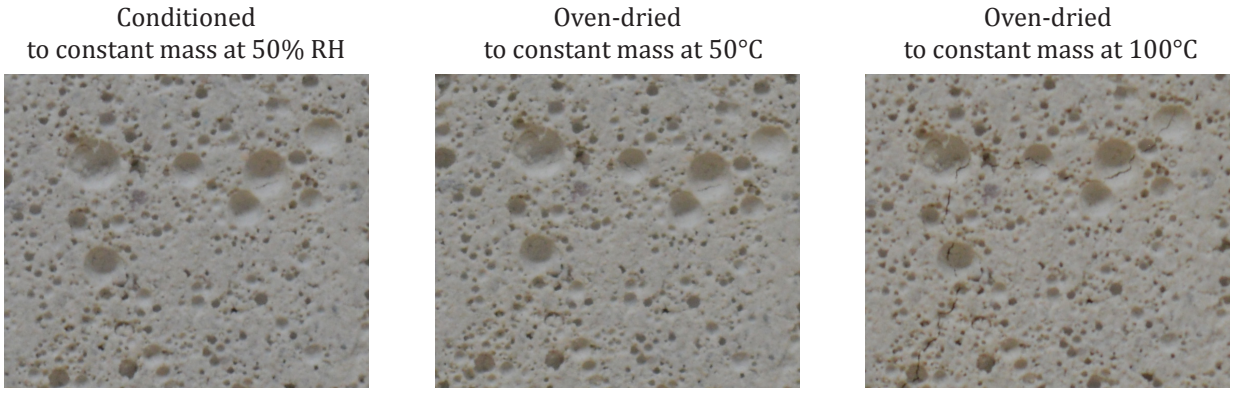

Figure 6.13c Drying at 100°C induced visible shrinkage cracking in 710kg/m^3 neat cement foam concrete. 4x magnification. (Refer also to Figures 6.14k and 6.14m.)

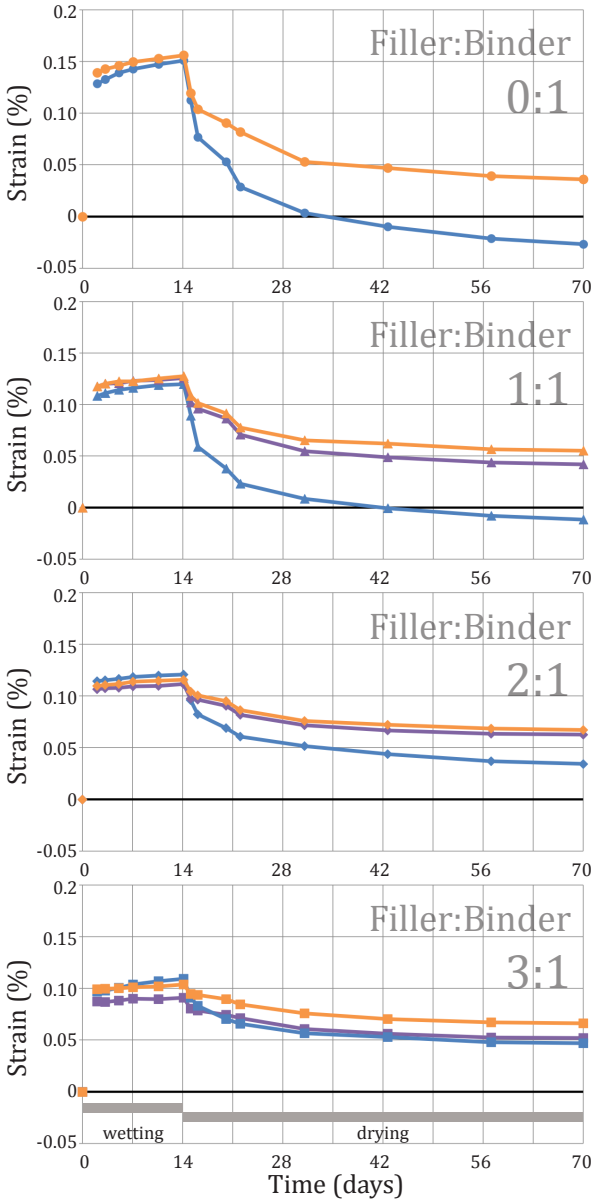

Figure 6.13d Change in length of specimens subjected to wetting, then drying.

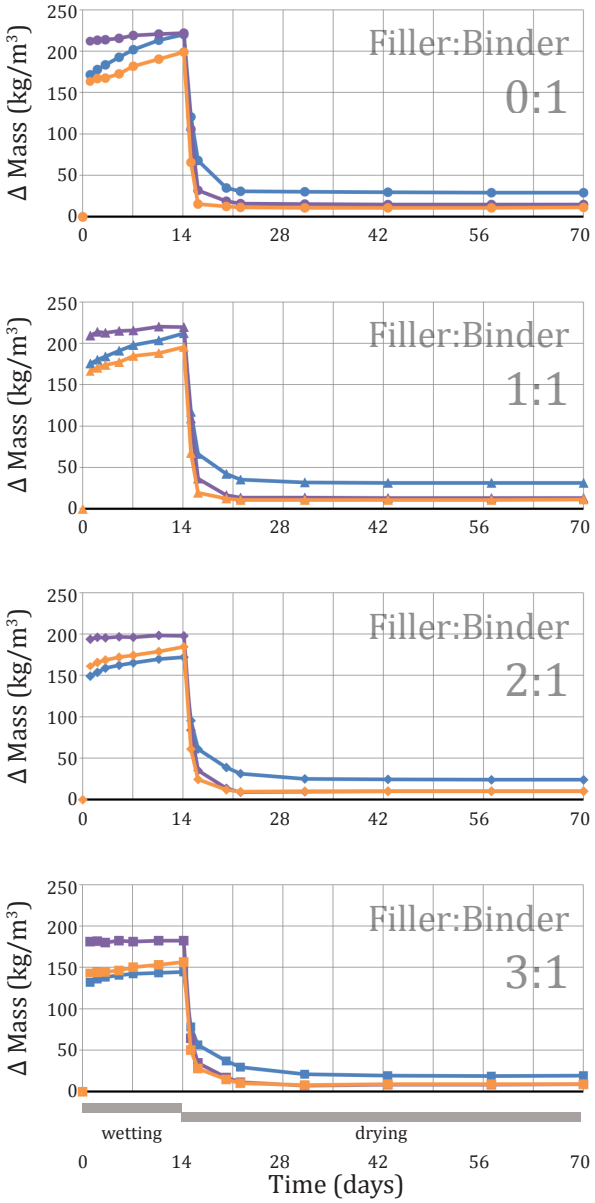

Figure 6.13e Change in mass of specimens subjected to wetting, then drying.

6.14 Capillary Water Uptake

Previous foam concrete researchers conditioned capillary water uptake (CWU) testing specimens in an oven at approximately 105°C, to drive off free water.[1] Figures 6.**14d** to 6.**14f** are based on this methodology, except that specimens were dried at 50°C until constant mass, to reduce damage to the air void system caused by shrinkage cracking.

For low-density mixes with no filler, the pattern of initial water uptake against the root of time was non-linear, indicating that water uptake was not purely one-dimensional. For example, cracking in the bulk material (e.g. due to drying shrinkage cracking during conditioning, or differential strain upon partial wetting), or damage to cell walls, would create significant paths for capillary flow (Figures 6.**14a**).

For sanded mixes, the pattern of initial water uptake against the root of time appeared to be more linear, until a nick-point time at which liquid water reached the top surface of the specimens.[2] This result is consistent with lower interconnectivity of voids.

For all cementitious blends, mixes with a filler-binder ratio of 2:1 (i.e. nominal density of 1400 kg/m^3) appeared to be optimal for suppressing CWU. At this density, interconnectivity of the air-void system is low, minimizing capillary suction. Closed air voids act as obstructions to the ingress of water, producing a tortuous path for capillary flow (Figures 6.**14b**).[3] Mixes with filler-binder ratios of 3:1 had higher water-binder ratios, and thus an increased volume of sorbing paste, increasing capillary flow[4] (Figure 6.**14c**).

Figure 6.14a CWU paths, 0:1 f/b.
Capillary suction of interconnected air voids results in high rate of CWU.

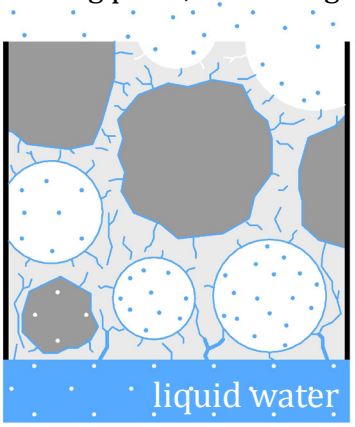

Figure 6.14b CWU paths, 2:1 f/b.
Low interconnectivity between air-voids results in lower rate of CWU.

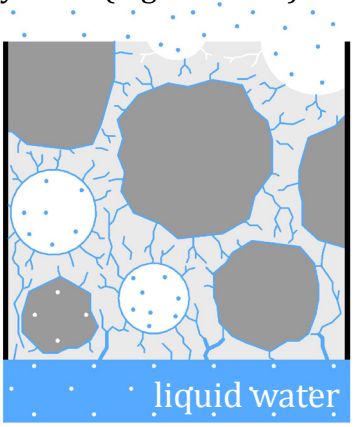

Figure 6.14c CWU paths, 3:1 f/b.
High water-binder ratios result in increased capillarity of paste.

1 Liu et al. (2014) 240, Nambiar and Ramamurthy (2007b) 1343.
2 Cf. Fagerlund (1977) 225, ISO 15148 (2002) Section 8.
3 Cf. Prim and Wittmann (1983) 66, Nambiar and Ramamurthy (2007b) 1345.
4 A similar pattern of high moisture storage was apparent for 3:1 specimens in 80% RH. Refer to Figure 6.12e.

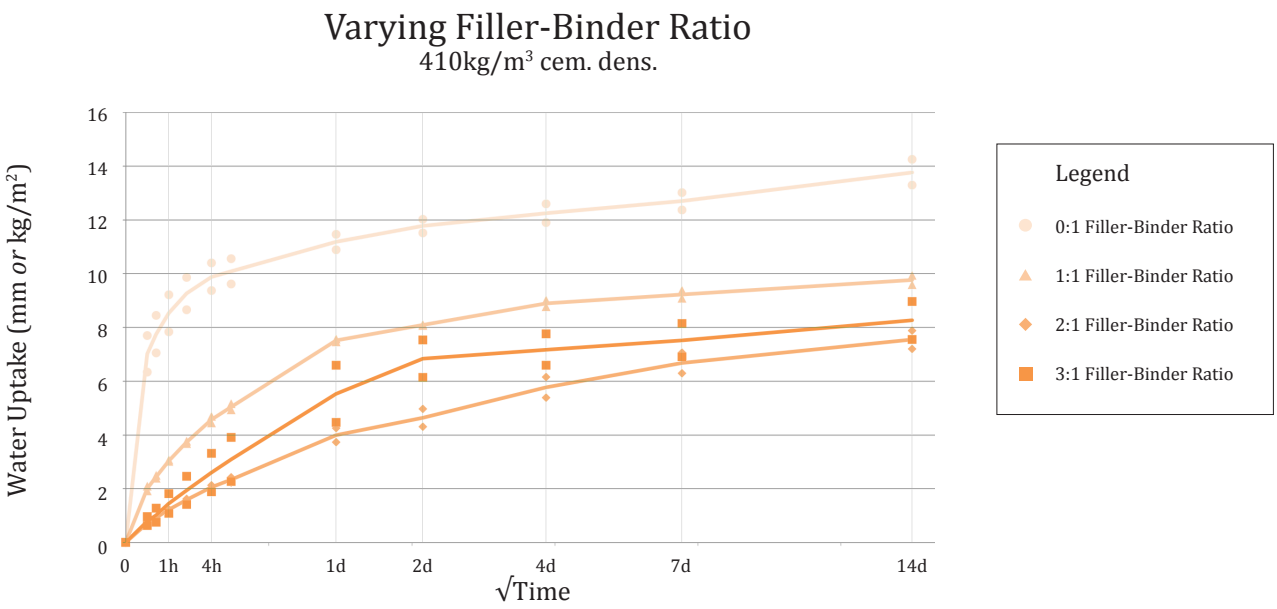

Figure 6.14d CWU of slag specimens conditioned at 50°C until constant mass.

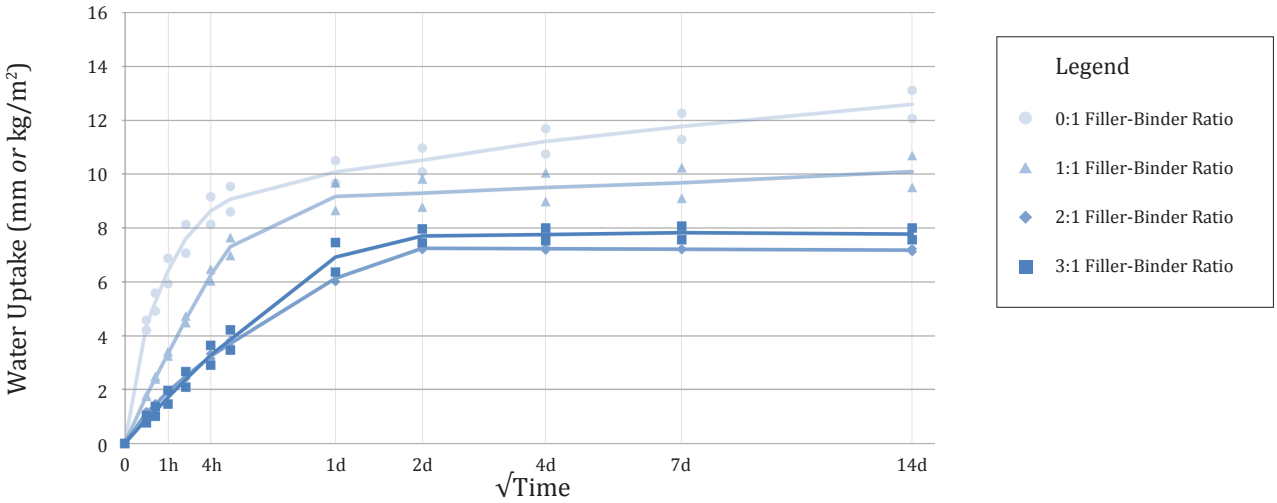

Figure 6.14e CWU of Portland cement specimens conditioned at 50°C until constant mass.

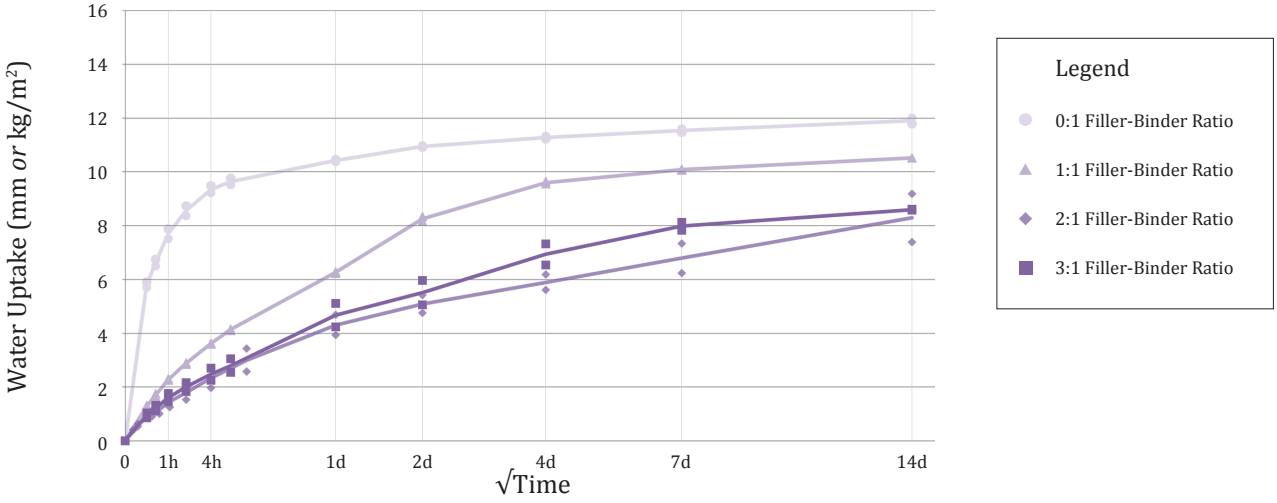

Figure 6.14f CWU of silica fume specimens conditioned at 50°C until constant mass.

Rates of CWU, during the first 0.5 hours of partial immersion, are plotted against porosity for various mixes Figure 6.**14g**. Figure 6.**14h** shows the rate of CWU following an initial period of stabilization (typically 30 minutes), until the nick-point time, i.e. the time at which water reaches the top surface of the specimen and the rate of CWU sharply decreases. Correlation coefficients were highest for sanded Portland cement and slag mixes. Note that for mixes with no filler, plots of moisture accumulation against the root of time were smoothly curved. Straight-line slopes could not be determined; instead, the rate of uptake was determined in accordance with ISO 15148[5] based on the accumulated mass 24 hours after the start of the test.

For sanded mixes, CWU was suppressed with the addition of SCMs, which may be attributed to increased impermeability resulting from improved particle packing and pozzolanic reactions (refer to Section 6.6.2). It is possible that Portland cement mixes had a higher open porosity, due to damage at the plateau boundaries (refer to Section 6.17).

For mixes with no filler, rates of CWU were higher for SCM mixes than for 100% Portland cement mixes. This effect may be a consequence of increased drying shrinkage cracking (refer to Sections 6.11 and 6.13), increasing the number of major capillary paths in the dry foamed material.

Accumulated moisture content from CWU after 1 day is plotted against porosity, in Figure 6.**14i**. Moisture content increased with porosity, except that moisture content was relatively high in mixes with a filler-binder ratio of 3:1. This trend may be due to the high water-binder ratios used for these mixes (refer to Figure 6.**14j**), which, for a given cementitious density, increase the volume of capillary-rich C-S-H sorbing paste. Moisture content at 1 day was suppressed by the use of SCMs.

Accumulated moisture content after 28 days is plotted against porosity, in Figure 6.**14k**. Patterns of moisture content at this testing time appeared to be independent of the cementitious blend used. Trends in Figures 6.**14d** to 6.**14f** indicate that for longer periods, the moisture content in SCM mixes may eventually be higher than in PC mixes.

The accumulated moisture content due to CWU is relevant for the freeze-thaw resistance of the material in-service, as elaborated in Section 6.16.

---

[5] ISO 15148 (2002), Section 8. Refer to Appendix M for further discussion.

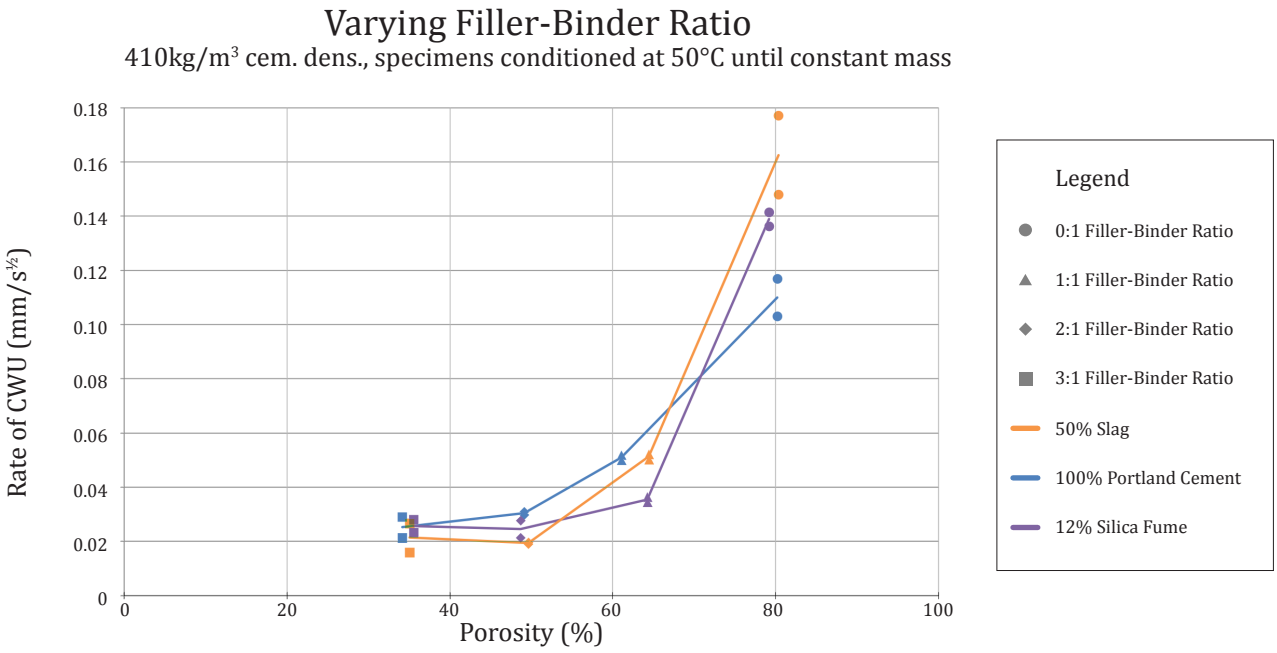

Figure 6.14g Initial rate of water uptake (0 to 0.5 hours)

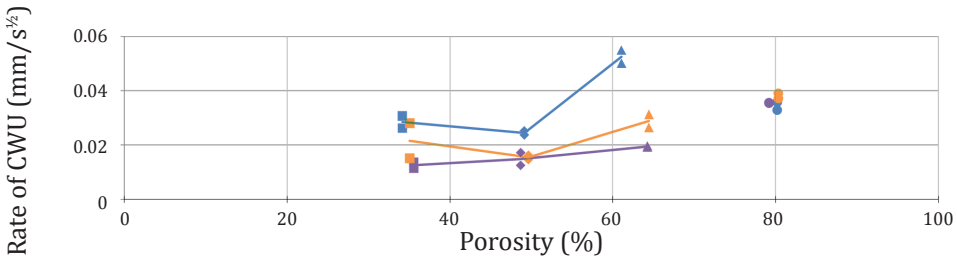

Figure 6.14h Rate of water uptake, after initial stabilization (0.5 to 4 hours)

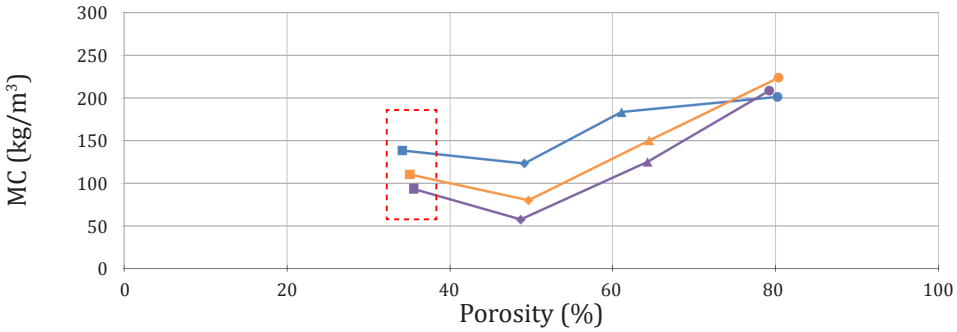

Figure 6.14i Accumulated moisture after 24 hours.

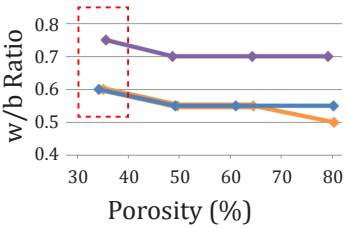

Figure 6.14j High water-binder ratios result in an increased volume of sorbing paste, which may help explain the increased CWU observed in the densest mixes.

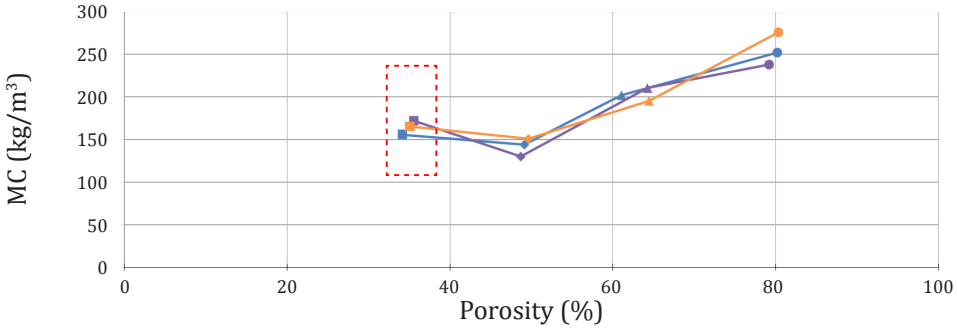

Figure 6.14k Accumulated moisture after 14 days.

Tests of capillary water uptake were repeated for other specimens, subjected to less harsh conditioning regimes.

The CWU procedure for concrete recommended in ASTM C1585 includes conditioning at 50°C and 80% RH, in order to generate internal relative humidities of between 50 and 70%.[6] Given the high permeability of foam concrete observed in Section 6.11,[7] specimens were instead stored in ambient lab conditions (23±3°C and 60±10% RH) for 3 months prior to the start of the test, achieving internal RH representative of normal indoor conditions in the field, while reducing the risk of damage from exposure to heat.

CWU of ambient-dried specimens are shown in Figure 6.**14l**, and are lower than for constant mass oven-dried specimens (Figure 6.**14n**). Three hypotheses are proposed to explain the suppression of CWU in ambient-dried specimens. First, capillary pores may have already been partially filled with moisture, thus there would be less room available for water uptake. Second, results from Section 6.12 suggest that any capillary condensation could promote sealing of interior air voids, slowing the ingress of water (refer to Figures 6.**12a** and 6.**12b**). Most significantly, damage to cell walls and drying shrinkage cracking are reduced for the ambient-dried specimens, resulting in greater closed porosity and minimizing large capillary channels. (Refer to the photographed cross-sections.)

Figure 6.**14m** depicts the CWU of specimens subjected to 3 days of oven-drying at 50°C, as an intermediate conditioning regime between ambient drying and oven-drying at 50°C to constant mass. Rates of CWU were between the results of the other two tests.

Notably, in both Figure 6.**14l** and 6.**14m**, the rate of CWU increased with porosity, while in Figure 6.**14n**, the rate of CWU was minimized at 1400 kg/m^3 nominal density. It is possible that the densest of mixes retained higher internal moisture during the mild conditioning regimes, suppressing CWU. A greater sample size would be required to more clearly discern trends. In general, the plots indicate that the conditioning regime has a significant effect on CWU of foam concrete. Where saturation values are critical determinants of performance (e.g. for evaluations of freeze-thaw resistance, cf. Section 6.16), tests should replicate conditions of CWU in the field as closely as possible.

---

6 ASTM C1585-13, Note 4.

7 Most moist- and water-cured specimens of 50mm diameter specimens desorbed fully to a 50% RH environment within approximately 56 days. 28-day water-cured specimens of 1400 kg/m^3 nominal density took up to 100 days to fully desorb. Cf. Figures 6.**11q** to 6.**11s**.

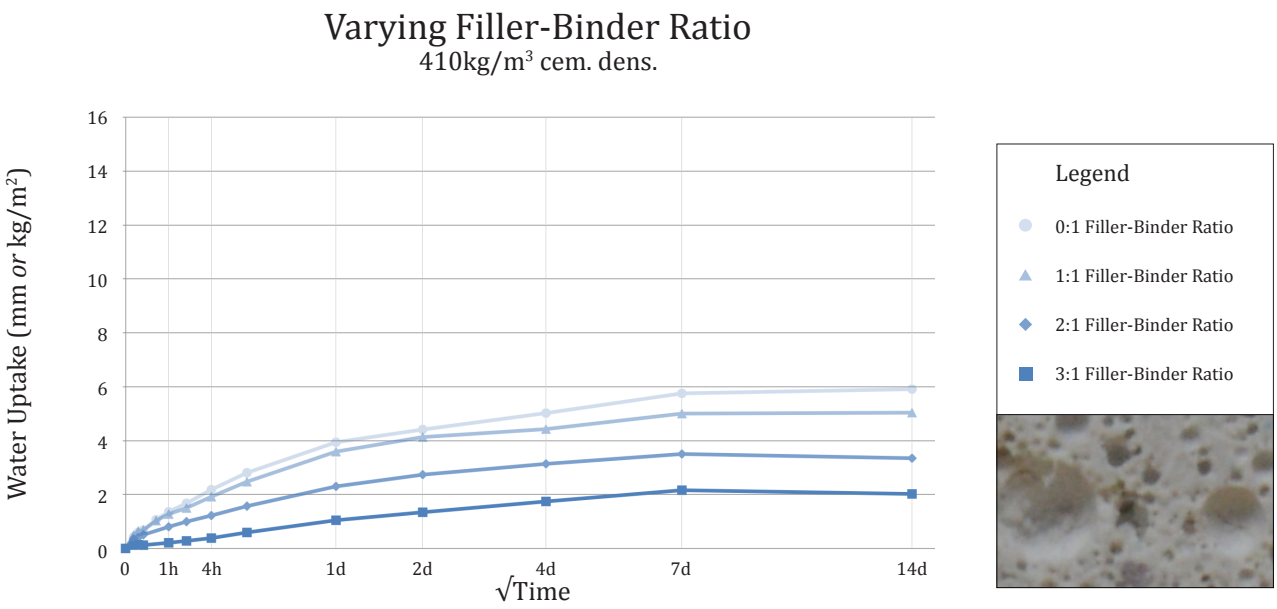

Figure 6.14l CWU of specimens conditioned in ambient lab for 3 months. Cross-section at 8x magnification.

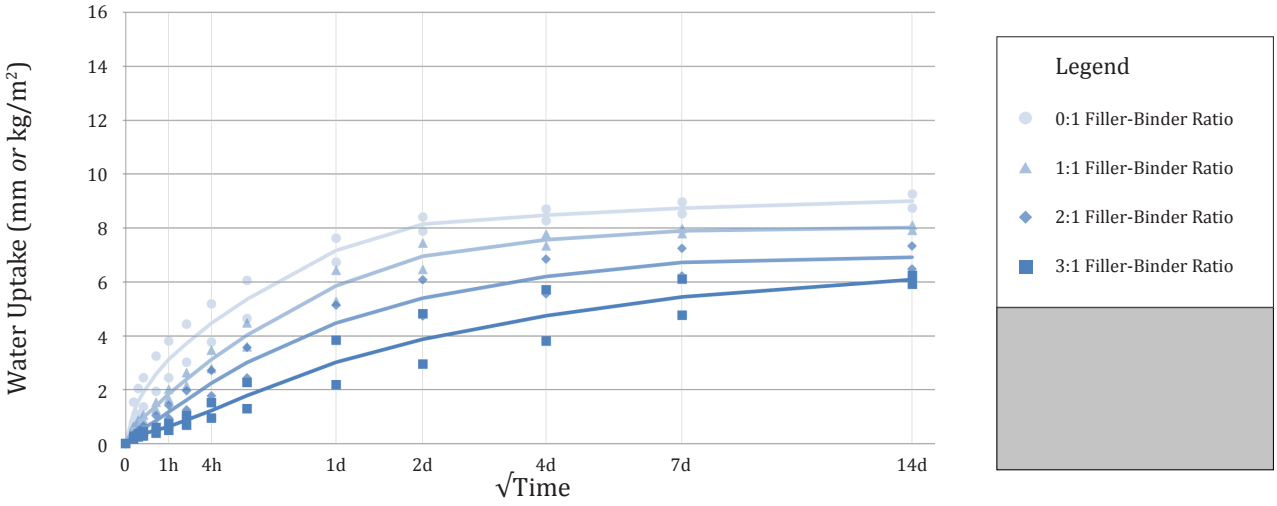

Figure 6.14m CWU of specimens conditioned at 50°C for 3 days.

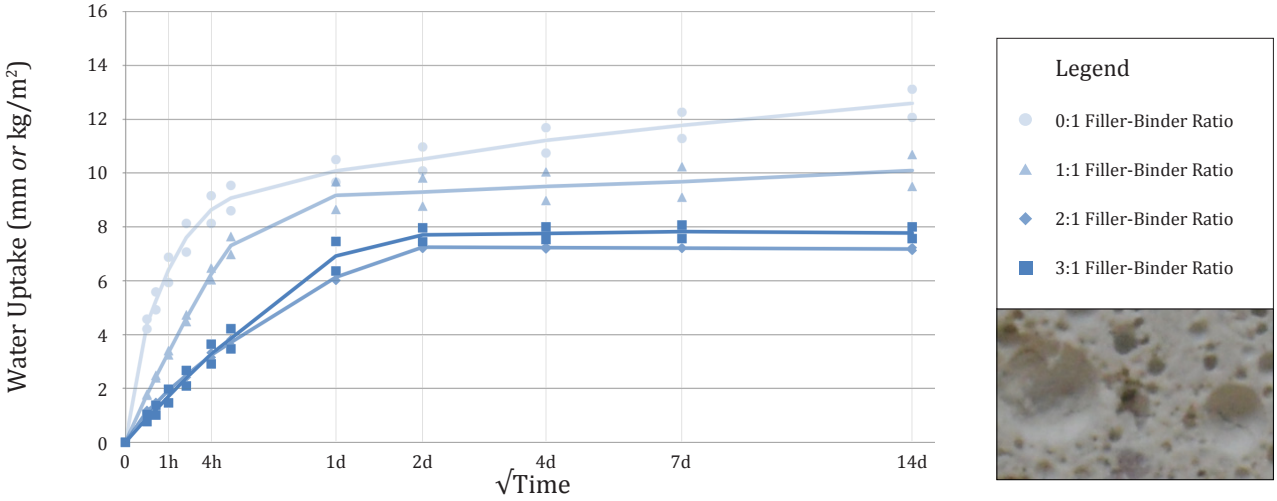

Figure 6.14n CWU of specimens conditioned at 50°C until constant mass. Cross-section at 8x magnification.

6.15 Thermal Conductivity

As for all materials, thermal conductivity of foam concrete is strongly dominated by density, as shown in Figure 6.**15a**.[1] The lowest density mix tested had a dry density of 550 kg/m^3, and thermal conductivity of 0.12 W/m·K (resistance of 8.2 m·K/W; R-1.2 per inch). The densest mix tested, with a dry density of 1775 kg/m^3, had a thermal conductivity of 0.58 W/m·K (resistance of 1.6 m·K/W; R-0.25 per inch).

Variations in mix composition did not significantly influence thermal resistance. The especially fine air voids present in silica fume mixes had no obvious effect on thermal resistivity for a given density; nor did variations in cementitious density.

Theoretical values for neat cement and sanded foam concrete, as provided in ACI Report 122,[2] are plotted on Figure 6.**15a** with a grey and black line, respectively. Thermal resistivity values from the experimental program were close to theoretical values for neat cement foam concrete. The relatively low thermal conductivity of sanded mixes in the experimental program, compared to theoretical values for sanded mixes, may be attributed to high cementitious density, and fine air-voids, creating many interruptions to radiative heat transfer.[3] Mix design is unlikely to significantly affect thermal conductivity of conventional foam concrete; factors such as moisture ingress may be more influential.[4]

Foam concrete specimens were also tested with varying hot and cold plate setpoints. Thermal resistivity decreased with increasing mean temperature, as shown in Figure 6.**15b**. This effect can be attributed principally to radiative heat transfer, q_r, which increases significantly with increasing temperature, per the Stefan–Boltzmann law:

$$q_r = \varepsilon\sigma(T_1^4 - T_2^4)$$

where ε is the emissivity of the material, σ is the Stefan–Boltzmann constant, and T_1 and T_2 are the respective temperatures of facing surfaces. By contrast, conductive heat flow is linearly dependent on the temperature gradient, and convection is negligible in foam concrete.[5] Temperature-dependent reductions in thermal resistivity may be significant for applications involving elevated temperatures (refer to Appendix A, Section 6.3.5d).

---

1 The plot shows measured values from tests with an average temperature value of 24°C (hot plate setpoint of 38°C; cold plate setpoint of 10°C). Refer to Section 5.6.1.
2 ACI 122R-02 Section 2.1
3 ACI 122R-02 does not clarify what assumptions were used in calculating theoretical values.
4 Cf. ACI 122R-02 Section 2.2
5 Refer to Appendix A, Section 6.3.4a

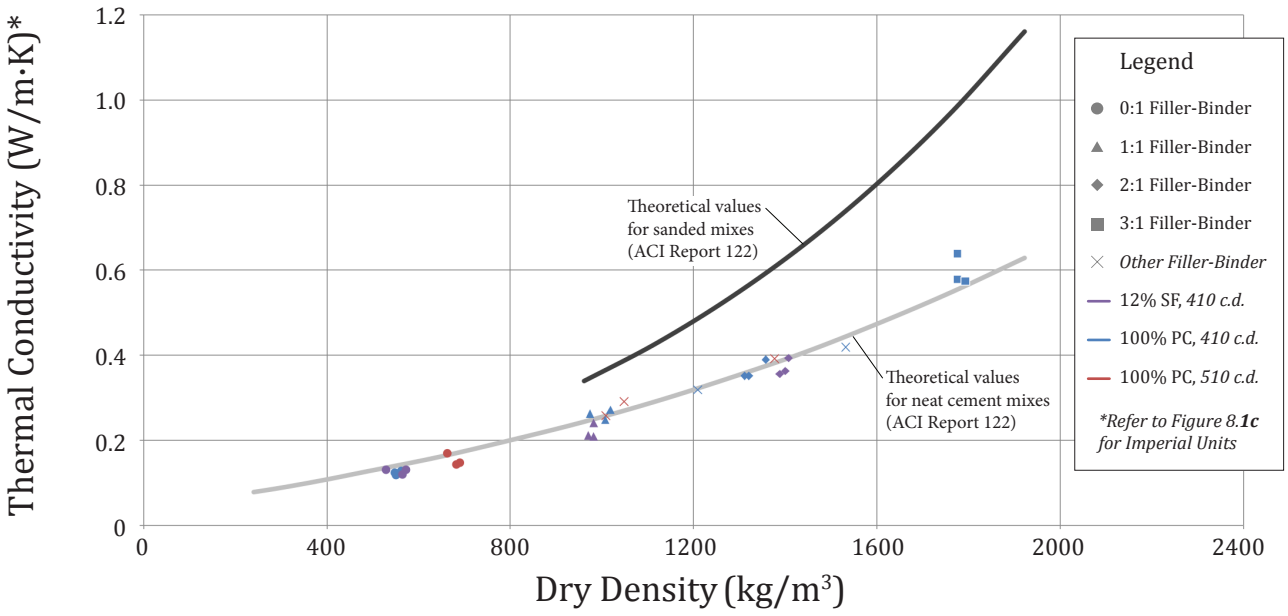

Figure 6.15a Thermal conductivity vs. dry density.

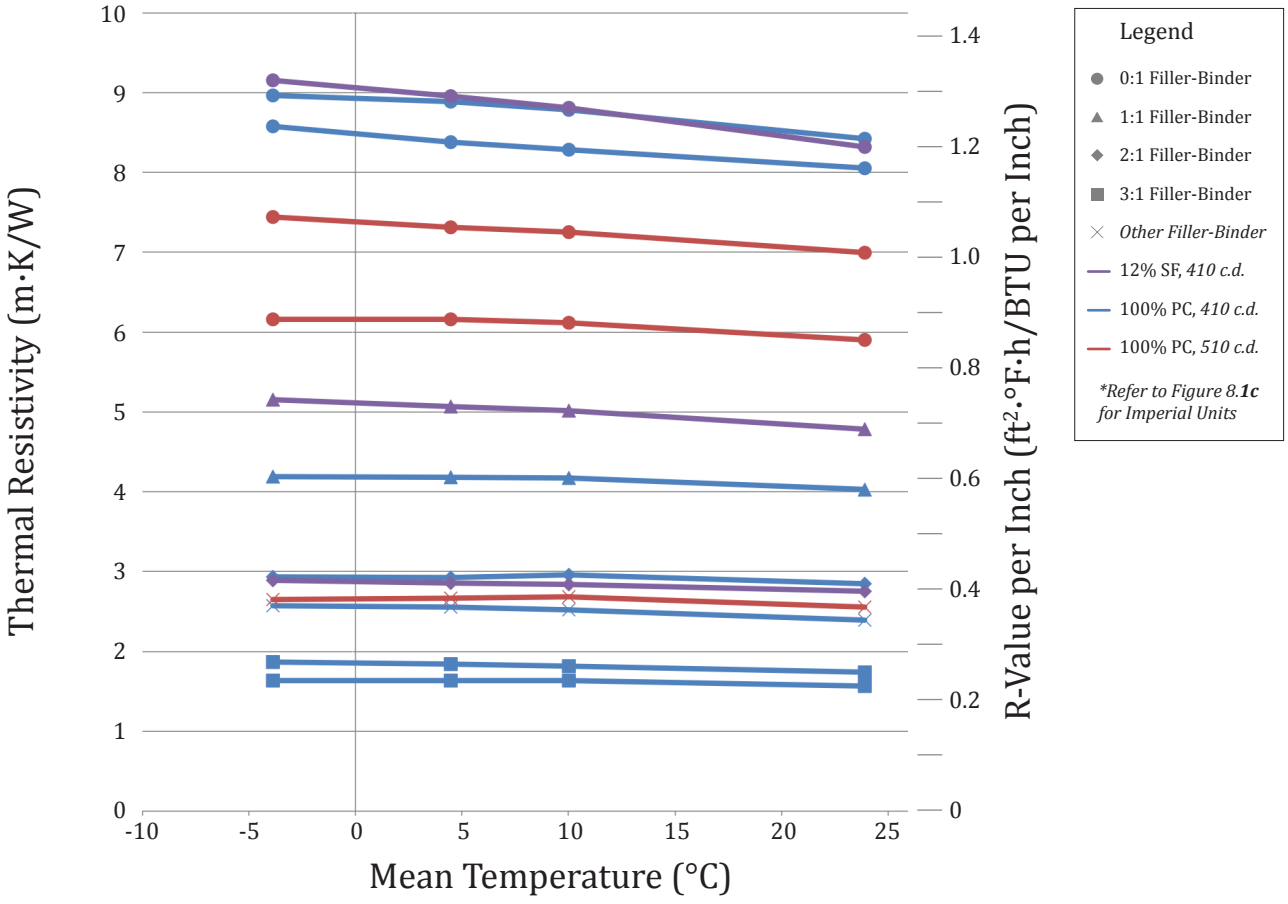

Figure 6.15b Dependence of thermal resistivity on mean temperature.

6.16 Freeze-Thaw Resistance

6.16.1 Freeze-Thaw Susceptibility: Degree of Saturation

Dilation due to freeze-thaw action is plotted against volumetric moisture content in Figures 6.**16.1a** and 6.**16.1b**, for specimens of 600 and 1400 kg/m^3 nominal density, respectively. Maximum 'safe' thresholds for moisture content, at which freeze-thaw damage was not detected, are indicated on the figures with vertical lines.

Portland cement, silica fume, and slag specimens of 1400 kg/m^3 nominal density did not experience obvious dilation for any of the moisture contents considered. Among 600 kg/m^3 nominal density mixes, slag specimens showed evidence of dilation at the lowest moisture content, above approximately 200 kg/m^3. Portland cement mixes showed signs of dilation above approximately 225 kg/m^3 M.C., while silica fume mixes dilated only after the M.C. exceeded 330 kg/m^3.

Based on the strategy articulated by Fagerlund,[1] maximum acceptable thresholds for moisture content can be compared to the actual moisture content of a material in a given situation, in order to assess the risk of freeze-thaw damage.

Anticipating the in-service moisture content of foam concrete can be a challenge. Low-density mixes, in particular, have a large volume of air voids, and a large potential for moisture storage. The actual accumulation of water will be a function of the duration of exposure to moisture; the presence of cracks (e.g. due to drying shrinkage of differential strain upon wetting); damage to cell walls, and the degree of open porosity (which is related to aging of the foamed material); pressure gradients; and numerous other factors. Sources of drainage or drying should also be considered.

Moisture accumulations during laboratory-controlled tests are shown in Figures 6.**16.1c** and 6.**16.1d**, for full and partial immersion (refer to Sections 6.12 to 6.14). MC thresholds for freeze-thaw damage are registered with a horizontal line. 18 month old 600 kg/m^3 slag, PC, and SF specimens exceeded saturation limits at 0.5, 4.4, and 8.5 days of full immersion, respectively. Notably, water ingress was slower in 12 month-old specimens with reduced head, likely due to reduced pressure and reduced aging (microcracking).

[1] Fagerlund (1977)

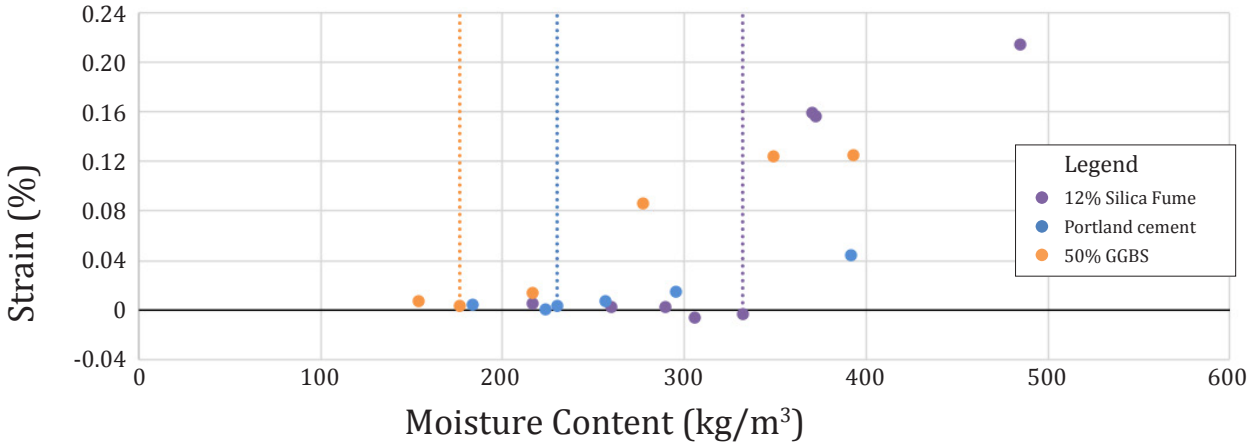

Figure 6.16.1a Freeze-thaw dilation of 600 kg/m³ specimens of varying moisture contents.

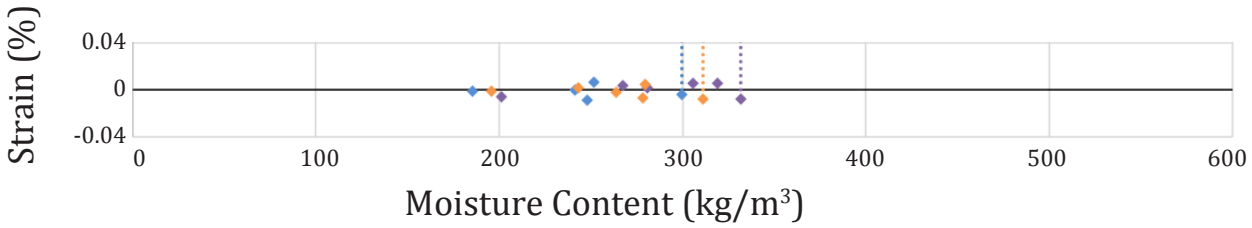

Figure 6.16.1b Freeze-thaw dilation of 1400 kg/m³ specimens of varying moisture contents.

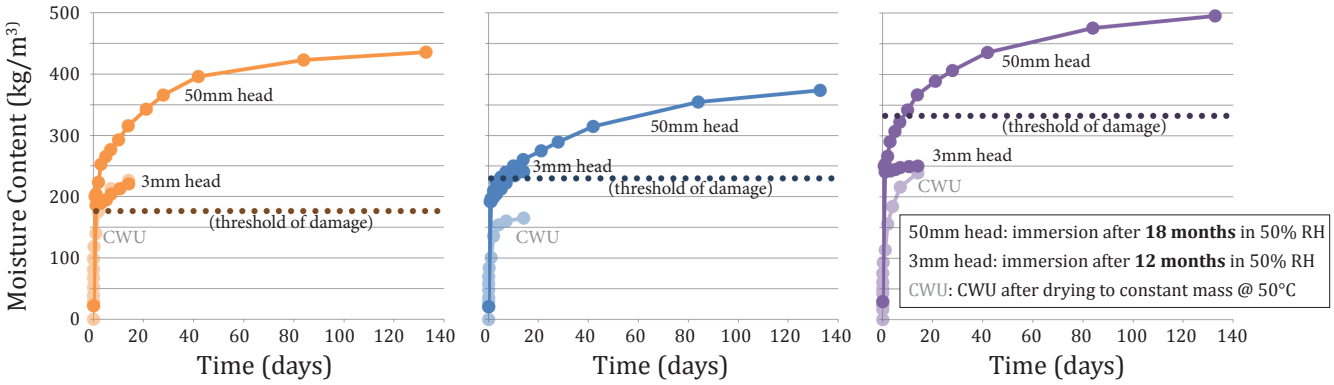

Figure 6.16.1c Moisture accumulation in 600 kg/m³ specimens during CWU and liquid immersion.

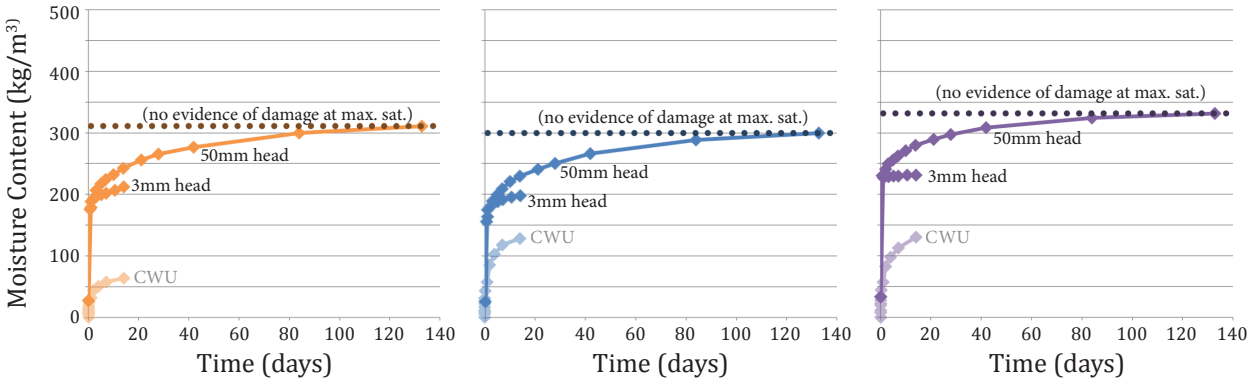

Figure 6.16.1d Moisture accumulation in 1400 kg/m³ specimens during CWU and liquid immersion.

1400 kg/m^3 specimens did not exceed saturation limits during months of full immersion.

Foam concrete appears to have special hygroscopic properties. Resulting gradations of moisture through the material should also be considered in assessing risk of freeze-thaw damage.

The pore size distribution of foam concrete strongly affects moisture transport and distribution. Foam concrete typically includes a large proportion of both capillaries and air voids. The porosity is thus bimodal ('gap graded'), with no significant porosity between 3 and 50 μm diameter (refer to Figure 6.**16.1e**). Previous work in this experimental program has indicated that when dry foam concrete is exposed to liquid water, capillary pores fill readily. Conversely, isolated air voids surrounded by saturated capillaries initially resist water ingress, but may eventually fill under hydraulic pressure, as air gases diffuse out of the voids via the capillary water (refer to Sections 6.12, 6.14 and 7.3.7).

Due to this diffusion process, the air voids closest to the surface of the concrete will tend to fill with water most quickly, while interior voids remain relatively dry. Moisture content does not appear to equilibrate readily through the specimens during wetting.

When a wetted specimen is exposed to freezing temperatures, ice crystals will thus form in saturated (or partially saturated) air voids near the surface. Water that is rigidly held in fine capillaries and gel pores cannot rearrange to form ice at normal freezing temperatures, however. This high-energy, supercooled liquid water is in thermodynamic disequilibrium with frozen water in larger pores, and will tend to migrate to low-energy, ice bearing regions.[2] The ice crystal in an air void therefore grows not only because of volumetric expansion as water transforms into ice, but also because of the ingress of supercooled water, inducing internal pressure and expansion at an unfrozen, supercoooled water layer between the ice crystal and the cell wall (Figure 6.**16.1f**).[3]

Figures 6.**16.1g** and 6.**16.1h** show images of the spalled surfaces of foam concrete, following freeze-thaw testing. Damage is apparent at the surface of the specimen, where air voids would tend to be most saturated.

It is possible that dry interiors of dilated specimens remained undamaged, since interior moisture contents may not have been high enough to fill interior air voids with ice.

---

2 Mehta (1986) 123.

3 Valenza and Scherer (2006) 1164-1165

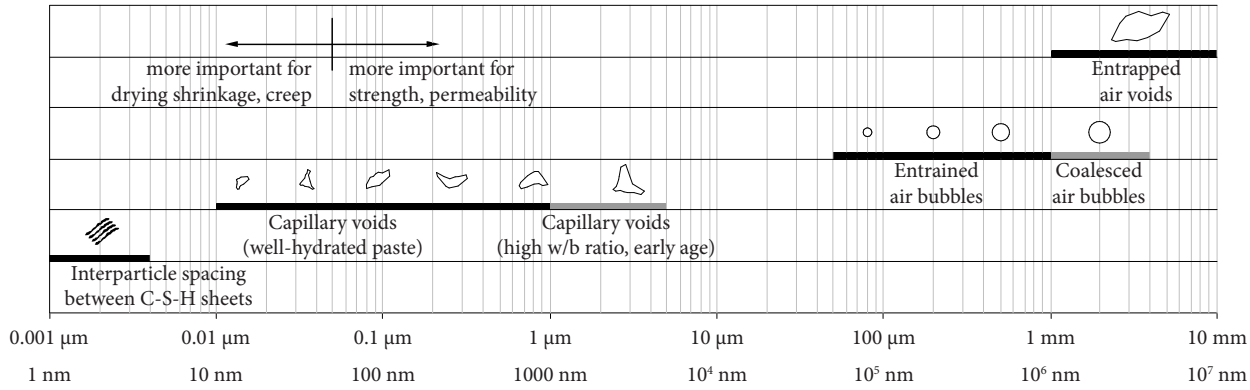

Figure 6.16.1e Scale of voids in concrete. Refer to Appendix A, Section 6.2.3. After Mehta (1986).

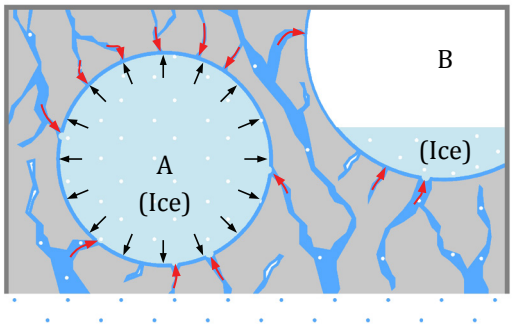

Specimen initially conditioned to 50% RH.
All available surfaces exposed to liquid water.
Specimen exposed to freezing temperatures.

Air voids closest to the specimen surface will tend to fill with water most quickly (A), while interior voids remain relatively dry (B). Ice crystals form in the saturated air voids. Supercooled liquid from surrounding capillaries migrates to the low-energy frozen sites (red arrows), contributing to tensile hoop stresses in the air-void wall (black arrows).

Figure 6.16.1f Proposed model of freezing event, following long-term immersion in water.

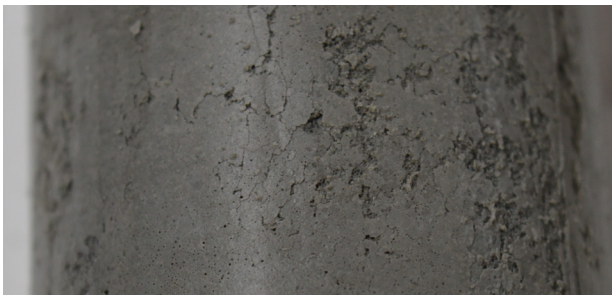

Figure 6.16.1g Scaled surface, 600 kg/m^3 specimen.

Figure 6.16.1h Scaled surface, 1400 kg/m^3 specimen.

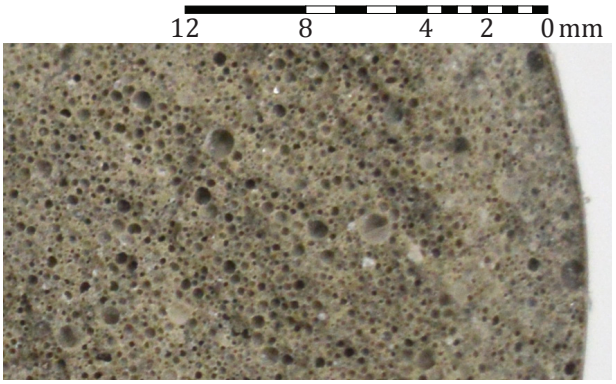

Figure 6.16.1i Specimen immersed 140 days, frozen, and fractured. 4x magnification.

Figure 6.16.1j Scaled surface near DEMEC disc, 600 kg/m^3 specimen.

Figure 6.**16.1i** shows the cross-section of a specimen that was immersed in water for 140 days, blotted with a damp cloth to remove excess moisture, frozen, and then fractured. Water is obvious in the air-voids near the surface, while interior air-voids are drier.

Rather, measured dilation is likely due to expansion of the foam concrete near the surface, where the DEMEC locating discs were epoxied to the specimen. Figure 6.**16.1j** shows freeze-thaw damage in the region of the epoxied DEMEC locating discs at the specimen surface, where the local degree of saturation would be high.

Alterations to the experimental setup were considered, to facilitate more consistent saturation throughout the air-void system of a specimen. For example, a smaller specimen size could reduce variability in moisture content through the specimen cross-section. Alternatively, a process of vacuum saturation, followed by drying to a given mass, may encourage more even distribution of moisture in the air void system: ingress of water into a dry foam concrete specimen is resisted for the reasons explained above, but migration of water out of a saturated specimen occurs more readily, since internal water can diffuse out via relatively dry, open capillary paths. (Refer to Figures 6.**16.1k** and 6.**16.1l**.)

These changes would incur certain disadvantages, however. Microcracking may occur with cutting and handling of thin pieces, affecting capillary flow. Furthermore, Figure 6.**16.1i** indicates that saturation may only progress a few millimeters deep, even after a long period of immersion, requiring exceptionally thin specimens. A process involving vacuum saturation would introduce water in voids that might not fill in normal wetting situations, therefore moisture distribution may not be realistic.

The experimental program, as conducted, serves to exhibit the freeze-thaw damage mechanism of foam concrete exposed to normal wetting. Data and photographs indicate that even when foam concrete is exposed to a source of liquid water for a very long time, only the specimen surface becomes sufficiently saturated to facilitate freeze-thaw damage.

Fortunately, despite uncertainty about the exact moisture distribution through specimens, Figures 6.**16.1c** and 6.**16.1d** are nevertheless useful for estimating maximum recommended immersion times. Moisture ingress increased with time, and upon reaching critical local degrees of saturation at the surface, freeze-thaw damage was registered at the DEMEC gauges. Maximum recommended immersion times are plotted in Figure 6.**16.1m**.

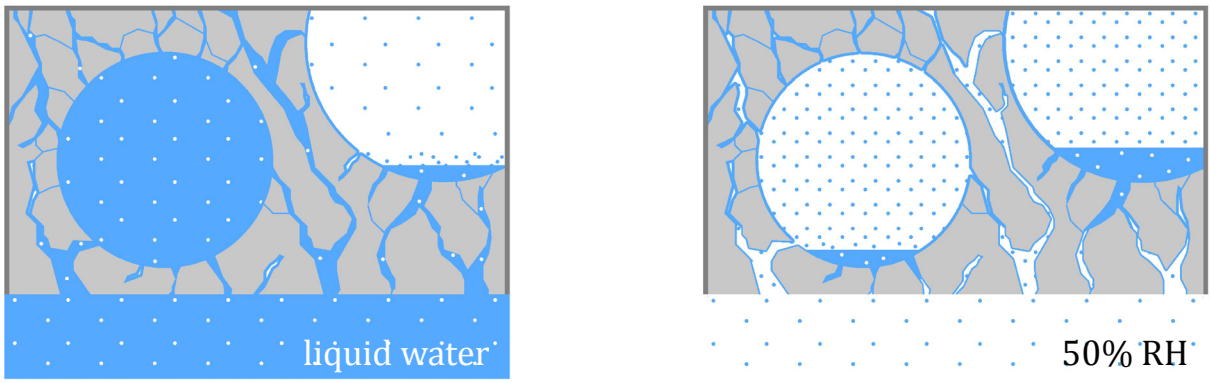

Figure 6.16.1k Moisture is concentrated near the specimen surface during long term immersion in water (left). Moisture diffuses more readily throughout the specimen during drying after vacuum saturation, via relatively dry capillary paths (right).

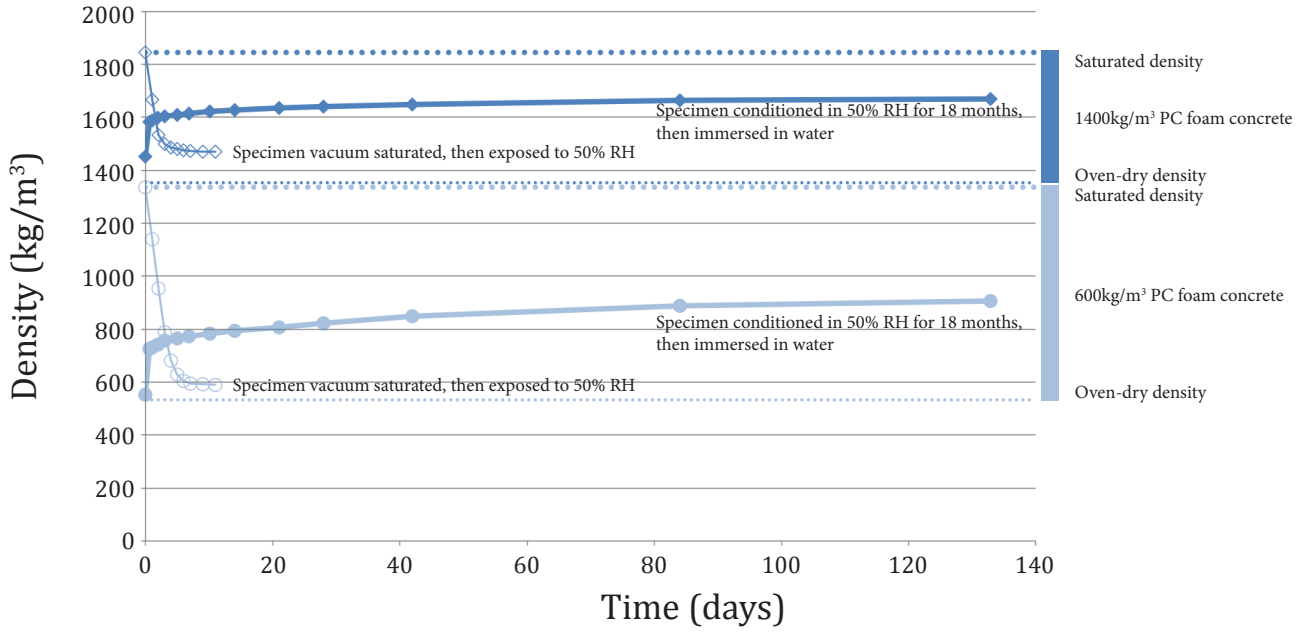

Figure 6.16.1l Changes in density upon wetting and drying for 600 and 1400 kg/m³ PC specimens. Vacuum saturated specimens release moisture readily via open capillary paths, while moisture ingress into dry specimens is slow after capillary saturation, since air voids are 'sealed'.

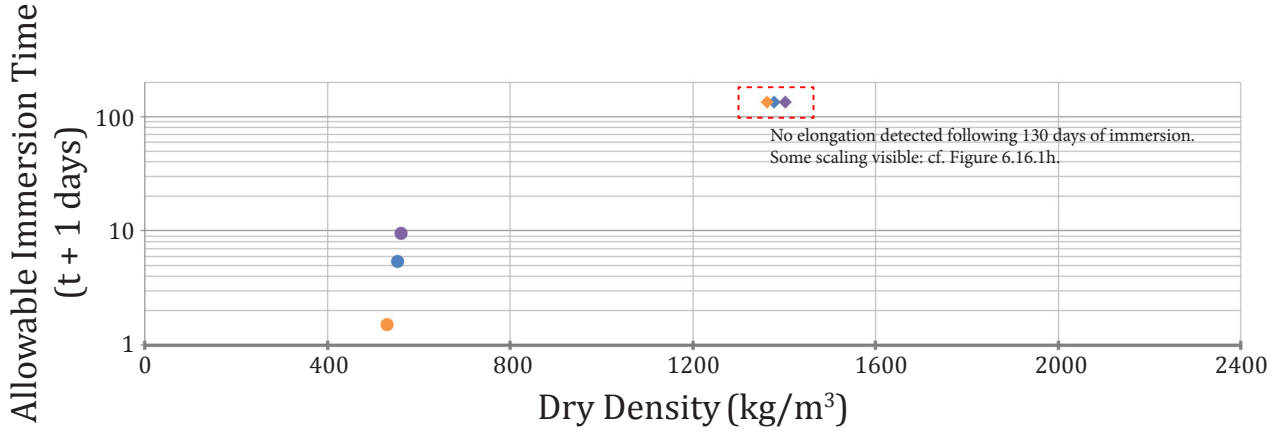

Figure 6.16.1m Allowable immersion time (without risk of freeze-thaw damage) vs. dry density, 50mm head.

6.16.2 Freeze-Thaw Susceptibility: Saline Scaling

Susceptibility to salt scaling does not correlate with susceptibility to internal frost action. Valenza and Scherer[1] have shown that while internal frost action is a function of crystallization pressures within pores, salt scaling is better explained as the result of a glue-spall mechanism, where a thermal expansion mismatch between the ice and the concrete induces stresses along the interface of the composite solid.

This mechanism is consistent with the high rates of scaling observed for foam concrete in Figure 6.**16.2a**. The interfacial bond between foam concrete and surface ice will typically be very strong, due to the high degree of saturation in capillaries and air-voids at the foam concrete surface. Brine pockets in the ice promote cracking of the ice, which propagates into the surface of the concrete. The foam concrete matrix has very little capacity to resist the resultant tensile and shearing stresses.

Particle packing effects will tend to increase the proportion of paste in the upper surface of a slab, and upward migration of water and bubbles during mixing will tend to make upper regions especially porous. These microstructural characteristics may account for the fast initial rate of mass loss observed. Within 10 cycles, three of the four slabs tested had already exceeded the 0.80 kg/m^2 limit for assessments of normal density concrete made with coarse aggregate.[2] Subsequent reduction in the rate of scaling may be attributed to reduced permeability, enriched salt concentration (i.e. above the 'pessimistic' concentration at which freeze-thaw damage is maximized[3]) due to the sublimation of water into the environment of the freezing chamber and replacement of solute water, or restraint provided by exposed aggregate (arresting cracks in the ice).

Average loss of depth was calculated based on the oven-dry mass of the scale, and is presented in Figure 6.**16.2b**. The progress of damage is shown in Figures 6.**16.2d** to 6.**16.2f**. Notably, specimens in distilled water experienced a slow rate of damage, despite high degrees of saturation at the surface. The slow rate of cooling would have provided more time for moisture transport than in Section 6.16.1, facilitating safe accumulation of super-cooled water in ice-bearing air-voids. (Refer to Figures 6.**16.2c** and 6.**16.1c**).

---

1 Valenza and Scherer (2006) 1164-1165

2 OPSS 1002, Section 1002.05.03.02.01. Cf. results for air-entrained normal density concrete, Appendix M.

3 The pessimistic concentration for saline scaling is approximately 3% by weight, independent of the solute used (inorganic salt, urea, or ethyl alcohol). Cf. Verbeck and Klieger (1957), Valenza and Scherer (2006) 1161

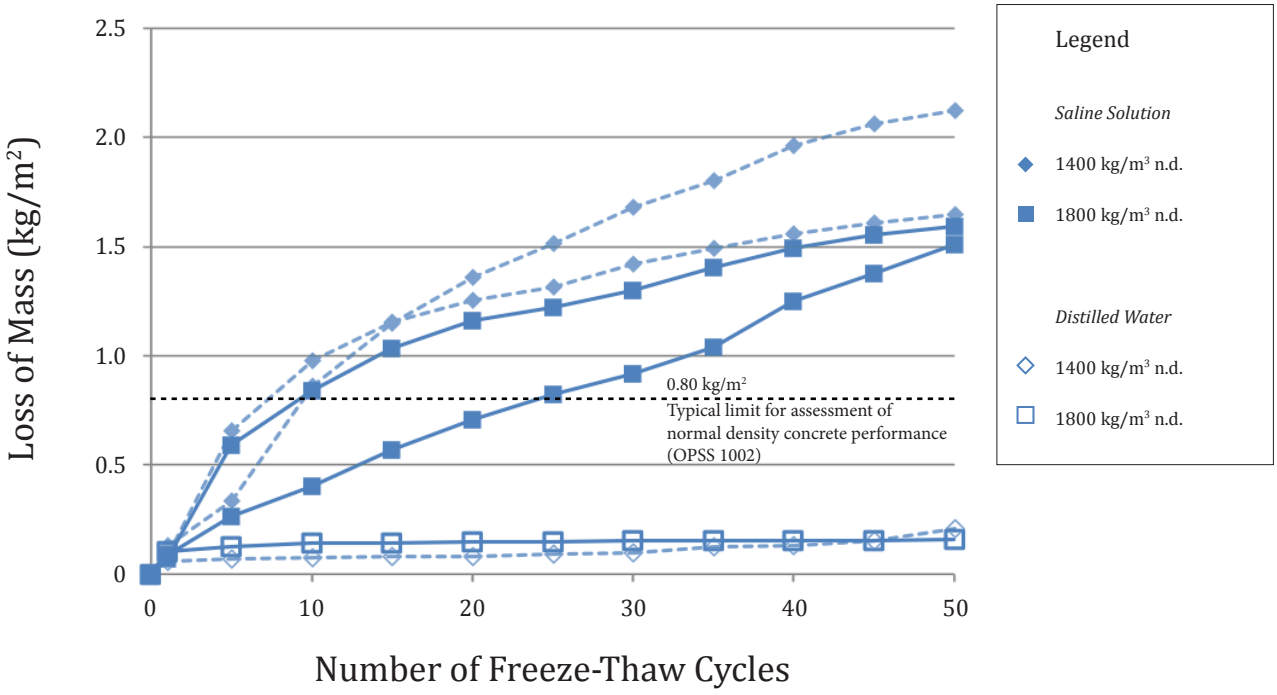

Figure 6.16.2a Loss of mass due to saline freeze-thaw scaling.

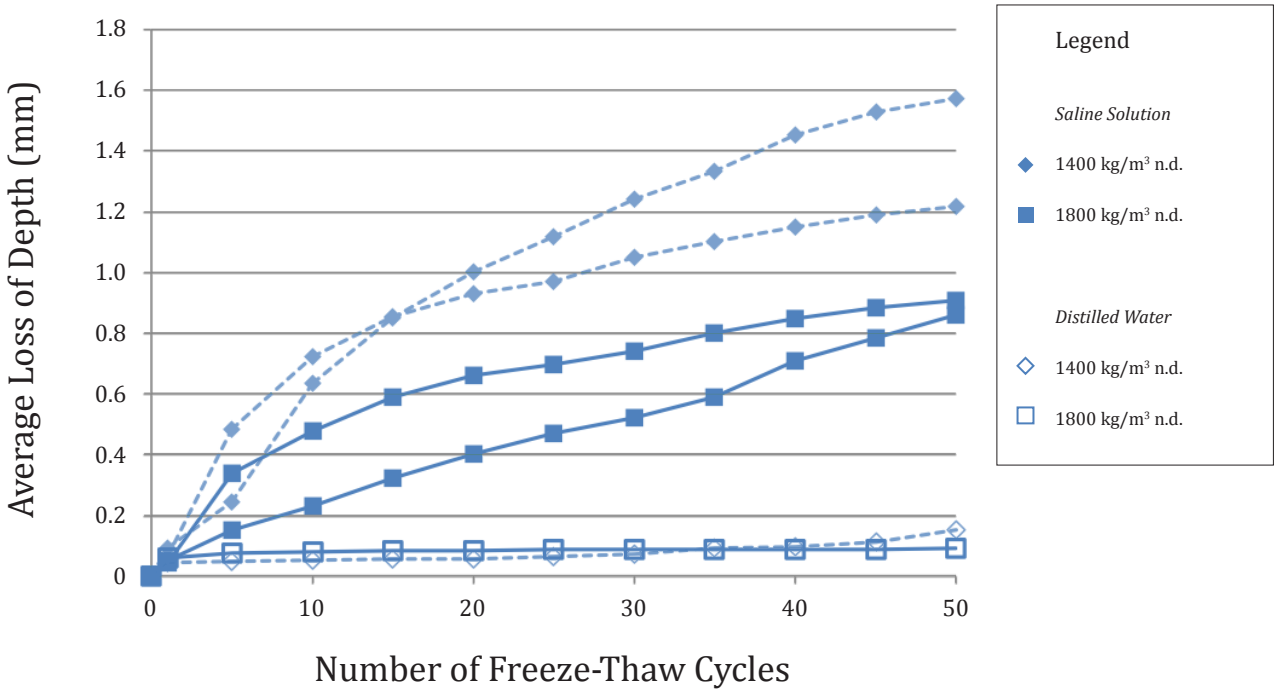

Figure 6.16.2b Average loss of depth due to saline freeze-thaw scaling.

1400 kg/m^3 n.d.

2:1 Filler-binder ratio
410 kg/m^3 c.d.

0 Cycles | 5 Cycles | 10 Cycles

Distilled Water

Figure 6.16.2c

Saline Solution

Figure 6.16.2d

1800 kg/m^3 n.d.

3:1 Filler-binder ratio
410 kg/m^3 c.d.

0 Cycles | 5 Cycles | 10 Cycles

Distilled Water

Figure 6.16.2e

Saline Solution

Figure 6.16.2f

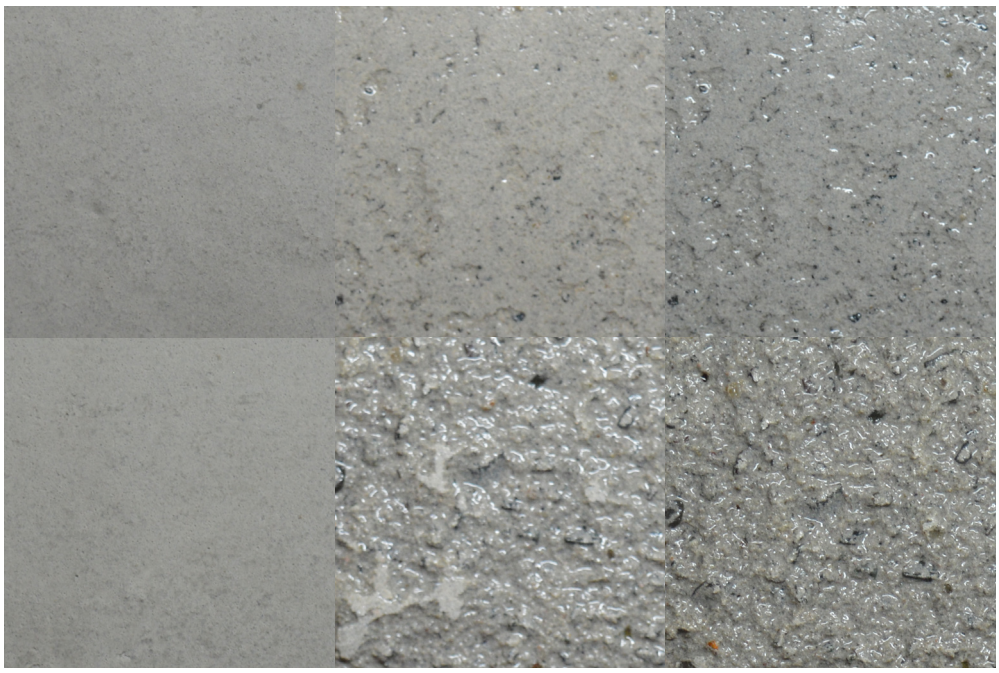

All Images at 1x Magnification

0 8 16 32 48 mm

20 Cycles 30 Cycles 40 Cycles 50 Cycles

20 Cycles 30 Cycles 40 Cycles 50 Cycles

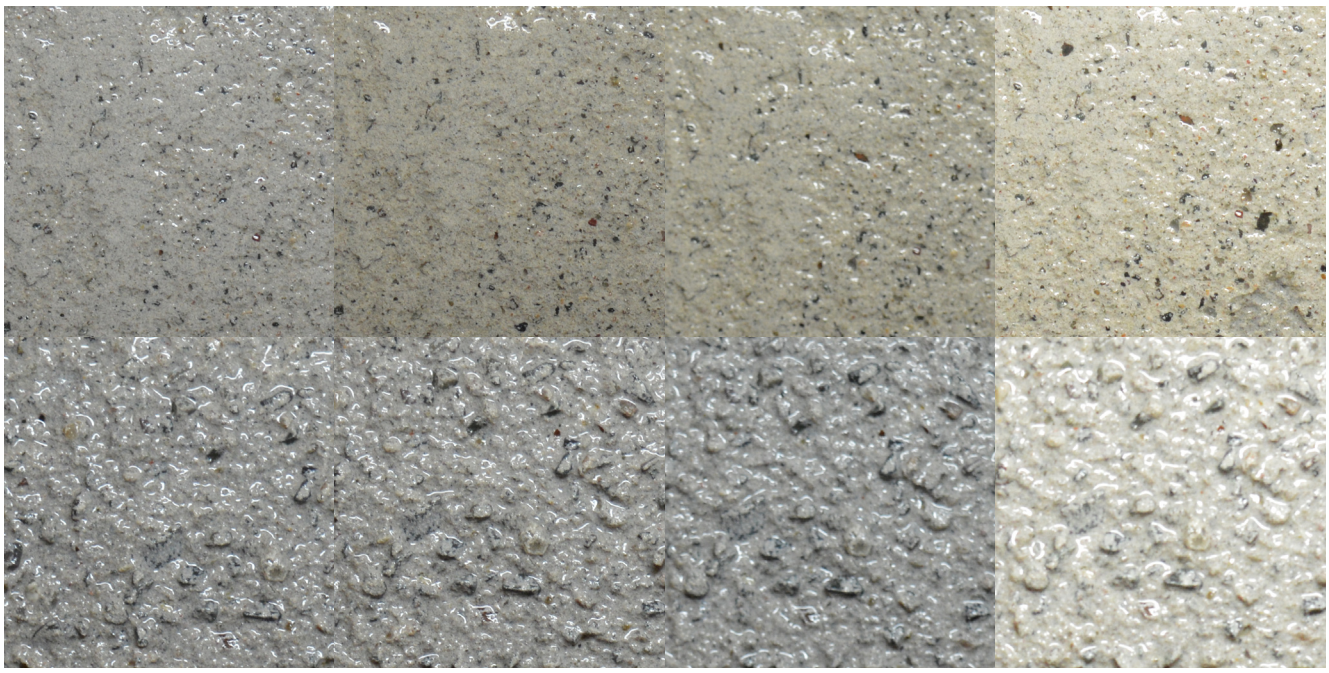

All Images at 1x Magnification

0 8 16 32 48 mm

6.17 Microstructural Analysis

6.17.1 Qualitative Analysis

Images of specimens oven-dried to 105°C are given in Figures 6.**17.1a** to 6.**17.1d**, at magnification levels of 1x, 2x, 4x, and 8x, respectively, as indicated. Photographs show the relative size distribution and circularity of air-voids, and indicate the effects of strong drying on shrinkage cracking and interconnectedness of air void systems.

At 1x magnification (Figures 6.**17.1a**), significant cracking of the bulk material is obvious in mixes with no filler. Cracking due to oven-drying affects properties such as permeability and capillary water uptake (refer to Section 6.14).

Rough surfaces are evident in Portland binder mixes with filler-binder ratios of 1:1 or 1.5:1, where the circular saw blade for cutting the samples has pushed fine aggregate across the weak surface of the mix, inscribing grooves. Photos of denser sanded mixes reveal that large grains of sand are well distributed.

Images at 2x magnification (Figure 6.**17.1b**) show that air void size diminishes with increasing filler content. It appears that the largest voids are present in mixes with 100% Portland binder or 30% slag, and no filler. These large voids are flaws in the matrix, and may be especially detrimental to mechanical strength, according to the Griffith criterion of fracture. High proportions of fine SCMs in other mixes may improve particle packing, promoting the production of a strong skeletal skin during concrete set up and reducing bubble coalescence.

At 4x magnification (Figure 6.**17.1c**), holes and cracking are visible in the cell walls of mixes with no filler, especially the Portland binder and 30% slag mixes. Cracking increases the interconnectivity of the air-void structure, with implications on permeability and capillary water uptake. This damage is likely due in large part to the oven-drying regime (refer to Section 6.13). Irregular voids are visible on the surface of mixes with filler-binder ratios from 1:1 to 2:1, where large sand particles have been eroded from the weak paste by the specimen cutting blade. Mixes with filler-binder ratios of 3:1 appear to be strong enough to resist the erosion of large sand particles. In these densest mixes, the average pore size appears to be very small; there are also regions of hardened paste with no apparent air voids, for example, in the mixes with 6 and 12% silica fume.

At 8x magnification, the degree of circularity of air voids may be observed qualitatively, especially in mixes with filler cement ratios of 0:1 and 3:1, where the visible surface is least damaged. Small voids appear to be highly spherical, while some larger, coalesced air voids are slightly oblong or irregular. In general, however, the air voids are reasonably circular.

6.17.2 Quantitative Analysis

The sequence of converting scanned cross-sections into air-void size distribution data is demonstrated in Figures 6.**17.2a** to 6.**17.2c**. Refer to Section 5.8.2 for a written description of this process. The resulting plot of air-void distribution for Portland cement, slag, and silica fume mixes with no filler is presented in Figure 6.**17.2d**.

When 'dry foam'[1] bubbles are first produced, they may be as small as 0.1 mm in diameter. Significantly larger voids may result while the foam is mixed into the cementitious slurry, due to coalescence.[2]

The air-void distribution plot indicates that bubble coalescence was relatively low in slag and silica fume mixes. Almost 30% of these air-void systems was composed of voids less than 0.5 mm in diameter, and approximately 75% of these air-void systems was composed of voids less than 1.0 mm in diameter. As suggested previously in this chapter, the fine particle sizes of the SCMs likely contribute to good particle packing, allowing for the creation of an even coating of solids around individual bubbles. High water-binder ratios used in the silica fume mix may facilitate through-solution hydration, rapidly reducing the scale of cementitious solids in the mix and further improving particle packing.

By contrast, significant coalescence was apparent in the Portland cement specimen. Only 40% of the area of the air-void system was composed of voids less than 1.0 mm in diameter. Approximately 20% of the area of the air-void system was composed of voids larger than 2.0 mm in diameter. Foam instability may be attributed to the coarseness or dryness of solids, or particle charges that upset the electrostatic balance of the surfactant.

The largest air voids detected were 4.2, 3.5, and 2.8mm, for Portland cement, slag, and silica fume specimens, respectively. These sizes correlate with the respective

1 Refer to Appendix A, Section 5.2.1b.
2 Brady et al. (2001) 2

Filler-Binder Ratio	0	0.5	1
Cementitious Blend			
12% Silica Fume			
6% Silica Fume			
100% Portland			
30% Slag			
50% Slag			

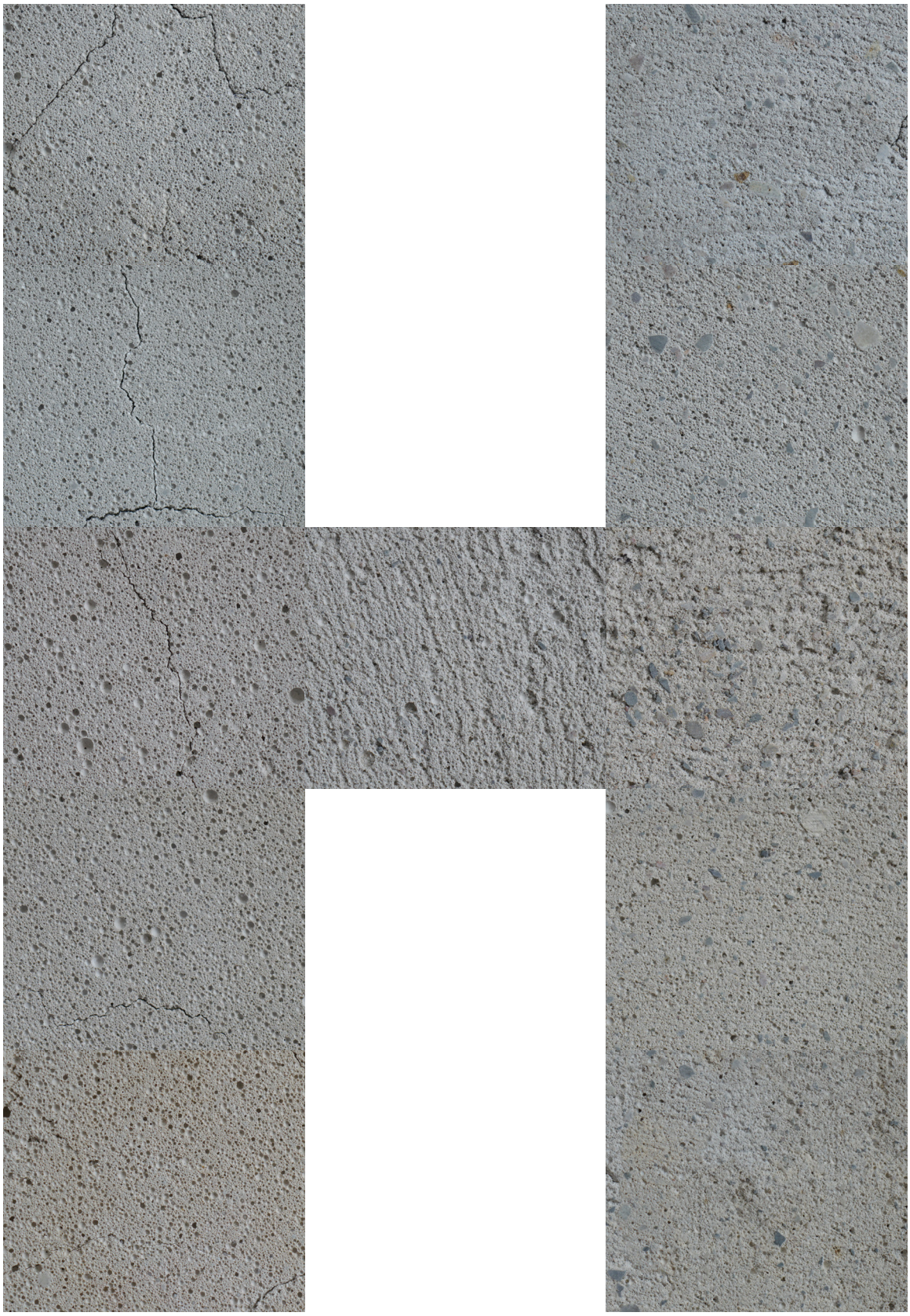

Figure 6.17.1a Foam concrete specimen sections at 1x magnification.

Foam Concrete Specimen Sections

All Images at 1x Magnification

0 8 16 32 48 mm

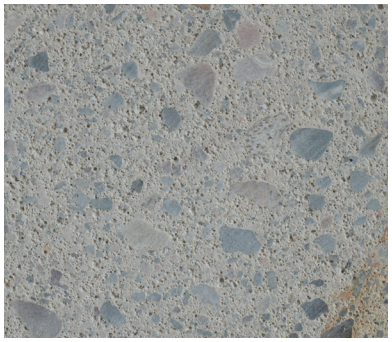

Figure 6.17.1b Foam concrete specimen sections at 2x magnification.

Foam Concrete Specimen Sections

All Images at 2x Magnification

0 4 8 16 24 mm

Filler-Binder Ratio	0	0.5	1
Cementitious Blend			
12% Silica Fume			
6% Silica Fume			
100% Portland			
30% Slag			
50% Slag			

Figure 6.17.1c Foam concrete specimen sections at 4x magnification.

Foam Concrete Specimen Sections

All Images at 4x Magnification

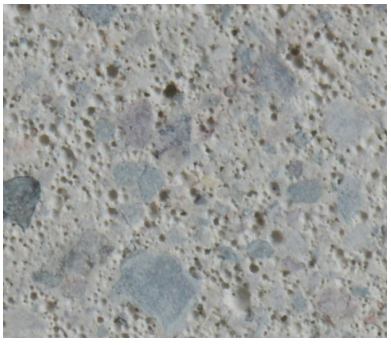

Filler-Binder Ratio	0	0.5	1
Cementitious Blend			
12% Silica Fume	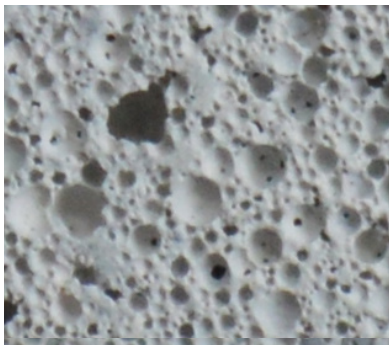		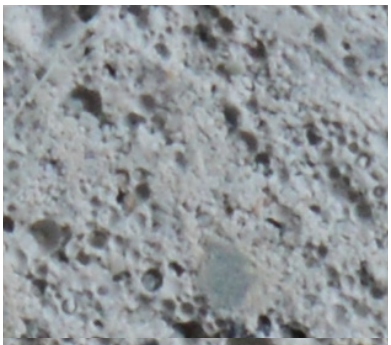
6% Silica Fume			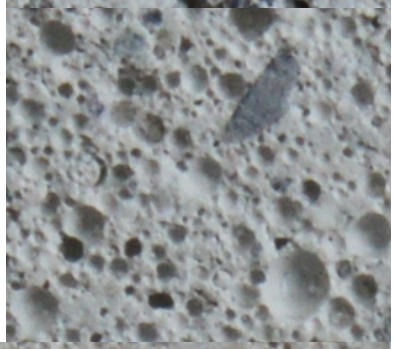
100% Portland		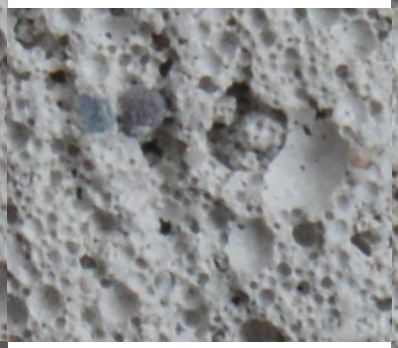	
30% Slag			
50% Slag	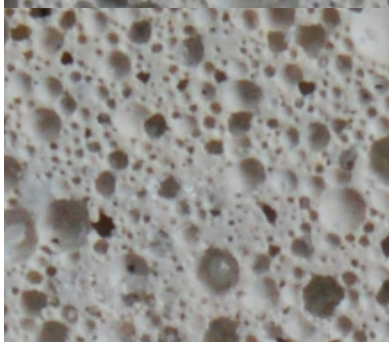		

Figure 6.17.1d Foam concrete specimen sections at 8x magnification.

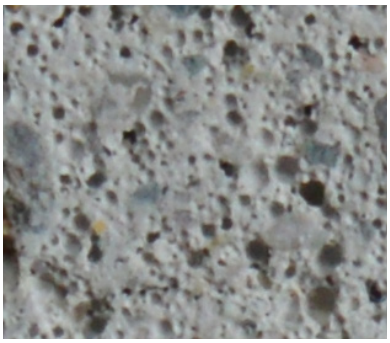

Foam Concrete Specimen Sections

All Images at 8x Magnification

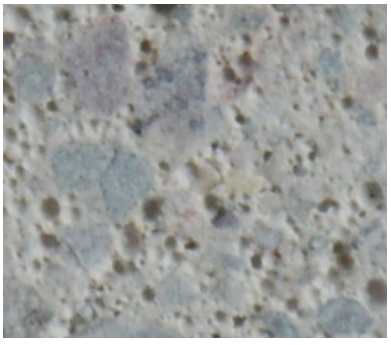

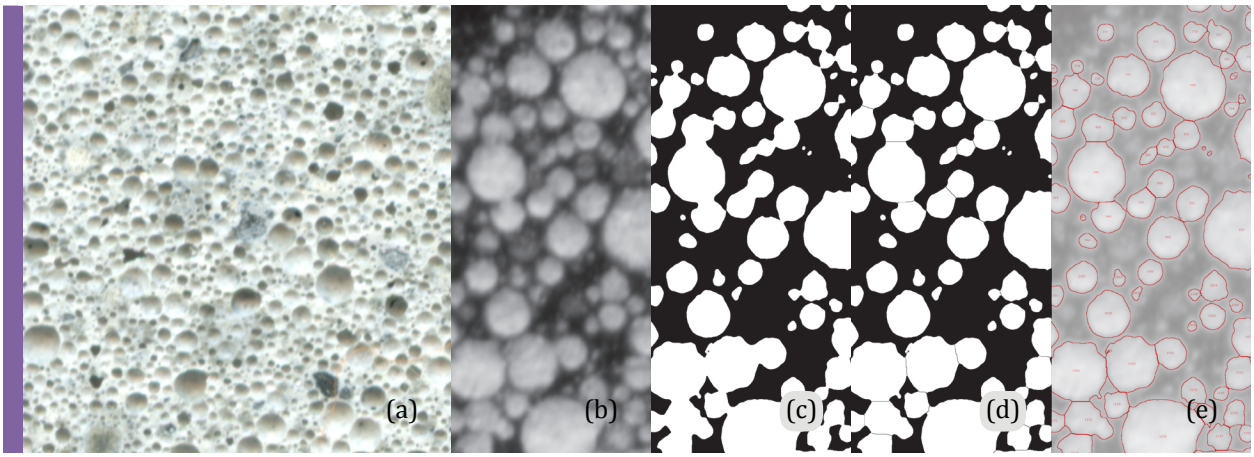

Figure 6.17.2a Silica fume photograph (a), scan (b), threshold of 108 (c), watershed (d), and outline (e). Photograph at 4x magnification; scan and manipulations at 8x magnification.

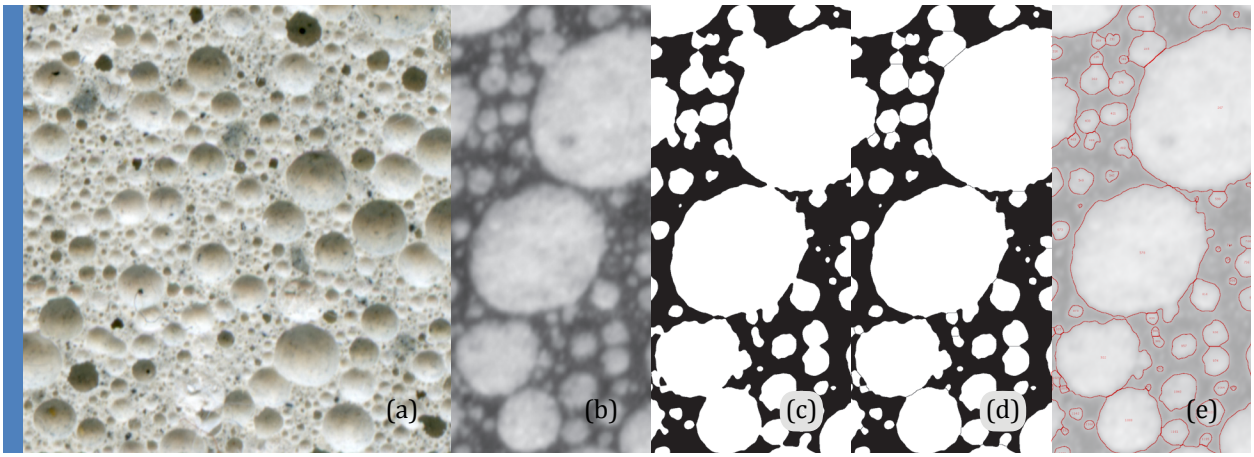

Figure 6.17.2b Portland cement photograph (a), scan (b), threshold of 108 (c), watershed (d), and outline (e). Photograph at 4x magnification; scan and manipulations at 8x magnification.

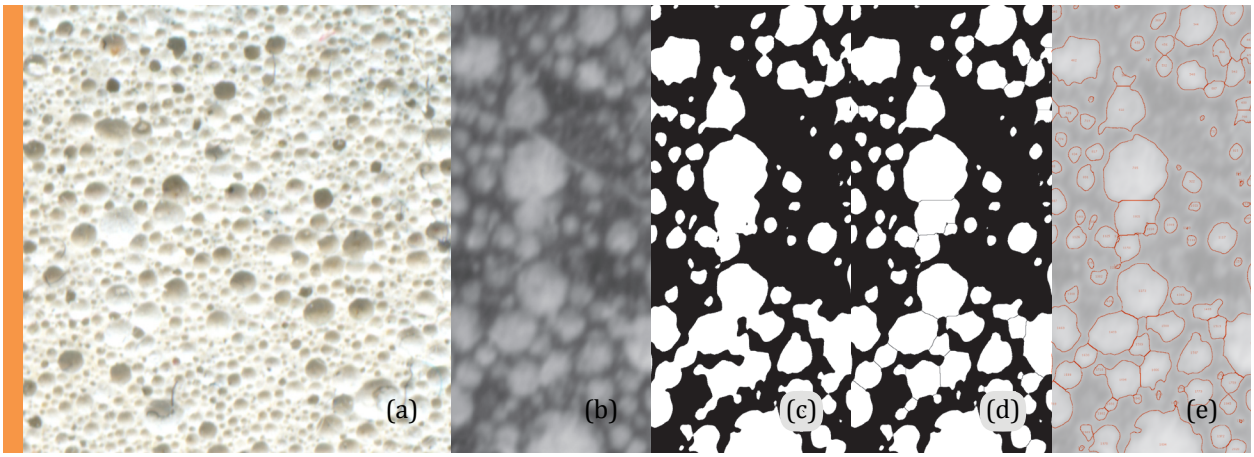

Figure 6.17.2c Slag photograph (a), scan (b), threshold of 108 (c), watershed (d), and outline (e). Photograph at 4x magnification; scan and manipulations at 8x magnification.

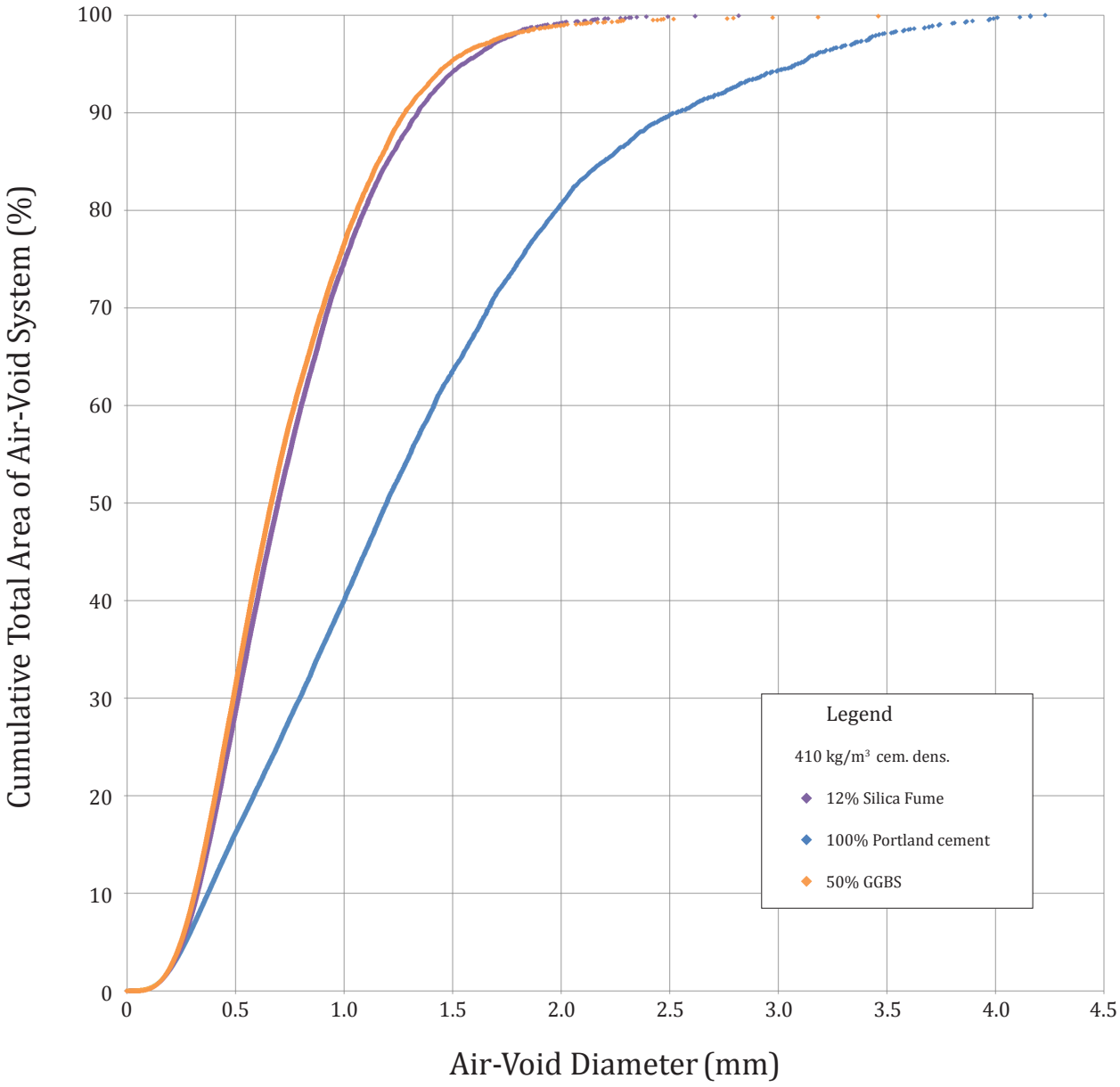

Figure 6.17.2d Cumulative area of air-void system vs. air-void diameter, for mixes with 0:1 filler-binder ratios.

compressive strengths of these mixes (refer to Figure 6.**6.1.2b**). Large flaws are critical Griffith flaws under load, and limit ultimate compressive strength.

Quantitative air void analysis results are consistent with visual analysis of the photographs of specimens with 0:1 filler-binder ratios given in Section 6.17.1. A large number of coalesced bubbles may be observed in the Portland cement cross-section, while the air-void size distribution in 12% silica fume or 50% slag mixes is more consistently fine-grained.

Several attempts to polish sanded foam concrete specimens were also undertaken. Despite using a variety of techniques and equipment from two different laboratories, partially polished particles of sand tended to tear out of the soft foamed matrix during polishing, marring the specimen surface. Application of lacquer and acetone as a stiffener did not penetrate sufficiently far into the specimen to mitigate this problem. The surfaces of the sanded foam concrete specimens were unsatisfactory for analysis, and data from these specimens are not included in this thesis.

Impregnation of sanded specimens with a resin under vacuum may produce better results for future work, sufficiently stiffening the matrix of sanded foam concrete specimens to allow for a high-resolution finish.

7

Proposed Micromechanical Model

Analysis of foam concrete at a fine scale can offer insight into its behaviour at a larger scale.

Three scales of analysis are commonly considered in concrete research, as established by Wittman[1]: *micro level*, which includes physical and chemical processes of molecules in hardened cement paste; *meso level*, which includes interactions of aggregate, pores, and cracks; and *macro level*, which describes concrete behaviour according to simplified laws.

In this chapter, the term microstructure is used to refer both micro and meso level interactions. A proposed qualitative microstructural model explains mechanisms that occur within foam concrete aerated with dry-foam methods during plastic, curing, and hardened states. Analysis is based on the literature review (available in Appendix A), as well as significant trends observed during the experimental program (Chapter 6).

7.1 Plastic Phase

The production of foam concrete begins with the preparation of a base mix from cement

1 Wittman (1987)
2 Refer to Appendix A, Section 5.2.1b.
3 Refer to Section 5.1.1 and Appendix A, Section 5.2.1b.
4 She et al. (2014b) 63
5 Appendix A, Section 6.1.2
6 Appendix A, Section 5.1.7
7 For this reason, approximately 25% of synthetic surfactants are non-ionic. Having no electrical charge can promote

and water. Fine aggregate, coarse lightweight aggregate, and fibre reinforcing may also be included. It is important that solid ingredients are completely wetted in the base mix, since dry solid ingredients added later to the foamed mix may draw water out of the diluted surfactant, causing collapse of bubble films. Ingredients should be well-graded and thoroughly blended for homogeneity and particle packing, to help achieve a uniform air-void system.

As dry foam[2] is added to the mix, the consistency of the mix will change. Typically, the slump flow (i.e. spread rate) of low- and medium-density mixes will decrease with increasing foam volume. This effect is due to the reduced self-weight of the mix (Figure 7.**1a**), as well as the high surface area of the foam, which is typically hydrophilic and capable of adsorbing layers of water. Conversely, the spread rate of denser foam concrete mixes (e.g. 1800 kg/m^3 n.d.) may increase: the aqueous surfactant solution of the foam appreciably increases the total amount of water available in the mix, and the bubbles may act as small 'ball-bearings', improving workability in a manner similar to the effect of air entrainment in retarded mortar systems (Figure 7.**1b**).[3]

If the mix is too stiff, a large proportion of the bubbles will break. This phenomenon results in increased density; it also increases the proportion of available water in the mix, which can help to reduce stiffness and avoid further bubble collapse. In this way, foam concrete mix designs can be self-correcting, to some extent, as long as additional preformed foam is available to restore the desired density.

If the mix is too fluid or is strongly vibrated, sand grains or cement particles may drop to the bottom of the casting during mixing, producing segregation. This problem is common in lower-density mixes, where thin bubble films cannot support relatively large, dense particles. In fluid mixes, bubbles or bleedwater may migrate upwards in the paste, creating a weak zone near the top of the casting and making the foam concrete difficult to finish. Fortunately, many foam surfactants produce bubbles with hydrophilic outer surfaces, which can adsorb layers of water of varying thickness, reducing bleeding and accounting in part for the tolerance of foam concrete to varying water-binder ratios (refer to Figure 7.**1c**).

---

2 Refer to Appendix A, Section 5.2.1b.
3 Refer to Section 5.1.1 and Appendix A, Section 5.2.1b.

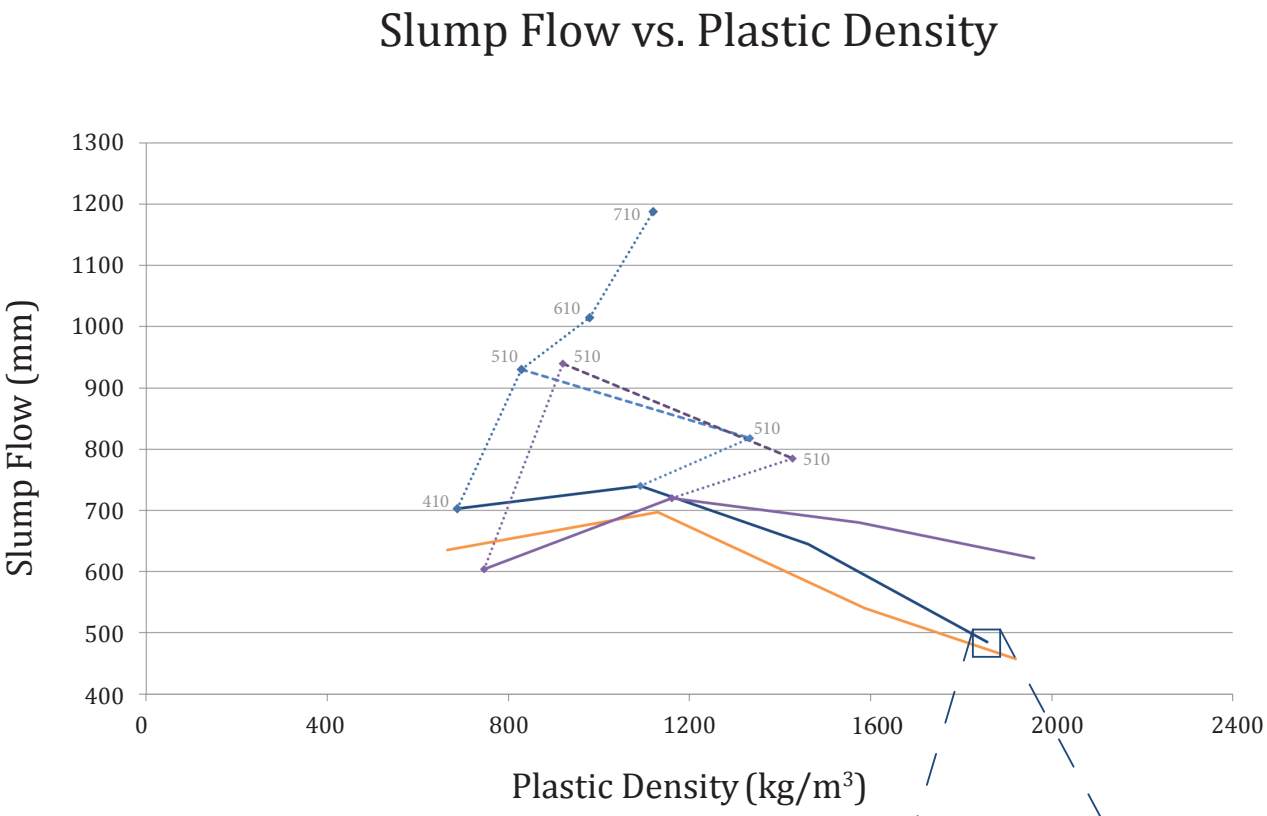

Figure 7.1a For low-density mixes,
workability *decreases* with added foam volume:
hydrophilic foam adsorbs layers of water,
and slump flow decreases with reduced self-weight.

3:1 filler-binder ratio, 0% foam (base mix) 3:1 filler-binder ratio, 7% foam by volume 3:1 filler-binder ratio, 15% foam by volume

Figure 7.1b For dense foam concrete mixes,
workability *increases* with foam volume:
the aqueous surfactant increases the amount of water in the mix,
and air bubbles act as spherical 'ball-bearings'.

If the foam is not evenly distributed throughout the mix, local segregation may occur in regions of especially low density. Dense particles of sand may sink in that region, further reducing density of the remaining foamed paste. It may be difficult to remix foam concrete into a homogenous paste after such segregation has occurred: dense, isolated particles will rupture the foam, where there is limited support from surrounding solid particles. Adding foam incrementally, and blending it thoroughly, helps to avoid this issue.

The thin surfactant films in fresh foam concrete are highly vulnerable during mixing and setting, with numerous sources of disequilibrium in the mix. Bubbles must maintain an appropriate and consistent size to impart desired hardened properties. They must resist coalescence, and must be durable during mixing and pouring, despite the flow of liquid free water in the mix, and the pressures of solid particles against the bubble film. The surface tension of the bubbles must be sufficient to support the self-weight of the foam concrete above.[4]

Spherical particles, such as silica fume or fly ash, and flexible fibres, such as polypropylene, will be physically compatible with fresh foam concrete. Sharp, angular particles, such as ground granulated blast furnace slag, and stiff fibres such as metal fibre reinforcing, are more likely to physically rupture the foam.[5]

The foam surfactant must also be resistant to damage from chemical interactions. Most synthetic surfactants are anionic:[6] the hydrophile group carries a negative charge, which stabilizes air bubbles in an alkaline environment of predominantly positively charged cementitious surfaces, as shown in Figure 7.**1d**, Bubble "A". However, the surfaces of cement particles also have regions of negative charges, which can upset the balance of electrostatic repulsive forces at the ionic heads of the surfactant molecules (Bubble "B").[7] Furthermore, fine particles with low surface energy, such as activated carbon, can disrupt the bubble surface by inserting themselves within the hydrophobic portion of the film (Bubble "C").[8]

---

4 She et al. (2014b) 63
5 Appendix A, Section 6.1.2
6 Appendix A, Section 5.1.7
7 For this reason, approximately 25% of synthetic surfactants are non-ionic. Having no electrical charge can promote stability in an environment with both positive and negative charges. Cf. Brady et al. (2001), C4.
8 Jolicoeur et al. (2009) 20

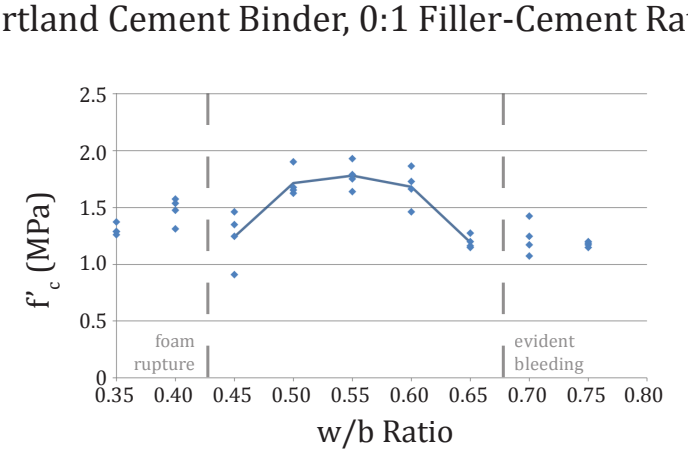

Figure 7.1c Tolerance of neat cement foam concrete to varying water-binder ratios. The hydrophilic outer surfaces of bubbles can adsorb layers of water of varying thickness, increasing tolerance to variation. Refer also to Figures 6.**1.1.1a** to 6.**1.1.4f**.

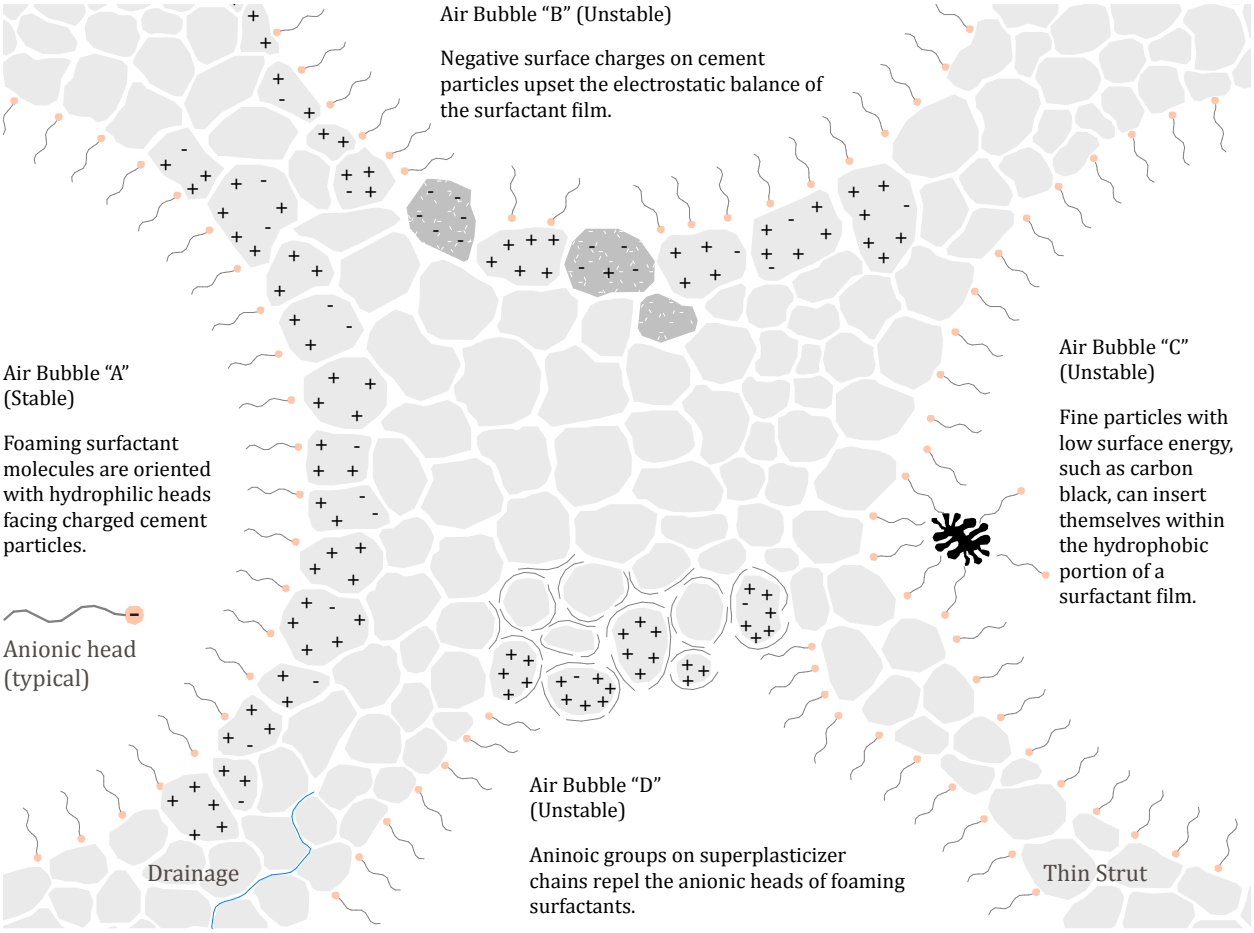

Figure 7.1d Causes of surfactant instability.

The surfactant must not only accommodate the concrete chemistry at the time of mixing, but must also be capable of tolerating an increasingly alkaline environment, especially as calcium hydroxide is produced during cement hydration.

The presence of other chemical admixtures can be problematic. Superplasticizers, for example, typically consist of long chains with anionic (polar) groups. Many polar groups adhere to positively-charged portions of the cement surface, while the remainder of the polar groups face outward. Consequently, the modified cement particles exert negative charges on the surrounding environment: they repel each other, reducing colloidal flocs, and they are attracted to the positive (hydrogen) ends of the surrounding water molecules, reducing surface tension (Figure 7.**1d**, Bubble "D"). While these chemical chains are helpful for creating a dispersed system, they undermine the ability of foam surfactants to arrange themselves as resilient bubbles, with charged heads attached to layers of cement particles, which will eventually form a skeletal skin.[9]

An inability of the bubble films to accommodate any of these effects can cause collapse of bubbles. This collapse will increase the mix density, and will add additional water to the mix, increasing the water-binder ratio. Overly high water-binder ratios can result in segregation, high permeability, high drying shrinkage, and various other effects discussed elsewhere in this chapter.

The paste must eventually solidify to form the structure of hardened foam concrete. Accordingly, the bubble film must host a sufficient density of cementitious particles or ions, and must also include a sufficient quantity of water for hydration.

Water-binder ratios are typically very high in foam concrete mixes. Consequently, 'through-solution hydration' mechanisms will tend to dominate over 'topochemical hydration' mechanisms; that is, anhydrous compounds in the cement particles will, to a large degree, dissolve into the surrounding water as ions, rather than merely hosting chemical reactions at their surfaces.[10] Local water-binder ratios are especially high adjacent to the hydrophilic bubbles;[11] consequently, dissociated calcium, sulfate, aluminate

[9] Superplasticizer is seldom used in commercially produced foam concrete. Refer to Appendix A, Section 5.1.6.
[10] Mehta (1986) 182, van Breuge (1992) 7
[11] Liu et al. (2016) 6

ions migrate easily and are distributed evenly along bubble walls, available to be reconstituted entirely into the desired air-void system form.

7.2 Curing Phase

Surface tension of the bubbles must be maintained until solid cementitious structures develop that are capable of carrying the foam concrete self-weight. Hydration products will accumulate mainly in dense struts along Plateau borders.[12] The plastic mix initially stiffens with the production of thin calcium sulfoaluminate crystals (i.e. ettringite). Within hours, large crystal blocks of calcium hydroxide form, alongside an emerging fibrous network of calcium silica hydrate (C-S-H). As the primary reaction product of cement hydration, C-S-H continuously binds the paste, providing strength via van der Waal forces. This compound of CaO, SiO_2, and H_2O varies considerably in its morphology in concrete. In an environment with a high water-binder ratio and available space for growth, such as in foam concrete, the C-S-H will tend to be needle-like and low-density.[13] Due to the availability of calcium, sulfate, and aluminate ions at the bubble walls, relatively high proportions of calcium hydroxide and ettringite may accumulate at the air-void shells.[14]

Generating a skeletal structure quickly reduces the risk that bubbles will collapse or coalesce, or be damaged by drainage, drying shrinkage or other mechanisms. Problematically, the rate of hardening in foam concrete is typically less than for normal density concrete, and decreases with decreasing density. The porous structure of foam concrete can limit the availability of reaction ingredients at certain locations, particularly where the cell wall is thinnest. Although a high water-binder ratio will permit cementitious materials to dissolve quickly and thoroughly, the average distance between reactants in solution increases with water-binder ratio, hindering the creation of connections between solid phases in the hydrating mix. Additionally, some foaming agents, particularly protein-based foams, appear to retard hydration.[15] The agent may physically separate the reaction ingredients, or interfere with electrostatic attraction; furthermore, in some regions, water

[12] That is, the edges where the soap films intersect. Cf. Figure 7.3.1b, Lu and Qin (2014) 5, Liu et al. (2016) 7.
[13] Zhang et al. (2018) 86
[14] Lu and Qin (2014) 8
[15] Pan et al. (2014) 257-258

adhered to the hydrophilic portion of a surfactant may be unavailable for reaction during early hydration stages.[16]

The setting speed of foam concrete may be increased in a number of ways. Physically, materials may be chosen and proportioned to ensure the production of an even, continuous skeleton structure, with good particle packing and sufficient water for dissolution and hydration.[17] Use of ultra-fine materials such as silica fume provides more physical sites for the nucleation of hydrates.[18]

Chemically, accelerators (such as calcium chloride[19]) or fast setting cements (such as aluminate cement[20] or calcium oxide[21]) may be used to promote dissolution of the cations and anions from the cement during the early hydration period.[22] Increasing the fineness of the cementitious materials, or increasing cementitious density, will similarly increase the density of ions available in the short term for the production of hydrates.

Higher curing temperatures promote faster chemical reactions, increasing the speed and frequency of reactant collisions. The temperature of the curing mix may be increased by increasing cement content,[23] thereby developing more heat through exothermic hydration reactions; by using insulated formwork to retain exothermic heat;[24] or by raising the ambient temperature.[25]

Temperature development occurs differently in foam concrete than in normal density concrete. The presence of air voids has a significant insulating effect, reducing the dissipation of heat.[26] Simultaneously, a lower mix density corresponds to a lower heat capacity. Consequently, low-density foam concrete mixes are especially subject to temperature rise. Moreover, foam concrete mix designs often incorporate relatively large

16 Brady et al. (2001) C10
17 Van Deijk (1991) 49
18 Berodier and Scrivener (2014)
19 Brady et al. (2001) C4
20 Huang et al. (2015) 390
21 Chen et al. (2014) 137
22 Mehta (1986) 259
23 Jones and McCarthy (2006) 1035
24 Van Deijk (1991) 49
25 She et al. (2014b) 71
26 Tarasov et al. (2010) 905

proportions of cementitious content in order to achieve sufficient strength, resulting in greater amounts of reaction energy generated per unit volume.

Foam concrete is often produced for large-volume applications, such as in-situ void-filling. At such scales, there can be significant variation between core and surface temperatures. Since foam concrete cures faster at elevated temperatures, the exothermic reaction will occur even faster nearer the core, intensifying the thermal gradient.[27]

During placement and set-up, heat of hydration may be helpful in void-filling applications: the air in the foam will expand slightly, ensuring good contact between the foam concrete and the surrounding surfaces.[28] During curing, control over temperature development is important to avoid differential strain and cracking caused by temperature gradients.[29] Cracking induced by thermal strains can have negative effects on important properties such as mechanical strength, water uptake, impermeability to gases, and resistance to chemical attack.

In extreme cases, high temperatures are capable of causing the evaporation of water, reducing the amount of liquid water available for reaction.[30] If internal temperatures exceed 90°C, protein coagulation may cause protein-based foams to collapse; or the expansion of heated air may rupture bubble structures.[31] Delayed formation of ettringite should be considered: if the mineral is inhibited from crystallizing until after the mix has stiffened or set due to high early temperatures, its eventual growth may expand and crack the concrete.[32] The risks associated with delayed ettringite formations (DEF) may be reduced somewhat in foam concrete, as the air voids can accommodate expansion.

Temperature rise may be slowed by reducing the rate of the hydration reaction, reversing the acceleration strategies described above. Additionally, hydraulic ingredients may be replaced with pozzolanic materials, such as fly ash or slag. With less hydraulic material, the speed of the hydraulic reaction will be slowed. Secondary pozzolanic reactions will only commence after calcium hydroxide is produced by the hydraulic

---

27 Tarasov et al. (2010) 905.
28 Barnes (2009) 7
29 Jones and McCarthy (2005b) 24
30 Cf. Mehta (1986) 331, Jones and McCarthy (2006) 1036
31 Tarasov et al. (2010) 899
32 Kosmatka et al. (2002) 17-18

reactions. Additionally, the finely divided pozzolans adsorb water, limiting the amount of water readily available for cement hydration.

Like temperature, humidity also has an important influence on foam concrete microstructure during curing. An in-depth discussion of concrete drying shrinkage mechanisms is presented in Appendix A, Section 6.2.3, for reference.

Conventional foam concrete is highly susceptible to drying shrinkage. High water-binder ratios result in a large volume of capillary pores,[33] promoting capillary tension as the water evaporates (down to approximately 40% RH). Relatively high cementitious densities, combined with significant water volume, result in a large amount of C-S-H gel, with a large surface area, which is subject to the effects of surface tension and disjoining pressures (from 40 to 11% RH).[34] In the event of strong drying (below 11% RH), the large volume of C-S-H compresses significantly as interlayer water is removed from mineral sheets.

Drying shrinkage varies with the use of supplementary cementitious materials, due in part to their influence on water demand. Fine particles, such as silica fume, require a relatively high water-binder ratio for workability, as the large surface area must be adequately wetted: drying shrinkage is typically significantly increased, due to the greater resultant volume of paste and capillary pores. The presence of SCMs will also affect the size distribution of capillary pores in a paste via particle packing, with consequent effects on rates and amount of shrinkage strain. For example, smaller capillaries will hold water more rigidly, and will only participate in capillary tension at low RH (Figure 7.**2c**). For further discussion, refer to Sections 6.11 and 7.3.6.

Drying shrinkage is reduced with the addition of aggregate. Stiff filler resists volumetric shrinkage of the surrounding matrix, and larger aggregate allows for a leaner mix, reducing the volume of C-S-H.[35] Unhydrated grains of cementitious materials may also restrain drying shrinkage: such effects are negligible in normal density concrete,[36] but may be more consequential for foam concrete. Foam concrete aggregate (FCA) may be

[33] Nambiar (2007b) 1346
[34] Cf. Georgiades (1991), in which pore surface area is related to drying shrinkage in AAC
[35] Neville (1963) 288
[36] Neville (1963) 292

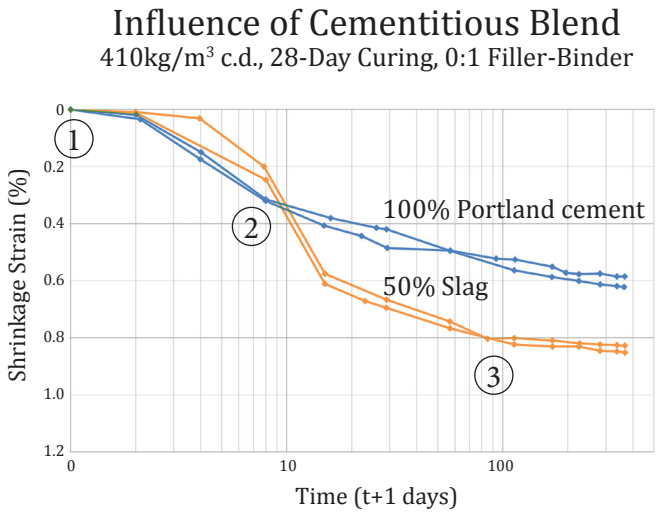

Figure 7.2a Influence of cem. blend on D.S.

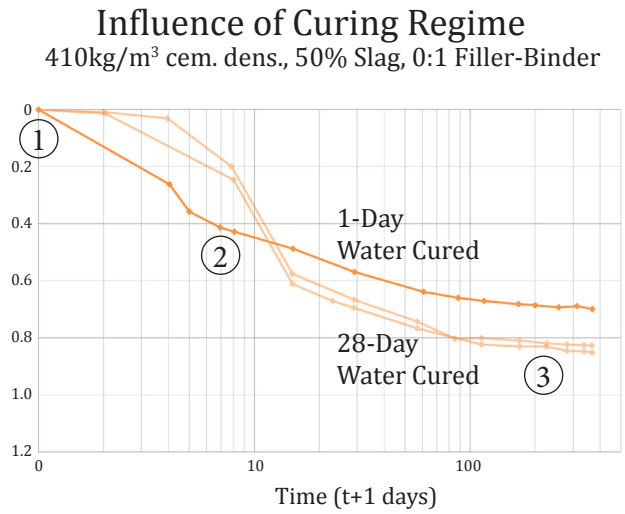

Figure 7.2b Influence of curing regime on D.S.

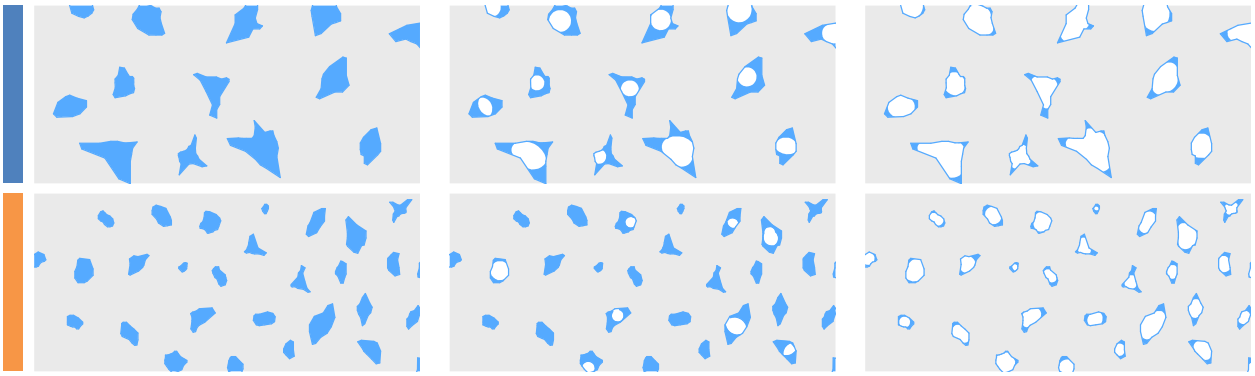

1 Specimens are saturated, with no capillary tension.

2 Only large pores are engaged in capillary tension at high RH. Portland cement mixes have a larger proportion of large capillaries than slag mixes, and experience greater shrinkage.

3 Small pores are engaged in capillary tension at lower RH. The high shrinkage strain in slag mixes may be due in part to the accumuated capillary tension induced by many fine pores.

Figure 7.2c Differences in drying shrinkage patterns may be attributed in part to differences in pore size distribution, which can be influenced by cementitious blend (Figure 7.2a) or curing regime (Figure 7.2b).

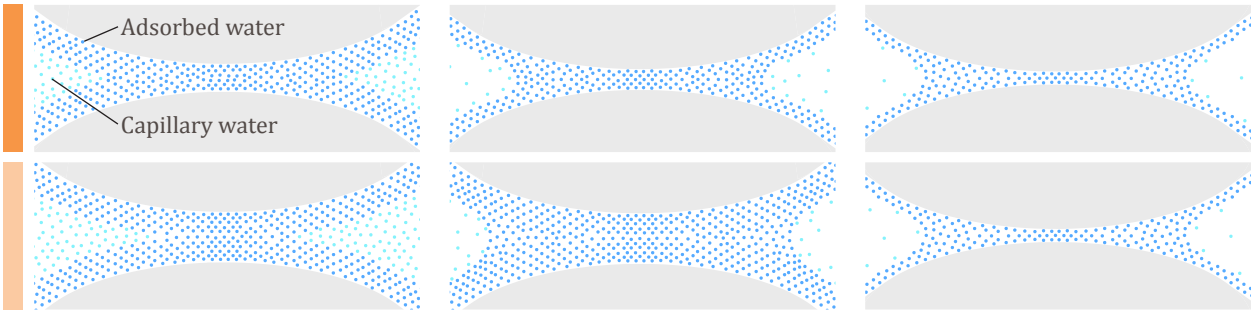

1 Disjoining pressures keep (or force) proximate solid surfaces apart during long periods of curing in high RH (lower graphic).

2 Internal RH remains higher, longer, in more saturated specimens (lower graphic), delaying shrinkage.

3 At low RH, disjoining pressures are relieved and surfaces draw close. Total shrinkage strain is greater for specimens with longer curing regimes.

Figure 7.2d Duration of curing in high humidity may affect drying shrinkage patterns by inducing swelling of the C-S-H at areas of hindered absorption during hydration.

used to reduce short-term drying shrinkage, since the crushed material has already undergone volumetric contraction during curing, and is relatively inert. FCA will be especially effective during initial drying shrinkage. However, FCA will continue to shrink as internal RH decreases and as water is removed from very fine capillary pores, with similar shrinkage strain to conventional foam concrete of the same density and cementitious density, after one year.[37]

The curing regime of foam concrete influences drying shrinkage patterns. When foam concrete is cured in high RH for a long time, air-voids take on some moisture.[38] The additional water preserves a high internal RH and thus reduces initial rates of moisture movement during drying, compared to foam concrete cured in high RH for shorter times (Figure 7.**2b**).

However, long-term drying strain is higher when specimens are cured for a longer time in high RH. This phenomenon may be explained as follows. First, as noted above, unhydrated cement grains in specimens with short curing regimes provide restraint to drying shrinkage. Secondly, capillary pore size diminishes with increasing degree of hydration, and these small pores may engage in capillary tension most effectively when internal RH becomes low (Figure 7.**2c**). Third, the curing regime may have an effect on disjoining pressures. In a curing specimen, adsorbed layer of water on internal surfaces will tend to be of a consistent thickness, to produce the lowest energy state. The thickness of this layer will increase with RH. During curing in high RH, proximate solid surfaces are kept apart to accommodate the appropriate thickness of adsorbed water. Adsorbed layers will remain thicker for longer with an extended high RH curing regime, affecting the emerging microstructure, and possibly promoting local disjoining strains. When specimens dry, disjoining pressures decrease. The surfaces draw close, and the volume of the sample is decreased.[39] Total contraction is greatest when foam concrete has been subjected to a high RH during early curing: water-curing for a long duration has an appreciable effect (Figure 7.**2d**, refer also to Section 6.11).

---

37 Cf. Section 6.11.
38 Cf. Section 6.12.
39 Powers (1965), Idiart (2009) 46-47

7.3 Hardened Phase

Load is transmitted through foam concrete via the hardened cement paste around air voids. At a large scale, the primary factor for many mechanical properties is the total cross-sectional area available to contribute to the support of load on a specimen. Just as average cross-sectional area increases at an increasing rate with increasing density, so modulus of elasticity, compressive strength, and other properties increase at an increasing rate with increasing density (Figures 7.**3a** to 7.**3c**).[40] At a finer scale, and especially at lower densities, the geometry and material properties of the cell walls, and the presences of flaws, become important for understanding the mechanical behaviour of foam concrete.

The following six sections consider the microstructural behaviour of hardened foam concrete subject to simple (uniaxial) compression. Patterns of moisture movement are reviewed in Section 7.3.7, and freeze-thaw mechanisms are discussed in Section 7.3.8.

7.3.1 Geometric Considerations

In extremely low-density foam concrete, a large proportion of paste volume will be in the form of struts, created at the Plateau borders where material is drawn via surface tension during curing. If cell walls are very fragile or discontinuous,[41] the open-cell structure will be essentially reticulated, and the buckling of struts will strongly influence behaviour[42] (Figure 7.**3.1a**).

Most modern, commercially-produced foam concrete is sufficiently dense and well-formed to produce a high proportion of closed cells. For closed-cell foam concrete, the stiffness of Plateau border struts continues to be important: the strut cross-section will vary as the cell walls become less likely to rupture, affecting radius of gyration (Figure 7.**3.1b**)[43]. The degree of fixity of the struts may increase, affecting strut buckling behaviour, since the nodes and tapered strut bases at the intersections of Plateau borders

---

40 Refer to Appendix A, Chapter 6.1 for a detailed discussion about strength-density relationships proposed by Ryshwik, Balshwin, etc.

41 Reactants along the thin film may be limited, and hindered from forming hydrates due to high concentrations of water or surfactant. In such cases, 'windows' may be produced between air voids.

42 Warren and Kraynik (1988) have demonstrated a linear elastic response for a theoretical open cell microstructure. The reticulated strut model may be most relevant for foam concrete with greater than 90% porosity, cf. Akthar (2010) 356, Gibson and Ashby (2010) 183.

43 After Warren and Kraynik (1988) 344

can account for a significant portion of the paste volume. Additionally, the cell walls begin to play a meaningful structural role via membrane stresses. As the material is strained, the cell wall will be placed in compression in one direction, and in tension at 90-degrees. Even very thin cell walls will not buckle in the tension direction, and will provide some resistance to deformation (Figure 7.**3.1c**).

With greater density, the cell walls thicken, providing increasing shear and axial resistance in the compression direction. As density is increased further, cell walls will tend to strain axially in compression, rather than bend. These effects will swiftly dominate mechanical properties, as the micromechanics behave less like a system of framing members and membranes, and more like a solid material with many small flaws[44] (Figure 7.**3.1d**).

7.3.2 Elastic Regime

Within the elastic regime, porosity is a key parameter, affecting the total amount of paste available for resisting strain, and shaping to what extent the microstructure strains via flexural or axial compression.[45] The strong dependence of elastic modulus on porosity across mix designs is evident in Figure 7.**3.2a**.

A second major parameter is the intrinsic elastic modulus of the paste, i.e. the modulus of the cell walls.

For neat, low-density foam concrete, the paste is dominated by C-S-H phases. The paste will tend to strain most easily where phases are less dense due to high local water-binder ratios during curing (e.g. at transition zones around air-voids).

Where the density of the paste is held constant,[46] the elastic modulus of the C-S-H will increase with a decreasing calcium/silicon (Ca/Si) ratio, due to an increasing length of

---

44 Porosity of approximately 70% may represent the lower limit of bending-dominated behaviour, cf. Gibson and Ashby (2010) 205, Tonan and Gibson (1992) 6377. Most sanded mixes and very dense neat cement mixes of foam concrete will have porosity less than 70%.

45 Both elastic modulus and shear modulus may be subject to strut bending, since these deformations involve distortion. Bulk modulus, however, will tend to be dominated by simple compression of members, even at low densities, since microstructural transformations are affine. Cf. Warren and Kraynik (1988) 345.

46 Patterns of C-S-H phases in normal density concrete would suggest that the surface of the bubble walls in foam concrete will tend to be low density with a low Ca/Si ratio (a 'loose fibril morphology'): while interior portions of the paste will tend to be denser, with a higher Ca/Si ratio ('aggregations of calcium ions and short silicate chains'). Despite a low Ca/Si ratio , the paste at the bubble wall will typically be the least stiff, due to its lower density. Cf. Hou et al. (2013) 3, Pelisser et al. (2012) 17221.

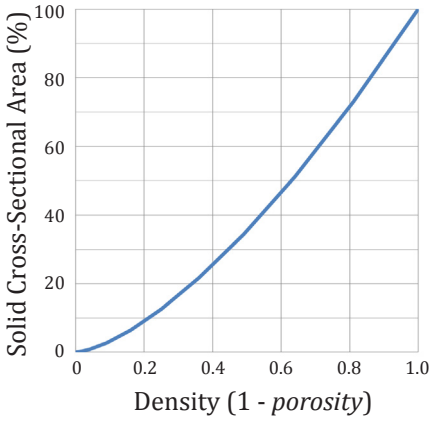

Figure 7.3a Area vs. density.

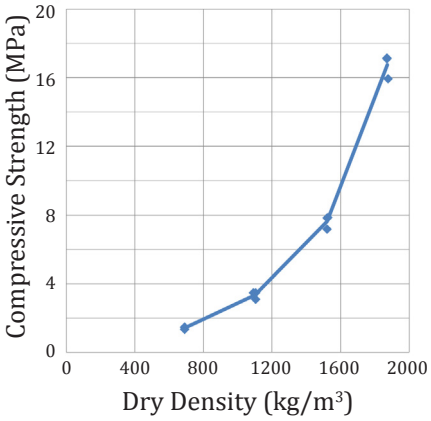

Figure 7.3b Strength vs. density.

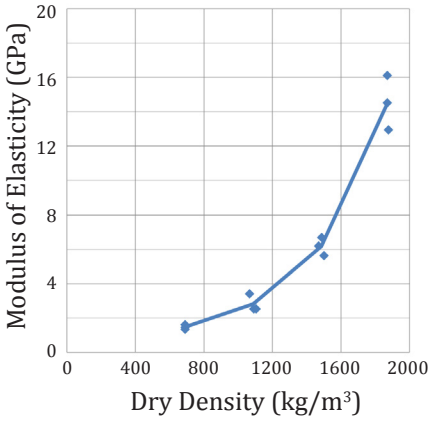

Figure 7.3c MOE vs. density.

Mechanical properties of a porous solid are partially dependent on cross-sectional area available to transmit load. Just as average cross-sectional area increases at an increasing rate with increasing density (Figure 7.3a), so modulus of elasticity, compressive strength, and other properties follow similar trends (Figures 7.3b and 7.3c).

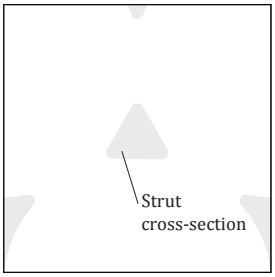

Figure 7.3.1a
Low density mix, with film ruptured during solidification. Strut surface area is reduced, tending towards a circular cross-section.

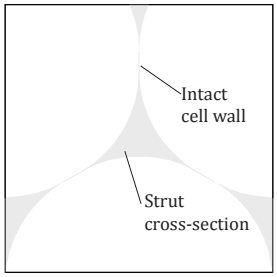

Figure 7.3.1b
Low density mix, with surfactant films remaining intact during solidification. Nodes account for a significant volume of the total paste, affecting fixity of struts.

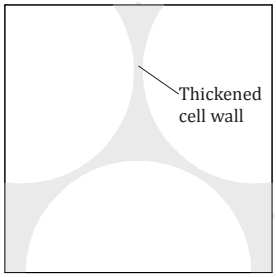

Figure 7.3.1c
Thickened cells wall provide increased shear and axial resistance in the compression direction.

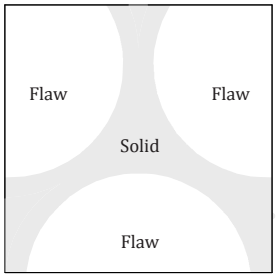

Figure 7.3.1d
As density increases, the porous material behaves less like a foam (i.e. a system of framing members and membranes), and more like a solid with many flaws.

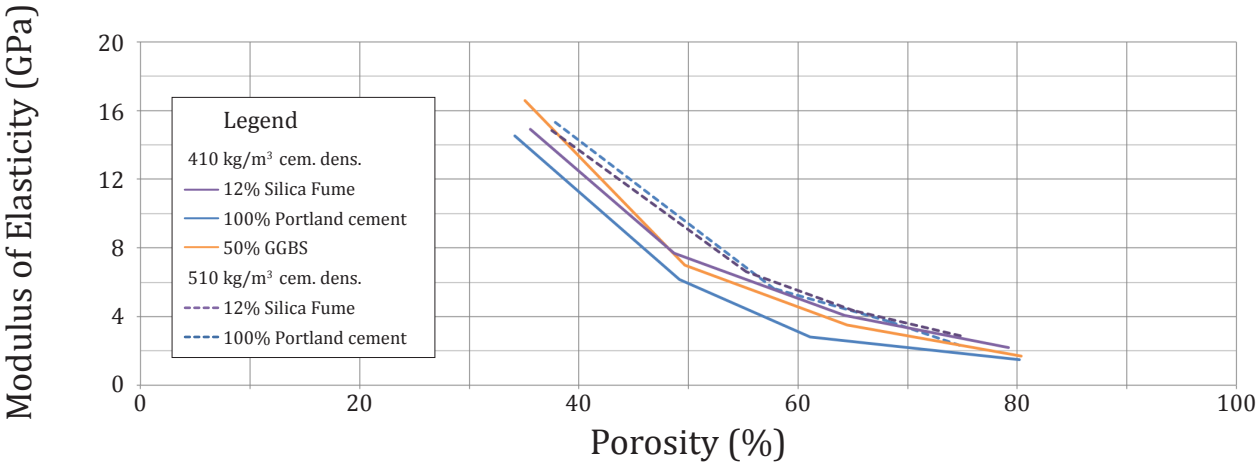

Figure 7.3.2a MOE vs. porosity, 56 days moist-cured.

silicate chains and subsequent effects on bonding[47] and induced distances between C-S-H sheets.[48] The Ca/Si ratio of C-S-H is reduced with the inclusion of silica-rich SCMs, including silica fume, fly ash, and even blast-furnace slag, if used in sufficient quantity.[49] The effects of SCMs on Ca/Si ratios may account for some of the apparent improvement in elastic modulus of and silica fume mixes, compared to foam concrete made with Portland-only binder.

SCMs also consume CH through pozzolanic activity during the curing process, replacing it with C-S-H, which is somewhat stiffer.[50] The effect of this reaction on modulus appears to be minor, however, since increasing the curing age of the foam concrete from 28 to 56 days did not significantly affect results.[51]

Moisture content will influence the paste's elastic modulus. Adsorbed water in the C-S-H will bear load, increasing the modulus. Conversely, microcracking caused by drying shrinkage can degrade the stiffness of the paste. Specimens with high initial water-binder ratios (such as silica fume mixes) will be especially subject to these effects, dependent upon whether they are kept moist or permitted to dry.[52]

Adding cementitious material or aggregate to a mix will increase paste volume, contributing to stiffness. Notably, for a given density, mixes with greater cementitious material and less aggregate tend to have greater stiffness (Figures 7.**3.2b** and 7.**3.2c**). The increase in heterogeneity in a mix with more sand may correspond to an increase in microcracking in the paste, degrading stiffness, as discussed more extensively below. Furthermore, in mixes between 1000 and 1400 kg/m^3, discrete particles of dense, stiff sand will increase mix density, but may not proportionally increase stiffness, since the elastic modulus of the composite will continue to be dominated by the thick surrounding C-S-H matrix. However, when very high proportions of sand are used, the inherent stiffness of

47 Manzano et al. (2009) 1671, Hou et al. (2013)
48 Pelisser et al. (2012) 17219, 17223.
49 Lothenbach et al. (2001) 1245
50 Manzano et al. (2009) 1670
51 In contrast, increasing curing age did have an effect on strength, likely due to pozzolanic reaction, as discussed below.
52 Specimens with a high initial water-binder ratio and low vapour permeability may benefit from these effects during testing or service. Refer to Section 6.7. Note that fully saturating air voids with water will also increase the elastic modulus of foam concrete, through fluid support of cell walls in closed cells, or through dynamic viscousity through open pore systems. Cf. Gibson and Ashby (1999) 252-257. The presence of air gases at atmospheric pressure will not contribute significantly to the mechanical properties of foam concrete, cf. Gibson and Ashby (1999) 250.

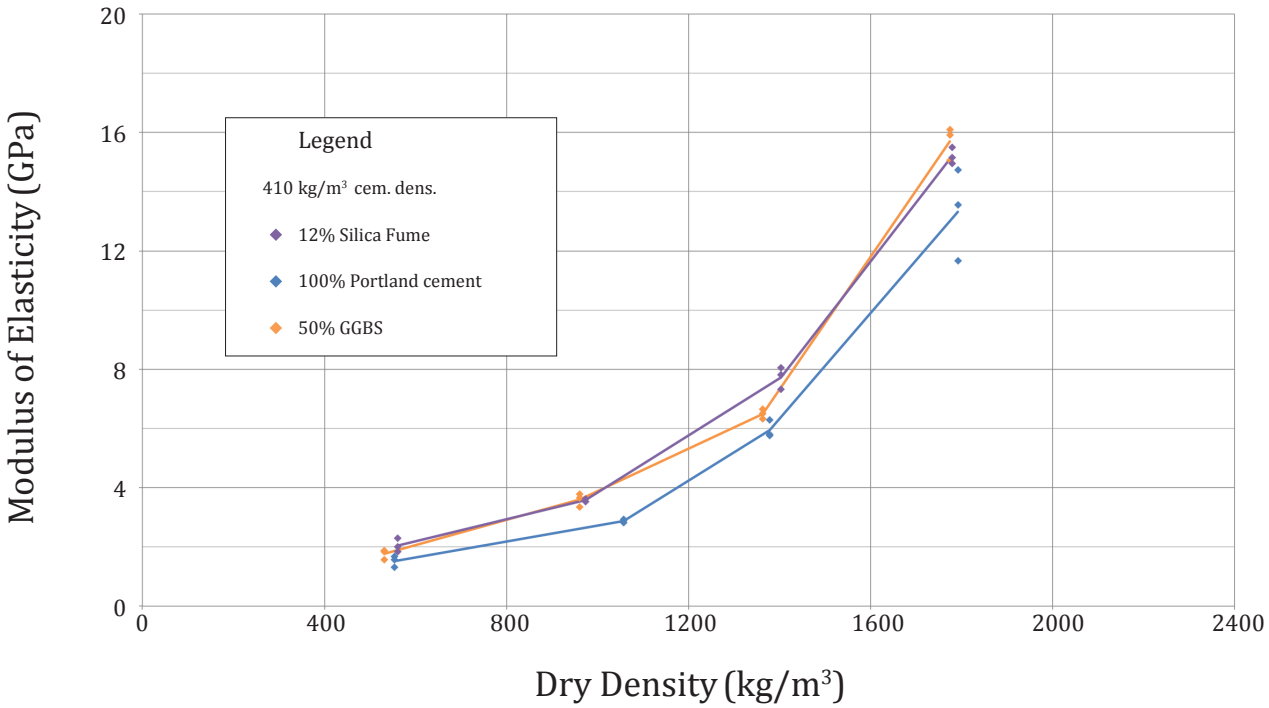

Figure 7.3.2b Modulus of elasticity vs. dry density, 28 days moist-cured. Varying cementitious blend.

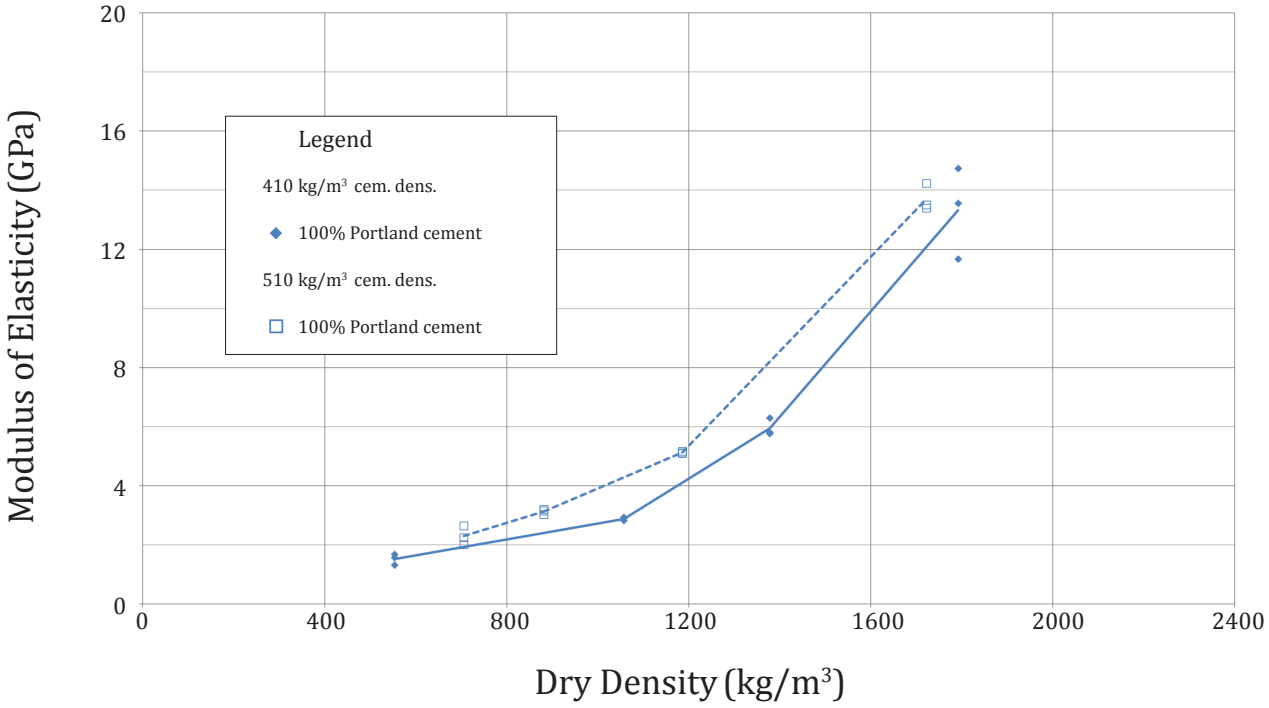

Figure 7.3.2c Modulus of elasticity vs. dry density, 28 days moist-cured. Varying cementitious density.

the sand is better utilized as aggregate bears more directly against other aggregate. For example, for the two Portland mixes of 1800 kg/m^3 nominal density in Figure 7.**3.2a**, the elastic modulus of the cement-poor mix is almost as high as that of the cement-rich mix.

The elastic regime is highly linear in well-formed foam concretes of varying density, cementitious density, and cementitious blends (Figure 7.**3.2d**). There are no obvious curves at the beginning of the stress-strain plots, indicating that the air-void system is consistent and regular: closing pressures are not needed to compress any secondary soft system of flaws.[53] Cyclical loading up to 40% of f'_c demonstrates no obvious change in elasticity for neat cement or sanded specimens (Figure 7.**3.2e**).

7.3.3 Plastic Regime and Peak Load

As stresses approach ultimate compressive limits, stress-strain relationships become non-linear. This plastic deformation can be explained in light of fracture mechanics.[54]

Fracture in concrete initiates at microcracks present at the interfaces of heterogeneous materials. In foam concrete, differences in elastic modulii[55] and in volumetric shrinkage during curing will induce microcracking between the C-S-H matrix and any fine aggregate, comparable to the interfacial cracks in the transition zone between dense aggregate and concrete paste in normal density concrete.[56] More significantly, microcracking may originate around air-voids, where the C-S-H phases are of relatively low density and stiffness with relatively high disjoining pressures, inducing differential shrinkage during curing.

These microcracks will not propagate significantly at low applications of load. As deformation progresses, however, the microcracks grow, according to three distinct internal conditions.

For very low-density foam concrete, tensile forces are induced along the tension side of buckled struts. Microcracks will grow rapidly where the tension is high and the paste is weak, until the strut fractures (Figure 7.**3.3g**).

---

53 Van Mier (2009) 285
54 Vonk (1992) 2
55 Note that air-voids can be conceived of as an aggregate having zero density.
56 Slate and Hover (1984) 137-159

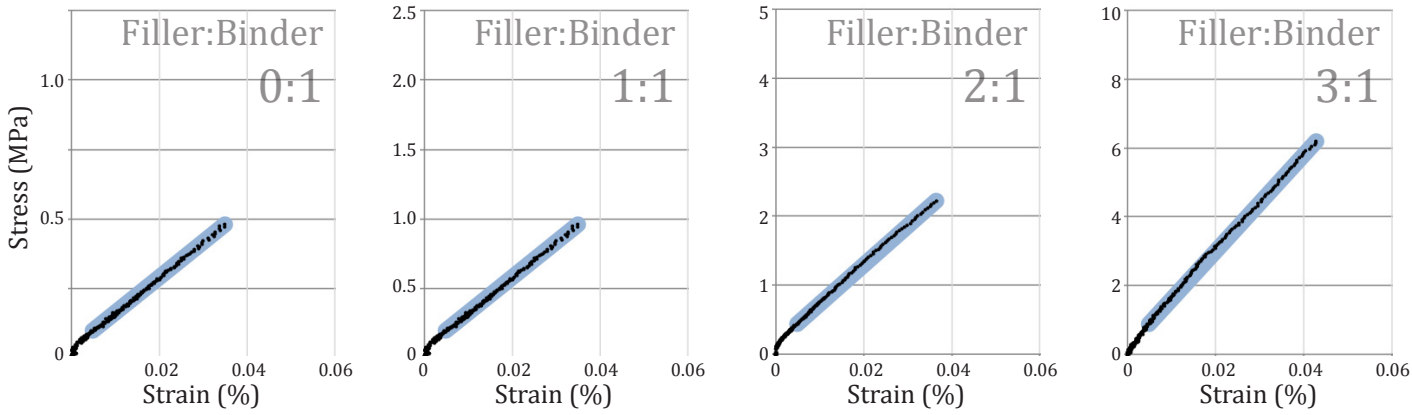

Figure 7.3.2d Stress-strain relationships for Portland cement specimens, varying filler-binder ratio.

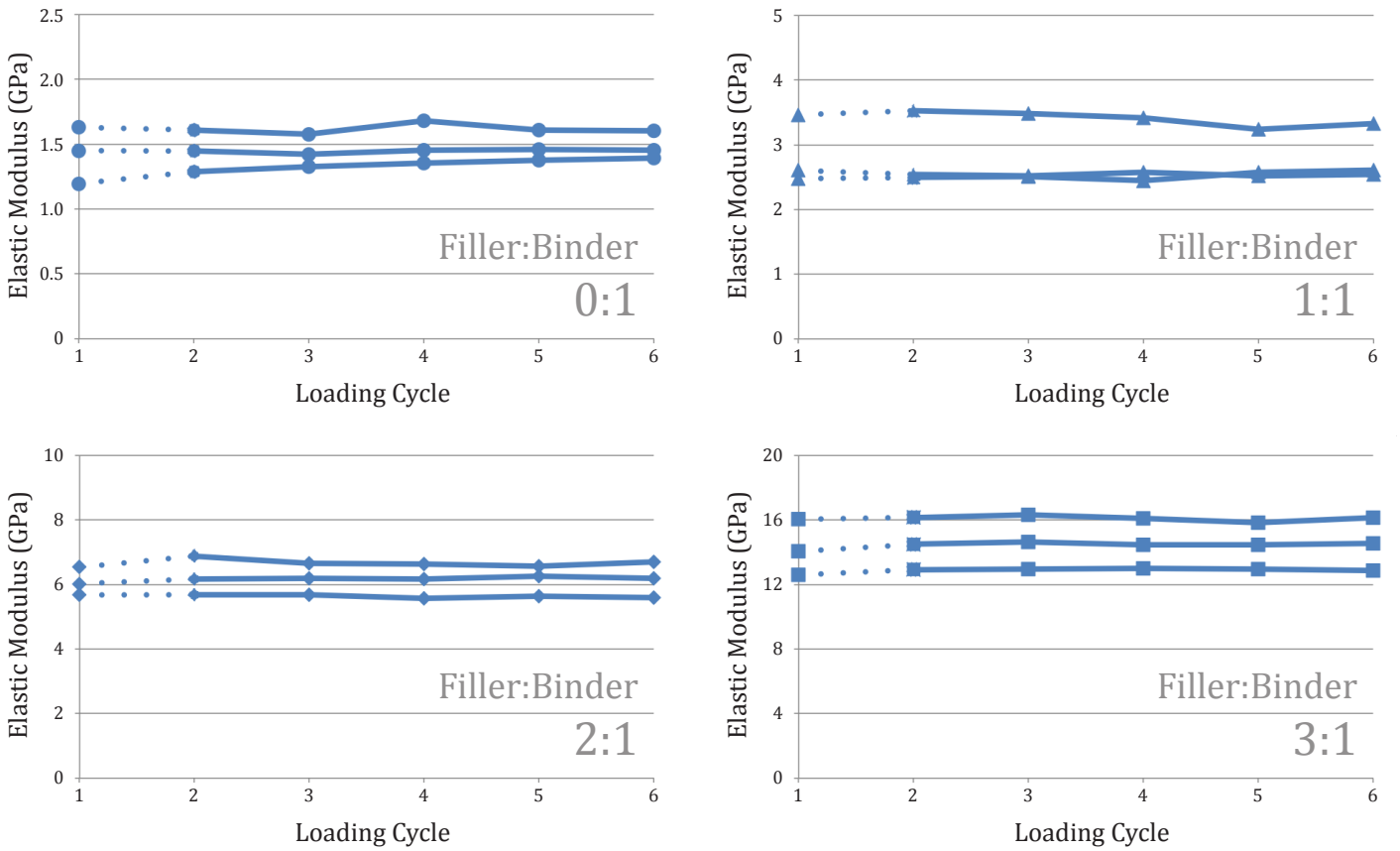

Figure 7.3.2e Effects of cyclical loading on MOE of Portland cement specimens, varying filler-binder ratio.

For denser foam concrete, with thicker cell walls, compression induces tensile stresses at the north and south poles of air voids.[57] Microcracks at these locations will widen and extend, curving to becoming approximately parallel with the direction of compression[58] (Figure 7.**3.3h**).

For sanded foam concrete in simple compression, microcracks grow not only at the poles of air voids, but also at the interfacial zones around fine aggregate particles. Differences in elastic moduli of paste and aggregate will induce splitting and shear stresses at bond interfaces, approximately parallel to the direction of compression[59] (Figure 7.**3.3i**). With further deformation, the distributed cracks will extend into the C-S-H paste.

These three mechanisms shape patterns of global failure.

In very low-density mixes, vulnerable struts and walls will fail at a critical load, triggering progressive collapse through a weak stratum in the specimen. There is minimal capacity for the fine microstructure to dissipate stresses through microcracking in the paste, and the plastic regime is very short.

At low density, for a given porosity, the vulnerability of cell walls and struts will generally be controlled by two major parameters: the geometry of the air-void system, and the modulus of rupture of the paste. A matrix of fine, evenly-spaced voids produces foam with short cell walls and consistent cross-sectional dimensions of microstructural elements. Loading is distributed relatively uniformly. By contrast, large, coalesced and irregularly spaced air-voids produce variability in the microstructure, including thinner, longer struts and walls, supporting greater tributary areas. Greater tensile stresses will develop as these irregular microstructural elements are loaded and flexed, and when tensile stresses reach the modulus of rupture of the paste, the elements will fail (Figure 7.**3.3m**).

The modulus of rupture of C-S-H is a function of its morphology and density. Roughness and heterogeneity of the pore surface increases stress concentrations. Low density C-S-H resulting from high local water-binder ratios, hindered hydration due to

[57] Sammis and Ashby (1986) 518
[58] Sammis and Ashby (1986) 519, Brace and Bombolakis (1963) 3712
[59] Vonk (1992) 104

410kg/m³ cem. dens.
0:1 Filler-Binder Ratio

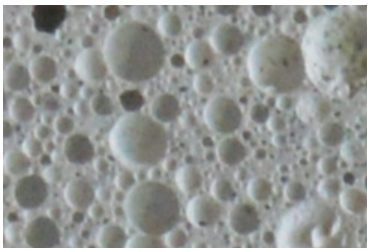

Figure 7.3.3a
Polished surface, 8x magnification

710kg/m³ cem. dens.
0:1 Filler-Binder Ratio

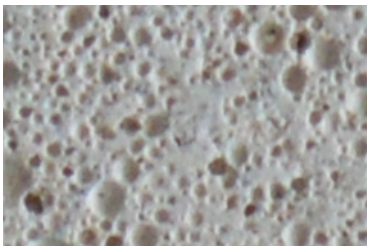

Figure 7.3.3b
Polished surface, 8x magnification

410kg/m³ cem. dens.
3:1 Filler-Binder Ratio

Figure 7.3.3c
Polished surface, 8x magnification

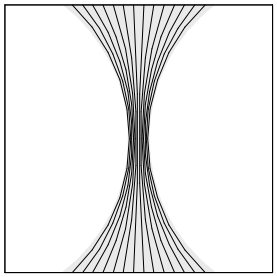

Figure 7.3.3d
Compressive stress
field at slender strut

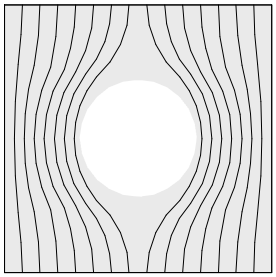

Figure 7.3.3e
Compressive stress
field at spherical void

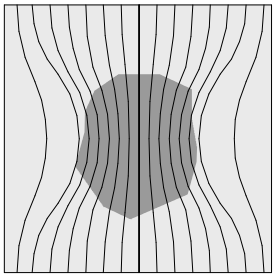

Figure 7.3.3f
Compressive stress field
at aggregate inclusion

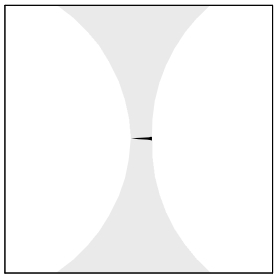

Figure 7.3.3g
Mode of fracture
at slender strut

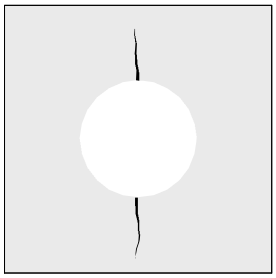

Figure 7.3.3h
Mode of fracture
at spherical void

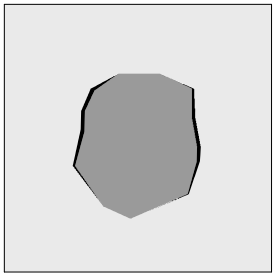

Figure 7.3.3i
Mode of fracture
at aggregate inclusion

Figure 7.3.3j
Horizontal fracture surface
was filled with debris
for 410kg/m³ cem. dens.,
0:1 filler-binder ratio mix.
4x magnification

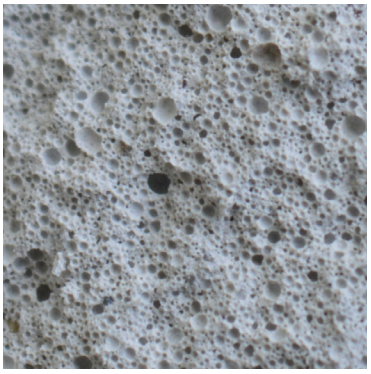

Figure 7.3.3k
Vertical fracture surface was
highly planar
for 710kg/m³ cem. dens.,
0:1 filler-binder ratio mix.
4x magnification

Figure 7.3.3l
Diagonal fracture surface was
highly irregular
for 410kg/m³ cem. dens.,
3:1 filler-binder ratio mix.
4x magnification

interference from foam surfactants,[60] and thermal, mechanical, or hygral-induced microcracks will each degrade the modulus of rupture.[61] The density and smoothness of the C-S-H may be improved through the use of curing regimes that supply water to any unreacted cement grains[62] or limit decomposition due to carbonation,[63] or through the use of pozzolanic materials, which convert calcium hydroxide crystals into C-S-H phases, replacing structural discontinuities in the paste with strong reaction products.

The frequency of failure types among a dozen specimens is shown in Figure 7.**3.3m**. A common fracture pattern for low-density neat Portland cement foam concrete is shown in Figure 7.**3.3o**. Because failure tends to occur in horizontal strata, a failed specimen may not appear to be obviously damaged upon inspection. For fluid foam concrete mixes, the weakest strata are often near the top of the casting, where bubbles have migrated upwards, reducing density. In such cases specimens may fail with a 'quasi-Type 6' break failure, as shown.

Fracture in denser foam concrete is more protracted. With a greater volume of material available to be fractured and rearranged, strain energy can be relieved through microcracking of the paste during loading, without inducing global failure of the air-void system.

As compressive stresses are increased above 40% of f'_c, microcracks will grow in length and number. Cracks will be stable: in a compressive stress field, tension cracks parallel to the applied force will only propagate when loading is increased.[64] Cracks will initially be distributed, and may be temporarily arrested where they intersect with stiff aggregate, strong paste, round voids (where the low curvature reduces the stress concentration), or cracks oriented in other directions.

For neat cement mixes, plastic non-linear behaviour becomes apparent in the stress-strain plot at about 80% or more of the ultimate compressive. Neighbouring branch fractures will not readily intersect, but will instead avoid direct collision due to

---

60 Pan et al. (2014) 258
61 For further discussion, refer to the discussion on air void size in Appendix A, Section 6.3.1b.
62 E.g moist-curing.
63 E.g. seal-curing, cf. Jiang et al. (2016) 957
64 Van Mier 2009

Failure Type Frequency	Typical Microstructural Fracture Pattern	Typical Global Fracture Pattern

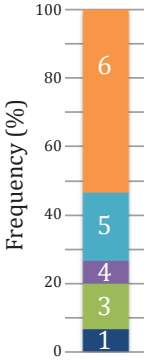

Figure 7.3.3m

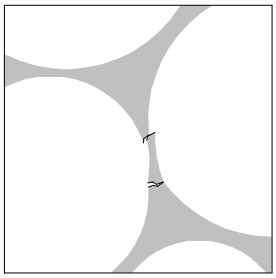

Figure 7.3.3n

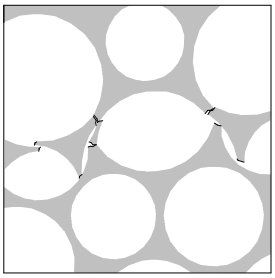

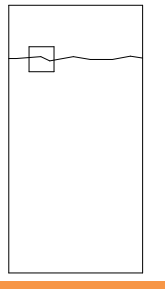

Figure 7.3.3o

Neat cement foam concrete, 410 kg/m^3 c.d., 100% Portland cement binder

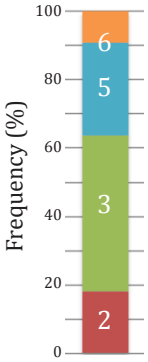

Figure 7.3.3p

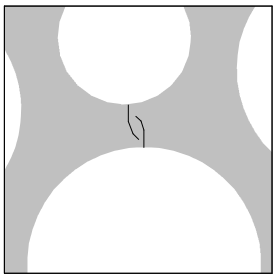

Figure 7.3.3q

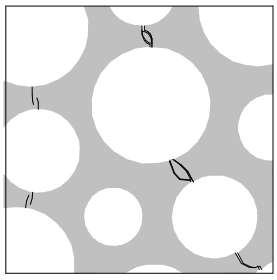

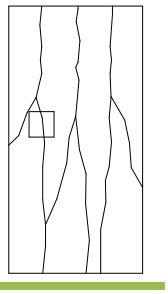

Figure 7.3.3r

Neat cement foam concrete, 710 kg/m^3 c.d., 100% Portland cement binder

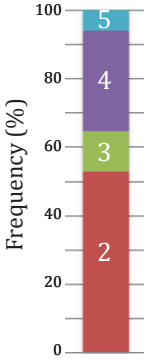

Figure 7.3.3s

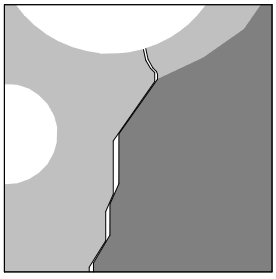

Figure 7.3.3t

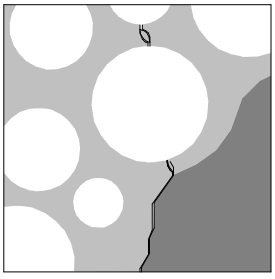

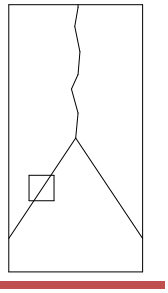

Figure 7.3.3u

Sanded foam concrete, 1800 kg/m^3 n.d., 100% Portland cement binder

interference of stress fields.[65] After the tips of the cracks pass each other, the ligament between the cracks will be subject to bending and buckling.[66] The crack tips will curve towards and eventually intersect with adjacent cracks (Figure 7.**3.3q**). The distance between crack tips is typically small in foam concrete due to the high air-void volume and small space between air voids. However, as density and the spacing between bubbles increases, some apparent ductility may arise from mutual avoidance of crack tips.

With greater heterogeneity, there will be a greater zone of damage, resulting in even more ductile behaviour. This pattern is evident in sanded mixes. A greater quantity of discontinuities in the solid provides a greater number of sites from which cracks may readily nucleate. Furthermore, cracks are forced to go around the fine aggregate, making the crack pattern more tortuous and discontinuous (Figure 7.**3.3t**), and increasing the fracture energy required for global failure.[67] In sanded Portland cement and slag mixes, plastic behaviour apparently begins at about 50% of the compressive stress. In sanded silica fume mixes, plastic behaviour begins at 60% or more of the ultimate compressive strength, likely due to the increased toughness of the paste, resisting initial fracture.

Internal bonds continue to fail as damage zones connect, and stiffness of the material decreases until it is zero at peak load. At this point, deformation localizes into unstable macro-cracks, which coalesce into a continuous system of fracture through the material.[68]

The final cracking pattern of relatively dense, neat cement foam concrete is characterized by columnar cracking, as shown in Figure 7.**3.3r**. Consistently spaced vertical splitting cracks dominate, with some slight curvature due to mutual avoidance of advancing crack tips. Some slender columns may be fractured laterally by buckling. By contrast, the final cracking pattern of sanded foam concrete includes random and steep triangular and conical fragments, resulting from a combination of vertical splitting cracks and inclined shear cracks. Where cracks have been arrested by the presence of aggregate or dense paste, there may be spreading patterns. Type 2 and Type 4 fractures are common, as shown in Figures 7.**3.3s** and 7.**3.3u**.

---

65 Brace and Bombolakis (1963) 3712, Cotterell and Rice (1980), Melin (1983), Simha et al. (1986) 248
66 Sammis and Ashby (1986) 522
67 Vonk (1992) 14
68 Vonk (1992) 104, 108

Crushing and Frictional Restraint

100% Portland binder, 56 days moist-cured

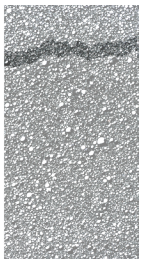

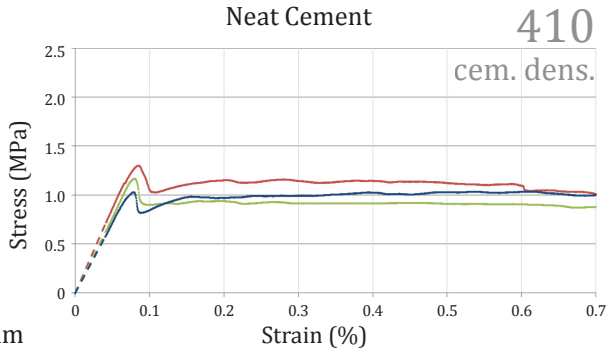

Figure 7.3.4a Weak strata collapse and densify in neat foam concrete of low density. The damage zone increases indefinitely with displacement.

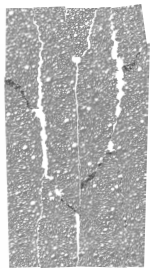

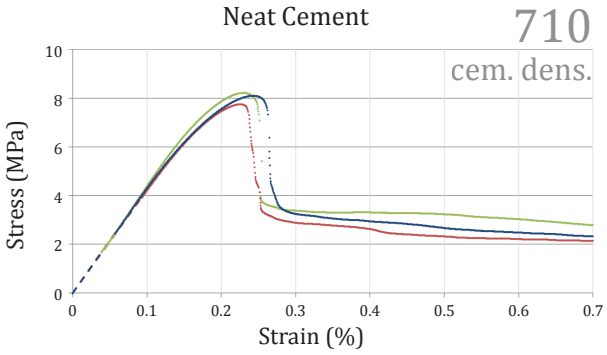

Figure 7.3.4b Neat foam concrete with high density fractures as columnar fragments, which buckle readily. Frictional restraint is minimal.

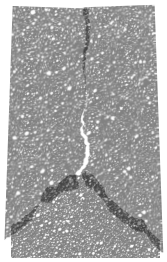

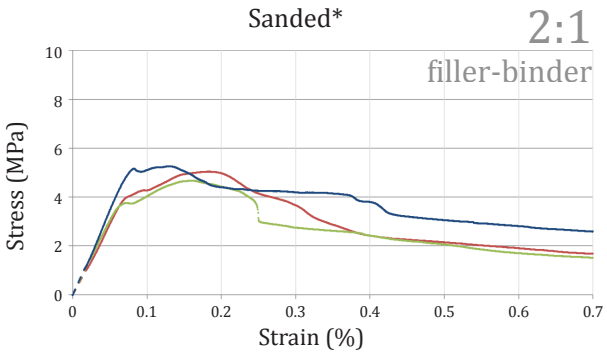

Figure 7.3.4c At medium densities, fractured surfaces 'catch' and conform at points of contact, increasing the damage zone.

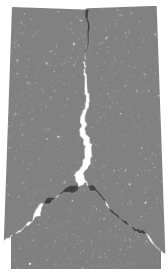

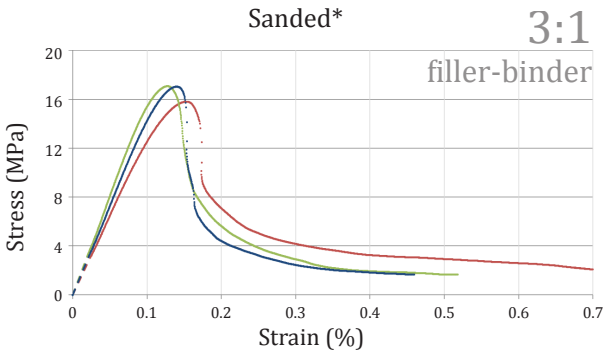

Figure 7.3.4d In dense foam concrete, fragments push apart at points of contact, reducing frictional retraint. Failure is brittle.

*410 kg/m^3 cem. dens.

Ultimate compressive strength increases with density, cementitious density, and the addition of SCMs. Slag binder improves particle packing, and converts calcium hydroxide into C-S-H through pozzolanic reactions. For a given density, the ultimate compressive strength is highest in silica fume mixes: in addition to pozzolanic reactions, the fine solid material promotes the production of an air-void system with fine, evenly-spaced bubbles.

7.3.4 Crushing Phase

Stress-strain relationships reveal various mechanical phenomena beyond peak load.

In low-density neat cement mixes, cycles of rising and falling stress indicate that weak strata are collapsing and densifying. As the weakest strata are eliminated, loading may increase above the levels that triggered the initial collapse (Figure 7.**3.4a**). In most cases, however, the jagged fractured surface will readily pierce adjacent intact cell walls, facilitating continued compaction with less load than was required to initiate collapse of the stable air-void system (Figure 7.**3.4b**).

For low-density Portland binder mixes, stress peaks slightly at the ultimate compressive strength; thereafter, fracture energy is released continually and consistently, as the debris material crushes through soft paste into adjacent void spaces. In many low-density slag or sanded specimens subjected to simple compression, stress continues to rise post-failure, as fractured surfaces catch and transfer shear via interlocking of angular slag or sand particles.

For strong and dense mixes, the initial condition of the hardened paste is the most stable, and fracture causes a decrease in mechanical resistance, i.e. softening. The specimen's capacity to support load diminishes as macrocracks continue to propagate through the failed cross-section.

Irregularity in the descending branch of the stress-strain curve may be attributed to a non-uniform cracking process.[69] Macrocracks are arrested and elongated in different regions of the specimen, as the stress field changes continually. Frictional restraint at points of contact between fractured surfaces contributes significantly to the pattern of

[69] In some cases, softening irregularity may be attributed to the control of the application of load. For example, snap-back may occur when deformation control is not sufficiently steady. Refer to the discussion in Section 6.9. Vonk (1992) 16

damage. An irregular pattern of softening tends to occur in specimens with soft paste and high air-void volumes. Fractured surface geometries tend to 'catch' and interlock, while conforming readily to each other by local crushing of exposed cell walls (Figure 7.**3.4c**). With many points of contact, the damage zone is enlarged, and ductility is increased.

Brittleness will be higher where fractured surfaces are pushed apart at points of contact, rather than conforming to each other (Figure 7.**3.4d**). This pattern occurs in denser mixes, where there is less air-void space available for debris, and therefore less crushing. Greater homogeneity also reduces the tendency for frictional restraint. Where the stiffness of the paste is closer to the stiffness of the aggregate, vertical splitting cracks at the air-void will dominate fracture behaviour, rather than shear cracks at the aggregate bond interface. Similarly, dense or especially strong neat cement mixes will fracture cleanly into discrete columnar fragments. In all of these cases, damage will be mainly concentrated along the fracture paths of the original localized macrocracks. The brittleness of specimens is signified by a steep slope in the stress-strain curve, post-peak.

The softening curve becomes smoother after global facture. Crack growth is no longer significant; instead, friction at contacts provides the residual mechanical resistance. The load-bearing capacity of the remaining material diminishes as resistance at the contacts is degraded by shear cracking (i.e. shear softening);[70] simultaneously, the number of contacts rapidly decreases as the crack pattern opens with increasing deformation.

7.3.5 Lateral Response/Dilation

Values obtained for the Poisson's ratio of foam concrete have a high degree of variability (Figure 7.**3.5a**). This variability may be due in part to the difficulty of accurate measurement, but it may also be due to the nature of the material itself, both in its pore structure, and as a heterogeneous composite of fine aggregate and hardened cement paste.

Young's, shear, and bulk moduli (E, G, and K, respectively) decrease monotonically with increasing porosity in an isotropic solid. The relationship between porosity and Poisson's ratio, ν, appears to be more complex. Poisson's ratio can be given as a function of any two other elastic moduli (e.g. $\nu = E/2G - 1$, $\nu = 0.5 - E/6K$), and the relative

[70] Vonk (1992) 108

dependence of these other moduli on porosity will affect how Poisson's ratio varies with porosity.

Based on Mori-Tanaka theory for heterogeneous materials, Dunn and Ledbetter[71] have demonstrated mathematically that Poisson's ratio may increase, decrease, or remain unchanged with increasing porosity, depending on the pore shape and on the Poisson's ratio of the defect-free bulk solid. Interconnection of pores may also influence Poisson's ratio.[72]

The dependence of Poisson's ratio on porosity may be readily appreciated at low densities. As noted in Section 7.2.1, even at high porosities, bulk modulus may be dominated by simple compression of members, since microstructural transformations are affine. Young's modulus and shear modulus, however, may be subject to significant strut bending with decreasing density, since these deformations involve distortion. These elastic moduli will vary to differing degrees with increasing porosity, with consequences for Poisson's ratio. In an empirical study, Ashkin et al.[73] detected a dependence on microstructure for Poisson's ratio of cellular materials with low relative density (i.e. PR between 0.15 and 0.4), which may be due to localized bending within the porous material. In their study, the Poisson's ratio of porous silica ceramic with spherical voids ranged from 0.26 at 80% porosity, diminishing to 0.16 as porosity was reduced to 0%.

The presence of aggregate further complicates Poisson's ratio. For normal density concrete, the volume fraction of aggregate in the mix is known to influence on Poisson's ratio. Models[74] and experimental data[75] suggest that Poisson's ratio will decrease with increasing heterogeneity, as stiff aggregate inclusions restrain lateral expansion of the more compliant matrix.

Observed PR values for foam concrete range from 0.33 to 0.15. PR is generally lowest in dense, sanded mixes. Sand aggregate is stiffer than the C-S-H, and restrains lateral

71 Dunn and Ledbetter (1995)
72 Cf. Wang (1984)
73 Ashkin et al. (1990)
74 Allos and Martin (1981)
75 Anson and Newman (1966) 119, Swarmy (1971) 567

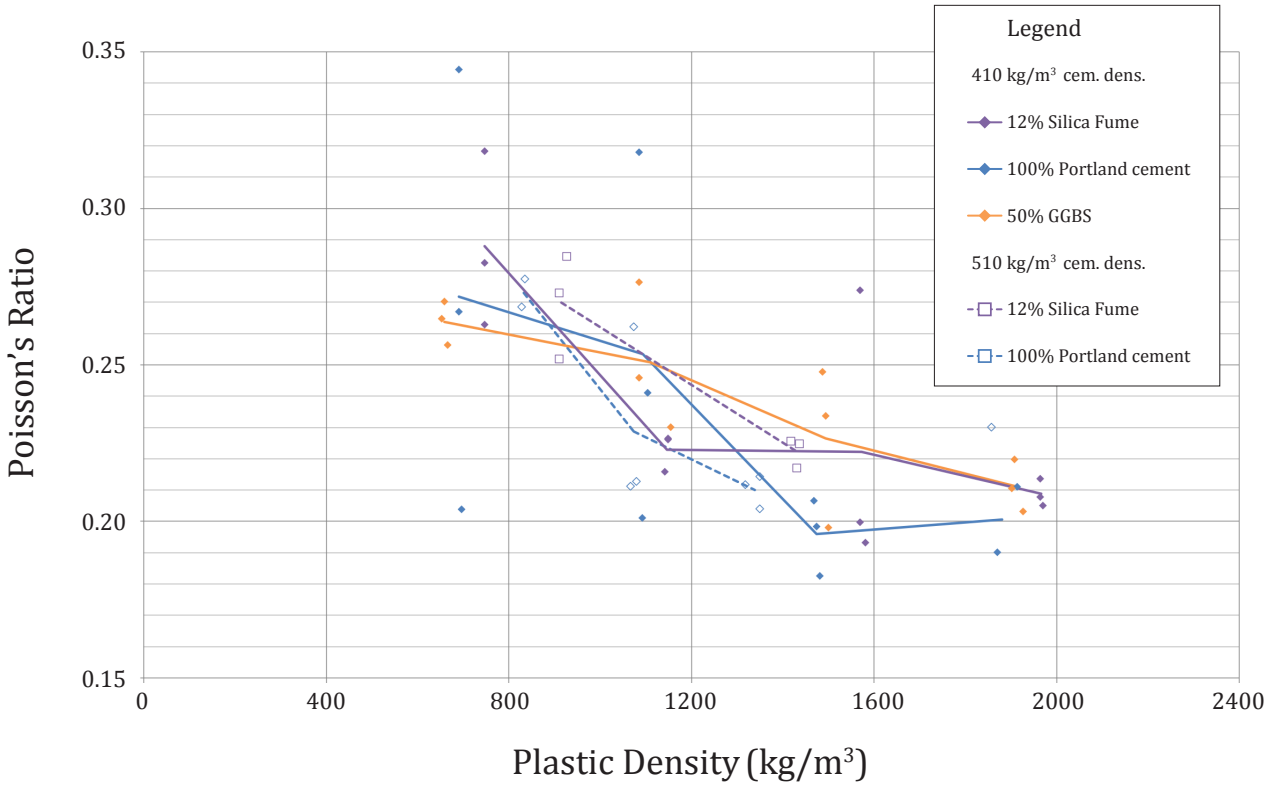

Figure 7.3.5a Poisson's ratio vs. plastic density, 28 days moist-cured.

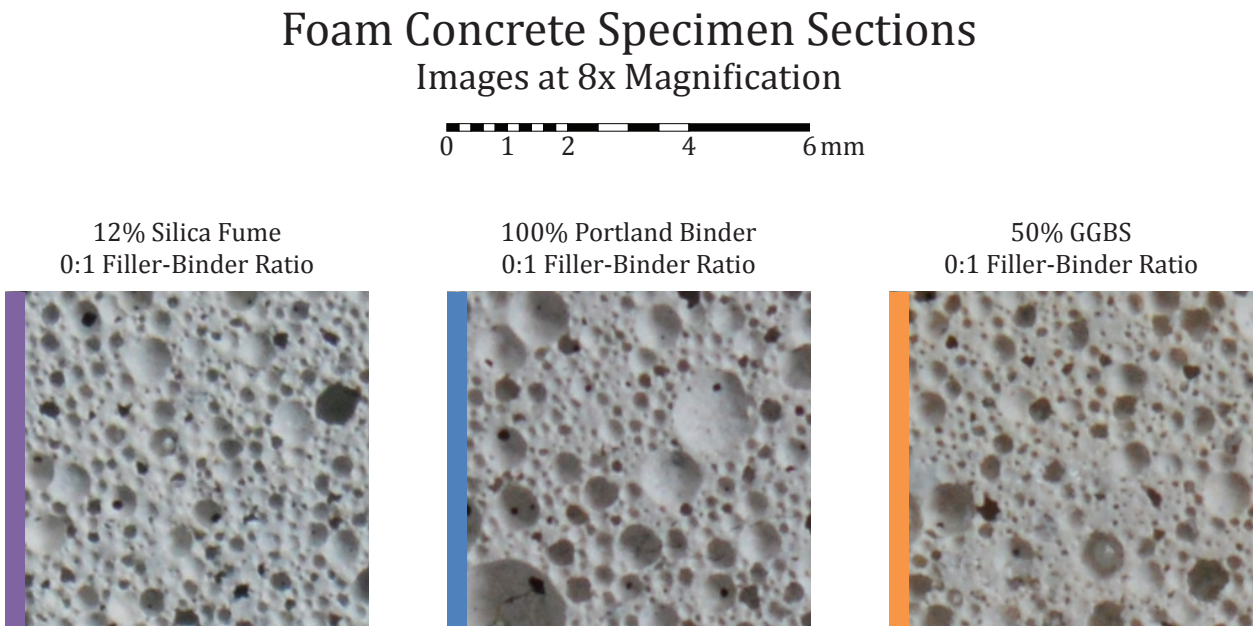

Figure 7.3.5b Microstructural images for mixes with no filler. Variability within microstructures account for some of the variability in Poisson's ratio, as the shape and orientation of interconnected voids influences lateral response.

expansion of the matrix (Figure 7.**3.5c**). The air-void system includes small, consistently sized pores, which may contribute to relatively low variability among specimens.

PR is highest in neat cement foam concrete. The compliant C-S-H is not restrained by aggregate inclusions. Furthermore, flexure of the fine microstructure may contribute to lateral expansion. The geometry of the air-void system is more variable with decreasing density, due to increased coalescence of air voids during plastic state (refer to Section 7.1); variability of the microstructure may help explain some of the variability in PR, as the shape and orientation of interconnected voids strongly influences lateral response.[76]

PR appeared to be highest in low-density mixes with silica fume. This pattern may be related to the chemistry of the paste, the geometry of the air-void system, or both. Chemically, pozzolanic activity eliminates stiff calcium hydroxide crystal. With fewer stiff restraining inclusions, the C-S-H paste can expand laterally more easily. Geometrically, a fine and consistent air-void system minimizes local microcracking in regions of high stress. Applied axial stress is thus translated into lateral deformation, rather than inducing stress-relieving fracture.

Considerable scatter in the data makes it difficult to define additional trends with certainty. It is possible that Poisson's ratio is generally slightly higher in 28-day specimens than in 56 days, which could be due to decreasing porosity with age (i.e., a higher gel-space ratio from continued hydration). However, further study would be necessary to confirm this trend.

For stresses up to 40% of f'c, the ratio of axial to lateral strain is highly linear in well-formed specimens (Figure 7.**3.5d**). At somewhat higher stresses, microcracks will form within the specimens, approximately parallel to the direction of compressive stress, inducing plastic lateral deformation. Foam concrete dilates at an increasing rate during localization, and undergoes rapid lateral expansion after global fracture due to longitudinal cracking.

[76] Cf. Dunn and Ledbetter (1995)

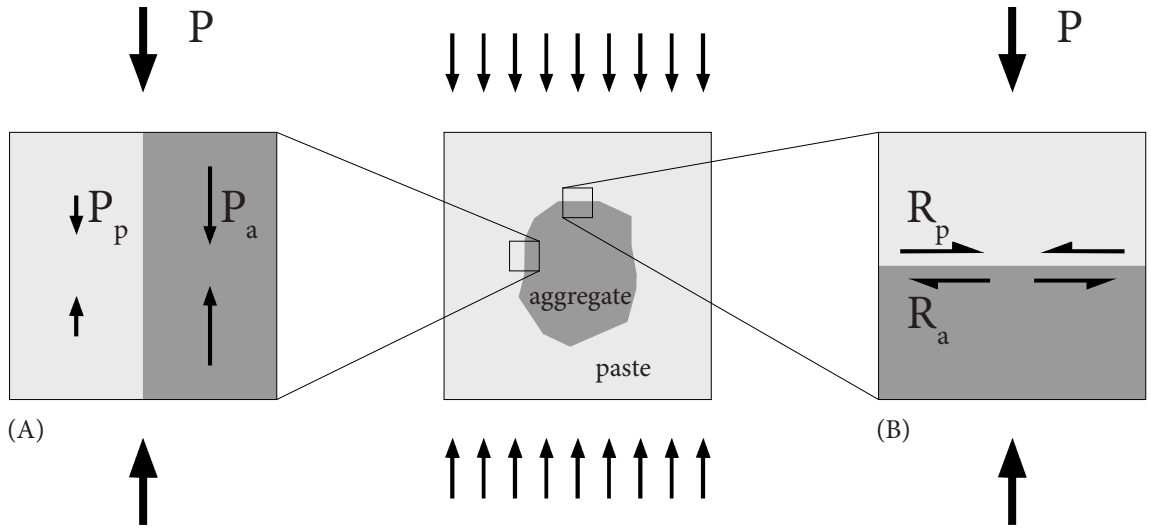

(A) Finite element at vertical interface. Despite varying elastic moduli, paste and aggregate undergo the same axial strain, with the stiff aggregate carrying proportionally more load (P_a).

The introduction of stiff aggregate reduces the load on the adjacent paste. Axial strain in the paste is therefore reduced; and transverse strain is reduced proportionally, according to the Poisson's ratio of the paste.

(B) Finite element at horizontal interface. Paste and aggregate experience the same vertical compressive force. Despite varying Poisson's ratios, the two materials undergo the same transverse strain, due to internal restraint at the bond.

Lateral expansion of the paste is restrained by the aggregate. The restraining force in the paste is designated 'R_p'.

Figure 7.3.5c Effect of aggregate inclusions on Poisson's ratio.

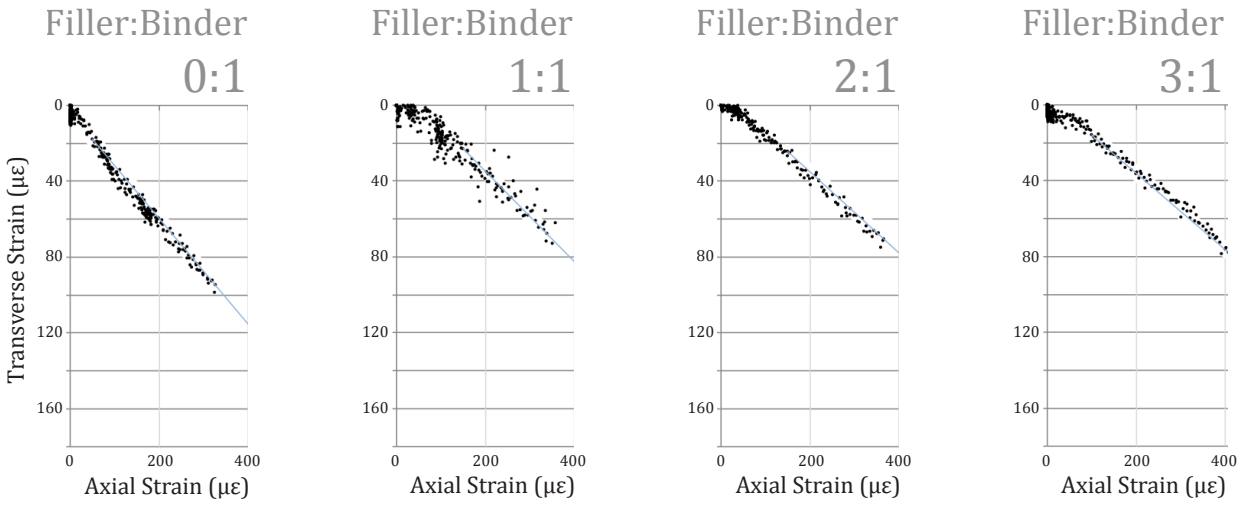

Figure 7.3.5d Relationship of axial strain to tranverse strain for Portland cement specimens.

7.3.6 Creep

Creep is the slow increase in strain induced by applied stress, which is separate from spontaneous elastic deformation. Creep is a property of all viscoelastic materials. However, unlike metals and polymers, concrete changes significantly as it ages, in chemistry, internal relative humidity, mechanical properties and microstructure, affecting creep behaviour. For foam concrete, creep behaviour is even more complex due to the geometry of the air-void system.

Concrete creep is largely due to the viscoelastic and viscoplastic properties of C-S-H, while the creep deformation of secondary cementitious reactants or aggregate are less significant.[77] Various models have been proposed to explain complex restructuring of C-S-H, based on i) expulsion of water, ii) shear slippage of solid phases, or iii) chemical dissolution and precipitation. These are summarized briefly below.

i) Powers' seepage theory[78] proposes that under long-term loading, load-bearing adsorbed water (notably in hindered absorption regions) is gradually expelled into non-loadbearing regions. Load is increasingly transferred via solid phases as the specimen reduces in volume. Bažant[79] extended this theory in a thermodynamic model to include the role of capillary and interlayer water. Research by Acker[80] suggests that C-S-H sheets collapse into compact structures through largely irreversible drainage processes.

ii) Slippage has been proposed both for granular and layered models of C-S-H. Reutz[81] hypothesized that C-S-H particles shear or 'slip' past each other, with adsorbed water acting as a lubricant. Jennings[82] proposed that creep occurs through the shearing of C-S-H 'globules', as intergranular bonds rupture and reform; Vandamme and Ulm[83] determined that creep is a function of the packing and jamming of three distinct densities of nanoscale C-S-H particles. Feldman[84] suggested that compressive stress initially induces expulsion of interlayer hydrate water from C-S-H sheets, but that long-term creep is due to

77 Acker (2001), Acker (2004) 241
78 Powers (1968)
79 Bažant (1972) 505, Bažant (1975) 31
80 Acker (2004) 241
81 Ruetz (1968) Cf. Vichit-Vadakan and Scherer (2001), Alizadeh et al. (2010)
82 Jennings (2004)
83 Vandamme and Ulm (2009)
84 Feldman (1972)

the subsequent shear or tensional stresses on the layers, resulting in shear slippage, microcracking, and breaking and reformation of bonds. Following this model, various researchers[85] have argued for a theory of sliding C-S-H sheets.

iii) As early as 1972, Bazant[86] postulated that moving water molecules might force Ca^{+} ions or other solutes to move with them, driving solids out of load-bearing regions and intensifying creep. Pignatelli et al.[87] have recently found direct evidence for a dissolution-precipitation creep mechanism for C-S-H in greater than 50% RH. In their model, pressure on the C-S-H promotes its solubility. Dissolved species of C-S-H diffuse through liquid or adsorbed water, following Fickian diffusion, removing solids from load-bearing regions.

The causes of creep in concrete are a subject of continued debate. It is plausible that collapse-drainage, shear slippage, and dissolution-precipitation mechanisms of concrete creep can each operate simultaneously or within a unifying theory.[88]

For foam concrete, the expulsion of load bearing water may be an important early creep mechanism.[89] Mixes typically have high water-binder ratios, which would tend to produce low-density solid phases with high surface areas, thick layers of adsorbed water, significant regions of hindered adsorption and high capillarity. Load-bearing water may be compressed out of small voids or interlayer regions, into the surrounding air voids.

Shear deformation is also a plausible creep mechanism in the saturated, low-density microstructures of young foam concrete. In Jenning's colloidal model, low-density phases shear readily, without significantly altering intergranular (i.e. inter-globular) bonding.[90] Large proportions of creep should therefore be recoverable. Based on the Feldman-Sereda model, the presence of interlayer water in moist foam concrete would contribute to slippage of C-S-H layers.[91] Low-density structures at sites of hindered water absorption could easily become overstressed, and these bridges in the C-S-H could allow shear slip.[92]

---

85 Bažant et al. (1997), Alizadeh et al. (2010)
86 Bažant (1972) 505
87 Pignatelli et al. (2016)
88 Cf. Bažant (1972) 479, Feldman (1972) 522, Kondo and Daimon (1974), Wittman (1982) 131, 147, Vandamme and Ulm (2009) 10552, Alizadeh et al. (2010) 369, Šmilauer and Bažant (2010) 198, Pignatelli et al. (2016) 9.
89 Cf. Wittman (1982) 147
90 Jennings (2004)
91 Alizadeh et al. (2010) 375
92 Bažant et al. (1997) 1190

Dissolution under stress is perhaps less likely to be a significant factor in foam concrete creep, since applied stresses are limited by fracture and crushing of the foamed structure, and are typically low. However, it is possible that high stresses may develop through the bending of fine microstructural elements.

For low-density foam concrete, the air-void structure will likely play a significant role in creep behaviour. Under loading, thin struts may buckle slightly (refer to Section 7.3.1). The deflected shape of a strut will initially have large radii of curvature. However, at high stress, creep of C-S-H is non-linear,[93] therefore curvature will tend to become concentrated near the mid-point of the strut where stress is greatest (Figure 7.**3.6a**).[94] This phenomenon will reduce local load-bearing capacity, promote increased stress (and therefore increased creep) in other regions of the cross-section, and may induce progressive collapse.

The air-void structure also influences aging effects of the C-S-H. Permeability increases with air-void volume and interconnectivity, and the transport of gasses through the foam will influence rates of drying, carbonation and continued hydration. Each of these processes can affect creep behaviour. For example, rapid drying will remove water needed for hydration, limiting the continued solidification and stiffening of the foam, which normally helps resist creep.[95] Rapid drying shrinkage[96] or carbonation[97] will introduce residual stresses in the C-S-H, creating overstressed sites where creep may be facilitated.

Given the material and geometric properties described above, it is unsurprising that creep rates of foam concrete are very high, relative to normal density concrete. Specific creep after one year was approximately 12,000 μstrain/MPa (i.e. 1.2%/MPa) for unsealed 600 kg/m^3 foam concrete specimens, and between 1000 and 2000 μstrain/MPa in 1400 kg/m^3 foam concrete. In comparison, values for normal density concrete typically lie between 100 and 200 μstrain/MPa.[98] Since applied loads for foam concrete are less than

93 Neville (1959), Bažant (1988) 147-149, Ashby et al. (2014) 334.
94 Gibson and Ashby (1999) 127
95 Cf. Bažant and Prasannan 1989a
96 Thomas and Jennings (2001)
97 Jiang et al. (2016b) 958
98 Mehta (1986) 93

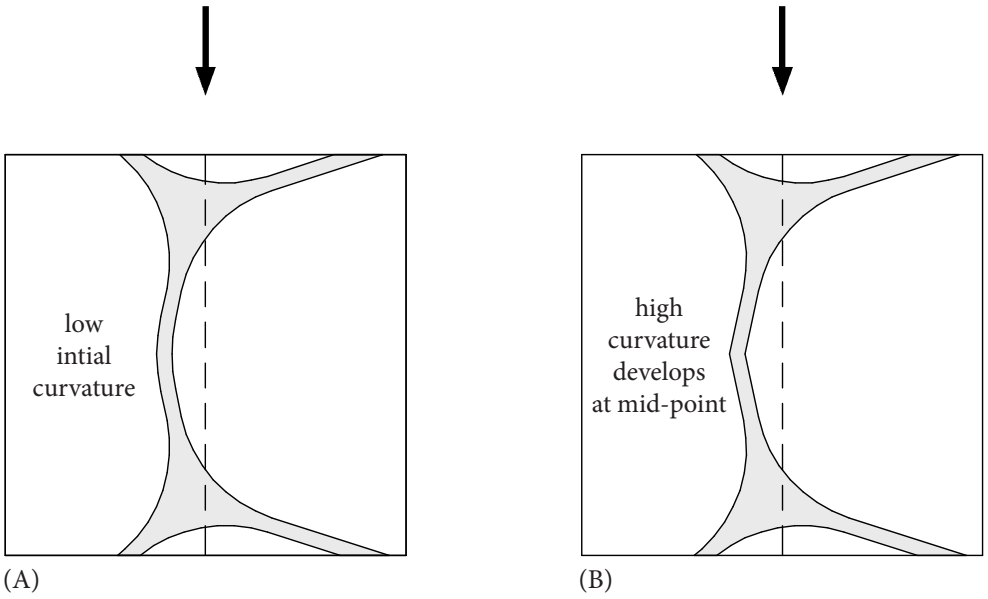

Figure 7.3.6a The creep behaviour of foam concrete is influenced by the buckling of thin struts. Deflection of struts will initially be sinusoidal (A), but non-linear creep will tend to concentrate curvature near the mid-point (B), reducing load-bearing capacity and promoting buckling. After Gibson and Ashby (1999) 127.

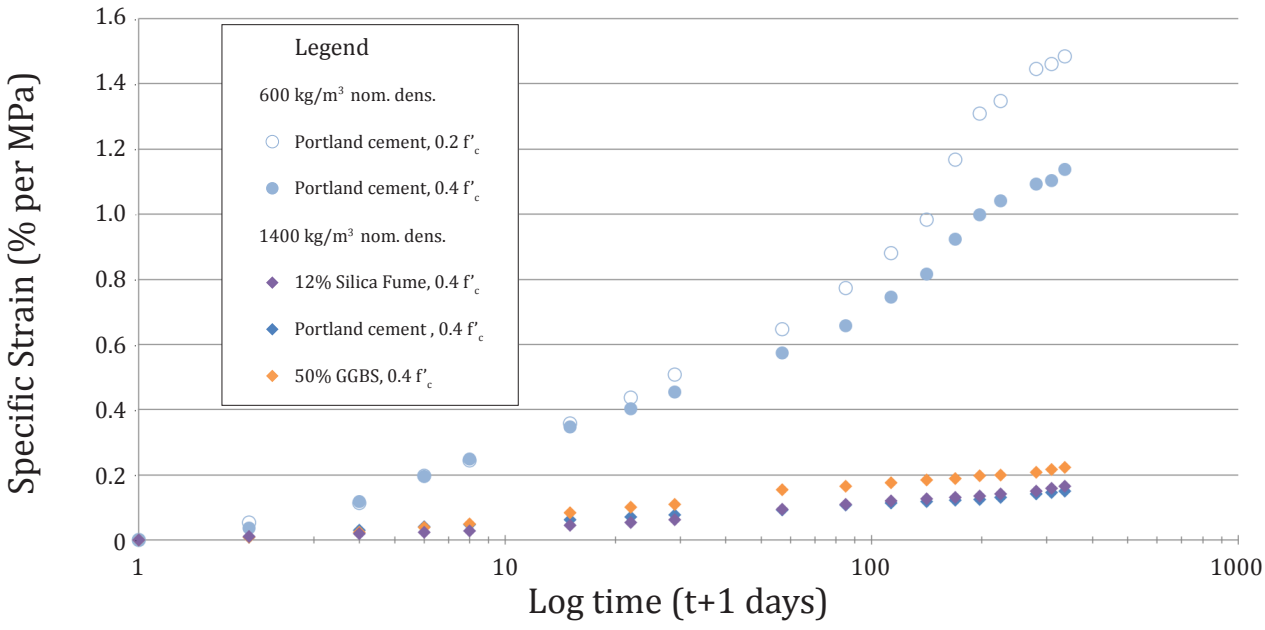

Figure 7.3.6b Specific creep strain of foam concrete specimens, not including strain induced immediately after loading.

for normal density concrete, differences in actual deformation in-service would be less extreme. Importantly, creep values from the experimental program are higher than those determined by other researchers for sealed specimens.[99]

Many trends in the data may be understood in light of microstructural interactions. Most obviously, the addition of aggregate reduces creep rates considerably (cf. 600 and 1400 kg/m^3 Portland cement mixes in Figure 7.**3.6b**). The non-aging, non-viscous aggregate phase elastically restrains[100] creep deformations, resisting the viscous flow of the C-S-H matrix (Figure 7.**3.6c**).[101] Creep will decrease with increasing aggregate stiffness,[102] and with a higher volume fraction of aggregate.[103] In mixes with very high volume fractions of aggregate, compliant C-S-H between the aggregate particles will creep initially to relieve internal stresses, but creep will slow as the aggregates pack and jam, densifying the C-S-H at contact points and creating load paths through the hardened cement paste via contiguous stiff sand particles.[104]

Creep rates for denser mixer appear to adhere closely to a logarithmic function, while lower density foam concrete mixes appear fluctuate more significantly in creep rate (Figure 7.**3.6d**). The relatively low permeability of denser foam concrete reduces the rate and abruptness of change within specimens.[105] For example, Figure 7.**3.6e** indicates that moisture is released at a slower rate with higher density, which would result in more constant internal relative humidity and reduced drying effects. Similarly, the progress of carbonation will be reduced with decreasing permeability. Stable internal conditions reduce changes in creep rate associated with humidity and chemical change.

Notably, the plot of creep for 600 kg/m^3 foam concrete shows a slight point of inflection after 56 days (Figure 7.**3.6d**), with an apparent acceleration in the rate of creep on a semi-log plot. It is possible that early rates of creep are suppressed slightly by

---

99 Kearsley (1999b) 153-156, Brady et al. (2001) C12

100 Šmilauer and Bažant (2010) 198

101 The rigid inclusion and the C-S-H matrix will tend to undergo the same deformation at their interface, resulting in a resistance to creep. Rigid aggregate inclusions similarly restrain axial and lateral deformations under load. Refer to Sections 7.3.2 and 7.3.5, respectively.

102 Troxell et al. (1958)

103 Scheiner and Hellmich (2009) 308

104 Acker (2004) proposes a similar compacted contact zone between hydrating cement grains, p. 238.

105 Cf. Troxell et al. (1958). Long-term creep specimens subjected to load in 100% RH exhibited close adherence to a logarithmic function, while specimens subjected to drying appeared to fluctuate more significantly in creep rate. Also compare Neville (1963) 302, Bažant (1975) 49.

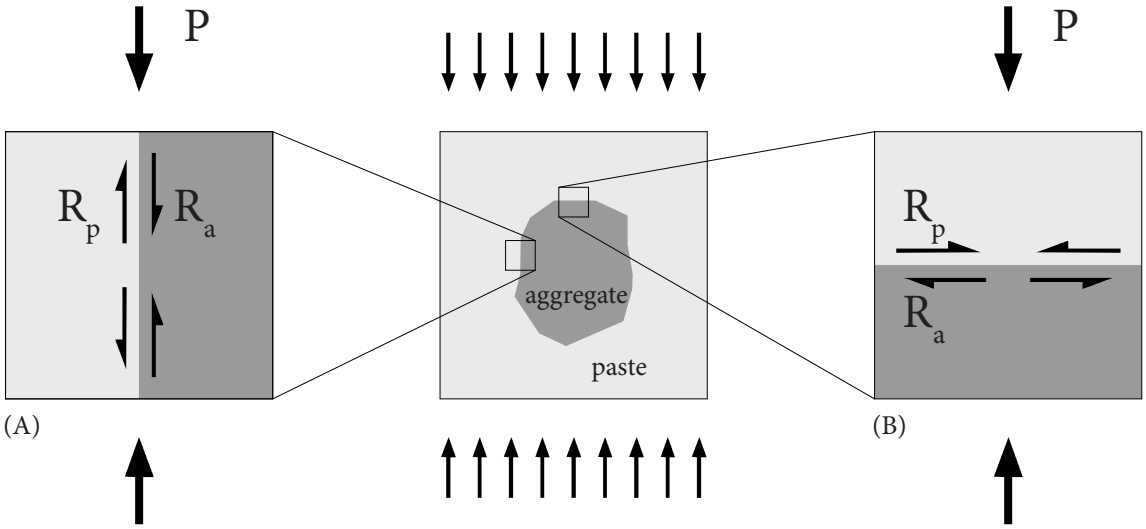

Figure 7.3.6c Finite elements at (A) horizontal and (B) vertical paste-aggregate interfaces. The stiff aggregate resists the viscous flow the C-S-H paste, inducing restraining forces, R_p.

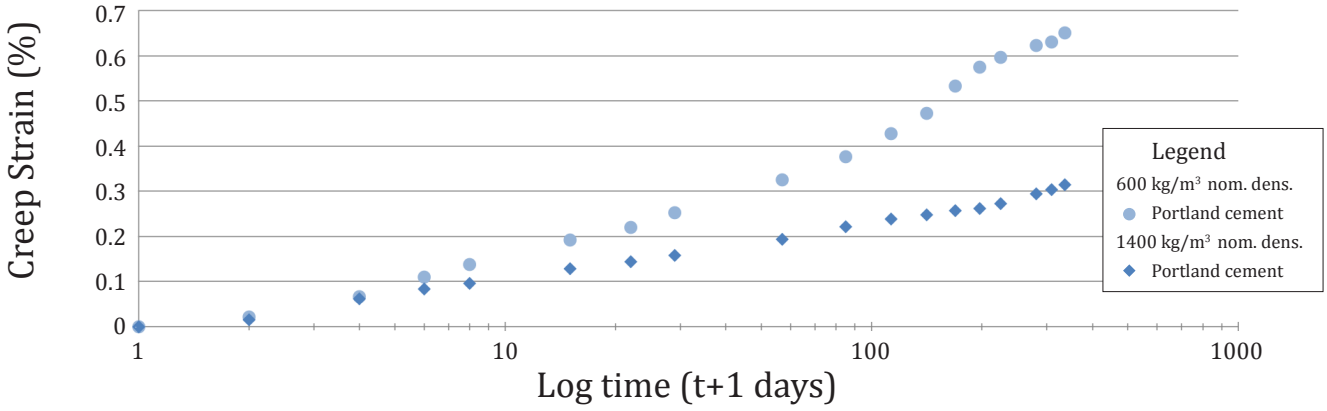

Figure 7.3.6d Creep strain of 600 and 1400 kg/m³ Portland cement foam concrete mixes, loaded to 0.4 f'_c.

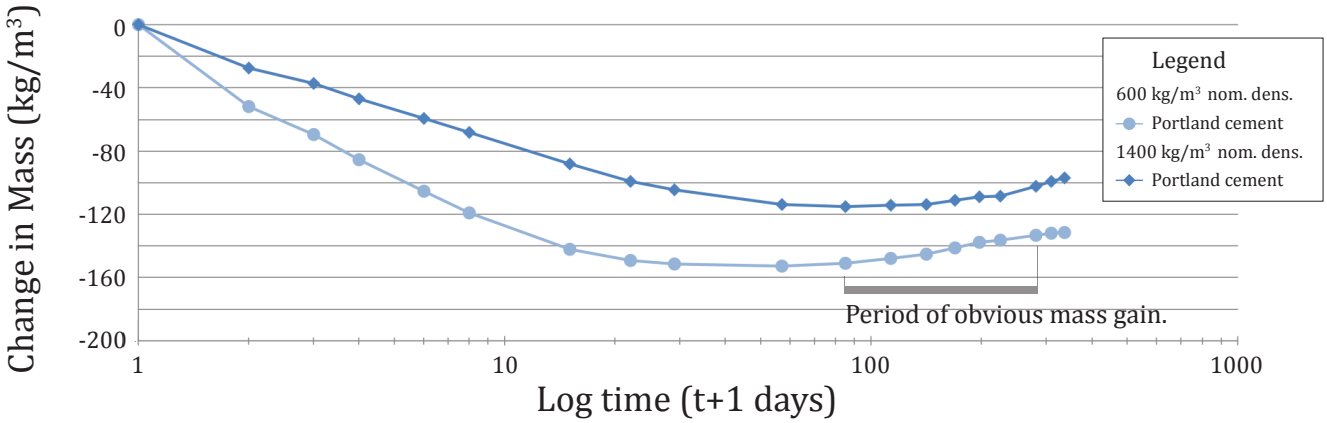

Figure 7.3.6e Change in mass of 600 and 1400 kg/m³ Portland cement foam concrete mixes during drying in 50% RH. The lower permeability of denser mixes promotes more stable internal conditions, reducing abrupt changes in creep rate.

continued hydration, with the deposition of new calcium silica hydrates increasing stiffness and viscosity of the C-S-H during this period.[106] The foam concrete appears to reach equilibrium moisture content with the 50% RH environment between 28 and 56 days, at which point further contribution of hydration to solidification may be more limited.

It is also possible that carbonation contributes to the accelerated creep rate evident after approximately 56 days. Maximum carbonation occurs in environments of approximately 50% RH,[107] and test specimens continued to increase in density after 56 days of creep testing, indicating that this process may have been active in the highly permeable material (Figure 7.**3.6e**). Carbon dioxide dissolves in water to form carbonic acid, which reacts with calcium hydroxide to form soluble calcium bi-carbonate. Calcium carbonate precipitates out with further interaction:

$$H_2O + CO_2 \rightarrow H_2CO_3$$

$$H_2CO_3 + Ca(OH)_2 \rightarrow Ca(HCO_3)_2 \text{ (soluble)}$$

$$H_2CO_3 + Ca(HCO_3)_2 \rightarrow H_2O + CaCO_3 \text{ (precipitate)}$$

This dissolution-precipitation mechanism facilitates creep, as calcium carbonate is deposited in spaces free from stress, and compressibility of the remaining load-bearing paste is increased.[108]

Diminished creep rates, as observed around 200 days, may be related in part to densification and the thickening of cell walls via carbonation and hydration processes. More significantly,[109] creep rate will tend to decrease as weak regions within the foam concrete microstructure are eliminated through crushing.[110]

For low-density foam concrete, the relationship of creep and stress is approximately linear for short times, but non-linear for longer times (Figure 7.**3.6g**). Non-linearity is common in concrete specimens subject to humidity variation (e.g. drying), due to non-additive strains.[111] Interestingly, specific creep is generally higher for a loading of 0.2 f'c

---

106 Bažant and Prasannan (1989a). Cited in Bažant et al. (1997)

107 Verbeck (1958) 24

108 Neville (1963) 298

109 Creep data from Kearsley (1999b), for low-density sealed foam concrete specimens shows a reduction in creep rate at approximately 200 to 300 days, similar to the pattern shown here. It is reasonable to conclude that densification through physical crushing is more significant to the reduction of creep than densification through chemical change, since chemical changes in the sealed specimens at this late age would have been low.

110 Cf. Gibson and Ashby (1999) 177, regarding the densification regime in compression of brittle-elastic foam.

111 Bažant (1975) 5 Theory of Creep and Shrinkage in 'Concrete Structures: A Precis of Recent Developments, Bažant (1988) 236 mathematical modelling of creep and shrinkage

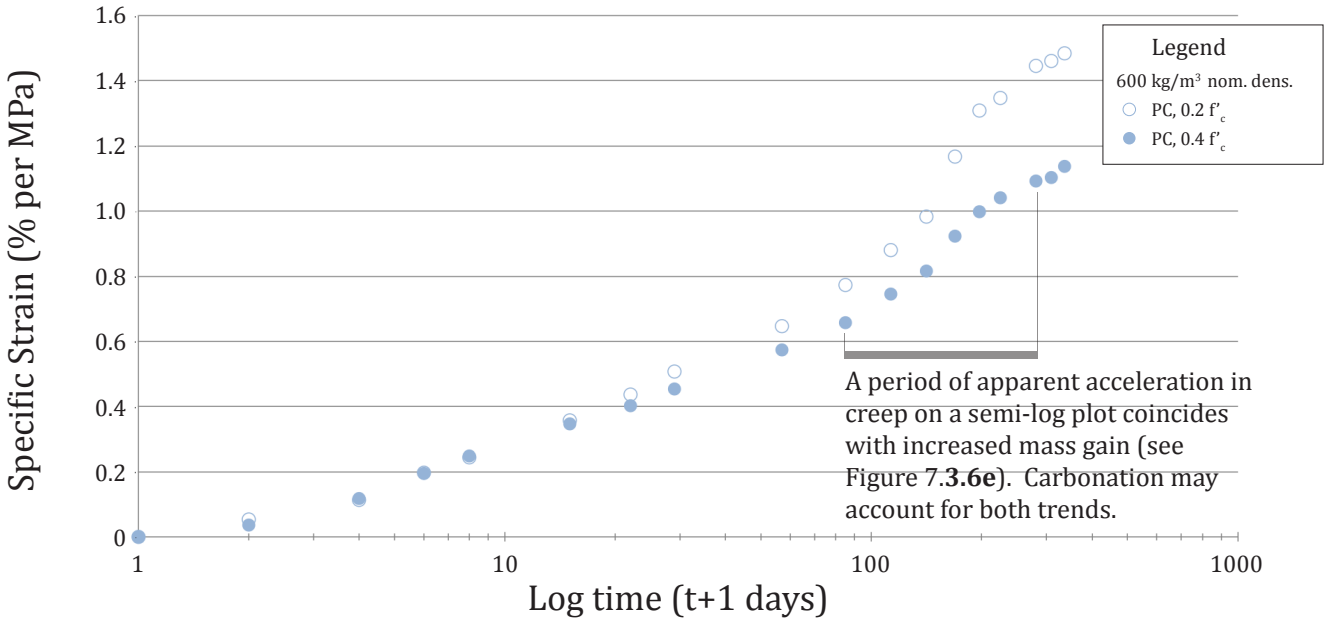

Figure 7.3.6f Specific creep strain plotted against time for 600 kg/m^3 Portland cement foam concrete with applied loads of 0.2 and 0.4 f'$_c$.

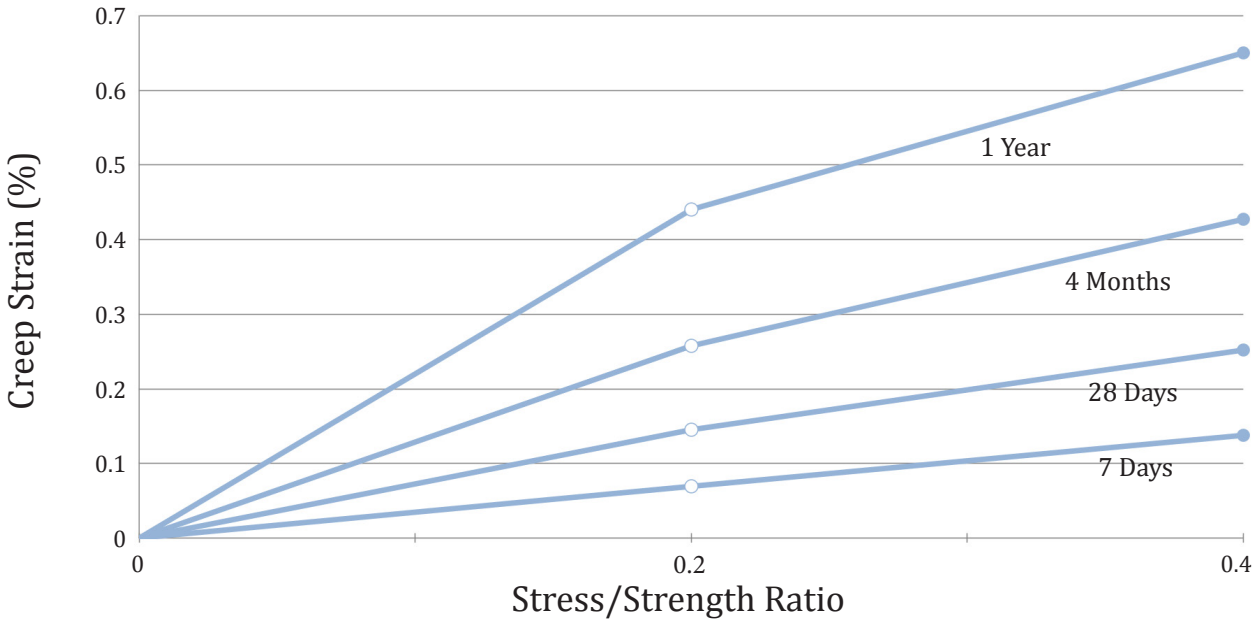

Figure 7.3.6g Creep strain plotted against stress-strength ratio, for various loading times of 600 kg/m^3 nominal density Portland cement specimens. The relationship between creep applied stress was approximately linear for short times, but was non-linear for long times.

than for a loading 0.4 f'c. Initially, this phenomenon appears contradictory to the Pickett effect,[112] which is the observation that the sum of pure creep and pure shrinkage is less than the deformation caused by simultaneous compression and drying. In this case, lower load produces higher apparent specific strain.

Two possible explanations for this trend are considered below. The first hypothesis is that moderate compression suppresses tensile cracking caused by differential drying shrinkage[113] or carbonation. Thus, the application of compressive stress eliminates an expansive strain from the total deformation. Assuming that loadings of 0.2 f'_c and 0.4 f'_c are equally sufficient to suppress tensile cracking, the reduction in expansive strain would have a more obvious effect on the apparent creep strain of the lightly loaded specimen.

This proposal is illustrated in Figure 7.**3.6h**. An unloaded specimen is subject to shrinkage cracking, which is suppressed in specimens loaded to 0.2 f'_c and 0.4 f'_c. If the effect of shrinkage cracking were eliminated from the creep strain of the unloaded specimens, a linear relationship between stress and creep strain would be apparent (dashed line). Instead, non-linearity arises when the expansive deformation of the unloaded companion specimens is included in the calculation of basic creep (solid line).

This mechanism may play a minor role in explaining non-linearity, but does not account for all of the trends. For example, tensile cracking would normally be greatest at early times, during the most extreme drying; however the relationship between creep and stress is most linear at short times.

A second hypothesis posits that even modest compression (e.g. 0.2 f'_c) is sufficient to cause instabilities in low-density foam concrete, since the geometry of fine microstructures will tend to generate highly stressed regions in bending. For example, threshold stresses may be exceeded in the buckling of struts. In the high-stress range, C-S-H creep is non-linear; thus, thin-walled cellular geometries can facilitate long-term damage and deformation that is disproportionate to the stress applied (Figure 7.**3.6i**).

The process of cell wall creep buckling is represented in Figure 7.**3.6j**: (A) a cell wall has an initial defect which induces bending under load; (B) the curvature is increasingly

[112] Pickett (1942)
[113] Wittman and Roelfstra (1980) 602, cf. Acker and Ulm (2001) 145

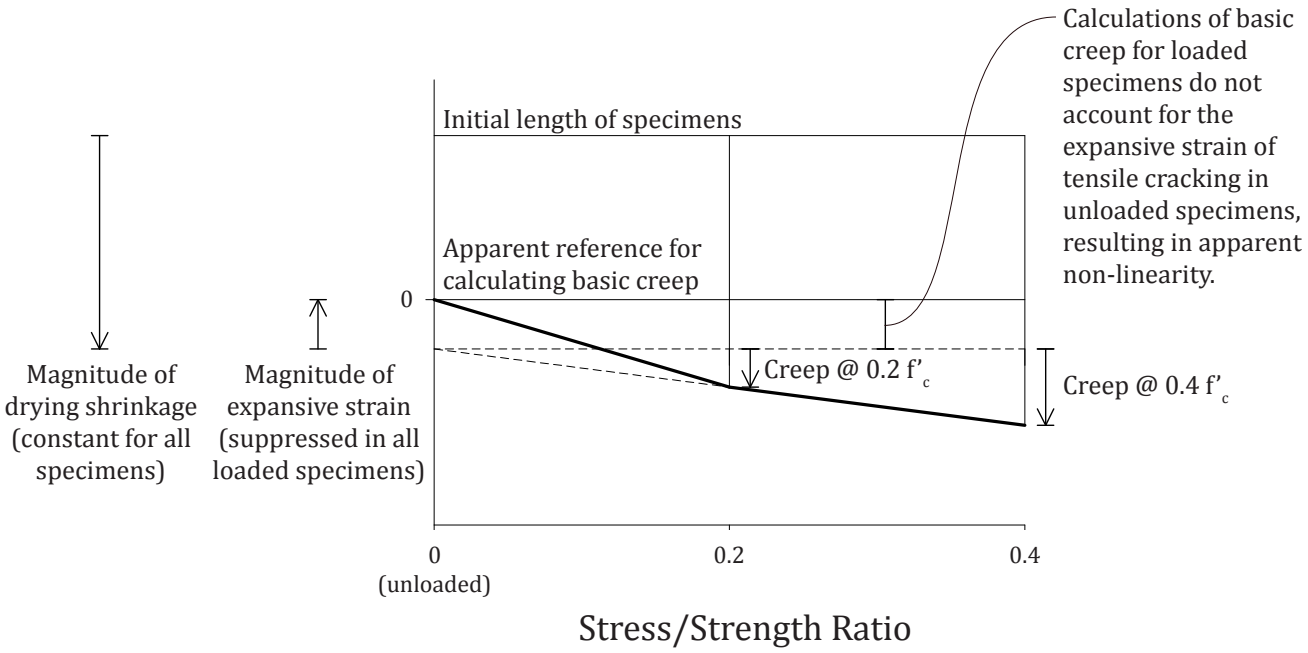

Figure 7.3.6h Diagram of first proposed explanation for non-linear creep behaviour in foam concrete. An expansive strain is present in unloaded companion specimens, due to tensile shrinkage cracking, but this strain is suppressed in loaded specimens. Calculations of basic creep for loaded specimens do not account for the expansive strain, resulting in apparent non-linearity (heavy line). This hypothesis may contribute to non-linearity, but does not fully explain the trends observed.

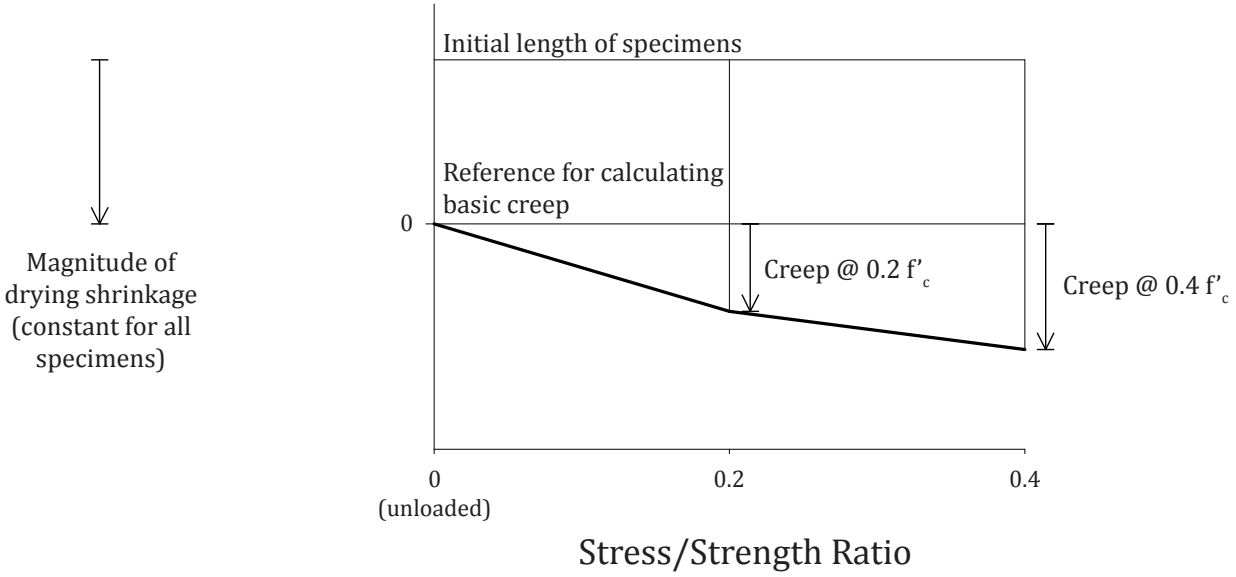

Figure 7.3.6i Diagram of second proposed explanation for non-linear creep behaviour. Modest compression (e.g. 0.2 f'_c) is sufficient to cause instabilities in low-density foam concrete, since the geometry of fine microstructures will tend to generate highly stressed regions in bending. Since C-S-H creep is non-linear in the high-stress range, thin-walled cellular geometries can facilitate long-term damage and deformation that is disproportionate to the stress applied.

concentrated at the midspan, due to non-linear creep of the solid material at this highly stressed site; and (C) deflection will increase until catastrophic buckling.

When applied stress is much below the buckling stress of the cell wall, and the creep exponent of the cell wall material is small, Gibson and Ashby[114] have demonstrated that the ratio of the creep buckling stress, σ_{cb}, to the elastic buckling stress, σ_{el}, can be related to the solid material's creep stress constant, elastic modulus and creep strain rate (σ_{0s}, E_s, and $\dot{\epsilon}_{0s}$, respectively); the ratio of the finite upper limit of deflection (a_u) and the initial deflection (a_0); and the time-to-buckling (t_b):

$$\frac{\sigma_{cb}}{\sigma_{el}} \propto \frac{B}{1+B} \qquad \textbf{Eqn. 1}$$

where

$$B = \frac{\sigma_{0s}}{E_s \dot{\epsilon}_{0s} t_b} \ln\left(\frac{a_u}{a_0}\right) \qquad \textbf{Eqn. 2}$$

For a given strut or wall, material and geometric variables will be constant. By implication,

$$\frac{\sigma_{cb}}{\sigma_{el}} \propto \frac{1}{t_b \cdot \left(1 + \frac{1}{t_b}\right)} = \frac{1}{1+t_b} \qquad \textbf{Eqn. 3}$$

Note that the creep buckling stress, σ_{cb} will diminish indefinitely with increasing time. Gibson and Ashby's work implies that any microstructural element capable of buckling elastically will ultimately fail in creep buckling, even from the smallest of loads, provided the load is applied for a sufficiently long time.

Building on this work, the time until buckling may be related to applied stress as follows:

$$t_b \propto \frac{1 - \frac{\sigma}{\sigma_{el}}}{\frac{\sigma}{\sigma_{el}}} \qquad \textbf{Eqn. 4}$$

If the applied stress is very small relative to the elastic buckling stress, i.e. $\frac{\sigma}{\sigma_{el}} \to 0$,

$$t_b \propto \frac{1}{\left(\frac{\sigma}{\sigma_{el}}\right)} \qquad \textbf{Eqn. 5}$$

[114] Gibson and Ashby (1999) 245

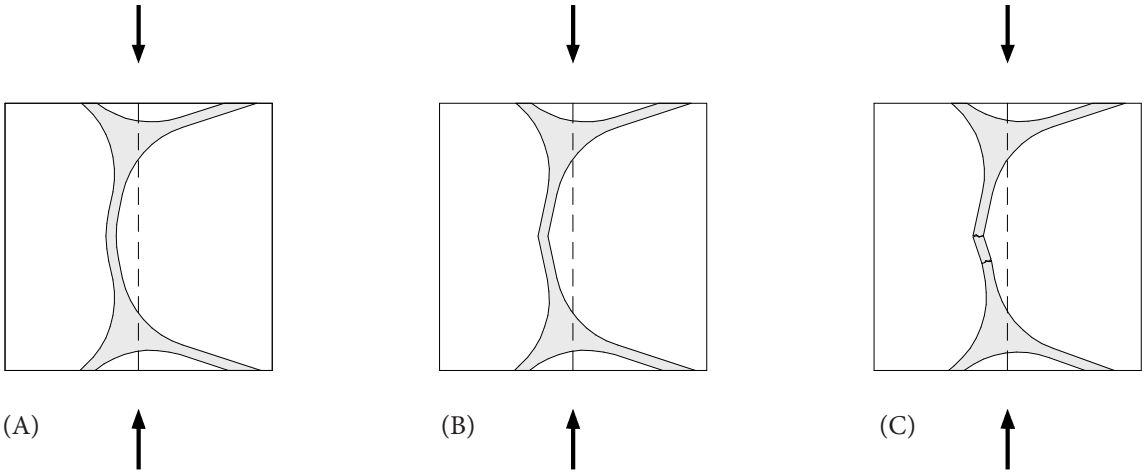

Figure 7.3.6j Process of cell wall creep buckling: (A) a cell wall has an initial defect which induces bending under load; (B) the curvature is increasingly concentrated at the midspan, due to non-linear creep of the solid material at this highly stressed site; and (C) deflection will increase until catastrophic buckling. After Gibson and Ashby (1999) 127.

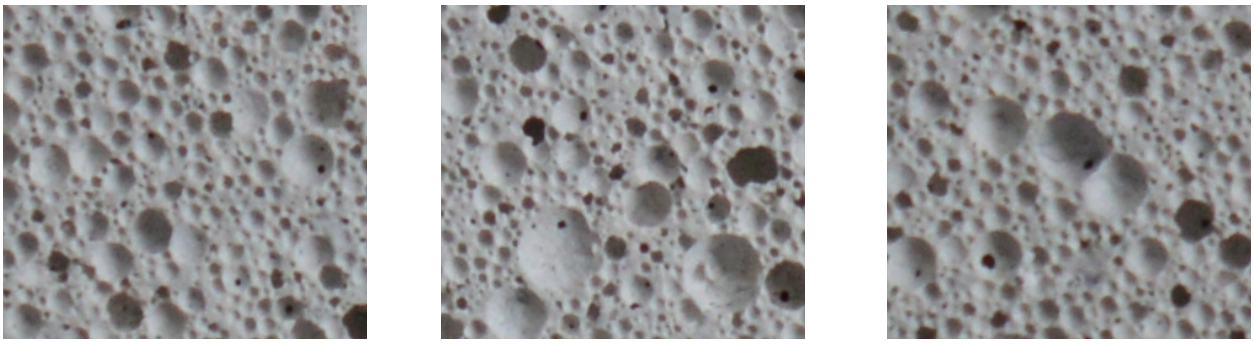

Figure 7.3.6k Photographic images of thin cell walls in 600kg/m^3 neat cement foam concrete, 8x magnification. Creep buckling mechanics suggest that any microstructural element capable of buckling elastically will ultimately fail in creep buckling, even from the smallest of loads, provided the load is applied for a sufficiently long time

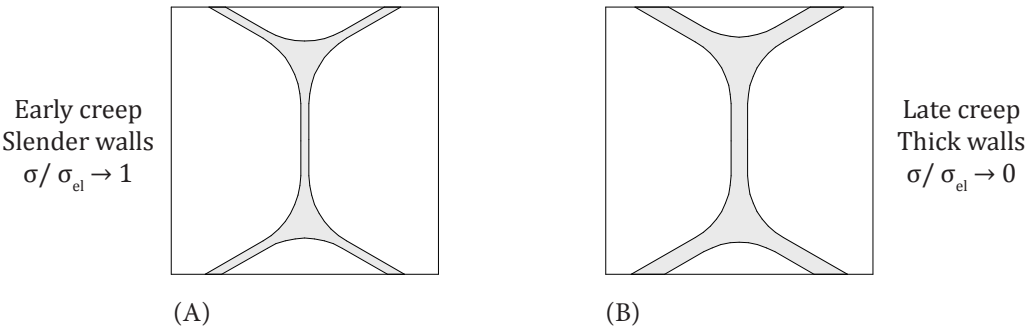

Figure 7.3.6l Time-to-buckling varies with slenderness. (A) At early creep times, creep buckling is dominated by failure of slender struts and walls: applied stress is high relative to the elastic buckling stress. (B) At later times, creep buckling is dominated by remaining, thicker struts and walls: applied stress is small relative to the elastic buckling stress, i.e. $\sigma/\sigma_{el} \rightarrow 0$.

For any given microstructural element, the elastic buckling stress does not vary with time or applied stress, thus

$$t_b \propto \frac{1}{\sigma} \qquad \text{Eqn. 6}$$

Based on this inverse proportionality, Figure 7.**3.6m** plots creep strain against *specific time*, that is, time multiplied by applied stress. (Note that this approach varies from convention, which plots specific creep against time.)

Three major patterns may be observed. Firstly, creep strain is consistently higher with greater applied stress. This result is in agreement with Equation 4, since a higher applied stress will suppress the numerator somewhat, reducing the time-to-buckling.

Secondly, the creep rate is especially high with greater applied stress at early times. The microstructure of foam concrete may be envisaged as a series of struts and walls, which vary in their resistances to buckling, and in applied stress. Equation 4 implies that creep deformation in a foamed specimen at early ages is controlled by those microstructural elements which have relatively high ratios of applied stress to elastic buckling stress, i.e. slender elements subject to high local stresses. Note also that high local stresses are likely to be present during early ages, e.g. due to drying shrinkage, prior to stress redistribution via creep. Where $\frac{\sigma}{\sigma_{el}}$ is already high for the relevant microstructural elements, increases in the applied stress will disproportionately accelerate the time until buckling, again via suppression of the numerator in Equation 4.

Finally, it is at later times, the plots converge. At these late times, creep deformation is controlled by remaining, less slender microstructural elements, with small values of $\frac{\sigma}{\sigma_{el}}$. An increase in applied stress will produce an almost proportional decrease in the time until buckling, per Equation 5.

Divergence in the final data points may be related to the influence of other chemical effects, such as carbonation processes. Accelerated rates of creep and mass gain are shown in Figures 7.**3.6n** and 7.**3.6o**, respectively, indicating that these processes may be active in the specimens, as previously discussed.

Based on these results, it appears likely that the non-linear relation of stress and creep strain in low-density foam concrete is at least partly a consequence of creep buckling

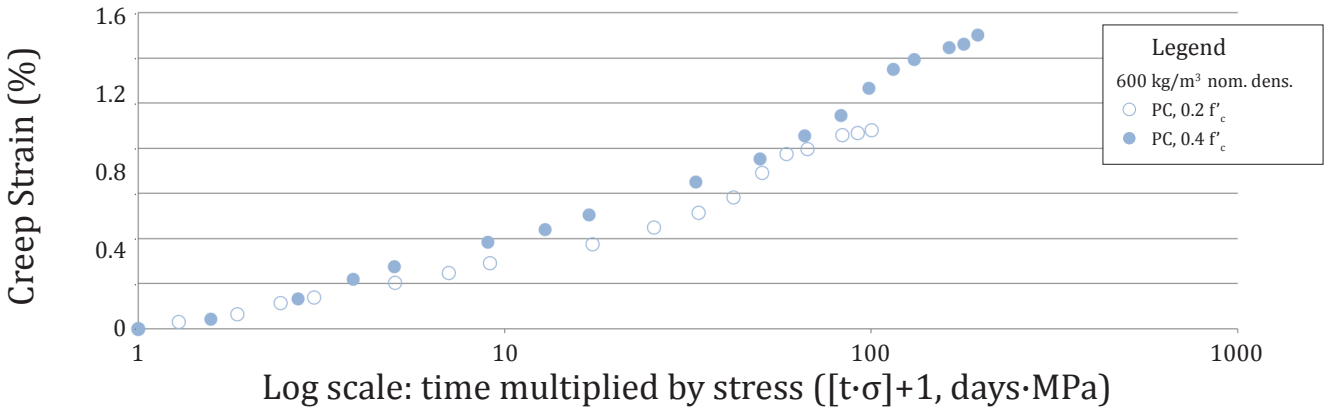

Figure 7.3.6m Creep strain plotted against *specific time* (time multiplied by stress) for 600 kg/m³ Portland cement foam concrete with applied loads of 0.2 and 0.4 f'_c.

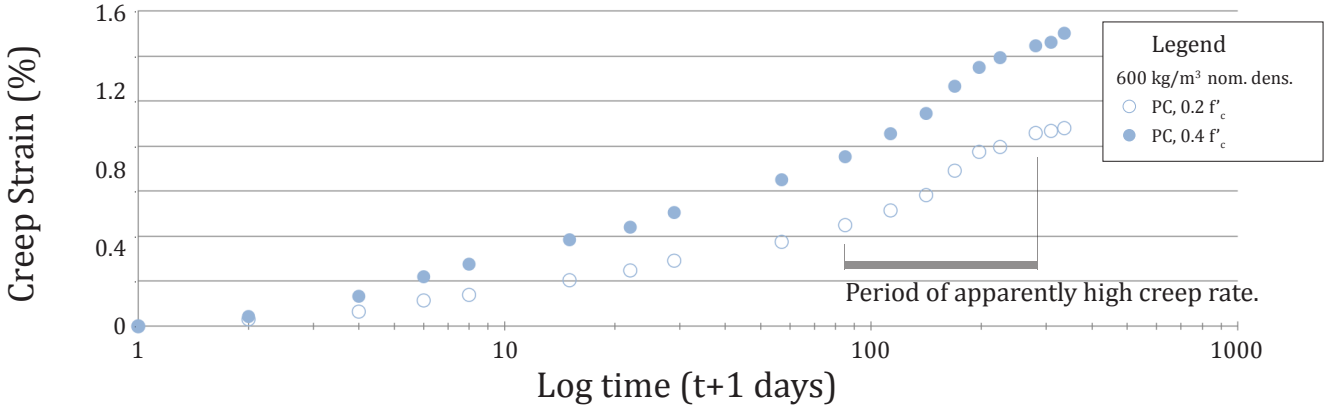

Figure 7.3.6n Creep strain plotted against time for 600 kg/m³ Portland cement foam concrete with applied loads of 0.2 and 0.4 f'_c.

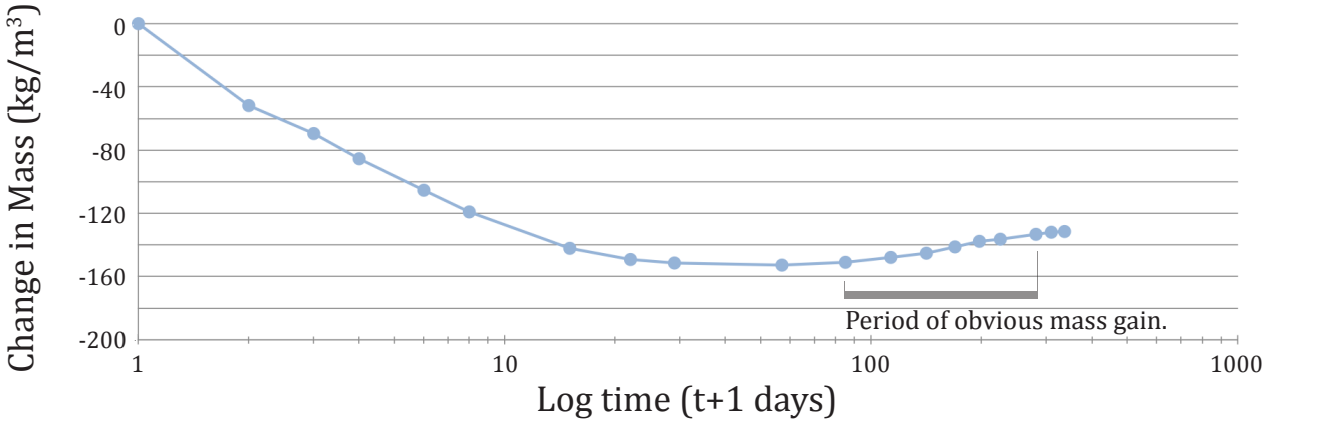

Figure 7.3.6o Change in mass plotted against time for 600 kg/m³ Portland cement foam concrete.

mechanics. Other effects such as hydration-solidification, drying, carbonation, shrinkage cracking, damage caused by creep,[115] and densification may play secondary roles in affecting creep rates, and could introduce additional non-linearities.

In addition to the creep buckling mechanism described above, it should be remembered that during early creep times, much of the strain observed may be due to creeping of thick members under simple compression. Thus, strain will tend to be proportional to applied stress, as is evident from zero to seven days in Figures 7.**3.6f** and 7.**3.6g**. Buckling mechanics of major structural members becomes increasingly relevant at long times.

For denser specimens, the experimental program indicates how binder composition may affect creep of foam concrete. For 1400 kg/m^3 nominal density mixes, partial replacement of Portland binder with silica fume SCM had a minor influence on specific creep strain.

For PC and SF mixes, there appear to be strong correlations in patterns of specific creep, mass loss (i.e. moisture content), and drying shrinkage as shown in Figures 7.**3.6k**, 7.**3.6l**, and 7.**3.6m**, respectively. Initial rates of change were highest for the Portland cement binder mix, but long-term values were highest for the SF mix. The point of intersection in trend lines was around approximately 56 days. Such correlation of humidity levels, drying shrinkage and creep is to be expected where drying shrinkage introduces residual stresses in the C-S-H, creating overstressed sites that facilitate creep.

As specimens are dried from high humidity conditions to 50% RH, loss of mass is dominated by the removal of adsorbed water from the surfaces of internal voids. The presence of capillary voids in concrete is especially significant to moisture storage at this humidity range, in part due to the high surface area-to-volume ratio of capillary voids; while larger air voids are comparatively less important, since their surface area-to-volume ratio may be several orders of magnitude lower.

Differences among specimens in rates of moisture loss, shrinkage, and thus creep can likely be attributed to differences in capillary pore size distribution. Given the higher initial water-binder ratio used to produce SF specimens, as well as the enhanced particle

[115] Bažant (1988) 237 mathematical modelling of creep and shrinkage

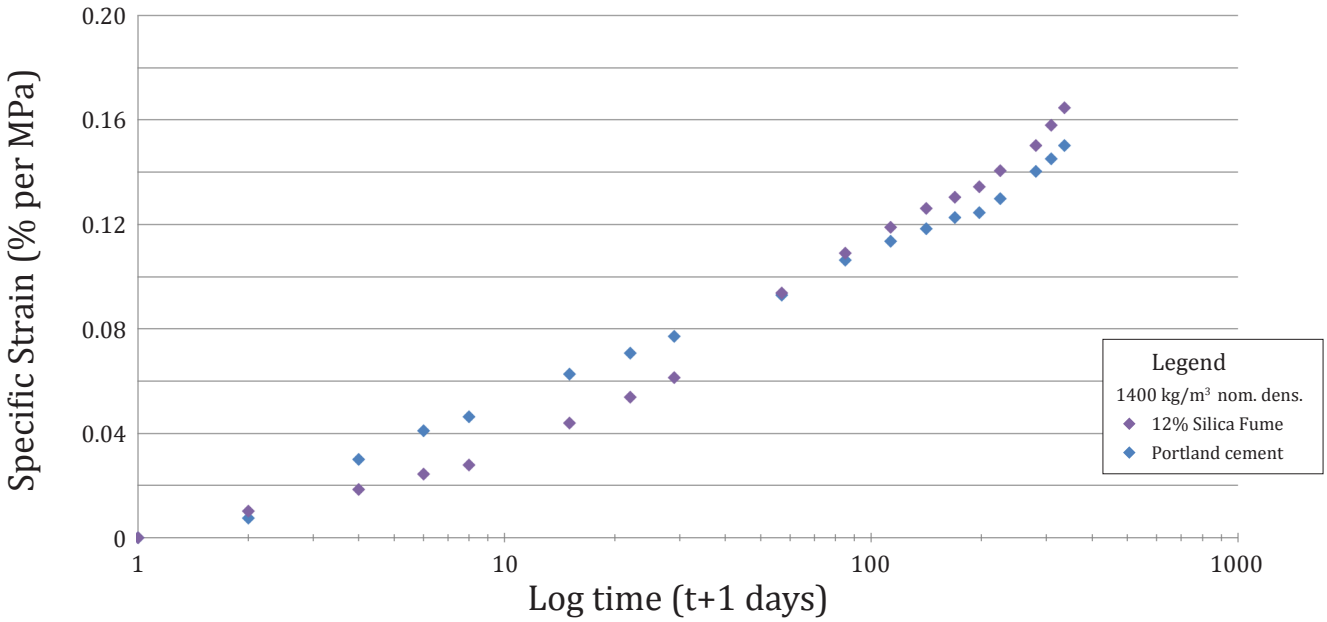

Figure 7.3.6p Specific creep strain for 1400 kg/m³ Portland cement and silica fume mixes.

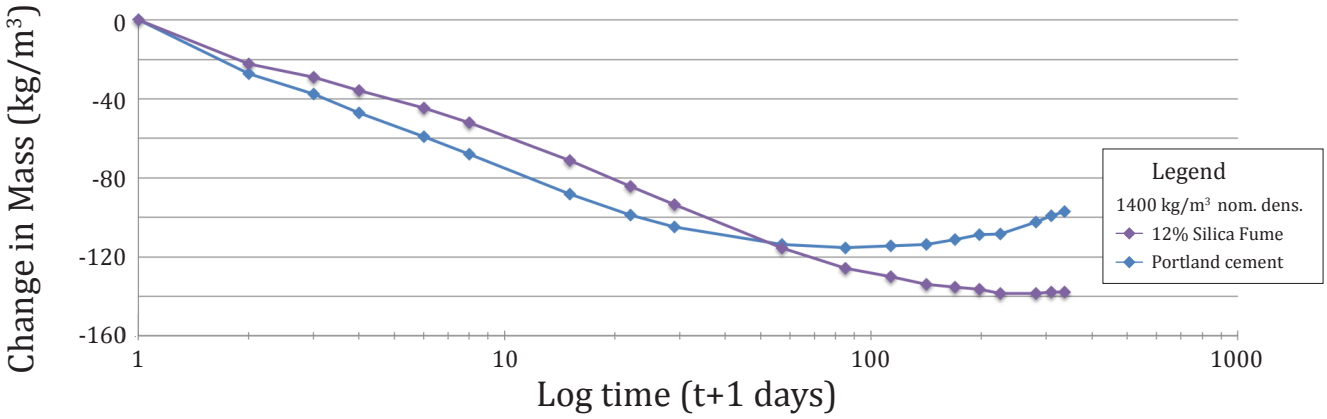

Figure 7.3.6q Change in mass of 1400 kg/m³ Portland cement and silica fume mixes.

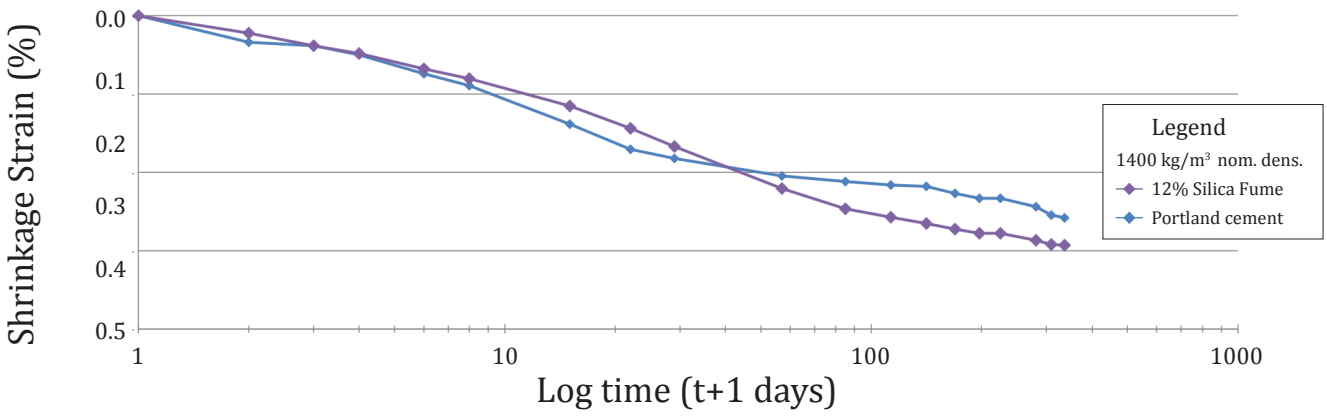

Figure 7.3.6r Drying shrinkage strain of 1400 kg/m³ Portland cement and silica fume mixes.

packing due to the small particle size of silica fume, it is probable that these specimens have a relatively high volume of small capillary pores. These smaller pores retain adsorbed water for longer in a drying environment, slowing the loss of mass and drying shrinkage. As water is eventually desorbed, there are a large number of capillary voids available to participate in capillary tension, resulting in high shrinkage and inducing high rates of creep. Refer to Section 7.2 for further discussion regarding the influence of capillary pore size distribution on shrinkage.

The high proportions of silica introduced by silica fume SCM will also tend to increase creep rate, due to influences on the stoichiometry of the C-S-H. For a given density, low Ca/Si ratios are associated with increased compressive strength and stiffness,[116] due to the presence of long silicate chains,[117] a high degree of polymerization,[118] and the production of skeletal (fibril) structures;[119] however, microindentation data indicates that creep increases with decreasing Ca/Si ratios.[120] This effect is perhaps due to the tendency for long, highly polymerized silicate chains to induce distance between C-S-H sheets,[121] facilitating slip. Local structural disorder induced by polymerization[122] would create additional pressure on molecular bonds, conducive to creep.

Patterns of mass loss, drying shrinkage, and creep are less obvious for the slag specimens (Figures 7.**3.6n**, 7.**3.6o**, and 7.**3.6p**). For example, while the initial loss of mass upon drying was consistent with other specimens, slag specimens experienced minimal shrinkage prior to Day 7. Specific creep was approximately 30% higher for slag specimens than for other mixes, after one year.

Three explanations for these trends are considered below. First, building on the discussion of drying shrinkage offered in Sections 6.11 and 7.2, it is possible that minimal early movement in 28-day water cured slag mixes may be attributed to a low proportion of

116 Confusion can arise here, since low density 'outer products' often have low Ca/Si ratios, while denser 'inner products' have high Ca/Si ratios. Statements are based on constant density. Cf. Pelisser et al. (2012) 17220.
117 Chen et al. (2004) 1508, 1510
118 Yu et al. (1999) 743
119 Hou et al. (2013) 10
120 Nuygen et al. (2014) 126
121 Pelisser et al. (2012) 17223
122 Yu et al. (1999) 746

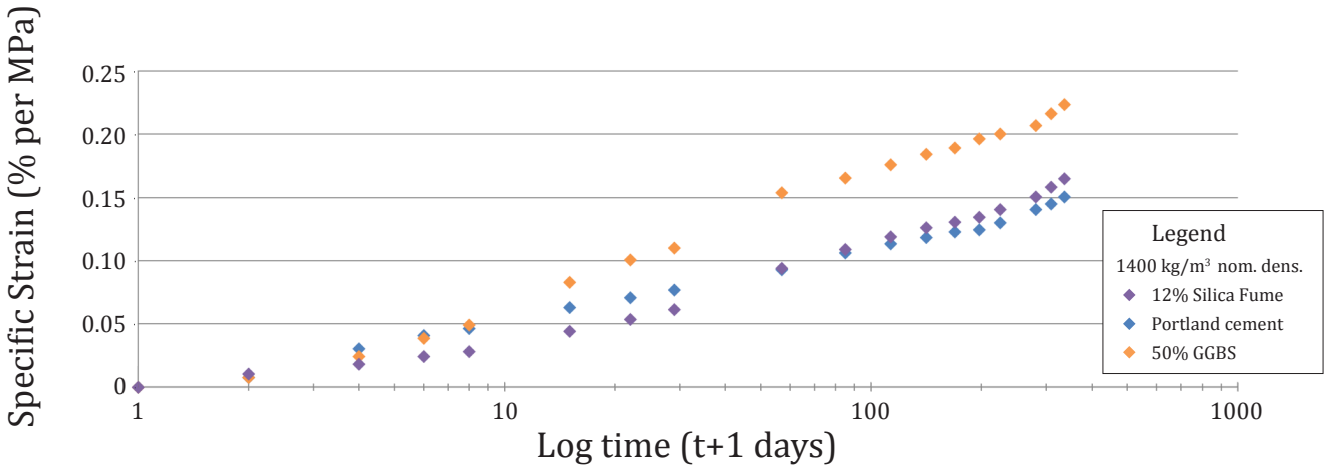

Figure 7.3.6s Specific creep strain for 1400 kg/m³ Portland cement, silica fume, and slag mixes.

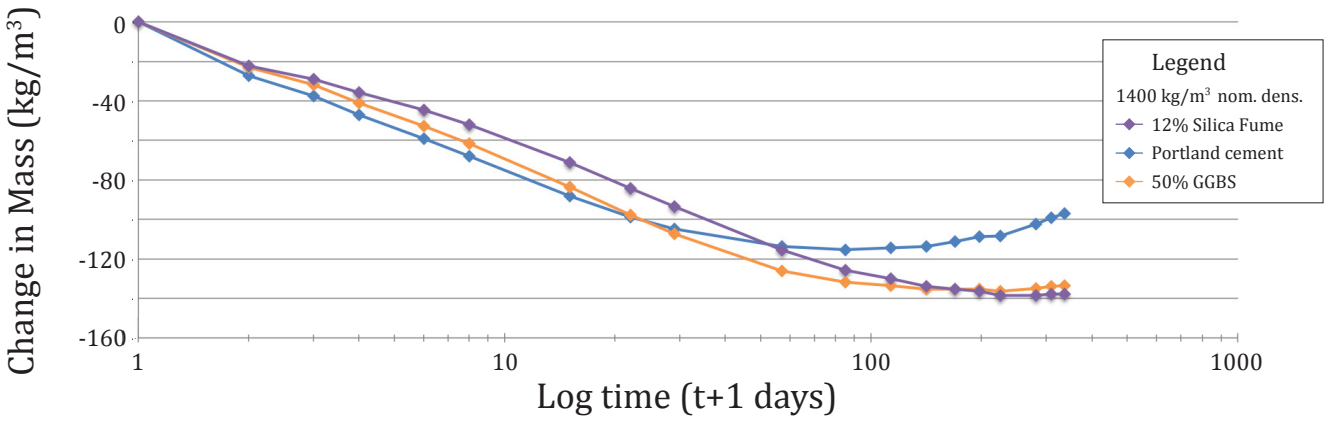

Figure 7.3.6t Change in mass of 1400 kg/m³ Portland cement, silica fume, and slag mixes.

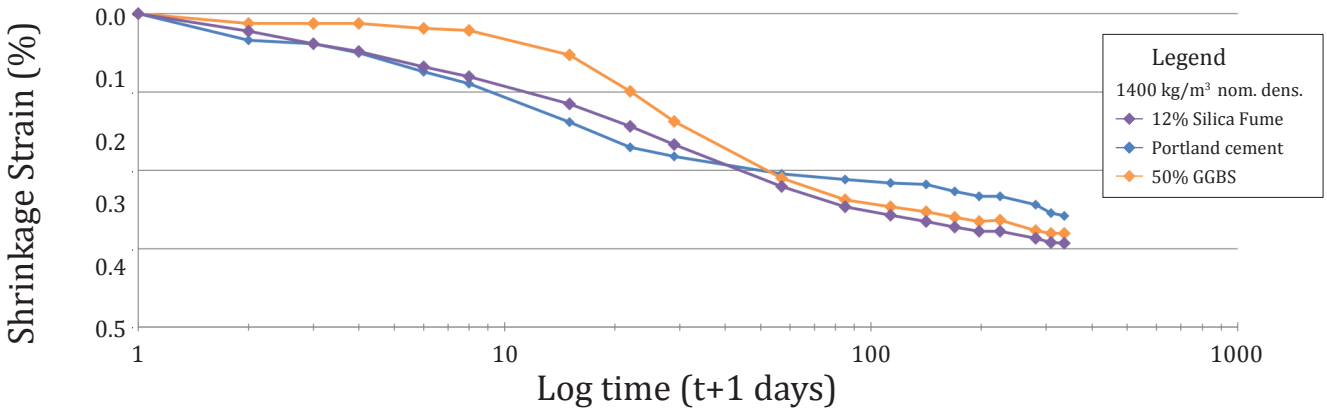

Figure 7.3.6u Drying shrinkage strain of 1400 kg/m³ Portland cement, silica fume, and slag mixes.

large capillary voids, due to relatively low water-binder ratios used in mix design, and a high degree of hydration.[123] At high RH (i.e. early drying times), smaller voids remain fully filled, and there would be few partially filled voids present to contribute to capillary tension via capillary menisci. Consequently, unloaded specimens will experience minimal contraction. However, with applied stress, capillary water may be driven into proximate air-voids, facilitating high apparent rates of basic creep.

Second, it is possible that relatively large volumes of water are absorbed into the slag specimens during the moist-curing regime. This hypothesis is supported by the observation that the total loss of mass (water) of slag specimens on drying in 50% RH is consistent with the total loss of mass of silica fume specimens, despite the higher initial water-binder ratio of the silica fume specimens (Figure 7.**3.6o**). In this proposed model, a large amount of free water would remain present in air voids of unloaded slag specimens, preserving a high internal RH and reducing capillary tension (and therefore shrinkage) during the early period of exposure to 50% RH. Under load, however, capillary water may be driven into proximate air-voids, facilitating compression of the specimens.

Third, the stoichiometry of the slag mix may help explain the high creep rates observed. Slag cement has relatively high proportions of alumina.[124] The incorporation of alumina into C-S-H leads to the formation of C-A-S-H, and is associated with a higher degree of crystallinity.[125] In normal density concrete, the high crystallization grade can help resist creep;[126] in foam concrete, however, struts and wall composed with C-A-S-H may be more brittle than those with greater proportions of C-S-H, increasing the rate of creep buckling. Additionally, slag cement has less calcium oxide and more silica than Portland cement, [127] which will produce C-S-H with a low Ca/Si ratio, contributing to creep as previously discussed.

---

123 'Through-solution' hydration mechanisms may tend to be high for mixes that include fine slag particles, promoting high interstitial mass between cement grains. By contrast, topochemical growth of C-S-H may be somewhat more significant for mixes that only include larger Portland cement particles, resulting in a slower degree of hydration with more space between cement grains. Cf. Section 7.1, Gruskovnjak et al. (2006) 126.

124 Thomas et al. (2016)

125 Gruskovnjak et al. (2006) 126.

126 Ma and Dehn (2016) 808.

127 Thomas et al. (2016)

This page intentionally left blank.

7.3.7 Patterns of Moisture Transport

Results from the experimental program described in Sections 6.11 to 6.14 offer insight into patterns of moisture transport through hardened foam concrete. Moisture transport can have an influence on various micromechanical phenomena, such as creep, as discussed briefly in Section 7.3.6; likewise, an understanding of moisture ingress is critical to the analysis of freeze-thaw deterioration, as discussed in the following section. Proposed explanations for major trends are summarized here for reference, for a variety of wetting or drying scenarios.

Mass accumulates slowly in hardened foam concrete specimens maintained in 50% RH. It is probable that gaseous moisture in the air within specimens becomes chemically bonded to anhydrous cement grains via topochemical reactions, at a slow rate (Figure 7.**3.7a**). As specimens self-desiccate, internal RH decreases. Moisture from the surrounding environment will continually diffuse into the specimen to maintain moisture equilibrium, via the relatively open porosity of dry foam concrete. The mass gain evident in Figure 6.**11i** may be due in part to this mechanism of ongoing hydration.[128]

When specimens conditioned to 50% RH are placed in 80% RH, moisture accumulation is relatively rapid. Moisture diffuses via the capillaries of the foam concrete and adsorbs to the internal surface area, displacing internal air (Figure 7.**3.7b**).

By contrast, when specimens conditioned to 50% RH are placed in 90% RH, moisture accumulation appears to be suppressed. It is possible that capillary condensation in the C-S-H matrix 'seals' the outside surface of the specimens, creating impediments to the exfiltration of internal air. Air must diffuse out via liquid water, which is a slow process (Figure 7.**3.7c**).

When specimens conditioned to 50% RH are immersed in water, capillaries in the C-S-H matrix fill rapidly. Large discrete air-voids, however, will not readily fill, since the surrounding saturated C-S-H matrix 'seals' the air bubbles, creating impediments to the exfiltration of trapped air (Figure 7.**3.7d**). Results for mixes with the same cementitious density but varying ratios of foam volume to filler suggest that both solid aggregate and discrete air-voids may be similarly competent at resisting water ingress in the short-term

[128] Carbonation may also contribute to mass gain, as discussed in Section 7.3.6.

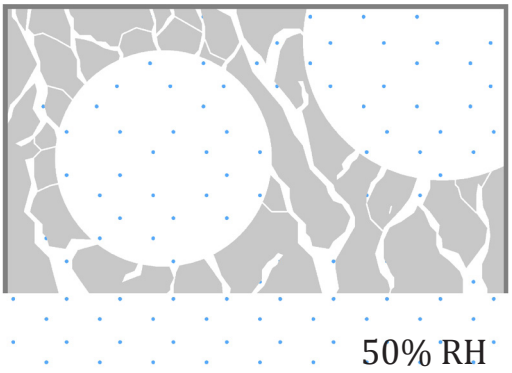

Figure 7.3.7a **Storage in 50% RH Environment**
Specimen initially conditioned to 50% RH.
All available surface exposed to 50% RH.

Internal RH decreases as water vapour is chemically bonded to anhydrous cement in the specimen. New moisture from the environment diffuses into the specimen to maintain equilibrium. Mass increases at a slow rate.

See also Figure 6.**11i.**

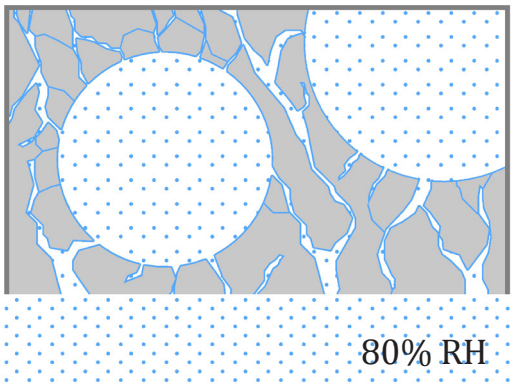

Figure 7.3.7b **Exposure to 80% RH**
Specimen initially conditioned to 50% RH.
All available surface exposed to 80% RH.

High RH air progresses through the highly permeable material. Water adsorbs on available internal surface area.

See also Figure 6.**12c.**

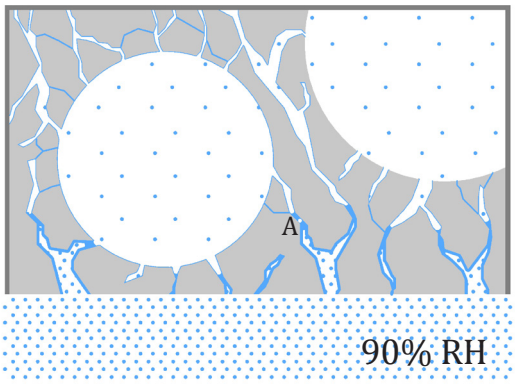

Figure 7.3.7c **Exposure to 90% RH**
Specimen initially conditioned to 50% RH.
All available surface exposed to 90% RH.

Moisture adsorbs on available internal surfaces. Vapour condenses in small diameter capillaries near the exposed surface of the material. Interior air is 'trapped'. Interior air can only evacuate the specimen via diffision through capillary condensation water (A).

See also Figure 6.**12c.**

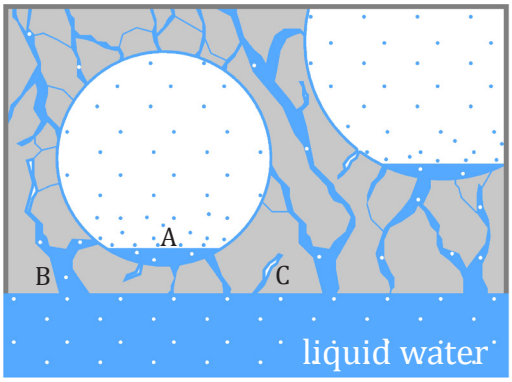

Figure 7.3.7d **Immersion in Liquid Water**
Specimen initially conditioned to 50% RH.
All available surface exposed to liquid water.

Water is drawn into the specimen under strong capillary suction. Before the air voids can fill (A), they are surrounded by saturated capillaries. Interior air is 'trapped'. Pneumatic pressure limits further ingress of water. Interior air can only evacuate the specimen via diffision through saturated capillary paths (B).

Like air voids, 'dead-end' capillaries may also remain filled with trapped air (C).

See also Figure 6.**12e.**

(cf. Figure 6.**12e**). Eventually, the air voids closest to the source of liquid water may become saturated, as air is displaced from the large void under hydraulic pressure, diffusing through the water in the surrounding C-S-H matrix along saturated capillary paths. (Refer to Figure 7.**3.8a** in the following section.)

Similarly, water will rise rapidly in the C-S-H matrix of specimens subjected to partial immersion. If air voids are discrete, they will remain air-filled in the short term, acting as obstructions to capillary flow. If air voids are interconnected (e.g. due to shrinkage cracking or aging of the foam), they may participate in capillary suction (Figure 7.**3.7e**).

When dry specimens are subjected to vacuum saturation, both air voids and capillary voids will tend to be completely filled (Figure 7.**3.7f**). Liquid water will be drawn by vacuum pressure into all available porosity, including dead end capillaries. It is possible that air will remain within the specimens only if air has not been completely evacuated from some pores: for example, very fine and discrete capillary pores.

'Wet cup' testing[129] was not conducted as part of the experimental program. The mechanisms of moisture movement discussed above suggest that a specimen with opposite sides exposed to high and low relative humidities would experience more rapid transport, as compared to a specimen immersed in a humid environment. When immersed in high RH, pneumatic pressure of 'trapped' air may suppress moisture ingress, whereas in a wet cup scenario, air may diffuse readily out of the dry side of the specimen. Capillary condensation could also contribute to the advancement of moisture in the specimen via wicking, readily displacing internal air (Figure 7.**3.7g**).

[129] Cf. ASTM E96/E96M–16, Section 12

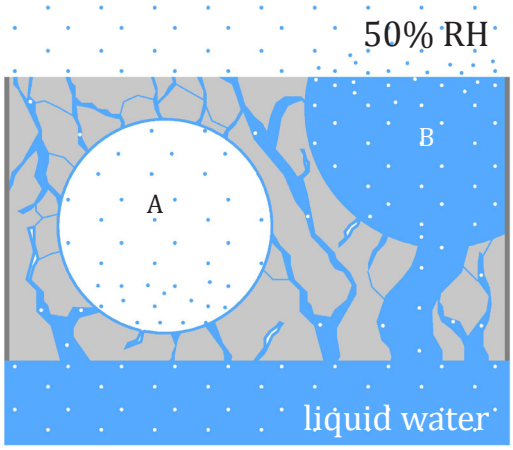

Figure 7.3.7e **Partial Immersion in Liquid Water**
Specimen initially conditioned to 50% RH. One surface exposed to liquid water; one surface exposed to air.

Most air voids are surrounded by saturated capillaries, and act as obstructions to capillary flow (A). Paths of interconnected air voids (e.g. along shrinkage cracks) will participate in capillary suction (B).

See also Figure 6.**14i.**

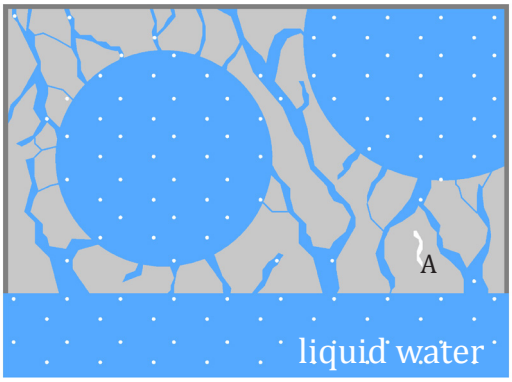

Figure 7.3.7f **Vacuum Saturation**
Specimen dried, then vacuum saturated.

All spaces accessible to vaccuum are filled, including air voids and 'dead-end' capillaries. It is possible that discrete capillaries would remain inaccessible (A).

See also Figure 6.**12e.**

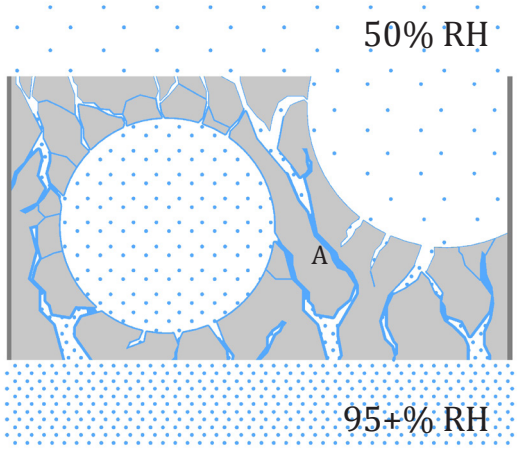

Figure 7.3.7g **'Wet Cup'**
Specimen with exposed to high RH on one side, and low RH on opposite side

Water transport would tend to be rapid in a wet cup scenario, since drier air may diffuse readily out of the dry side of the specimen (cf. Figures 7.**3.7b** and 7.**3.7c**). Capillary condensation could also contribute to the advancement of moisture in the specimen via wicking, readily displacing internal air (A).

See also Figure 6.**12c.**

7.3.8 Freeze-Thaw Damage

As depicted in Figure 7.**3.7d**, when dry foam concrete is exposed to liquid water, capillary pores fill readily. Conversely, isolated air voids surrounded by saturated capillaries initially resist water ingress, but may eventually begin to fill under hydraulic pressure, as air gases diffuse out of the voids via the capillary water.

Due to this diffusion process, the air voids closest to the surface of the concrete will tend to fill with water most quickly, while interior voids remain relatively dry. Moisture content does not appear to equilibrate readily through the specimens during wetting (Figure 7.**3.7a**).

When a wetted specimen is exposed to freezing temperatures, ice crystals will form in saturated (or partially saturated) air voids near the surface. Water that is rigidly held in fine capillaries and gel pores cannot rearrange to form ice at normal freezing temperatures, however. This high-energy, supercooled liquid water is in thermodynamic disequilibrium with frozen water in larger pores, and will tend to migrate to low-energy, ice bearing regions.[130] The ice crystal in an air void therefore grows not only because of volumetric expansion as water transforms into ice, but also because of the ingress of supercooled water, inducing internal pressure and expansion at an unfrozen, supercoooled water layer between the ice crystal and the cell wall (Figure 7.**3.7b**).[131] While spalling occurs at the specimen surface, interiors of specimens may remain undamaged, since interior moisture contents are lower: dry interior air voids have sufficient room for accumulation of moisture from the surrounding capillaries during freezing.

---

[130] Mehta (1986) 123.
[131] Valenza and Scherer (2006) 1164-1165

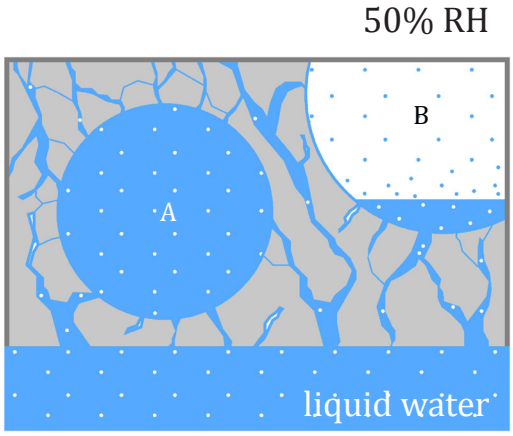

(Refer to Figure 6.**14i**.)

Figure 7.3.8a **Long-term Exposure to Liquid Water**
Specimens initially conditioned to 50% RH, then exposed to liquid water, for a long period.

Over a long period, air within air voids evacuates the specimen via diffusion through saturated capillary paths, driven by hydraulic and capillary pressures. Water will eventually fill the air-voids closest to the specimen surface (A), while more interior air voids may remain drier for a longer time (B).

See also Figures 6.**16.1g** to 6.**16.1g**, 6.**16.1l**.

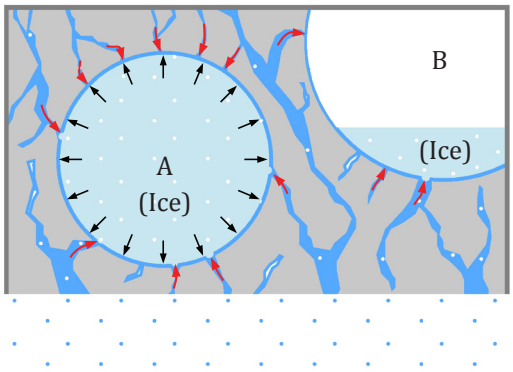

Figure 7.3.8b **Freezing of Specimen after Long-term Exposure to Liquid Water**
Specimen initially conditioned to 50% RH. All available surfaces exposed to liquid water. Specimen exposed to freezing temperatures.

Ice crystals form in the saturated air voids near the specimen surface (A). Supercooled liquid from surrounding capillaries migrates to the low-energy frozen sites (red arrows), contributing to tensile hoop stresses in the air-void wall (black arrows). Interior regions may remain undamaged, since drier interior air voids have sufficient room for accumulation of moisture upon freezing (B).

See also Figures **6.16.1c, 6.16.1d**.

8

Proposed Approaches to Mix Design

This chapter is intended to assist a mix designer in efficiently developing appropriate foam concrete mixes for various applications. Objectives include minimizing trial-and-error testing, avoiding omission of relevant considerations, establishing recommended tolerances for batching, and diagnosing and correcting issues.

In Section 8.1, key mix properties are plotted against density, and presented as a preliminary reference. A designer may quickly determine the approximate density and mix proportions necessary to achieve desired strength, stiffness, drying shrinkage and creep criterion for plain foam concrete.

Section 8.2 offers a more detailed protocol for developing foam concrete mix designs, for five distinct applications. Major performance considerations are prioritized according to their anticipated influence on mix design, to facilitate an efficient iterative process. Relevant test results and portions of the literature review are cited for further information and clarification.

Section 8.3 describes a computer application developed based on research from this thesis, and available for industry use. A user may define desired parameters, and the program will return possible mix designs, based on interpolated data from the

experimental program. Although the program is not included as part of this thesis, the essential logic and functionality of the software is explained.

Section 8.4 provides a troubleshooting guide. Common issues encountered during the production and placing of foam concrete are identified, and a diagnostic process is presented to isolate and correct the causes of deficiencies.

Finally, Sections 8.5 and 8.6 establish recommended tolerances for mix proportions and acceptance criteria for quality control, respectively.

8.1 Preliminary Graphic Reference for Mix Design

Properties of plastic and dry density, slump flow, drying shrinkage strain, thermal resistivity, compressive strength, static modulus of elasticity, and specific creep are plotted as a preliminary reference. The feasibility of a proposed use can be rapidly assessed, and appropriate mix designs can be approximated for a broad range of parameters. The preliminary graphic reference begins on **Page 258**.

8.2 Detailed Protocol for Foam Concrete Mix Design

The properties of foam concrete vary significantly. Relatively small modifications to mix design can meaningfully affect the density, mechanical response, transport properties, durability, and thermal performance of the material. When designing foam concrete for a particular application, it is often necessary to consider numerous parameters, to confirm the suitability of a proposed recipe.

In this approach, five distinct applications for foam concrete are identified. A customized design protocol is proposed for each application. Critical material properties are introduced in order of priority of their anticipated influence on mix design. Various methods of controlling the relevant properties are listed, to provide multiple paths for achieving design targets.

The five applications are characterized below, starting on **Page 260**. These applications cover a large proportion of major uses for foam concrete. The proposed design protocols may be adapted for other uses of foam concrete as required.

This page intentionally left blank.

Refer to Figures for Sections 8.1 and 8.2

on the following pages.

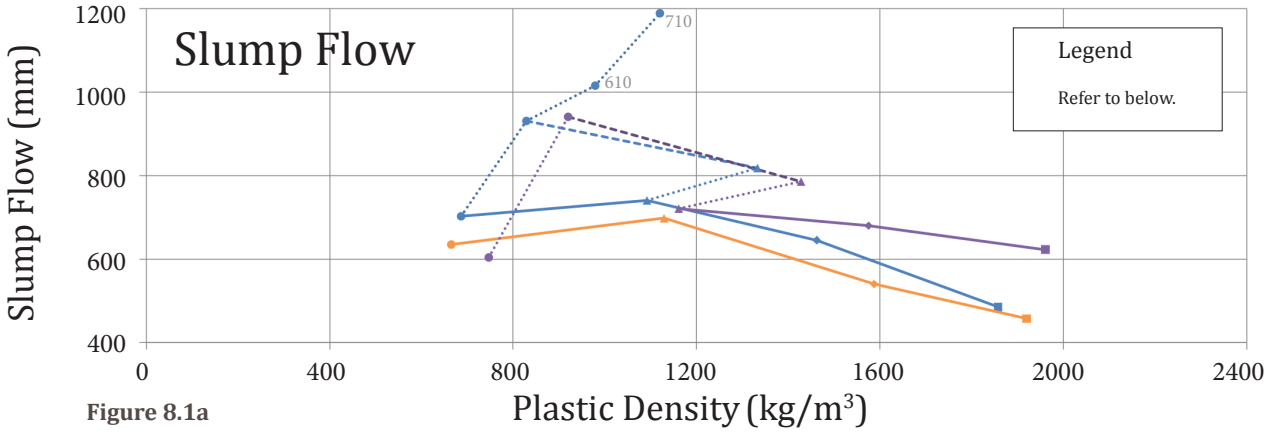

Figure 8.1a

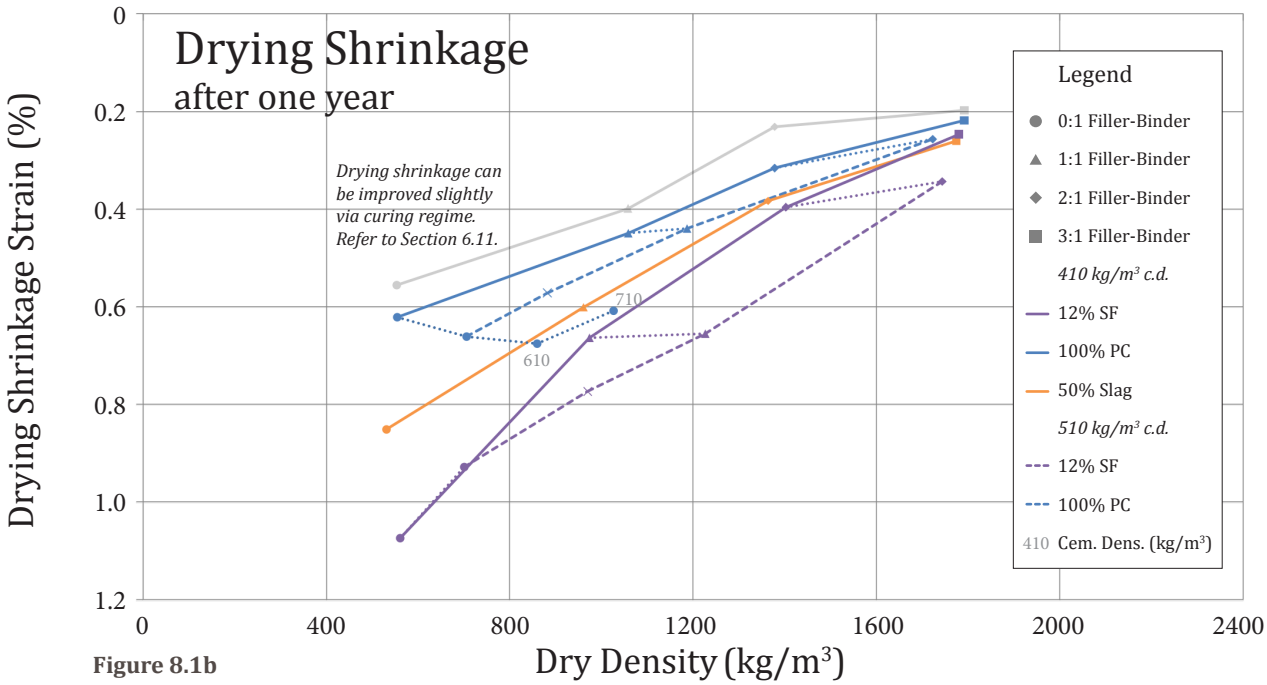

Figure 8.1b

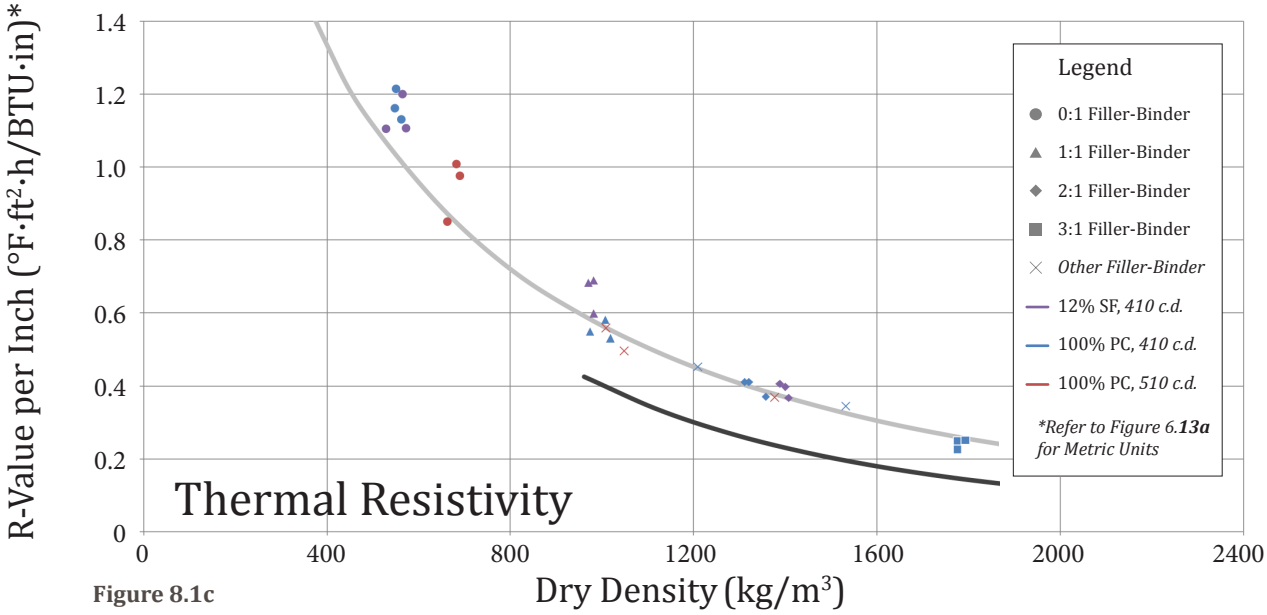

Figure 8.1c

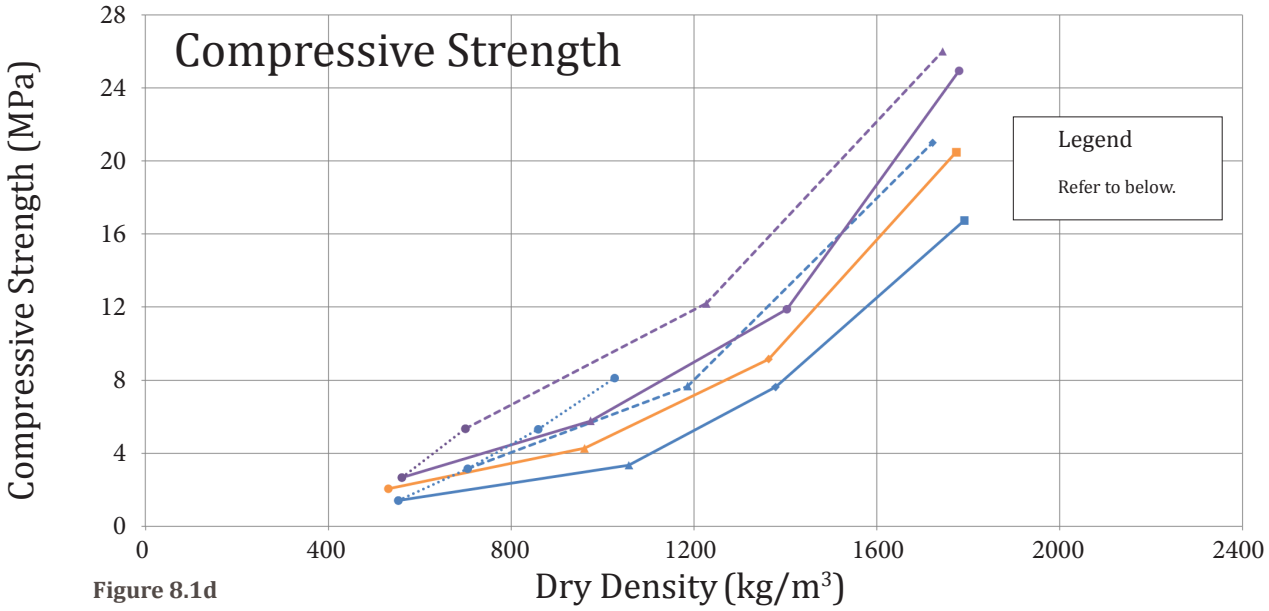

Figure 8.1d

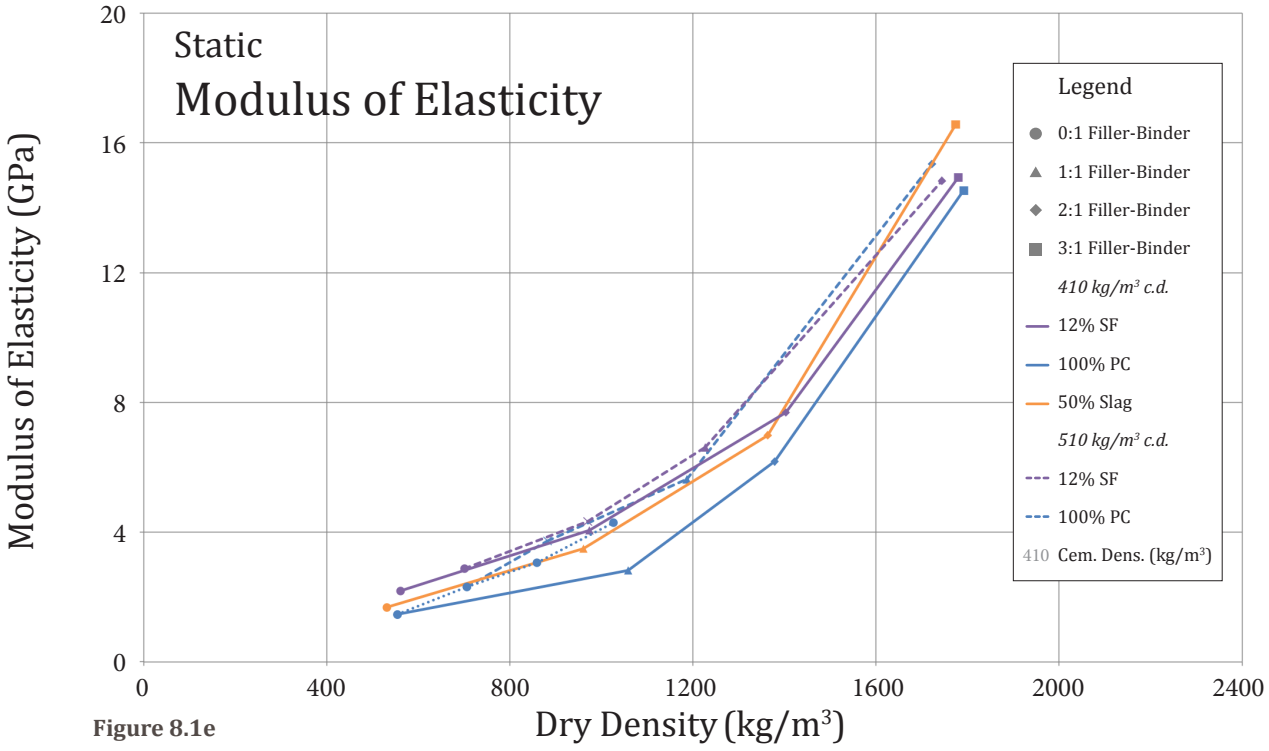

Figure 8.1e

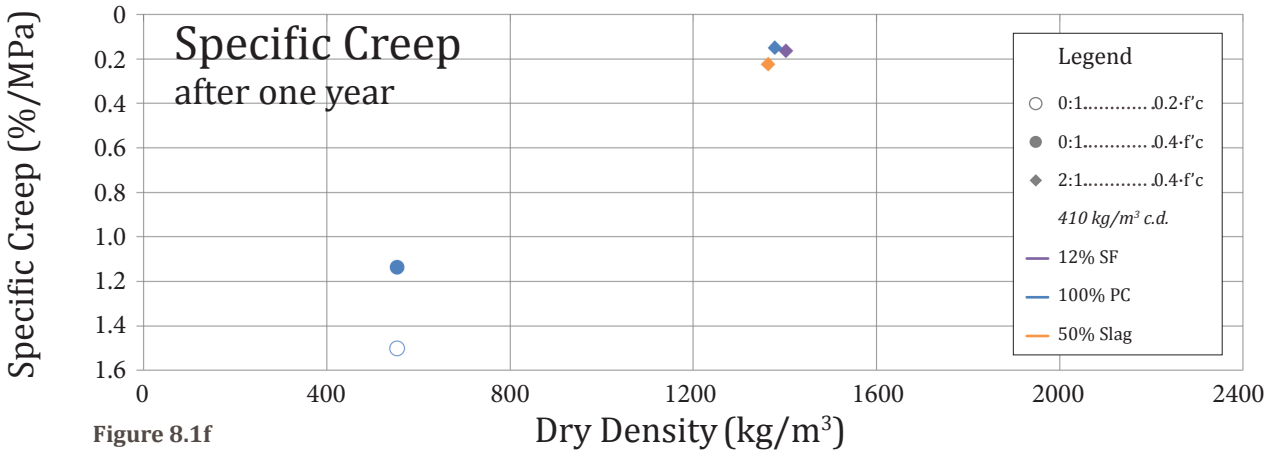

Figure 8.1f

Geotechnical fill, generic

Figure 8.2a

The protocol below presents design consideration and controls for foam concrete geotechnical fill. Note that not all parameters listed will be relevant for all applications.

Possible applications for foam concrete geotechnical fill include the following:

Non-settling fill, cohesive fill, buoyant fill, emergency void-filling, soil stabilization, soil replacement, road sub-base, concrete blinding, annular grouting, bridge abutments, fill for spandrels of masonry arch bridges, bulk fill for mines or subways, backfill of redundant sewers or tanks, air-tight grouting of coal mines, containment of hazardous waste. (Refer to Appendix A, Section 8.1)

Control of mix ingredient and proportions (additions) ○
Control of mix ingredient and proportions (subtractions) ●
Control of curing or placing environment □
Controls which are not recommended ×

Relevant Figures 6.**1a**
Relevant notes from the Appendices *A-6.1*

Long-term strength	Increase for anticipated loading	○ increase volume of filler……6.**6.1.1a** ○ increase cementitious density……6.**6.1.1a** ○ increase proportion of slag or silica fume……6.**6.1.1a** □ increase curing age (SCM mixes)……6.**6.4a** to 6.**6.4f**
	Decrease for ease of future excavation	● reduce density, cementitious density……6.**6.1.1a** ● reduce SCMs……6.**6.1.1a**
Density	Decrease	○ decrease filler, increase cementitious as required……6.**6.1.1a**
Void Filling		
Spread flow	Increase for constricted void-filling applications	○ increase cementitious density……6.**2b** ○ increase water content……6.**2b** × avoid use of superplasticizers……*Appendix P*
Void Filling		
Early-age stiffness	Decrease for large and constricted void-filling	● decrease cementitious density……6.**6.4a** to 6.**6.4f** ○ increase proportion of slag……6.**6.4a** to 6.**6.4f**
	Increase for walkability, safety of public	○ use FCA……*Appendix E* ○ increase volume of filler……6.**6.4a** to 6.**6.4f** ○ increase cementitious density……6.**6.4a** to 6.**6.4f** ○ increase proportion of silica fume……6.**6.4a** to 6.**6.4f** ● reduce proportion of slag……6.**6.4a** to 6.**6.4f**
Modulus of elasticity	Increase	○ increase cementitious density……6.**7b**, 6.**7c** ○ increase use of SCMs……6.**7b**, 6.**7c** Note: Use of slag SCM provides a high stiffness-to-strength ratio……6.**7i**

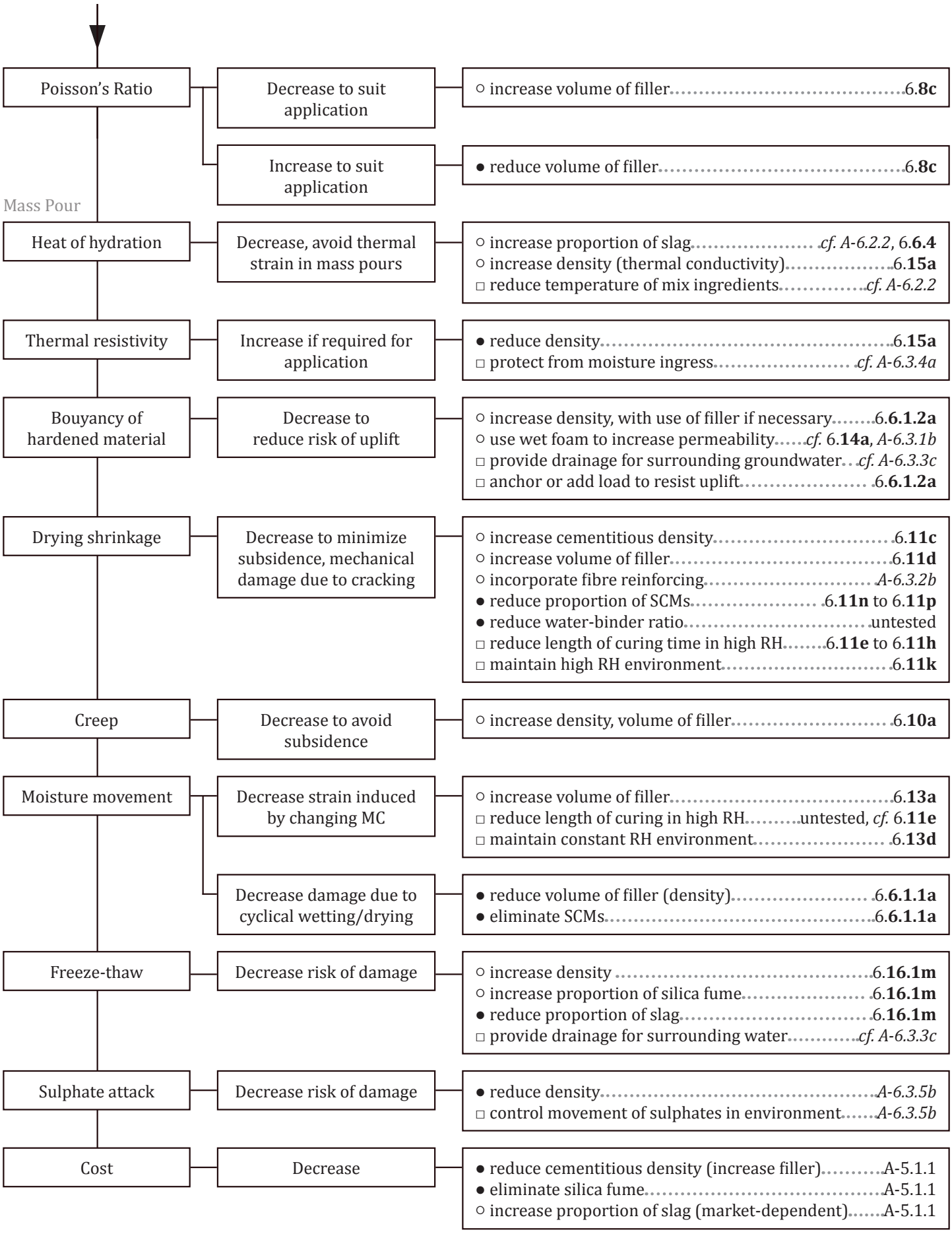
Poisson's Ratio
Decrease to suit application
○ increase volume of filler 6.8c
Increase to suit application
● reduce volume of filler 6.8c
Mass Pour
Heat of hydration
Decrease, avoid thermal strain in mass pours
○ increase proportion of slag cf. A-6.2.2, 6.6.4
○ increase density (thermal conductivity) 6.15a
□ reduce temperature of mix ingredients cf. A-6.2.2
Thermal resistivity
Increase if required for application
● reduce density 6.15a
□ protect from moisture ingress cf. A-6.3.4a
Bouyancy of hardened material
Decrease to reduce risk of uplift
○ increase density, with use of filler if necessary 6.6.1.2a
○ use wet foam to increase permeability cf. 6.14a, A-6.3.1b
□ provide drainage for surrounding groundwater cf. A-6.3.3c
□ anchor or add load to resist uplift 6.6.1.2a
Drying shrinkage
Decrease to minimize subsidence, mechanical damage due to cracking
○ increase cementitious density 6.11c
○ increase volume of filler 6.11d
○ incorporate fibre reinforcing A-6.3.2b
● reduce proportion of SCMs 6.11n to 6.11p
● reduce water-binder ratio untested
□ reduce length of curing time in high RH 6.11e to 6.11h
□ maintain high RH environment 6.11k
Creep
Decrease to avoid subsidence
○ increase density, volume of filler 6.10a
Moisture movement
Decrease strain induced by changing MC
○ increase volume of filler 6.13a
□ reduce length of curing in high RH untested, cf. 6.11e
□ maintain constant RH environment 6.13d
Decrease damage due to cyclical wetting/drying
● reduce volume of filler (density) 6.6.1.1a
● eliminate SCMs 6.6.1.1a
Freeze-thaw
Decrease risk of damage
○ increase density 6.16.1m
○ increase proportion of silica fume 6.16.1m
● reduce proportion of slag 6.16.1m
□ provide drainage for surrounding water cf. A-6.3.3c
Sulphate attack
Decrease risk of damage
● reduce density A-6.3.5b
□ control movement of sulphates in environment A-6.3.5b
Cost
Decrease
● reduce cementitious density (increase filler) A-5.1.1
● eliminate silica fume A-5.1.1
○ increase proportion of slag (market-dependent) A-5.1.1

Backfill for linear utilities

Figure 8.2b

Backfill for linear utilities is a special case of geotechnical fill. A distinct set of considerations is necessitated by fragile or buoyant utilities, length of the pour, proximity to the public, etc.

This protocol may be appropriate for the following foam concrete applications:

Trench reinstatement, bedding material to absorb stresses for differential movement or settlement, insulation and support for pipelines installed over permafrost, support for existing pipes. (Refer to Appendix A, Section 8.1)

Control of mix ingredient and proportions (additions) ○
Control of mix ingredient and proportions (subtractions) ●
Control of curing or placing environment □
Controls which are not recommended ×

Relevant Figures 6.**1a**
Relevant notes from the Appendices *A-6.1*

Early-age stiffness	Increase for walkability, safety of public	○ use FCA ..... *Appendix E* ○ increase volume of filler ..... 6.**6.4a** to 6.**6.4f** ○ increase cementitious density ..... 6.**6.4a** to 6.**6.4f** ○ increase proportion of silica fume ..... 6.**6.4a** to 6.**6.4f** ● reduce proportion of slag ..... 6.**6.4a** to 6.**6.4f**
Long-term strength	Increase for anticipated loading	○ increase volume of filler ..... 6.**6.1.1a** ○ increase cementitious density ..... 6.**6.1.1a** ○ increase proportion of slag or silica fume ..... 6.**6.1.1a** □ increase curing age (SCM mixes) ..... 6.**6.4a** to 6.**6.4f**
	Decrease for ease of future excavation	● reduce density, cementitious density ..... 6.**6.1.1a** ● reduce SCMs 6.**6.1.1a**
Bouyancy of hardened material	Decrease, avoid damage by hydrostatic pressure	○ increase density, with use of filler if necessary ..... 6.**6.1.2a** ○ use wet foam to increase permeability ..... *cf.* 6.**14a**, *A-6.3.1b* □ provide drainage for surrounding groundwater ..... *cf. A-6.3.3c*
Hydrostatic pressure of plastic mix	Decrease to reduce bouyant force on pipes during placement	○ use FCA ..... *Appendix E* ● reduce (plastic) density ..... 6.**6.1.1a** ○ increase slag and reduce w/b ratio 6.**1.1.6a**, 6.**6.1.1a**
Modulus of elasticity	Decrease to minimize local stress on utilities	● reduce cementitious density ..... 6.**7b**, 6.**7c** ● reduce SCMs 6.**7b**, 6.**7c**

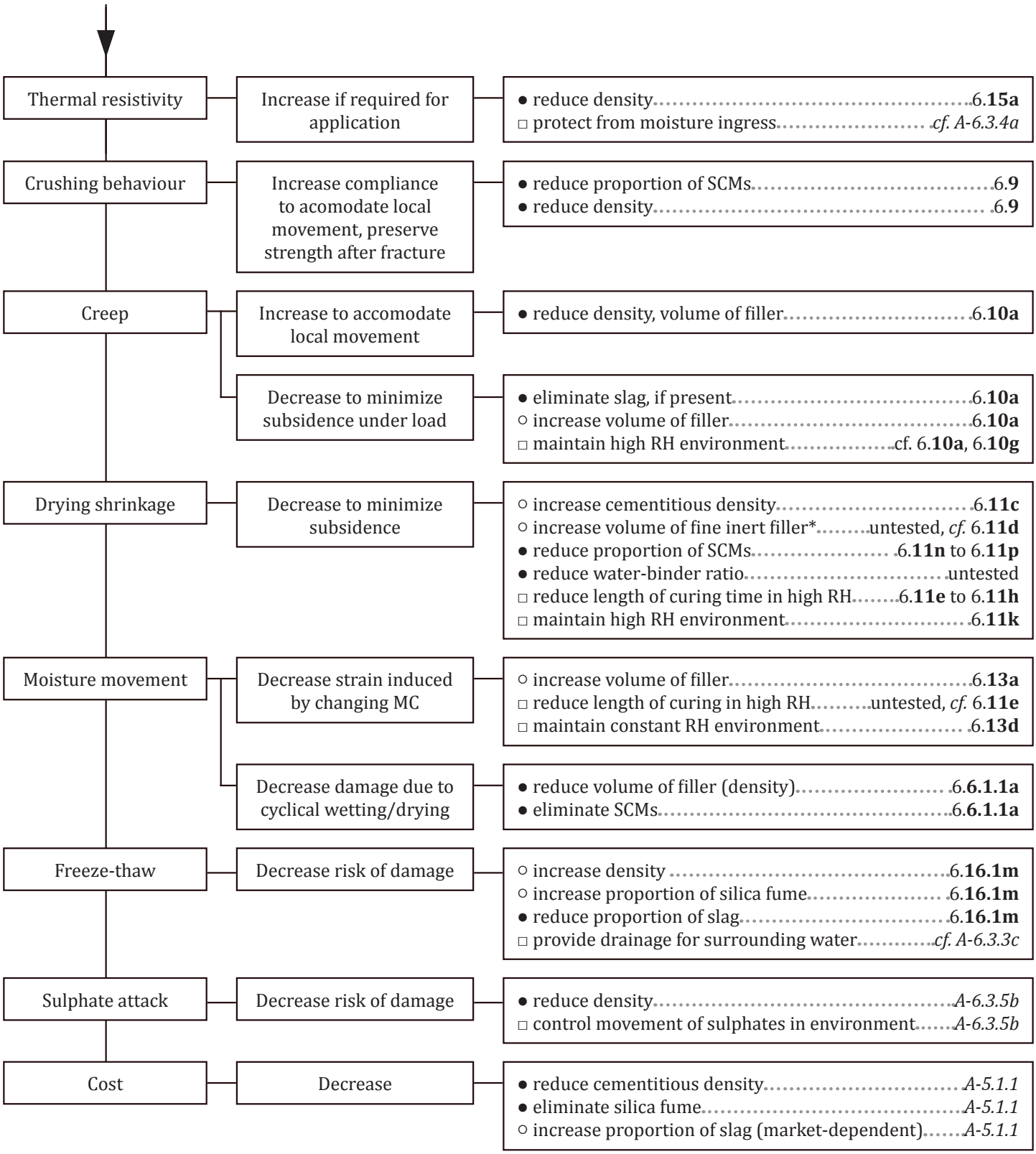
Thermal resistivity
Increase if required for application
● reduce density 6.15a
□ protect from moisture ingress cf. A-6.3.4a
Crushing behaviour
Increase compliance to acomodate local movement, preserve strength after fracture
● reduce proportion of SCMs 6.9
● reduce density 6.9
Creep
Increase to accomodate local movement
● reduce density, volume of filler 6.10a
Decrease to minimize subsidence under load
● eliminate slag, if present 6.10a
○ increase volume of filler 6.10a
□ maintain high RH environment cf. 6.10a, 6.10g
Drying shrinkage
Decrease to minimize subsidence
○ increase cementitious density 6.11c
○ increase volume of fine inert filler* untested, cf. 6.11d
● reduce proportion of SCMs 6.11n to 6.11p
● reduce water-binder ratio untested
□ reduce length of curing time in high RH 6.11e to 6.11h
□ maintain high RH environment 6.11k
Moisture movement
Decrease strain induced by changing MC
○ increase volume of filler 6.13a
□ reduce length of curing in high RH untested, cf. 6.11e
□ maintain constant RH environment 6.13d
Decrease damage due to cyclical wetting/drying
● reduce volume of filler (density) 6.6.1.1a
● eliminate SCMs 6.6.1.1a
Freeze-thaw
Decrease risk of damage
○ increase density 6.16.1m
○ increase proportion of silica fume 6.16.1m
● reduce proportion of slag 6.16.1m
□ provide drainage for surrounding water cf. A-6.3.3c
Sulphate attack
Decrease risk of damage
● reduce density A-6.3.5b
□ control movement of sulphates in environment A-6.3.5b
Cost
Decrease
● reduce cementitious density A-5.1.1
● eliminate silica fume A-5.1.1
○ increase proportion of slag (market-dependent) A-5.1.1

Profiling for floors or roofs

Figure 8.2c

With high worakability and low density, foam concrete may be suitable for use in overpour applications. Finished surfaces may be horizontal or slightly sloped, as required. Foam concrete provides thermal resistance to control heat flow through enclosure assemblies, or under heated slabs.

This protocol may be appropriate for the following foam concrete applications:

Floor leveling, insulating layer below heated slabs, slopes for flat roofs.
(Refer to Appendix A, Section 8.1.)

Control of mix ingredient and proportions (additions)	○
Control of mix ingredient and proportions (subtractions)	●
Control of curing or placing environment	□
Controls which are not recommended	×
Relevant Figures	6.**1a**
Relevant notes from the Appendices	*A-6.1*

Long-term strength	Increase for anticipated loading	○ increase volume of filler……6.**6.1.1a** ○ increase cementitious density……6.**6.1.1a** ○ increase proportion of slag or silica fume……6.**6.1.1a** □ increase curing age (SCM mixes)……6.**6.4a** to 6.**6.4f** □ install dense finishing screed or coverboard……6.**6.1.1a**
Density	Decrease	○ decrease filler, increase cementitious as required……6.**6.1.1a**
Spread flow	Decrease for ability to form slope	○ increase volume of filler……6.**2b** ● reduce water content……6.**2b** ○ incorporate fibre reinforcing……*A-5.1.5*
Stability	Resist segregation of water, paste, aggregate	● maintain low water-binder ratio……*cf.* 6.**2b** □ avoid overworking……*A-7.2.1* □ seal substrate, avoid leakage of water……6.**6.1.1a**
Drying shrinkage	Decrease for compatibility with substrate, avoid cracking	○ increase cementitious density……6.**11c** ○ increase volume of filler……6.**11d** ○ incorporate fibre reinforcing……*A-6.3.2b* ● reduce proportion of SCMs……6.**11n** to 6.**11p** ● reduce water-binder ratio……untested □ reduce length of curing time in high RH……6.**11e** to 6.**11h**
Thermal resistivity	Increase if required for application	● reduce density……6.**15a** □ protect from moisture ingress……*cf. A-6.3.4a*

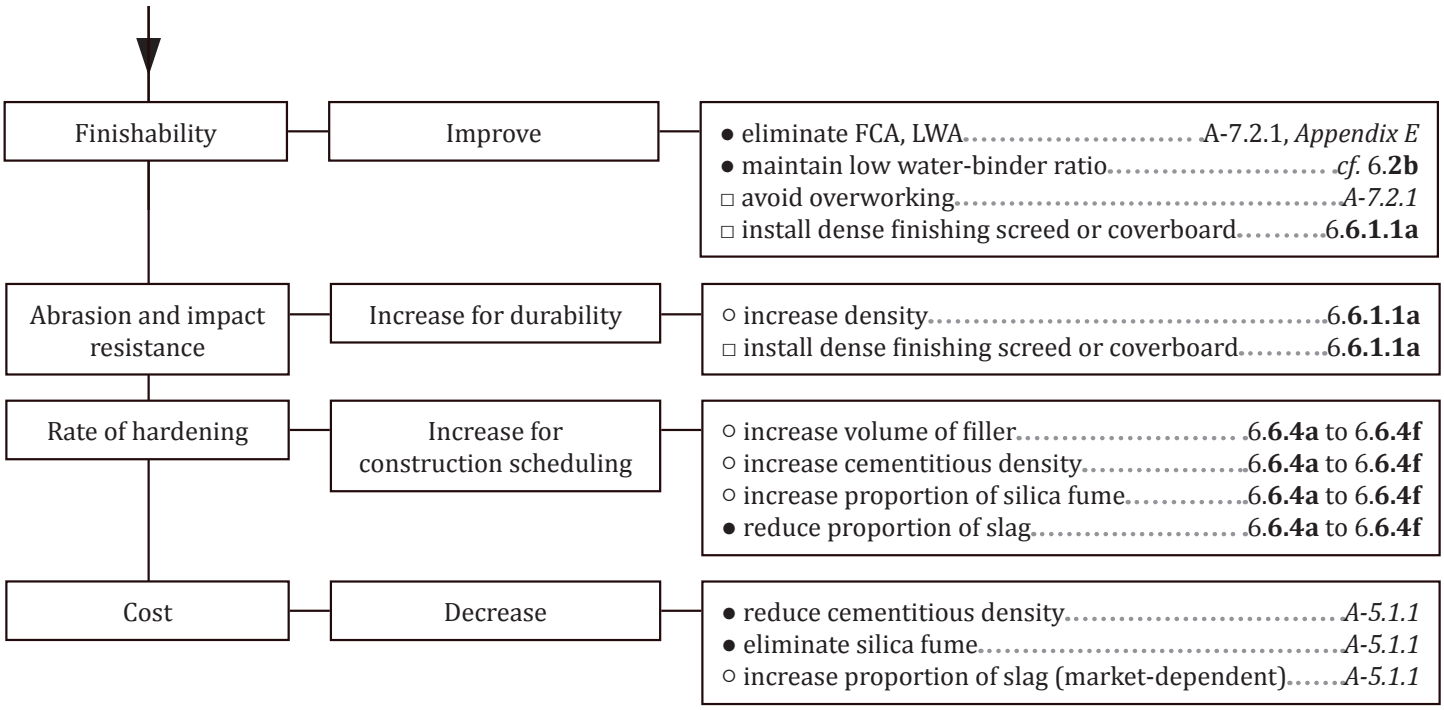
Finishability
Improve
● eliminate FCA, LWA A-7.2.1, *Appendix E*
● maintain low water-binder ratio *cf.* 6.**2b**
□ avoid overworking *A-7.2.1*
□ install dense finishing screed or coverboard 6.**6.1.1a**
Abrasion and impact resistance
Increase for durability
○ increase density 6.**6.1.1a**
□ install dense finishing screed or coverboard 6.**6.1.1a**
Rate of hardening
Increase for construction scheduling
○ increase volume of filler 6.**6.4a** to 6.**6.4f**
○ increase cementitious density 6.**6.4a** to 6.**6.4f**
○ increase proportion of silica fume 6.**6.4a** to 6.**6.4f**
● reduce proportion of slag 6.**6.4a** to 6.**6.4f**
Cost
Decrease
● reduce cementitious density *A-5.1.1*
● eliminate silica fume *A-5.1.1*
○ increase proportion of slag (market-dependent) *A-5.1.1*

Impact absorbing material

Figure 8.2d

Foam concrete can dissapate energy through crushing. The protocol given below may be appropriate for the following impact-absorbing foam concrete applications:

Crash barriers, stopping pads, defensive structures, bullet traps, explosion prevention, protection of pipelines from rockfall, cribbing for seismically active mines, blast walls. (Refer to Appendix A, Section 8.1.)

Note that additonal design considerations are given for slab formats, materials exposed to the outdoors, and materials in contact with the ground.

Control of mix ingredient and proportions (additions) ○
Control of mix ingredient and proportions (subtractions) ●
Control of curing or placing environment □
Controls which are not recommended ×

Relevant Figures 6.**1a**
Relevant notes from the Appendices *A-6.1*

Crushing behaviour

- Stress remains consistent during crushing
  - ● reduce proportion of SCMs 6.**9**
  - ● reduce density 6.**9**
  - Note: Study plots in Section 6.9 to select mix design with desired crushing characteristics 6.**9**
- Crushing properties do not vary with age
  - Note: Portland cement mixes appear to densify with increased age. Further investigation is necessary 6.**11r**

Compressive strength

- Increase for support of normal, non-impact loads
  - ○ increase volume of filler 6.**6.1.1a**
  - ○ increase cementitious density 6.**6.1.1a**
  - ○ increase proportion of slag or silica fume 6.**6.1.1a**
  - □ increase curing age (SCM mixes) ..... 6.**6.4a** to 6.**6.4f**

Tensile strength

- Increase for preserving integrity of material during crushing
  - ○ add fibre reinforcing ..... *cf. A-5.1.5, A-6.3.2b*

Poisson's Ratio

- Decrease to suit application
  - ○ increase volume of filler 6.**8c**
- Increase to suit application
  - ● reduce volume of filler 6.**8c**

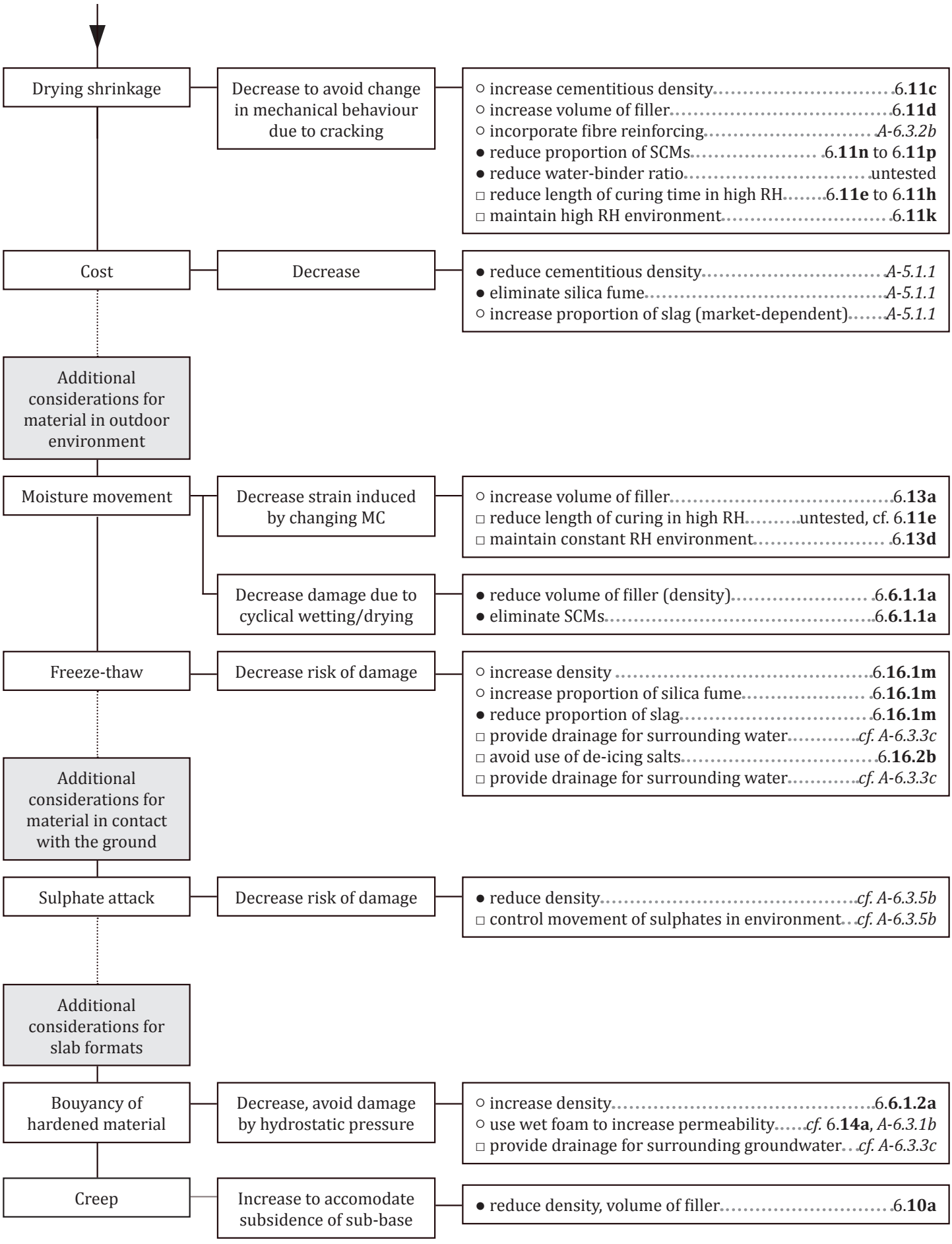
Drying shrinkage
Decrease to avoid change in mechanical behaviour due to cracking
○ increase cementitious density 6.11c
○ increase volume of filler 6.11d
○ incorporate fibre reinforcing A-6.3.2b
● reduce proportion of SCMs 6.11n to 6.11p
● reduce water-binder ratio untested
□ reduce length of curing time in high RH 6.11e to 6.11h
□ maintain high RH environment 6.11k
Cost
Decrease
● reduce cementitious density A-5.1.1
● eliminate silica fume A-5.1.1
○ increase proportion of slag (market-dependent) A-5.1.1
Additional considerations for material in outdoor environment
Moisture movement
Decrease strain induced by changing MC
○ increase volume of filler 6.13a
□ reduce length of curing in high RH untested, cf. 6.11e
□ maintain constant RH environment 6.13d
Decrease damage due to cyclical wetting/drying
● reduce volume of filler (density) 6.6.1.1a
● eliminate SCMs 6.6.1.1a
Freeze-thaw
Decrease risk of damage
○ increase density 6.16.1m
○ increase proportion of silica fume 6.16.1m
● reduce proportion of slag 6.16.1m
□ provide drainage for surrounding water cf. A-6.3.3c
□ avoid use of de-icing salts 6.16.2b
□ provide drainage for surrounding water cf. A-6.3.3c
Additional considerations for material in contact with the ground
Sulphate attack
Decrease risk of damage
● reduce density cf. A-6.3.5b
□ control movement of sulphates in environment cf. A-6.3.5b
Additional considerations for slab formats
Bouyancy of hardened material
Decrease, avoid damage by hydrostatic pressure
○ increase density 6.6.1.2a
○ use wet foam to increase permeability cf. 6.14a, A-6.3.1b
□ provide drainage for surrounding groundwater cf. A-6.3.3c
Creep
Increase to accomodate subsidence of sub-base
● reduce density, volume of filler 6.10a

Structural lightweight concrete

Figure 8.2e

Foam concrete may be produced with sufficient strength for some structural applications. The mix design protocol given below provides guidance for the following uses:

Structural beams, structural slabs, walls, blocks, sandwich panels, precast elements. (Refer to Appendix A, Section 8.1.)

Note that additonal design considerations are given for structural lightweight elements exposed to the outdoors or placed in contact with the ground.

Control of mix ingredient and proportions (additions) ○
Control of mix ingredient and proportions (subtractions) ●
Control of curing or placing environment □
Controls which are not recommended ×

Relevant Figures 6.**1a**
Relevant notes from the Appendices *A-6.1*

Long-term strength	Increase for anticipated loading	○ increase volume of filler ..... 6.**6.1.1a** ○ increase cementitious density ..... 6.**6.1.1a** ○ increase proportion of slag or silica fume ..... 6.**6.1.1a** □ increase curing age (SCM mixes) ..... 6.**6.4a** to 6.**6.4f**
Density	Decrease	○ decrease filler, increase cementitious as required 6.**6.1.1a**
Modulus of elasticity	Increase	○ increase cementitious density ..... 6.**7b**, 6.**7c** ○ reduce proportion of slag 6.**7b**, 6.**7c**
Drying shrinkage	Decrease to minimize mechanical damage, strain	○ increase cementitious density ..... 6.**11c** ○ increase volume of filler ..... 6.**11d** ○ incorporate fibre reinforcing ..... *A-6.3.2b* ● reduce proportion of SCMs ..... 6.**11n** to 6.**11p** ● reduce water-binder ratio ..... untested □ reduce length of curing time in high RH ..... 6.**11e** to 6.**11h** □ maintain high RH environment 6.**11k**
Creep	Decrease	● eliminate slag, if present ..... 6.**10a** ○ increase volume of filler ..... 6.**10a** □ maintain high RH environment ..... cf. 6.**10a**, 6.**10g**
Carbonation	Decrease	○ increase cementitious density ..... 6.**12f**, *A-6.3.5a* ○ increase density ..... 6.**12b**, *A-6.3.5a* ○ increase SCM (reduce permeability) ..... 6.**12b**, *A-6.3.5a* □ avoid use of steel reinforcing ..... *A-6.3.5a* □ increase RH to above 70% ..... 6.**12b**, *A-6.3.5a* □ decrease RH to below 50% ..... 6.**12g**, *A-6.3.5a* □ seal to resist ingress of moisture *A-6.3.5a*

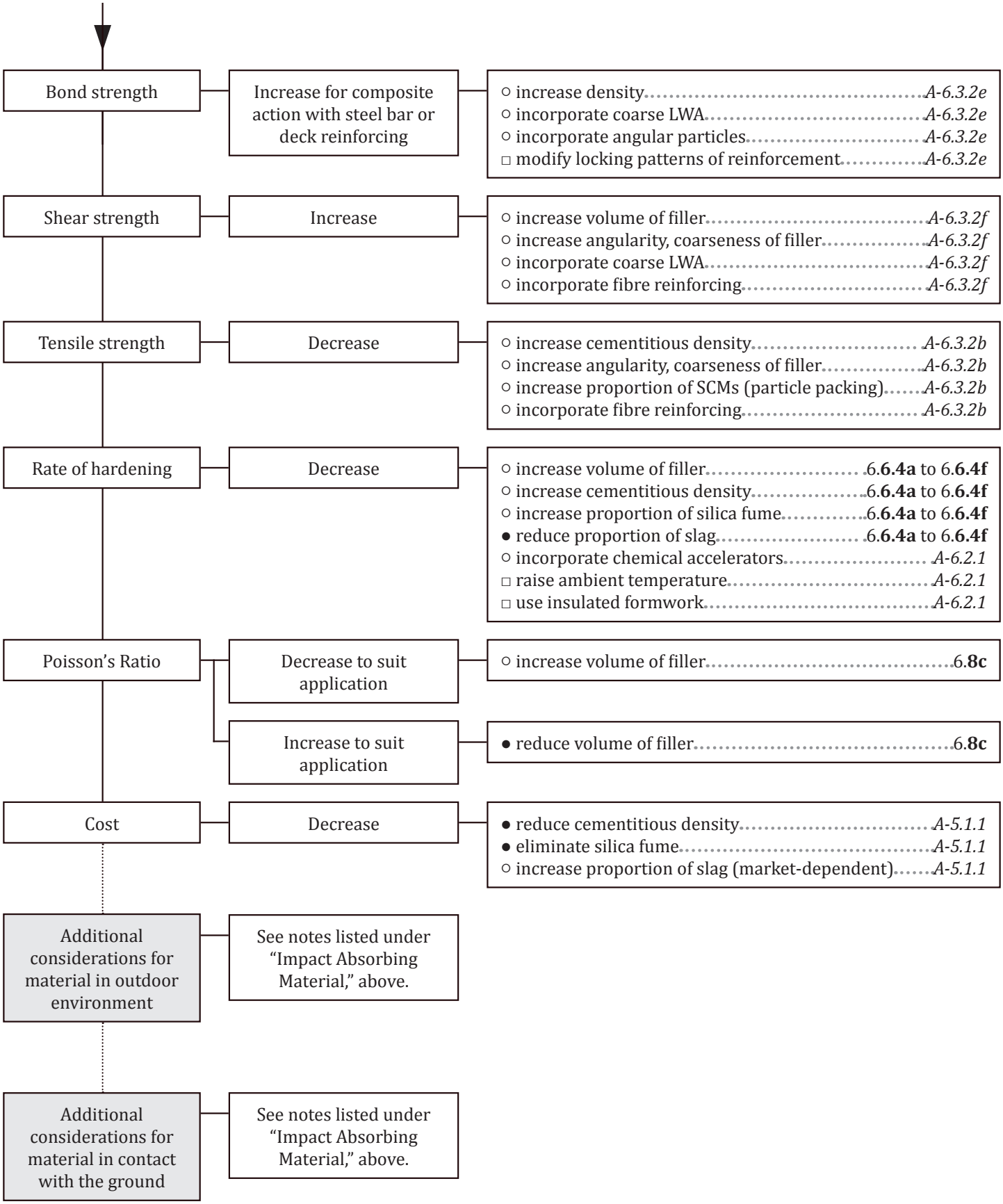
Bond strength
Increase for composite action with steel bar or deck reinforcing
○ increase density A-6.3.2e
○ incorporate coarse LWA A-6.3.2e
○ incorporate angular particles A-6.3.2e
□ modify locking patterns of reinforcement A-6.3.2e
Shear strength
Increase
○ increase volume of filler A-6.3.2f
○ increase angularity, coarseness of filler A-6.3.2f
○ incorporate coarse LWA A-6.3.2f
○ incorporate fibre reinforcing A-6.3.2f
Tensile strength
Decrease
○ increase cementitious density A-6.3.2b
○ increase angularity, coarseness of filler A-6.3.2b
○ increase proportion of SCMs (particle packing) A-6.3.2b
○ incorporate fibre reinforcing A-6.3.2b
Rate of hardening
Decrease
○ increase volume of filler 6.6.4a to 6.6.4f
○ increase cementitious density 6.6.4a to 6.6.4f
○ increase proportion of silica fume 6.6.4a to 6.6.4f
● reduce proportion of slag 6.6.4a to 6.6.4f
○ incorporate chemical accelerators A-6.2.1
□ raise ambient temperature A-6.2.1
□ use insulated formwork A-6.2.1
Poisson's Ratio
Decrease to suit application
○ increase volume of filler 6.8c
Increase to suit application
● reduce volume of filler 6.8c
Cost
Decrease
● reduce cementitious density A-5.1.1
● eliminate silica fume A-5.1.1
○ increase proportion of slag (market-dependent) A-5.1.1
Additional considerations for material in outdoor environment
See notes listed under "Impact Absorbing Material," above.
Additional considerations for material in contact with the ground
See notes listed under "Impact Absorbing Material," above.

8.3 Foam Concrete Mix Design Computer Application

Matrices or graphs typically display only two or three dimensions of information. In this thesis, a large number of parameters have been considered. As noted in the section above, multiple parameters may need to be considered and constrained for certain foam concrete applications. In order to simplify this procedure, a computer program has been developed.

While the computer program is not a part of this publicly available thesis, the user interface and underlying framework are described below.

8.3.1 User Interface

1) The mix designer identifies which cementitious ingredients are available at the batching facility.
2) The mix designer identifies whether foam concrete aggregate is available at the batching facility.
3) The designer may update cost information for materials as required.
4) The designer identifies limiting values (minimum or maximum) for various properties:
    - compressive strength at 7, 28, or 56 days
    - plastic, dry, or oven-dry density
    - specific creep at one year, for 0.4 f'_c
    - drying shrinkage at one year
    - cost
5) The program presents possible mix designs in the database that meet the design parameters.
6) Mixes can be further refined by porosity, within available limits defined by the constraints in Step 4.
7) The program will provide mix ingredient proportions per cubic meter of foam concrete for the selected recipe. Material costs will be provided based on user inputs in Step 3.

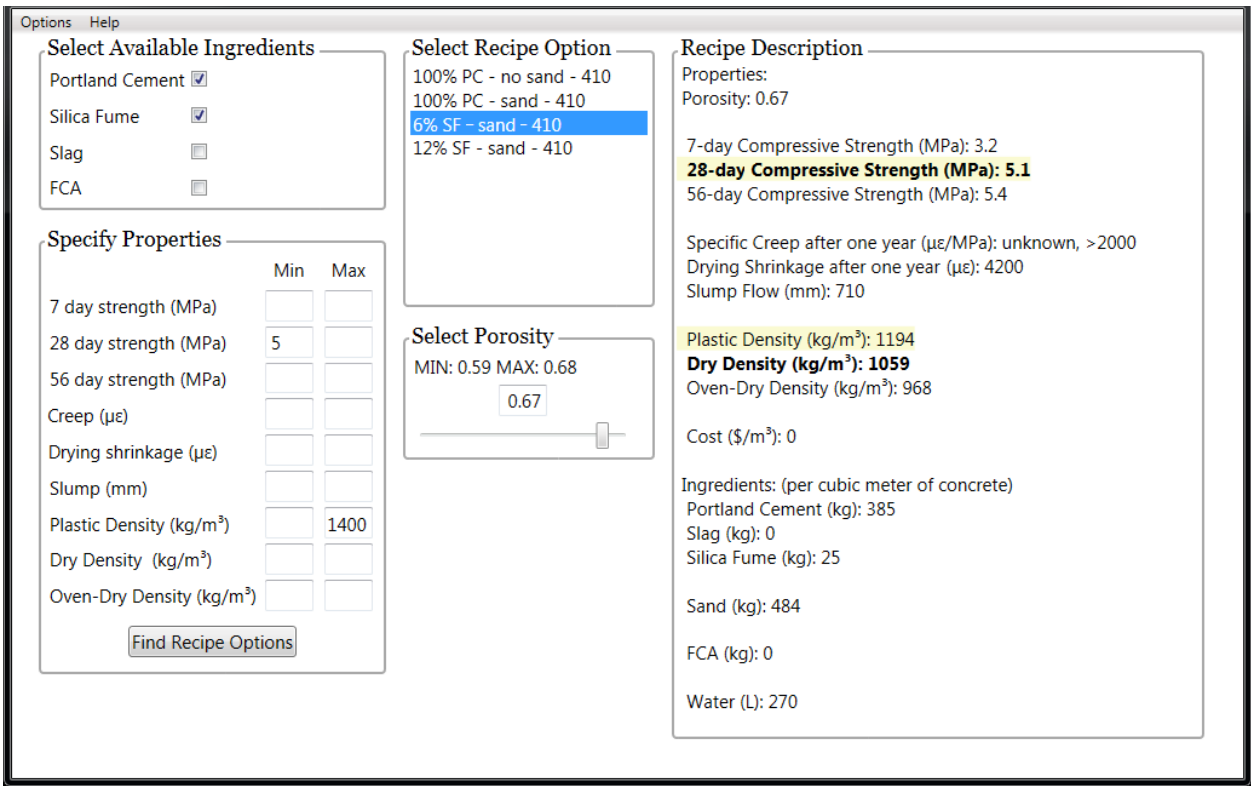

Figure 8.3.2a Screenshot of user interface for application, showing available parameters and controls.

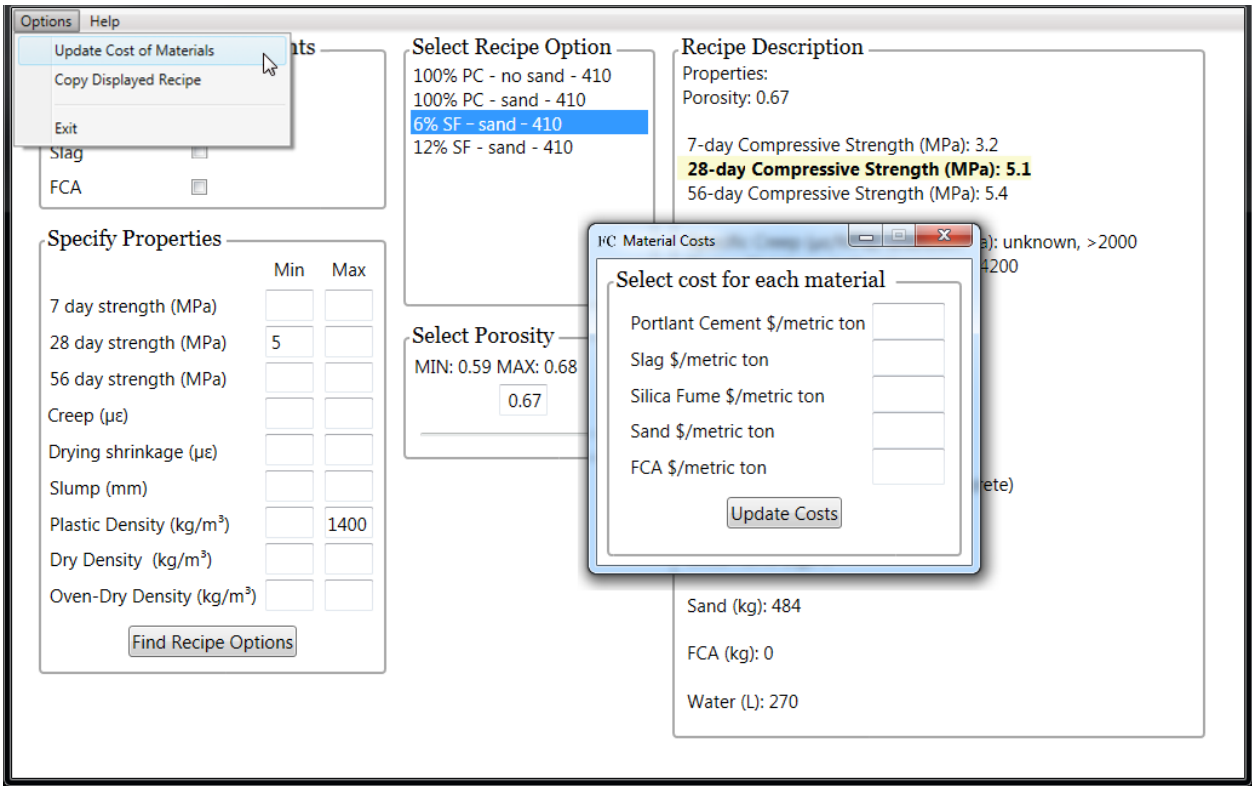

Figure 8.3.2b User interface for inputting costing information.

8.3.2 Underlying Framework

All data from the experimental program was organized in numerous overlapping mix subsets, in which two of the following three mix design parameters were constant:[1]

- Cementitious density
- Binder composition
- Filler-binder ratio

For each mix subset, the properties and quantities in Tables 8.3.2a and 8.3.2b were plotted against porosity, *P*. These properties and quantities were then expressed as functions of *P*, interpolating between known points.

The program evaluates the functions associated with each mix subset, and returns all mix subsets for which there is a domain of *P* that satisfies user-defined constraints.

When a mix subset is selected, the available domain of *P* is limited by the user-defined constraints. As *P* is varied, the program returns quantities of mix ingredients, calculated as a function of *P*. Cost is calculated as the sum of each mix ingredient, multiplied by its respective cost.

Mix Properties		**Units**
Physical Properties	Plastic density	kg/m^3
	Dry density	kg/m^3
	Oven-dry density	kg/m^3
Mechanical Properties	7-day compressive strength	MPa
	28-day compressive strength	MPa
	56-day compressive strength	MPa
	Specific creep after one year, at 0.4 f'c, in 50% RH	με/MPa
Drying Shrinkage Properties	Drying shrinkage after one year, in 50% RH	με
Workability Properties	Slump Flow	mm

Table 8.3.2a Mix properties plotted as a function of porosity, *P*, for computer program.

[1] For example, one mix subset included all mixes with 100% Portland binder and 410kg/m^3 cementitious density; the filler-binder ratio varied with density. Another subset included all mixes with 12% silica fume binder and a filler-binder ratio of 2:1; the cementitious density varied with density. Mixes incorporating FCA were also organized in separate mix subsets.

Mix Quantities, per cubic meter of fresh foamed mix		Unit
Solids	Portland Cement	kg/m^3
	Silica Fume	kg/m^3
	Slag	kg/m^3
	Sand	kg/m^3
	FCA	kg/m^3
Water	Drying shrinkage after one year	L/m^3
Foam	Foam Volume	L/m^3
	Surfactant	kg/m^3
Cost	Cost of mix ingredients[2]	$/m^3

Table 8.3.2b Mix quantities plotted as a function of porosity, P, for computer program.

8.3.3 On-going Developments

A number of updates to the program are currently in development. Most significantly, the updated program includes curated plots of key properties, such as compressive strength vs. dry density. Plots are updated in real-time, showing the data points and segments of trendlines that satisfy user-defined constraints. These plots enable the designer to compare mix options graphically, and indicate a level of reliability for the stated mix design, by showing actual scatter of data from the experimental program. These improvements reduce the tendency for the computer program to be used as a black box.

These intuitive tools for assessing reliability will be supplemented by statistical analysis.[3] Additionally, the updated program will include commentary on allowable tolerances to water-binder ratio and mixing time.

8.4 Mix Design Troubleshooting Guide

Various problems may arise during the batching, placing or curing of foam concrete. Possible causes and solutions for common issues are provided in the diagnostic diagrams shown in Figures 8.**4a** to 8.**4c**, below.

[2] Cost was expressed as a function of mix ingredients, which are each expressed as a function of porosity.
[3] E.g. coefficient of variation. Refer to Section 6.5.

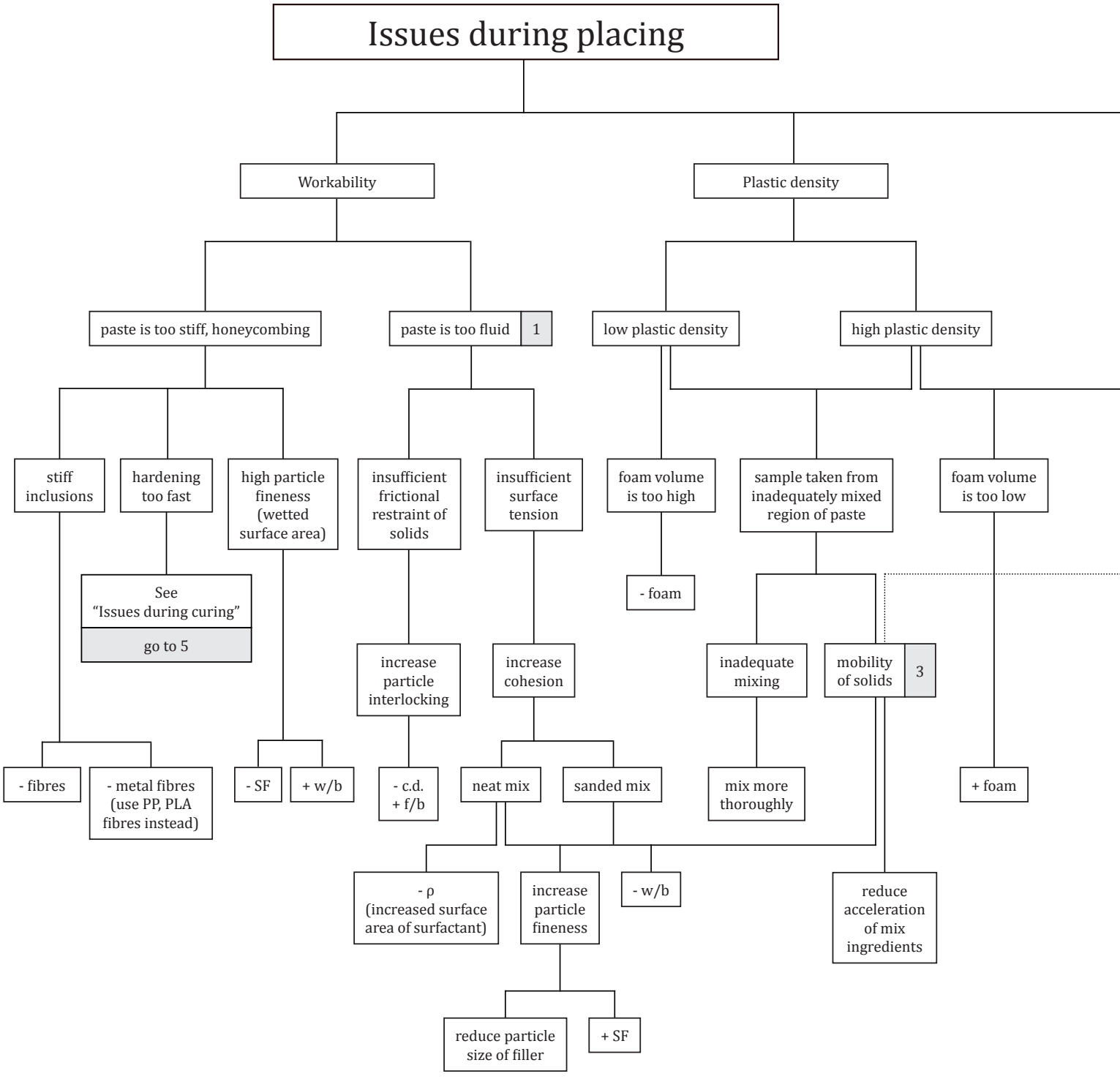

Figure 8.4a Diagnostic diagram for issues encountered during placing.

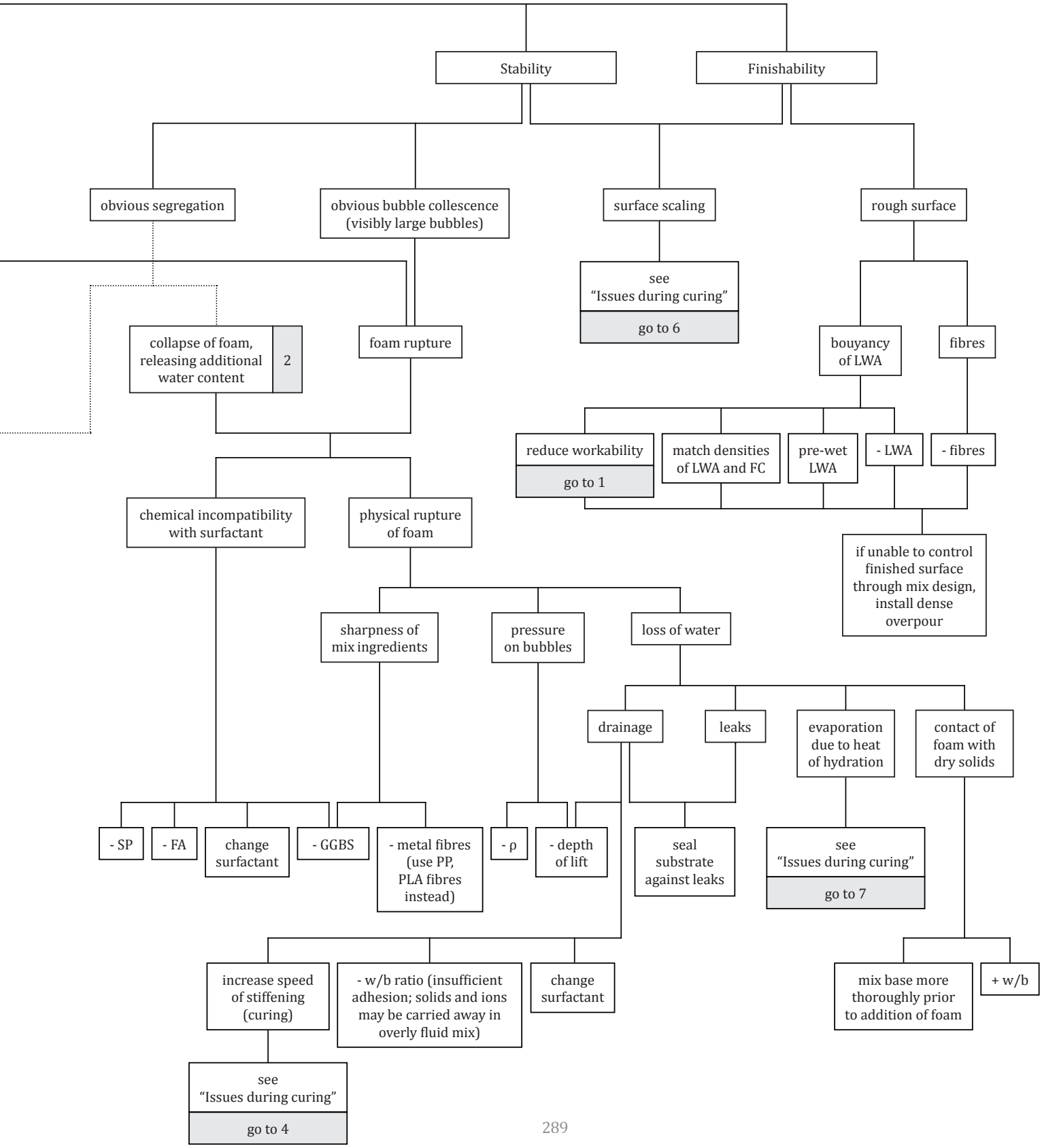
Stability
Finishability
obvious segregation
obvious bubble collescence (visibly large bubbles)
surface scaling
rough surface
see "Issues during curing"
go to 6
collapse of foam, releasing additional water content
2
foam rupture
bouyancy of LWA
fibres
reduce workability
go to 1
match densities of LWA and FC
pre-wet LWA
- LWA
- fibres
chemical incompatibility with surfactant
physical rupture of foam
if unable to control finished surface through mix design, install dense overpour
sharpness of mix ingredients
pressure on bubbles
loss of water
drainage
leaks
evaporation due to heat of hydration
contact of foam with dry solids
- SP
- FA
change surfactant
- GGBS
- metal fibres (use PP, PLA fibres instead)
- ρ
- depth of lift
seal substrate against leaks
see "Issues during curing"
go to 7
increase speed of stiffening (curing)
- w/b ratio (insufficient adhesion; solids and ions may be carried away in overly fluid mix)
change surfactant
mix base more thoroughly prior to addition of foam
+ w/b
see "Issues during curing"
go to 4

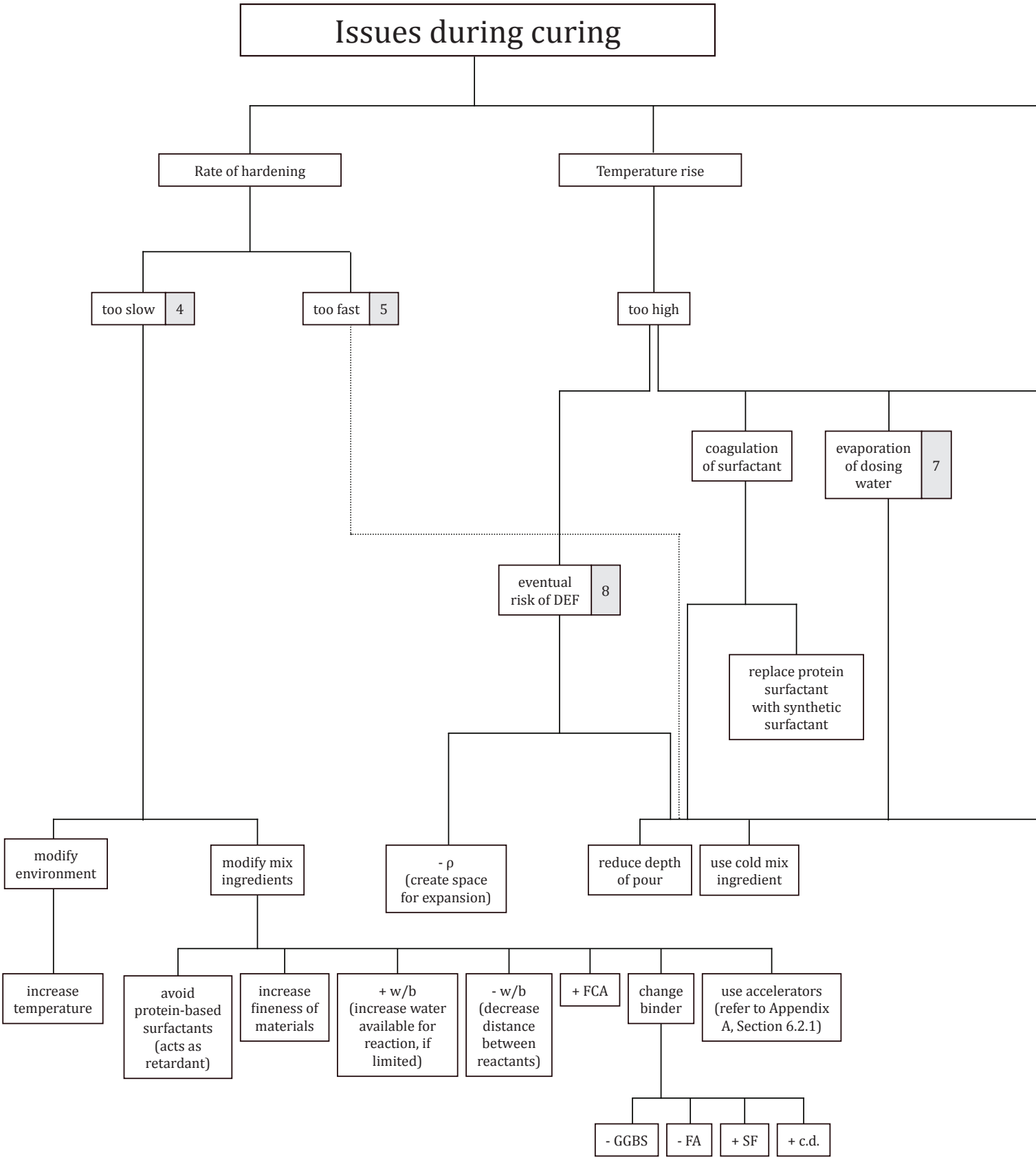

Figure 8.4b Diagnostic diagram for issues encountered during curing.

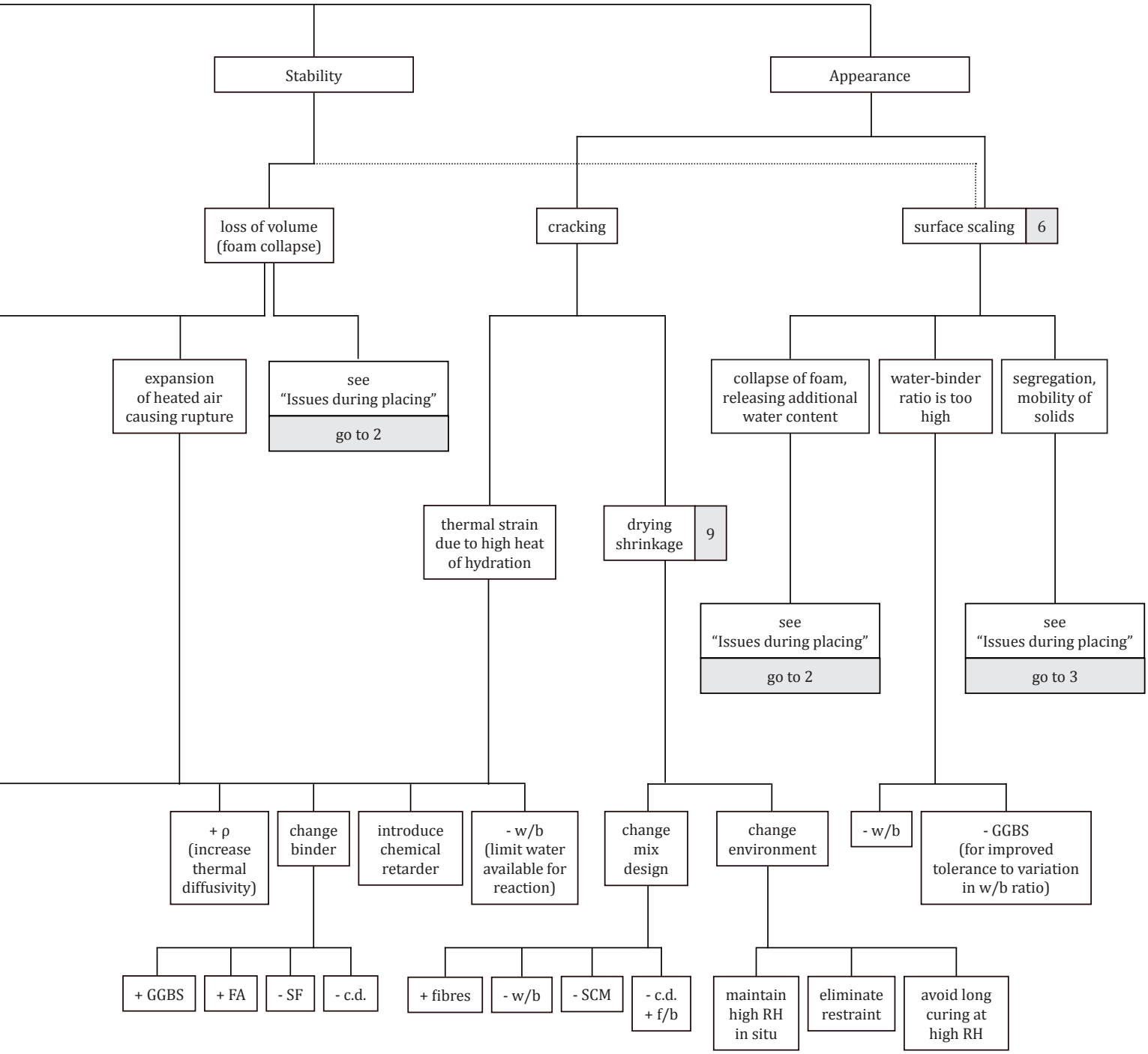
Stability
Appearance
loss of volume (foam collapse)
cracking
surface scaling
6
expansion of heated air causing rupture
see "Issues during placing"
go to 2
thermal strain due to high heat of hydration
drying shrinkage
9
collapse of foam, releasing additional water content
water-binder ratio is too high
segregation, mobility of solids
see "Issues during placing"
go to 2
see "Issues during placing"
go to 3
+ ρ (increase thermal diffusivity)
change binder
introduce chemical retarder
- w/b (limit water available for reaction)
change mix design
change environment
- w/b
- GGBS (for improved tolerance to variation in w/b ratio)
+ GGBS
+ FA
- SF
- c.d.
+ fibres
- w/b
- SCM
- c.d. + f/b
maintain high RH in situ
eliminate restraint
avoid long curing at high RH

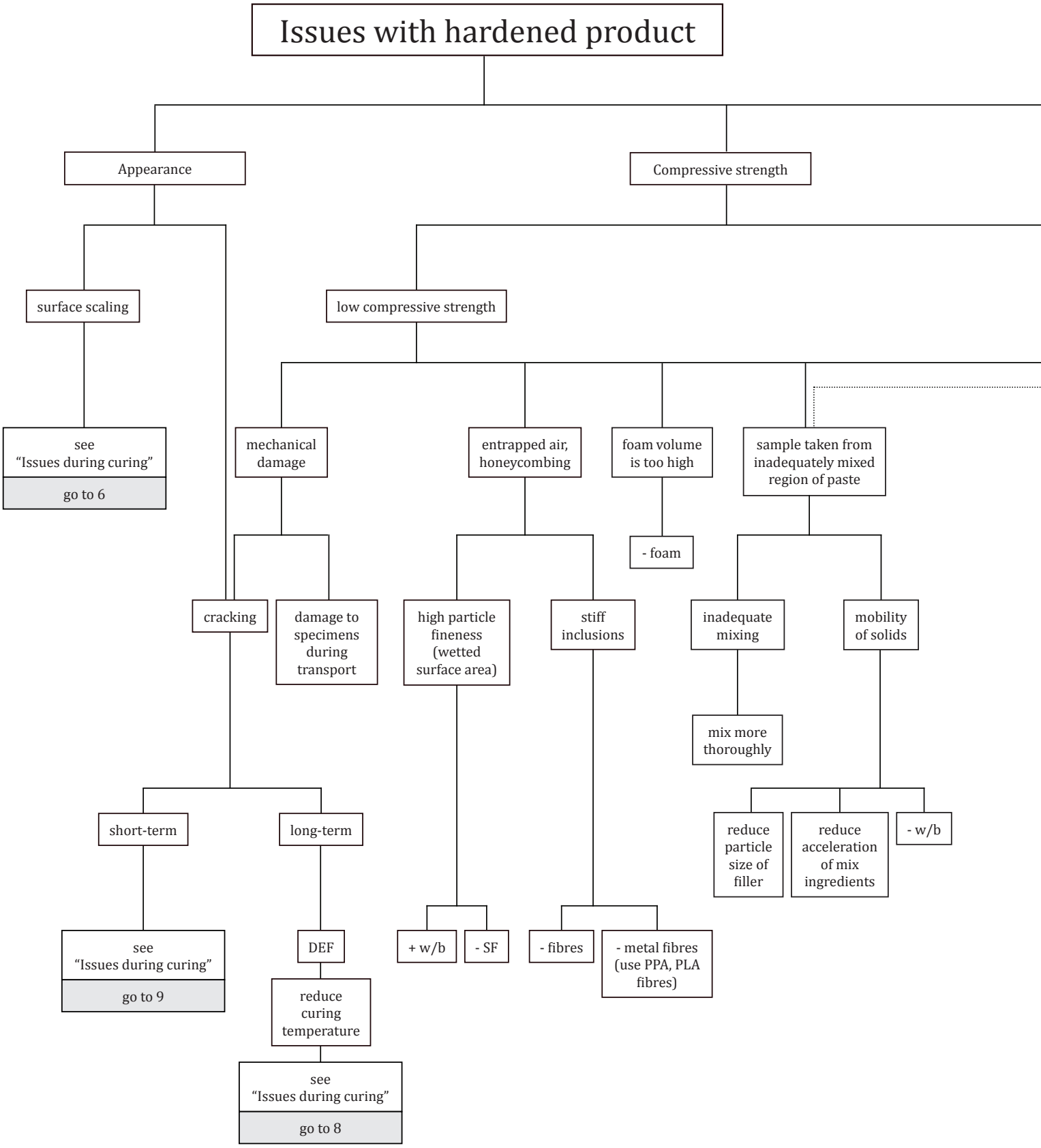

Figure 8.4c Diagnostic diagram for issues encountered with hardened product.

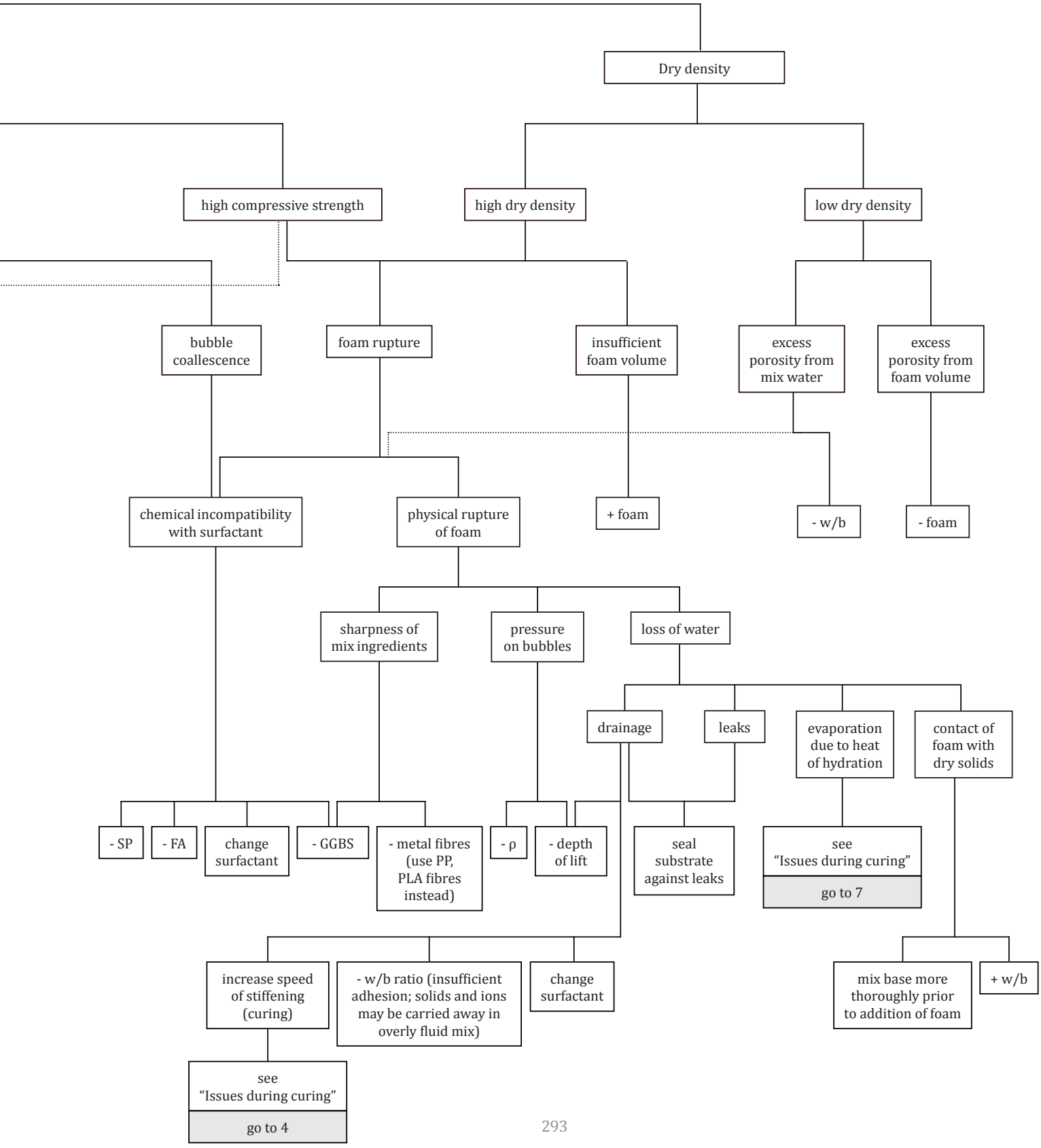
Dry density
high compressive strength
high dry density
low dry density
bubble coallescence
foam rupture
insufficient foam volume
excess porosity from mix water
excess porosity from foam volume
chemical incompatibility with surfactant
physical rupture of foam
+ foam
- w/b
- foam
sharpness of mix ingredients
pressure on bubbles
loss of water
drainage
leaks
evaporation due to heat of hydration
contact of foam with dry solids
- SP
- FA
change surfactant
- GGBS
- metal fibres (use PP, PLA fibres instead)
- ρ
- depth of lift
seal substrate against leaks
see "Issues during curing"
go to 7
increase speed of stiffening (curing)
- w/b ratio (insufficient adhesion; solids and ions may be carried away in overly fluid mix)
change surfactant
mix base more thoroughly prior to addition of foam
+ w/b
see "Issues during curing"
go to 4

8.5 Recommended Tolerances for Mix Proportioning

Recommended tolerances are given in the table below, for both research and industry purposes.

These proposed tolerances have been found practicable during the experimental program, and appear to be reasonable based on accumulated data. Supporting analysis is provided in Appendix S. Note that the cumulative effects of parameter variance should also be considered.

Mix parameter		Tolerance for research[4]	Tolerance for industry		Notes
			Critical[5]	Non-Critical[6]	
Foam density		±2 g/L	±2 g/L	±2 g/L	Foam density calibration is typically straightforward. Adjust per manufacturer instructions. See Appendix G.
Quantity of binder		±0.5%	±5 kg/m^3	±10 kg/m^3	If variance is suspected, consult figures in Appendix S to estimate impact on mix properties.
Quantity of filler		±0.5%	±10 kg/m^3	±20 kg/m^3	If variance is suspected, consult figures in Appendix S to estimate impact on mix properties.
Sand, moisture content		±0.2%	±1%	±1%	It is critical to account for MC in dense (sanded) mixes.
Water-Binder Ratio	PC	±0.01	±0.05	±0.05	Tolerance to hydration varies with the use of SCMs. Tighter tolerances are recommended with increased cementitious density.
	Slag	±0.01	±0.02	±0.02	
	SF	±0.01	±0.02	±0.02	
Plastic Density		±10 kg/m^3	±25 kg/m^3	±50 kg/m^3	Deviations of ±50kg/m^3 from target density are permitted per ASTM C796, Section 7.3.1. Closer tolerances req'd for low density mixes. Refer to Appendix S.

Table 8.5 Recommended tolerances for mix proportioning.

4 Small-scale batching is assumed, in order to achieve the proposed tolerances.
5 Average compressive strength within approximately 10% of target. Refer to Appendix S.
6 Average compressive strength within approximately 15-18% of target. Refer to Appendix S.

8.6 Recommended Acceptance Criteria for Quality Control

The following section provides guidance for quality assurance measures. This guidance is specifically intended for foam concrete produced from dry foam, and delivered to site as prefoamed mortar. Refer to Appendix A, Sections 5.2.1 and 5.2.2 for further discussion on alternative methods of aeration and delivery of foam concrete.

Checks of quality should occur at various stages of foam concrete production, to identify issues early in production, and to facilitate corrections to the mix where possible. Recommended tests are as summarized in the table below.

Production Stage	Parameter to Check	Recommended QC Metrics and Notes	References
Preparation of materials	Temperature of materials	Industry applications: 0 to 30°C Research: 18 to 24°C	CSA A23.2, 5.2.5.4.2; ASTM C157 8.2
	Grading of filler	No particles greater than 5mm diameter	Appendix A, §5.1.3
	Foam density	Per manufacturer. Relatively easy to adjust. Should normally be within 5% of stated value.	Table 8.5
	Foam stability	No obvious collapse	Appendix A, §6.1.2
	Moisture content of sand	Calibrate proportions of sand and mix water accordingly	Appendix D
Production of base mix	Temperature of base mix	10 to 30°C for depths of <1m 5 to 20°C for depths of >1m	CSA A23.2, Table 14
	Plastic density of base mix (optional)	Typically should be ±25 kg/m^3 of target density	Appendix S
	Slump of base mix (optional)	Note that workability may be very low, relative to foamed mix. Slumps of 75 to 100mm are common.	Figure 7.1b
Production of foamed mix	Stability	Plastic density dev. from target: ±50 kg/m^3	Table 8.5
		No obvious bubble coalescence	
		No obvious foam coalescence	
	Segregation	Plastic density dev. from mean: ±50 kg/m^3	Appendix A, §6.1.3

		Spread flow test: No halo (indication of low segregation)	Appendix A, §6.1.3
	Plastic density	Limit deviation per Table 8.5, to achieve desired tolerance. Each truck should be tested.	Table 8.5
	Slump flow	Normally between 600 and 700mm. May vary from 400 to 1200mm.	§6.2; Figure 8.**1a**.
Analysis of hardened product	Compressive strength	Per requirements. Variances as high as 15% may be expected, especially for medium density (highly heterogonous) mixes. Produce three cylinders for every 50m^3. For some applications, it may be desirable to produce specimens from every truck.	§6.5
	Soundness (optional)	Indentation of less than 5mm	Brady et al. (2001) 8
	Segregation (optional)	dev. from mean: ±50 kg/m^3	Appendix A, §6.1.3

Table 8.6 Recommended acceptance criteria for quality control.

9

Conclusions and Recommendations

This thesis presents a systematic, rational framework for understanding foam concrete behaviour, and how it may be controlled.

By evaluating material properties in a tightly controlled study conducted by a single operator, it has become possible to confidently characterize foam concrete over a broad range of mix parameters. The simultaneous study of diverse properties such as compressive strength, crushing behaviour, creep, drying shrinkage, and air-void size distribution has allowed the creation of a detailed micromechanical model, which explains many interrelated trends. New data for critical engineering properties, together with new design and diagnostic tools, have broken down barriers to advancement in the field of foam concrete research.

Several major research contributions are described in Section 9.1, below. A selection of conclusions from the experimental program data is provided in Section 9.2. Competitive market niches for foam concrete are summarized in Section 9.3.

Proposed standards for a methodologically consistent research framework are described in Section 9.4, as a resource for future work.

Finally, recommended topics for further study are identified in Section 9.5.

9.1 Major Research Contributions

9.1.1 Comprehensive Literature Review

An exhaustive review of hundreds of articles, papers and reports related to foam concrete is available in Appendix A. The review helps to clarify what has been previously reported in the open, English-language literature, including the following:

- history of foam concrete from the late 1800s to the present day;
- contemporary production and curing methods;
- use of ingredients, including binders, fillers, surfactants, and reinforcing;
- influence of mix design parameters on fresh, curing, and hardened properties;
- sustainability considerations;
- comparisons to other lightweight inorganic materials;
- lists of actual and proposed applications for foam concrete, significant foam concrete projects; and use of foam concrete in regions around the world.

9.1.2 Large Dataset of Strategic Mix Parameters and Properties

The literature is augmented with new data from thousands of specimens, manufactured and conditioned according to well-defined and tightly controlled variables, produced and tested by a single operator. Measures of uniformity and repeatability have been established through multiple iterations of testing.

The dataset is based on a strategic matrix of mix designs, with nominal densities ranging from 600 to 1800 kg/m^3, cementitious densities from 410 to 710 kg/m^3, and cementitious blends which include varying proportions of Portland cement, silica fume, and ground granulated blast furnace slag.

Specimens have been tested for numerous properties, including the following:

- density (plastic, dry, and oven-dry);
- compressive strength (7-, 28-, and 56-day);
- slump flow;
- segregation;
- porosity;
- static modulus of elasticity;

- Poisson's ratio;
- crushing behaviour;
- creep;
- drying shrinkage;
- moisture storage (50, 80, 90% RH; liquid immersion);
- moisture movement (i.e. hygral expansion);
- capillary water uptake;
- thermal conductivity;
- freeze-thaw resistance; and
- air-void interconnectivity and size distribution.

9.1.3 Trends for Optimizing Water-Binder Ratios

The water content of foam concrete is not typically constrained by workability requirements; however, providing an appropriate volume of mix water is critical for foam stability and consistency. In some foam concrete studies, water-binder ratios are assumed without exploration, which may affect the reliability of the conclusions. Furthermore, tolerance to under- or over-hydration is important knowledge for industry. The present research indicates appropriate water-binder ratios for a wide range of mixes.

9.1.4 Quantified Influence of SCMs and Cementitious Density

Supplementary cementitious materials may be used in foam concrete to improve mechanical performance, reduce costs, or reduce ecological impact. Through this research, the effect of incorporating silica fume or slag has been quantified for numerous engineering properties, and compared to the effects of increasing the total cementitious density.

9.1.5 Creep Data for Unsealed Specimens

Only two studies of creep were discovered in the prior literature. Both studies were for sealed, sanded mixes, with densities of between 1000 and 1750 kg/m^3. The thesis has contributed data for unsealed specimens of 600 and 1400 kg/m^3. The new data includes variations in loading, and variations in cementitious blend.

9.1.6 Extensive Drying Shrinkage Data

Foam concrete use can be limited by high drying shrinkage, since cracking affects mechanical, transport and durability properties. Experimental results indicate how drying shrinkage is influenced by density (i.e. volume of restraining filler); cementitious blend, cementitious density, curing regime, and size effects.

9.1.7 Micromechanical Model

Interrelated trends from experimental program and information from the literature review were combined in a proposed micromechanical model, to explain observed behaviour of foam concrete at a micromechanical scale during, plastic, curing, and hardened phases.

9.1.8 Detailed Mix Protocols

A detailed design protocol prioritizes critical design considerations according to their influence on mix design, for five major foam concrete applications. Various methods of controlling the relevant properties are listed, to provide multiple paths for achieving design targets. Relevant thesis subsections are noted in the protocols, for further guidance.

9.1.9 Computer Application for Mix Design

A computer application described in this thesis provides mix designs and batching tolerances based on interpolated data from the testing results. The program is constrained to return only mix designs which fulfill any number of the following user-defined parameters: available materials; compressive strength at 7, 28, or 56 days; plastic, dry, or oven-dry densities; specific creep after one year under loading of 0.4 f'_c; drying shrinkage at one year; and cost.

9.1.10 Diagnostic Diagrams

A series of diagnostic diagrams identify common issues encountered during the production, placing, and curing of foam concrete, and guide a user in isolating and correcting deficiencies.

9.2 Selection of Specific Conclusions

9.2.1 Influence of Mix Design on Water Demand

- Water-binder ratios may be optimized for a foam concrete mix, to achieve the highest possible strength for a given dry density.

- If water content is insufficient, dilution water may be extracted from the aqueous foam to wet the surface of solid particles, causing coalescence and collapse of bubbles; moreover, an especially stiff mix may cause rupture of bubbles. Conversely, if water content is excessive, bubbles will migrate upwards and dense particles will fall in the fluid mix, resulting in a weak upper region in the specimen.

- Water demand tended to increase slightly with filler content, since solids in the mix must be sufficiently wetted and sufficiently workable to avoid rupture and coalescence of bubbles during placement.

- Water demand for optimal compressive strength varies widely in relation to the presence of supplementary cementitious materials. Water demand was highest for silica fume mixes (with optimal water-binder ratios of up to 0.75); while water demand was lowest for slag mixes (with water-binder ratios as low as 0.45). The apparent water demand for good quality mixes with Portland cement binder was between 0.55 and 0.6. The fineness and surface textures of the solid cementitious particles appear to have a significant influence on the adsorption of mix water.

- At nominal densities of 1400 kg/m^3 or greater, mixes appeared to be relatively tolerant to variations in water-binder ratio, based on compressive strength results. This trend may be due to the relatively high solid surface area available to adsorb additional layers of water, as well as to the relatively thick and resilient cell walls in these denser mixes. Greater precision in water-binder ratios was required in order to achieve optimal strength for mixes with nominal densities of 1000 kg/m^3 or less. Use of slag and silica fume binders also generally necessitated greater precision in water-binder ratios.

- The reduced water demand of foam concrete made using slag may be exploited to reduce the self-weight of foam concrete: a slag mix will contain less water, and a greater proportion air bubbles, as compared to a Portland cement mix of equivalent compressive strength. The proportional reduction in self-weight is especially significant among mixes with no filler (600 kg/m^3 nominal density). This lower self-weight may have some use in applications where restrictions on construction loads or hydrostatic pressures are critical.

- Water-binder ratios for sanded Portland cement binder mixes (1400 and 1800 kg/m^3) do not appear to vary greatly with changes in cementitious density. However, total water demand increases with increasing cementitious density.

- Optimal water-binder ratios determined through laboratory testing may need to be reduced slightly when batching at a larger scales, to avoid segregation. Increased paste stiffness helps reduce the mobility of dense sand particles as they are accelerated in large mixers. This effect is most obvious for mixes in the range of 1000 to 1400 kg/m^3.

9.2.2 Slump Flow

- The slump flow of well-proportioned fresh foam concrete is typically between 500 and 700 mm for mixes with 410 kg/m^3 cementitious density. Slump flow may be slightly higher with increased cementitious density, due to higher absolute water contents, and increased smoothness of the paste.

- For low-density mixes, slump flow tends decreases with added foam volume, since self-weight is reduced. The hydrophilic foam may also contribute to the cohesiveness of the fresh mix by adsorbing layers of water.

- For dense foam concrete mixes, workability increases with foam volume: the aqueous surfactant increases the amount of water in the mix, and foam bubbles may act as spherical 'ball-bearings', similar to the entrained bubbles in retarded mortar systems.

- The fineness and roundness of silica fume particles may improve the smoothness and workability of a mix somewhat. By contrast, the angular particles of ground granulated blast furnace slag tend to produce relatively harsher mixes, corresponding to slightly reduced slump flow measurements.

9.2.3 Segregation

- Segregation results indicated a high degree of foam stability for well-proportioned mixes, with minimal migration of buoyant air bubbles or dense sand particles.

9.2.4 Porosity

- Measured porosity slightly exceeded predicted values for most mixes, which may be due to increased capillarity from collapsed foam dilution water. Variance was within 3% for well-proportioned plain foam concrete mixes.

9.2.5 Uniformity and Repeatability

- Relative to normal density concrete, foam concrete exhibits high variability in compressive strength. This effect can be attributed to variability in the air-void system, as coalesced air-voids or other large Griffith flaws govern failure.

- For a given batch, the coefficient of variation among three or four specimens was typically less than 15%. The CoV was lower for very dense batches, and for silica fume mixes, which typically have relatively small voids with minimal coalescence.

- Variability in drying shrinkage strain was typically very low among specimens from the same batch. Coefficients of variation for one year drying shrinkage values were 0.85, 1.95, and 2.95%, for 600 kg/m^3 nominal density slag, Portland cement, and silica fume mixes, respectively. Coefficients of variation were 0.50, 0.71, and 1.48%, for 1400 kg/m^3 nominal density slag, Portland cement, and silica fume mixes, respectively.

9.2.6 Influences on Compressive Strength

- The relationship between strength and density of foam concrete is non-linear. Rather, small increases in density can strongly increase compressive strength. Density may be added by increasing cementitious content, or by increasing the volume of filler in a mix.

- Strength-porosity relationships conformed well to the power model proposed by Balshin.[1]

- Partial replacement of Portland cement binder with slag and silica fume supplementary cementitious materials improved 28-day compressive strength, for all densities and combinations tested.

- Mixes with 12% silica fume binder replacement exhibited the greatest strength. The excellent performance of silica fume mixes may be partially attributed to the small average grain size of silica fume, improving particle packing around foam bubbles and distributing reactants for pozzolanic activity through the paste. The compressive strength of slag mixes was typically lower than for Portland binder only mixes at 7 days, and higher at 56 days, which may be explained with respect to pozzolanic reactions in the paste.

- The inclusion of silica fume contributes meaningfully to strength gain, even at low densities, if supplied in sufficient quantities and with sufficient mix water. Previous studies have suggested that silica fume is not appropriate for low-density mixes.[2]

- Increasing cementitious density up to 610 kg/m^3 has a meaningful influence on compressive strength, which is higher than the strength ceiling of 500 kg/m^3 suggested previously.[3] However, in many cases, partial replacement of Portland cement binder with supplementary cementitious materials may be a more effective strategy for strength gain than increasing cementitious content. For example, in

1 Balshin (1949)
2 Cf. Brady et al. (2001), Zulkarnain and Ramli (2011)
3 Cf. Brady et al. (2001) B1, C1.

mixes of approximately 1400 and 1800 kg/m^3 plastic density, 12% silica fume binder replacement offered greater strength improvement than the addition of 200 kg/m^3 cementitious density.

9.2.7 Static Modulus of Elasticity

- Stress-strain relationships were highly linear for mixes across a range of densities and cementitious blends, for stresses of up to 0.4 f'c. Furthermore, specimens did not obviously stiffen or soften when subjected to multiple loading cycles up to 0.4 f'c, suggesting that deformation was mainly elastic.

- For a given density, use of silica fume and slag improved the modulus of elasticity. Improvements over 100% Portland cement mixes range between 9 and 35%. Silica-rich SCMs may improve the stiffness of the paste by promoting the creation of long of silica chains. The fineness of SCM particles, especially silica fume, may contribute to stiffness by promoting dense particle-packing

- The presence of load-bearing water may also contribute to stiffness. The liquid mass of water in capillaries adds density and may also increase stiffness, especially for mixes with high water-binder ratios, such as silica fume mixes.

- Increasing curing time from 28 to 56 days did not significantly improve modulus of elasticity. Factors such as cracking due to autogenous or drying shrinkage may explain minor loss of stiffness with increased curing age for some mixes.

- Slag mixes offered the highest stiffness-to-strength ratio. This trend may be related to the crystalline properties of the C-A-S-H, produced in slag mixes because of the large proportion of aluminates present in the supplementary cementitious binder.

9.2.8 Poisson's Ratio

- Reasonably linear trends were observed in the relationships between axial and transverse strain for foam concrete specimens under uniaxial compression across a range of densities and cementitious blends, for stresses of up to 0.4 f'c.

- Observed PR values for foam concrete range from 0.33 to 0.15. Considerable scatter in the data may be due in part to the difficulty of accurate measurement, but it may also be due to the nature of the material itself, both in its pore structure, and as a heterogeneous composite of fine aggregate and hardened cement paste.

- Average PR values were lowest in dense, sanded mixes. Sand aggregate is stiffer than the C-S-H, and restrains lateral expansion of the matrix. PR was highest for neat cement foam concrete. The compliant C-S-H is not restrained by aggregate inclusions. Furthermore, flexure of the fine microstructure may contribute to lateral expansion. The geometry of the air-void system is more variable with decreasing density, due to coalescence of air voids during plastic state.

9.2.9 Crushing Behaviour

- Type 6 failure tends to dominate for the weakest of mixes. The strata near the top of the casting may be slightly weaker than the remainder of the specimen, due to upward migration of bubbles; side fractures near the top of the cylinder result in a pointed form. In some cases, failure can occur as collapse of horizontal strata near the top of the cast. In such cases, failure of the specimen may not be visibly obvious upon inspection, even though the specimen has experienced peak load.

- Columnar Type 3 cracking tends to dominate in denser, neat cement foam concrete. Vertical splitting cracks nucleate at air-voids as Mode I fracture, and propagate parallel to the compressive stress field, with no stiff aggregate present to arrest or divert the cracks. The resulting slender columns fracture laterally by buckling.

- The cracking pattern of sanded foam concrete includes random and steep triangular and conical fragments, resulting from a combination of vertical splitting cracks and inclined shear cracks. Where cracks have been arrested by the presence of aggregate or dense paste, there may be spreading patterns. Type 2 fractures are common. Very dense mixes, and sanded silica fume mixes, include especially small air-voids (refer to Section 6.17). Type 4 failure is common among these specimens, and may be related to the greater homogeneity of the paste, with fewer weak sites, resulting in more concentrated localization along the shear plane.

- For low-density mixes, the plastic regime was especially short, suggesting that once initiated, damage quickly propagated (localized) through the entire specimen.

- For higher density specimens, the plastic regime was more obvious. With a greater volume of material available to be fractured and rearranged, strain energy could be relieved through microcracking of the paste during loading, without inducing large-scale failure of the air-void system.

- High cementitious contents provided an increased volume of compliant C-S-H, which accommodated greater plastic deformation than lean mixes.

- Crushing characteristics of neat Portland cement foam concrete are especially favourable for impact absorbing applications, compared to mixes with slag, silica fume, or sand filler.

9.2.10 Creep

- The specific creep of foam concrete is very high, relative to normal density concrete. Specific creep after one year was approximately 12,000 μstrain/MPa (1.2%/MPa) for 600 kg/m^3 foam concrete, and between 1000 and 2000 μstrain/MPa (0.1 to 0.2%/MPa) for 1400 kg/m^3 foam concrete.

- Basic creep values for the drying specimens were higher than values for sealed specimens of similar density, determined previously by other researchers.[4] Exposure to drying conditions apparently had a strong effect on creep rate.

- Results for low-density foam concrete indicate that creep is not linearly dependent on stress. A lower load produced a higher specific strain. This phenomenon can be attributed to the time dependence of microstructural buckling mechanics.

- The addition of aggregate reduces specific creep rates considerably, as the non-viscous aggregate phase elastically restrains creep deformations in the surrounding viscous C-S-H matrix.

- For PC and SF mixes, there appeared to be strong correlations in patterns of specific creep, drying shrinkage, and mass loss (i.e. change in moisture content). Such correlation of humidity levels, drying shrinkage and creep is to be expected where drying shrinkage introduces residual stresses in the C-S-H, creating overstressed sites that facilitate creep. Patterns of mass loss, drying shrinkage, and creep were less obvious for the slag specimens. Trends for the slag specimens may be related to properties of C-A-S-H.

9.2.11 Drying Shrinkage

- The drying shrinkage of foam concrete is very high, relative to normal density concrete.

- Drying shrinkage decreased with increasing density. The inclusion of stiff fine aggregate restrained the shrinking C-S-H matrix.

- In the short term, longer periods of high humidity curing tended to reduce drying shrinkage. This pattern is especially evident for low-density mixes, and for slag mixes, and may be due to greater internal saturation of specimens, which preserves

[4] Kearsley (1999b) 153-156, Brady et al. (2001) C12. Refer to Appendix A, 6.3.2g.

a high internal RH for longer, delaying the volumetric contraction due to capillary tension in partially filled capillary voids.

- In the long term (i.e. after one year), longer periods of high humidity curing tended to increase total drying shrinkage. Long curing periods may have introduced significant disjoining pressures in the C-S-H. Alternatively, long curing periods may have facilitated the production of large portions of small capillary voids, which contribute to contraction via capillary tension at the 50% relative humidity of the storage environment.

- Shrinkage patterns were very similar for specimens that were water-cured for 28 days, and specimens that were moist-cured for 28-days. The availability of calcium for water-cured specimens did not appear to have an appreciable effect on shrinkage patterns.

- Rates of moisture loss decreased with longer curing times. This phenomenon may be due to increased impermeability, related to an increased degree of hydration. Alternatively, longer exposure to high RH during curing may have increased the proportion of fine capillary pores: finer capillary pores would retain water for longer during drying.

- Notably, at long times of exposure to 50% RH, specimens continued to gain mass due to ongoing hydration, especially in Portland cement specimens. As internal water chemically bonds and forms C-S-H, interior RH decreases, and additional moisture is drawn from the controlled 50% RH environment to maintain equilibrium. Density would also increase with ongoing carbonation.

- Negligible expansive strains observed during various curing regimens indicate that differences in shrinkage strain due to curing regime is not simply a consequence of global swelling that is reversed upon drying. Rather, variations in shrinkage behaviour are related to internal microstructural changes that have relatively negligible effects on volume during curing.

- Use of SCMs increased drying shrinkage. Higher volumes of fine capillary porosity in these specimens may contribute to increased shrinkage via capillary tension.

- Shrinkage strain rates were reduced with increased specimen size.

9.2.12 Moisture Storage

- At 50 and 80% RH, moisture storage was primarily a function of paste volume: that is, a function of cementitious density and water-binder ratio. Moisture storage increased with cementitious density, due to increased available capillary void volume. The inclusion of aggregate had a relatively small influence on moisture storage, due to its low surface area in comparison with capillary-rich C-S-H.

- Specimens in 80% RH gained mass at a decreasing rate until approximately four months. Total mass gain was typically lowest for slag mixes. This trend may be due in part to the low water-binder ratios used, resulting in relatively low capillary porosity and thus low internal surface area for water absorption. Mass gain was higher for Portland cement and silica fume mixes, reflecting a higher internal surface area resulting from many fine capillary voids.

- Specimens in 90% RH gained mass at a slower rate than specimens in 80% RH. It is possible that significant capillary condensation in the paste at the exterior surface of the specimens 'sealed' the specimens, creating a barrier to diffusion of air and slowing the ingress of moisture.

- In the first set of water absorption tests, moisture storage did not vary significantly with porosity, which suggests that both solid aggregate and discrete air-voids were similarly competent at resisting water ingress during the 14 days of immersion. It is possible that rapid capillary flow through the paste matrix seals discrete air-voids, creating a barrier to the exfiltration of air, and slowing the ingress of moisture.

- In the second set of water absorption tests, conducted over a longer period with older foam concrete, the increase in moisture storage with increasing porosity was

more pronounced. The older foam concrete may have had a higher open porosity due to damage from shrinkage cracking and chemical aging of the cell walls. At 14 and 28 days, moisture storage was highest in both slag and silica fume mixes, which may relate to cracking due to moisture movement in these SCM mixes. Nevertheless, air voids continued to obstruct water ingress relatively successfully, with water occupying less than 20% of the total available porosity after 28 days, for the lowest density mixes.

- In both the first and second set of water absorption tests, patterns of moisture storage at 24 hours for varying cementitious blends were similar, and broadly corresponded to mix water-binder ratios, indicating that capillary porosity was dominant in early stages of water absorption. The degree of interconnectivity of pores due to cracking or aging of cell walls appears to be more important for longer periods of immersion. Some cracking may occur during immersion, due to disjoining pressures and relief of capillary tension as the internal RH is increased.

9.2.13 Moisture Movement

- Approximately 50 to 70% of the total elongation experienced upon immersion occurred within the first 24 hours of wetting. Capillary pores readily absorbed water, promoting expansion via disjoining pressures and relief of capillary tension.

- Moisture movement decreased with the addition of filler, due to the restraining effect of the inert aggregate on the C-S-H phase. Elongation upon 28-day immersion was between 1000 and 1200 μstrain (0.10 to 0.12%) for mixes with no filler (600 kg/m^3 nominal density), compared to approximately 500 μstrain (0.05%) for mixes with filler-binder ratios of 3:1 (1800 kg/m^3 nominal density).

- Elongation due to wetting increased slightly with increased cementitious density, for neat cement foam concrete, due to the higher volume of C-S-H and resultant increase in disjoining pressures.

- Elongation due to 28-day immersion typically represented less than 25% of the original drying shrinkage strain, for each given mix.

- The addition of silica fume or slag as partial binder replacement did not have a significant influence on the wetting strain of foam concrete.

- Measured expansive strains upon wetting indicate that dry, rigidly constrained foam concrete could expand with sufficient force to induce crushing of the material, when soaked with water. Further study is recommended to assess this damage mechanism.

- Mature foam concrete specimens subjected to a single wetting and drying cycle exhibited residual mass gain of between approximately 10 kg/m^3 for SCM mixes, and approximately 30 kg/m^3 for Portland cement mixes. Residual elongation was highest for SCM mixes, at approximately 0.05%. Mass gain may be due to hydration and/or carbonation, while elongation may be due to microcracking due to differential strain upon partial wetting, or creep from wetting strain. Moisture-related damage mechanisms in foam concrete should be studied further.

- The magnitude of contraction induced by oven drying was less than the magnitude of expansion due to wetting, due to limitations of physical space between solids. Change in cementitious density did not significant affect shrinkage strain of neat cement mixes.

- Oven drying at 100°C can introduce significant shrinkage cracking in specimens. Where testing protocols requiring driving free water from a specimen, a drying environment with a lower temperature (e.g. 50°C) is preferred, in order to minimize significant physical changes to the air-void system.

9.2.14 Capillary Water Uptake

- For specimens subjected to oven drying, plots of water uptake for specimens with no filler (nominal density of 600 kg/m^3) indicated that capillary water uptake was

not one-dimensional. Observed interconnectivity of air-voids (e.g. due to drying shrinkage cracking or damage to cell walls) contributed to capillary flow.

- Plots of water uptake in specimens of 1400 kg/m^3 or greater indicated that capillary water uptake was one-dimensional, and not significantly influenced by interconnectivity of large air-voids.

- Rates of capillary water uptake appeared to be at a minimum for mixes with a nominal density of 1400 kg/m^3. These mixes include a significant volume of discrete air-voids capable of acting as obstructions to the ingress of water, creating a tortuous path for water ingress. Denser mixes had higher volumes of sorbing paste for capillary flow, due to higher water-binder ratios used for workability.

- For specimens with no filler, use of SCMs slightly increased the water uptake, compared to a 100% Portland cement mix. Increased drying shrinkage cracking in SCM mixes may have contributed to increased capillary flow.

- For sanded mixes, the rate of water uptake was suppressed with the incorporation of silica fume or slag. Use of silica fume binder replacement provided the greatest reduction in water uptake. This phenomenon may be due to the improved particle packing of solids in the mix, increasing impermeability: small capillary voids will tend to fill more slowly than large capillaries. Furthermore, visual inspection of specimen sections indicated that Portland cement mixes had a higher open porosity due to damage at the plateau boundaries.

- After 14 days of partial immersion, the volume of water in dense specimens filled approximately 42% of the specimens' apparent porosity, as determined by vacuum saturation. The volume of water in low-density specimens filled approximately 32% of the specimens' apparent porosity. Results suggest that rapid capillary flow through the paste matrix sealed discrete air-voids, creating a barrier to the exfiltration of air, and slowing the ingress of additional liquid into the remaining void space.

9.2.15 Thermal Conductivity

- Thermal conductivity increases at an increasing rate with a rise in density. Test results were similar to previously published values, including theoretical values for neat cement foam concrete published in ACI Report 122.[5]

- The lowest density mixes tested had a dry density of 550 kg/m^3 and a thermal conductivity of 0.12 W/m·K,.

- Modest variations in cementitious density had a negligible effect on thermal conductivity for the specimens tested.

- Use of silica fume to produce especially fine air-voids had a negligible effect on thermal conductivity, for the temperature range considered.

- Thermal conductivity increased by approximately 5% as the mean temperature was increased from −4 to 24°C. This phenomenon can be attributed to increased radiative heat transfer. Temperature-dependent reductions in thermal resistivity may be significant for foam concrete applications involving elevated temperatures.

9.2.16 Freeze-Thaw Resistance

- Specimen surfaces saturated with brine water exhibited significant scaling with freeze-thaw cycling. The interfacial bond between foam concrete and an ice layer will typically be very strong due to the permeability of the foam concrete, facilitating a significant glue-spall mechanism.

- Scaling was especially significant during the first 10 cycles of the test, which may be due to especially high permeability of the upper paste region.

- Foam concrete specimens of 1400 kg/m^3 and 1800 kg/m^3 nominal density had a loss of mass of more than 1.5 kg/m^2 after 50 cycles, exceeding the 0.80 kg/m^2 limit for assessments of normal density concrete made with coarse aggregate.[6]

[5] ACI 122R-02 Section 2.1

- Loss of mass and average loss of depth were lower for 1800 kg/m^3 specimens than for 1400 kg/m^3 specimens, which may be related to improved paste strength and reduced permeability.

- Specimens surfaces immersed in distilled water exhibited excellent resistance to scaling upon freeze-thaw cycling, despite high degrees of saturation. Stress in the pure ice layer is relieved through creep, reducing glue-spall cracking; and the slow rate of cooling of specimens helps facilitate the safe accumulation of super-cooled water in ice-bearing air voids, reducing the effects of crystallization pressures in capillary pores.

9.2.17 Microstructural Analysis

- Large, coalesced voids were visible in mixes with no filler (600 kg/m^3 nominal density), likely due to the fragility of the thin walls during set-up of the concrete. Coalescence was reduced with the addition of silica fume, or large proportions of slag. The maximum observed pore size diminished with increasing density, since the increased volume of filler provided thicker walls around discrete bubbles, reducing coalescence.

- Cracking the bulk was visually evident in all mixes with no filler, after oven-drying. Similarly, interconnectivity between air voids was visible on at a macroscopic level in mixes with no filler. This interconnectivity of voids is likely to dominate transport properties in particular.

- Small voids appear to be highly spherical, while some larger, coalesced air voids were slightly oblong or irregular.

- For a given density, air void sizes were smallest in silica fume mixes. This may be attributed to the fine particle size of silica fume, resulting in improved particle packing.

---

[6] OPSS 1002, Section 1002.05.03.02.01. Cf. results for air-entrained normal density concrete, Appendix M.

9.3 Summary of Competitive Niches for Foam Concrete

Key observations about favourable contexts for foam concrete are noted below. Further information can be found in Appendix A, Chapters 7 and 8.

- Foam concrete is versatile material. With appropriate knowledge and control over mix design, a wide range of properties can be 'dialed in'. Foam concrete can be catered to achieve project-specific criteria, while manufactured products such as aerated autoclaved concrete, foam glass, or porous brick are typically produced to established performance specifications, which are not readily altered.

- Foam concrete may also be cast *in situ*, without the need for special curing conditions, making it an attractive option for void-filling applications.

- Foam concrete is relatively well suited to the production of extremely low-density mixes. A fine-grain mixture of water, foam, and cementitious particles allows for the production of highly porous concrete with a homogenous structure. Foam concrete may be better suited to extremely light-weight applications than either LWAC, which uses large aggregate particles, or autoclaved aerated concrete, which relies on the presence of sand particles for the production of calcium silicate hydrate crystal. Low-density foam glass offers similar performance to foam concrete, but has significant limitations of manufacture. Ultra low-density foam concrete mixes have potential in thermally insulating purposes.[7]

- For mixes from 300 to 800 kg/m^3, autoclaved aerated concrete and insulating brick perform especially well. However, these materials cannot be cast *in situ*. Cement-bonded wood fibre products, such as Durisol block, may be considered a form of lightweight aggregate no-fines concrete, and also appear to perform well within this density range.

- For mixes between 1000 kg/m^3 and 1400 kg/m^3, foam concrete mixes vary greatly in compressive strength. By contrast, LWAC is more constrained in mix design, both

[7] Pan et al. (2014) 256

by efficient ratios of aggregate-to-mortar volume, and by available densities of aggregate. Substituting lightweight fine aggregate for normal density aggregates, [8] blending lightweight and normal density aggregates,[9] altering the aggregate size,[10] or increasing air entrainment in the mortar,[11] gives LWAC mix designers somewhat more latitude in varying compression strength and density characteristics; nevertheless, as a heterogeneous composite, LWAC is subject to certain limitations.[12] Consequently, foam concrete may be especially valuable outside of the normal strength-density parameters of LWAC design. Medium density, low-strength mixes with low cement content and low cost may be useful for some fill applications. Conversely, certain special niches may require the medium-density, high-strength properties that foam concrete with a high cementitious content can provide.

- For higher density, high strength mixes, LWACs is likely to prove more cost effective than foam concrete in most situations. Many LWAC mixes between 1600 and 1900 kg/m^3 density are capable of achieving strength higher than 40MPa,[13] while reports of foam concrete with strength greater than 40 MPa are relatively uncommon, and at present have only been achieved in laboratory conditions.

- Foam concrete mixes are typically stronger than no-fines concrete of the same density; however foam concrete will also normally have a higher cost due to its greater cementitious density.

- With compressive strengths in excess of 20 MPa at 1800 kg/m^3 dry density, or 10 MPa at 1400 kg/m^3 dry density, foam concrete recipes tested in the experimental program meet minimum strength requirements for various structural applications, including structural masonry units, load bearing walls, and composite steel deck. However, other properties of foam concrete, such as bond strength, stiffness, drying shrinkage, and resistance to carbonation, may necessitate modifications to

8 ACI 213-03 Section 2.3.6
9 ACI 213-03 Section 3.2.1.2
10 ACI 213-03 Section 2.3.4.1
11 ACI 213-03 Section 3.2.1.5
12 ACI 213-03 Section 3.4
13 Lotfy et al. (2015) 189

conventional systems to allow foam concrete to be used successfully: direct substitution of foam concrete for normal density structural concrete is unlikely.

- Relatively high cementitious densities were used in all mixes tested in the experimental program, while the compressive strengths of foam concrete specimens were low compared to the strength of normal density concrete. The cost of foam concrete should be expected to be high in comparison with the strength of normal density concrete.

9.4 Proposed Standards for Future Testing

Comparison of foam concrete mixes from varying researchers is difficult due to inconsistent reporting conventions, and inconsistent preparation and testing methodologies. Proposed standards for foam concrete research are provided below.

9.4.1 Minimum Notation for Production of Specimens

Details of mixing, casting, and curing are frequently neglected in the literature, but can have meaningful implications for the material properties of foam concrete. At a minimum, the key parameters described below should be recorded to enable comparison of research results. (Parameters that are typically of lesser significance are in grey.)

Mix Ingredients	Material Data	Quantification for mix design
Water	Source	Water-binder ratio; or ρ* (kg/m^3) *Note: If quantified as water-binder ratio, indicate whether dilution water from foam is included.*
Binder	Type(s), specification	ρ* (kg/m^3)
Filler	Type, specification, maximum particle size	ρ* (kg/m^3)
Foam	Type, dilution ratio, foam density	ρ* (kg/m^3)
Fibres	Type, length	ρ* (kg/m^3) *Note: If quantified as a volume fraction, also provide the material density of the fibres*
Chemical admixtures	Type	ρ* (kg/m^3) *Note: If quantified by volume, also provide the density of the solution*
		*indicate density as mass of material per unit volume of fresh foam concrete

Plastic density, target	ρ (kg/m^3)
Plastic density, actual	ρ (kg/m^3)

Table 9.4.1 Minimum recommended notation for mix design.

Notable casting parameters include specimen format (e.g. cube or cylinder), and specimen dimensions. Curing parameters such as time, temperature, relative humidity, and pressure should be documented from the time of initial hydration, until testing. Methods of sealing specimens, and the timing of demoulding, may be especially relevant for low-density mixes.

9.4.2 Standardized Increments for Mix Design

Increments for mix design parameters used throughout the experimental program provide broad coverage of possible foam concrete properties, at an appropriate resolution, given the material variability of foam concrete. Building on the framework of this experimental program in future research, by perpetuating systematic values for mix design parameters, will facilitate convenient comparison of testing results.

Recommended increments for cementitious density, filler-binder ratio, and water-binder ratio are summarized in Figure 9.**5.2a**, below. Major increments are in bold. Increments may be further subdivided as required.

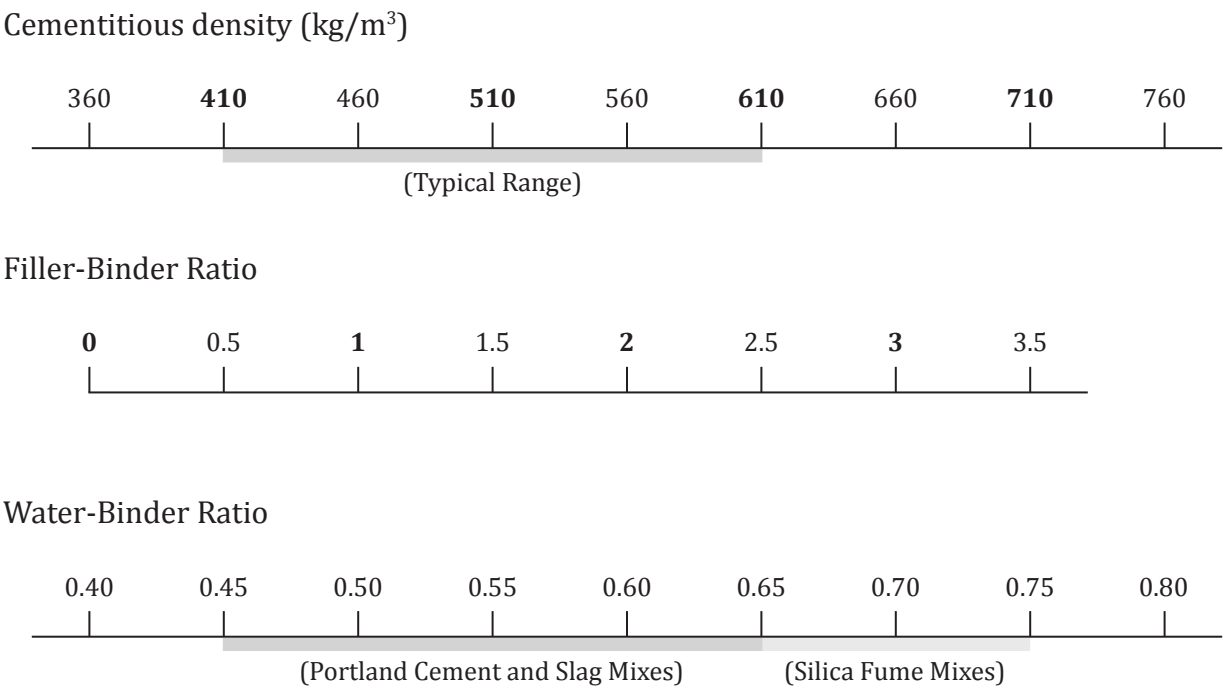

Figure 9.4.2a Standardized increments for mix design parameters.

9.4.3 Standardized Methodologies

During the course of this research, techniques for producing and testing foam concrete have been investigated, developed, and refined. Testing protocols can be reviewed in Chapter 5; alternative testing methods are described in Appendix M for comparison. Significant notes and recommendations for a variety of tests are included in the table

below, as a convenient reference for future research and to promote methodological consistency.

Test	Relevant Standards *Thesis References*	Important notes and recommendations for future research and testing
Mix proportioning	ASTM C796 *§5.1.2, Appendix B*	• Given the high volume of sand in some foam concrete mixes, the moisture content of the sand can have a major effect on actual mix proportions, and must be taken into account. Refer to Appendix D. • It is recommended to maintain a plastic density tolerance of ±25kg/m^3 for research, relative to target plastic density, rather than the tolerance of ±50kg/m^3 recommended by ASTM C796 and other researchers.[1]
Casting and demoulding	ASTM C495 *§5.1.4*	• Demoulding may be delayed for up to seven days for fragile specimens.
Porosity	Fagerlund (1977) *§5.2*	• Time required under vacuum pressure may be higher than that required for other materials of similar density, due to the highly closed porosity typical of foam concrete. Time under vacuum pressure should be adjusted to account for specimen size and density. • Low-density specimens placed in the vacuum chamber should be weighted with stainless steel masses as required. Small amounts of air within specimens in near-vacuum conditions may be sufficient to keep some specimens buoyant when water is introduced into the chamber. • Volume may be determined gravimetrically. Refer to Appendix J.
Dry Density	*§5.2*	• It is recommended to determine dry density at 50% RH and 25°C, conditioned until constant mass.
Oven dry density	*§5.2*	• Oven-drying at 100°C can significantly affect the pore structure and transport properties of foam concrete, especially by inducing bulk cracking. If subsequent testing of hygroscopic properties will be conducted, oven-drying temperature should be limited to 50°C, or other methods of drying or conditioning should be considered (e.g. freeze drying, use of desiccants, etc.).[2]
Segregation testing	*§5.3.2*	• Eliminate slices from top and bottom of specimens, to eliminate effects of particle packing at cast surfaces and unevenness at free surfaces.
Compressive strength, other properties tested	*§5.4*	• Conceptually, capping specimen ends with sulphur or neat cement is preferred to end-grinding, due to the tendency for free edges of

1 Cf. Brady et al. (2001) 8
2 Cf. Korpa and Trettin (2005)

under uniaxial compression		cell walls to buckle under load. However, actual differences in compressive strength were not obviously significant (refer to Figures 6.**6.1.1a** and 6.**6.1.1b**). Further testing and statistical analyses should be undertaken. • The effects of capping on lateral restraint should be considered, especially for low-density specimens and for measurements of Poisson's ratio.
Static modulus of elasticity	*§5.4.2*	• Creep effects on modulus measurements should be considered, especially for very low-density specimens.
Poisson's ratio	*§5.4.3*	• Measuring Poisson's ratio across a single diameter appears to significant scatter in the data. Measuring dilation circumferentially may yield more representative values for Poisson's ratios by flattening local effects. • Sources of lateral restraint should be considered (e.g. sealing, capping, bearing conditions), especially for very low-density specimens.
Creep	*§5.4.4*	• Given the Poisson's ratio and low strength of many foam concrete mixes, methods of seal-curing should be considered carefully to avoid inducing lateral restraint on specimens. • Given the low strength of foam concrete, it may be possible to use gravity loads for creep tests, for greater constancy of force. Refer to Appendix M.
Drying shrinkage	*§5.5.1*	• Conditions of both the curing regime and the drying regime appear to have significant influence on shrinkage strain, and should be carefully controlled. • Size effects appear to be significant, and should be considered in comparison of results.
Moisture storage	*§5.5.2*	• Express moisture content in absolute terms (e.g. kg/m^3)
Moisture movement	*§5.5.3*	• Condition specimens to 50% RH and 25°C, prior to immersion.
Capillary water uptake	Fagerlund (1977), ISO 15148, ASTM C1585 *§5.5.4*	• Condition specimens in a manner that will not damage the C-S-H, prior to immersion. Do not oven-dry specimens, as this can significantly affect results via the introduction of cracks in the bulk. • Express moisture content in absolute terms (e.g. kg/m^3).
Thermal conductivity	ASTM C177, ASTM C518 *§5.6.1*	• Foam concrete surfaces may be rough and uneven. Ensure surfaces in contact with hot and cold plates are planar, or use appropriate facers as required, to ensure consistent conductivity.
Freeze-thaw susceptibility	Fagerlund (1977) *§5.7.1*	• Avoid vacuum-saturating foam concrete specimens to be used in freeze-thaw testing, to preclude unrealistic distribution of moisture. Refer to discussion in Section 5.7.1. • Carefully seal specimens against moisture loss

		or gain, as moisture movement may be more significant than dilation due to freezing. Determine moisture content via oven-drying after the conclusion of the freeze-thaw cycles. • Express moisture content in absolute terms (e.g. kg/m^3). • Osmotic pressures strongly affect freeze-thaw susceptibility. The source of water used for mixing, curing, and saturating specimens should be considered.
Saline freeze-thaw testing	LS-412 (MTO) ASTM C1262 *§5.7.2*	• Maintaining brine water on upper surface of specimen may be impractical for many foam concrete mixes, due to high capillarity and rapid deterioration of the foamed paste. Instead, immerse the lower surface of specimen in brine water, elevating the specimen to avoid contact.with the bottom of the pan as required.
Microstructural analysis	ASTM C457, EN 480-11 *§5.8.2*	• Specimens with no aggregate may be successfully polished and lapped without reinforcement of the paste. • Specimens with aggregate will typically require lacquer for reinforcement of the paste.

Table 9.4.3 Notes and recommendations for future research and testing.

9.5 Recommended Topics for Further Research

Two areas of foam concrete research are especially critical for the continued expansion and refinement of a comprehensive mix design framework for foam concrete.

Firstly, a large-scale study of reinforcing for foam concrete should be considered as a major supplementary project to the present work. In practice, testing results for plain foam concrete have already been used to design fibre-reinforced foam concrete mixes, with good success. However, the inclusion of fibre reinforcing has an influence on water-demand, workability and mechanical properties in particular, which should be methodically quantified. Use of fibre reinforcing will expand the performance envelope and potential uses of foam concrete.[3]

Secondly, aging of foam concrete should be more thoroughly investigated. Given the highly hygroscopic nature of foam concrete, the influence of humidity, wetting, and drying on long-term properties of foam concrete merits further attention:

- Specimens with high internal relative humidities were tested for compressive strength, modulus or elasticity, and Poisson's ratio (Sections 6.6, 6.7, and 6.8). Tests should be repeated on dry specimens, to anticipate the effects of drying shrinkage cracking and the loss of load-bearing water on mechanical properties.

- Specific creep values for the unsealed specimens in this experimental program were significantly higher than for sealed specimens of similar density tested by other researchers (Section 6.10). Further work should be done to quantify this Pickett effect for various drying environments, to anticipate creep of specimens according to in situ drying conditions.

- Long-term drying shrinkage strain increases with long periods of high RH during curing (Section 6.11). The effects of curing regime on long-term properties, including mechanical properties, should be considered.

- Preliminary investigations indicate that wetting and drying cycles can cause damage to specimens (Section 6.13). Damage due to cyclical wetting and drying should be quantified. The expansive force due to wetting may also be relevant as a damage

[3] The literature review in Appendix A provides a starting point for the research of fibre reinforcing in foam concrete. Refer to Section 5.1.5 on Reinforcing, Section 6.2.3 on Drying Shrinkage, and Section 6.3.2a on Tensile Strength.

mechanism for foam concrete that is highly restrained, for example in void-filling applications.

- Long-term mass gain in a constant environment (Section 6.11) indicates continued hydration or carbonation. The effects of these chemical changes on mechanical, durability, and transport properties should be assessed.

Other causes of degradation, such as sulfate attack[4] or chloride ingress[5] may be relevant for fill applications. Further research into long-term durability is important for foam concrete used in ground engineering work, since later remediation will prove difficult.

In addition to these two major areas of foam concrete research, mixes will continue to be produced using new combinations of ingredients (e.g. binders, SCMs, fillers, surfactants), and tested for other properties (e.g. resistance to fire and elevated temperatures), as required for particular applications. Where feasible, researchers are advised to follow the recommendations of Section 9.4 to promote methodological consistency and to facilitate straightforward comparison of results from separate studies.

A supplementary list of recommended topics for further research is provided in Appendix T.

[4] Cf. Appendix A, Section 6.3.5b.
[5] Cf. Appendix A, Section 7.3.2.

A

Bibliography

Abdollahnejad Z, Pacheco-Torgal F, Félix T, Tahri W, de Aguiar JB (2015). Mix design, properties and cost analysis of fly ash-based geopolymer foam. *Construction and Building Materials, 80*, 18-30.

ACI 122R-02, *Guide to thermal properties of concrete and masonry systems*.

ACI 212-63, *Admixtures for Concrete.*

ACI 213-03, *Guide for structural lightweight aggregate concrete*.

ACI 213-67, *Guide for structural lightweight aggregate concrete*, 433-469.

ACI 213-79, *Guide for structural lightweight aggregate concrete,* 1-4.

ACI 318-11, *Building Code Requirements for Structural Concrete.*

ACI 544-96, *Report on Fiber Reinforced Concrete.*

Acker P (2001). Micromechanical analysis of creep and shrinkage mechanisms. *Creep, Shrinkage and Durability Mechanics of Concrete and other quasi-brittle Materials, Cambridge, MA*, 15-25.

Acker P (2004). Swelling, shrinkage and creep: a mechanical approach to cement hydration. *Materials and Structures*, *37*(4), 237-243.

Acker P, Ulm FJ (2001). Creep and shrinkage of concrete: physical origins and practical measurements. *Nuclear Engineering and Design*, *203*(2-3), 143-158.

Ahmed RM, Takach NE, Khan UM, Taoutaou S, James S, Saasen A, Godøy R (2009). Rheology of foamed cement. *Cement and Concrete Research, 39*(4), 353-361.

Akhtaruzzaman AA (1989). Behaviour of foamed slag concrete at high temperatures. *Cement and Concrete Research, 19*(3), 345-354.

Akkari AK (2014). *Thermal diffusivity and freeze thaw behavior of pervious concrete pavements.* (Doctoral dissertation.) University of Minnesota.

Akroyd T (1962). *Concrete: Properties and Manufacture.* Oxford: Permagon Press.

Akthar FK, Evans JRG (2010). High porosity (>90%) cementitious foams. *Cement and Concrete Research, 40*(2), 352-358.

Al Bakri Abdullah MM, Hussin K, Bnhussain M, Ismail KN, Yahya Z, Razak RA (2012). Fly ash-based geopolymer lightweight concrete using foaming agent. *International Journal of Molecular Sciences*, *13*(6), 7186-7198.

Al-khalaf MN, Yousif HA (1986). Compatibility of no-fines concrete. *International Journal of Cement Composites and Lightweight Concrete, 8*(1), 45-50.

Al-Noury SI, Mirza WH, Huq S (1990). Density and strength characteristics of lightweight mortar. *Cement and Concrete Composites, 12*(2), 79-86.

Alawad OA, Alhozaimy A, Jaafar MS, Aziz FNA, Al-Negheimish A (2015). Effect of Autoclave Curing on the Microstructure of Blended Cement Mixture Incorporating Ground Dune Sand and Ground Granulated Blast Furnace Slag. *International Journal of Concrete Structures and Materials, 9*(3), 381-390.

Aldridge D (2005). Introduction to foamed concrete (What, Why, How?). In *Proceedings of the International Conference on the Use of Foamed Concrete in Construction; Dundee, Scotland; 5 July 2005,* 1-14.

Aldridge D, Ansell T (2001). Foamed concrete: production and equipment design, properties, applications and potential. In *Proceedings of the One-Day Seminar on Foamed Concrete: Properties, Applications and Latest Technological Developments; Leicestershire, UK; July 2001,* 1-7.

Ali I, Kesler CE (1965). *Rheology of concrete: a review of research*. University of Illinois at Urbana Champaign, College of Engineering. Engineering Experiment Station.

Aliabdo AA, Abd-Elmoaty AM, Hassan HH (2014). Utilization of crushed clay brick in cellular concrete production. *Alexandria Engineering Journal, 53*(1), 119-130.

Alizadeh R, Beaudoin JJ, Raki L (2010). Viscoelastic nature of calcium silicate hydrate. *Cement and Concrete Composites*, *32*(5), 369-376. ASTM International.

Allos AE, Martin LH (1981). Factors affecting Poisson's ratio for concrete. *Building and Environment*, *16*(1), 1-9.

Alobaidi IM, Ghataora GS, Billam J, Coombs R (2000). The use of permeable materials for backfilling trenches. *Proceedings of the Institution of Civil Engineers-Transport, 141(3).* Thomas Telford Ltd. 151-159.

Amran YHM, Abang Ali AA, Rashid RSM, Hejazi F, Safiee NA (2016). Structural behavior of axially loaded precast foamed concrete sandwich panels. *Construction and Building Materials, 107*, 307-320.

Amran YHM, Farzadnia N, Abang Ali AA (2015). Properties and applications of foamed concrete; A review. *Construction and Building Materials, 101*, 990-1005.

Anon. (1989). Foamed concrete for trench reinstatement. *Construction and Building Materials, 3*(1), 54.

Anon. (1999) American Eagle Saab 340 Stopped by an Arrestor Bed Made of Foam Concrete. *Aviation Week & Space Technology, 150*(20), 21.

Anson M, Newman K. (1966). The effect of mix proportions and method of testing on Poisson's ratio for mortars and concretes. *Magazine of Concrete Research*, *18*(56), 115-130.

Arasteh AR (1988). *Structural applications of lightweight aggregate foamed concrete.* (Doctoral dissertation.) Polytechnic of Central London.

Arnold M, Boccaccini AR, Ondracek G (1996). Prediction of the Poisson's ratio of porous materials. *Journal of materials science*, *31*(6), 1643-1646.

Ashby MF (2009). *Materials and the Environment: Eco-Informed Material Choice.* Burlington, MA: Butterworth-Heinemann.

Ashton LA, Bigmore RH (1954). The fire-resistance of no-fines concrete walls. *Fire Research Notes*, *44*, 1-8.

Ashworth T, Hooper A, O'Connor B, Miller E, Jarratt A (2013). Foamed concrete facilitates decommissioning of nuclear plant. *Proceedings of the Institution of Civil Engineers: Energy, 166*(2), 58-66.

ASO Group (2010). *Construction with Aerated Concrete*. Retrieved from https://www.asofoam.co.jp/english/jigyou/kihou/air.html

ASTM C1202-19, *Standard Test Method for Electrical Indication of Concrete's Ability to Resist Chloride Ion Penetration*.

ASTM C1240-15, *Standard Specification for Silica Fume Used in Cementitious Mixtures.*

ASTM C1262-10, *Standard Test Method for Evaluating the Freeze-Thaw Durability of Dry-Cast Segmental Retaining Wall Units and Related Concrete Units.*

ASTM C136/C136M-14, *Standard Test Method for Sieve Analysis of Fine and Coarse Aggregates.*

ASTM C143/C143M-15a, *Standard Test Method for Slump of Hydraulic-Cement Concrete.*

ASTM C150/C150M-16, *Standard Specification for Portland Cement*.

ASTM C1585-13, *Standard Test Method for Measurement of Rate of Absorption of Water by Hydraulic-Cement Concretes.*

ASTM C1611/C1611M-14, *Standard Test Method for Slump Flow of Self-Consolidating Concrete.*

ASTM C1645/C1645M-15, *Standard Test Method for Freeze-thaw and De-icing Salt Durability of Solid Concrete Interlocking Paving Units.*

ASTM C1693-11, *Standard Specification for Autoclaved Aerated Concrete (AAC).*

ASTM C172/C172M-14, *Standard Practice for Sampling Freshly Mixed Concrete.*

ASTM C1754/C1754M-12, *Standard Test Method for Density and Void Content of Hardened Pervious Concrete*.

ASTM C1757-13, *Standard Test Method for Determination of One-Point, Bulk Water Sorption of Dried Concrete.*

ASTM C177-13, *Standard Test Method for Steady-State Heat Flux Measurements and Thermal Transmission Properties by Means of the Guarded-Hot-Plate Apparatus.*

ASTM C177-19. *Standard test method for steady-state heat flux measurements and thermal transmission properties by means of the guarded-hot-plate apparatus*.

ASTM C230 / C230M-14, *Standard Specification for Flow Table for Use in Tests of Hydraulic Cement.*

ASTM C260 / C260M-10, *Standard Specification for Air-Entraining Admixtures for Concrete.*

ASTM C33/C33M-16, *Standard Specification for Concrete Aggregates*.

ASTM C330/C330M-14, *Standard Specification for Lightweight Aggregates for Structural Concrete.*

ASTM C331/C331M-14, *Standard Specification for Lightweight Aggregates for Concrete Masonry Units.*

ASTM C469/C469M-14, *Standard Test Method for Static Modulus of Elasticity and Poisson's Ratio of Concrete in Compression.*

ASTM C495/C495M-12*, Standard Test Method for Compressive Strength of Lightweight Insulating Concrete.*

ASTM C496/C496M-11, *Standard test method for splitting tensile strength of cylindrical concrete specimens.*

ASTM C512-15, *Standard Test Method for Creep of Concrete in Compression*.

ASTM C518-15, *Standard Test Method for Steady-state Thermal Transmission Properties by Means of the Heat Flow Meter Apparatus.*

ASTM C518-17, *Standard test method for steady-state thermal transmission properties by means of the heat flow meter apparatus. ASTM International*.

ASTM C567/C567M-11, *Standard Test Method for Determining Density of Structural Lightweight Concrete.*

ASTM C617 / C617M-15, *Practice for Capping Cylindrical Concrete Specimens*.

ASTM C642-13, *Standard Test Method for Density, Absorption, and Voids in Hardened Concrete.*

ASTM C796/C796M-12, *Standard Test Method for Foaming Agents for Use in Producing Cellular Concrete Using Preformed Foam*.

ASTM C830-00, *Standard Test Methods for Apparent Porosity, Liquid Absorption, Apparent Specific Gravity, and Bulk Density of Refractory Shapes by Vacuum Pressure. ASTM International*.

ASTM C989/C989M-14, *Standard Specification for Slag Cement for Use in Concrete and Mortars*.

ASTM D4716/D4716M-14, *Standard Test Method for Determining the (In-plane) Flow Rate per Unit Width and Hydraulic Transmissivity of a Geosynthetic Using a Constant Head.*

ASTM E122-09*, Standard Practice for Calculating Sample Size to Estimate, With Specified Precision, the Average for a Characteristic of a Lot or Process*.

ASTM E96/E96M-16, *Standard Test Methods for Water Vapor Transmission of Materials.*

Atzeni C, Massidda L, Sanna U (1987). Effect of pore size distribution on strength of hardened cement pastes. In *Proceedings of the 1st international RILEM Congress on Pore Structure and Material Properties, Versailles, France; September 1987,* 195-202.

Awang H, Ahmad MH (2014). Durability properties of foamed concrete with fiber inclusion. *International Journal of Civil, Environmental, Structural, Construction and Architectural Engineering*, *8*(3), 273-276.

Ayudhya BIN (2011). Compressive and splitting tensile strength of autoclaved aerated concrete (AAC) containing perlite aggregate and polypropylene fiber subjected to high temperatures. *Sonklanakarin Journal of Science and Technology*, *33*(5), 555.

Bahafid S, Ghabezloo S, Duc M, Faure P, Sulem J (2017). Effect of the hydration temperature on the microstructure of Class G cement: CSH composition and density. *Cement and Concrete Research*, *95*, 270-281.

Balevičius R, Dulinskas E (2010). On the prediction of non-linear creep strains. *Journal of Civil Engineering and Management*, *16*(3), 382-386.

Balevičius R, Marčiukaitis G (2013). Linear and Non-linear Creep models for a multi-layered concrete composite. *Archives of civil and mechanical engineering*, *13*(4), 472-490.

Balshin MY (1949). Relation of mechanical properties of powder metals and their porosity and the ultimate properties of porous metal-ceramic materials. *Doklady Akademii Nauk SSSR (Proceedings of the Russian Academy of Sciences) 67*(5), 831-834.

Baozhen S, Erda S (1987). Relation between properties of aerated concrete and its porosity and hydrates. In *Proceedings of the 1st international RILEM Congress on Pore Structure and Material Properties; Versailles, France; September 1987,* 232-237

Barnes RA (2009). Foamed concrete: Application and specification. In *Excellence in Concrete Construction through Innovation: Proceedings of the International Conference on Concrete Construction; London, United Kingdom; 9-10 September 2008,* 3-9.

Basiurski J, Wells D (2001). The use of foamed concrete in construction and civil engineering. *Conspectus*, 64-73.

Bath & North East Somerset Council (2010a). Interesting stats. *Combe Down Stone Mines.* Retrieved from http://www.combedownstoneminesproject.co.uk/subcategory/stabilising_the_mines/article/interesting_stats

Bath & North East Somerset Council (2010b). Stabilisation phases and techniques. *Combe Down Stone Mines.* Retrieved from

http://www.combedownstoneminesproject.co.uk/subcategory/stabilising_the_mines/article/stabilidation_techniques

Baud P, Wong TF, & Zhu W (2014). Effects of porosity and crack density on the compressive strength of rocks. *International Journal of Rock Mechanics and Mining Sciences*, *67*, 202-211.

Bave G (1980). Aerated lightweight concrete—Current technology. In *Proceedings of the Second International Symposium on Lightweight Concretes; London, England; 14-15 April 1980,* 28-35.

Bayer EC (1931). *U.S. Patent No. 1,794,272*. Washington, DC: U.S. Patent and Trademark Office.

Bayuaji R, Nuruddin MFB (2008). Prediction of compressive strength for foamed concrete using neural network. In *National Postgraduate Conference on Engineering, Science and Technology; Petronas, Malaysia; 2008*.

Bažant ZP (1972). Thermodynamics of interacting continua with surfaces and creep analysis of concrete structures. *Nuclear engineering and design*, *20*(2), 477-505.

Bažant ZP (1975). Theory of creep and shrinkage in concrete structures: A precis of recent developments. *Mechanics today*, *2*, 1-93.

Bažant ZP (1988). *Mathematical modeling of creep and shrinkage of concrete*. Wiley.

Bažant ZP, Hauggaard AB, Baweja S, Ulm FJ (1997). Microprestress-solidification theory for concrete creep. I: Aging and drying effects. *Journal of Engineering Mechanics*, *123*(11), 1188-1194.

Bažant ZP, Murphy WP (1995). Creep and shrinkage prediction model for analysis and design of concrete structures-model B3. *Materials and Structures*, *28*(180), 357-365.

Bazzaz-Bonabi S, Kahani-Khabushan J, Kahani R, Honarbakhsh-Raouf A (2014). Fabrication of metallic composite foam using ceramic porous spheres “light expanded clay aggregate” via casting process. *Materials and Design, 64*, 310-315.

Beaudoin JJ (1983). Comparison of mechanical properties of compacted calcium hydroxide and Portland cement paste systems. Cement and Concrete Research, 13(3), 319-324.

Beaudoin JJ, Gu P, Myers RE (1998). The Fracture of CSH and CSH/CH Mixtures 1. Cement and concrete research, 28(3), 341-347.

Beaudoin, JJ (2000). Calcium hydroxide in cement matrices: physico-mechanical and physico-chemical contributions. In *Workshop on Role of Calcium Hydroxide in Hydration and Deterioration of Concrete*, 131-132.

Bederina M, Gotteicha M, Belhadj B, Dheily RM, Khenfer MM, Quéneudec M (2012). Drying shrinkage studies of wood sand concrete—effect of different wood treatments. *Construction and Building Materials, 36*, 1066-1075.

Bederina M, Laidoudi B, Goullieux A, Khenfer MM, Bali A, Quéneudec M (2009). Effect of the treatment of wood shavings on the physico-mechanical characteristics of wood sand concretes. *Construction and Building Materials, 23*(3), 1311-1315.

Bederina M, Marmoret L, Mezreb K, Khenfer MM, Bali A, Quéneudec M (2007). Effect of the addition of wood shavings on thermal conductivity of sand concretes: Experimental study and modelling. *Construction and Building Materials, 21*(3), 662-668.

Ben Fraj A, Kismi M, Mounanga P (2010). Valorization of coarse rigid polyurethane foam waste in lightweight aggregate concrete. *Construction and Building Materials, 24*(6), 1069-1077.

Benazzouk A, Douzane O, Mezreb K, Quéneudec M (2006). Physico-mechanical properties of aerated cement composites containing shredded rubber waste. *Cement and Concrete Composites, 28*(7), 650-657.

Bienvenu Y (2014). Application and future of solid foams. *Comptes rendus—Physique, 15*(8-9), 719-730.

Bindiganavile V, Hoseini M (2008). Foamed concrete. In Mindess S (Ed.), *Developments in the Formulation and Reinforcement of Concrete.* Cambridge, England: Woodhead Publishing Ltd., 231-255.

Bing C, Zhen W, Ning L (2012). Experimental research on properties of high-strength foamed concrete. *Journal of Materials in Civil Engineering*, *24*(1), 113-118.

Boughrarou R, Cale SA (2005). Stabilisation of Old Mine Workings: A Case Study of the Use of Foamed Concrete in Combe Down Stone Mines. In *Proceedings of the International Conference on the Use of Foamed Concrete in Construction; Dundee, Scotland; 5 July 2005,* 133-142.

Brady KC, Watts GR, Jones MR (2001). *Specification for Foamed Concrete.* Crowthorne Berkshire, UK: TRL Limited.

British Cement Association (1991). *Foamed Concrete for Improved Trench Reinstatements. Report Reference 46.043.* Slough, UK: BCA.

British Cement Association (1994). *Foamed Concrete; Composition and Properties. Report Reference 46.042.* Slough, UK: BCA.

Brookby HE, Gough FJ (1931). *U.S. Patent No. 1,818,376*. Washington, DC: U.S. Patent and Trademark Office.

Brouwers HJH (2004). The work of Powers and Brownyard revisited: Part 1. *Cement and Concrete Research, 34*(9), 1697-1716.

Bumanis G, Bajare D, Korjakins A (2013). Mechanical and thermal properties of lightweight concrete made from expanded glass. *Journal of Sustainable Architecture and Civil Engineering*, *2*(3), 19-25.

Bumanis G, Bajare D, Locs J, Korjakins A (2013). Alkali-silica reactivity of foam glass granules in structure of lightweight concrete. *Construction and Building Materials, 47*, 274-281.

Burg RG, Ost BW (1992). *Engineering properties of commercially available high-strength concretes* (No. RD104T).

Bush AL, Bryan DP, Hack DR (2006). Lightweight aggregates. In Kogel JE, Trivedi NC, Barker JM, Krukowski WT (Eds.), *Industrial Minerals & Rocks: Commodities, Markets, and Uses, 7th Edition*. Littletown, Colorado: Society for Mining, Metallurgy and Exploration, Inc., 181-194.

Byun KJ, Song HW, Park SS (1998). Development of structural lightweight foamed concrete using polymer foam agent. In *Proceedings of the 9th International Congress on Polymers in Concrete; Bologna, Italy.*

Cabrillac R, Fiorio B, Beaucour AL, Dumontet H, Ortola S (2006). Experimental study of the mechanical anisotropy of aerated concretes and of the adjustment parameters of the introduced porosity. *Construction and Building Materials*, *20*(5), 286-295.

CAN/CSA-A23.3-04. *Design of Concrete Structures.* Mississauga, Ontario: Canadian Standards Association.

CAN/CSA-A3001-18. *Cementitious Materials for Use in Concrete.* Mississauga, Ontario: Canadian Standards Association.

Carlson J, Sutter LL, Van Dam T, Peterson K (2005). *Advancement on the Application of a Flat-Bed Scanner for Hardened Portland Cement Concrete Air Void Analysis* (Doctoral dissertation.) Michigan Technological University.

Cellular Concrete Solutions (n.d.). *White Paper: Smart Foam Liquid Concentrate Solutions Series*. Retrieved from http://www.idc-online.com/technical_references/pdfs/chemical_engineering/wicc_wp.pdf

Cellular Concrete Technologies (2011). *Stable air foaming agent brochure.* Irvine, California.

Cellular Concrete Technologies (2012). Aerator check list prior to shipping. Irvine, California.

Cellular Concrete Technologies (2013a). *Stable air foam concentrate: Material safety and data sheet.* Irvine, California. 14 January 2013.

Cellular Concrete Technologies (2013b). *Stable air foam concentrate: Material safety and data sheet.* Irvine, California. 22 January 2013.

Cematrix Corportation (2016). *Cematrix Production Units*. Retrieved from http://www.cematrix.com/production.html

Cematrix Corportation (n.d.). *Generic Cematrix Cellular Concrete Specification.* Retrieved from http://www.cematrix.com/app_technical.html

Cement Admixtures Association (2012a). *Admixture Technical Sheet: ATS 5, Air-Entraining Admixtures.* Retrieved from http://www.admixtures.org.uk

Cement Admixtures Association (2012b). *Admixture Technical Sheet: ATS 7, Retarded Ready-to-use Mortars.* Retrieved from http://www.admixtures.org.uk

Cement Association of Canada (2016). CAC members. *Cement Association of Canada Website.* Retrieved from http://www.cement.ca/en/CAC-Members.html

Chatterji S (2001). A discussion of the paper" Mercury porosimetry-an inappropriate method for the measurement of pore size distributions in cement-based materials" by S. Diamond. *Cement and concrete research*, *31*(2001), 1657-1658.

Chen B, Liu J (2004). Properties of lightweight expanded polystyrene concrete reinforced with steel fiber. *Cement and Concrete Research*, *34*(7), 1259-1263.

Chen JJ, Thomas JJ, Taylor HF, Jennings HM (2004). Solubility and structure of calcium silicate hydrate. *Cement and concrete research*, *34*(9), 1499-1519.

Chen X, Wu S, Zhou J (2013). Influence of porosity on compressive and tensile strength of cement mortar. *Construction and Building Materials, 40*, 869-874.

Chen X, Yan Y, Liu Y, Hu Z (2014). Utilization of circulating fluidized bed fly ash for the preparation of foam concrete. *Construction and Building Materials, 54*, 137-146.

Chen Y, Peng M, Zhang Y, Liu Y (2013). Mechanical properties of autoclaved aerated concrete with different densities. *Advances in Civil Engineering Materials, 2*(1), 441-456.

Chia KS (2006). *Workability and stability of lightweight aggregate concrete from rheology perspective.* (Doctoral dissertation.) National University of Singapore.

Chindaprasirt P, Nuaklong P, Zaetang Y, Sujumnongtokul P, Sata V (2015). Mechanical and thermal properties of recycling lightweight pervious concrete. *Arabian Journal for Science and Engineering*, *40*(2), 443-450.

Cho BS, Lee HH, Choi YC (2017). Effects of aluminate rich slag on compressive strength, drying shrinkage and microstructure of blast furnace slag cement. *Construction and Building Materials*, *140*, 293-300.

Choi H, Ma S (2015). An optimal lightweight foamed mortar mix suitable for tunnel drainage carried out using the composite lining method. *Tunnelling and Underground Space Technology Incorporating Trenchless Technology Research, 47*, 93-105.

Christiani and Nielsen v. Rice, Supreme Court of Canada (1930). Retrieved from https://scc-csc.lexum.com/scc-csc/scc-csc/en/item/8930/index.do

Christiani FR, Nielson A (1925). Cell concrete, its properties and applications. *Circular, 22*(I), 45.

Claisse PA, El-Sayad HI, Ganjian E (2009). Water vapour and liquid permeability measurements in mortar samples. *Advances in Cement Research*, *21*(2), 83-89.

Coatanlem P, Jauberthie R, Rendell F (2006). Lightweight wood chipping concrete durability. *Construction and Building Materials, 20*(9), 776-781.

Colaizzi GJ (2004). Prevention, control and/or extinguishment of coal seam fires using cellular grout. *International Journal of Coal Geology, 59*, 75-81.

Collins F, Sanjayan JG (2000). Effect of pore size distribution on drying shrinking of alkali-activated slag concrete. *Cement and Concrete Research*, *30*(9), 1401-1406.

Collishaw PG, Evans JRG (1994). An assessment of expressions for the apparent thermal conductivity of cellular materials. *Journal of materials science*, *29*(9), 2261-2273.

Comité Euro-International du Beton (1978). *CEB manual of autoclaved aerated concrete: design and technology*. Lancaster, New York: Construction Press.

Cong M, Bing C (2014). Properties of a foamed concrete with soil as filler. *Construction and Building Materials, 76*, 61-69.

Constantinides G, Ulm FJ (2007). The nanogranular nature of C–S–H. *Journal of the Mechanics and Physics of Solids*, *55*(1), 64-90.

Constantinides G, Ulm FJ, Van Vliet K (2003). On the use of nanoindentation for cementitious materials. *Materials and structures*, *36*(3), 191-196.

Corathers LA (2004). Silicon. *U.S. Geological Survey Minerals Yearbook.* Washington, DC: U.S. Department of the Interior. Retrieved from http://minerals.usgs.gov/minerals/pubs/commodity/silicon/silicmyb04.pdf

Ćosić K, Korat L, Ducman V, Netinger I (2015). Influence of aggregate type and size on properties of pervious concrete. *Construction and Building Materials, 78*, 69-76.

Cotterell B, Rice J (1980). Slightly curved or kinked cracks. *International journal of fracture*, *16*(2), 155-169.

Cox L (2005). Major road and bridge projects with foam concrete. In *Proceedings of the International Conference on the Use of Foamed Concrete in Construction; Dundee, Scotland; 5 July 2005,* 105-112.

Daimon M, Abo-El-Enein SA, Rosara G, Goto S, Kondo R (1977). Pore structure of calcium silicate hydrate in hydrated tricalcium silicate. *Journal of the American Ceramic Society*, *60*(3-4), 110-114.

Darcy H (1856). *Les Fontaines publiques de la ville de Dijon. Exposition et application des principes à suivre et des formules à employer dans les questions de distribution d'eau, etc*. Paris, France: Librairie des corps impériaux des ponts et chaussées et des mines.

Davidovits J (1999). Chemistry of geopolymeric systems, terminology. *Geopolymer, 99*, 9-40.

De Schutter G (1999). Degree of hydration based Kelvin model for the basic creep of early age concrete. *Materials and Structures*, *32*(4), 260.

De Schutter G, Taerwe L (1995). Specific heat and thermal diffusivity of hardening concrete. *Magazine of Concrete Research*, *47*(172), 203-208.

Dharmawardhana CC, Misra A, & Ching WY (2018). Theoretical investigation of C-(A)-SH (I) cement hydrates. *Construction and Building Materials*, *184*, 536-548.

Dhir RK, Hewlett PC, Chan YN (1989). Near surface characteristics of concrete: intrinsic permeability. *Magazine of Concrete Research*, *41*(147), 87-97.

Dhir RK, Jackson N (1989). Concrete admixtures. In Jackson N, Dhir RK (Eds.), *Structural Engineering Materials, 4th Edition.* Hong Kong: Hemisphere Publishing Corp., 132-139.

Dhir RK, Levitt M, Wang J (1989). Membrane curing of concrete: water vapour permeability of curing membranes. *Magazine of Concrete Research*, *41*(149), 221-228.

Dixon JJS, Geyer GB (1958). *U.S. Patent No. 2,864,714*. Washington, DC: U.S. Patent and Trademark Office.

Dolton B, Hannah C (2006). Cellular concrete: Engineering and technological advancement for construction in cold climates. *The 2006 Annual General Conference of the Canadian Society for Civil Engineering*.

Doniec A (2008). A cellular concrete material used for thorough cleaning of wastewater generated in electroplating process. *Clean Technologies and Environmental Policy*, *10*(3), 263-268.

Dransfield JM (2000). Foamed concrete: Introduction to the product and its properties. In *Proceedings of the One-Day Awareness Seminar on Foamed Concrete: Properties, Applications and Potential; Dundee, Scotland; March 2000,* 1-11.

Du L, Folliard KJ (2005). Mechanisms of air entrainment in concrete. Cement and concrete research, 35(8), 1463-1471.

Ducman V, Mirtic B (2009). The applicability of different waste materials for the production of lightweight aggregates. *Waste Management, 29*(8), 2361-2368.

Dunn ML, Ledbetter H (1995). Poisson's ratio of porous and microcracked solids: theory and application to oxide superconductors. *Journal of materials research*, *10*(11), 2715-2722.

Ekrami N, Kamel RS, Garat A, Amirirad A, Fung AS (2015). Applications of active hollow core slabs and insulated concrete foam walls as thermal storage in cold climate residential buildings. *Energy Procedia, 78*, 459-464.

Eliche-Quesada D, Martínez-Martínez S, Pérez-Villarejo L, Iglesias-Godino FJ, Martínez-García C, Corpas-Iglesias, FA (2012). Valorization of biodiesel production residues in making porous clay brick. *Fuel processing technology*, *103*, 166-173.

Emiko L, Thamaraikkannan V, Wee TH, Thangayah T (2011). Shear transfer in lightweight concrete. *Magazine of Concrete Research, 63*(6), 393-400.

Environment and Climate Change Canada (2013). *Environmental Code of Practice for Integrated Steel Mills*. Gatineau, Quebec: Environment Canada. Retrieved from https://www.ec.gc.ca/lcpe-cepa/default.asp?lang=En&n=30360F3C-1&offset=5&toc=show

Environment and Climate Change Canada (2015). *Code of Practice to Reduce Fugitive Emissions of Total Particulate Matter and Volatile Organic Compounds from the Iron, Steel and Ilmenite Sector.* Gatineau, Quebec: Environment Canada, 2. Retrieved from https://www.ec.gc.ca/lcpe-cepa/C8DD8207-98B0-453A-931C-760CF9C22255/CoPSteel-CdPFer-2015Dec_eng.pdf

Erasmus PN, Smit J (2005). Assessment of pre-cast foamed concrete as support medium in deep level mining. In *Proceedings of the International Conference on the Use of Foamed Concrete in Construction; Dundee, Scotland; 5 July 2005,* 121-132.

Erdem TK, Meral C, Tokyay M, Erdogan TY (2007). Use of perlite as a pozzolanic addition in producing blended cements. *Cement and Concrete Composites, 29*(1), 13-21.

Esmaily H, Nuranian H (2012). Non-autoclaved high strength cellular concrete from alkali activated slag. *Construction and Building Materials, 26*(1), 200-206.

Evans AG, Biswas DR, Fulrath RM (1979). Accept/reject criteria for structural ceramics: Some effects of cavities in the fracture of ceramics-spherical cavities. In *Proceedings of the ARPA/AFML Review of Progress in Quantitative Nondestructive Evaluation; La Jolla, CA; 8-13 July 1979,* 171-177

Everett DH (1961). The thermodynamics of frost damage to porous solids. *Transactions of the Faraday society*, *57*, 1541-1551.

Expanded Shale Clay and Slate Institute (2007). *Reference Manual for the Properties and Applications of Expanded Shale, Clay and Slate Lightweight Aggregate.* Retrieved from http://www.escsi.org/ContentPage.aspx?id=1124

Fabian GL, O'Donnell RH, Tom JG, Malone PG (1996). Use of shock-absorbing concrete (SACON) as an environmentally compatible bullet-trapping medium on small-arms training ranges. In *Proceedings of the Tri-Service Environmental Technology Workshop "Enhancing Readiness Through Environmental Quality Technology"; Hershey, Pennsylvania; 20-22 May 1996*; 187-196.

Fadila R, Suleiman MZ (2008). Paper fiber reinforced foam concrete wall paneling system. In *2nd International Conference on Built Environment in Developing Countries; Penang, Malaysia; 3-4 December 2008, 527-540.*

Fagerlund G (1973). Strength and porosity of concrete. In *Proceedings of the International Symposium RILEM/IUPAC on Pore Structure and Properties of Materials; Prague, Czech Republic; September 1973,* D51-D141.

Fagerlund G (1977). *The critical degree of saturation method of assessing the freeze/thaw resistance of concrete.* Stockholm: Swedish Cement and Concrete Research Institute.

Famy C, Scrivener, KL, Atkinson A, Brough AR (2001). Influence of the storage conditions on the dimensional changes of heat-cured mortars. *Cement and Concrete Research*, *31*(5), 795-803.

Fan D, Yang S (2018). Mechanical properties of CSH globules and interfaces by molecular dynamics simulation. Construction and Building Materials, 176, 573-582.

Farghal Maree A, Hilal Riad K (2014). Analytical and experimental investigation for bond behaviour of newly developed polystyrene foam particles' lightweight concrete. *Engineering Structures, 58*, 1-11.

Federal Aviation Administration (2012). *Advisory Circular 150/5220-22B, Engineered Materials Arresting System (EMAS) for Aircraft Overruns.* Washington, DC: US Department of Transport.

Feldman RF (1972). Mechanism of creep of hydrated Portland cement paste. *Cement and concrete research*, *2*(5), 521-540.

Feldman RF, Sereda PJ (1970). A new model for hydrated Portland cement and its practical implications. *Engineering Journal*, *53*(8/9), 53-59.

Ficker T (2008). Fractal strength of cement gels and universal dimension of fracture surfaces. *Theoretical and Applied Fracture Mechanics*, *50*(2), 167-171.

Fidjestøl, P and Dåstøl, M (n.d.). *The history of silica fume in concrete—From novelty to key ingredient in high performance concrete.* Oslo, Norway: Elkem Materials, Norway. Retrieved from http://www.ibracon.org.br/eventos/50cbc/plenarias/per_fidjestol.pdf

Finney E (1944). *Air-Entrained Concrete.* Michigan: Michigan State Highway Department.

Fiore V, Scalici T, Di Bella G, Valenza A (2015). A review on basalt fibre and its composites. *Composites Part B, 74*, 74-94.

Flores-Johnson EA, Li QM (2012). Structural behaviour of composite sandwich panels with plain and fibre-reinforced foamed concrete cores and corrugated steel faces. *Composite Structures, 94*(5), 1555-1563.

Floyd RW, Hale WM, Bymaster JC (2015). Effect of aggregate and cementitious material on properties of lightweight self-consolidating concrete for prestressed members. *Construction and Building Materials, 85*, 91-99.

Fonseca PC, Jennings HM (2010). The effect of drying on early-age morphology of C–S–H as observed in environmental SEM. *Cement and Concrete research*, *40*(12), 1673-1680.

Fouad FH (2006). Cellular concrete. In Lamond JF (Ed.), *Significance of Tests and Properties of Concrete and Concrete-Making Materials*. West Conschhocken, Pennsylvania: ASTM International, 561-569.

Frickland P, Cleland E, Hasegawa T (1981). *Evaluation of the effects of a freeze/thaw environment on cellular glass.* Pasadena, California: Jet Propulsion Laboratory, California Institute of Technology.

Fujiwara H, Sawada E, Ishikawa Y (1995). Manufacturing of high strength aerated concrete containing silica fume. In *Proceedings of fifth international conference on fly ash, silica fume, slag and natural pozzolana in concrete (ACI SP-153, Vol. 2)*; *Milwaukee, Wisconsin; June 1995,* 779–91.

Funke K, Eliasson B (1978). *Hoegisolerande laettbetong som baerande element (High-insulation aerated concrete as bearing elements).* Stockholm, Sweden: Byggdok, 369

Gan MS (1997). *Cement and concrete.* London: Chapman and Hall.

Gao L, Zhang J, Xu C (2015). National standards of the People's Republic of China: Thoughts of revision on technical specification for application of autoclaved aerated concrete (Nationale Standards der Volksrepublik China: Gedanken zur Überarbeitung der technischen Spezifikationen für die Anwendung von dampfgehärtetem Porenbeton). *Mauerwerk, 19*(3), 214-227.

Gdoutos EE (1984). Growth predictions of two interacting cracks. *Theoretical and applied fracture mechanics*, *1*(2), 133-137.

Georgiades A, Ftikos C, Marinos J (1991). Effect of micropore structure on autoclaved aerated concrete shrinkage. *Cement and Concrete Research, 21*(4), 655-662.

Ghafoori N, Dutta S (1995a). Development of no-fines concrete pavement applications. *Journal of Transportation Engineering, 121*(3), 283-288.

Ghafoori N, Dutta S (1995b). Laboratory investigation of compacted no-fines concrete for paving materials. *Journal of Materials in Civil Engineering, 7*(3), 183-191.

Giannakou A, Jones MR (2002). Potentials of foamed concrete to enhance the thermal performance of low rise dwellings. *Innovations and development in concrete materials and construction: Proceedings of the International Congress 'Challenges of Concrete Construction'; Dundee, Scotland; September 2002,* 533-544.

Gibson LJ, Ashby MF (1999). *Cellular solids: structure and properties, 2nd edition.* Cambridge, UK: Cambridge University Press.

Giovan M, Adams M (1979). *Evaluation of cellular glasses for solar mirror panel applications.* Pasadena, California: Jet Propulsion Laboratory, California Institute of Technology.

Goguen C (2013). Weighing in on high-density concrete. *National Precast Association Website.* Retrieved from http://precast.org/2013/04/weighing-in-on-high-density-concrete/

Gonçalves M, Molina-Sabio M, Rodriguez-Reinoso F (2010). Modification of activated carbon hydrophobicity by pyrolysis of propene. Journal of Analytical and Applied Pyrolysis, 89(1), 17-21.

Görhan G, Şimşek O (2013). Porous clay bricks manufactured with rice husks. *Construction and Building Materials*, *40*, 390-396.

Grassl P, Wong HS, Buenfeld NR (2010). Influence of aggregate size and volume fraction on shrinkage induced micro-cracking of concrete and mortar. Cement and concrete research, 40(1), 85-93.

Graybeal BA (2006). *Material property characterization of ultra-high performance concrete* (No. FHWA-HRT-06-103). United States. Federal Highway Administration. Office of Infrastructure Research and Development.

Gruskovnjak A, Lothenbach B, Holzer L, Figi R, Winnefeld F (2006). Hydration of alkali-activated slag: comparison with ordinary Portland cement. *Advances in cement research*, *18*(3), 119-128.

Gunasekaran K, Annadurai R, Kumar PS (2013). Study on reinforced lightweight coconut shell concrete beam behavior under shear. *Materials & Design, 50*, 293-301.

Gunawan P, Busra S (2014). Foamed lightweight concrete tech using galvalum Az 150 fiber. *Procedia Engineering, 95*, 433-441.

Gunduz L (2008). The effects of pumice aggregate/cement ratios on the low-strength concrete properties. *Construction and Building Materials, 22*(5), 721-728.

Guo H, Guo W, Shi Y (2015). Computational modeling of the mechanical response of lightweight foamed concrete over a wide range of temperatures and strain rates. *Construction and Building Materials, 96*, 622-631.

Hall C (1989). Water sorptivity of mortars and concretes: a review. *Magazine of concrete research*, *41(147),* 51-61.

Hall C, Yau MHR (1987). Water movement in porous building materials—IX. the water absorption and sorptivity of concretes. *Building and Environment, 22*(1), 77-82.

Hamad AJ (2014). Materials, production, properties and application of aerated lightweight concrete: Review. *International Journal of Materials Science and Engineering, 2*(2), 152-157.

Hamidah MS, Azmi I, Ruslan MRA, Kartini K, Fadhil NM (2005). Optimisation of foamed concrete mix of different sand-cement ratio and curing conditions. In *Proceedings of the International Conference on the Use of Foamed Concrete in Construction; Dundee, Scotland; 5 July 2005,* 37-44.

Hanle LJ, Jayaraman KR, Smith JS (2004). CO2 emissions profile of the US cement industry. In *Proceedings of the 13th International Emission Inventory Conference; Clearwater, Florida; 8-10 June 2004*, 8. Retrieved from https://www3.epa.gov/ttn/chief/conference/ei13/ghg/hanle.pdf

Hannant DJ (1968). The mechanism of creep in concrete. *Matériaux et Construction*, *1*(5), 403-410.

Hanžič L, Ilić R (2003). Relationship between liquid sorptivity and capillarity in concrete. *Cement and Concrete Research, 33*(9), 1385-1388.

Hasselman DPH (1963). Relation between effects of porosity on strength and on Young's modulus of elasticity of polycrystalline materials. *Journal of the American Ceramic Society*, *46*(11), 564-565.

Hatton-Jones S, Teah M (2015). Case analysis of the do-it-yourself industry. *Asia Pacific Journal of Marketing and Logistics*, *27*(5), 826-838.

He Y, Zhang X, Zhang Y, Zhou Y (2014). Effects of particle characteristics of lightweight aggregate on mechanical properties of lightweight aggregate concrete. *Construction and Building Materials, 72*, 270-282.

Hearn N, Hooton RD, Mills RH (1994). Pore structure and permeability. In Klieger P, Lamond JF (Eds.), *Significance of Tests and Properties of Concrete and Concrete-Making Materials*. West Conschhocken, PA: ASTM International, 240-244.

Hebel (1982). *Hebel Technical Handbook*. Tokyo, Japan: Asahi Kasei Kenzai Construction Materials Corporation, 274.

Hebel New Zeeland (2010). *The History of AAC*. Retrieved from https://web.archive.org/web/20101104001651/http://www.hebel.co.nz/about/hebel%20history.php

Hengst RR, Tressler RE (1983). Fracture of foamed Portland cements. *Cement and Concrete Research, 13*(1), 127-134.

Hess JA, Kincl L, Amasay T, Wolfe P (2010). Ergonomic evaluation of masons laying concrete masonry units and autoclaved aerated concrete. *Applied Ergonomics, 41*(3), 477-483.

Hilal AA, Thom NH, Dawson AR (2014a). Pore structure and permeation characteristics of foamed concrete. *Journal of Advanced Concrete Technology*, *12*(12), 535-544.

Hilal AA, Thom NH, Dawson AR (2014b). Effect of additives on void structure of foamed concrete. In *Proceedings from the 34th Cement and Concrete Science Conference; Sheffield, UK; 14-17 September 2014.*

Hilal AA, Thom NH, Dawson AR (2015a). On entrained pore size distribution of foamed concrete. *Construction and Building Materials, 75*, 227-233.

Hilal AA, Thom NH, Dawson AR (2015b). On void structure and strength of foamed concrete made without/with additives. *Construction and Building Materials, 85*, 157-164.

Hilal AA, Thom NH, Dawson AR (2015c). The use of additives to enhance properties of pre-formed foamed concrete. *International Journal of Engineering and Technology*, *7*(4), 286-293.

Hlavácek P, Šmilauer V, Škvára F, Kopecký L, Šulc R (2015). Inorganic foams made from alkali-activated fly ash: Mechanical, chemical and physical properties. *Journal of the European Ceramic Society, 35*(2), 703-709.

Hoarty JT, Hodgkinson L (1990). Improved air-entraining agents for use in concretes containing pulverized fuel ashes. In *Admixtures for Concrete—Improvement of Properties: Proceedings of the International Symposium held by RILEM; Barcelona, Spain; 14-17 May 1990,* 490-499.

Hoek E, Bieniawski ZT (1965). Brittle fracture propagation in rock under compression. *International Journal of Fracture Mechanics*, *1*(3), 137-155.

Hoff GC (1972). Porosity-strength considerations for cellular concrete. *Cement and Concrete Research, 2*, 91-100.

Hooimeijer FL (2011). *The tradition of making: polder cities.* (Doctoral dissertation.) Delft University of Technology.

Hooton RD, Vassilev D (2012). *Deicer scaling resistance of concrete mixtures containing slag cement. Phase 2: evaluation of different laboratory scaling test methods* (No. InTrans Project 10-374). Iowa State University. Institute for Transportation.

Hossain KMA (2004a). Properties of volcanic pumice based cement and lightweight concrete. *Cement and Concrete Research, 34*(2), 283-291.

Hossain KMA (2004b). Properties of volcanic scoria based lightweight concrete. *Magazine of Concrete Research, 56*(2), 111-120.

Hossain KMA, Ahmed S, Lachemi M (2011). Lightweight concrete incorporating pumice based blended cement and aggregate: Mechanical and durability characteristics. *Construction and Building Materials, 25*(3), 1186-1195.

Hou D (2014). Molecular simulation on the Calcium Silicate Hydrate (CSH) gel. Hong Kong University of Science and Technology (Hong Kong).

Hou D, Ma H, Li Z (2015). Morphology of calcium silicate hydrate (CSH) gel: a molecular dynamic study. Advances in Cement Research, 27(3), 135-146.

Huang Z, Zhang T, Wen Z (2015). Proportioning and characterization of Portland cement-based ultra-lightweight foam concretes. *Construction and Building Materials, 79*, 390-396.

Hwang C, Tran V (2015). A study of the properties of foamed lightweight aggregate for self-consolidating concrete. *Construction and Building Materials, 87*, 78-85.

Hyun SK, Murakami K, Nakajima H (2001). Anisotropic mechanical properties of porous copper fabricated by unidirectional solidification. *Materials Science and Engineering: A (Structural Materials: Properties, Microstructure and Processing)*, *299*(1), 241-248.

Ibrahim NM, Salehuddin S, Amat RC, Rahim NL, Izhar TNT (2013). Performance of lightweight foamed concrete with waste clay brick as coarse aggregate. In

Proceedings of the 4th International Conference on Environmental Science and Development; Dubai, United Arab Emirates; 19-20 January 2013, 497-501.

Ibrahim W, Haziman M, Jamaluddin N, Juki MI, Adnan SH (2014). Compressive and flexural strength of foamed concrete containing polyolefin fibers. *Advanced Material Research, 9*(11), 489–493.

Idiart AE (2009). *Coupled analysis of degradation processes in concrete specimens at the meso-level*. (Doctoral dissertation.) Universitat Politècnica de Catalunya.

Ikponmwosa E, Fapohunda C, Kolajo O, Eyo O (2015). Structural behaviour of bamboo-reinforced foamed concrete slab containing polyvinyl wastes (PW) as partial replacement of fine aggregate. *Journal of King Saud University, Engineering Sciences*.

India Autoclaved Aerated Concrete Producers Association (2014). *History and Evolution.* Retrieved from http://www.magicrete.in/iaacpa.org/history.php

Isida M, Nemat-Nasser S (1987). On mechanics of crack growth and its effects on the overall response of brittle porous solids. *Acta metallurgica*, *35*(12), 2887-2898.

ISO 15148 (2002). *Hygrothermal performance of building materials and products — Determination of water absorption coefficient by partial immersion.* Geneva, Switzerland: International Standards Organization.

Jahjah J (1942). *U.S. Patent No. 2,282,190*. Washington, DC: U.S. Patent and Trademark Office.

Jansen DC, Shah SP (1997). Effect of length on compressive strain softening of concrete. *Journal of Engineering Mechanics*, *123*(1), 25-35.

Jasiczak J, Zielinski K (2006). Effect of protein additive on properties of mortar. *Cement and Concrete Composites*, *28*(5), 451-457.

Jennings HM (2004). Colloid model of C-S-H and implications to the problem of creep and shrinkage. *Materials and structures*, *37*(1), 59-70.

Jerman M, Keppert M, Výborný J, Černý R (2013). Hygric, thermal and durability properties of autoclaved aerated concrete. *Construction and Building Materials, 41*, 352-359.

Jiang J, Lu Z, Niu Y, Li J, Zhang Y (2016). Study on the preparation and properties of high-porosity foamed concretes based on ordinary Portland cement. Materials & Design, 92, 949-959.

Jiang J, Lu Z, Niu Y, Li J, Zhang Y (2016a). Investigation of the properties of high-porosity cement foams based on ternary Portland cement–metakaolin–silica fume blends. *Construction and Building Materials*, *107*, 181-190.

Jiang J, Lu Z, Niu Y, Li J, Zhang Y (2016b). Study on the preparation and properties of high-porosity foamed concretes based on ordinary Portland cement. *Materials & Design, 92*, 949-959.

Jiang Q, Zhang J (2011). Anti-seismic capability and property optimization of foam concrete in tunnel as isolation layer. *Advanced Science Letters*, *4*(3), 691-695.

Jirásek M, Havlásek P (2014). Microprestress-solidification theory of concrete creep: Reformulation and improvement. *Cement and Concrete Research*, *60*, 51-62.

Jitchaiyaphum K, Sinsiri T, Chindaprasirt P (2011). Cellular lightweight concrete containing pozzolan materials. *Procedia Engineering*, *14*, 1157-1164.

Jolicoeur C, To TC, Benoît É, Hill R, Zhang Z, Pagé M (2009). Fly-ash carbon effects on concrete air-entrainment: fundamental studies on their origin and chemical mitigation. In *9th ACI international conference on superplasticizers and other chemical admixtures in concrete, Seville, Spain: ACI, SP-262*.

Jones MR (2000). Foamed concrete for structural use. In *Proceedings of the One-Day Awareness Seminar on Foamed Concrete: Properties, Applications and Potential; Dundee, Scotland; March 2000,* 54-79

Jones MR, Giannakou A (2004). Thermally insulating foundations and ground slabs using highly-foamed concrete. *Journal of ASTM International, 1*(6), 1-13.

Jones MR, McCarthy A (2005a). Behaviour and Assessment of Foamed Concrete for Fill and Highway Applications. In *Proceedings of the International Conference on the Use of Foamed Concrete in Construction; Dundee, Scotland; 5 July 2005,* 61-88.

Jones MR, McCarthy A (2005b). Preliminary views on the potential of foamed concrete as a structural material. *Magazine of Concrete Research, 57*(1), 21-31.

Jones MR, McCarthy A (2005c). Utilising unprocessed low-lime coal fly ash in foamed concrete. *Fuel, 84*(11), 1398-1409.

Jones MR, McCarthy A (2006). Heat of hydration in foamed concrete: Effect of mix constituents and plastic density. *Cement and Concrete Research, 36*(6), 1032-1041.

Jones MR, Zheng L (2013). Energy absorption of foamed concrete from low-velocity impacts. *Magazine of Concrete Research, 65*(4), 209-219.

Jones MR, Zheng L, Yerramala A, Rao KS (2012). Use of recycled and secondary aggregates in foamed concretes. *Magazine of Concrete Research, 64*(6), 513-525.

Just A, Middendorf B (2009). Microstructure of high-strength foam concrete. *Materials Characterization, 60*(7), 741-748.

Kan A, Demirboğa R (2009). A novel material for lightweight concrete production. *Cement and Concrete Composites, 31*(7), 489-495.

Kaneko Y, Mihashi H, Ishihara S (2004). Shear failure of plain concrete in strain localized area. In *Proceeding of the Fifth International Conference on Fracture Mechanics of Concrete and Concrete Structures, Colorado, USA,* Vol. 1, 383-390.

Kang J (2015). Composite and non-composite behaviors of foam-insulated concrete sandwich panels. *Composites Part B, 68*, 153-161.

Kaplan P (1940). *U.S. Patent No. 2,215,812*. Washington, DC: U.S. Patent and Trademark Office.

Kasten I (2011). *Concrete Technology for Concrete Pumps.* Stuttgart, Germany: Putzmeister Concrete Pumps GmbH.

Kearsley EP (1996). The use of Foamcrete for affordable development in third world countries. In *Proceedings of the International Conference on Concrete in the Service of Mankind, Volume 3: Appropriate Concrete Technology; Dundee, Scotland; June 1996,* 232.

Kearsley EP (1999). Just Foamed Concrete—An Overview. In *Specialist techniques and materials for concrete construction*, 227-237. Thomas Telford Publishing.

Kearsley EP (1999a). Just foamed concrete—An overview. In *Specialist techniques and materials for construction: Proceedings of the International Conference 'Creating with Concrete'; Dundee, Scotland; September 1999*, 227-237.

Kearsley EP (1999b). *The effect of high volumes of ungraded fly ash on the properties of foamed concrete.* (Doctoral dissertation). University of Leeds.

Kearsley EP, Booysens P (1998). Reinforced foamed concrete—Can it be durable? *Concrete Beton, 91,* 5-9.

Kearsley EP, Mostert HF (1997). The use of foamcrete in Southern Africa. In *Proceedings of the Thrid CANMET/ACI International Conference on High Performance Concrete; Lumpur, Malaysia; 2-5 December 1997,* 919-934.

Kearsley EP, Mostert HF (2005a). Designing mix composition of foamed concrete with high fly ash contents. In *Proceedings of the International Conference on the Use of Foamed Concrete in Construction; Dundee, Scotland; 5 July 2005,* 29-36.

Kearsley EP, Mostert HF (2005b). Opportunities for expanding the use of foamed concrete in the construction industry. In *Proceedings of the International Conference on the Use of Foamed Concrete in Construction; Dundee, Scotland; 5 July 2005,* 143-155.

Kearsley EP, Mostert HF (2005c). The use of foamed concrete in refractories. In *Proceedings of the International Conference on the Use of Foamed Concrete in Construction; Dundee, Scotland; 5 July 2005,* 89-96.

Kearsley EP, Visagie M (1999). Micro-properties of foamed concrete. In *Specialist techniques and materials for construction: Proceedings of the International Conference 'Creating with Concrete'; Dundee, Scotland; September 1999*, 173-184.

Kearsley EP, Visagie M. (2002). Properties of foamed concrete as influenced by air-void parameters. *Concrete Beton*, *101*, 9-13.

Kearsley EP, Wainwright PJ (2001a). Porosity and permeability of foamed concrete. *Cement and Concrete Research, 31*(5), 805-812.

Kearsley EP, Wainwright PJ (2001b). The effect of high fly ash content on the compressive strength of foamed concrete. *Cement and Concrete Research, 31*(1), 105-112.

Kearsley EP, Wainwright PJ (2002). The effect of porosity on the strength of foamed concrete. *Cement and Concrete Research, 32*(2), 233-239.

Kevern JT, Wang K, Schaefer VR (2009). Effect of coarse aggregate on the freeze-thaw durability of pervious concrete. *Journal of Materials in Civil Engineering*, *22*(5), 469-475.

Khan MI (2014). *Experimental investigation on mechanical characterization of fiber reinforced foamed concrete.* (Doctoral dissertation.) University of Akron.

Kim DI, Jung SC, Lee JE, Chang SH (2006). Parametric study on design of composite-foam-resin concrete sandwich structures for precision machine tool structures. *Composite Structures, 75*(1-4), 408-414.

Kockal NU, Ozturan T (2011). Durability of lightweight concretes with lightweight fly ash aggregates. *Construction and Building Materials, 25*(3), 1430-1438.

Kohler, N. (1983). Global energetic budget of aerated concrete. In Wittmann FH (Ed.), *Autoclaved Aerated Concrete: Moisture and Properties.* Amsterdam, Netherlands: Elsevier Scientific Publishing Co., 13-26.

Kollek JJ (1989). The determination of the permeability of concrete to oxygen by the Cembureau method—a recommendation. *Materials and structures*, *22*(3), 225-230.

Kondo R, Daimon M (1974). 'Phase composition of hardened cement pa te', Proc. 5th Int. Congr. on the Chemistry of Cement, Moscow. (See abo: Daimon, M., Abo-El-Enein, S. A., Hosaka, G., Goto, S., and Kondo, R. (1977).

König J, Petersen RR, Yue Y (2016). Influence of the glass particle size on the foaming process and physical characteristics of foam glasses. *Journal of Non-Crystalline Solids*, *447*, 190-197.

Königsberger M, Irfan-ul-Hassan M, Pichler B, Hellmich C (2016). Downscaling based identification of nonaging power-law creep of cement hydrates. *Journal of Engineering Mechanics*, *142*(12), 04016106.

Koronthalyova O (2011). Moisture storage capacity and microstructure of ceramic brick and autoclaved aerated concrete. *Construction and Building Materials*, *25*(2), 879-885.

Korpa A, Trettin R (2006). The influence of different drying methods on cement paste microstructures as reflected by gas adsorption: comparison between freeze-drying (F-drying), D-drying, P-drying and oven-drying methods. *Cement and Concrete Research*, *36*(4), 634-649.

Kosmatka SH, Kerkhoff B, Panarese WC, MacLeod NF, McGrath RJ (2002). *Design and Control of Concrete Mixtures, 7th Edition.* Ottawa: Portland Cement Association.

Kotronis P, Al Holo S, Bésuelle P, Chambon R (2008). Shear softening and localization: Modelling the evolution of the width of the shear zone. *Acta geotechnica*, *3*(2), 85-97.

Koudelka T, Kruis J, Madera J (2015). Coupled shrinkage and damage analysis of autoclaved aerated concrete. *Applied Mathematics and Computation, 267*, 427-435.

Kováčik J (2006). Correlation between Poisson's ratio and porosity in porous materials. *Journal of materials science*, *41*(4), 1247-1249.

Kovler K, Zhutovsky S (2006). Overview and Future Trends of Shrinkage Research. *Materials and Structures 39*(9), 827-847.

Kozłowski M, Kadela M, Kukiełka A (2015). Fracture energy of foamed concrete based on three-point bending test on notched beams. *Procedia Engineering, 108*, 349-354.

Krämer C, Schauerte M, Kowald TL, Trettin RHF (2015). Three-phase-foams for foam concrete application. *Materials Characterization, 102*, 173-179.

Kramer DA, Papp JF, LaTurno NM, Gambogi J (1998). Mine and mineral processing plant locations—Supplemental information for USGS Map I-2654. *U.S. Geological Survey Minerals Yearbook.* Washington, DC: U.S. Department of the Interior. Retrieved from http://minerals.usgs.gov/minerals/pubs/mapdata/

Kreft O, Haussmann J, Hubálková J, Aneziris CG, Straube B, Schoch T (2011). *Pore size distribution effects on the thermal conductivity of light weight autoclaved aerated concrete.* Kloster Lehnin, Germany: Xella Technologie- und Forschugsgesellschaft

mbH, 257-264. Retrieved from https://www.xella.com/de/docs/SKMBT_C253_12091713151.pdf

Krivenko PV, Yu Kovalchuk G, Yu Kovalchuk O (2005). Heat-Resistant Cellular Concretes Based on Alkaline Cements. In *Proceedings of the International Conference on the Use of Foamed Concrete in Construction; Dundee, Scotland; 5 July 2005,* 97-104.

Kumar EM, Ramamurthy K (2015). Effect of fineness and dosage of aluminium powder on the properties of moist-cured aerated concrete. *Construction and Building Materials*, *95*, 486-496.

Kumar R, Bhattacharjee B (2003). Porosity, pore size distribution and in situ strength of concrete. *Cement and Concrete Research, 33*(1), 155-164.

Kunther W, Ferreiro S, Skibsted J (2017). Influence of the Ca/Si ratio on the compressive strength of cementitious calcium–silicate–hydrate binders. *Journal of Materials Chemistry A*, *5*(33), 17401-17412.

Kuosa H, Ferreira M, Leivo M (2013). *Freeze-thaw testing*. *VTT Technical Research Centre of Finland, Finland*.

LaBarca IK, Foley RD, Cramer SM (2007). *Effects of Ground Granulated Blast Furnace Slag in Portland Cement Concrete: Expanded Study*. Wisconsin Highway Research Program.

Laforest G, Duchesne J (2005). Immobilization of chromium (VI) evaluated by binding isotherms for ground granulated blast furnace slag and ordinary Portland cement. *Cement and concrete research*, *35*(12), 2322-2332.

Lajtai EZ (1974). Brittle fracture in compression. *International Journal of Fracture*, *10*(4), 525-536.

Laukaitis A, Fiks B (2006). Acoustical properties of aerated autoclaved concrete. *Applied Acoustics, 67*(3), 284-296.

Laukaitis A, Kerienė J, Mikulskis D, Sinica M, Sezemanas G (2009). Influence of fibrous additives on properties of aerated autoclaved concrete forming mixtures and strength characteristics of products. *Construction and Building Materials, 23*(9), 3034-3042.

Laukaitis A, Žurauskas R, Kerienė J. (2005). The effect of foam polystyrene granules on cement composite properties. *Cement and Concrete Composites, 27*(1), 41-47.

Laurent JP (1991). La conductivité thermique 'à sec'des bétons cellulaires autoclavés: un modèle conceptuel. *Materials and Structures*, *24*(3), 221-226.

Łazniewska-Piekarczyk B (2014). The methodology for assessing the impact of new generation superplasticizers on air content in self-compacting concrete. *Construction and Building Materials, 53*, 488-502.

Lee DH, Jun MH, Ko JS (2001). Physical properties and quality control of foamed concrete with fly ash for cast-in-site. *Journal of the Korea Concrete Institute 13*(1), 69-76.

Lee KG (2010). *Performance of foamed concrete using laterite as sand replacement* (Bachelor thesis.) Universiti Malaysia Pahang.

Lee YL, Hung YT (2005). Exploitation of solid wastes in foamed concret—Challenges ahead. *Proceedings of the International Conference on the Use of Foamed Concrete in Construction; Dundee, Scotland; 5 July 2005,* 15-22.

Leitch FN (1980). The properties of aerated concrete in service. In *Proceedings of the 2nd International Conference on Lightweight Concretes; London, UK; April 1980.*

Li Q, Wang H, Zhang Z, Reid A (2013). Numerical simulation of porosity on thermal properties and fire resistance of foamed concrete. *Journal of Sustainable Cement-Based Materials, 2*(1), 13-19.

Lian C, Zhuge Y, Beecham S (2011). The relationship between porosity and strength for porous concrete. *Construction and Building Materials, 25*(11), 4294-4298.

Liew ACM (2005). New innovative lightweight foam concrete technology. In *Proceedings of the International Conference on the Use of Foamed Concrete in Construction; Dundee, Scotland; 5 July 2005,* 45-50.

Lim SK, Tan CS, Lim OY, Lee YL (2013). Fresh and hardened properties of lightweight foamed concrete with palm oil fuel ash as filler. *Construction and Building Materials, 46*, 39-47.

Limbachiya M, Meddah MS, Fotiadou S (2012). Performance of granulated foam glass concrete. *Construction and Building Materials, 28*(1), 759-768.

Liu MYJ, Alengaram UJ, Jumaat MZ, Mo KH (2014). Evaluation of thermal conductivity, mechanical and transport properties of lightweight aggregate foamed geopolymer concrete. *Energy & Buildings, 72*, 238-245.

Liu MYJ, Alengaram UJ, Santhanam M, Jumaat MZ, Mo KH (2016). Microstructural investigations of palm oil fuel ash and fly ash based binders in lightweight aggregate foamed geopolymer concrete. *Construction and Building Materials, 120*, 112-122.

Liu Z, Zhao K, Hu C, Tang Y (2016). Effect of water-cement ratio on pore structure and strength of foam concrete. Advances in Materials Science and Engineering, 2016.

London A (1949). Transmission of reverberant sound through single walls. *Journal of Research of the National Bureau of Standards*, *42*(605), 2.

London A (1950). Transmission of reverberant sound through double walls. *The Journal of the Acoustical Society of America*, *22*(2), 270-279.

London A (1949). Transmission of reverberant sound through single walls. *Journal of Research of the National Bureau of Standards*, *42*(605), 2.

Loo YH, Peterson JS, Swaddiwudhipong S, Tam CT (1995). Application of the layering method on large concrete pours. *Magazine of Concrete Research, 47*(172), 209-217.

Lopez de Murphy M, Lissenden C, Xiao C (2009). *Technology evaluation on characterization of the air void system in concrete* (No. FHWA-PA-2009-013-PSU 020). Pennsylvania. Dept. of Transportation. Bureau of Planning and Research.

Lotfy A, Hossain KM, Lachemi M (2015). Lightweight self-consolidating concrete with expanded shale aggregates: Modelling and Optimization. *International Journal of Concrete Structures and Materials*, *9*(2), 185-206.

Lothenbach B, Scrivener K, Hooton RD (2011). Supplementary cementitious materials. Cement and Concrete Research, 41(12), 1244-1256.

Loudon AG (1979). The thermal properties of lightweight concretes. *International Journal of Cement Composites and Lightweight Concrete*, *1*(2), 71-85.

Lu Y, Qin B (2015). Experimental investigation of closed porosity of inorganic solidified foam designed to prevent coal fires. *Advances in Materials Science and Engineering*, *2015*.

Lucideon Ltd. (2014). *Technical Report and Design Guidance for the Use of Porotherm Blocks in the UK.* Stoke-on-Trent, Staffordshire.

Ludwig NC (1950). *U.S. Patent No. 2,521,073*. Washington, DC: U.S. Patent and Trademark Office.

Ma J, Dehn F (2017). Shrinkage and creep behavior of an alkali-activated slag concrete. *Structural Concrete*, *18*(5), 801-810.

Mackenzie JK (1950). The elastic constants of a solid containing spherical holes. *Proceedings of the Physical Society. Section B*, *63*(1), 2.

Makul N, Sua-iam G (2016). Characteristics and utilization of sugarcane filter cake waste in the production of lightweight foamed concrete. *Journal of Cleaner Production, 126*, 118-133.

Mamun M, Batool F, Bindiganavile V (2014). Thermo-mechanical properties of fibre reinforced cement-based foam exposed to sulphate. *Construction and Building Materials, 61*, 312-319.

Mamun M, Bindiganavile V (2011). Sulphate resistance of fibre reinforced cement-based foams. *Construction and Building Materials*, *25*(8), 3427-3442.

Manzano H, Dolado JS, Ayuela A (2009). Elastic properties of the main species present in Portland cement pastes. Acta Materialia, 57(5), 1666-1674.

Masloff B, Palladino R (2012). *U.S. Patent No. 8,172,937*. Washington, DC: U.S. Patent and Trademark Office.

Massazza F (1998). Pozzolana and pozzolanic cements. *Lea's chemistry of cement and concrete*, *4*, 471-636.

Mazloom M (2008). Estimating long-term creep and shrinkage of high-strength concrete. *Cement and Concrete Composites*, *30*(4), 316-326.

Mazloom M, Ramezanianpour AA, Brooks JJ (2004). Effect of silica fume on mechanical properties of high-strength concrete. *Cement and Concrete Composites*, *26*(4), 347-357.

McLellan BC, Williams RP, Lay J, Van Riessen A, Corder GD (2011). Costs and carbon emissions for geopolymer pastes in comparison to ordinary Portland cement. *Journal of Cleaner Production*, *19*(9), 1080-1090.

Mehta PK (1986). *Concrete Structure, Properties and Materials.* New Jersey: Prentice-Hall Inc.

Melin S (1983). Why do cracks avoid each other?. *International Journal of Fracture*, *23*(1), 37-45.

Mendes JC, Moro TK, Figueiredo AS, do Carmo Silva KD, Silva GC, Silva GJB, Peixoto RAF (2017). Mechanical, rheological and morphological analysis of cement-based composites with a new LAS-based air entraining agent. *Construction and Building Materials, 145*, 648-661.

Meyer D, van Mier JGM (2006). The influence of the foam behaviour on the properties of foamed cement paste. In *Proceedings of the 6th International PhD Symposium in Civil Engineering; Zurich, Switzerland; 23-26 August 2006*, 96-97.

Meyer D, van Mier JGM (2007). Influence of different PVA fibres on the crack behaviour of foamed cement paste. In *Proceedings of 6th International Conference on Fracture Mechanics of Concrete Structures; Catania, Italy; 17-22 June 2007;* 1359-1365.

Mielenz RC, Wolkodoff VE, Backstrom JE, Flack HL (1958). Origin, Evolution, and Effects of the Air Void System in Concrete. Part 1: Entrained Air in Unhardened Concrete. *American Concrete Institute Journal Proceedings* 55(7), 95-121.

Mineral Products Association (2016). Lightweight concrete. *The Concrete Centre: Special Concrete.* Retrieved from http://www.concretecentre.com/Performance-Sustainability-(1)/Special-Concrete/lightweight-concrete.aspx

Minerals and Metals Sector NRCAN, National Energy Board (2012). Principal mineral areas of Canada / Principales régions minières du Canada. *Geological Survey of Canada Map 900A (66th edition).* doi:10.4095/292216. Retrieved from http://geoscan.nrcan.gc.ca/starweb/geoscan/servlet.starweb?path=geoscan/downloade.web&search1=R=292216

Ming TL (2009). *Engineering properties of lightweight foam concrete using saw dust as a filler replacement*. Kuantan, Pahang: Universiti Malaysia Pahang.

Mohammad M (2011). *Development of foamed concrete: enabling and supporting design.* (Doctoral dissertation.) University of Dundee.

Mostofinejad D, Nozhati M (2005). Prediction of the modulus of elasticity of high strength concrete. *Iranian Journal of Science & Technology, Transaction B, Engineering*, *29*(B3), 311-321.

Mounanga P, Gbongbon W, Poullain P, Turcry P (2008). Proportioning and characterization of lightweight concrete mixtures made with rigid polyurethane foam wastes. *Cement and Concrete Composites, 30*(9), 806-814.

MTO LS-412 (1997). Methods of test for scaling resistance of concrete surfaces exposed to deicing chemicals. In *Laboratory Testing Manual.* Ontario: Ministry of Transportation.

Munir A, Huzaim A, Safwan SI (2015). Utilization of palm oil fuel ash (POFA) in producing lightweight foamed concrete for non-structural building material. *Procedia Engineering, 125*, 739-746.

Mydin MAO, Wang YC (2011). Structural performance of lightweight steel-foamed concrete–steel composite walling system under compression. *Thin-Walled Structures, 49*(1), 66-76.

Mydin MAO, Wang YC (2012a). Mechanical properties of foamed concrete exposed to high temperatures. *Construction and Building Materials, 26*(1), 638-654.

Mydin MAO, Wang YC (2012b). Thermal and mechanical properties of lightweight foamed concrete at elevated temperatures. *Magazine of Concrete Research, 64*(3), 213-224.

Mydin MO, Sudin MAS, Sani NM (2014). Axial compressive strength of foamcrete with different profiles and dimensions. In *Building Surveying, Facilities Management and Engineering Conference; Perak, Malaysia; 27 August 2014, 139-145*.

Nadeem M, Pofale AD (2012). Utilization of industrial waste slag as aggregate in concrete applications by adopting Taguchi's approach for optimization. *Open Journal of Civil Engineering*, *2,* 96-105.

Nambiar EKK, Ramamurthy K (2006a). Influence of filler type on the properties of foam concrete. *Cement and Concrete Composites, 28*(5), 475-480.

Nambiar EKK, Ramamurthy K (2006b). Models relating mixture composition to the density and strength of foam concrete using response surface methodology. *Cement and Concrete Composites, 28*(9), 752-760.

Nambiar EKK, Ramamurthy K (2007a). Air-void characterisation of foam concrete. *Cement and Concrete Research, 37*(2), 221-230.

Nambiar EKK, Ramamurthy K (2007b). Sorption characteristics of foam concrete. *Cement and Concrete Research*, *37*(9), 1341-1347.

Nambiar EKK, Ramamurthy K (2008). Fresh state characteristics of foam concrete. *Journal of Materials in Civil Engineering, 20*(2), 111-117.

Nambiar EKK, Ramamurthy K (2009). Shrinkage behavior of foam concrete. *Journal of Materials in Civil Engineering, 21*(11), 631-636.

Nandi S, Chatterjee A, Samanta P, Hansda T (2016). Cellular concrete and its facets of application in civil engineering. *International Journal of Engineering Research, 5*(1), 37-43.

Narayanan JS, Ramamurthy K (2012). Identification of set-accelerator for enhancing the productivity of foam concrete block manufacture. *Construction and Building Materials, 37*, 144-152.

Narayanan N, Ramamurthy K (2000a). Microstructural investigations on aerated concrete. *Cement and Concrete Research, 30,* 457–64.

Narayanan N, Ramamurthy K (2000b). Structure and properties of aerated concrete: A review. *Cement and Concrete Composites, 22*(5), 321-329.

National Ready Mixed Concrete Association (2003). *Concrete in practice.* Retrieved from http://www.nrmca.org/aboutconcrete/cips/

Nehdi M, Djebbar Y, Khan A (2001). Neural network model for preformed-foam cellular concrete. *Materials Journal*, *98*(5), 402-409.

Nehdi M, Djebbar Y, Khan A (2001). Neural network model for preformed-foam cellular concrete. Materials Journal, 98(5), 402-409.

Neto AAM, Cincotto MA, Repette W (2008). Drying and autogenous shrinkage of pastes and mortars with activated slag cement. *Cement and Concrete Research*, *38*(4), 565-574.

Neufeld R, Vallejo L, Hu W, Latona M, Carson C, Kelly C (1994). Properties of high fly ash content cellular concrete. *Journal of Energy Engineering, 120*(1), 35-48.

Neville AM (1963). *Properties of Concrete.* New York: John Wiley and Sons Inc.

Neville AM (2006). *Concrete: Neville's insights and issues.* London: Thomas Telford Publishing.

Neville AM (1959). Role of cement in the creep of mortar. In *Journal Proceedings, 55*(3), 963-984.

Neville AM (1960). Recovery of creep and observations on the mechanism of creep of concrete. *Applied Scientific Research*, *9*(1), 71.

Ng SC, Low KS, Lim SK (2011). Thermal insulation performance of aerated lightweight concrete. *Proceedings of the Institution of Civil Engineers—Construction Materials*, *164*(4), 181-189.

Nguyen DT (2014). *Microindentation creep of calcium-silicate-hydrate and secondary hydrated cement systems* (Doctoral dissertation). University of Ottawa.

Nguyen DT, Alizadeh R, Beaudoin JJ, Pourbeik P, Raki L (2014). Microindentation creep of monophasic calcium-silicate-hydrates. *Cement and Concrete Composites*, *48*, 118-126.

O'Reilly D (2009). Lightweight Cellular Concrete Debuts in Ontario Road Project. *Journal of Commerce*, 16-17.

Odler I, Abdul-Maula S (1987). Investigations on the relationship between porosity structure and strength of hydrated Portland cement pastes III. effect of clinker composition and gypsum addition. *Cement and Concrete Research, 17*(1), 22-30.

Odler I, Rößler M (1985). Investigations on the relationship between porosity, structure and strength of hydrated Portland cement pastes: II. Effect of pore structure and of degree of hydration. *Cement and Concrete Research, 15*(3), 401-410.

Oliver A (1994). Rush to Stabilize Heathrow Chasm. *New Civil Engineer*, 4-5.

OPSS 1352 (1989). *Material Specification For Precast Concrete Barriers.* Ontario: Ontario Provincial Standards for Roads and Public Works.

Ozawa M (1983). *Internal Report on Aerated Autoclaved Concrete*. Tokyo, Japan: Misawa Homes Institute of Research and Development.

Pade C, Jakobsen UH, Elsen J (2002). A new automatic analysis system for analyzing the air void system in hardened concrete. *International cement microscopy association, Metropolis, Illinois Proceedings*, 204-213.

Pan Z, Fujiwara H, Wee TH (2007). Preparation of high performance foamed concrete from cement, sand and mineral admixtures. *Journal of Wuhan University of Technology—Material Science Edition, 22*(2), 295-298.

Pan Z, Li H, Liu W (2014). Preparation and characterization of super low density foamed concrete from Portland cement and admixtures. *Construction and Building Materials, 72*, 256-261.

Panesar DK (2013). Cellular concrete properties and the effect of synthetic and protein foaming agents. *Construction and Building Materials, 44*, 575-584.

Papayianni I, Milud IA (2005). Production of foamed concrete with high calcium fly ash. In *Proceedings of the International Conference on the Use of Foamed Concrete in Construction; Dundee, Scotland; 5 July 2005,* 23-28.

Park CH, Bobet A (2009). Crack coalescence in specimens with open and closed flaws: a comparison. *International Journal of Rock Mechanics and Mining Sciences*, *46*(5), 819-829.

Park SB, Yoon ES, Lee BI (1999). Effects of processing and materials variations on mechanical properties of lightweight cement composites. *Cement and Concrete Research, 29*(2), 193-200.

Pavoine A, Brunetaud X, Divet L (2012). The impact of cement parameters on Delayed Ettringite Formation. *Cement and Concrete Composites*, *34*(4), 521-528.

Pelisser F, Gleize PJP, Mikowski A (2012). Effect of the Ca/Si molar ratio on the micro/nanomechanical properties of synthetic CSH measured by nanoindentation. The Journal of Physical Chemistry C, 116(32), 17219-17227.

Pellenq RJM, Kushima A, Shahsavari R, Van Vliet KJ, Buehler MJ, Yip S, Ulm FJ (2009). A realistic molecular model of cement hydrates. *Proceedings of the National Academy of Sciences*, *106*(38), 16102-16107.

Persson B (1999). Poisson's ratio of high-performance concrete. *Cement and concrete research*, *29*(10), 1647-1653.

Petit P, Javierre I, Jézéquel P, Biance A (2014). Generation and stability of bubbles in a cement based slurry. *Cement and Concrete Research, 60*, 37-44.

Petrov I, Schlegel E (1994). Application of automatic image analysis for the investigation of autoclaved aerated concrete structure. *Cement and concrete research*, *24*(5), 830-840.

Phani KK (1996a). Porosity-dependence of elastic properties and ultrasonic velocity in polycrystalline alumina—a model based on cylindrical pores. *Journal of materials science*, *31*(1), 262-266.

Phani KK (1996b). Porosity-dependence of ultrasonic velocity in sintered materials—a model based on the self-consistent spheroidal inclusion theory. *Journal of materials science*, *31*(1), 272-279.

Phani KK, Sanyal D (2005). Critical reevaluation of the prediction of effective Poisson's ratio for porous materials. *Journal of materials science*, *40*(21), 5685-5690.

Philip JR (1957). The theory of infiltration: 4. Sorptivity and algebraic infiltration equations. *Soil science*, *84(3)*, 257-264.

Philip JR (1969). Theory of infiltration. *Advances in Hydroscience*, *5*, 215-296.

Pickett G (1942). The effect of change in moisture-content on the crepe of concrete under a sustained load. In *Journal Proceedings, 38*, 333-356.

Pickford C, Crompton S (1996). Foamed concrete in bridge construction. *Concrete, 30*(6), 14-15.

Pignatelli I, Kumar, A, Alizadeh R, Le Pape Y, Bauchy M, Sant G (2016). A dissolution-precipitation mechanism is at the origin of concrete creep in moist environments. *The Journal of chemical physics*, *145*(5), 054701.

Pitroda J, Umrigar FS (2013). Evaluation of sorptivity and water absorption of concrete with partial replacement of cement by thermal industry waste (fly ash). *International Journal of Engineering and Innovative*, *2*(7), 245-249.

Pittsburg Corning (2009). *Foamglas® Insulation Systems: Industrial Applications.* Retrieved from http://www.insulation.org/mtl/pdfs/000256_494.pdf

Pittsburgh Corning (2013). *Foamglas® Wall Board T4+ Product Data Sheet.* Retrieved from http://www.foamglas.com/en/building/products/product_overview/foamglas_boards/#2-1-0

Pittsburgh Corning (n.d.). *Foamglas® Building: Corporate Brochure.* Retrieved from http://uk.foamglas.com/en/building/downloads/documentation/brochures

Plassard C, Lesniewska E, Pochard I, Nonat A (2007). Intrinsic elastic properties of Calcium Silicate Hydrates by nanoindentation. In *12th International Congress on the Chemistry of Cement*, 44.

Popovics S (1998). *Strength and related properties of concrete: A quantitative approach*. Hoboken, NJ: John Wiley & Sons.

Portland Cement Association (2001). *Ettringite formation and the performance of concrete* (No. 2166). Portland Cement Association.

Portland Cement Association (2015a). *Freeze-thaw resistance*. Retrieved from http://www.cement.org/for-concrete-books-learning/concrete-technology/durability/freeze-thaw-resistance

Portland Cement Association (2015b). *Ultra-high performance concrete.* Retrieved from http://www.cement.org/for-concrete-books-learning/concrete-technology/concrete-design-production/ultra-high-performance-concrete

Posi P, Ridtirud C, Ekvong C, Chammanee D, Janthowong K, Chindaprasirt P (2015). Properties of lightweight high calcium fly ash geopolymer concretes containing recycled packaging foam. *Construction and Building Materials, 94*, 408-413.

Powers TC (1949). The nonevaporable water content of hardened Portland-cement paste—Its significance for concrete research and its method of determination. *ASTM Bulletin 158*, 68-76.

Powers TC (1954). Void space as a basis for producing air-entrained concrete. *American Concrete Institute Journal Proceedings 50(5)*, 741-760.

Powers TC (1958a). Structure and physical properties of hardened Portland cement paste. *Journal of the American Ceramic Society 41*(1), 1-6.

Powers TC (1958b). The physical structure and engineering properties of concrete*. Portland Cement Association Research and Development Bulletin No. 90*. Chicago, Illinois: PCA.

Powers TC (1968). The thermodynamics of volume change and creep. *Matériaux et Construction, 1*(6), 487–507

Powers TC, Brownyard TL (1946). Studies of the physical properties of hardened Portland cement paste. *American Concrete Institute Journal Proceedings 43 (9)*, 101-132.

Powers TC, Copeland LE, Mann HM (1959). Capillary continuity or discontinuity in cement pastes. *Journal of the Portland Cement Research and Development Laboratories, 1*(2), 38-48.

Powers TC, Helmuth RA (1953). Theory of volume changes in hardened portland-cement paste during freezing. In *Highway research board proceedings, 46*.

Powers TC, Willis TF (1949). The air requirement of frost resistant concrete. In *Highway Research Board Proceedings, 29*, 184–211.

Prim P, Wittmann FH (1983). Structure and water absorption of aerated concrete. *Autoclaved aerated concrete, moisture and properties*, 55-69.

Proshin A, Beregovoi VA, Beregovoi AM, Eremkin AI (2005). Unautoclaved foam concrete and its constructions, adopted to the regional conditions. In *Proceedings of the International Conference on the Use of Foamed Concrete in Construction; Dundee, Scotland; 5 July 2005,* 113-120.

Qin B, Lu Y (2015). Experimental investigation of closed porosity of inorganic solidified foam designed to prevent coal fires. *Advances in Materials Science and Engineering*, 1-9.

Raden MAMA, Hamidah MS (2012). Strength characteristic of foamed geopolymer concrete. In *Proceedings of the 11th International Conference on Concrete Engineering and Technology*; *Putrajaya, Malaysia; 11-14 June 2012.*

Ramamurthy K, Nambiar EKK, Indu Siva Ranjani G (2009). A classification of studies on properties of foam concrete. *Cement and Concrete Composites, 31*(6), 388-396.

Ramamurthy K, Narayanan N (2000a). Factors influencing the density and compressive strength of aerated concrete. *Magazine of Concrete Research, 52*(3), 163-168.

Ramamurthy K, Narayanan N (2000b). Influence of composition and curing on drying shrinkage of aerated concrete. *Materials and Structures*, *33*(4), 243-250.

Regan PE, Arasteh AR (1984). Lightweight aggregate foamed concrete. *Low-cost and energy saving materials, 42(1)*, 123-138.

Regan PE, Arasteh AR (1990). Lightweight aggregate foamed concrete. *Structural Engineer*, *68*, 167-73.

Remadnia A, Dheilly RM, Laidoudi B, Quéneudec M (2009). Use of animal proteins as foaming agent in cementitious concrete composites manufactured with recycled PET aggregates. *Construction and Building Materials*, *23(10),* 3118-3123.

Rice JA (1929). *U.S. Patent No. 1,717,319*. Washington, DC: U.S. Patent and Trademark Office.

Rice JA (1930). *U.S. Patent No. 1,749,508*. Washington, DC: U.S. Patent and Trademark Office.

Rice JA (1930). *U.S. Patent No. 1,769,275*. Washington, DC: U.S. Patent and Trademark Office.

Rice JA (1931). *U.S. Patent No. 1,788,592*. Washington, DC: U.S. Patent and Trademark Office.

Rice JA (1931). *U.S. Patent No. 1,826,897*. Washington, DC: U.S. Patent and Trademark Office.

Rice JA (1932). *U.S. Patent No. 1,856,294*. Washington, DC: U.S. Patent and Trademark Office.

Rice JA (1936). *U.S. Patent No. 2,053,842*. Washington, DC: U.S. Patent and Trademark Office.

Rice JA (1937). *U.S. Patent No. 2,069,078*. Washington, DC: U.S. Patent and Trademark Office.

Rice JA (1937). *U.S. Patent No. 2,089,813*. Washington, DC: U.S. Patent and Trademark Office.

Rice RW (1977). Microstructure dependence of mechanical behavior of ceramics. *Treatise on Materials Science and Technology 11*, 199-381.

Rice RW (1993). Comparison of stress concentration versus minimum solid area based mechanical property-porosity relations. *Journal of materials science*, *28*(8), 2187-2190.

Richard AO, Ramli M (2013). Experimental production of sustainable lightweight foamed concrete. *British Journal of Applied Science & Technology*, *3*(4), 994.

Richard T, Dobogai J, Gerhardt T, Young W (1975). Cellular concrete: A potential load-bearing insulation for cryogenic applications? *IEEE Transactions on Magnetics*, *11*(2), 500-503.

Richardson IG (2014). Model structures for C-(A)-S-H(I). *Acta Crystallographica Section B: Structural Science, Crystal Engineering and Materials*, *70*(6), 903-923.

Rickard EM, Rice JA (1929). *U.S. Patent No. 1,716,932*. Washington, DC: U.S. Patent and Trademark Office.

Riding KA, Esmaeily A, Vosahlik J (2015). *Air void clustering* (No. K-TRAN: KSU-13-6). Kansas Department of Transportation.

RILEM Technical Committees 78-MCA and 51-ALC (1993). *Autoclaved Aerated Concrete: Properties, Testing and Design.* London: E & FN Spon.

Ringot E, Bascoul A (2001). About the analysis of microcracking in concrete. *Cement and concrete composites*, *23*(2-3), 261-266.

Roslan AF, Awang H, Mydin MAO (2013). Effects of various additives on drying shrinkage, compressive and flexural strength of lightweight foamed concrete (LFC). *Advanced Materials Research* (626), 594-604.

Ross AD (1936). *Creep of concrete under load with special reference to the use of Portland-blast furnace cement.* (Doctoral dissertation.) Edinburgh University.

Rossen JE, Lothenbach B, Scrivener KL (2015). Composition of C-S-H in pastes with increasing levels of silica fume addition. *Cement and Concrete Research*, *75*, 14-22.

Rößler M, Odler I (1985). Investigations on the relationship between porosity, structure and strength of hydrated Portland cement pastes: I. Effect of porosity. *Cement and Concrete Research, 15*(2), 320-330.

Roy DM, Grutzeck MW, Shi D, Lui G (1993). *Cement paste aggregate interface microstructure.* Washington, DC: National Research Council.

Ruetz W (1968). A hypothesis for the creep of hardened cement paste and the influence of simultaneous shrinkage. *Proceedings of the Structure of Concrete and its Behavior under Load*, 365-387.

Ruiwen K (2004). *Properties of high-strength foam concrete* (Masters thesis.) National University of Singapore.

Ruiz MF, Muttoni A, Gambarova PG (2007). Relationship between nonlinear creep and cracking of concrete under uniaxial compression. *Journal of Advanced Concrete Technology*, *5*(3), 383-393.

Russell HG, Graybeal BA, Russell HG (2013). *Ultra-high performance concrete: a state-of-the-art report for the bridge community* (No. FHWA-HRT-13-060). United States. Federal Highway Administration. Office of Infrastructure Research and Development.

Ryshkewitch E (1953). Compression strength of porous sintered alumina and zirconia. *Journal of the American Ceramic Society*, *36*(2), 65-68.

Safiuddin M, Hearn N (2005). Comparison of ASTM saturation techniques for measuring the permeable porosity of concrete. *Cement and Concrete Research*, *35*(5), 1008-1013.

Saikia N, de Brito J (2014). Mechanical properties and abrasion behaviour of concrete containing shredded PET bottle waste as a partial substitution of natural aggregate. *Construction and Building Materials, 52*, 236-244.

Salvoldi BG, Beushausen H, Alexander MG (2015). Oxygen permeability of concrete and its relation to carbonation. *Construction and Building Materials, 85*, 30-37.

Sammis CG, Ashby MF (1986). The failure of brittle porous solids under compressive stress states. *Acta metallurgica*, *34*(3), 511-526.

Sas J (2015). The common sense proposition of phasing out Alberta's coal plants. *The Broadbent Institute.* Retrieved from http://www.broadbentinstitute.ca/50417/the_common_sense_proposition_of_phasing_out_alberta_s_coal_plants

Sayadi AA, Vilches TJ, Neitzert TR, Clifton GC (2016a). Effectiveness of foamed concrete density and locking patterns on bond strength of galvanized strip. *Construction and Building Materials, 115*, 221-229.

Sayadi AA, Vilches TJ, Neitzert TR, Clifton GC (2016b). Effects of expanded polystyrene (EPS) particles on fire resistance, thermal conductivity and compressive strength of foamed concrete. *Construction and Building Materials, 112*, 716-724.

Sayadi AA, Vilches TJ, Neitzert TR, Clifton GC (2016c). Strength of bearing area and locking area of galvanized strips in foamed concrete. *Construction and Building Materials, 114*, 56-65.

Schackow A, Effting C, Folgueras MV, Güths S, Mendes GA (2014). Mechanical and thermal properties of lightweight concretes with vermiculite and EPS using air-entraining agent. *Construction and Building Materials, 57*, 190-197.

Scheiner S, Hellmich C (2009). Continuum microviscoelasticity model for aging basic creep of early-age concrete. *Journal of engineering mechanics*, *135*(4), 307-323.

Schiller KK (1971). Strength of porous materials. *Cement and Concrete Research*, *1*(4), 419-422.

Schober G (1992). Effect of size distribution of air pores in AAC on compressive strength. In *Proceedings of the 3rd International Symposium on autoclaved aerated concrete: Advances in Autoclaved Aerated Concrete; Zurich, Switzerland;* 77-81.

Scrivener K (2004). Preface. In *Proceedings of the International RILEM TC 186-ISA Workshop on Internal Sulfate attack and Delayed Ettringite Formation; Villars, Swizterland; 4-6 September 2002, XI-XIII*.

Scrivener KL, Crumbie AK, Laugesen P (2004). The interfacial transition zone (ITZ) between cement paste and aggregate in concrete. *Interface science*, *12*(4), 411-421.

Senbu O, Kamada E (1990). Mechanism and evaluation method of frost deterioration of cellular concrete, durability of building materials and components. In *Proceedings of the 5th International Conference on the Durability of Building Materials and Components; Brighton, United Kingdom; 7-9 November 1990;* 241-246.

Sengul O, Azizi S, Karaosmanoglu F, Tasdemir MA (2011). Effect of expanded perlite on the mechanical properties and thermal conductivity of lightweight concrete. *Energy & Buildings, 43*(2-3), 671-676.

Shah SP, Choi S, Jansen DC (1996). Strain softening of concrete in compression. *Proceedings of Fracture Mechanics of Concrete Structures*, *3*, 1827-1841.

Shah SP, Slate FO (1968). Internal microcracking, mortar-aggregate bond and the stress-strain curve of concrete. *Proceedings of International Conference of the Cement & Concrete Association*, 82-92.

Shams A, Horstmann M, Hegger J (2014). Experimental investigations on textile-reinforced concrete (TRC) sandwich sections. *Composite Structures, 118*, 643-653.

Shams A, Stark A, Hoogen F, Hegger J, Schneider H (2015). Innovative sandwich structures made of high performance concrete and foamed polyurethane. *Composite Structures, 121*, 271-279.

Sharipudin SS, Ridzuan ARM, Saman HM (2012). Performance of foamed concrete with waste paper sludge ash (WPSA) and fine recycled concrete aggregate (FRCA) contents. *International Journal of Sustainable Civil Engineering 1*(2), 19-27

She W, Chen Y, Zhang Y, Jones MR (2013). Characterization and simulation of microstructure and thermal properties of foamed concrete. *Construction and Building Materials, 47*, 1278-1291.

She W, Zhang Y, Jones MR (2014a). Three-dimensional numerical modeling and simulation of the thermal properties of foamed concrete. *Construction and Building Materials, 50*, 421-431.

She W, Zhang Y, Jones MR (2014b). Using the ultrasonic wave transmission method to study the setting behavior of foamed concrete. *Construction and Building Materials, 51*, 62-74.

She W, Zhang Y, Jones MR, Guo P (2013). In-situ monitoring the setting behavior of foamed concrete using ultrasonic pulse velocity method. *Journal of Wuhan University of Technology—Material Science Edition, 28*(6), 1146-1154.

Shebl FA, Helmy FM, Ludwig U (1985). A new approach on the hydration mechanism of tricalcium silicate. *Cement and Concrete Research*, *15*(5), 747-757.

Shi C (2002). *U.S. Patent No. 6,488,762*. Washington, DC: U.S. Patent and Trademark Office.

Shi X, She W, Zhou H, Zhang Y, Shi F, Chen W (2012). Thermal upgrading of hui-style vernacular dwellings in china using foam concrete. *Frontiers of Architectural Research, 1*, 23-33.

Short A, Kinniburgh W (1978). *Lightweight Concrete, 3rd Edition.* Essex: Applied Science Publishers Ltd.

Shu X, Huang B, Wu H, Dong Q, Burdette EG (2011). Performance comparison of laboratory and field produced pervious concrete mixtures. *Construction and Building Materials*, *25*(8), 3187-3192.

Shuraim AB, Aslam F, Rizwan Hussain R, Alhozaimy AM (2016). Coupled effect of coarse aggregate type and silica fume on creep coefficients of high-strength concrete. *Journal of Materials in Civil Engineering*, *28*(12), 04016159.

Siddique R (2011). Utilization of silica fume in concrete: Review of hardened properties. *Resources, Conservation and Recycling*, *55*(11), 923-932.

Simha KRY, Fourney WL, Barker DB, Dick RD (1986). Dynamic photoelastic investigation of two pressurized cracks approaching one another. *Engineering fracture mechanics*, *23*(1), 237-249.

Sinha D (2014). Evaluation of Cementing Efficiency of Flyash in Concrete. *International Journal of Emerging Technology and Advanced Engineering, 4*(5), 44-49.

Sinica M, Dudik A, Laukaitis A, Sezeman G (2000). Reinforcement influence on non-autoclave foam cement concrete strength characteristics. *Statyba, 6*(3), 169-174.

Siram KKB (2013). Foam Concrete: the present generation's building solution. *International Journal of Civil, Structural, Environmental and Infrastructure Engineering Research and Development 3*(4), 59-62.

Slate FO, Hover KC (1984). Microcracking in concrete. In: *Fracture mechanics of concrete: Material characterization and testing.* Carpinteri A., Ingraffea A.R. (eds). Engineering Application of Fracture Mechanics, 3. Springer, Dordrecht.

Šmilauer V, Bažant ZP (2010). Identification of viscoelastic CSH behavior in mature cement paste by FFT-based homogenization method. *Cement and Concrete Research*, *40*(2), 197-207.

Smith J (2014). McInnis Cement Update. *Cement Americas News.* Retrieved from http://www.cementamericas.com/features/835-mcinnis-cement-update.html

Sommerville J, Craig N, Charles A (2010). The performance characteristics of no-fines concrete in social housing. In *Construction, Building and Real Estate Research Conference of the Royal Institution of Chartered Surveyors; Paris, France; 2-3 September 2010.*

Song G, Wang L, Deng L, Yin HM (2015). Mechanical characterization and inclusion based boundary element modeling of lightweight concrete containing foam particles. *Mechanics of Materials, 91*, 208-225.

Song Y (2014). *Analysis of air-void system in hardened concrete from a three-dimensional perspective.* (Masters thesis.) University of Illinois.

Stengel T, Reger J, Heinz D. (2009). Life cycle assessment of geopolymer concrete: what is the environmental benefit? In *Proceeding of the 24th Biennial Conference of the Concrete Institute of Australia; Sydney, Australia; 17-19 September 2009.*

Stoll R, Holm T (1985). Expanded shale lightweight fill: Geotechnical properties. *Journal of Geotechnical Engineering, 111*(8), 1023-1027.

Straube B, Walther H (2011). *AAC with low thermal conductivity*. Kloster Lehnin, Germany: Xella Technologie- und Forschugsgesellschaft mbH, 371-374. Retrieved from https://www.xella.com/de/docs/SKMBT_C253_12091713140.pdf

Straube JF (2011). *BSD-011: Thermal Control in Buildings*. Retrieved from http://buildingscience.com/documents/digests/bsd-011-thermal-control-in-buildings

Su L, Wang YF, Mei SQ, Li PF (2017). Experimental investigation on the fundamental behavior of concrete creep. *Construction and Building Materials*, *152*, 250-258.

Sun J (2013). Strength criterion for ecological light porous concrete under multiaxial stress. *Construction and Building Materials, 44*, 663-670.

Superbuild International Limited (2013). *History: Autoclaved Aerated Concrete*. Retrieved from http://www.superbuild.co.nz/about/history_AAC.html

Sutcu M, Ozturk S, Yalamac E, Gencel O (2016). Effect of olive mill waste addition on the properties of porous fired clay bricks using Taguchi method. *Journal of Environmental Management*, *181*, 185-192.

Swamy RN (1971). Dynamic Poisson's ratio of portland cement paste, mortar and concrete. *Cement and Concrete Research*, *1*(5), 559-583.

Tada S (1986). Material design of aerated concrete—An optimum performance design. *Materials and Structures, 19*(1), 21-26.

Tam CT, Lim TY, Sri Ravindrarajah R, Lee SL (1987). Relationship between strength and volumetric composition of moist-cured cellular concrete. *Magazine of Concrete Research, 39*(138), 12-18.

Tang WC, Lo Y, Nadeem A (2008). Mechanical and drying shrinkage properties of structural-graded polystyrene aggregate concrete. *Cement and Concrete Composites, 30*(5), 403-409.

Tang ZB, Zhao YL, Kong DS, Kan D (2013). Study and application of a new type of foamed concrete wall in coal mines. *Journal of Coal Science and Engineering (China), 19*(3), 345-352.

Tanyildizi H (2014). Post-fire behavior of structural lightweight concrete designed by Taguchi method. *Construction and Building Materials, 68*, 565-571.

Tapia JV (2013). *The development of novel infill materials for composite structural assemblies.* (Master thesis.) Auckland University of Technology.

Tarasov AS, Kearsley EP, Kolomatskiy AS, Mostert HF (2010). Heat evolution due to cement hydration in foamed concrete. *Magazine of Concrete Research, 62*(12), 895-906.

Tarasov AS, Lesovik VS and Kolomatskiy AS (2005). Industrial manufacture of foamed concrete products. In *Proceedings of the International Conference "Poreconcrete 2005"; Belgorod, Russia,* 128–143.

Tasdemir C (2003). Combined effects of mineral admixtures and curing conditions on the sorptivity coefficient of concrete. *Cement and Concrete Research, 33*(10), 1637-1642.

Taylor HFW, Famy C, Scrivener KL (2001). Delayed ettringite formation. *Cement and concrete research*, *31*(5), 683-693.

Taylor RW (1991). *Foamed Concrete for Improved Trench Reinstatements*. British Cement Association.

TEC Services Inc. (2011). *Final report: Stable Air, air-entraining admixture—Compliance verification.* Lawrenceville, Georgia.

The Aberdeen Group (1961). *Publication #C610196: No fines concrete.* Boston, Massachusetts: The Aberdeen Group.

The Aberdeen Group (1981). *Publication #C810247: At the high end of the lightweight concrete spectrum: Structural lightweight concrete.* Boston, Massachusetts: The Aberdeen Group.

The Concrete Society (2016a). *Delayed ettringite formation (DEF)*. Retrieved from http://www.concrete.org.uk/fingertips-nuggets.asp?cmd=display&id=932

The Concrete Society (2016b). *Foamed concrete: Examples of use*. Retrieved from http://www.concrete.org.uk/fingertips-nuggets.asp?cmd=display&id=359

Thomas JJ, Jennings HM (2001). Chemical Aging and the Colloidal Structure of the CSH-Gel: Implications for creep and shrinkage. In *Proceedings of The Sixth International Conference on creep, shrinkage and durability mechanics of concrete and other quasi-brittle materials; 20-22 August 2001; Cambridge, Massachusetts*; 33-38.

Thomas RJ, Ye H, Radlinska A, Peethamparan S (2016). Alkali-activated slag cement concrete. *Concr. Int*, *38*(1), 33-38.

Thunuguntla CS, Rao TG (2018). Effect of mix design parameters on mechanical and durability properties of alkali activated slag concrete. *Construction and Building Materials*, *193*, 173-188.

Tian T, Yan Y, Hu Z, Xu Y, Chen Y, Shi J (2016). Utilization of original phosphogypsum for the preparation of foam concrete. *Construction and Building Materials, 115*, 143-152.

Tian X, Zhang D, Niu Y (2016). Mechanical and energy absorption properties of foamed concrete under one-dimension strain compression. *Modern Applied Science*, *10*(7), 195.

Tikalsky PJ, Pospisil J, MacDonald W (2004). A method for assessment of the freeze–thaw resistance of preformed foam cellular concrete. *Cement and concrete research*, *34*(5), 889-893.

Tittarelli F, Carsana M, Bellezze T (2013). Corrosion behavior of reinforced no-fines concrete. *Corrosion Science, 70*, 119-126.

Tittarelli F, Carsana M, Ruello ML (2014). Effect of hydrophobic admixture and recycled aggregate on physical–mechanical properties and durability aspects of no-fines concrete. *Construction and Building Materials, 66*, 30-37.

Tom J, Weiss C Jr, Malone P, Virostek A (2003). Durable roadside protective structures for low-volume roads. *Transportation Research Record: Journal of the Transportation Research Board*, (1819), 221-224.

Tong S, Li H, Zingre KT, Wan MP, Chang VWC, Wong SK, Toh WBT, Lee IYL (2014). Thermal performance of concrete-based roofs in tropical climate. *Energy & Buildings, 76*, 392-401.

Tonyan T, Gibson L (1992a). Strengthening of cement foams. *Journal of Materials Science, 27*(23), 6379-6386.

Tonyan T, Gibson L (1992b). Structure and mechanics of cement foams. *Journal of Materials Science, 27*(23), 6371-6378.

Topcu İB, Işikdağ B (2007). Manufacture of high heat conductivity resistant clay bricks containing perlite. *Building and Environment, 42*(10), 3540-3546.

Topcu İB, Işikdağ B (2008). Effect of expanded perlite aggregate on the properties of lightweight concrete. *Journal of Materials Processing Technology, 204*, 34-38.

Torrans PH, Ivey DL (1968). Review Of Literature on Air Entrained Concrete. Texas: Texas Transportation Institute, A&M University.

Troxell GE (1958). Long-time creep and shrinkage tests of plain and reinforced concrete. In *ASTM Proceedings 58*, 1101-1120.

Tulin LG (1965). *Creep of a Portland cement mortar as a function of stress-level and time.* (Doctoral dissertation). Iowa State University.

Turner M (2001). Fast set foamed concrete for same day reinstatement of openings in highways. In *Proceedings of One-Day Seminar on Foamed Concrete: Properties, Applications and Latest Technological developments; Leicestershire, UK; July 2001,* 12-18.

Uddin N, Fouad F, Vaidya UK, Khotpal A, Serrano-Perez JC (2006). Structural characterization of hybrid fiber reinforced polymer (FRP)-autoclave aerated concrete (AAC) panels. *Journal of reinforced plastics and composites*, *25*(9), 981-999.

UK Aircrete Products Association (2016). *Aircrete Sustainable Building Blocks*. Retrieved from http://www.aircrete.co.uk/

Ulm FJ, Le Maou F, Boulay C (1999). Creep and shrinkage coupling: new review of some evidence. *Revue française de génie civil*, *3*(3-4), 21-37.

US Department of Commerce (2016). *US and World Population Clock.* Retrieved from http://www.census.gov/popclock/

US Energy Information Administration (2016). Layer: Coal Power Plants. *U.S. Energy Mapping System.* Retrieved from http://www.eia.gov/state/maps.cfm

Valenza JJ, Scherer GW (2006). Mechanism for salt scaling. *Journal of the American Ceramic Society*, *89*(4), 1161-1179.

Valore RC (1954a). Cellular Concretes: Part 1, Composition and Methods of Preparation. *Journal of the American Concrete Institute*, 773-796.

Valore RC (1954b). Cellular Concretes: Part 2, Physical Properties. *Journal of the American Concrete Institute*, 817-836.

Valore RC (1961). Foam and gas concretes. In *Structural Foams: Procedings of the Building Research Institute; Washington, DC; Fall 1960;* National Academy of Sciences—National Research Council, 5-29

Valore RC (1980). Calculation of U-values of hollow concrete masonry. *Concrete International, 2*(2)*,* 40-63.

Valori A, McDonald PJ, Scrivener KL (2013). The morphology of C–S–H: Lessons from 1H nuclear magnetic resonance relaxometry. *Cement and Concrete Research*, *49*, 65-81.

Van Breugel K (1995). Numerical simulation of hydration and microstructural development in hardening cement-based materials (I) theory. *Cement and concrete research*, *25*(2), 319-331.

Van Deijk S (1991). Foam concrete: A review of the Netherlands approach to the use of foam concrete in Holland and at Canary Wharf. *Concrete, 25*(5), 49-54.

Van Mier JG, Man HK (2009). Some notes on microcracking, softening, localization, and size effects. *International Journal of Damage Mechanics, 18*(3), 283-309.

Van Mier JGM, Shah SP, Arnaud M, Balayssac JP, Bascoul A, Choi S, Karihaloo BL (1997). Strain-softening of concrete in uniaxial compression. *Materials and Structures*, *30*(4), 195-209.

van Oss HG (2004). Slag—iron and steel. *U.S. Geological Survey Minerals Yearbook.* Washington, DC: U.S. Department of the Interior. Retrieved from http://minerals.usgs.gov/minerals/pubs/commodity/iron_&_steel_slag/islagmyb04.pdf

Vandamme M, Ulm FJ (2009). Nanogranular origin of concrete creep. *Proceedings of the National Academy of Sciences*, *106*(26), 10552-10557.

Vandamme M, Ulm FJ (2013). Nanoindentation investigation of creep properties of calcium silicate hydrates. *Cement and Concrete Research*, *52*, 38-52.

Vassilev DG (2012). *Evaluation of Test Methods for De-icer Scaling Resistance of Concrete* (Doctoral dissertation). University of Toronto.

Verbeck G (1958). Carbonation of hydrated Portland cement. In *Cement and Concrete*. ASTM International.

Verbeck GJ, Klieger P (1957). Studies of 'salt' scaling of concrete. *Highway Research Board Bulletin, 150*, 1-13.

Vonk RA (1992). *Softening of concrete loaded in compression.* (Doctoral dissertation.) Technische Universiteit Eindhoven.

Vonk RA (1993). *A Micromechanical Investigation of Softening of Concrete Loaded in Compression*. Stevin-Laboratory of the Faculty of Civil Engineering, University of Technology. Technische Universiteit Eindhoven.

Wahlman T (1991). Skumbetong i mark: Latt och stabil. (Foam concrete in soil: Light and stable.) *Cementa* (1). Retrieved from http://www.aercrete.se/eng/down1.html

Walter E (1935). *U.S. Patent No. 2,006,425*. Washington, DC: U.S. Patent and Trademark Office.

Wang EZ, Shrive NG (1993). On the Griffith criteria for brittle fracture in compression. *Engineering fracture mechanics*, *46*(1), 15-26.

Wang H, Chen W, Tan X, Tian H, Cao J (2012). Development of a new type of foam concrete and its application on stability analysis of large-span soft rock tunnel. *Journal of Central South University, 19*(11), 3305-3310.

Wang JC (1984a). Young's modulus of porous materials, Part 1: Theoretical derivation of modulus-porosity correlation. *Journal of materials science*, *19*(3), 801-808.

Wang JC (1984b). Young's modulus of porous materials, Part 2: Young's modulus of porous alumina with changing pore structure. *Journal of material science*, *19*(3), 809-814.

Warnock ACC (1985). Factors affecting sound transmission loss. *Canadian Building Digest 239*. Ottawa, Ontario: National Research Council of Canada.

Warren WE, Kraynik AM (1988). The linear elastic properties of open-cell foams. *Journal of Applied Mechanics, 55*(2), 341-346.

Warren WE, Kraynik AM (1991). The nonlinear elastic behavior of open-cell foams. *Journal of Applied Mechanics, 58*(2), 376-381.

Wee TH (2005). Recent developments in high-strength lightweight concrete with and without aggregates. In *Proceedings of the 3rd International Conference on Construction Materials: Performance, Innovations and Structural Implications and Mindess Symposium*; *Vancouver, Canada; 22-24 August 2005*.

Wee TH, Babu DS, Tamilselvan T, Lim HS (2006). Air-void system of foamed concrete and its effect on mechanical properties. *American Concrete Institute Materials Journal*, *103*(1), 45-52.

Wee TH, Daneti SB, Tamilselvan T (2011). Effect of w/c ratio on air-void system of foamed concrete and their influence on mechanical properties. *Magazine of Concrete Research, 63*(8), 583-595.

Weigler H, Karl S (1980). Structural lightweight aggregate concrete with reduced density: Lightweight aggregate foamed concrete. *The International Journal of Lightweight Concrete, 2*(2), 101-104.

Weil M, Dombrowski K, Buchawald A (2009). Life-cycle analysis of geopolymers. *Geopolymers, Structure, Processing, Properties and Applications.* Cambridge, UK: Woodhead Publishing Limited, 194-210.

Werkema T, Lovett W, Valore RC, Yntema LF (1961). Open forum discussion. In *Structural Foams: Procedings of the Building Research Institute; Washington, DC; Fall 1960;* National Academy of Sciences—National Research Council, 35-39.

WHD Microanalysis Consultants Ltd. (2016). *Autoclaved aerated concrete (AAC, Aircrete)*. Retrieved from http://www.understanding-cement.com/autoclaved-aerated-concrete.html

White JC, Agrawal SK (1993). *Soft ground arresting system for airports (DOT/FAA/CT-93/80).* Atlantic City, NJ: Federal Aviation Administration Technical Center.

Wienerberger Building Material Solutions (2014). *Porotherm Wall Solutions: Precision-made clay block walling system.* Cheadle, Cheshire, UK: Weinerberger Building Material Solutions.

Wienerberger Building Material Solutions (2016). *Product range Porotherm* . Retrieved from http://www.wienerberger.com/brands-products/porotherm-bricks-ceiling-system/product-range-porotherm

Wienerberger Building Material Solutions (n.d.). *Porotherm Best Practise Guide.* Dalton, North Yorkshire: Weinerberger Building Material Solutions. Retrieved from http://wienerberger.co.uk/about-us/porotherm-best-practice-guide.

Wilbur WW (1935). *U.S. Patent No. 2,023,800*. Washington, DC: U.S. Patent and Trademark Office.

Wimmer SA, Karr DG (1996). Compressive failure of microcracked porous brittle solids. *Mechanics of materials*, *22*(4), 265-277.

Wittmann FH (1973), Interaction of hardened cement paste and water, *American Ceramic Society, 56(8)*, 96-117.

Wittmann FH (1976). The structure of hardened cement-paste: A basis for a better understanding of the material properties. In *Hydraulic Cement Pastes: Their Structure and Properties: Proceedings of the Cement and Concrete Association Conference; Sheffield, England; 8-9 April 1976*, 96-117.

Wittmann FH (1982). Creep and shrinkage mechanisms. *Creep and shrinkage in concrete structures*, 129-161.

Wittmann FH (1983). Structure and Water Absorption of Aerated Concrete.

Wittmann FH (1986). Estimation of the modulus of elasticity of calcium hydroxide. *Cement and Concrete Research, 16*(6), 971-972.

Wittmann FH (1987). Structure of concrete and crack formation. In *Fracture of non-metallic materials*, Herrmann K.P., Larsson L.H. (eds), 309-340. Springer, Dordrecht.

Wittmann FH, Englert G (1968). Water in hardened cement paste. *Matériaux et Constructions, 1(6),* 535-546.

Wittmann FH, Roelfstra PE (1980). Total deformation of loaded drying concrete. *Cement and Concrete Research*, *10*(5), 601-610.

Wittmann FH, Roelfstra PE (1980). Total deformation of loaded drying concrete. *Cement and Concrete Research*, *10*(5), 601-610.

Wong JM, Glasser FP, Imbabi MS (2007). Evaluation of thermal conductivity in air permeable concrete for dynamic breathing wall construction. *Cement and Concrete Composites*, *29*(9), 647-655.

Wu Z, Chen B, Liu N (2013). Fabrication and compressive properties of expanded polystyrene foamed concrete: Experimental research and modeling. *Journal of Shanghai Jiaotong University (Science), 18*(1), 61-69.

Xella Aircrete North America, Inc. (2010). *Technical Manual for Builders and Architects.* Retrieved from http://www.hebel-usa.com/en/content/technical_manual_1795.php

Yakovlev G, Kerienė J, Gailius A, Girnienė I (2006). Cement based foam concrete reinforced by carbon nanotubes. *Materials Science [Medžiagotyra]*, *12*(2), 147-151.

Yakub I, Du J, Soboyejo WO (2012). Mechanical properties, modeling and design of porous clay ceramics. *Materials Science and Engineering: A*, *558*, 21-29.

Yamamoto M, Honda Y, Ogawa A, Rokugo K (2006). Fiber reinforced foamed mortar with multiple cracks in flexure. In Fischer G, Li VC (Eds.), *International RILEM Workshop on High Performance Fiber Reinforced Cementitious Composites in Structural Applications.* Bagneux, France: RILEM Publications SARL, 75-82.

Yang J, Jiang G (2003). Experimental study on properties of pervious concrete pavement materials. *Cement and Concrete Research, 33*(3), 381-386.

Yang KH, Lee KH (2015). Tests on high-performance aerated concrete with a lower density. *Construction and Building Materials, 74*, 109-117.

Yang KH, Lee KH, Song JK, Gong MH (2014). Properties and sustainability of alkali-activated slag foamed concrete. *Journal of Cleaner Production, 68*, 226-233.

Yap SP, Bu CH, Alengaram UJ, Mo KH, Jumaat MZ (2014). Flexural toughness characteristics of steel–polypropylene hybrid fibre-reinforced oil palm shell concrete, *Materials & Design, 57*, 652–659.

Ye H (2015). Creep mechanisms of calcium–silicate–hydrate: an overview of recent advances and challenges. *International Journal of Concrete Structures and Materials*, *9*(4), 453-462.

Ye H, Cartwright C, Rajabipour F, Radlińska A (2014). Effect of drying rate on shrinkage of alkali-activated slag cements. *4th International Conference on the Durability of Concrete Structures 24–26 July 2014*. Purdue University, West Lafayette, IN.

Ye H, Radlińska A (2017). Shrinkage mitigation strategies in alkali-activated slag. *Cement and Concrete Research*, *101*, 131-143.

Young JF, Mindess S, Gray RJ, Bentur A (1998). *The Science and Technology of Civil Engineering Materials.* Engelwood Cliffs, NJ: Prentice Hall, 221-222.

Yu C (2015). Foam Concrete Performance Study Based on Experimental Analysis. In *MATEC Web of Conferences, 25*, 04005. EDP Sciences.

Yu P, Kirkpatrick RJ, Poe B, McMillan PF, Cong X (1999). Structure of calcium silicate hydrate (C-S-H): near-, mid-, and far-infrared spectroscopy. *Journal of the American Ceramic Society*, *82*(3), 742-748.

Yu XG, Luo SS, Gao YN, Xiao H, Li DJ, Xu HC, Li F (2012). Microstructure, mineral phases and strength of foam concrete. In *Key Engineering Materials, 492*, 484-488.

Yuan J, Lindquist WD, Darwin D, Browning J (2015). Effect of slag cement on drying shrinkage of concrete. *Materials Journal, 112*(2), 267-276.

Yuan XH, Chen W, Lu ZA, Chen H (2014). Shrinkage compensation of alkali-activated slag concrete and microstructural analysis. *Construction and building materials*, *66*, 422-428.

Yue L, Bing C (2015). New type of super-lightweight magnesium phosphate cement foamed concrete. *Journal of Materials in Civil Engineering, 27*(1), 04014112.

Zaetang Y, Wongsa A, Sata V, Chindaprasirt P (2013). Use of lightweight aggregates in pervious concrete. *Construction and Building Materials*, *48*, 585-591.

Zawada JM (1998). *U.S. Patent No. 5,782,970*. Washington, DC: U.S. Patent and Trademark Office.

Zhang Y, Davy CA, Tricot G, Albert-Mercier C, Henry N, Bertier P, Cazaux F, Damidot D, Bourbon X (2017). On shrinkage and structure changes of pure and blended Portland concretes. *Journal of the American Ceramic Society*, *100*(9), 4131-4152.

Zhang YM, Jia LT, Mei H, Cui Q, Zhang PG, Sun ZM (2016). Fabrication, microstructure and properties of bricks fired from lake sediment, cinder and sewage sludge. *Construction and Building Materials*, *121*, 154-160.

Zhang Z, Provis JL, Reid A, Wang H (2014). Geopolymer foam concrete: An emerging material for sustainable construction. *Construction and Building Materials, 56*, 113-127.

Zhang Z, Provis JL, Reid A, Wang H (2015). Mechanical, thermal insulation, thermal resistance and acoustic absorption properties of geopolymer foam concrete. *Cement and Concrete Composites, 62*, 97-105.

Zhang Z, Scherer GW, Bauer A (2018). Morphology of cementitious material during early hydration. *Cement and Concrete Research, 107*, 85-100

Zhang Z, Wang H, Reid A, Aravinthan T (2011). Effects of fly ash source and curing procedure on strength development of geopolymers. In *Proceedings of the 21st Australasian Conference on the Mechanics of Structures and Materials (ACMSM 21); Melbourne, Australia,* 855-859.

Zhang ZQ, Yang JL, Li QM (2013). An analytical model of foamed concrete aircraft arresting system. *International Journal of Impact Engineering, 61*, 1-12.

Zhao X, Lim SK, Tan CS, Li B, Ling TC, Huang R, Wang Q (2015). Properties of Foamed Mortar Prepared with Granulated Blast-Furnace Slag. *Materials*, *8*(2), 462-473.

Zhao YH, Tandon GP, Weng GJ (1989). Elastic moduli for a class of porous materials. *Acta Mechanica*, *76*(1-2), 105-131.

Zhou J, Qian P, Chen X (2014). Stress-strain behavior of cementitious materials with different sizes. *The Scientific World Journal*, 2014.

Zimmerman RW (1992). Hashin-Shtrikman bounds on the Poisson ratio of a composite material. *Mechanics research communications*, *19*(6), 563-569.

Zollo RF, Hays CD (1998). Engineering Material Properties of a Fiber Reinforced Cellular Concrete. *ACI Materials Journal, 95(5)*, 631-635.

Zulkarnain F, Ramli M (2011). Durability of performance foamed concrete mix design with silica fume for housing development. *Journal of Materials Science and Engineering*, *5*(5).

Appendix A

Comprehensive Literature Review

Table of Contents

for Appendix A: Comprehensive Literature Review

List of Figures

List of Tables

A-1

Introduction

The following seven chapters provide a comprehensive state-of the art review for foam concrete.

Fundamentals of concrete mix design are reviewed in Chapter A-2. Chapter A-3 defines foam concrete in relation to other low-density cementitious products; and a history of foam concrete is provided in Chapter A-4. Chapter A-5 reviews the constituent ingredients, methods of foam production, and curing regimes used in the manufacture of foam concrete.

Chapter A-6 offers a summary of foam concrete properties, in plastic, curing, and hardened states, and summarizes what is known about controlling these parameters through mix design.

Chapter A-7 offers a comparison of several lightweight, mineral-bound materials which may be competitors for foam concrete in certain markets.

Finally, Chapter A-8 tabulates applications for foam concrete, significant foam concrete projects, and available data on the use of foam concrete in regions around the world.

A-2

Fundamentals of Concrete

A fundamental understanding of 'normal' concrete is helpful to the study of foam concrete. The characteristics of normal density, normal strength concrete are well researched, and relatively well understood. This established literature provides a basis for comprehending foam concrete chemistry, opportunities, and limitations.

As a general material class, concrete is the most used manufactured material in the modern world. By mass, its usage globally is second only to water. Each year humans use twice as much concrete than the total mass of all other building materials combined, including wood, steel, plastic and aluminum.[1] Approximately two tonnes of concrete are poured annually for each living human being, in structures such as roads, bridges, buildings, and mines.[2]

The vast majority of concrete has a density of approximately 2200 kg/m^3, and a compressive strength of between approximately 15 and 35 MPa, suitable for structural applications. The section below provides a general review of the constituents of normal density structural concrete, and their interactions during hydration and curing.

---

1 Ashby (2009) 17
2 Ashby (2009) 13, US Department of Commerce (2016)

2.1 Composition of Normal Density Structural Concrete

Concrete is classically understood as a composite of two parts: paste, and aggregate. The paste is a mixture of cementitious material, water, and air. A matrix of this paste surrounds and binds the loose aggregates, which are commonly classified as either 'coarse' or 'fine', based on grain size.

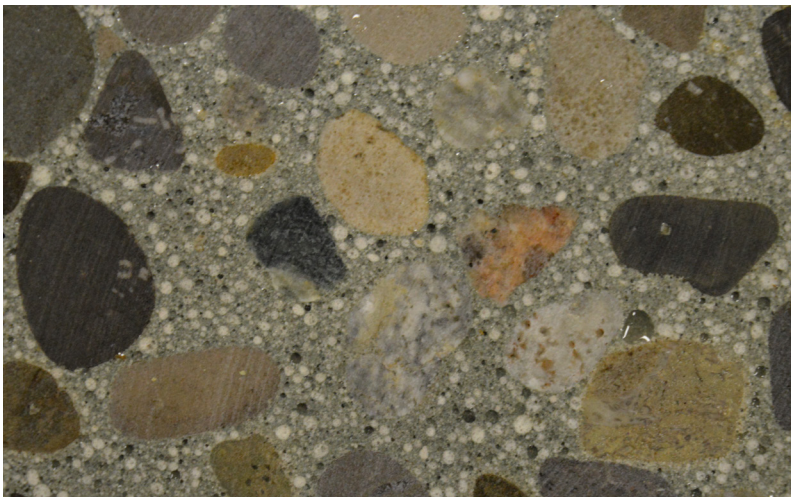

Figure A-2.1a Paste and aggregate visible in concrete section.

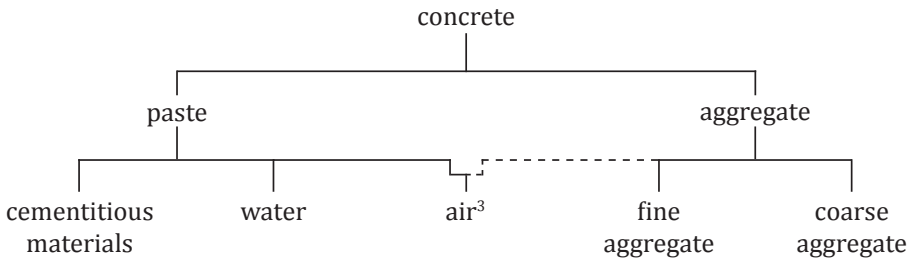

Figure A-2.1b Concrete as a composite of paste and aggregate.

The word *concrete* is derived from the Latin *concretus*, past participle of *concrescere*, 'to grow together.' The ingredients of concrete are bound together into a cohesive mass over time. The chemical reactions of the binders are especially vital to this process.

[3] Air is typically considered as part of the paste in concrete. Note, however, that air voids can be conceptualized as aggregate with zero density to help explain certain phenomena, e.g. the transition zones around air voids. Cf. Appendix A, Section 6.1.3b.

2.1.1 Binder

Portland cement

The typical, principal binder in most concrete production is Portland cement. It is produced by combining clay with chalk or limestone to produce a cement slurry; heating the slurry in a kiln to dry it, drive off carbon dioxide, and ultimately to recombine it chemically into clinker material;[4] and then grinding the clinker into angular particles between 1 and 50 μm in size.[5] The powder material consists primarily of calcium silicates (40 to 60% C_3S and 15 to 30% C_2S), and lesser proportions of calcium aluminates (C_3A and C_4AF). Quantities of gypsum (calcium sulfate) are added to the mix to prevent flash-setting of the other materials.

These anhydrous compounds react readily with water. As cement powder is mixed with water, a solution rich in calcium, sulfate, aluminate, and hydroxyl ions is produced.[6] Within minutes, thin calcium sulfoaluminate hydrate crystals, known as ettringite, begin to grow. Within hours, large crystal blocks of calcium hydroxide form, alongside an emerging fibrous network of calcium silica hydrates (C-S-H). The hydration reactions continue as long as moisture is present and temperature is favourable, causing the mix to stiffen and strengthen.

Ultimately, the network of calcium silicate hydrate (C-S-H) is the primary reaction product of cement hydration, accounting for up to 60 percent of the volume of cement paste. This compound of CaO, SiO_2, and H_2O varies significantly in its exact composition, and its internal crystal structure is uncertain.[7] However, it is responsible for many properties of concrete, as it continuously binds the concrete mix. Its strength is understood to be due to van der Waal attraction between layers with vast surface areas in the order of 700 m^2/g.[8]

Other crystalline compounds, and even unhydrated grains of cement, coated with crystals, may also exist within the cement paste. On their own, these hydration products are not as significant as C-S-H in influencing concrete properties. However, the presence of

4 Neville (1963) 4
5 Mehta (1986) 23
6 Mehta (1986) 23
7 Cf. Fabian (2006) 189, Mehta (1986) 24
8 Mehta (1986) 24

calcium hydroxide, which comprises 15% to 25% of the solid volume of a hardened Portland cement paste,[9] is significant when mixes include certain supplementary cementitious materials.

Supplementary cementitious materials

Supplementary cementitious materials (SCMs), also known as mineral admixtures, are powdered materials blended into a mix in addition to, or as a partial replacement for, Portland cement. SMCs include natural pozzolans, which are earth materials such as calcinated clay or shale, ground at normal temperatures,[10] and industry by-products such as fly ash, slag, and silica fume. Some SCMs contribute to the hardening of concrete through a hydraulic reaction, but many also contribute partially or entirely through pozzolanic activity.

In a pozzolanic reaction, fine siliceous or alumininosilicieous particles react with calcium hydroxide in the presence of water, to produce C-S-H and other compounds. Thus, the calcium hydroxide is transformed into a more beneficial reaction product within the concrete paste. Because this transformation of calcium hydroxide is a secondary reaction, for a given mix, replacing a portion of Portland with an SCM will often result in a slower hardening process, although in the long-term the strength may be greater.

In addition to their contribution to the production of C-S-H, SCMs offer further advantages to the mechanical, durability and transport properties of concrete. Slower setting reactions may help to suppress temperature rise due to heat of hydration, reducing risk of delayed ettringite formation. Spherically shaped particles may be a workability or pumping aid. Fine particles can improve particle packing, improving abrasion resistance, impermeability, and corrosion resistance of a hardened paste.

Risk of alkali-silica reactivity may be reduced with the use of SCMs. Alkali hydroxides are consumed by pozzolanic reaction in the early stages of hardening; subsequently, they are not available in the hardened paste to react with silica and form expansive reaction products that cause deterioration.[11]

---

9 Kosmatka et al. (2002) 40
10 Neville (1963) 1
11 Kosmatka et al. (2002) 135

There may also be economic and environmental benefits to using SCMs. For example, the most common SCMs in use today are derived from the byproducts of industrial processes, which would otherwise be landfilled.

The origins of various supplementary cementitious materials are noted below.

Fly ash production

Fly ash is produced by from the combustion of coal in electrical power generation plants. Carbon-based compounds are burned off to produce energy, while some incombustible impurities, such as minerals from clay, shale, or quartz, remain suspended is the exhaust gases. These impurities fuse into solid and hollow spherical particle, which may be collected electrostatically or through physical filters.

600 million kg of fly ash are produced worldwide each year. The majority of fly ash is disposed of in landfills and ash lagoons, while 20 to 30% is diverted and recycled, mainly in the production of concrete or plaster.

Two types of fly ash are differentiated in the North American concrete industry. Class F fly ash is derived from hard types of coal (i.e., Anthracite and Bituminous), producing low proportions of CaO (less than 20%). It is pozzolanic, and requires a cementing agent or a chemical activator to make a cementitious contribution. Class C fly ash is produced from less dense coal (i.e., Lignite and Sub-bituminous). It is pozzolanic, and it can also be self-cementing, as it contains higher proportions of CaO.

Due to variations in combustion and coal contents, the particle size distribution of fly ash varies significantly, with particles ranging in size from 0.5 to 300 μm. Typically, 70 to 90% of the mass of a sample consists of particles under 45 μm.

Ground granulated blast furnace slag production

Ground granulated blast furnace slag is created from iron blast furnace slag. Molten slag is rapidly chilled with streams of water or air to produce a sand-like glassy granulated material, which is then ground into particles of less than 45 μm in diameter. Rapid chilling produces a structure that is more disordered, and thus more reactive;[12] quenching and

[12] Mehta (1986) 272

chilling in water produces material with hydraulic properties.[13] Ground granulated blast furnace slag cooled with air requires an activator, such as NaOH or CaOH, to hydrate and set.

Silica fume production

Silica fume is the finest of particles. Like fly ash, this airbourne material has a spherical shape. It is collected from the manufacture of silicon or ferrosilicon alloys, when high purity quartz is reduced with coal in an electric arc furnace. The oxidized vapour rises, cools, condenses, and is collected in cloth bags.[14]

Ferrosilicon is used to deoxidize steel and ferroalloys to avoid loss of carbon content from molten steel; is utilized as an additive in the manufacture of cast iron to control silicone content, helping to promote a stable iron-graphite structure; and is used in electrode coating, electric motors, and transformer cores, among various other uses. Silicon is used in semi-conductor electronics, as well as in steel refining and aluminum casting.

Globally, production of silica fume is estimated at 1.5 million tons per year. Possibly 70 to 80% of this value will be filtered, collected, and available to industry. Most silica fume is produced in China, with additional production in Norway, Canada, the USA, South Aftrica, Spain, Russia, and France.[15]

Production of natural pozzolans

The most common natural pozzolans are calcinated clay, calcinated shale, and metakaolin. These materials are mined, processed in a kiln, and then ground into fine powder. As with all cementing materials, the crystal structures must be destroyed in order to produce good hydraulic or reactive properties.[16]

Agricultral wastes, such as, rice husk ash, may also be combusted to produce pozzolanic materials.[17]

---

13 Kosmatka et al. (2002) 59
14 Kosmatka et al. (2002) 60
15 Fidjestøl and Dåstøl (n.d.)
16 Mehta (1986) 269
17 Mehta (1986) 273

Properties of cementitious materials are summarized in the table below.

Additionally, Canadian and U.S. sources of Portland cement, fly ash, ground granulated blast furnace slag, and silica fume, are mapped in Appendix C.

	Portland Cement (type 10)		Fly Ash (class F)		Ground Granulated Blast Furnace Slag		Silica Fume	
Particle Size (µm)[18]	1 to 50		1 (low) 1-20 (typ) 100 (high)		less than 45		.1 (avg) 1 (high)	
Shape of Particles	Angular, solid		Spherical, solid or hollow		Angular, solid		Spherical	
Surface Area (m^2/kg)[19]	300-400		200 (low) 300-500 (typ) 700 (high)		400-600		15,000 (low) 20,000 30,000 (high)	
Specific gravity (relative density)[20]	3.15		2.38		2.85-2.95		2.20-2.25 (typ) 2.5 (high)	
Chemical composition (%)[21]	**SiO_2** Al_2O_3 Fe_2O_3 **CaO** SO_3 MgO	**20.5** 5.4 2.6 **63.9** 3.0 2.1	**SiO_2** **Al_2O_3** Fe_2O_3 CaO SO_3	**52** **23** 11 5 0.8	**SiO_2** Al_2O_3 Fe_2O_3 **CaO** SO_3	**35** 12 1 **40** 9	**SiO_2** Al_2O_3 Fe_2O_3 CaO SO_3	**90** 0.4 0.4 1.6 0.4
Effect on water demand[22]	N/A		-10% to +5%		-10% to -1%		increases	

Table A-2.1.1 Physical properties of various cementitious materials.

2.1.2 Water

Water is supplied in normal density concrete for cement hydration and for workability.

The proportion of water to cement in a mix, know as the water-cement ratio, significantly affects concrete quality.

Powers[23] established 0.26 as a theoretical optimal water-cement ratio for ordinary Portland cement concrete. Modern analysis of cement composition and reaction products indicates that for Type 10 cement, complete hydration will require a water-cement ratio

18 Kosmatka et al. (2002) 58-60, Mehta (1986) 23
19 Kosmatka et al. (2002) 58-60
20 Kosmatka et al. (2002) 62
21 Kosmatka et al. (2002) 42, 62
22 Kosmatka et al. (2002) 62
23 Powers (1949)

between 0.22 and 0.25.[24] In the industry, however, w/c values of approximately 0.40 are more typical, improving workability and increasing tolerance for real-life effects (e.g. evaporation during transport), ensuring that all cement grains are exposed to water. However, as water is added to a mix beyond the amount necessary for hydration, there is an increase in the total volume of the mix, and subsequently in the eventual porosity of the hardened paste, reducing strength.

Water exists in various forms within the cement paste: as capillary water, including 'free water' in relatively large pores, and water held in capillary tension in smaller pores; as adsorbed at solid surfaces; as interlayer water between sheets of C-S-H, held with hydrogen bonding; and as chemically combined water within the C-S-H phases themselves.[25] In smaller spaces water is most restrained, which affects patterns of drying shrinkage and freeze-thaw behaviour, as discussed in Sections 6.2.3 and 6.3.5d.

2.1.3 Aggregate

Despite its strength, hardened cement paste by itself is not a viable mass building material due to its high cost and the dimensional instability of C-S-H structures. Rather, aggregate must be incorporated into concrete as an inert filler material. Aggregates typically occupy 60 to 75% of the volume of concrete, and represent 70 to 85% of the mass.[26] Rock materials, such as sand and gravel, are commonly used, although various recycled and alternative materials may also be incorporated.

To produce strong concrete, each aggregate particle should be continuously surrounded by paste. Subsequently, a continuous gradation from fine to coarse particles makes efficient use of the cementitious paste in the mix.

[24] Kosmatka et al. (2002) 43
[25] Mehta (1986) 29
[26] Kosmatka et al. (2002) 79

Fine aggregate

Fine aggregate is usually 35 to 45% by mass or volume of the total aggregate content.[27] Natural sand, or crushed stone with most particles smaller than 4 or 5 mm, is typically used in normal density concrete.[28]

Fine aggregate must meet specific grading limits, which are related the intended purpose of the concrete, the richness of the mixture, and the maximum particle size of the coarse aggregate.[29]

Coarse Aggregates

Coarse aggregate typically represents 40 to 55% by mass or 35 to 50% by absolute volume of hardened concrete.[30] Ideally, the coarse aggregate particles should be of approximately the same strength and stiffness as the hardened cement paste. Natural gravel or crushed stone may be used, as well as various recycled crushed materials.

Particle shape and surface area has a strong influence on the properties of freshly mixed concrete. Mixes with angular, rough, elongated, or poorly graded aggregates may require a greater volume of paste to achieve the same workability as mixes with smooth or rounded aggregates.[31] However, with appropriate grading, angular or rounded aggregates offer essentially similar strength in hardened concrete, for the same aggregate type and cementitious density.

The transition zone between the coarse aggregates and paste is often critical to the strength of normal density concrete. High local water contents may be present at this interface, adjacent to the impervious aggregate, increasing the local porosity of the paste.[32] Use of larger aggregate tends to increase the local water content of the transition zone, and will typically reduce the strength of a mix, compared to a mix with the same total volume of smaller aggregates

The resistance of the aggregate to freeze-thaw action, acid and corrosive substances, and abrasion must be considered for certain concrete applications. Aggregate should also

---

27 Kosmatka et al. (2002) 80
28 Brady et al. (2001), Kosmatka et al. (2002) 79
29 Kosmatka et al. (2002) 83
30 Kosmatka et al. (2002) 80
31 Kosmatka et al. (2002) 87
32 Mehta (1986) 47

have a compatible wetting and drying properties to avoid developing strain in the paste or aggregate.[33]

	Fine Aggregate	Coarse Aggregate
Particle Size (μm)[34]	160 μm (low) <5 mm (typ) 10 mm (high)	1.25 mm (low) 10-40mm (typ) 112 mm (high)
Shape of Particles[35]	Angular improves bonding	Angular or rounded
Specific gravity (relative density)[36]	2.4 to 2.9 (typ)	2.4 to 2.9 (typ)

Table A-2.1.3 Physical properties of typical fine and coarse aggregate.

2.1.4 Air

Voids may exist at multiple scales within a concrete casting. At the largest scale, honeycombing may occur due to insufficient workability of concrete placed in a constricted form. Within the paste, air may be entrapped during mixing, leaving voids of up to 3 mm in size, if the concrete is not adequately consolidated. Deliberately introduced, spherical air voids, ranging in size from 50μm to 1mm, may be added to a mix for reasons of workability or durability.

Capillary voids remain when excess mix water evaporated from hardened cement paste. In pastes with low water-cement ratios, voids will typically range in size from 10 to 50 nm; in mixes with high water-cement ratios, capillary voids may be as large as 3 to 5μm, especially in early stages of hydration.[37]

Air is the weakest component within concrete,[38] especially in the form of voids greater than 50 nm in size.[39] The total air void content of normal density concrete is typically not greater than 8%.

[33] Kosmatka et al. (2002) 88
[34] Kosmatka et al. (2002) 79, 81
[35] Kosmatka et al. (2002) 87
[36] Kosmatka et al. (2002) 89
[37] Mehta (1986) 27
[38] Neville (2006) 190
[39] Mehta (1986) 27

2.1.4 Other Ingredients

Numerous types of chemical admixtures may be used in normal density structural concrete to enhance durability, workability, or strength. Fibre reinforcing helps to overcome the relatively weak strength on concrete in tension, and is often used to resist dying shrinkage cracking. (Refer to Appendix A, Section 5.1.5 for further discussion.)

2.2 Alternative Types of Concrete

The behaviour of normal density structural concrete has been intensively studied. While normal density structural concrete may vary somewhat in its performance based on mix design, it provides a generally predictable product, with a relatively high compressive strength, low tensile strength, and high density.

Other types of concrete exist with dramatically altered properties. For example, ultra-high performance concrete (UHPC) combines various strategies for strength improvement, including the elimination of coarse aggregates and substitution of fine sands and hard quartz flour for efficient aggregate particle packing; introduction of extremely fine supplementary cementitious materials such as silica fume to improve cement particle packing; minimization of water-cement ratio through the use of water-reducing agents; and addition of steel or organic reinforcing fibers to improve ductility. Ultra high performance concrete may offer compressive strengths in excess of 150 MPa, and flexural strengths of 15 to 25 MPa.[40]

For other applications, High Density (HD) concrete may be appropriate. Heavy aggregates such as magnetite, ilmenite, hematite and barite are used for concrete with densities of 3500 kg/m^3; and aggregates such as iron punchings or ferrophosphorous may be used to produce concrete with densities greater than 4800 kg/m^3.[41] HD concrete is used in nuclear applications for radiation shielding; in offshore pipelines, breakwater structures and counterweights for resistance to buoyancy; and in applications requiring vibration dampening/attenuation.[42]

---

40 Portland Cement Association (2015b), cf. Graybeal (2006) 4
41 Kosmatka et al. (2002) 320
42 Goguen (2013)

Conversely, other concretes trade compressive strength in favour of lighter weight, by incorporating significant volumes of void.

The introduction of large volumes of void can have a dramatic influence on many aspects of concrete performance. Although some of the materials and their interactions remain the same, when large volumes are air are included in a mix, proportions and principals that have been well established for normal density concrete must be thoroughly re-reconsidered and refined.

A-3

Definition of Foam Concrete

Foam concrete is a low-density cementitious material, produced by entrapping significant volumes of air void within a mortar paste by means of a foaming agent. Bubbles remain stable during the stiffening and curing of the concrete, resulting in a relatively homogenous distribution of macroscopic pores throughout the hardened mass.

There is no universal agreement as to how dense or porous a mortar must be to qualify as foam concrete. The volume of air void is cited variously at 'up to 50 percent',[1] 'up to 75 percent',[2] '40 to 80 percent,'[3] 'more than 20 percent',[4] or '10 to 70 percent.'[5] Mixes have also been attempted with greater than 90% porosity.[6]

Confusion may arise due to imprecise, redundant, or conflicting terminology in technical and promotional literature. Foam concrete may variously be identified as 'foamed mortar',[7] 'foamed cement paste',[8] 'foamcrete,'[9] 'aerated concrete',[10] 'aerated

1 Mineral Products Association (2016)
2 Basiurski and Wells (2001) 66
3 Mydin et al. (2014)
4 Barnes (2009) 3, Van Deijk (1991) 49
5 Panesar (2013) 575
6 Akthar and Evans (2010)
7 Zhao et al. (2015), Yamamoto et al. (2006), Choi and Ma (2015) 93
8 Meyer and van Mier (2007)
9 Kearsley (1996)

lightweight concrete'[11] 'cellular concrete,'[12] 'cellular lightweight concrete' (CLC),[13] 'neat cement cellular concrete',[14] 'sanded cellular concrete',[15] 'cement foam',[16] 'inorganic solidified foam',[17] 'lightweight mortar',[18] or 'air-mixed mortar'.[19] Other lightweight cementitious products may be called by similar names, such as porous concrete,[20] gas concrete,[21] or aircrete,[22] in addition to a variety of trade names; misleadingly, these materials may be classified as 'foamed' cementitious products,[23] or even as types of foam concrete.[24]

The following section will distinguish foam concrete from various other porous cementitious mortars, and help to clarify and classify common terms. Porous cementitious materials may be differentiated according to their method of pore formation, and according to their volume of air-void;[25] highly porous mixes are also commonly classified with respect to their curing regimes.

Pore formation and stabilization

At the broadest level, pores may be introduced into a mortar in two ways:

1) from within, by inducing a chemical reaction to produce a gas from materials in the mix; or
2) from without, drawing air bubbles into a plastic mortar through mixing, or manufacturing foam bubbles outside of the paste and then incorporating them.

Gas bubbles may be generated in a cement paste through a variety of mechanisms. One of the earliest methods used the reaction of hydrochloric acid and limestone. A 1917 Dutch

10 Yang (2015). Foam concrete is termed 'aerated concrete' to differentiate it from AAC.
11 Ng et al (2011)
12 Panesar (2013)
13 Jitchaiyaphum et al. (2011)
14 Fouad (2006) 562
15 Fouad (2006) 562
16 Tonyan and Gibson (1992) 6371
17 Lu and Qin (2015)
18 Soliman (1990) 79
19 ASO Group (2010)
20 India Autoclaved Aerated Concrete Producers Association (2014), Valore (1954a) 774
21 Laukaitis and Fiks (2005) 284
22 UK Aircrete Products Association (2016)
23 Neufeld et al. (1994), Abdollahnejad (2015)
24 Zollo and Hays (1998) 631, Just and Middendorf (2009), Pan et al. (2014) 256
25 Barnes (2009) 3

patent utilized yeast to produce an early form of porous concrete through the formation of carbon dioxide.[26] Since 1929, the use of hydrogen peroxide in reaction with bleaching powder has been used to produce oxygen gas, and this technique has been used in commercial production. Today, however, the most widespread commercial method of producing co-called 'gas concrete' is the reaction of metal powder and lime to evolve hydrogen gas, first developed in 1914.[27] Aluminum powder is most common; zinc powder may also be used.[28] Such additives are known as 'gas-forming agents'. Aerated concrete produced with gas forming agents is often referred to as 'gas concrete', particularly in Europe.[29]

Air that is incorporated into a paste through mixing is known as 'entrained air'. The word 'entrain' is derived from the French verb '*trainer*', to drag along: bubbles are drawn into the mix and distributed throughout the paste.

Normally, bubbles in a mortar will coalesce and be driven up to the surface of the paste by buoyant force.[30] However, a surfactant, or 'surface active agent', can be used to stabilize the bubbles. Surfactants lower the surface tension of a liquid, permitting bubbles to be produced with less work, and inhibiting their coalescence. The stiffness of cement paste is typically sufficient to resist the buoyant force of these fine bubbles, resulting in a relatively homogenous distribution.

It should be noted that, strictly speaking, the term 'air-entraining agent' refers to a surfactant that enables fine air bubbles to be formed and maintained in a paste through mechanical mixing ('entrainment').[31] In practice, however, the term is often used to refer to any additive used to form or stabilize air bubbles in concrete mix design. Thus, gas-forming agents are sometimes referred to as 'air-entraining agents'.[32]

---

26 Superbuild International Ltd. (2013), Hebel New Zeeland (2010)
27 Valore (1954a) 774
28 Short and Kinniburgh (1978) 294-295
29 Valore (1954a) 774
30 Torrans and Ivey (1968) 2
31 Torrans and Ivey (1968) 2-3
32 Dhir and Jackson (1989) 134, Finney (1944) 63

When air-entraining agents are used with normal mixing procedures, relatively modest volumes of air are entrained. However, large volumes of air may be incorporated through the use of a 'foaming agent'.

A foaming agent may be combined with a paste in one of two ways. In the most common procedure, the surfactant is first diluted and aerated to produce preformed foam. This foam is then blended into a cementitious base mix. In the second method, liquid foaming agent is added to the base mix, and the paste is then aerated by high-speed mixing, entraining large volumes of air.

It is sometimes suggested that only the former method, in which foam is created outside of the paste, produces 'true' foam concrete.[33] Most authors, however, agree that foam concrete may be produced by either of these methods.[34] According to the first interpretation, 'foaming agent' refers to the stable preformed surfactant foam. In the second case, 'foaming agent' may be a more general term which simply suggests that the surfactant is capable of stabilizing a large volume of air from outside the mix as fine, evenly distributed bubbles within the paste.[35]

These methods of 'pre-foaming' and 'high-speed mixing' will be elaborated in greater detail in Chapter 4.

Reactive metal powders[36] or chemicals[37] that evolve gas bubbles are occasionally also referred to as 'foaming agents'. However, it is more precise (and more well-defined) to refer to these gas-forming additives as 'gassing agents', as described above.

Additionally, a hybrid form of foaming agent is available commercially, in which a specialized preformed foam produces additional bubbles in the presence of cementitious materials.[38] However, there is little information available on so-called "smart foam" in open academic literature.[39]

---

33 Barnes (2009) 3
34 Valore (1954a) 785, Akroyd (1962) 302, Short and Kinniburgh (1978) 301, Fouad (2006) 561
35 Valore (1961) 14
36 Baspinar et al. (2014) 48
37 Abdollahnejad et al. (2015) 19
38 Cellular Concrete Solutions (n.d.)
39 Siram (2013) 59, Nandi (2016) 42

Degree of porosity

The agents described above are used in mix design to produce three major groups of porous cementitious materials. In order of increasing porosity, these materials are normal density air-entrained concrete, retarded mortar systems, and cellular concrete. Each material group corresponds to a primary purpose for incorporating air-voids: air voids in normal density air-entrained concrete improve durability; air voids in retarded mortar systems principally augment workability; and air voids in cellular concrete are principally for the purpose of reducing density.

Normal Density Air-Entrained Concrete

The first modern air entraining agents were used on the pavements of New York in the 1930s. The accidental incorporation of beef tallow, a lubricant used in the pulverization of Portland cement, was identified to be the cause of reduced surface scaling in concrete sidewalks. Similarly, Portland cement 'contaminated' by oil leaked from crusher bearings was observed to give excellent weathering properties.[40]

Subsequent experimentation, beginning in 1938, established the practice of air entrainment. Traditionally, tallows, fish oil stearate, or resins were used; that is, abietic acid salts and fatty acid salts. In the ancient world, Romans used ox blood as an air entrainer.[41] Today, synthetic surfactants are used, such as alkyl sulphates; olefin sulphonates; diethanolamines; alcohol ethoxylates; or betaines.[42]

Air voids stabilized by these substances are captured in the hardened concrete. They provide space for water to accumulate as it freezes, reducing the internal pressures within the hardened concrete and avoiding effects such as spalling.[43] Osmotic pressures are similarly reduced, minimizing damage from de-icing salts.[44] The spherical bubbles also act as 'ball bearings' within the plastic mix, improving workability while reducing issues of segregation and bleeding.[45]

---

40 Torrans (1968) 1
41 Jasiczak and Zielinski (2006) 451
42 Kosmatka et al. (2002) 106
43 Cement Admixtures Association (2012a) 3
44 Cement Admixtures Association (2012a) 3
45 Kosmatka et al. (2002) 107

Because air-entraining agents often rely on air being folded into the paste through ordinary mixing, the volume of air introduced is limited. Typically, air entrainment of between 4 and 8% of concrete volume is sufficient for improving durability performance, and commercial air-entraining admixtures are capable of providing these volumes of air void.

Even such modest reductions in density have significant influence on mechanical strength, however. As an approximate guideline, at these normal densities, compressive strength is estimated to drop 5% for every 1% increase in air entrainment.[46]

Retarded Mortar Systems

Another application for air entraining admixtures is found in retarded mortar systems. In this approach, a mortar retarder is combined with a mortar plasticizer. Air entraining agent in the plasticizer forms stable, microscopic air bubbles within a mortar mix, accounting for 15 to 22% of the mortar volume.[47] The spherical bubbles are a workability aid. Water requirement is reduced: subsequently, inevitable evaporation of water from the mix has a diminished influence on consistency. With the help of the retarder, mortar lasts in a usable state for up to 72 hours, making it feasible for readymix suppliers to deliver large quantities of well-proportioned mortar to a site. This system eliminates the requirements of mixing equipment or on-site storage, and can improve worker productivity. When a masonry unit is bedded on the freshly placed mortar, it absorbs excess water and mortar retarder, and hydration and stiffening ensue.

A retarded mortar system also increases the resistance of mortar to attack by frost and de-icing salts, increases mortar yield, and can help produce a mortar which is less stiff that the brick, ensuring that if the wall deforms under a load, the mortar will crack sacrificially, while the brick will be preserved.

While the amount of retarder controls the setting time of mortar, the amount of air entrainer has the greatest influence in maintaining proper workability. A reduction of as little as 2% air content in the mix may result in loss of consistency.[48]

---

46 Cement Admixtures Association (2012a) 3
47 Barnes (2009) 3
48 Cement Admixtures Association (2012b) 3

Cellular Concrete

Very porous mixes, whether formed through vigorous air-entrainment, preformed bubbles, or the evolution of a gas, may collectively be referred to as 'cellular concrete.' Cellular concrete is typically desired for its low density, or a property that derives from low density, such as thermal insulation, impact absorption, or lower compressive strength.

As noted above, foam concrete may be produced with porosity as low as 10%,[49] to more than 90%.[50] Most foam concrete has between 40 and 80% porosity, corresponding to a density of approximately 500 to 1500 kg/m^3.

It is possible to manufacture gas concrete with a similar range of densities, as low as 200[51] and as high as 1700 kg/m^3.[52] Most commercially manufactured gas concrete, however, is produced with between 300 and 600 kg/m^3 density, which offers a good balance between performance, manufacturing efficiency, and minimized energy consumption.[53]

In industry practice, cellular concretes are commonly distinguished according to their curing regimes. The method of pore formation typically has a strong correlation with the chosen curing method.

Curing Methods

Porous mortar materials are commonly identified according to whether or not they are autoclaved.

Autoclaving Curing Methods

Autoclaving is the curing of concrete under pressurized steam.[54] Both foam concrete and gas concrete may be autoclaved.[55] Commercial production of autoclaved foam concrete is relatively uncommon, however,[56] and autoclaving tends to be associated with gas concrete.

---

49 Panesar (2013)
50 Akthar and Evans (2010)
51 RILEM Technical Committees 78-MCA and 51-ALC (1993) 4
52 Ramamurthy and Narayanan (2000) 166 Factors
53 Kohler (1983), RILEM Technical Committees 78-MCA and 51-ALC (1993) 9
54 Kosmatka et al. (2002) 319
55 Valore (1954a) 791, Laukaitis and Fiks (2005) 284
56 Short and Kinniburgh (1978) 295

Gas concrete is normally favoured over foam concrete for the production of autoclaved cellular concrete products for a variety of reasons. For example, gas concrete may be produced with a lower w/c ratio than foam concrete, resulting in a less pervious mortar matrix, with minimal capillary voids. The density of the matrix contributes to strength.[57]

Furthermore, the manufacturing processes for gas concrete production and autoclaved curing are compatible. For commercial production, autoclaving must be conducted in a factory setting, with large autoclaves. Gas concrete production is also suited to the large-scale manufacture and the high quality control provided by a factory setting. Ingredients may be processed, weighed, and combined according to precise tolerances. Expansion due to the gas-forming agents may be predicted with a high degree of certainty, and accommodated. Routine procedures yield a consistent product with minimal waste. Finally, many gas concrete mixes produced from metal powder also rely on autoclaving for strength development, due to the role of lime. The production of gas relies on a reaction between the metal and hydrated lime, as illustrated in the reaction equation of aluminum below:

$$\underset{\text{Aluminum}}{2Al} + \underset{\text{hydrated lime}}{2Ca(OH)_2} + \underset{\text{water}}{6H_2O} \rightarrow \underset{\text{tricalcium aluminate hydrate}}{3CaO \cdot Al_2O_3 \cdot 6H_2O} + \underset{\text{hydrogen gas}}{3H_2}$$

The required lime may be supplied through the setting of Portland cement, with the evolution of hydrogen gas as a secondary reaction. Often, however, the Portland cement may be replaced partially or wholly with lime as a binder, providing material for the immediate production of gas.[58]

As explained in Section 2.3, calcium-silicate-hydrate (C-S-H) is the crucial reaction product for strength development in concrete. Portland cement will produce this product though hydration. Lime, however, will not produce C-H-S through hydration alone, but lime can be reacted with siliceous material under autoclaving conditions to produce C-H-S. Thus, the strength of Portland mixes will be improved by autoclaving; but autoclaving is essential for strength-gain in lime-based mixes.[59]

---

57 Just and Middendorf (2009) 742
58 Short and Kinniburgh (1978) 295
59 Short and Kinniburgh (1978) 295

Consequently, while some gas concrete recipes may be cured at a normal temperature and pressure,[60] it is often most effective to produce gas concrete in a factory setting where it may be autoclaved.

Factory castings may wirecut or milled into appropriate precast formats while the concrete is still 'green' (soft), before transporting the material into large autoclaves, typically 2.4 m in diameter and 24 m in length.[61] Cellular concrete that is autoclaved may be referred to as autoclaved cellular concrete (ACC), autoclaved aerated concrete (AAC), autoclaved lightweight concrete (ALC), or simply autoclaved concrete. Trade names include Y-TONG, Hebel Block, Siporex, AERCON, and many others. All of these manufacturers produce autoclaved gas concretes.

Non-Autoclaving Curing Methods

Cellular concretes which are cured at normal temperatures and pressures are referred to as 'non-autoclaved aerated concretes'. The curing regime may instead include air-curing, moist-curing, water-curing, or steam-curing at normal pressure. These methods are described in Section 5.3.1.

Foam concrete is usually not autoclaved; rather, it is well-suited for *in situ* placement, where curing occurs at relatively normal pressures and temperatures. Whereas gas concrete manufacturing procedures, once established, are typically perpetuated with rigid constancy,[62] foam concrete can accommodate a greater degree of variability, based on project requirements. Mix design may be adjusted relatively easily, without risk of disrupting a delicate chemical reaction or its timing. Quantities may be scaled intuitively, with greater tolerance for inexactness. Density may be fine-tuned during batching by adding more foam, or entraining more air. Additionally, equipment for producing foam concrete, such as foam generators, is usually portable and can be combined with a conventional concrete batching plant to produce material near the site where the concrete must be placed.[63]

---

60 Kumar and Ramamurthy (2015) 492, Ramamurthy and Narayanan (2000b) 243
61 Short and Kinniburgh (1978) 279
62 Short and Kinniburgh (1978) 299
63 Jiang et al. (2016b) 949

In reviewing the literature, it is important to note that cellular concrete produced by gas or foam methods may both be cured either by autoclaving non-autoclaving methods. Practically, however, use of the term 'aerated autoclaved concrete' in the industry generally implies 'gas concrete', and 'foam concrete' implies non-autoclaved curing. In Chapter 7, 'aerated autoclaved concrete' and 'foam concrete' will be contrasted as products, based on this understanding.

Figure A.**3** provides a graphic summary of the relationship between various cementitious mortars with deliberately introduced air voids.

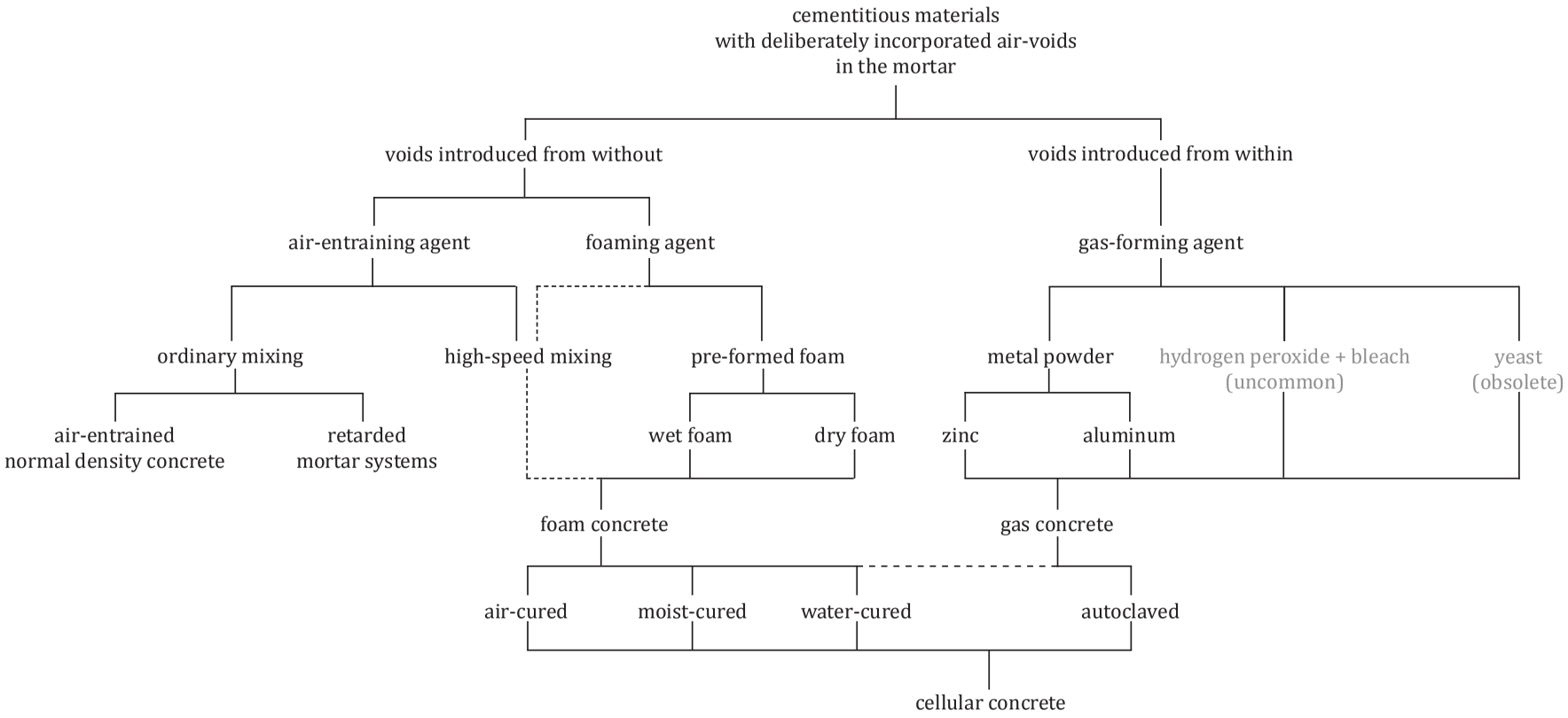

Figure A-3 Relationship between cementitious materials with deliberately introduced air-voids in the mortar.

A-4

History of Foam Concrete

Attempts to produce aerated, low density concrete are at least 125 years old. In 1889, a patent was registered for a lightweight concrete, with gas bubbles produced through the reaction of hydrochloric acid and limestone.[1] Patents for other forms of cellular concrete were registered through the 1910s and 1920s, using aluminum powder (1914), yeast (1917), or excess water (1923) to introduce significant volumes of air void into a mix.[2]

In 1923, autoclave curing of cellular concrete was discovered in Sweden, essentially by accident. Architecture lecturer Dr. Johan Axel Eriksson, from the Royal Institute of Technology in Stockholm, attempted to speed up the curing process of a sample of aluminum powder gas concrete by placing the mass in an autoclave oven. Under heat and pressure, limestone in the mix crystallized in a mineral form similar to the volcanic rock tobermite, resulting in unanticipated strength gain.[3] Autoclaving offered needed strength to help make many early cellular concretes viable.

In the same year, foaming processes were introduced. Erik Christian Bayer registered patents in Denmark, Germany, and the United States for a 'porous building

1 Hebel New Zealand (n.d)
2 Valore (1954a) 774
3 Hebel New Zealand (n.d)

material' produced by "mixing a tenacious foam with mortar, forming the building material therefrom."[4] The material was to be cured 'in steam under high pressure' for strength gain.

By 1926, moist-cured foam concrete had been produced commercially in Europe,[5] and within a short time was brought to North America.[6] A series of U.S. patents were filed between 1926 and 1938 by John A. Rice of the Bubblestone Company in California.[7] Producing stable foam was difficult: a Bubblestone patent filed in 1926 describes an apparatus by which foam could be "gently carried into the slurry and made to smoothly enter at its surface and without unnecessary agitation"[8] to avoid damaging the fragile bubbles.

A patent filed in 1927 described a machine that could produce foam concrete continuously. This 'cellular concrete machine' produced foam by beating a liquid with a 'foam whipper'; the bubbles could then be discharged into a slurry of water, cement, and sand.[9]

Nevertheless, early foam concrete remained of low strength, largely unsuitable for structural building products. Instead, non-structural applications were invented. A patent from 1931 proposed to use foam concrete "to produce masses and forms thereof having the appearance of natural rocks […] as will be attractive and useful for making rock gardens and containers having the appearance of having been made from natural rocks."[10] A patent from 1933 suggested using "light weight cellular cement mixtures however produced" in combination with finely shredded redwood bark to make a shock-resisting concrete, taking advantage of the material's low strength.[11] A Bubblestone patent filed in 1935 proposed to use foam concrete for acoustic surfaces. The text of the patent noted that existing "foaming compounds […] have not proved wholly satisfactory in commercial operation", as the surfactants were difficult to produce in concentrated forms for efficient transportation; were chemically unstable and degraded too quickly; and that they were generally

4 U.S. Patent 1794272 A
5 Christiani and Nielson (1925). Cited by Valore (1954a) 786.
6 *Christiani and Nielsen v. Rice*, Supreme Court of Canada (1930).
7 U.S. Patents 1717319, 1749508, 1769275, 1788592, 1826897, 1856294, 2053842, 2069078, etc.
8 U.S. Patent 1716932 A
9 U.S. Patent 1818376 A
10 U.S. Patent 2006425 A
11 U.S. Patent 2023800 A

inadequate for making 'proper, thick, viscid cellular mortar'.[12] Foam surfactants were a limiting factor in the production of strong, stable foam concrete for building purposes.

Research beginning in 1936 concerning air-foams for suppressing gasoline fires has been credited with improving foaming agents for foam concrete.[13] Indeed, Akroyd[14] notes that modern pre-foamed surfactant is 'much the same material' as that in a foam fire extinguisher, and is produced in a similar way. These improvements had a direct effect on the stability and strength of mixes, and increased their use.

A patent from 1939 acknowledged that up until that time, foam concrete, "[had] not found use in the building trades." Bubbles would collapse during mixing or while the cement was setting. However, the patents promise a "strong, tough foam having properties which cause it to persist or remain in place or existence for the greatly lengthened period of time required to permit a hydraulic cement to set."[15] Similar attempts to produce a highly stable surfactant were attempted throughout the 1940s and 1950s.[16]

In 1954, Valore[17] prepared a comprehensive report on cellular concrete based on literature from European sources, as well testing at the National Bureau of Standards in the United States. He commented on methods of production, use of pozzolans and accelerators, mixing speeds, and costs of gas and foamed concretes. He also compiled information on properties such as compressive and flexural strength, elasticity, bond strength, adsorption and capillarity, freeze-thaw resistance, drying shrinkage, thermal expansion, thermal conductivity. Valore noted that many trends were 'not well defined', and concluded that further research was needed, especially for moving from laboratory testing to commercial production.

In a 1960 publication on 'Foamed Materials,' Valore[18] noted that non-autoclaved concrete was still mostly used for non-structural applications, such as thermal insulation or fill. While precast planks had also been attempted, transportation and handling was difficult without excessive chipping and cracking.

---

12 U.S. Patent 2089813 A
13 Valore (1954a) 774
14 Akroyd (1962) 302
15 U.S. Patent 2282190 A
16 U.S. Patent 2521073, U.S. Patent 2215812, U.S. Patent 2864714
17 Valore (1954a) and Valore (1954b)
18 Valore (1961) 6

An extensive research program was carried out in the Netherlands during the late 1970s, using foam concrete for ground engineering applications.[19] By the 1980s and early 1990s, significant commercial projects had been undertaken based on this research, in the Netherlands and elsewhere. Foam concrete was used as soil replacement in areas of weak soils, as a form of soil stabilization on slopes, and as a void-filling material where low vertical or lateral load were required. Large volumes of foam concrete were sometimes demanded for these projects. For example, the Canary Wharf project, which converted the obsolete Docklands area in London into the city's largest business centre, utilized 33,000 m^3 of foam concrete between 1989 and 1990,[20] and an additional 20,000 m^3 for a second phase from 1996 to 2002.[21]

Additionally, beginning in the early 1990s, foam concrete was used for raft foundations, low-slope roofs, precast sandwich panels, and for permeable landscaping surfaces (for example, under sports fields and athletic tracks).[22] Foam concrete was also used as an insulating fill for fire-resistance, thermal resistance, or sound-proofing. By 2001, foam concrete use in the UK alone was estimated at 25,000 tonnes per year.[23] With a series of practical applications and notable projects, foam concrete was firmly established as a commercially viable material.

Since 2000, major topics of research for foam concrete have included the following:

- production of high-strength foam concrete for structural applications
- incorporation of lightweight aggregates, especially waste aggregates
- incorporation of alternative binders, especially from industrial by-products
- advanced methods of modeling and simulation (fire resistance, heat transfer, compressive strength, etc.)

Other properties such as heat evolution, sorptivity, rheology, and energy absorption have also been studied in the past decade. Moreover, research has been produced to support specialized applications for foam concrete, including projects as varied as

[19] Brady et al. (2001) 3
[20] Van Diejk (1991)
[21] Cox (2005) 107
[22] Van Deijk (1991)
[23] Van Deijk (1991)

decommissioning a nuclear facility,[24] retrofitting traditional dwellings,[25] and building extensions to runways to absorb energy and decelerate large planes.[26]

Foam concrete continues to fulfill increasingly diverse roles as its properties are recognized and refined.

[24] Ashworth et al. (2013)
[25] Shi et al. (2012)
[26] Jones and Zheng (2013)

A-5

Methods of Foam Concrete Production

5.1 Constituent Ingredients

A diverse assortment of materials has been tested in foam concrete mixes. Research concerning the use of binders, water, fillers, coarse aggregates, reinforcing, admixtures, and surfactants in foam concrete is summarized below.

5.1.1 Cementitious Materials

Portland cement

Portland cement is the principal binder in most foam concrete recipes. As in typical concrete, hydrates grow on the cement particles in the presence of water. These hydrates bond to other solid materials in the mix, and form a three-dimensional structural matrix around the surfactant bubbles during setup.

Typically, for foam concrete mixes using Portland cement, total cement content will be between 300 and 400 kg/m^3. It is unusual to include more than 500 kg/m^3 of cement, due to high heat development during curing and shrinkage problems in the concrete.

Furthermore, it is reported that cementing efficiency above 500 kg/m^3 is diminished; that is, the rate of strength gain is less for additional cementitious density.[1]

Fast-setting cements

In addition to ordinary Portland cement, fast setting cements, such as those incorporating aluminate cement[2] or calcium oxide,[3] may be used. More recently, foam concrete has also been prepared with magnesium phosphate cement, which also has quick hardening properties.[4]

Supplementary cementitious materials

Supplementary cementitious materials may be used in foam concrete. These ingredients contributing to strength gain as described in Section 2.2.1. Natural pozzolans mined from raw earth materials, such as calcinated shale, calcinated clay, or metakolin, are seldom discussed in foam concrete literature. However, industrial byproducts, such as fly ash, ground granulated blast furnace slag, or silica fume are commonly used, offering environmental benefits in addition to improved performance and reduced cost.

Fly ash (FA)

Fly ash has a significant range of particle sizes, including a significant portion of particles less than 20 μm.[5] While foam concrete is in a plastic state, the enhanced grading of the cementitious content may improve workability.[6] The spherical shape of the particles further contributes to improving consistency. Consequently, uniformity of the bubble structure is improved.[7] In normal density concrete, use of fly ash may improve the particle packing of a blend;[8] however, in foam concrete, the greater fineness and surface area of fly ash increases water demand, resulting in a less dense matrix phase.[9]

---

1 Brady et al. (2001) C1
2 Huang et al. (2015) 390
3 Chen et al (2014) 137
4 Yue and Bing (2015)
5 Kosmatka et al. (2002) 59
6 Jones and McCarthy (2005a) 66
7 Brady et al. (2001) C1
8 Kearsley (1999b) 32
9 Jones and Giannakou (2004) 6, Brady et al. (2001) C1

Because the pozzolanic reaction of fly ash occurs more slowly than the hydraulic reaction of Portland cement, the early strength of concrete with fly ash may be lower than a Portland cement. For the same reason, heat development is less, which may be beneficial in mass pours.[10] Foam concrete studies have shown that the inclusion of fly ash improves late (i.e., 56-day) compressive strength, due in part to this on-going pozzolanic reaction.[11]

PFA may make up 80% of the total cementitious content in some recipes.[12]

Ground granulated blast furnace slag (GGBS)

Whereas typical fly ash particles are mostly solid spheres or hollow cenospheres, ground granulated blast furnace slag particles are angular,[13] which tends to reduce workability.[14] Brady et al.[15] noted that GGBS particles may cause the collapse of foam in a foam concrete recipe, especially with certain types of surfactants. Jones and McCarthy[16] described additional difficulties with blended Portland cement-GGBS mixes, including inadequate incorporation of foam during mixing, excessive coalescence of bubbles, and foam-mortar segregation after placing. It is possible that GGBS is chemically incompatible with foam surfactants.[17]

Due in part to these difficulties, GGBS blends have been less studied than fly ash blends. (Refer to Appendix B.) Nevertheless, GGBS has been used at rate of between 10 and 50% of the total cementitious content in the literature.[18]

Silica fume (SF)

Silica fume is an extremely fine supplementary cementitious material. Like fly ash, this airbourne material has a spherical shape. The fine powder improves the grading of a concrete blend, which contributes to workability, bubble stability, and uniformity and

10 Jones and McCarthy (2006) 1040
11 Jones and McCarthy (2005b) 25
12 Brady et al. (2001) C1
13 Kosmatka et al. (2002) 58-59
14 Cf. Kearsley (1999) 31
15 Brady et al. (2001) C2
16 Jones and McCarthy (2006) 1036
17 Jones and McCarthy (2005a) 66
18 Ramamurthy et al. (2009) 388

circularity of pores.[19] Silica fume contributes to strength gain through pozzolanic reaction. In foam concrete recipes, silica fume has been reported to significantly increase strength in denser mixes, where foam content is up to 30% of mix volume. Brady et al.[20] suggest that for very low density mixes, strength improvement is less significant. However, Jun Jiang et al.[21] noted that fine silica fume improved the stability of foam concrete with porosity greater than 90%, although workability was reduced.

Metakaolin

Metakaolin is very fine. Like silica fume, it appears to improves stability in extremely low-density mixes. It has been used in comparison to and in combination with silica fume, in highly porous mixes.[22] Metakaolin may also be activated to produce geopolymer binders (see "Geopolymers", below).[23] However, metakaolin is not commonly mentioned in the open literature on foam concrete.

Ternary Blended Cement

Blends incorporating Portland cement and two or more supplementary cementitious materials have also been produced for foam concrete mixes. For example, Pan et al.[24] have produced high strength mixes with blended cement composed of 67% Portland, 8% silica fume, 15% slag, and 10% fly ash; or with 52% Portland, 8% slag, and 40% fly ash.

The Canadian National Standard CSA A3001[25] specifies maximum values of supplementary cement material content to be included in blended cements. The total SCM content for ternary blended cement, for example, is to be not more than 70% of the total mass of cementitious materials, with slag content less than 70%, fly ash content less than 40%, and silica fume content less than 10%.

---

19 Cong and Bing (2014) 68
20 Brady et al. (2001) C2
21 Jiang et al. (2016a) 181
22 Jiang et al. (2016a) 183
23 Zhang et al. (2014) 118
24 Pan et al. (2007)
25 CAN/CSA-A3001-18. Cf. Kosmatka et al. (2002) 32

Geopolymers

Recent research in foam concrete mix design has attempted to completely replace Portland cement with some of these normally 'supplementary' materials. Solid powders that are rich in silica and alumina, such as fly ash and calcinated clay,[26] may be activated as binders when they are dissolved in a strongly alkaline aqueous phase.[27] This process is known as 'geopolymerization'. Geopolymer concrete was first studied by Davidovits[28] in the late 1970s for its enhanced fire resistance;[29] today, geopolymer binders are of interest since they make effective use of industrial byproducts, reducing the ecological burden of the concrete industry.[30] Porous materials may be produced from geopolymers. Gassing agents may be used, including metal powders or hydrogen peroxide, to evolve hydrogen gas. The inclusion of silica fume in a mix will also release hydrogen gas as free silica is oxidized by water. Greater environmental benefits may be realized, however, through the use of preformed foam, due to its low embodied energy relative to typical gassing agents.[31]

Zhang et al.[32] investigated the use of geopolymer binder foam concrete derived from from Class F fly ash, while Al Bakri Abdullah et al.[33] used Class C fly ash. Liu et al.[34] studied the use of alkali activated low-calcium fly ash and of palm oil fuel ash. Yang et al.[35] have shown that ground granulated blast-furnace slag may also be used as a practical and cost-effective binder for foam concrete when activated with alkali activators. The tested GBSS specimens developed higher strength than Portland cement recipes of the same dry density.

Waste ashes, such as from rice-husks, sawdust, or palm oil fuel, often contain amorphous silica, and may therefore also be suitable for geopolymer foam concrete production. Liu et al.[36] used palm oil fuel ash in foam concrete, using flakes of sodium

[26] Zhang et al. (2014) 115
[27] Zhang et al. (2014) 118
[28] Davidovits (1999)
[29] Zhang et al. (2014)
[30] Zhang et al. (2014) 114-115
[31] Zhang et al. (2014) 121
[32] Zhang et al. (2014) 121
[33] Al Bakri Abdullah (2012)
[34] Liu et al. (2014)
[35] Yang et al. (2014)
[36] Liu et al. (2014) 239

hydroxide and aqueous sodium silicate as an alkaline activator. Similarly, geopolymer foam concrete may be produced using waste paper sludge ash.[37]

While there are many possible sources of reactive aluminosilicate, these sources are not quality controlled, but are rather heterogeneous, dependent on the composition of input materials and process operations. Mineralogical composition may vary widely, influencing the setting behaviour of the geopolymer binder product. Producing geopolymer foam concrete is complicated by this inconsistency, since setting behaviour has important implications for foam concrete stability and structure. Furthermore, while the mineral phases of solid geopolymer concrete have been studied, the effect of air void volume on geopolymer microstructures have not yet been well-characterized.[38] Nevertheless, converting these waste products into binders presents strong ecological and financial incentives.

5.1.2 Water

Water is necessary in a base mix to hydrate cement, and to achieve workability. The water-cement ratio of foam concrete mixes may vary significantly, from 0.4 or less, to more than 1.25, depending on density, as well as the total cementitious content and the fineness of solid particles in the mix.[39] Foam concrete recipes that include superplasticizer may have w/c ratios as low as 0.22.[40]

For normal density concrete, strength diminishes with increasing w/c ratio, as the water volume displaces solids, increasing porosity. In foam concrete mixes, however, the w/c ratios does not necessarily influence the final porosity of a hardened sample, as the water may displace air content, with the solids content remaining constant. Thus, changes to the w/c ratio of foam concrete may not influence foam concrete strength in the same way that would be expected for normal density concrete.[41]

Nevertheless, the w/c ratio of foam concrete must still be carefully calibrated for the mix. If there is too little water, the paste will be too stiff, causing air bubbles to break

[37] Raden and Hamidah (2012). Cited in Liu et al. (2014) 239. Cf. Sharipudin et al. (2012).
[38] Zhang (2014) 124
[39] Valore (1954a) 780
[40] Pan et al. (2007) 297
[41] Jones and McCarthy (2006)

during mixing.[42] As well, water may be drawn from the aqueous surfactant to hydrate the cement, causing collapse of the foam.[43] Kearsley and Mostert[44] suggested that a minimum water-cement ratio of 0.35 is necessary for a neat cement foam concrete mix to avoid extraction of water from foam for cement hydration.

Conversely, if the w/c ratio is too high, the highly fluid mix will tend to segregate, with solids sinking in the paste and buoyant foam rising to the surface. [45] Drying shrinkage is more pronounced in mixes with higher w/c ratios.[46] Furthermore, Wee et al.[47] have shown that maintaining a low w/c ratio helps reduce bubble coalesce and coarsening, resulting in small, consistent void sizes, with favourable mechanical properties.

In the past, Valore[48] suggested that water content in a mix was often determined by consistency, rather than by a fixed water-cement ratio or water-solids ratio. Workability was sometimes specified rather than water content.[49] However, current literature normally quantifies water content according to water-cement (w/c) or water-binder (w/b) ratios.[50] Sometimes water content is expressed according to a water-solids (w/s) ratio, which helps to identify the effect of various filler types on water demand.[51]

Occasionally, authors include the quantity of dosing water from the diluted foam surfactant in the total water-cement ratio. This addition may have a non-negligible effect on the reported w/c ratio, especially in low density mixes with a large volume of foam.[52] In denser mixes, the moisture content of any filler (e.g. sand) must be accounted for, especially since dense foam concrete recipes may include significantly more sand than normal density concrete recipes.

Potable water should be used in foam concrete recipes. Impurities such oils, acids, alkalis, salts, and organic materials may affect setting behaviour, strength, and other

42 Nambiar and Ramamurthy (2006a) 476
43 Brady et al. (2001) C3
44 Kearsley and Mostert (2005a) 31
45 Brady et al. (2001) C3
46 Brady et al. (2001) C3
47 Wee et al. (2011)
48 Valore (1954a) 781
49 Kearsley and Mostert (2005a) 31
50 Cf. Ramamurthy et al. (2009) 392
51 Nambiar and Ramamurthy (2006a) 477, Kearsley and Mostert (2005a) 31
52 Akroyd (1962) 302

properties.[53] Protein-based surfactants are especially susceptible to contamination, which may cause instability in the foam.[54]

Water-reducing admixtures or superplasticizers may be used to reduce water demand in normal density concrete. However, these chemical additives sometimes have anti-foaming properties, causing instability of air bubbles. Plasticizer molecules may take the place of foaming agent molecules in foam concrete, undermining the resilience of the bubble walls.[55] Consequently, although such additives have been used successfully in foam concrete, chemical compatibility should always be verified through batch testing.[56] Stability concerns appear to be most significant for low density mixes, and Fouad[57] suggested that water-reducing admixtures should only be used in mixes with with cast densities of 1440 kg/m^3 or greater, after establishing compatibility through trials.

5.1.3 Fine Aggregate (Fillers)

In low-density foam concrete recipes, solid ingredients typically include only Portland cement and finely divided pozzolans. Using these fine cementitious materials promotes strength gain, and also avoids segregation issues, as heavier filler particles would tend to settle in a highly foamed mix.

In denser mixes, however, a variety of fillers may be used to increase density and strength. Fine sand is most common,[58] used in foam concrete with a dry density of approximately 1200 kg/m^3 or greater. Well-graded sand with particles sizes no larger than 4 or 5 mm is suitable;[59] however, improved strength has been reported with the use of sand particle sizes no larger than 2 mm, and 60 to 90% passing through a 600-micron sieve.[60]

Alternatively, clay soil may be used as filler, with positive effects on thermal resistance.[61] Lee[62] determined that 5% replacement of sand with laterite improved

[53] Fouad (2006) 562
[54] Brady et al. (2001) C3
[55] Zhang et al. (2014) 116
[56] Brady et al. (2001) C3, Akroyd (1962) 302
[57] Fouad (2006) 563
[58] Brady et al. (2001) 2
[59] Brady et al. (2001) C2
[60] Barnes (2009) 5
[61] Cong and Bing (2014) 61

mechanical properties. Bentonite and diatomite have been reported to reduce permeability in hardened foam concrete; and diatomite reportedly also improves workability.[63]

Jones et al.[64] suggested that fine recycled secondary aggregates may be used effectively in foam concrete, since fresh properties are dominated by the foam and cementitious paste, rather than the aggregate. Proposed waste materials include demolition fines, incinerator bottom ash from municipal solid waste incineration facilities, foundry sand, China Clay sand recovered from the processing of china clay waste, crumb rubber,[65] glass fines recycled from building flat glass,[66] as well as crushed concrete.[67] Ground granite dust or mine tailings of a single particle size may be used,[68] although batch trials are especially necessary, as appropriate grading and particle size distribution appears to be significant in the production of foam concrete.[69]

Some fillers contribute to the binding capacity of a mix. Coarse pulverized fly ash is often classified as a filler for foam concrete.[70] It may be used as a partial or complete replacement for sand. Jones and Giannakou[71] reported positive effects on compressive strength due to pozzolanic reaction; however, active carbon in coarse fly ash may also destabilize air bubbles.[72] Use of limestone fines has been shown to accelerate setting when used in combination with pulverized fly ash.[73]

Other solid wastes, such as finely divided rice husks, paper sludge contaminated with heavy metals, or powdered waste plastics, may be incorporated into foam concrete to divert these materials from landfills.[74] Inclusion of shredded rubber less than 1mm in particle size is reported to have positive effects on sound absorption and vibration

---

62 Lee (2010) 55
63 U.S. Patent 5782970 A
64 Jones et al. (2012)
65 Jones et al. (2012)
66 U.S. Patent 6488762. Cited in Zhang (2014) 116
67 Aldridge and Ansell (2001). Cited in Ramamurthy et al. (2009) 388
68 Fouad (2006) 562
69 British Cement Association (1991). Cited in Brady et al. (2001) C2
70 Ramamurthy et al. (2009) 389 classification
71 Jones and Giannakou (2004) 6
72 Hoarty and Hodgkinson (1990) 490, 497. Cf. Brady et al. (2001) C2.
73 Brady et al. (2001) C2
74 Lee and Hung (2005) 18

dampening, in addition to producing adequate acceptable for bearing walls.[75] Sawdust may be used as filler, with the additional reported benefit of improving thermal resistance.[76]

Finally, for low density mixes, lightweight aggregate fines may also be used, including Lytag fines, made from expanded fly ash,[77] and expanded perlite fines.[78]

5.1.4 Coarse Aggregates

Most foam concrete recipes do not include any coarse aggregate. Where coarse aggregates are used, however, they should be of approximately the same density as the foamed paste to avoid segregation issues.[79] Normal density granite or limestone aggregates are usually too dense, and will sink, while extremely lightweight aggregates may be too buoyant for a given mix. The degree of adhesion between foamed paste and aggregate will also influence the tendency of a mix to segregate. Furthermore, it is important to account for the volume of water absorbed by the aggregates, especially porous aggregates, as this additional water demand can affect both cement hydration and bubble stability.[80]

Despite these additional complications, use of coarse aggregate can offer advantages of resisting drying shrinkage, reducing total cementitious density by displacing some of the cement paste, and incorporating waste materials.[81] Various manufactured, harvested, or waste lightweight aggregates may be used foam concrete.

Manufactured LWA

Several LWAs manufactured from earth materials have been used in foam concrete. Weigler and Karl[82] considered the use of expanded shale and clay aggregate, and Regan and Arasteh[83] provided an in-depth study of the use of expanded clay aggregate. These materials are typically produced for structural lightweight concrete, by pyroprocessing earth materials in rotary kilns or on traveling grate sintering machines.

---

75 Benazzouk et al. (2006) 656
76 U.S. Patent 5782970 A
77 Van Deijk (1991) 49
78 Zhang et al. (2014) 116
79 Brady et al. (2001) C2
80 Brady et al. (2001) C2
81 Ibrahim et al. (2013)
82 Weigler and Karl (1980)
83 Regan and Arasteh (1984), Arasteh (1988)

LWAs may also be manufactured for insulative value: ground vermiculite, perlite, and diatomite may be pyroprocessed to achieve very low densities. However, these aggregates do not appear to improve significantly on the insulating properties of neat cement foam concrete,[84] and there is little literature available on their use in foam concrete.

Industrial waste materials such as fly ash, expanded slag, organic cinders, and coke breeze may be processed into LWA, as well.[85] Lytag fines, produced from fly ash, have been used successfully in large-scale foam concrete pours.[86]

Harvested LWA

Earth materials may be mined, graded and used as lightweight aggregate. Typical aggregates for lightweight concrete include pumice, tuff, breccia, and volcanic cinders. However, no data is available concerning use of these LWAs in foam concrete.

LWA may also be harvested from waste sources. Graded clay brick, for example, has been proposed as coarse aggregate in foam concrete.[87] Aliabdo et al.[88] have examined the influence of fine crushed clay brick on mechanical properties, thermal conductivity, and sound attenuation for foam and gas concrete, with favourable results at between 25 and 50% filler replacement levels.

In addition to these inorganic materials, organic substances are sometimes also harvested for use in lightweight concrete. Waste organic materials, including sawdust,[89] rice husks, and plastics[90] may be used in foam concrete, especially when finely divided. Light aggregate derived from waste plastic bottles were reported to improve flowability of foam concrete paste.[91] Crushed oil palm shell has been used as lightweight coarse aggregate.[92]

---

84 ACI 122R-02 Table 2.1
85 Bush et al. (2006) 181
86 Van Deijk (1991)
87 Ibrahim et al. (2013)
88 Aliabdo et al. (2013)
89 Ming (2009)
90 Lee and Hung (2005) 18
91 Remadnia et al. (2009)
92 Liu et al. (2014) 239

Tonyan and Gibson[93] suggested that large diameter thin-walled spheres, in-filled with smaller foamed cement spheres, are more efficient at resisting bending loads than a homogenous structure of foamed cement. Consequently, low stiffness spherical aggregates, such as waste expanded polystyrene granules, may improve the mechanical properties of foam concrete. Laukaitis et al.[94] studied the thermal properties of foam concrete with waste crumbled polystyrene, and described a process to hydrophilizate the polystyrene to improve its adhesion to the paste, minimizing segregation. The consistency of a mix should be sufficient to resists the buoyant force of expanded polystyrene, in order to avoid segregation.[95]

Lightweight aggregates are categorized in the table below, according to source and processing. Lightweight aggregates and fillers that have been used in foam concrete mixes are written in bold.

.

		Material type and processing		
		Organic, harvested	Inorganic, harvested	Inorganic, manufactured
Source	natural materials	Straw, peat	Pumice, scoria, tuff, breccia, volcanic cinders	*Strength*: **Shale**,[96] **clay**,[97] or slate *Insulation*: ground vermiculite, perlite, and diatomite
	waste materials	**Sawdust**,[98] **rice husks**,[99] **PET**,[100] **foam granules**,[101] cigarette butts, wood chips, coconut shells,[102] **oil palm shell**[103]	**Waste brick**[104]	**Fly ash (Lytag)**,[105] expanded and granulated slag, cinders, and coke breeze[106]

Table A-5.1.4 Lightweight aggregates used in foam concrete mixes are indicated with bold text.

93 Tonyan and Gibson (1992a)
94 Laukaitis et al. (2005)
95 Cf. Chen and Liu (2004)
96 Weigler and Karl (1980)
97 Weigler and Karl (1980), Arasteh (1988)
98 Ming (2009)
99 Lee and Hung (2005) 18
100 Lee and Hung (2005) 18
101 Tonyan and Gibson (1992a), Laukaitis et al. (2005), Wu et al. (2013)
102 Gunasekaran et al. (2013)
103 Liu et al. (2014)
104 Ibrahim et al. (2013), Aliabdo et al. (2013)
105 Van Deijk (1991)
106 Bush et al. (2006) 181

5.1.5 Reinforcing

There appears to be strong potential for the use of fibre reinforcing and surface reinforcing with foam concrete, but the behaviour of reinforced cementitious foam has not been thoroughly characterized.[107] The review below summarizes work that has been initiated, and also identifies gaps in the open literature on this significant subject.

Reinforcing Bar

Steel reinforcing bar is not commonly used in foam concrete. According to Merril,[108] steel stirrups may improve foam concrete shear capacity, relative to unreinforced specimens. Jones and McCarthy[109] conducted preliminary tests of reinforced foam concrete beams with densities of 1400 and 1600 kg/m^3, which indicated that performance was satisfactory, with minimal bond slippage and failure in tension. However, in testing by Emiko et al.,[110] steel bar reinforced foam concrete and lightweight aggregate foam concrete did not appear to perform well in comparison to other lightweight concrete types. Shear transfer behaviour of lightweight aggregate concrete was similar to that of normal weight concrete. Conversely, foam concrete and lightweight aggregate foam concrete experienced sudden catastrophic failure, resulting in relatively low ultimate shear transfer strengths, compared to corresponding lightweight concrete specimens with the same reinforcing and similar compressive concrete strengths.

The porosity and permeability of foam concrete may also provide limited protection for steel reinforcing bar.[111] Kearsley and Booysens[112] have addressed the rate of reinforcement corrosion in foamed concrete in comparison with normal density concrete.

For aerated autoclaved gas concrete, steel reinforcing bar is sometimes encased first in a denser concrete, and then embedded in the lighter weight mortar.[113] No similar process for foam concrete has been reported in the open literature.

---

[107] Bindiganavile and Hoseini (2008) 252
[108] Brady et al. (2001) C12
[109] Jones and McCarthy (2005b) 29
[110] Emiko et al. (2011) 397
[111] Kearsley and Wainwright (2001a) 811
[112] Kearsley and Booysens (1998)
[113] Valore (1954b) 826

Bamboo strips are a possible low cost alternative to steel reinforcing bar for some applications. Ikponmwosa et al.[114] evaluated the density, compressive strength, and flexural strength of bamboo-reinforced foam concrete slabs. The bamboo was coated in bitumen to reduce water absorption, and wound with coir rope to produce a ribbed surface, increasing bond strength.

Reinforcing Fibre

Fibre reinforcing, evenly distributed through a foam concrete matrix, is reported to resist drying shrinkage,[115] prevent micro-cracks[116] (and thus improve durability performance[117]); increase tensile strength, shear capacity, and stiffness;[118] and increase capacity for energy absorption.[119] Behaviour of cellular concrete appears to transform from brittle to ductile plastic-elastic with the addition of fibres.[120] However, fibre reinforcing also reduces workability,[121] and an excess of fibres can introduce additional air voids and honeycombing, undermining mechanical properties.[122]

As is the case for aggregates, reinforcing fibres should ideally have a similar density to the hardened cement paste to avoid segregation issues. In their geometry and flexibility, fibres should be capable of mixing within the fresh pore structure without rupturing foam bubble walls. Use of fibres generally increases the thermal conductivity of a sample,[123] and natural or glass fibres appear to increase the rate of water absorption of a hardened foam concrete specimen.[124]

In mix design, the volume fraction of fibres is usually limited by workability. The optimal volume fraction of fibre reinforcing for in foam concrete of around 1000 to 1800 kg/m^3 appears to be between 0.25 and 0.50 percent for some metal,[125] synthetic,[126]

---

114 Ikponmwosa et al. (2015)
115 Brady et al. (2001) C9
116 Roslan et al. (2013) 602
117 Sinica et al. (2012) 173
118 Brady et al. (2001) C9
119 Fabian et al. (1996)
120 Zollo and Hays (1998) 632
121 Jones and JcCarthy (2005)
122 Roslan et al. (2013)
123 Awang and Ahmad (2014) 272
124 Awang and Ahmad (2014) 272
125 Gunawan and Busra (2014) 441
126 Awang and Ahmad (2014) 269

and natural fibres.[127] In highly porous mixes, volume fractions of up to approximately 1.5 to 2% may be appropriate.[128]

Metal Fibers

Steel fibres are generally not recommended for foam concrete due to their mass,[129] as the consistency and density of many foam concrete mixes will allow the steel to sink and segregate. Additionally, carbon steel is also susceptible to corrosion due to the permability of foam concrete to water vapour and carbon dioxide (CO_2).[130] Nevertheless, Awang and Ahmad[131] suggest that inclusion of 0.25 and 0.4% volume fraction of steel fibres contributed significantly to the compressive strength, flexural strength and tensile split strength of conventional and fly-ash foam concrete mixes having 1000 kg/m^3 plastic density. Elsewhere,[132] Awang and Ahmad observed that inclusion of steel fibre substantially increased the thermal conductivity of foam concrete. Steel fibres have been used in shock absorbing concrete (SACON) for military applications, resulting in foam concrete tensile strengths of greater than 3.4 MPa.[133]

Galvalum, produced from steel coated in zinc and aluminum for corrosion resistance, has also been used as a fibre reinforcement for foam concrete.[134] Relatively dense mixes, of between 1800 and 1900 kg/m^3 plastic density, increased by 34 and 47% in compressive strength and tensile strength, respectively, with an addition of 0.25% volume fraction of fibre.

Synthetic Fibres

Polypropylene fibres are commonly used for fibre reinforced foam concrete mixes. The flexibility of these fibres is an advantage during mixing, minimizing damage to foam bubbles. Jones and McCarthy[135] suggested that a volume fraction of 0.5% for 19.2 mm long

[127] Jones and McCarthy (2005b) 27
[128] Akthar and Evans (2010) 355
[129] Amran et al. (2015) 993
[130] Brady et al. (2001) 12
[131] Awang and Ahmad (2012)
[132] Awang and Ahmad (2014) 271
[133] Fabian et al. (1996) 118
[134] Gunawan and Busra (2014)
[135] Jones and McCarthy (2005b) 27

polypropelene fibres was an upper optimal limit for increasing tensile strength, compressive strength, stiffness, shear capacity, and reducing drying shrinkage, without undermining workability. 12 mm long polypropylene fibres have also been used.[136] Bing et al.[137] made concrete with a density of 800 to 1500 kg/m^3 and compressive strength of 10 to 50 MPa, respectively, with the use of polypropylene fibres and silica fume. Mamun et al.[138] studied the properties of polypropylene fibre-reinforced foam concrete exposed to a sulphate bath.

Similarly, Meyer and van Mier[139] demonstrated that polyvinyl alcohol fibres significantly improved the flexural strength and ductility of foamed concrete, with bending strength increasing by a factor of five compared to unreinforced foam concrete. 12 mm long fibres were found to perform better than either 3 mm or 6 mm fibres. Flores-Johnson and Li[140] noted that polyvinyl alcohol fibres significantly improved the mechanical properties of sandwich panels composed of a foam concrete core and corrugated steel faces. Yamamoto et al.[141] observed good bonding between polyvinyl alcohol fibres and the surrounding cement matrix at low and high densities. No slipped fibres were observed; rather, fibres ruptured in mixes with low air content, while the foamed cement matrix failed at a higher air content.

Carbon fibres are generally considered cost prohibitive for foam concrete, however they have been used in laboratory testing.[142] Sinicia et al.[143] reported an increase in flexural strength of 24.5% in a 900 kg/m^3 foam concrete mix with the addition of 0.4% volume fraction of carbon fibres. However, the adhesion between the carbon fibre and the foam concrete matrix was insufficient to completely prevent slippage. Notably, elsewhere[144] these authors report that carbon fibre has a superior binding strength to polypropene fibres, basalt fibres, or kaoline fibres in aerated autoclaved concrete.

136 Kearsley and Mostert (1997). Cited in Brady et al. (2001) C9
137 Bing et al. (2012)
138 Mamun et al. (2014)
139 Meyer and van Mier (2007)
140 Flores-Johnson and Li (2012) 1555
141 Yamamoto et al. (2006)
142 Amran et al (2015) 996
143 Sinica et al. (2000) 173
144 Laukaitis et al. (2009)

Yakovlev et al.[145] noted that the fineness of carbon nanotubes makes them especially suitable for reinforcing the cell walls of foam concrete. Nanotubes are significantly thinner than the cells walls in foam concrete, and thus tend to be incorporated entirely within the matrix, displaced by air voids, whereas thicker conventional fibres often span the void structure, with less benefit to mechanical properties.

Glass Fibre

Jones and McCarthy[146] suggested that glass fibres may be too rigid for use in foam concrete, stiffly intersecting the porous matrix structure rather than accommodating the presence of air void bubbles. However, Awang and Ahmad[147] reported that alkaline resistant glass provided highly effective control of foam drying shrinkage, superior to polypropylene, steel, kenaf or oil palm fibre. Akthar and Evans[148] used short staple alkali-resistant glass fibre of 6 mm in length to reinforce foam concrete with porosity greater than 90%, in order to achieve sufficient compressive strength.

Basalt fibre, derived from volcanic rock, is sometimes regarded as an alternative to glass fibre. It is processed in a similar manner, but consumes less energy and does not require additives, making it less expensive.[149] Khan[150] demonstrated that the flexural strength of basalt fibre reinforced foam concrete was nearly ten times greater than that of conventional foam concrete. Basalt fibre reinforced foam concrete also had a greater maximum load carrying capacity than either conventional or polypropylene fibre-reinforced foam concrete.

Natural fibres

Natural fibres were the earliest type of fibre to reinforce foam concrete: finely shredded redwood bark was used to make a shock-resisting foam concrete in a patent process from 1933.[151]

---

145 Yakovlev et al. (2006) 147
146 Jones and McCarthy (2005b)
147 Awang and Ahmad (2014) 270
148 Akthar and Evans (2010) 353
149 Fiore et al. (2015) 91
150 Khan (2014) 75-76
151 U.S. Patent 2023800 A

Modern day natural fibres include vegetable fibers, such as wood cellulose, bamboo, sisal, jute, rice husk, coconut husk, groundnut shell, and cotton stalk.[152] Mineral fibres such as asbestos fibers and basalt fibres, may also be considered natural fibres.[153]

Among these many options, only a few fibre types have been reported upon in the open literature concerning foam concrete. Awang and Ahmad[154] found that kenaf and oil palm fibres were effective in reducing drying shrinkage of foam concrete in mixes of approximately 1000 kg/m^3. Fadila et al.[155] produced foam concrete in the density range of range 800 to 900 kg/m^3, incorporating significant amounts of recycled paper fibre as reinforcement (i.e. 5 to 20%). The composite material reportedly had good sound absorption, and significantly improved flexural strength with 20% paper content.

Hybrid fibres.

Hybrid fibres, combining two or more materials or fibre dimensions for improved performance, have not been studied extensively in the open literature for foam concrete.

Surface reinforcement

Various authors have proposed the construction of sandwich panels with foam concrete cores, on account of their thermal properties and lightweight. Flores-Johnson and Li[156] tested corrugated steel faces with conventional and fibre-reinforced foamed concrete cores for uniaxial tensile and compression testing and flexural testing. Face-core debonding appeared to be a significant limiting factor. Mydin and Wang[157] proposed a similar assembly for low-rise residential buildings up to four storeys in height, to be constructed by manual workers in Malaysia without the use of machinery.

Wang et al.[158] found that the flexural capacity of foamed concrete beams reinforced with woven glass fiber sandwich fabrics increased by a factor of four. Failure of the composite was ductile, due to the ability of the glass fiber textiles to stretch. The

[152] Kosmatka et al. (2002) 123, Fadila (2008) 527
[153] ACI 544.1R-96, Fiore et al. (2015) 74
[154] Awang and Ahmad (2014)
[155] Fadila et al. (2008)
[156] Flores-Johnson and Li (2012) 1555
[157] Mydin and Wang (2011) 66
[158] Wang et al. (2016) 130

researchers noted that the use of textile reinforcing allowed the walls to be thinner, as concrete cover for reinforcing bar was not required. Similarly, Sinica et al.[159] installed a fiberglass fabric mesh with 2 mm of cover in non-autoclaved specimens, with significant improvement to flexural strength and impact resistance. Other similar assemblies have been proposed that incorporate aerated autoclaved concrete as a core material.[160]

5.1.6 Admixtures

Set controllers

Set controllers are highly useful admixtures in foam concrete applications. At a microstructural level, chemical accelerators allow cementitious skeletons to harden before liquid bubbles loose stability through coarsening and drainage. Practically, accelerators speed construction work, permitting reuse of formwork, traffic loads and further construction sooner. Dransfield[161] considered calcium chloride an effective accelerator for foam concrete, especially since carbon steel is rarely used for reinforcing. Huang et al.[162] noted that aluminate and sulphoaluminate cements are commonly used to control air-void stability. Chen et al.[163] studied the use of quicklime (calcium oxide) and aluminate cement in foam concrete mixes with fly ash, and determined that contents of 8% and 2%, respectively, were appropriate. Narayanan and Ramamurthy[164] attempted to minimize demoulding time for the production of foam concrete blocks. In order of decreasing set time, they used calcium chloride, triethanol amine, calcium nitrate, and alum. In the same study, Narayanan and Ramamurthy discussed the use of lithium salts and calcium formate.

Conversely, retarders allow time for transportation to site and can reduce the rate of temperature rise due to heat of hydration. Supplementary cementitious materials such as GGBS and fly ash are often used for this purpose.[165] Yue and Bing used a retarder in magnesium phosphate foam concrete to control the setting rate of the quick hardening cement.[166] Many foaming agents appear to also retard cement hydration.[167]

---

159 Sinica et al. (2000) 173
160 Uddin et al. 2006.
161 Dransfield (2000). Cited in Brady et al. (2001) C4
162 Huang et al. (2015) 390
163 Chen et al. (2014) 137
164 Narayanan and Ramamurthy (2012)
165 Jones and McCarthy (2006) 1036
166 Yue and Bing (2014) 1

Superplasticizers and water-reducing agents

As discussed above in Section 5.1.2 above, superplasticizers and water-reducing agents can cause instability in the foam. Compatibility of superplasticizers and water-reducing agents with surfactants should be confirmed through batch trials. Additionally, a mix must remain sufficiently stiff to resist the migration of bubbles, which leads to segregation.

Water reducing chemical admixtures, especially, are seldom used in the open literature.[168] Superplasticizers (that is, high-range water reducing admixtures) are used occasionally in the production of high strength foam concrete mixes, where they permit w/c ratios as low as 0.22 or 0.24.[169] Wee et al.[170] used a naphthalene-based superplasticiser at a dosage rate of 8 ml per kilogram of cement to reduce the w/c ratio to 0.22 for mixes with a range of densities. Amran et al.[171] reported that a popular plasticizer for foam concrete is fluorosurfactant, used at a dosage rate of between 0.45 and 5% of foam agent volume.

Other agents

Brady et al.[172] noted that waterproofing materials have been used in foam concrete mixes, and that thickening agents may be used to reduce the flowability of foam concrete once placed.

5.1.7 Surfactants

Foaming agents stabilize air bubbles by reducing surface tension in a mix: they are 'surface active agents', also known as 'surfactants'. Many surfactants are available for foam concrete production, and compatibility with cementitious materials, reactive fillers, and chemical admixtures should be confirmed. Surfactants are also vulnerable to the highly alkaline environment of the paste, and their stability may also be strongly affected by temperature,[173] so they must be selected carefully for the proposed mix and use. It is

[167] Tarasov et al. (2010) 902, Akthar and Evans (2010) 353
[168] Amran (2015) 991, Jones and McCarthy (2006) 1032
[169] Pan et al. (2007) 297
[170] Wee et al. (2011) 585
[171] Amran et al. (2015) 993
[172] Brady et al. (2001) C3
[173] Panesar (2013)

important that foaming agents produce regular, resilient bubbles.

Although various types of foaming agents have been used historically,[174] common modern foaming agents may be categorized as either synthetic or protein-based.

Synthetic surfactants

Synthetic agents may be classified based on the charge of their hydrophilic group. A survey by Brady et al.[175] found that a significant majority (approximately 70%) of percent of synthetic surfactants were anionic, with a negatively charged hydrophile group. Very few synthetic surfactants are cationic, in which the hydrophile group carries a positive charge, as these are less effective at sustaining surface tension around air bubbles in an alkaline environment. Non-ionic or polar surfactants are electrically neutral, and account for a minority of synthetic surfactants. Amphoteric surfactants can sustain either positive or negative charges based on the pH of the solution.

Cement particles have both positive and negative charges, but tend to become more negatively charged with the addition of pulverized fly ash. Amphoteric and non-ionic surfactants may be best for Portland cement-only mixes, due to the mix of positive and negative charges throughout the paste, while hydrophile groups with a single charge may perform better when fly ash is included in the mix design, due to the presence of reactive carbon. [176]

Synthetic surfactants have a longer storage life, and require less energy to aerate than protein-based foam.[177] They are typically less susceptible to degradation due to extremes in temperature than protein-based foams. Furthermore, unlike natural protein-based foams, synthetic surfactants are not susceptible to degradation by bacteria and other organisms.[178]

[174] Valore (1954a) 784
[175] Brady et al. (2001) C4
[176] Brady et al. (2001) C5
[177] Barnes (2009) 5
[178] Brady et al. (2001) C4

Protein-based surfactants

Despite certain advantages of synthetic agents, protein-based surfactants are more widely used. In general, protein-based surfactants produce mixes with superior mechanical properties, in the order of 80% stronger than that made by using synthetic surfactants.[179] Panesar[180] explained that protein-based surfactants are capable of producing stronger and smaller bubbles than synthetic surfactants. A resilient film is created around the bubbles due to the degradation of the proteins. The peptide linkages of large protein molecules break, resulting in smaller hydrophobic molecules, which cling to each other through hydrogen bonding. Brady et al.[181] noted that the stronger closed bubble structure may allow protein based surfactants to be used in higher-density mixes with less foam collapse. Furthermore, proteins retain water and release it into the cement paste at a slower rate, prolonging the hydration process and producing a denser crust around each air void, resulting in greater strength.[182] Van Deijk[183] suggested that because the proteins break down into hydrophobic molecules, they also impart some level of water repellence to the concrete.

In tests by Panesar,[184] protein-based mixes appeared to have better thermal resistance at low density, while synthetic foam mixes had better thermal resistance in higher density mixes. Choice of surfactant should be suited to context.

The dilution factor of the surfactant may also be optimized for a particular mix. It is important to hydrate the surfactant sufficiently so that it does not compete with the water-cement ratio of the mix; simultaneously, keeping the dilution ratio lower will help produce bubbles with strong, thick films. Surfactant manufacturers specify a dilution ratio with their foaming agent. Ratios of between 1:5 and 1:40 are common;[185] a rate of 1:25 is often considered optimal, but this ratio will be influenced by surfactant type and method of production.[186]

---

179 Aldridge (2005) 5
180 Panesar (2013) 583
181 Brady et al. (2001) C5
182 Brady et al. (2001) C10
183 Van Deijk (1991) 49
184 Panesar (2013) 583
185 Amran et al. (2015) 994
186 Brady et al. (2001) C5

5.2 Methods of Foaming

5.2.1 Aeration Methods

To produce foam concrete, a base mix is prepared from cementitious materials and water, as well as any fillers, coarse aggregate, reinforcing fibres, or chemical admixtures. This base mix is then aerated, and the bubbles stabilized with a surfactant. Aeration may be provided either through high-speed mixing, or through a pre-foaming method.

5.2.1a High-Speed Mixing

In the high speed mixing method, the liquid air entraining agent is added to a cementitious paste. The paste is then mixed at a high speed, drawing air into the mix through the shearing action of the mixer. The surfactant reduces the surface tension of the solution, stabilizing the bubbles. Concrete produced by high speed mixing tends to be used to produce heavier densities of aerated concrete. Controlled low-density fill may be produced in this way, for example.[1]

The composition of the base mix, mixing time, amount of foaming agent, and water temperature can affect the air void volume generated, making precise control of batch density difficult.[2] Paddles or screws that fold air into the mix are recommended, as these disperse air efficiently into the paste. If there is too little mixing, the paste will not be homogenous; but too much mixing will result in collapse of the foam.[3]

5.2.1b Pre-foaming

More commonly, however, a 'pre-foamed' method is employed. In this process, the surfactant is combined with water and aerated with compressed air to produce foam of shaving-gel-like consistency. The foam is then injected into the base mix slurry from a nozzle or via an inline mixer, and blended thoroughly. The bubbles remain suspended during the curing of the concrete. Pre-foaming is usually a more expensive method of

---

1 Akroyd (1962) 302
2 Fouad (2006) 561
3 Brady et al. (2001) C7

production,[4] and is often a slower method for introducing air voids,[5] but it typically offers better control and consistency than the foam concrete produced by mechanical beating.[6]

'Dry foam' and 'wet foam'

Surfactants may be pre-foamed either as 'dry foam' or 'wet foam'.

Wet foam has larger bubbles, and is not considered appropriate for the production of foam concrete with densities less than 1000 kg/m^3.[7] Wet foam may be produced in one of two ways. In the first, a surfactant solution is pressurized in a vessel; then allowed to escape from a small aperture. As it escapes the pressured vessel, relatively fine bubbles are produced. The device is called a 'foam gun.' In the second technique, the aqueous surfactant solution is sprayed onto a metallic gauze within a tube. When air is drawn through the tube, a vacuum is generated due to the Venturi effect, producing relatively large bubbles. The higher output of a Venturi generator may be desirable for some projects where large volumes of foam are demanded.[8] However, wet foam is not suitable for mixes which must be pumped, nor can it be poured do a great depth, due to the large, loose bubble structure.[9]

'Dry foam' is more uniform, more stable, and has smaller bubbles. It is also more costly to produce than foam made with a Venturi generator. To generate dry foam, compressed air is used to force surfactant solution through a metal or plastic gauze. Surfactants must have sufficiently stable structure to withstand the higher-pressure aeration process.[10] Once they have been produced, the more stable bubbles of dry foam may be more vigorously mixed within a batch than wet foam bubbles, making for easier blending.[11] Dry foam must always be used for inline mixing methods, described below.[12]

---

4 Panesar (2013) 576
5 Brady et al. (2001) C7
6 Fouad (2006) 561
7 Barnes (2009) 5
8 Brady et al. (2001) C17
9 Aldridge (2005) 3
10 Brady et al. (2001) C17
11 Panesar (2013) 576
12 Aldridge (2005) 6

Hybrid foaming agents

Each of the 'high speed mixing' and 'pre-foamed' methods of production described above rely on mechanical action for the formation of air bubbles. However, some recent foaming agents also use the chemical reaction of the surfactant with cementitious materials to introduce miniscule bubbles throughout the mix. Thus, surfactants for foam can also work in a similar manner to the chemical gassing agents described in Chapter 3. This so-called 'hybrid method' is relatively uncommon, however, and has not been reviewed extensively in the open literature.[13]

5.2.2 Delivery Methods

A load of preformed foam concrete may be delivered to site as a pre-foamed mortar, wet mortar, or dry mortar.

Pre-foamed Mortar Delivery

In this system, wet or dry foam is added to the base mix at the batching plant, delivered to site, and placed. Quality is controlled at the batching plant. Drawbacks to this system are (1) that homogeneity of the mix is dependent on the mixing action of the truck, which may not be designed for this application; (2) that the full volume of the aerated mix must be transported, rather than a more condensed volume of base mix; (3) that the quality and stability of the foam may diminish during transport; and (4) that density adjustments to the mix on site are unfeasible, and if the paste is out of specification, then the load must be rejected.[14]

Wet Mortar Delivery

In this system, a relatively wet base mix is delivered to site. Foam is produce on-site. It may be combined with the base mix the truck mixer; combined with the base mix in a special blender; or injected into flexible hoses through which the mortar is being pumped,

[13] Cellular Concrete Solutions (n.d.), Siram (2013) 59, Nandi et al. (2016) 42
[14] Alderidge (2005) 6

and blended with an in-line homogenizer.[15] An onboard density monitor confirms the quality of the foam.[16]

Using any of these three methods, a base mix may be expanded to between four and five times its original volume. Consequently, transportation costs are dramatically reduced.[17]

Dry Mortar Delivery (Dry Inline Mixing)

In this final method, dry materials are carried onboard in silos and aggregate bins. They are weighed, mixed, and hydrated on-site. The base mix is then combined with dry foam through a series of inline mixers, in a special blender.[18] Barnes[19] reported that one delivery is capable of producing 130 m^3 of concrete. These trucks are ideal for area where base mix materials are difficult to obtain, although the trucks themselves are often large, weighing up to 60 tonnes, making them unsuitable for congested urban areas. Additionally, significant amounts of water must be supplied on-site.[20]

Dry mortar delivery systems were developed in mainland Europe, where their use is relatively widespread.[21] Aldridge reported that they were gradually being accepted in the UK as of 2005.[22] Both dry mortar and wet mortar foam concrete systems are currently available in North America.[23]

---

15 Van Deijk (1991) 50
16 Alderidge (2005) 6
17 Barnes (2009) 5
18 Van Deijk (1991) 50
19 Barnes (2009) 5
20 Alderidge (2005) 7
21 Barnes (2009) 5
22 Aldridge (2005) 6
23 Cematrix Corporation (2016)

5.3 Methods of Curing

Although appropriate curing regimes for normal density concretes are well established, curing techniques for foam concrete continue to be investigated. Parameters of humidity, temperature, and pressure may be optimized for foam concrete mix designs. Curing time is also an important variable, especially for mixes with a high pozzolanic content, which may require more time to achieve ultimate strength.

5.3.1 Humidity

Humidity control is essential for good curing. Mehta[1] explained that hydration of cement grains proceeds only under highly saturated conditions, and that hydration virtually stops when relative humidity in void spaces is less than 80%. When cured hydration products surround anhydrous cement grains, further hydration is impeded. Water must be available continually for hydration to ensure that a maximum of hydration products are formed.

Foam concrete may be air-cured, seal-cured, moist-cured, or water-cured, to control the rate at which additional water evaporates from, or enters, a curing specimen. Accelerated curing techniques for cellular concrete that involve water and heat include hot water curing,[2] steam curing at atmospheric pressure,[3] or steam curing at high pressures, i.e. autoclaving;[4] however, these techniques are relatively uncommon for foam concrete.

In the past, Valore[5] suggested that non-autoclaved cellular concrete for structural applications was typically moist-cured for seven days before air-drying, while insulating and fill applications were moist-cured for between one and seven days. Studies of numerous foam concrete curing regimes by Kearsley[6] in the 1990s revealed that water-curing reduces strength relative to air-curing, while seal curing increases strength. It was also discovered that curing foamed concrete with a sealing membrane also reduces plastic shrinkage.[7] Subsequently, the seal curing method has frequently been adopted by foam concrete researchers, and data from seal cured foam concrete has been used to benchmark

1 Mehta (1986) 55
2 Park et al. (1999) 196
3 Chen et al. (2014) 138
4 Laukaitis and Fiks (2005) 284
5 Valore (1954a) 789
6 Kearsley (1996), Kearsley (1999a)
7 Brady et al. (2001) C9

the mechanical properties of Portland only mixes and fly ash mixes,[8] to study sorptivity indices,[9] to evaluate air void-systems,[10] and to speculate on the potential of foam concrete for structural applications.[11] Jones and McCarthy[12] stated that seal-curing with plastic film, from the time of demoulding until testing, is a typical industry practice for foamed concrete.

Recently, Jiang et al.[13] used X-ray diffraction measurements to evaluate the mineral phases of reaction products of foam concrete cured under various conditions: standard curing, with greater than 95% RH; natural curing, exposed to ambient conditions ranging from 18 °C to 35 °C and 30% RH to 95% RH; and humidity insulated curing, or seal curing. Seal curing was found to reduce carbonation, minimizing the decomposition of hydration products. As a result, seal cured mixes were denser, with smooth inner surfaces at a microstructural level, leading to greater mechanical strength.

However, ASTM standards C796[14] and C495[15] require that foam concrete specimens be moist cured from Day 2 to Day 25, and then air-dried at a relative humidity of 50±10%, until mechanical testing on Day 28.

The majority of commercially produced foam concrete is used for in-situ applications, as explained in Chapter 3. In these settings, humidity may be controlled by limiting evaporation with impervious paper, plastic sheets, formwork, or membrane coatings, or by supplying water to the surface of a pour through ponding, sprinkling, or wet fabric coverings.[16] The use of aggregates[17] or surfactants that retain and slowly release water into a mix during curing may be considered a form of internal moist curing, which appears to have a discernable effect on foam concrete strength.[18]

---

8 Jones and Giannakou (2004), Jones and McCarthy (2005c), Kearsley and Wainwright (2001a)
9 Kearsley and Wainwright (2001b)
10 Wee et al. (2006)
11 Jones and McCarthy (2005b)
12 Jones and McCarthy (2005b) 22
13 Jiang et al. (2016b) 958
14 ASTM C796/C796M-12
15 ASTM C495/C495M-12
16 Kosmatka et al. (2002) 215
17 ACI 213-03 Section 6.5
18 Brady et al. (2001) C10, Aldridge (2009) 5

5.3.2 Temperature

Foam concrete properties may also be improved with somewhat elevated curing temperatures. Van Deijk[19] suggested that higher temperatures increase the rate of hardening of foam concrete, speeding construction and reducing the need for liquid foam to remain stable for a long time during setup. A study by She et al.[20] recorded a significant reduction in setting time as the curing temperature was increased from 20°C to 80°C.

Abdullah et al.[21] noted that increasing the ambient temperature of geopolymer foam concrete produced from Class C fly ash by 60°C, for 24 hours, improved early strength properties, but had no significant impact on density, pore structure, or 28 day strength. However, Kearsley and Visagie[22] determined that curing temperature does influence ultimate strength, and that 40°C was an optimal temperature for strength gain in a 50% fly ash mix.

Jones and McCarthy[23] noted that although elevated temperatures can accelerate pozzolanic reaction and increase ultimate strength in normal density concrete, heat box-cured specimens with 30% fly ash were less strong than mixes cured at ambient temperatures. Jones and McCarthy asserted that while short periods of high temperatures may enhance early strength development, long-term exposure to elevated temperatures can be detrimental, distorting bubble structures and possibly producing an impermeable shell around cement grains before they are fully hydrated. Tarasov et al.[24] observed that if internal temperatures exceed 90°C, protein coagulation may cause protein-based foams to collapse; or the expansion of heated air may rupture bubble structures.

Fujiwara et al.[25] recommended a relatively detailed procedure for increasing compressive strength of pre-foamed aerated mortar made with silica fume and lightweight coarse aggregate, which involved curing samples in moist air for one day; then applying steam while increasing temperature the temperature to 65°C for 4 hours; and finally cooling the sample in ambient conditions.

---

19 Van Deijk (1991) 49
20 She et al. (2014b) 71
21 Al Bakri Abdullah (2012). Cited in Zhang (2014)
22 Kearsley and Visagie (1999). Cited in Amran et al. (2015) 996
23 Jones and McCarthy (2006) 1039
24 Tarasov (2010) 899
25 Fujiwara et al. (1995). Cited in Amran et al. (2015) 996.

The heat of foam concrete mixes may be controlled through the temperature of constituent ingredients,[26] the heat of hydration of binders, the use of insulated formwork,[27] external heat sinks or sources,[28] or evaporative cooling (e.g. of water at the surface of a specimen).[29] The inherent insulating property of foam concrete itself also influences heat retention.[30]

5.3.3 Pressure

Control over pressure is unfeasible for large scale and *in situ* foam concrete projects. Nevertheless, foam concrete may be autoclaved with heat, steam, and pressure in a laboratory or factory setting.[31] High pressure enables the steam to reach extremely high temperatures, contributing to the production of desirable reaction products.[32] Autoclaving significantly reduces drying shrinkage,[33] and improves mechanical properties. Today, however, commercial production of autoclaved foam concrete is relatively uncommon.[34]

5.3.4 Time

In general, foam concrete properties such as mechanical strength, durability, impermeability and freeze–thaw durability may be expected to improve with time, as long as the degree of hydration of the cementitious materials continues to increase.[35] Drying shrinkage will also increase with time.[36] Brady et al.[37] suggested that specifying a 56-day compressive strength, instead of a 28-day compressive strength, will greatly increase mix design options for 10 MPa applications. Specifying 56-day strengths is especially helpful in SCM mixes, as it allows additional time for secondary pozzolanic reactions to occur.[38]

---

26 Jones and McCarthy (2006)
27 Van Deijk (1991) 49
28 She et al. (2014b) 71
29 Kosmatka et al. (2002) 214
30 Tarasov et al. (2010) 905
31 Valore (1954a) 791
32 Short and Kinniburgh (1978) 295
33 Neville (1963) 448
34 Short and Kinniburgh (1978) 295
35 Powers and Brownyard (1948), Powers et al. (1959)
36 Jones et al. (2012) 520
37 Brady et al. (2001) 9
38 Jones and Giannakou (2004)

A-6

Properties of Foam Concrete

This survey of foam concrete studies summarizes key findings in developing desired fresh state, curing, and hardened properties, in Sections 6.1 to 6.3. For each property, the survey identifies ingredients that are known to influence performance, and references relevant literature for further information. Foam concrete properties that relate to sustainability are emphasized in Section 6.4.

6.1 Fresh State Properties

6.1.1 Consistency

Foam concrete is a highly flowable material. Unlike most normal density concrete, its rheology is not measured according to its slump. Rather, its consistency is often evaluated according to its 'spreadability' (also referred to as 'spread rate') using a standard flow cone[1], or its 'floawability' (also referred to as 'flow rate') using a modified Marsh cone test.[2] These measurements are taken as an indication of yield stress and plastic viscosity,

[1] Nambiar and Ramamurthy (2008) 111
[2] Cf. ASTM C230/C230M-14

respectively.[3] A lower yield stress (greater spread rate) corresponds to a lower plastic viscosity (faster flow rate); and for foam concrete, these properties have a good correlation.[4]

The consistency of foam concrete in a plastic state is very important for producing good quality foam concrete. If the mix is too stiff, a large proportion of bubbles will break, increasing the density and the water-binder ratio. If the mix is too thin, bubbles will rise through the paste, causing segregation. Good consistency is indicated by a density ratio close to unity; that is, when the theoretical density and the measured density of the plastic mix are nearly the same.[5]

Consistency increases as the water-to-solids ratio increases, or with the addition of superplasticizer. Consistency is reduced as the surface area of solids increases, e.g. with the addition of fine silica fume, and where more angular particles are introduced. As well, the addition of foam bubbles has been shown to reduce consistency measurements. This is partially due to adhesion between solid particles and bubbles, and partially due to the influence of self-weight, as gravity loads will produce a greater spread in denser mixes.[6]

A study by Nambiar and Ramamurthy[7] proposed a 'consistency requirement' in terms of a water-solids ratio for different densities and different filler types. A study by Jones et al.[8] included the slump flow spread for a variety of foam concrete mixes using recycled or secondary aggregates. Research at the University of Dundee[9] evaluated the influence of surfactant type on consistency, showing that protein-based surfactants tend to produce foam concrete with lower plastic viscosity. Ahmed et al.[10] evaluated the rheology of foam concrete using a flow-through rotational viscometer.

A spread rate of around 45% has been shown to indicate mixes of good consistency, where typical ingredients are used.[11] Most foam concrete mixes are self-leveling, although mixes may also be designed to provide slopes of up to 1%.[12]

---

3 Cf. Jones et al. (2003). Cited in Brady et al. (2001) C7
4 Nambiar and Ramamurthy (2008) 115
5 Nambiar and Ramamurthy (2006a) 477
6 Nambiar and Ramamurthy (2008) 115
7 Nambiar and Ramamurthy (2006a) 477
8 Jones et al. (2012)
9 Brady et al. (2001) C7
10 Ahmed et al. (2009)
11 Ramamurthy et al. (2009) 390
12 Van Deijk (1991) 49

6.1.2 Stability

Extraordinary performance is required from the bubbles in foam concrete. These thin films must remain stable despite numerous sources of disequilibrium within the mix. Bubbles must maintain an appropriate and consistent size to impart desired hardened properties. They must resist coalescence, and must be durable during mixing and pouring, despite the flow of liquid free water in the mix, and the pressures of solid particles against the bubble film. They must be capable of tolerating an increasingly alkaline environment, as calcium hydroxide is produced during cement hydration. The surface tension of the bubbles must be sufficient to support the self-weight of the foam concrete above.[13]

The liquid film must eventually solidify to form the structure of hardened foam concrete. Accordingly, the bubble film must contain a sufficient density of solid and cementitious particles, and must also contain a sufficient quantity of water for hydration. The bubble film must be highly resilient as it undergoes the solidification process, despite the production of reactive ions, the migration of water, the formation of new crystalline substances, and the volume shrinkage that accompanies hydration.

An inability of the bubble films to accommodate these any of these effects can cause collapse of bubbles. This collapse will increase the mix density, and will add additional water to the mix, increasing the water-binder ratio.[14] The stability of a mix is typically evaluated by comparing the theoretical and actual volumes of foam introduced into a mix to achieve a target plastic density, or by comparing actual and theoretical water-to-binder ratios.[15]

The method of foam production has a strong influence on mix stability. Pre-foamed methods produce the most stable bubbles, with dry foam being more stable than wet foam. High speed mixing produces the least stable bubbles.[16]

Naturally, the surfactant used to alter liquid surface tension is also highly important for producing stable bubbles. Brady et al.[17] provide a summary of the types of surfactants

[13] She et al. (2014b) 63
[14] Ramamurthy et al. (2009) 389
[15] Ramamurthy et al. (2009) 389
[16] Panesar (2013) 576
[17] Brady et al. (2001) C4

available. Surfactants should be compatible with the cementitious materials used.[18] Many admixtures, notably superplasticizers, are incompatible with foam concrete surfactants, and can cause bubble collapse.[19]

The surface charges, reactivity, and shape of solids should be considered. Fly ash has been found to cause bubble collapse, likely due to residual active carbon contents.[20] Angular, ground materials, such as Portland cement or ground granulated blast furnace slag, appear to be more likely to rupture bubble films than spherical particles, such as silica fume.[21]

An appropriate proportion of water is necessary for consistency and hydration. A mix with a stiff consistency may cause bubbles to break.[22] Additionally, if there is insufficient water in the mix to allow for complete hydration, water may be drawn from the diluted surfactant, to the detriment of maintaining strong bubble films. [23]

Achieving mix stability is especially difficult for extremely low-density mixes. Strength development is usually slower due to the reduced density of solids and binder, so liquid bubbles must be preserved for a longer time during the setting process. Quick hardening cementitious materials[24] or cement setting accelerators[25] have been shown to offer some improvements.

Producing mixes that are both highly stable and highly flowable is also a challenge. Some surfactants provide improved consistency; however, stability is often compromised. A faster stiffening and initial setting will help limit bubble collapse, but may reduce flow distance. A balance must be found for many grouting applications in particular.[26]

Petit et al.[27] provided a detailed study of the generation and stabilization of a single bubble in a cement-based slurry, with special consideration given to attachment of solid particles to the liquid film. Hilal et al.[28] described the phenomenon of bubble merging

---

18 Panesar (2013) 576
19 Cf. Brady et al. (2001) B1, Petit et al. (2014) 42
20 Jones and McCarthy (2006) 1035
21 Brady et al. (2001) C1
22 Nambiar and Ramamurthy (2006a) 476
23 Akroyd (1962) 302
24 Huang et al. (2015) 390
25 Pan et al. (2014)
26 Ashworth et al. (2013) 65
27 Petit et al. (2014) 40
28 Hilal et al. (2015a) 231

(coalescence) in foam concrete, and discussed its influence on air void size distribution. Lu et al.[29] have discussed foam stability in light of producing a maximum of closed pores.

6.1.3 Segregation and Bleeding

Three mechanisms of segregation may occur in foam concrete. Firstly, heavy particles may sink in the mix due to gravity forces. Secondly, air bubbles may rise due to buoyancy. Finally, water may migrate to a layer on top of the paste as 'bleed water', distinct from the rest of the mix.[30]

In each case, the ingredients no longer remain uniformly distributed within the paste. To avoid segregation, foam concrete should be produced with a stiff enough consistency to resist the buoyant forces of air bubbles, and the gravity forces of heavy particles. The paste should be cohesive, without excess water, to avoid bleeding. Typically, surfactants are designed to inhibit the bleeding of water.[31]

In their foam concrete specification, Brady et al.[32] suggested that segregation may be tested by casting a 100 mm diameter x 300 mm long cylinder, removing 25 mm thick slices from top and bottom of the cast, and ensuring that their oven dry densities do not vary by more than 50 kg/m^3.

6.1.4 Plastic Density

Plastic density is typically measured to confirm that the desired volume of volume of foam has been added to a mix.[33] Plastic density is readily tested during production and mixing, providing fine-level control over dry density, and thus hardened properties, of the foam concrete. Plastic density measurements also provide valuable information about the quality of a mix. Good stability and low segregation are assured where measured values of plastic density do not deviate significantly from theoretical values nor from mean values, respectively.

---

29 Lu and Qin (2015)
30 Brady et al. (2001) 5
31 Yue and Bing (2015)
32 Brady et al. (2001) 9
33 Giannakou and Jones (2002)

Brady et al.[34] proposed a tolerance of ±100 kg/m^3 from a target plastic density for dense foam concrete mixes, but suggested a more stringent tolerance of ±50 kg/m^3 for lightweight mixes, since hardened properties vary more significantly with density at lower densities. ASTM C796[35] permits a tolerance of ±50 kg/m^3 for a 640 kg/m^3 mix, in the standard test method for evaluating foaming agents used to make preformed foam for cellular concrete.

Reducing plastic density for a given hardened density may be advantageous for various applications. Lower plastic densities reduce vertical and hydrostatic loads during construction. Additionally, reducing the self-weight of fresh foam concrete may help to avoid the collapse of foam structures. Fresh density is typically 150 to 200 kg/m^3 higher than dry density.[36] However, fresh density may be reduced with minimal effect on hardened density or properties by adjusting three parameters: water content is minimized to reduce weight, while foam is added to maintain volume, and superplasticizer is added to maintain consistency.

Density of foam concrete will be discussed in greater detail later in this chapter, with respect to the dry density of hardened concrete. (Refer to Section 6.3.1a)

[34] Brady et al. (2001) 8
[35] ASTM C796/C796M-12, Section 7.3.1
[36] Brady et al. (2001) 2

6.2 Curing Properties

6.2.1 Rate of Hardening

The rate of hardening in foam concrete typically decreases with decreasing density. According to the results of one study, Portland-only mixes of 1000 kg/m^3 plastic density stiffen around 4.5 hours and begin to set at 12 hours, while mixes of 300 kg/m^3 stiffen at 10 hours and begin to set at 18 hours.[1] The porous structure of foam concrete may limit the availability of reaction ingredients at a given location, reducing the rate of hydrate nucleation; additionally, a slow rate of setting has been attributed to retarding properties of protein-based foams.[2] [3]

The setting behaviour of foam concrete has a strong influence on mix stability. Surface tension within the bubbles must be maintained, until solid cementitious structures develop that are capable of carrying the foam concrete self-weight. Generating these structures quickly reduces the risk that bubbles will collapse or coalesce.

Rapid hardening may also be desirable to speed construction. Traffic loads may be accommodated and additional lifts of material may be placed sooner.[4] Reducing the amount of time required for setting allows for faster demoulding and reuse of formwork, which is especially important for precasting operations.

The setting time of foam concrete may be reduced in a number of ways. Chemical accelerators, such as calcium chloride,[5] or fast setting cements, such as aluminate cement[6] or calcium oxide,[7] may be used. Fine binders[8] or fine fillers help to generate an even, continuous skeleton structure more quickly than when coarser solids are used.[9] Increasing cement content,[10] raising the ambient temperature,[11] or using insulated formwork to retain exothermic heat,[12] increases the speed of the hydration reaction in foam concrete. It has

1 She et al. (2014b) 69
2 Brady et al. (2001) C8, She et al. (2014b) 69
3 Pan et al. (2014) 257-258
4 Van Deijk (1991)
5 Brady et al. (2001) C4
6 Huang et al. (2015) 390
7 Chen et al. (2014) 137
8 Tarasov et al. (2010) 896
9 Van Deijk (1991) 49
10 Jones and McCarthy (2006) 1035
11 She et al. (2014b) 71
12 Van Deijk (1991) 49

been suggested that using superplasticizers to reduce the w/c ratio may also help produce a faster setting mix,[13] although other studies[14] indicate that higher w/c ratios may improve the set time. Presumably, the w/c ratio may be optimized for the desired rate of hardening. Narayanan and Ramamurthy[15] evaluated a variety of chemical accelerators to decrease demoulding time for the production of lightweight foam concrete blocks having approximately 1250 kg/m^3 plastic density. In the study, calcium chloride reduces mix stability and requires 4.5 hours to set up; triethanol amine requires more than 6.5 hours to set up; calcium nitrate requires more than 4 hours to set up; and alum requires 2 to 3 hours to set up, but is deemed uneconomical based on the required dosage. The authors also discuss the use of lithium salts and calcium formate.

Research by She et al.[16] employed an ultrasonic pulse velocity (UPV) method to characterize setting behaviour for mixes of varying composition and density. The study identifies a dormant stage, an acceleration stage, and a deceleration stages for each recipe. A marked reduction in setting time is observed as the curing temperature is increased from 20°C to 80°C.

6.2.2 Heat of Hydration

The hydration of cement is an exothermic reaction. Control over temperature development is important to avoid differential strain and cracking caused by temperature gradients.[17] In extreme cases, high temperatures are capable of causing the evaporation of water, reducing the amount of liquid water available for reaction.[18] If internal temperatures exceed 90°C, protein coagulation may cause protein-based foams to collapse; or the expansion of heated air may rupture bubble structures.[19] Another consequence of high early temperatures is the delayed formation of ettringite. If the mineral is inhibited from crystallizing until after the mix has stiffened or set, its eventual growth may expand and crack the concrete.[20]

---

13 Van Deijk (1991) 49
14 Tarasov et al. (2010) 896
15 Narayanan and Ramamurthy (2012)
16 She et al. (2014b)
17 Jones and McCarthy (2005b) 24
18 Cf. Mehta (1986) 331, Jones and McCarthy (2006) 1036
19 Tarasov et al. (2010) 899
20 Kosmatka et al. (2002) 17-18

Some authors[21] suggest that this phenomenon is not a major concern for foam concrete, as the air voids provide sufficient space to accommodate delayed ettringite formations (DEF); however, Jones and McCarthy note that certain mix compositions may be more susceptible to DEF, and recommend further research into the issue over a long period.[22]

Temperature development occurs differently in foam concrete than in normal density concrete. The presence of closed air voids has a significant insulating effect, reducing the dissipation of heat.[23] Simultaneously, a lower mix density corresponds with a lower heat capacity. Consequently, low-density foam concrete mixes are especially subject to temperature rise. Furthermore, foam concrete recipes often incorporate relatively large proportions of cementitious content in order to achieve sufficient strength, resulting in greater amounts of reaction energy generated per unit volume. For mixes with a dry density of less than approximately 800 kg/m^3,[24] sand is seldom used as filler due to segregation issues; rather, additional cementitious materials are included. High cementitious densities are also used to compensate for the inherently lower mechanical strength of the porous material. Cementitious densities may range from 300 to 600 kg/m^3 in foam concrete, resulting in internal temperatures as high as 62°C above ambient temperature,[25] or even higher.[26]

A final significant consideration is that the majority of foam concrete is used in large volume applications, such as in-situ void-filling, or the precasting of large masses. At such scales, there will be significant variation between core and surface temperatures. Since foam concrete cures faster at elevated temperatures, the exothermic reaction will occur even faster nearer the core, intensifying the thermal gradient;[27] the situation is exacerbated by foam concrete's limited capacity to absorb or dissipate heat. Cracking induced by thermal strains can have negative effects on important properties such as mechanical strength, water uptake, impermeability to gases, and resistance to chemical attack.

---

21 Brady et al. (2001) C8
22 Jones and McCarthy (2006)
23 Tarasov et al. (2010) 905
24 Fouad (2006) 562. A limit of 1200 kg/m^3 has also been suggested, cf. Brady et al. (2001) C2.
25 Jones and McCarthy (2006) 1037
26 Brady et al. (2001) C8
27 Tarasov et al. (2010) 905.

Temperature rise may be slowed by reducing the rate of the hydration reaction, reversing the strategies described in the section above. The fineness of materials may be adjusted, or a chemical retarder may be included. Alternatively, hydraulic ingredients may be replaced with pozzolanic materials, such as fly ash or slag. The pozzolanic reaction is delayed, as calcium hydroxide must first be produced by the hydraulic reaction of cement; additionally, the finely divided pozzolans adsorb water, limiting the amount of water readily available for cement hydration.

Since a rapid speed of hydration is often desirable, other approaches may be preferred. Parameters such as the temperature of mix ingredients and ambient curing temperature and humidity may be regulated to control the heat of hydration. Water has a very high heat capacity, so by increasing the amount of water in a mix, more energy will be absorbed per unit change in temperature.[28] Similarly, the heat capacity of binders and fillers may be considered.[29] Increasing density, or controlling the pore size distribution and connectivity[30] to facilitate heat transfer may be appropriate solutions for some applications.[31]

Jones and McCarthy[32] have studied the influence of plastic density, cementitious content, and inclusion of fly ash on foam concrete temperature development and concrete strength. Tarasov et al.[33] have developed some early mathematical models to predict temperature rise in foamed concrete. These models incorporate factors that are insignificant in normal density concrete, such as the heat capacity of each of the constituent materials.

6.2.3 Drying Shrinkage

Drying shrinkage is an important issue for foam concrete. The topic warrants a close study, including a review of several drying shrinkage mechanisms. Note that there is uncertainty and debate over the mechanisms of drying shrinkage, and the range of relative humidities

[28] Jones and McCarthy (2006) 1036
[29] Jones and McCarthy (2006) 1036
[30] Jones and McCarthy (2006) 1037
[31] Tarasov et al. (2010) 896
[32] Jones and McCarthy (2006)
[33] Tarasov et al. (2010)

in which they operate.[34] The discussion below serves as a brief introduction to this complex topic.

Water is held in various states in a hydrated cement paste. Larger voids hold the water relatively loosely, and may absorb or release water with little effect on the hydrated cement paste. Water is held more rigidly in smaller voids, and the removal of water from these locations causes drying shrinkage.

The first water to be lost from a drying concrete sample is free water, held in large cavities. Because this free water is not attached to the solidified concrete by physical or chemical bonding, its removal does not have a major influence on the mechanics or structure of the hydrated cement paste.[35]

As the relative humidity decreases, water is removed from smaller capillaries, between 5 and 50 nm in size.[36] In each partially filled capillary pore, a meniscus is formed over the residual water. Surface tension of the water induces a compressive stress on the walls of the capillary pore, causing shrinkage of the specimen. Much of this shrinkage is elastic, and as the relative humidity continues to decrease below 50 or 40%, a significant amount of this shrinkage strain will be relieved. This mechanism is known as *capillary tension*.[37]

Where the RH is below 40%, shrinkage strain is largely related to the removal of adsorbed water from the surface of cement gel particles. Mehta[38] suggested that the loss of adsorbed water is the main cause of drying shrinkage in hardened cement paste. This water is held by hydrogen bonding in layers up to six molecules deep. These layers are capable of causing volumetric change in two ways, as they affect *surface tension* and *disjoining pressures* in the cement gel.

Surface tension acts along the surfaces of solid materials. This tension exists due to lack of symmetry of intermolecular forces: whereas molecules inside the solid are held in

---

34 For example, Powers (1965) suggested that disjoining pressures operate at all relative humidities; the Munich model, developed by Wittmann (1968, 1973, 1978) proposed that disjoining pressures are important beyond 50% RH, and the Feldman-Sereda model (1970) did not account for this mechanism. Such diverse perspectives are reviewed by Hearn et al. (1994) and Kovler and Zhutovsky (2006). A conciliatory position today is that many mechanisms operate within respective humidity ranges, cf. Idiart (2009) 45.

35 Mehta (1986) 32

36 Mehta (1986) 29, 90

37 Idiart (2009) 46

38 Mehta (1986) 29

equilibrium by the attractive and repulsive forces of neighbouring particles, molecules at the surface of solids are exposed to dissimilar forces in interior and directions. In order to maintain equilibrium, there is a resultant force normal to the surface, which induces a contraction, or surface tension, in the plane of the surface. Cement gel has a high surface area to volume ratio, so this surface tension can have a significant effect on solid volume. When adsorbed layers of water are present on the solid surface, surface molecules exist in a state of greater equilibrium, reducing surface tension. However, as these adsorbed layers are removed during drying, surface disequilibrium increases, compressive stresses intensify, and solid volume is reduced.[39]

Disjoining pressures also influence volumetric change. Ideally, to produce the lowest energy state, the adsorbed layer of water on a surface should be of a consistent thickness, determined by the local RH and temperature. However, where two surfaces come close together, there may not be sufficient space between them to develop the appropriate thickness of the adsorbed layer. Swelling occurs at these areas of hindered adsorption, forcing the surfaces apart. When the sample dries, these disjoining pressures decrease. The surfaces draw close, and the volume of the sample is decreased.[40]

A final source of drying shrinkage occurs with the loss or *movement of interlayer water*. This film of water, one molecule thick, separates the solid layers, or 'sheets', of C-S-H. The water is held in place by strong hydrogen bonds, and will only be given up with extreme drying, below 11% RH. A small decrease in interlayer water brings about significant volumetric change.[41]

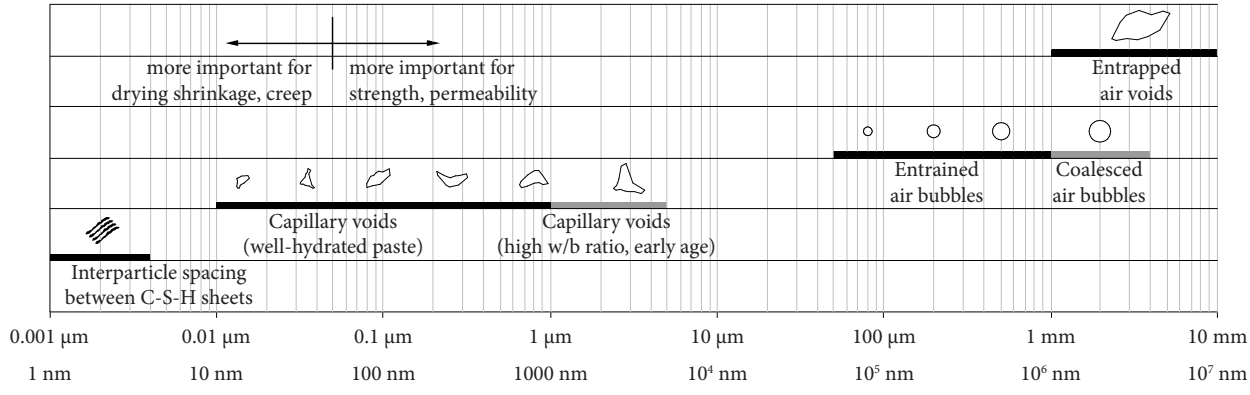

Figure A-6.2.3 Scale of voids in concrete. Water is held more rigidly in smaller voids. After Mehta (1986).

[39] Idiart (2009) 46
[40] Powers (1965), Idiart (2009) 46-47
[41] Mehta (1986) 29

In normal density concrete, drying shrinkage is reduced through two main strategies. Firstly, the inclusion of rigid aggregate physically restrains the shrinkage of the hydrated cement paste. Coarse aggregate is usually recommended: according to Neville, this is because the use of larger aggregate allows for a leaner mix.[42] Secondly, w/c ratios are kept to a minimum. Neville suggested that lower w/c ratios allow for the maximum volume of restraining aggregate; [43] additionally, reducing the w/c ratio helps to minimize the volume of capillary void in hardened cement paste,[44] by increasing the density of the paste and reducing residual spaces between cement grains.[45]

Foam concrete, however, is highly susceptible to drying shrinkage. High w/c values result in a large volume of capillary pores,[46] promoting capillary tension as the water evaporates. Relatively high cementitious densities combined with significant water volume results in a large amount of C-S-H gel with a large surface area, which is subject to the effects of surface tension and disjoining pressures.[47] In the event of strong drying, the large volume of C-S-H consists of mineral sheets that compress with the removal of interlayer water. Since foam concrete rarely contains coarse aggregate, and often contains no aggregate at all, the material typically possesses minimal capacity to mechanically resist drying shrinkage.

Foam concrete shrinkage may be an order of magnitude greater than that of normal density concrete.[48] Neat cement mixes may experience shrinkage as high as 3,300 to 4,400 μstrain.[49] Sanded foam concrete mixes may experience only 700 or 1,200 μstrain;[50] however, these values are still high compared to performance of normal density concrete with a low w/c ratio, which may only experience 200 to 400 μstrain.[51]

Numerous factors may be correlated with foam concrete shrinkage, from water content[52] to density[53] to pore size distribution.[54] A good understanding of drying shrinkage

---

42 Neville (1963) 288
43 Neville (1963) 289
44 Young et al. (1998) 221, Just and Middendorf (2009) 742, Jones et al. (2012) 520
45 Mehta (1986) 27
46 Nambiar (2007b) 1346
47 Cf. Georgiades (1991), in which pore surface area is related to drying shrinkage in AAC
48 Valore (1954b) 830
49 Neville (1963) 448
50 Nambiar and Ramamurthy (2009) 632
51 Neville (1963) 288
52 Jones et al. (2012) 520
53 British Cement Association (1994). Cited in Brady 2001, Table C5.

control for foam concrete may be gained by considering four major parameters: cementitious density, volume of filler, type of filler, and curing regime. Special foaming agents may also be used to reduce drying shrinkage.

Cementitious density

As would be expected from the mechanisms outlined above, a reduction in cementitious density helps to reduce drying density. Cement content may be reduced by replacing cement with increased void content, thus reducing density,[55] or by replacing cement with filler, maintaining density.[56] Reducing cementitious density from 400 to 300 kg/m^3 may result in approximately 20% less shrinkage in mixes of 1400 kg/m^3 plastic density, and approximately 10% and 11% less shrinkage at 1000 and 600 kg/m^3 plastic density, respectively.[57]

Filler volume

At densities less than 1400 kg/m^3, where cementitious density is kept constant, literature suggests that drying shrinkage increases with reduced density (i.e. reduced filler volume).[58] This effect is consistent with an understanding that rigid filler restrains drying shrinkage. Interestingly, however, in a study by Jones et al.,[59] mixes with a plastic density of 1400 kg/m^3 experienced less shrinkage than mixes of 1800 kg/m^3 plastic density, with cement content held constant. This effect may be due to the greater total volume of shrinkable mortar paste in the 1800 kg/m^3 mix.[60] It is also possible that the structure of the spherical air voids in foam concrete contributes to volumetric stability.[61] Yet another explanation is that the surfactant acts as a 'shrinkage reducing admixture', relieving water surface tension at the menisci of capillary pores:[62] an increase in surfactant concentration within a smaller volume of paste increases the efficacy of the 'admixture'.

---

54 Nambiar and Ramamurthy (2009) 633 , Cf. Georgiades (1991)
55 Ramamurthy et al. (2009) 390
56 Nambiar and Ramamurthy (2009) 632, Figure 1.
57 Jones et al. (2012) 520
58 Jones et al. (2012) 520
59 Jones and McCarthy (2005b) 25
60 Nambiar and Ramamurthy (2009) 632
61 Jones and McCarthy (2005b) 25
62 Nambiar and Ramamurthy (2009) 633

Filler type

The influence of filler type increases as filler content increases, i.e. in denser mixes.[63] In general, the influence of filler on drying shrinkage may be related to particle fineness. Fine particles have a diminished capacity to resist shrinkage. Additionally, they increase water demand due to their high surface area, resulting in greater capillarity and a thicker layer of adsorbed water,[64] which intensifies the effects of capillary tension, surface tension, and disjoining pressures.

Consequently, where coarse fly ash is used as a filler replacement for sand, greater shrinkage is experienced in mixes of the same dry density. The finer particles of fly ash have a lesser capacity to restrain shrinkage; and a greater volume of paste is produced. In this case, the volume of air voids is less, both since more water is required for good consistency, and since fly ash has a lower particle density than sand.[65] A 1400 kg/m^3 plastic density mix with 400 kg/m^3 cementitious density has been shown to have approximately 37% less shrinkage with sand than with coarse fly ash filler. However, as cementitious density is reduced, differences in shrinkage appear to become less significant, perhaps due to improved particle packing.[66]

Research into the use of various recycled and secondary aggregates in foam concrete has shown that mixes incorporating demolition fines, incinerator bottom ash, or china clay sand tend to experience even greater shrinkage strain than mixes with coarse fly ash. This has been attributed to high degree of water absorption in these filler types:[67] the higher water requirement likely results in a less compact hardened cement paste matrix, which perhaps incorporates an increased volume of capillary pores.[68]

Coarse lightweight aggregates may be used in foam concrete to provide effective restraint of drying shrinkage.[69] It has also been suggested that the incorporation of polypropylene fibres may help improve shrinkage performance; however, there is limited data available to support this proposal.[70]

---

63 Jones et al. (2012) 520
64 Nambiar and Ramamurthy (2009) 632
65 Nambiar and Ramamurthy (2009) 632
66 Jones et al. (2012) 520
67 Jones et al. (2012) 520
68 Just and Middendorf (2009) 742
69 Weigler and Karl (1980), Regan and Arasteh (1984), Regan and Arasteh (1990)
70 Jones and McCarthy (2005b) 27, Brady et al. (2001) C9, Papayianni and Milud (2005) 26

When fine fly ash is used as a partial replacement for Portland cement, shrinkage decreases. It is understood that unreacted grains of fine fly ash provide restraint, acting as a rigid aggregate.[71] By contrast, the incorporation of silica fume, which is extremely fine, is reported to have a relatively insignificant influence on drying shrinkage.[72]

Curing regime

Curing regime can have a significant influence on drying shrinkage. High pressure steam curing, or autoclaving, dramatically reduces shrinkage of cellular concrete[73] by improving the mineralogical composition and nanostructures of calcium silica hydrates in an appropriately proportioned mix.[74] Foam concrete is rarely cured in this manner, however, for reasons discussed in Chapter 2.[75] Among non-autoclaving curing techniques, seal-curing has been shown to reduce shrinkage.[76] The length of time during which a specimen is maintained in a curing environment with a high RH may influence drying shrinkage by increasing the degree of hydration and reducing capillarity, and thus capillary tension. Conversely, unhydrated cement grains also restrain shrinkage. These effects, which are negligible in normal density concrete,[77] may be more consequential in foam concrete, and require further study.

Foaming agents

Some foaming agents have been developed to reduce the drying shrinkage of foam concrete.[78] As described above, surfactants can reduce water surface tension at the menisci of capillary pores:[79] this approach, therefore, will be especially effective at reducing shrinkage while the sample dries from 50 to 40% internal relative humidity.

---

71 Jones and McCarthy (2005b) 25
72 Zhang et al. (2014) 117
73 Neville (1963) 454
74 Alawad et al. (2015) 382, Winter (2016), RILEM Technical Committees 78-MCA and 51-ALC (1993) 28
75 Short and Kinniburgh (1978) 295
76 Brady et al. (2001) C9
77 Neville (1963) 292
78 Brady et al. (2001) C12
79 Nambiar and Ramamurthy (2009) 633

6.3 Hardened State Properties

6.3.1 Physical Properties

6.3.1a Dry Density

Density is a key property of foam concrete. Low density is a critical consideration for many foam concrete applications; and density has a dominant effect on other mechanical, thermal, transport, and durability properties, as well.

A remarkable range of densities is possible. With porosities in excess of 90 percent or as low as 10 percent of volume, dry density measurements of foam concrete may range from only 140 kg/m^3,[1] to more than 1900 kg/m^3.[2] In most foam concrete mixes, dry density measurements are between 400 and 1600 kg/m^3.[3]

Density is principally controlled by foam volume. Less significantly, the proportions and particle densities of fillers and binders will also influence the density of the hardened cement paste.

The moisture content of a sample can have a strong influence on its measured density. Oven-dry values, determined through standardized testing methods, help facilitate comparisons among materials.[4] However, concrete in the field usually contains significantly more moisture than an equivalent oven-dry sample. More realistic dry density values may be determined by storing a sample at a specified temperature and relative humidity until equilibrium.[5] Often, authors may simply report material 'dry' density following a given curing/drying regime. Valore[6] suggested that "oven-dry" and "room-dry" densities of cellular concrete are typically close enough to permit comparison of reported properties from various sources.

Foam concrete mixes with especially high or low densities are subject to certain extra consideration. At high densities, designers must ensure that mixes are not too stiff, or else

1 Akthar and Evans (2010) 354
2 Fouad (2006) 562, Gunawan and Busra (2014) 436
3 Brady et al. (2001) 2
4 Cf. ASTM C796/C796M-12, Section 8.2
5 Cf. ASTM C1585-13, Note 4
6 Valore (1954b) 818-819

foam bubbles may be destroyed during mixing.[7] Very low-density mixes are subject to a number of challenges. During curing, stability is a significant concern: the plastic self-weight of foam must not exceed the structural capacity of the liquid bubbles. Curing is slow, since protein-based foams retard hydration,[8] and since cementitious content is low and dispersed in highly foamed mixes. Bubbles tend to coalesce in mixes with densities below 720 kg/m^3;[9] at densities of less than 240 kg/m^3, large voids with diameters of up to 3mm may form.[10] These larger bubbles are especially detrimental to mechanical properties.[11]

Use of preformed foam is more appropriate than high speed mixing for very low-density foam concrete, as it provides better control over density and cell structure.[12] Tonyan and Gibson[13] studied a variety of additions to the cement paste for stability at low density. A microsilica liquid admixture improved cohesiveness; superplasticizer reduced water requirements to minimize self-weight and improve hardened paste properties; and polyester fibres improved foam stability during curing. Stable mixes were possible with densities as low as 160 kg/m^3. Minimizing w/c ratio,[14] and ensuring the thickness and adhesiveness of the surfactant,[15] also appears to help generate a maximum of closed cells in low-density mixes.

Strategies to accelerate curing can help to counter slow strength development. (See Section 6.2.) Recently,[16] magnesium phosphate cement has been used to produce foamed concrete with densities between 250 and 400 kg/m^3. The success of these trials has been attributed in part to quick hardening and high early strength characteristics of the binder. Minimizing the amount of protein-based surfactant concentrate in a mix may also help reduce its retarding effects.[17] In an effort to produce 'super low density foamed concrete,' Pan et al.[18]

---

7 Nambiar and Ramamurthy (2006) 476
8 Pan et al. (2014) 258
9 Tonyan and Gibson (1992b) 6378
10 Tonyan and Gibson (1992b) 6371
11 Cf. Just and Middendorf (2014) 747
12 Tonyan and Gibson (1992b) 6371
13 Tonyan and Gibson (1992b) 6372
14 Pan et al. (2014) 258
15 Cf. Akthar and Evans (2010) 353, Lu and Qin (2015) 7. Iota carrageenan and gelatin were used as thickeners, respectively
16 Yue and Bing (2014)
17 Akthar and Evans (2010) 353

eliminated foam surfactants entirely, instead producing bubbles by evolving oxygen gas from hydrogen peroxide. Strictly speaking, the resulting product is 'gas concrete' rather than 'foam concrete', but the investigation does highlight the influence of the surfactant on strength development, and thus viability, of low density mixes.

6.3.1b Air-Void Systems

Mixes of equivalent foam volume and density may vary in their properties due to other characteristics of their air-void systems. The size and uniformity, shape, spacing, and interconnectivity of air voids are related parameters, and their influence on foam concrete properties is summarized briefly below.

Size

Air void size has a significant effect on mechanical properties.[19] For a given foam volume, a mix with finer voids will perform better: small bubbles are better at maintaining a round shape; [20] and, geometrically, they permit a greater minimum wall thickness between cells. Additionally, larger air voids tend to be surrounded a weaker, more porous C-S-H phase,[21] analogous to the interfacial zone that occurs between paste and coarse aggregate in normal density concrete.[22] Cracks may be initiated at these local areas of weakness.[23] Finally, singular, large voids create structural discontinuities within the paste matrix. Research by Hengst and Tressler[24] concluded that failure in foam concrete can be explained according the Griffith criterion for fracture, where strength is limited by the most critical flaw: according to this research, the 'strength-dominating parameter' in foam concrete is the maximum pore size.

Void size may have a minor role in sorptivity. Although closed air voids do not facilitate capillary movement of water, and in fact appear to obstruct it,[25] the interfacial phase around large air voids may be highly conducive to liquid moisture, due to the

---

18 Pan et al. (2014) 259
19 Nambiar and Ramamurthy (2007a) 228
20 Just and Middendorf (2009) 747, Hilal et al. (2015a) 232
21 Ramamurthy et al. (2009) 391
22 Mehta (1986) 37
23 Roy et al. (1993) 1
24 Hengst and Tressler (1983) 134
25 Nambiar and Ramamurthy (2007b) 1346, Ramamurthy et al. (2009) 393

presence of microcracks and significant volume of capillary pores.[26] Average pore size may also influence the tortuousity of the path of liquid water moving through the hardened cement paste, and thus the rate of water ingress.[27]

Finally, the interfacial zones associated with larger air voids[28] may also make a mix more susceptible to freeze-thaw damage, or chemical attack.[29]

Higher air-void contents tend to increase void coalescence, and thus air-void size, due to the proximity of adjacent bubbles and relative weakness of the intervening paste-bubble membrane.[30] Various authors have noted a 'transition point' in foam volume, above which coalescence increases significantly. In a study by Wee et al.,[31] this transitional air content value was 40%; in a study by She et al.,[32] the value was 52%. This point occurs when there is insufficient cement paste to prevent coalescence, and is dependent on the properties of the paste.

For mixes of the same density and foam volume, the air void size may be controlled by four main parameters: initial pore size; surface tension and fluidity of the mix; and fineness of the paste.

Initial pore size

Initial pore size is related to the method of air void generation. Preformed 'dry foam' is superior to preformed 'wet foam' or high speed mixing for producing small and uniform air voids.[33] Preformed dry foam bubbles are typically 0.10 mm in diameter, before entering the cementitious paste.[34] Air voids in hardened foam concrete typically range from 0.10 to 1.0 mm in diameter, due to coalescence; [35] [36] bubble splitting is not believed to occur during mixing. [37] In very lightweight mixes, of approximately 240 kg/m^3, coalesced air voids may

[26] Mehta (1986) 37, Liu et al. (2014) 243
[27] Nambiar and Ramamurthy (2007b) 1346
[28] Narayanan and Ramamurthy (2000a). Cited in Ramamurthy et al. (2009) 391
[29] Roy et al. (1993) 1
[30] Wee et al. (2011) 585
[31] Wee et al. (2011) 593
[32] She, Chen, Zhang and Jones (2013) 1282
[33] Tonyan and Gibson (1992b) 6371
[34] She, Chen, Zhang and Jones (2013) 1282
[35] Nambiar and Ramamurthy (2007a) 223
[36] She et al. (2014a) 423
[37] Hilal et al. (2015a) 231

be as large as 3 mm in diameter.[38] By contrast, preformed wet foam is produced with large bubbles, initially 2 to 5 mm in diameter,[39] and control over density, foam volume, and bubble size distribution is difficult with high speed mixing,[40]

Surface tension and fluidity

Good plastic viscosity and strong surface tension are necessary to maintain bubble size. If a mix is highly fluid, bubbles will migrate easily in the paste, collecting and coalescing due to the reduced yield stress.[41] A low surface tension reduces the capacity of the bubble film to resist disequilibrium pressures, which also tend to increase coalescence in the mix.[42] Viscosity and surface tension are reduced simultaneously with the addition of either water or superplasticizer. Work by Wee et al.[43] has shown that for a given air content, where the w/c ratio of a mix is varied from 0.3 to 0.5, air void size increases with w/c ratio. Air void size also increases with the use of superplasticizer, especially in mixes with high air content.[44] Conversely, Lu and Qin[45] have shown that incorporating gelatin in the mix increases viscosity, reducing gravitational drainage and coalescence.

Fineness of paste

Finally, the use of fine fillers[46] and binders[47] helps maintain uniform spacing, which is also an effective way to reduce coalescence and maintain small bubble size, as elaborated below.[48]

Wee et al.[49] suggested that optimal air-void size for foam concrete is 0.15mm, for attaining a maximum strength-to-density ratio. Note that preformed dry foam bubbles are only 0.10mm, so a minimum of coalescence is permitted. However, this optimal size, and its significance, may vary with composition of paste and surfactant type. For instance, Nambiar and Ramamurthy[50] noted that air void size appeared to be a more significant

38 Tonyan and Gibson (1992b) 6371
39 Aldridge (2005) 3
40 Akroyd (1962) 302
41 Wee et al. (2011) 587
42 Wee et al. (2011) 588
43 Wee et al. (2011) 585
44 Wee et al. (2011) 588
45 Lu and Qin (2015) 7
46 Ramamurthy et al. (2009) 391
47 Cf. Just and Middendorf (2009) 748
48 Wee et al. (2011) 588, Nambiar and Ramamurthy (2007a) 226
49 Wee et al. (2011) 590
50 Nambiar and Ramamurthy (2007a) 228

parameter in cement-sand mixes than in cement-fly ash mixes.

Shape

Spherical voids bubbles are preferred to elongated, flattened or irregular bubbles, for optimal mechanical properties,[51] since irregularities promote stress concentration under loading.

A shape factor, or circularity factor, may be defined as a function of perimeter and area of section through an air-void. Often the shape factor is normalized, so that a perfect circular gives a circularity factor of unity.[52] In the equation given below, the shape factor increases with irregularity:

$$F_{circ} = \frac{(Perimeter)^2}{4\pi(Area)}$$

Shape is closely related to bubble size, as larger bubbles formed by coalescence are more likely to be irregular. Consequently, irregular bubbles are more common in mixes with higher foam content.[53] Additionally, the self-weight of curing foam concrete can cause subsidence and flattening of bubbles during setting.[54] This effect should also be considered for low-density mixes in particular.

Maximizing surface tension helps to promote circularity, as incidences of coalescence are reduced, and deformations of bubbles during mixing and setting are resisted more strongly. Surface tension is maintained through the use of viscous surfactants, minimizing the w/c ratio, and avoiding the use of superplasticizers.

Finer solids also help to reduce coalescence and deformation of bubbles. A consistent coating of paste around each bubble is understood to reduce bubble merging.[55] Finer materials make the paste smooth during mixing and promote uniform distribution, helping the bubbles to be at greatest equilibrium in a spherical form.[56]

---

51 Valore (1954b) 817
52 Nambiar and Ramamurthy (2007a) 228
53 Hilal et al. (2015a) 232
54 Valore (1954b) 817
55 Nambiar and Ramamurthy (2007a) 226
56 Nambiar and Ramamurthy (2007a) 228

Uniformity

Consistency of bubble sizes has a beneficial effect on compressive strength.[57] Griffith's model of fracture suggests that maximum pore size, rather than average pore size, may limit strength in foam concrete;[58] thus, it is desirable to produce foam concrete with a narrow range of air void size distribution.

As could be expected from the explanations of coalescence mechanisms above, tighter air void size distribution is associated with low air content, [59] [60] low w/c ratio, no plasticizer, viscous mixes,[61] and use of fine solids. [62] If reinforcing fibers are used, they should be fine and relatively flexible, so as not to disrupt the uniformity of bubbles.[63]

Additionally, coarsening of the foam occurs at a greater rate in mixes that have a range of bubble sizes, than in mixes with consistent bubble sizes. Coarsening occurs due to differences in surface tension among bubbles of different sizes, resulting in different pressures within the bubbles: more highly pressurized air in smaller bubbles will tend to diffuse into an adjacent larger bubble.[64] For this reason, it is desirable to introduce highly consistent bubbles into a mix, such as are generated through preformed dry foam.

Spacing

Powers[65] proposed a spacing factor for air voids in the study of air-entrained concrete. By ensuring that every capillary pore in a paste is within 0.1 to 0.2 mm of an air void, freeze-thaw damage is reduced, since water may migrate to the escape boundary of the air void instead of building pressure within capillary pores during freezing.[66]

Spacing factors are not significant as indicators of freeze-thaw performance for foam concrete. Mixes with air content as low as 10% usually have spacing factors of 0.2mm or less, and mixes with high air contents have spacing factors an order of magnitude

57 Ramamurthy et al. (2009) 391
58 Hengst and Tressler (1983) 134, Lian et al. (2011) 4296
59 Nambiar and Ramamurthy (2007a) 226
60 She, Chen, Zhang and Jones (2013) 1282
61 Lu and Qin (2015) 7
62 Nambiar and Ramamurthy (2007a) 226
63 Amran et al. (2015) 997, Yakovlev et al. (2006) 147
64 Mielenz et al. (1958)
65 Powers (1954)
66 Mehta (1986) 125

lower.[67] Instead, in foam concrete, the spacing factor may be used as a measure of mean paste thickness,[68] indicating the resilience and strength of cell walls during fresh and hardened states, respectively.

In tests by Wee et al.,[69] a spacing factor of 0.02 mm appeared to be an approximate lower limit for foam concrete: thinner cell walls will collapse and bubbles will coalesce. Mechanical strength and modulus of elasticity diminished rapidly as the spacing factor was reduced below 0.05mm;[70] thus, a spacing factor of 0.05 mm was deemed to be optimal for achieving a high strength-to density ratios in the cement-slag mixes tested.

Use of fine solids is especially important for producing viable mixes with very small spacing factors. Fine solids make the paste more consistent at a fine scale, promoting uniform spacing and providing a uniform coating to the bubbles, with minimal discontinuities.[71] They also permit efficient particle packing, resulting in a dense and continuous mortar between cells.

At very fine spacing between air voids, the relative charges of surfactants and solid particles become increasingly important for the stability of bubble walls. In a colloidal model, the zeta potential is defined as the degree of electrostatic repulsion or attraction between a dispersion medium, and the electrical double layer (EDL) that adheres to a dispersed particle. A high zeta potential indicates that a mix is electrically stable, as it implies a strong repulsive force between dispersed particles. However, if the zeta potential is small, the repulsion forces of similarly charged dispersion particles may be overcome, leading to coalescence of dispersed particles. For a plastic foam concrete mix, a zeta potential exists between solids in the fresh paste, and surfactant molecules (the EDL) that surround each air void.[72] Foam films are stabilized by the strong adhesion between surfactant molecules and solid particles. Strong adhesion between surfactant and solids is especially critical where air-void spacing is low, in order to maintain a continuous thin film of solids that separates the ELDs of adjacent air voids. This solid layer is necessary to

[67] Wee et al. (2011) 586
[68] Wee et al. (2011) 588
[69] Wee et al. (2011) 588
[70] Wee et al. (2011) 591
[71] Nambiar and Ramamurthy (2007a) 226
[72] Lu and Qin (2015) 5

inhibit both coalescence and coarsening.[73] Thus, charges of surfactants and solid cementitious or filler particles must be calibrated to ensure stability of these extremely thin walls, in particular.

Interconnectivity

In foam concrete, interconnectivity between air voids occurs due to the rupture of the liquid bubble wall, after the stiff solid skeleton framework has already begun to set. The interconnected bubbles are restrained from forming a more spherical shape by the stiffened paste, resulting in two or more identifiable but connected pores, rather than one single pore. Aging mechanisms in liquid foam promote interconnectivity: gravity drainage removes water needed for hydration from the cell wall, as well as suspended cementitious particles needed for solidification; and gas transfer between adjacent bubbles during coarsening may apply additional strains on bubble walls, contributing to their rupture.[74] Additionally, cement reactivity, the growth of hydration products, and shrinkage may destabilize bubble films during setting, increasing interconnectivity,[75] and the thermal expansion of air bubbles within cement paste, due to heat of hydration, may induce the formation of micro-cracks.[76]

Interconnectivity of air-voids influences numerous hardened and fresh-state properties. As could be expected, compressive strength is reduced, since an interconnected pore is essentially a larger flaw within the solid matrix, subject to a lower failure stress.[77]

Fluid transport increases with interconnectivity. In foam concrete, isolated voids dampen sorptivity, and often will not be filled through water absorption at normal pressures.[78] This isolation of air voids helps explain why a foam concrete sample with a specific gravity less than unity will float in water for long periods of time. As cells become more interconnected, penetrability to fluids increases, with influences on other properties as well.[79] Freeze-thaw damage may increase due to the greater ingress of water into an

[73] Petit et al. (2014) 37
[74] Petit et al. (2014) 37
[75] Petit et al. (2014) 38
[76] Kearsley and Mostert (2005b) 144
[77] Petit et al. (2014) 37
[78] Nambiar and Ramamurthy (2007b) 1341
[79] Brady et al. (2001) C13

interconnected microstructure structure.[80] Fluids may carry ions more easily into the porous body, increasing chemical attack.[81] Greater saturation of the porous body results in lower thermal resistance.[82]

In some cases, porosity of foam concrete is a desirable characteristic, for example, as a permeable fill underneath sports fields and athletic tracks.[83]

Similarly, permeability to gases increases with interconnectivity.[84] This property is important in applications where foam concrete is required to create an air seal, for example, in fire control in mines.[85] Permeability to gases also has an effect on thermal resistance, as a more interconnected air-void structure facilitates a greater degree of convective heat transfer.[86]

Interconnectivity of air voids in foam concrete is understood to have an influence on its acoustic performance,[87] since interconnected voids are better at absorbing sound.[88]

Interconnectivity of pores will affect not only hardened properties, but also curing properties of foam concrete. It has been proposed that higher rates of heat loss from interconnected cells may reduce temperature rise due to heat of hydration.[89] Similarly, fluid transport rates and vapour permeability will presumably have an effect on drying rates, which in turn may affect drying shrinkage and mechanical properties. These effects may be non-negligible in large-scale pours. These effects are discussed in Sections 6.1 and 6.2.

Interconnectivity can be controlled through many of the strategies described above to minimize coalescence. Interconnectivity is increases with air content:[90] just as Wee et al.[91]

---

80 Jones and Giannakou (2004) 8
81 Jones and McCarthy (2005c) 1406
82 Cf. Yang and Lee (2015) 110
83 Van Deijk (1991) 51
84 Brady et al. (2001) C13
85 Lu and Qin (2015)
86 Petit et al. (2014) 37
87 Petit et al. (2014) 37
88 Ramamurthy et al. (2009) 391
89 Jones and McCarthy (2006) 1037
90 Jones and McCarthy (2006) 1037
91 Wee et al. (2011) 593

and She et al.[92] reported a threshold air content above which coalescence increases dramatically, Jones and McCarthy[93] noted a critical threshold of about 50% air content, above which interconnectivity becomes evident. Interconnectivity is reduced when w/c ratio is minimized.[94] Use of resilient, adhesive surfactants helps to produce closed cell: protein-based foams have a good record of producing closed cell structure,[95] and the viscosity of surfactants may be increased with gelatin[96] or other substances[97] for a greater proportion of closed cells. Furthermore, the use of fine solids like silica fume increases the proportion of closed air voids.[98]

Since interconnectivity of air voids occurs as bubble walls break during curing, changes to the mix during hydration must be considered as well. The aging mechanisms of liquid foam, and the interaction of a surfactant with products of hydration, are important considerations. Accelerators can help to solidify cell walls before they are damaged by drainage, drying shrinkage, or other destabilizing effects during curing.[99] However, holes may also exist in pore walls that have hydrated too quickly, as explained by Lu and Qin.[100]

Work by Petit et al.[101] and Lu and Qin[102] has shown how calibrating the electrostatic adhesion between surfactants and solid particles in a cementitious slurry can create a film layer that is highly resistant to collapse, inhibiting coarsening and coalescence of bubbles, while also allowing wetting of the cement for hydration, thus maximizing the number of closed air-voids. It is evident from this work that the electrical charges of the surfactant, of cementitious materials, and of any fillers must be coordinated for precise control over interconnectivity in foam concrete, especially in low-density mixes with thin cell walls.

92 She, Chen, Zhang and Jones (2013) 1282
93 Jones et al. (2012) 521
94 Pan et al. (2014) 258
95 Brady et al. (2001) C14
96 Lu and Qin (2015) 7
97 Akthar and Evans (2010) 353
98 Cong and Bing (2014) 68
99 Lu and Qin (2015) 1
100 Lu and Qin (2015) 5
101 Petit et al. (2014) 37
102 Lu and Qin (2015) 3

6.3.2 Mechanical Properties

6.3.2a *Compressive Strength*

In general, the strength of a porous material diminishes with increasing porosity. Numerous researchers have sought to precisely establish the fundamental inverse relationship between porosity and strength of solid materials.[1]

In concrete, both air content and excess water content contribute to the porosity of a mix. These influences are captured in Feret's formula[2] for the strength of a cement-paste, from 1896:

$$S = k_F \left(\frac{c}{c + w + a}\right)^n$$

where *c*, *w* and *a* are the absolute volumes of cement, water, and air respectively, *n* is an empirical constant (*n=2* for normal density concrete), and k_F is a constant that takes into account every factor that influences concrete strength, other than the cement-paste ratio.[3]

Feret's formula, however, fails to account for many important factors, such as the degree of hydration and physical and chemical properties of the cement.[4] In 1958, Powers[5] proposed that strength could be related more precisely to the gel/space ratio in a mortar; that is, the ratio of hydrated cement paste volume, to the total specimen volume. He suggested that concrete strength be expressed as

$$S = S_0 x^3$$

where S_0 is the intrinsic strength of the material with no porosity, and *x* is the gel/space ratio, or fraction of solids.

Powers' formula indicates that small changes in density can powerfully influence compressive strength. Furthermore, it suggests that there are two major parameters by which compressive strength of a mortar may be improved: reduce porosity, or improve the intrinsic strength of the paste.

A third major parameter controlling the strength of porous materials concerns the presence of flaws within the mix. Powers' formula above assumes material homogeneity of

---

1 Mehta (1986) 44
2 Neville (1963) 216
3 Popovics (1998) 374
4 Neville (1963) 221
5 Powers (1958a) 3

cement paste, but cracks, micro-cracks, areas of insufficiently hydrated paste and large, irregular, or interconnected voids create locations of weakness where stresses may be concentrated, and fracture initiated.

These three parameters of porosity, paste strength, and presence of flaws, provide a good basis for understanding the compressive strength of foam concrete. The strength of foam concrete varies dramatically with porosity. Low density mixes of 160 kg/m^3 offer compressive strengths of only 0.04 MPa, while mixes of 1600 kg/m^3 may offer 25 MPa. Mixes of similar composition, with varying porosity, will generally conform to fundamental relationships between strength and porosity. However, for a given density, widely diverse values of compression strength are reported for mixes of different compositions.[6] A 1600 kg/m^3 mix may have a compressive strength as low as 2 MPa, or as high as 60 MPa.[7] This variation may be largely attributed to differences in the intrinsic strength of the cement paste, as well as the presence of flaws in the matrix.

Research into the compressive strength of foam concrete may be generally organized according to these three parameters, as well. Models relate strength to porosity, paste strength, and flaw size; and attempts to improve concrete strength for a given density must either improve paste strength, or minimize the severity of flaws.

Mathematical Models: Strength and Porosity

Historically, several forms of equation have been proposed to relate strength and porosity in homogenous, isotropic materials.[8] In his research on polycrystalline refractory materials, Hasselman[9] proposed a linear relationship:

$$S = S_0 - k_H p$$

where p is porosity and k_H is a material constant, however this relationship appears to be oversimplified for cement-bound materials.[10]

Both Feret's and Powers' formulae are modified or specific cases of Balshin's[11] strength-porosity relation developed for metal ceramics:

---

6 Pan et al. (2007)
7 Wee (2005). Cited in Wee et al. (2011) 584
8 Röβler and Odler (1985) 323
9 Hasselman (1963)
10 Kumar and Bhattacharjee (2003) 158
11 Balshin (1949)

$$S = S_0(1-p)^{k_B}$$

Ryshkewitch[12] proposed an exponential relation for ceramics and rock,

$$S = S_0 e^{-k_R p}$$

while Schiller[13] proposed a logarithmic relationship for non-metallic brittle materials:

$$S = k_S \ln\left(\frac{p_0}{p}\right)$$

where p_0 is the porosity of a material at zero strength. Material constants are given as k_B, k_R, and k_S respectively in the equations above.

Experimental data from porous cement materials may be fitted to these data.[14] Note that the intrinsic strength constant, S_0, and the porosity at zero strength constant, p_0, account for microstructural features, such the specific density solid particles and C–S–H, particle and void size distribution, and the presence of flaws.[15]

Röβler and Odler determined that a linear plot was most appropriate for strength-porosity relationship of cement pastes with between 5 and 23% porosity.[16] However, many relationships developed for cellular concrete raise the solids/porosity ratio by a power. For example, for moist-cured, aerated concrete, Tam et al.[17] proposed a modified Feret formula, which incorporated Powers gel/space ratio concept, using α to indicate the degree of hydration:

$$f_c = k_T \left(\frac{\alpha c}{\alpha c + w + a}\right)^n$$

where k_T and n are constants, found to be 4490 Mpa and 3.36, respectively. More recently, Wee et al.[18] expressed cube compressive strength of foam concrete, f_{cu}, as a function of cube compressive strength of paste, $f_{cu,p}$, and air content, A.

$$f_{cu} = 1.048\, f_{cu,p}(1-A)^{2.793}$$

Thus, Wee et al. include the effect of gel and capillary porosity in the compressive strength of the paste.

---

12 Ryshkevitch (1953)
13 Schiller (1971)
14 Chen, Wu and Zhou (2013) 870, Lian et al. (2011) 4295, Kumar and Bhattacharjee (2003) 160
15 Chen, Wu and Zhou (2013) 870
16 Röβler and Odler (1985) 323
17 Tam et al. (1987) 17
18 Wee et al. (2011)

More sophisticated models attempt incorporate additional factors related to the composition of the paste. Hoff[19] developed a formula for moist-cured cellular concrete, which accounts for the specific gravity of the cement used, among other factors. Anticipating a hydration water-to-cement ratio of 0.2, he proposed that

$$S = S_0 \left(\frac{d_c}{1 + \frac{w}{c}} \right)^{k_B} \left(\frac{1 + 0.2 p_c}{p_c \gamma_w} \right)^{k_B}$$

where d_c density of the concrete, $\frac{w}{c}$ is the water-cement ratio, p_c is the specific gravity of the cement used, γ_w is the unit weight of water, and k_B is an empirical constant, following Balshin. Hoff corroborated his model with experimental testing of cellular concrete made from three different types of Portland cement at various porosities and w/c ratios, with good correlations. Kearsey and Wainwright[20] have shown that this equation is also appropriate for foam concrete made with blended cements of Portland and high proportions of fly-ash, where specific density of cement is taken as the mass-weighted average of the specific gravity of the cementitious materials used.

Fagerlund[21] observed that different equations appear to be necessary at high and low porosities, to describe strength-porosity relationship in concrete. This assertion is supported by research of aerated concrete by Baozhen and Erda,[22] who found it necessary to vary the exponent Balshin's equation between 1 and 2.2 according to porosity. Tonyan and Gibson[23] proposed that at high densities, the exponent is reduced due to the contribution of axial and shear stresses in the cell wall. Including porosity in the exponent, following Ryshkewitch, may therefore be useful developing an equation that applies at high and low densities.

The equations above allow various parameters of the mix design to be included in anticipating strength design, however they are still subject to some considerable limitations. In each of the formulae, the intrinsic properties of the paste represented by S_0, p_0, k_F, or k_T, $f_{cu,p}$, must be determined empirically. Moreover, these intrinsic properties

[19] Hoff (1972)
[20] Kearsley and Wainwright (2002) 239
[21] Fagerlund (1973). Cited in Kearsley and Wainwright (2002) 234
[22] Baozhen and Erda (1987) Cited in Kearsley and Wainwright (2002) 234
[23] Tonyan and Gibson (1992b) 6377

will vary with each mix design. Finally, each of the formulae developed for cellular concrete have been designed for mixes composed of water, air, and cementitious materials only. Adding fillers and chemical admixtures will add complexity and require further alterations of these models.

Mathematical Models: Strength and Severity of Flaw

Another approach to modeling the strength of a porous cement-based material is to recognize the contribution of flaw severity. According to the Griffith criteria of fracture, the propagation of the most severe defect will govern the mechanical failure of a sample. An early study by Röβler and Odler[24] attempted to model the influence of different pore size groups on strength for cement pastes, in the form

$$S = S_0 - ap_{largepores} - bp_{mediumpores} - cp_{smallpores} \cdots$$

where a, b, and c are coefficients that allow the detriment of porosity on strength to be varied according to pore size. However, Atzeni et al.[25] rejected this model, since regression analysis of actual data can yield negative coefficients, which are difficult to explain. Atzeni et al. instead proposed a model based on a 'mean distribution radius', r_m, which is a function of the average radius and total pore volume of each pore size group.

$$S = S_0 \frac{k_A(1-p)}{\sqrt{r_m}}$$

As demonstrated by Kumar et al., Atzeni's formula can be related to Griffith's model,

$$\sigma_t = \sqrt{\frac{2ET}{\pi c_1}}$$

By employing the simple relationships $E = E_0(1-p)$ and $T = T_0(1-p)$, and assuming that the effective half-crack length, c_1, is equal to the mean distribution radius of the pores, r_m, the following formula is derived:

$$\sigma_t = \sqrt{\frac{2E_0T_0}{\pi}} \cdot \frac{(1-p)}{\sqrt{r_m}}$$

Since uniaxial compressive strength is proportional to tensile fracture strength, and since E_0, T_0, etc. may also be collected within an empirical constant, k_G, we have

[24] Röβler and Odler (1985b). Cited by Kumar and Bhattacharjee (2003) 159
[25] Atzeni et al. (1987). Cited by Kumar and Bhattacharjee (2003) 160

$$S = k_G \frac{(1-p)}{\sqrt{r_m}}$$

Tonyan has developed an approach based on work by Gibson and Ashby and others for modeling the compressive strength of cement foams, which accounts for the presence of large coalesced voids:

$$S = k_t \sigma_{fs} \left(\frac{\rho}{\rho_s}\right)^m e^{-k_R p}$$

The size of the largest crack (i.e. void) and fracture toughness are thereby incorporated into the value of the modulus of rupture, σ_{fs}; while $\left(\frac{\rho}{\rho_s}\right)$ is the relative density of the cement foam, m is a constant between 1 and 2, k_t is an empirical constant, and k_R is a constant following Ryshkewitch which appears to vary with porosity.[26] Tonyan's model assumes that all voids are closed cells, i.e. no interconnectivity between pores.

Other studies, such as those by Ficker,[27] have attempted to account for the degree of pore randomness or clustering of pores. Hyun et al.[28] proposed that the constant k_B in Balshin's model may be related to the stress concentration developed around pores, which could help incorporate aspects of pore geometry into a model of strength-porosity for cellular concrete.

Early work by Hengst and Tressler[29] indicated that the most significant parameter for foam concrete strength is flaw size, in accordance with the Griffith criteria. To date, much research related to propagation of defects has been developed for cement mortar and concrete, with porosity often controlled through the use of excess water, degree of hydration, or aggressive chemicals.[30] Lian et al.[31] developed a strength model for porous concrete with large macroscopic pores and up to 35% void, derived from Griffith's model, which offered significant improvement over a simple porosity-based exponential equation. Numerous studies on the fracture of brittle materials with spherical cavities[32] or on the

[26] Tonyan and Gibson (1992b) 6377
[27] Ficker (2008). Cited by Chen, Wu and Zhou (2013) 871
[28] Hyun et al. (2001). Cited by Chen, Wu and Zhou (2013) 871
[29] Hengst and Tressler (1983)
[30] Kumar and Bhattacharjee (2003) 155
[31] Lian et al. (2011) 4298
[32] Evans et al. (1979)

failure of cellular solids[33] are available. More work is needed to extend this research into developing models that account for the severity of flaws in cellular concrete. Total porosity and paste strength do not appear to be sufficient parameters to explain foam concrete strength, since empirical evidence suggests that large,[34] irregular,[35] or interconnected[36] voids can also have a strong influence on mechanical properties.

Statistical Models: Predicting Strength from Empirical Results

Predictive models for compressive strength may be generated based on empirical results from systematically designed trials. Nehdi et al.[37] and Bayuaji and Nuruddin[38] proposed the use of Artificial Neural Networks for foam concrete, and Nambiar and Ramamurthy[39] used statistical treatment of experimental results to generate response surfaces, relating parameters such as filler-cement ratio, fly ash replacement, density, and compressive strength. However, these statistical analyses do not readily yield insight for improving the performance envelope of foam concrete from an understanding of its microstructure, but only summarize results from mixes that have already been tested.

Mix Design

As indicated in many of the models above, the strength of porous materials can be readily improved by reducing porosity. The challenge in foam concrete mix design is rather to improve strength, at a given density. This may be accomplished by improving the intrinsic strength of the paste, or by reducing the severity of flaws.

Intrinsic strength of paste is governed by the type and amount of binder, the type and amount of filler, the w/c ratio and the use of plasticizer.

Binder type has a strong influence on paste strength. The hydraulic reaction of cement produces C-H-S, which imparts strength due to Van der Waal attraction forces between sheets with high ratios of surface area to volume. Use of cementitious pozzolans, such as fly ash and silica fume, facilitates the conversion of hydration products like calcium

---

33 Rice (1977), Gibson and Ashby (1988)
34 Nambiar and Ramamurthy (2007a) 228
35 Valore (1954b) 817
36 Petit et al. (2014)
37 Nehdi et al. (2001)
38 Bayuaji and Nuruddin (2008)
39 Nambiar and Ramamurthy (2006b)

hydroxide, which do not contribute significantly to strength, into these valuable C-H-S sheets. Furthermore, use of finely divided pozzolans can improve particle packing of the paste, minimizing discontinuities in the paste itself.

Foam concrete mixes made using ordinary Portland cement binders are typically used as a baseline for strength properties.[40] Numerous studies have included pozzolans as additives, or as partial replacements for Portland. The influence of fly ash in foam concrete has been studied by Kearsley and Wainwright[41] and Jones and Giannakou,[42] among others. Wee et al.[43] incorporated ground granulated blastfurnace slag. Hilal et al.[44] used silica fume and fly ash separately and in combination, while Tonyan and Gibson[45] and Akthar and Evans[46] used silica fume as an additive in highly porous mixes made using preformed foams. Pan et al.[47] evaluated the strength performance of foam concrete made from blended cements of fly ash, slag, and silica fume. Increasingly, the use of alkali-activated geopolymers as binders is of interest for environmental and economic reasons. Zhang et al.[48] and Liu et al.[49] have studied the mechanical strength of these binders.

Strength of the bond between the binder and the filler is important, and the strength of the interfacial zone surrounding larger aggregates may be an area of localized weakness.[50] Fillers that have rough surfaces promote good mechanical bonding, and slightly reactive fillers may also bond chemically with the binder.[51]

Sand is the typical filler used in foam concrete. However, Jones and McCarthy[52] have used coarse fly ash, and more recently, Jones et al.[53] compared the strength of foam concrete made with various recycled aggregates, including demolition fines, incinerator bottom ash aggregate, glass fines, foundry sand, china clay sand, conditioned fly ash and

40 Brady et al. (2001) Table C5
41 Kearsley and Wainwright (2001b)
42 Jones and Giannakou (2004)
43 Wee et al. (2011)
44 Hilal et al. (2014b)
45 Tonyan and Gibson (1992b)
46 Akthar and Evans (2010)
47 Pan et al. (2007)
48 Zhang et al. (2015)
49 Liu et al. (2014)
50 Mehta (1986) 37, Roy et al. (1993) 1
51 Jones and McCarthy (2005c) 1398, 1404
52 Jones and McCarthy (2005c)
53 Jones et al. (2012)

crumb rubber. Aliabdo et al.[54] studied the strength of foam and concrete made with crushed clay brick, and Lim et al.[55] used palm oil fuel ash as a filler. Tonyan and Gibson[56] considered the structural efficiencies of using XPS granules as a lightweight aggregates for foam concrete.

Significant flaws in a foam concrete sample may include areas of incomplete hydration, cracks or micro-cracks, and the geometry of air void systems. The degree of hydration of a foam concrete paste can be influenced by w/c ratio, curing conditions,[57] and the use of accelerators.[58] Cracks may be caused by thermal stresses, drying shrinkage stresses,[59] freeze-thaw action, or aggressive chemicals.[60] Use of various reinforcing fibres, discussed in Section 5.1.5b, can help prevent cracking and the propagation of flaws. The geometry of air-void systems includes 'flaws' such as interconnected pores and large pore sizes: mix design influences on air void systems are discussed in detail in Section 6.3.1.

Schober[61] has emphasized that the condition of the pore shells is especially important in cellular concrete.

6.3.2b Tensile Strength

Compressive strength is the most commonly studied mechanical property of foam concrete, due to its immediate practical importance, and ease of testing. Tensile and flexural strengths are less well-studied, but are nevertheless significant. ASTM C869[62] indicates that foamed concrete should have a minimum tensile strength of 0.17 N/mm^2 for adequate in-service performance.

According to Valore,[63] flexural strength of neat cement mixes varies significantly due to shrinkage cracking, with ratios of flexural to compressive strength as low as 0.05. The flexural strength of some very low-density mixes was reported to be negligible. Other

54 Aliabdo et al. (2014)
55 Lim et al. (2013)
56 Tonyan and Gibson (1992a)
57 Tam et al. (1987), Jiang et al. (2016) 957-959
58 Lu and Qin (2015) 5 ("During [the curing] process, if the pore wall was able to coagulate and hydrate quickly, the liquid could not carry the fly ash and cement particles to the Plateau borders and thus left the hole.")
59 Valore (1954b) 826
60 Jones and Giannakou (2004) 6
61 Schober (1992). Cited in Hamidah et al. (2005) 43.
62 ASTM C869/C869M-11, Table 1
63 Valore (1954b) 825

commercial sources cited by Valore reported flexural to compressive strength ratios of between 0.2 and 0.35 for cellular concrete; Graf[64] suggested that their relationship could be described approximately by the following equation:

$$f_c = 0.75\left(f_y\right) + 0.005\left(f_y\right)^2$$

Neville[65] observed that the addition of air entrainment was more detrimental to compressive strength than to tensile strength; recent research by Chen et al.[66] affirmed that the ratio of compressive to tensile strength in porous cement-bound materials appears to be porosity dependent.

Pozzolans appear to affect flexural strength similarly to how they influence compressive strength. Roslan et al.[67] reported that use of fine fly-ash as a pozzolan gives good long term flexural performance, but that fly-ash mixes may be less strong than Portland-only in the short term. Ruiwen[68] noted that the correlation between compression strength and flexural strength for slag mixes was similar to the correlation for conventional foam concrete, between 0.12 and 0.26. Similarly, Liu et al.[69] evaluated the tensile strength of foam concrete composed of geopolymer binder and lightweight coarse aggregate, and found the flexural strength to compression strength ratio of between 0.12 and 0.18. The ratio of splitting tensile strength to compressive strength has been found to be between 0.06 and 0.11 for mixes with slag,[70] between 0.05 and 0.07 for mixes with coarse fly ash, and between 0.06 and 0.09 for conventional sanded foam concrete mixes.[71]

Jones and McCarthy[72] noted that sand filler mixes had higher tensile strengths than coarse fly ash filler mixes at 28 days, which was attributed to improved shear capacity between the sand particles and the paste. The use of palm oil fuel ash as a replacement for sand filler improved flexural strength, apparently due to the production of additional C-H-S through pozzolanic reaction.[73]

Accelerating or water reducing admixtures may be beneficial in the development of

64 Graf (1949). Cited by Valore (1954b) 825
65 Neville (1963) 238
66 Chen, Wu and Zhou (2013) 869
67 Roslan et al. (2013) 603
68 Ruiwen (2004) 93
69 Liu et al. (2014) 243
70 Ruiwen (2004) 93
71 Jones and McCarthy (2005b) 26
72 Jones and McCarthy (2005b) 26
73 Lim et al. (2013) 46

tensile strength. Roslan et al.[74] demonstrated that lime may be used as an accelerator for early flexural strength. Research by Ruiwen[75] indicated that increasing the water-binder ratio may be more detrimental to compressive strength than to flexural strength.

Reinforcing fibres can improve tensile strength by reducing cracking during plastic and drying shrinkage, and increasing ductility.[76] The addition of polypropylene fibres at a dosage of 0.50% of mix volume improved flexural strength by up to 58% in mixes of between 1400 and 1800kg/m^3.[77] In a study of ultra-lightweight foam concrete, Huang et al.[78] determined that densities as low as 150 kg/m^3 can maintain an acceptable tensile strength through the use of polypropylene fibres. Byun et al.[79] reported 104% improvement of tensile strength in mixes using vynylon fibres, and 30% improvement in flexural strength. Gunawan and Busra[80] reported that use of galvalum fibres increased tensile strength by 47% in a 1900 kg/m^3 mix.

Finally, Mydin and Yang[81] have studied how flexural strength of foam concrete decreases with exposure to high temperatures.

6.3.2c Modulus of Elasticity

According research by the British Cement Association,[82] the modulus of elasticity of foam concrete ranges from 1 to 12 GPa for foam concrete with dry densities between 500 and 1600 kg/m^3, respectively. By comparison, the elasticity modulus of structural concrete may be 30 GPa or more.

Van Deijk[83] provided information on both the static and dynamic modulus of elasticity for mixes between 600 and 1500 kg/m^3 for sand-cement mixes and for sand-cement-coarse fly ash mixes, determined at 56 days. Fly-ash mixes appear to have a higher static elasticity modulus than sand mixes, by a factor of more than two. Brady et al.[84]

---

74 Roslan et al. (2013) 600
75 Ruiwen (2004) 93
76 Amran et al. (2015) 997
77 Jones and McCarthy (2005b) 27
78 Huang et al. (2015)
79 Byun et al. (1998)
80 Gunawan and Busra (2014)
81 Mydin and Yang (2012a) 644-645
82 British Cement Association (1994). Cited in Brady et al. (2001) C11, Table C5
83 Van Deijk (1991) 50
84 Brady et al. (2001) C11

suggested that fly ash mixes are stiffer for a given density, due to improved particle packing and interlocking of the fine aggregate. Jones and McCarthy[85] found that mixes with coarse fly ash mixes were less stiff than sand mixes for a given compressive strength, and proposed the following relationships:

Sand Mixes: $E = 0.42 f_c^{1.18}$

Coarse Fly ash mixes: $E = 0.99 f_c^{0.67}$

where E is the static modulus of elasticity in GPa and f_c is 28-day compressive strength in MPa. For comparison, for normal weight concrete with compressive strengths between 20 and 40 MPa, the elasticity modulus may be estimated using the formula below:[86]

Normal density concrete: $E = 4.5 f_c^{0.5}$

Several relationships are plotted in the figure below, for reference.

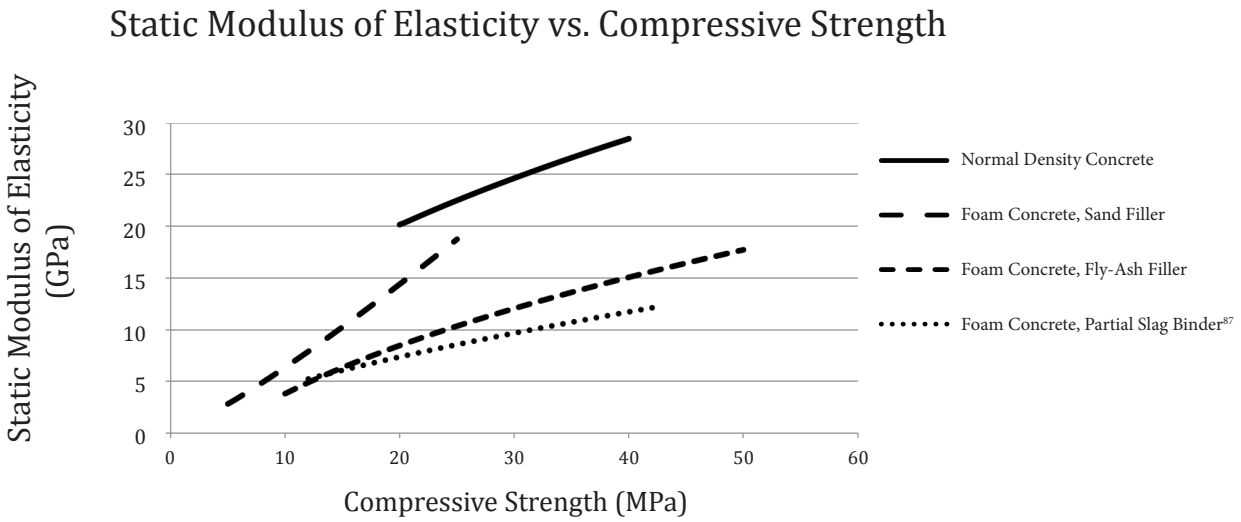

Figure A-6.3.2 Static elasticity modulus vs. compressive strength for various mixes.

Röβler and Odlin[88] compiled a series of relationships for elasticity modulus and porosity based on the models of Hasselmen, Balshin, Ryshkevitch, and Schiller respectively, which show good correlations to actual data from cement pastes with up to 35% porosity. Tonyan and Gibson[89] developed a relationship for elasticity modulus and porosity for foam

85 Jones and McCarthy (2005b) 26
86 CAN/CSA-A23.3-04, Section 8.6.2.3.
87 Ruiwen (2004) 94
88 Röβler and Odlin (1985)
89 Tonyan and Gibson (1992b) 6376

concrete based on Ryshkevitch's empirical equation, correlated with data from mixes of between 230 and 1680 kg/m^3 density.

The addition of fibres can contribute greatly to foam concrete stiffness. Brady et al.[90] reported that adding 0.5% polypropylene fiber content to a sample of 1400 kg/m^3 plastic density increased the elasticity modulus by 70%. Gunawan and Setiono[91] observed that the addition of 0.5% galvalum fibres increased the modulus of elasticity by 26% in a 1900 kg/m^3 mix, to 74 GPa.

6.3.2d *Poisson's Ratio*

Poisson's ratio, υ, describes the expansion of a material under compression, perpendicular to the direction in which it is being compressed. The ratio may be determined from the modulus of elasticity, E, and shear modulus, G:

$$\upsilon = \frac{E}{2G} - 1$$

The Poisson's ratio of foam concrete is seldom reported in the literature. Wee et al.[92] reported a Poisson's ratio of 0.2, obtained experimentally from mixes with a binder of 50% Portland cement and 50% slag. In mixes of 1300 kg/m^3 density, Lim et al.[93] found that the Poisson's ratio of foam concrete with sand filler had a Poisson's ratio of 0.327, while mixes with 10 and 20% pal oil fuel ash filler replacement had lower Poisson's ratios of 0.216 and 0.261, respectively. This phenomenon may be related to particle packing. Byun et al.[94] used silica fume, fly ash, and expanded polystyrene aggregate to produce foam concrete with a densities between 390 and 640 kg/m^3 having a Poisson's ratio of 0.2.

Tang et al.[95] used a ratio of 0.22 for numerical analysis of a conventional foam concrete mix with a dry density of 730 kg/m^3. Zhen et al.[96] used a ratio of 0.15 in numerical analysis of foam concrete with expanded polystyrene granules aggregate and densities between 300 and 500 kg/m^3.

---

90 Brady et al. (2001) Table C7
91 Gunawan and Busra (2014) 433–441
92 Wee et al. (2011) 591
93 Lim et al. (2013) 46
94 Byun et al. (1998)
95 Tang et al. (2013) 347
96 Zhen et al. (2013) 68

Arnold et al.[97], Kováčik[98], and Phani and Sanyal[99] have discussed the relationship between Poisson's relationship and porosity in porous materials. Researchers are divided over whether Poisson's ratio is a function of porosity.[100]

6.3.2e Bond Strength

The bonding behaviour of embedded components within foam concrete has not been extensively researched.

Valore[101] commented that information on the bond strength of cellular concretes was difficult to find. For prefoamed moist-cured cement-sand concrete, the ratio of "push-out" bond strength to compressive strength was between 0.25 and 0.38 for mixes of varying densities and cement-filler ratios.

Jones and McCarthy[102] tested full-scale foam concrete beams with longitudinal and shear steel reinforcing. The plastic densities of the selected cement-sand-coarse fly-ash mixes were 1400 and 1600 kg/m^3, respectively. The beams were subjected to four-point bending until failure. Following failure, the beams were broken apart in order to examine the concrete surrounding the reinforcing. There was no evidence of local crushing, indicating that bond slip was minimal or negligible.

Similarly, Regan and Arasteh[103] reported minimal bond slip in their study of lightweight aggregate foam concrete. Weigler and Karl[104] observed that bond strength in lightweight aggregate foam concrete decreased in the same proportion as compressive strength, for increasing air content. Bond strength of the bottom bars appeared to be at least as high as in normal density concrete of the same strength; however, bond strength of the top bars was sometimes lower than in normal density concrete of the same strength.

Sayadi et al.[105] studied the bond strength of galvanized strips embedded in foam concrete, for the purposes of designing composite sandwich panels. The authors developed

---

97 Arnold et al. (1996)
98 Kováčik (2006)
99 Phani and Sanyal (2005)
100 Phani and Sanyal (2005) 5685
101 Valore (1954b) 826
102 Jones and McCarthy (2005) 29
103 Regan and Arasteh (1984). Cited in Jones and McCarthy (2005b) 29
104 Weigler and Karl (1980) 103
105 Sayadi et al. (2016a) and Sayadi et al. (2016c)

equations to describe slip behaviour based on experimental results, varying the length, width and thickness of the embedded strips, as well as the number and total areas of holes in the strip.[106] The authors have also tested the influence of foam concrete density on bonding behaviour, with mixes of between 800 and 1200 kg/m^3. Foam concrete with a density of less than 1000 kg/m^3 was deemed unsuitable for the locking pattern systems under investigation.[107]

6.3.2f Shear Strength and Shear Transfer

Emiko et al.[108] compared shear transfer in normal density concrete, lightweight aggregate concrete, foam concrete, and lightweight aggregate foam concrete. Shear transfer behaviour of lightweight aggregate concrete was similar to that of normal weight concrete. Conversely, foam concrete and lightweight aggregate foam concrete experienced sudden catastrophic failure without first exhibiting a non-linear stress-strain response. Ultimate shear transfer strength was lower in foam concrete samples than in lightweight aggregate concrete samples with the same reinforcing and similar compressive strength.

Brady et al.[109] noted that the foam concrete's relatively poor performance in shear resistance may be attributed to the lack of coarse aggregate. Jones and McCarthy[110] suggested that sand filler particles may offer improved shear capacity, in comparison to fly ash filler particles.

The shear strength of foam concrete is seldom reported in the open literature. Tonyan and Gibson[111] determined that the shear strength of foam concrete with 430kg/m^3 density averaged 0.145 MPa. In a study on foam concrete sandwich panels, Flores-Johnson and Li[112] observed that even after a foam concrete core failed in shear, it was still capable of separating corrugated steel face panels, extending the total bending resistance of the composite panel.

---

106 Sayadi et al. (2016c)
107 Sayadi et al. (2016a)
108 Emiko et al. (2011) 397
109 Brady et al. (2001) C12
110 Jones and McCarthy (2005b) 26
111 Tonyan and Gibson (1992b) 6376
112 Flores-Johnson and Li (2012) 1560

6.3.2g Creep

Studies of foam concrete creep are rare in the open literature. Brady et al.[113] recorded the creep strain of three mix designs, with specific creep strain between 300 and 100 μstrain/MPa after three months for densities between 1330 and 1750 kg/m^3. Kearsley[114] included the results of preliminary creep tests in a thesis on fly ash foam concrete. After two years, specific creep was between 1400 and 200 μstrain/MPa for specimens with nominal densities between 1000 and 1500 kg/m^3. Specimens in both sets of tests were sealed to retain moisture. No creep data is available for specimens exposed to drying, nor for specimens without filler.

[113] Brady et al. (2001) C12
[114] Kearsley (1999b) 153-156.

6.3.3 Transport Properties

6.3.3a Capillary Water Uptake

Capillary water uptake describes the capacity of a porous medium to absorb or desorb liquid by capillary action. The concept was introduced by Philip,[1] who called the phenomenon "sorptivity," and developed formulas for the one-dimensional infiltration of liquid through a porous body in horizontal and vertical directions.[2] Hall[3] presented the formula for vertical sorptivity, S, in mortar and concrete as

$$i = A + S\sqrt{t}$$

where i is the cumulative volume absorbed per unit area of inflow surface, A is the original mass of the sample, and $\sqrt{t}$ is the root of time. In practice, sorptivity is determined from the line of best fit obtained from a plot of i against $\sqrt{t}$. ISO Standard 15148[4] provides guidance in the event that the graph takes the form of a curve, rather than a straight line.

The term 'capillary water uptake' is preferred to 'sorptivity', as it avoids confusion with other forms of water absorption and adsorption. However, the original term continues to be commonly used in foam concrete literature.

Capillary water uptake indices are a useful parameter for anticipating the ingress and accumulation of moisture in porous building materials exposed to liquid moisture. The size, spacing and continuity of capillary voids, and the tortuosity of the path of liquid influence the rate of transmission. In foam concrete, uptake is controlled by physical properties of the air void system, and of the paste.

Physical Properties of the Air-Void System

Research by Nambiar and Ramamurthy[5] indicated that increasing the foam volume in a mix reduced capillary water uptake. The authors determined that water migrated readily through highly pervious pastes that contain a large volume of capillary voids, while the closed air voids did not to facilitate capillary movement.[6] According to their model, air

---

1 Philip (1957)
2 Philip (1969)
3 Hall (1989)
4 ISO 15148 (2002), Section 8
5 Nambiar and Ramamurthy (2007b)
6 Cf. Neville (1963) 454

voids remain as chambers of air, undisplaced by the ingress of water. A reduction in paste volume results in a reduction of cross-sectional area through which the water is capable of progressing. Furthermore, the air voids are obstacles that increase the length of the path the water must travel to fill the sample.[7]

However, research by Liu et al.[8] and Panesar[9] suggested that capillary water uptake increased with increasing foam volume. The discrepancy between these results may be due to additional characteristics of the air void system, other than total foam volume. Interconnectivity of voids, for example, would negate the capacity of air voids to remain isolated and air-filled.[10]

Physical Properties of the Paste

Whether or not air voids contribute to sorptivity, it is certain that the capillary voids in the paste have a strong influence on the uptake of liquid. It is desirable to reduce the volume of capillary voids in the paste, i.e. improve the density of the matrix, to reduce capillary action.[11] Additionally, making the matrix dense will improve its impermeability to gases: it is possible that this impermeability helps to entrap air in the hardened concrete voids, rather than allowing it to diffuse out, preventing the air from being easily displaced by liquid water. Increasing the density of the matrix may be accomplished by a number of mechanisms, including reducing the water-cement ratio, improving the particle packing of solids, and ensuring full hydration.[12]

Reducing the w/c ratio

The amount of water in a foam concrete mix is typically governed by the requirements of stability and workability. Some binders and fillers require a higher w/c ratio, resulting in a greater volume of capillary pores. For example, Nambiar and Ramamurthy[13] demonstrated that replacing sand filler with coarse fly-ash filler resulted in higher sorptivity indices. The higher water demand of the coarse fly-ash mixes resulted in a greater volume of more

7 Nambiar and Ramamurthy (2007b) 1345
8 Liu et al. (2014) 244
9 Panesar (2013) 580
10 Cf. Yang and Lee (2015)
11 Hall and Yau (1987) 78
12 Cf. Hall and Yau (1987)
13 Nambiar and Ramamurthy (2007b) 1345

pervious paste for a given density.

Improving particle packing

Use of fine binders and fillers reduces discontinuities in a matrix. The influence of silica fume and other mineral admixtures on sorptivity of normal density concrete has been studied.[14] Similar results may be anticipated for foam concrete, provided water requirements can be kept to a minimum.[15]

Ensuring full hydration

Capillary porosity decreases with degree of hydration of cementitious content, as per Power's gel/space ratio concept.[16] The influence of air-, moist-, and water curing regimes on the sorptivity of normal density concrete has been evaluated.[17] An equivalent study has not been conducted for foam concrete; however, a study by Jiang et al.[18] used X-ray diffraction to evaluate the mineral phases of reaction products of foam concrete cured under various curing regimes. Seal curing was found to produce dense paste phases.

Other considerations

Water-cement ratio, particle packing, and degree of hydration may also be influenced by the use of chemical admixtures. For example, the use of superplasticizer may affect w/c ratio and particle packing, while accelerators may prevent complete hydration in porous mixes.[19] Hanžič and Ilić[20] demonstrated how capillarity and sorptivity decrease with the use of superplasticizer in normal density concrete. Panesar[21] studied the effects of various protein and synthetic foaming agents on sorptivity, concluding that some foaming agents tend to result in a higher capillary pore volume. Foam concrete made using such surfactants may be unsuitable for outdoor applications where they will be exposed to moisture, freezing temperatures, and ions capable of inducing osmatic pressures.

Furthermore, an interfacial zone may exist around large air voids, similar to the interfacial zone around aggregates in normal density concrete.[22] This zone is especially

14 Tasdemir (2003)
15 Cf. Brady et al. (2001) C1
16 Powers (1958)
17 Tasdemir (2003)
18 Jiang et al. (2016) 958
19 Lu and Qin (2015) 5
20 Hanžič and Ilić (2003)
21 Panesar (2013) 575
22 Ramamurthy et al. (2009) 391

pervious, and thus may increase sorptivity. Therefore, applying strategies to maintain small air bubbles may also help to dampen water uptake.

Finally, the presence of cracks will significantly increase the rate of water ingress, as fractures provide long, continuous paths for liquid transport. For this reason, it is important to limit drying shrinkage and extreme thermal gradients due to heat of hydration during curing, and to avoid damage due to frost action or aggressive chemicals after hardening.

For sand-cement mixes with between 10 and 50% air void, Nambiar and Ramamurthy[23] reported sorptivity values ranging between 0.626 and 0.360 mm/min$^{0.5}$ respectively. Similar sand-cement-coarse fly ash mixes ranged from 0.627 to 0.447 mm/min$^{0.5}$, respectively. Liu et al.[24] reported that for geopolymer foam concrete composed of fly ash and palm oil fuel ash binder, and oil palm shell lightweight aggregate, cured at high temperatures, with foam volumes between 16.5 and 31.7%, sorptivity indices were between 0.109 and 0.142 mm/min$^{0.5}$ respectively.

6.3.3b Water Absorption

Water absorption is usually expressed as the percent difference in mass between and oven-dried specimen, and an identical specimen immersed in water. Absorption measurements may be taken after a given period of time (for instance 24 or 48 hours),[25] or until constant mass.[26] Absorption may be measured by immersing a specimen in water at normal pressures as an indicator of in-service performance; or by vacuum saturating the specimen[27] or using boiling water[28] to fill all pores as completely as possible with liquid, to determine total porousity.

For foam concrete, water absorption should be expressed as a percent of volume, rather than of mass, as the highly variable weight of foam concrete does not allow for consistent comparison based on specimen mass.[29]

---

23 Nambiar and Ramamurthy (2007b) 1345
24 Liu et al. (2014)
25 ASTM C796/C796M-12
26 ASTM C642/C642M-13
27 Fagerlund (1977)
28 ASTM C642-13, Kosmatka et al. (2002) 285
29 Kearsley and Wainwright (2001a) 809, Nambiar and Ramamurthy (2007b) 1343

According to Nambiar and Ramamurthy,[30] lower density foam concrete may initially absorb less water than higher density foam concrete under normal conditions. As described in the previous section, if the voids can be isolated, they will not readily fill with liquid by capillarity.[31] The impermeability of the matrix limits the diffusion of gas from the air voids, so water is not permitted to swiftly displace the air and fill the air voids. Based on the model proposed by Nambiar and Ramamurthy, the same techniques used to dampen sorptivity will also reduce water absorption under normal pressure. The matrix should be dense, with a low volume of capillary voids, and voids should be small and isolated, rather than interconnected.

In a study by Kearsley and Wainwright,[32] lower density foam concrete mixes absorbed only slightly more water than those with higher densities. As discussed in the previous section, other aspects of the air void system will have an effect on the capacity of the air voids to remain inaccessible to water uptake. It is important to note, for instance, that Kearsley and Wainwright maintained a constant w/b ratio in all mixes,[33] while Nambiar and Ramamurthy varied the w/c ratio in response to the demands of workability and stability.[34] Kearsley and Wainwright concluded that only some of the air voids in the samples were filled or partly filled during testing.[35]

Nambiar and Ramamurthy[36] reported that sand-cement mixes with between 10 and 50% foam volume, immersed in water for 7 days, absorbed between 21 and 25% liquid by volume, respectively. Sand-cement-coarse fly ash mixes with between 10 and 50% foam volume absorbed between 29 and 32.5% water under the same conditions. This discrepancy can be attributed to the additional water required for stability and workability in the coarse fly ash mix. The higher volume of water results in less foam volume, more paste volume, and a greater volume of capillary pores in the paste. Kearsley and Wainwright[37] reported that replacing up to 75% of the mass of cement with pulverized fly ash or pozz-fill binders did not have a meaningful effect on water absorption; significantly,

30 Nambiar and Ramamurthy (2007b) 1343
31 Neville (1962) 454
32 Kearsley and Wainwright (2001a) 809
33 Kearsley and Wainwright (2001a) 807
34 Nambiar and Ramamurthy (2007b) 1342
35 Kearsley and Wainwright (2001a) 810
36 Nambiar and Ramamurthy (2007b) 1344
37 Kearsley and Wainwright (2001) 810

the authors did not alter the w/b ratio according to filler type, so the ratio of foam volume to paste volume remained practically unchanged. Research by Cong and Bing[38] suggested that use of silica fume was capable of initially suppressing water absorption.

It is important to note that absorption values for foam concrete are very high relative to normal density concrete. Kosmatka et al.[39] listed data for a series of normal density concrete recipes. Absorption after immersion varied from 2.43% to 5.81% by mass; and absorption after immersion and boiling varied from 2.56% to 5.90% by mass. Subjecting foam concrete specimens to vacuum saturation or boiling will allow an even greater amount of water to the specimen than indicated in the absorption values cited above. [40]

6.3.3c *Liquid Water Permeability*

Liquid water permeability is a measure of the flow of liquid water under pressure through a saturated porous medium.[41] It may determined according to Darcy's law,[42]

$$\kappa = \upsilon \frac{\mu \Delta x}{\Delta P}$$

where κ is the permeability of a medium, υ is the superficial fluid flow velocity, μ is the dynamic viscosity of the fluid, Δx is the thickness of the porous medium, and ΔP is the pressure gradient applied to the medium.

Permeability is an important parameter for foam concrete in applications where it must drain. Where foam concrete is used as a backfill replacement for sand or granular materials, subgrade drainage is important to avoid issues such as ponding or surface runoff.

Van Deijk[43] noted that foam concrete may be suitable as a subbase for sports fields. For example, foam concrete with a density of 600 to 650 kg/m^3 and a hydraulic conductivity of 300 mm/h has been used for outdoor tennis courts and soccer fields. Choi

38 Cong and Bing (2014) 65
39 Kosmatka et al. (2002) 285
40 Nambiar and Ramamurthy (2007b) 1344
41 Nambiar and Ramamurthy (2007b) 1341
42 Darcy (1856)
43 Van Deijk (1991) 51

and Ma[44] studied the use of foam concrete for drainage courses in long tunnels, which may perform better than geotextiles, as it is less likely to be clogged by fine soils. Foam concrete has been proposed for stormwater detention applications,[45] and for filtering wastewater.[46]

In a study on permeable backfills for utility trenches, Alobaidi et al.[47] reported that foam concrete in the UK was often of low permeability, which had to be compensated by including a layer of sand at the bottom of the trench. If a fill with a specific gravity of less than unity resisted the ingress of water under pressure, a buoyant force could result, potentially damaging utilities.

Soft ground arresting systems, such as those used for aircraft[48] or ground vehicles, may use a layer of crushable foam concrete over a large area to absorb kinetic energy. Managing drainage is necessary to avoid compromising the superficial friction and crushing response of the material.[49]

Permeability is largely dependent on porosity characteristics of a material. Interconnected voids in foam concrete provide paths for rapid movement of water. Voids may be connected by rupture of an intervening cell wall during setting,[50] by microcracking, or by large scale cracking the bulk material. Since the presence of fractures due to drying shrinkage, etc. can strongly contribute to a higher permeability, curing regime may have a dominant effect on penetrability.[51] Although water progresses most readily through voids, water will also drain through the paste, thus the perviousness of the matrix material is important: characteristics of the matrix may be controlled by w/b ratio, particle packing, and degree of hydration, as previously discussed. Thin cell walls will allow water to migrate from cell to cell more easily than thick cell walls. According to research by Brady,[52] foam concrete may be more than one hundred times more permeable to water that normal density concrete.

---

44 Choi and Ma (2015)
45 U.S. Patent 8172937 B2
46 Doniec (2008) 264
47 Alobaidi et al. (2000) 151-159.
48 Zhang et al. (2013)
49 Federal Aviation Administration (2012) 5
50 Petit et al. (2014) 37
51 Brady et al. (2001) C13
52 Brady (2000). Cited by Brady et al. (2001) C14

The use of lightweight aggregate may also have a significant effect on the permeability of foam concrete, [53] due to the permeability of the aggregate itself, as well as the properties of the interfacial zone.[54] Byun et al.[55] proposed that the permeability coefficient for foam concrete made with polymer foaming agent and expanded polystyrene lightweight aggregate, with 59 to 75% porosity, was inversely proportional to density.

6.3.3d *Gas Permeability*

The permeability of foam concrete to gases such as water vapour and oxygen is strongly dependent on total void volume, and interconnectivity of pores. A dense matrix, as controlled by w/b ratio, particle packing, and degree of hydration, will reduce permeability. The presence of cracking can have a dominant effect on permeability; consequently, curing regime may have a considerable influence.[56]

Water vapour

The rate of movement of water vapour from a concrete specimen has implications for drying rates and curing behaviour. Additionally, water vapour transport is a critical factor for many issues of durability, such as carbonation. [57]

Kearsley and Wainwright[58] compared the vapour permeability of highly porous cement pastes, with pore volume introduced either by preformed foam, or by high w/b ratios. Vapour permeability increased with total porosity, regardless of whether the pores were predominately air-voids or capillary pores. Kearsley and Wainwright concluded that all voids participate in the transport of water vapour through the specimen.[59] By contrast, as discussed in Section 6.3.3b, capillary pores have a dominant influence on sorptivity and water absorption. The authors further determined that the partial replacement of cement binder with up to 75% fine fly ash or pozz fill, did not make an appreciable difference to

[53] Ćosić et al. (2015)
[54] Metha (1986) 37
[55] Byun et al. (1998) 8
[56] Brady et al. (2001) 10, C13
[57] Brady et al. (2001) 10
[58] Kearsley and Wainwright (2001a)
[59] Kearsley and Wainwright (2001a) 810

water vapour permeability. [60]

Conversely, the use of coarse fly ash as a replacement for sand filler does appear to influence vapour permeability. Dhir et al.[61] reported that the rate of diffusivity for a cement-fly ash mix was half of that for a cement-sand mix, with both samples manufactured to be 1400 kg/m^3 dry density. Kearsley and Booyens[62] reported similar findings.

Brady et al.[63] reproduced data for the influence of w/b ratio and surfactant type on the vapour permeability of foam concrete specimens with 1400 kg/m^3 plastic density and 500 kg/m^3 cementitious density. Values ranged from 2.53 to 3.20 g/mm/s x 10^{-13}. These values are approximately twice as high as for normal density concrete with compressive strengths of 40 to 50 MPa.[64]

Oxygen gas

Oxygen gas is a useful permeating medium for concrete. As it does not modify pore structure, tests are repeatable and reproducible.[65] Oxygen permeability may be correlated with carbonation depth to help predict the durability of reinforcing steel in concrete.[66]

Oxygen permeability is typically very high in foam concrete, and increases with porosity. For foam concrete with a plastic density of 1800 kg/m^3 and 500 kg/m^3 cementitious density, Dhir et al.[67] reported values an order of magnitude higher than for normal density concrete. Brady[68] produced low-density foam concrete mixes with permeability values two orders of magnitude higher than for normal density concrete.

However, Kearsley and Booyens[69] reported that use of coarse fly ash filler as a complete replacement for sand filler could significantly reduce oxygen permeability. In their study, foam concrete with a dry density of 1500 kg/m^3 was less permeable to oxygen than normal density structural concrete with 25 MPa compressive strength, indicating

60 Kearsley and Wainwright (2001a) 811
61 Dhir et al. (1989). Cited in Brady (2001) C14.
62 Kearsley and Booyens (1998)
63 Brady et al. (2001) Table C1
64 Brady et al. (2001) C14
65 Kollek (1989) 225
66 Kearsley and Booyens (1998), Kearsley (1999b) 23-24, Salvoldi et al. (2015)
67 Dhir et al. (1989). Cited in Brady et al. (2001) C14.
68 Brady (2000). Cited in Brady et al. (2001) C15.
69 Kearsley and Booyens (1998)

foam concrete may be capable of providing adequate protection for carbon steel reinforcing bar.[70]

[70] Kearsley and Booyens (1998)

6.3.4 Thermal Properties

6.3.4a Thermal Conductivity

Thermal conductivity is a measure of the rate at which heat energy flows through a unit area of a material of a unit thickness with a one degree temperature gradient. In SI units, thermal conductivity, *k*, is expressed in W/m^2K. Heat transfer occurs via three mechanisms: conduction, convection and radiation. Conduction is the flow of heat by molecular contact, and usually dominates heat transfer in solids. Convection is the transfer of heat through the displacement of liquid or gas molecules. Radiation is the transfer of heat via electromagnetic radiation through a gas or vacuum, and can be an important form of heat transfer in porous solids.[1]

Heat transfer through solids tends to decrease with an increase in porosity. The path of heat transfer via conduction is made longer and more tortuous, and entrapped air is inhibited from convecting, making for excellent thermal resistance. At very high porosities, the movement of heat through void spaces via convection and radiation may become more dominant than conductive heat transfer, and an optimal density must be determined to minimize the total flow of heat.[2] However, conductivity remains the dominant form of heat transfer in even very low-density concretes at normal temperatures.[3]

Valore[4] determined a logarithmic relationship between thermal conductivity and oven dry density for lightweight concrete, expressed in the equation

$$k_c = 0.072e^{0.00125d}$$

where k_c is the thermal conductivity of concrete in W/m·K and d is the oven-dry density of a sample in in kg/m^3. Thus, conductivity increases at an increasing rate with higher density.

However, distinct types of lightweight concrete may have differing thermal performance for a given density, based on the microstructure and materials used. Values may be somewhat higher or lower than anticipated by Valore's formula. Based on the data

1 Straube (2011)
2 Straube (2011), Gibson and Ashby (1999) 287
3 Gibson and Ashby (1999) 286. The lowest density concretes are more than and order of magnitude above critical density values, e.g 160 kg/m^3 foam concrete vs. 16 kg/m^3 typical critical density, cf. Straube (2011).
4 Valore (1980)

compiled by ACI Committee 122,[5] foam concrete conductivity is slightly lower than many other lightweight concrete materials. Among very low-density concretes, neat cement foam concrete has only slightly higher thermal conductivity than AAC and natural pumice LWA concrete, for the same density. Among medium-low density concretes, neat cement foam concrete is less conductive than expanded clay, shale, and slate LWA concrete, volcanic slag and scoria LWA concrete, and fired clay brick; only expanded slag is less conductive for a given density.[6] (Refer to Chapter 7.) Neat cement foam concrete of 240, 480, 960, and 1920 kg/m^3 dry density will have k_c values of approximately 0.078, 0.125, 0.244, 0.629 W/m·K, respectively.[7] By comparison, the thermal conductivity of normal density concrete is approximately 1.1 to 1.4 W/m·K.[8]

Air-void System

The relative success of foam concrete as a thermal insulator may be attributed largely to the air-void system, which is composed generally of closed, evenly distributed cells. A matrix of relatively thin cells walls produces a tortuous path for heat transfer by conduction. Low interconnectivity of air voids suppresses convection and radiative heat transfer.[9] Air voids in foam concrete are sufficiently small to fully suppress convection.[10]

The size of pores influence heat transfer. Small voids are desirable for increasing the tortuousity of the heat flow path via conductance for a given density.[11] Small voids also reduce convective looping within the cells, although convection is not believed to be a significant form of heat transfer in most foam concrete mixes, since the molecular mean path length within a void is significantly less than the length of a sample (i.e., the Knudsen number is much lower than unity).[12] Radiation is a non-negligible heat transfer mechanism in highly porous mixes, with its influence diminishing with decreasing porosity;[13] smaller voids will increase the number of interruptions to radiative heat transfer over a given

5 ACI 122R-02 Section 2.1
6 ACI 122R-02 Table 2.1
7 ACI 122R-02 Table 2.1
8 Brady et al. (2001) C16
9 Petit et al. (2014) 37, Huang et al. (2015) 396, Gibson and Ashby (1999) 287
10 Gibson and Ashby (1999) 287
11 Cf. Bave (1980). Cited in Narayanan and Ramamurthy (2000b) 327, and Yue and Bing (2014) 7
12 Kreft et al. (2011) 263, cf. Gibson and Ashby (1999) 287
13 She, Chen, Zhang and Jones (2013) 1278

specimen length.

Kreft et al.[14] studied thermal conductivity with respect to various air void characteristic of lightweight autoclaved aerated concrete, and determined that slightly thinner partition walls between cells, as controlled via a surfactant, contributed to a reduced conductivity value. Similarly, Panesar[15] suggested that surfactant type had an influence on thermal resistance of foamed concrete. In the study, it appeared that synthetic surfactant mixes had an advantageous thermal resistance at higher densities, while protein-based surfactant mixes had a greater thermal resistance at low densities. However, further research is necessary to understand the influences of these surfactants on foam concrete microstructure and air void systems.

Use of accelerators such as quicklime may cause fracture of foam cell walls, reducing thermal resistance in foam concrete, as studied by Cong and Bing.[16]

Binder

According to Jones and Giannakou,[17] replacement of Portland cement with 30% fine fly ash reduced thermal conductivity by 12 to 38% in mixes of 1000 to 1400 kg/m^3 plastic density. The lower particle density reduces the thermal conductance of fine fly ash as compared to Portland cement; additionally, the cenospheric shape of fly ash particles increases the tortuousity of the heat flow path by conductance.

Yang et al.[18] used alkali activated foam concrete as a thermal insulation material for in-floor heating systems of buildings.

Yue and Bing[19] reported that magnesium phosphate cement binder improved thermal resistance, compared to conventional Portland cement foam concrete. The addition of fly ash further improved the mix, such that at dry densities of 200 and 355 kg/m^3, thermal conductivity values of 0.049 and 0.062 W/mK were achievable, respectively. By comparison, a Portland cement mix of 355 kg/m^3 dry density might offer

14 Kreft et al. (2011) 263
15 Panesar (2013) 583
16 Cong and Bing (2014) 64
17 Jones and Giannakou (2004) 10
18 Yang et al. (2014)
19 Yue and Bing (2015) 6

thermal resistance of approximately 0.095 W/mK.[20] Yue and Bing[21] indicated that magnesium phosphate cement may help to maintain finer closed pores than Portland cement.

Cong and Bing[22] compared thermal performance of fine clay soil with and without silica fume addition. The mixes with silica fume had a lower thermal conductivity, which was attributed to the capacity of fine solids to maintain finer pores. However, the use of pozzolans does not necessary ensure better thermal performance. Pan et al.[23] documented the thermal conductivity of high performance mixes designed for strength, which included silica fume, slag and fly ash, as well as mixes with sand. Significant improvement in thermal resistance of the pozzolan mixes is not evident. Mix values are also very similar to those provided by ACI Committee 122[24] for sanded foam concrete mixes.

Filler

The addition of sand filler to a mix increases thermal conductivity, compared to a neat cement mix.[25] Sanded foam concrete may be somewhat more conductive than LWA concretes for a given density, depending on the binder-filler ratio. Sanded foam concrete may be between 11 and 84% more conductive than neat cement foam concrete for densities from 480 to 1920 kg/m^3, respectively; this discrepancy will vary with binder-filler ratio.

Ng et al.[26] replaced sand with fine clay soil in foam concrete mixes of between approximately 1100 and 1800 kg/m^3 density. Improved thermal resistance in the soil mixes was attributed to the differences in the thermal conductivity of the soil particles compared to the sand, as well as particle packing properties. Angular sand particles interlock in a dense matrix, while round soil particles are thought to produce interstitial voids at a nanostructural scale, reducing heat transfer by conduction. Simultaneously, the fineness of the soil particles may help minimize coalescence, maintaining small bubble

[20] ACI 122R-02 Table 2.1
[21] Yue and Bing (2015) 6
[22] Cong and Bing (2015) 63
[23] Pan et al. (2007) 3
[24] ACI 122R-02 Table 2.1
[25] ACI 122R-02 Table 2.1
[26] Ng et al. (2011) 185

sizes with the attendant thermal insulation benefits described above. Research by Cong and Bing[27] also suggested that clay soil foam concrete has a lower thermal conductivity than conventional concrete.

Aliabdo et al.[28] reported that thermal conductivity was reduced with the incorporation of fine aggregate crushed clay brick to replace sand. The porous fine aggregate increased the total porosity of the mix. However, data presented by Jones et al.[29] for foam concrete made from recycled and secondary aggregates indicated that replacement of sand filler with demolition fines, incinerator bottom ash, China clay sand, or conditioned fly ash, did not have a significant effect on thermal conductivity values.

Lightweight Aggregate and Fibre Reinforcing

Weigler and Karl[30] proposed that foamed lightweight aggregate concrete could provide excellent thermal resistance, in comparison with normal LWA concrete of similar strength. Proshin et al.[31] introduced polystyrene granules into foam concrete mixes for a density of 200 to 650 kg/m^3 and a thermal conductivity of 0.06 to 0.16 W/mK, respectively.

Liu et al.[32] determined that geopolymer foam concrete created with fuel ash and oil palm shell LWA had a thermal conductivity of 0.47 W/mK for a 1300 kg/m^3 density mix. This value lies between 0.348 and 0.536 W/mK reported by ACI Committee 122[33] for neat cement and sanded foam concrete mixes of approximately the same density, respectively. 1300 and 1500 kg/m^3 mixes could be classified both as structural concrete and as insulating concrete.

Yakovlev et al.[34] studied the thermal conductivity of foam concrete mixes reinforced with carbon nanotubes. The reinforcing produced greater pore uniformity, smaller pore size, and less interconnectedness compared to an unreinforced mix, resulting in improved thermal resistance.

---

27 Cong and Bing (2015) 63
28 Aliabdo et al. (2014)
29 Jones et al. (2012) 524
30 Weigler and Karl (1980) 104
31 Proshin et al. (2005) 116
32 Liu et al. (2014) 244
33 ACI 122R-02 Table 2.1
34 Yakovlev et al. (2006) 150

Ultra-Low Density Mixes

Foaming agents may inhibit solidification at extremely low densities, as discussed previously. (Refer to Section 6.3.1.) Consequently, hydrogen peroxide is sometimes employed as a gassing agent, instead. Huang et al.[35] produced ultra lightweight cellular concrete using the decomposition of hydrogen peroxide in a Portland cement-fly ash blend. A mix with an apparent density of 102 kg/m^3 had a thermal conductivity of 0.043 W/mK, which is comparable to the thermal conductivity of mineral wool insulation of between 0.036 and 0.041 W/mK. Huang et al. noted that almost all of the air voids were non-connected. 71.3% of voids were between 2.0 and 4.0 mm in diameter; 25.6% were larger, and the remainder were smaller. The average shell thickness was 41.6μm, compared to 63.7μm in a similar mix of 307 kg/m^3 dry density.

Similarly, Pan et al.[36] produced Portland cement-slag cellular concrete using hydrogen peroxide as a gassing agent, producing a mix with a measured dry density of 153 kg/m^3 and a thermal conductivity of 0.050 W/mK.

Influence of Moisture

The presence of moisture in a porous concrete can have a significant influence on its thermal conductivity.[37] Valore[38] suggested that the value of k_c may be increased by 6% for each increase of 1% moisture by weight. Thus,

$$k_c' = k_c \left[1 + \left(\frac{6d_m - d_o}{d_o}\right)\right]$$

where k_c' is a moisture-corrected value for thermal conductivity, and d_m and d_o are moist and oven-dry specimens, respectively. Consequently, the internal humidity, as well as the sorptivity of foam concrete in service conditions, should be taken into account to accurately anticipate the actual thermal performance of foam concrete.[39]

[35] Huang et al. (2015) 395
[36] Pan et al. (2014)
[37] ACI 122R-02 Table 2.1
[38] Valore (1980)
[39] Cf. Yang and Lee (2015) 110

Mathematical Models

In research on highly porous cementitious foams, Akthar and Evans used a formula[40] for the apparent thermal conductivity of foam concrete, k_{fc}, as a function of the thermal conductivity of an unfoamed paste, k_s, the thermal conductivity of the gas in the air voids, k_g, and the volume fraction of gas in a specimen, V_g:

$$k_{fc} = k_s(1 - A) + k_g A$$

where

$$A = \frac{2^n}{2^n - 1}\left(1 - \frac{1}{\left(1 + V_g\right)^n}\right)$$

with n=2. However, Akthar and Evans suggest that incorporating heat transfer by radiation is an important consideration for further investigation.[41]

She et al.[42] conducted two-dimensional numerical predictions for foam concrete with densities of 300 to 1700 kg/m^3, with good results for mixes with porosities of less than 35%. In another study, She et al.[43] have shown that three-dimensional numerical modeling and simulation of foam concrete thermal properties are in good agreement with experimental results across a range of porosities, while thermal conductivity is underestimated by two-dimensional models, since additional heat paths in the third dimension are suppressed.

Thermal Uses in Various Regions and Unusual Applications

Jones and Giannakou[44] recommended foam concrete as a form of Controlled Thermal Fill (CTF) for trench fill foundations and ground-supported slabs for housing in the UK. Dolton and Hannah[45] suggested that cellular concrete may be useful in extremely cold climates: for example, on permafrost, foam concrete may provide superior insulation and bearing performance to traditional granular fills. Shi et al.[46] proposed filling the hollow walls of Hui-style vernacular dwellings in China with foam concrete, to improve their thermal

40 Cf. Collishaw and Evans (1994). Cited in Akthar and Evans (2010) 357
41 Akthar and Evans (2010) 357
42 She, Chen, Zhang and Jones (2013) 1290
43 She et al. (2014a) 430
44 Jones and Giannakou (2004) 10
45 Dolton and Hannah (2006) 7
46 Shi et al. (2012) 23

performance without compromising architectural heritage. Tada[47] developed a parametric strategy for determining optimum density and wall thickness for cellular concrete building enclosures, based on local conditions and including thermal performance as a criteria.

Richard et al.[48] studied the potential for foam concrete in as a load bearing material in cryogenic applications, noting that thermal conductivity may be reduced by up to 26% when the mean testing temperature is reduced from 22°C to –196°C. Extreme cooling was also accompanied by an increase in strength, as is usual for structural material. Tested mix densities varied from 640 to 1440 kg/m^3.

6.3.4b Heat Capacity

Specific heat capacity is the amount of heat energy required to raise the temperature of a mass by one degree.[49] In SI units, specific heat capacity may be measured in $J/kg \cdot K$. For foam concrete, density is a major variable. Consequently, it may be more helpful to measure specific heat capacity on a volumetric basis, rather than a mass basis. Volumetric heat capacity is the product of density and specific heat capacity, measured in $J/m^3 \cdot K$.

Volumetric heat capacity increases with density. The total heat capacity of a volume of foam concrete may be taken as the sum of the heat capacities of all of its constituents.[50] Thus, the type and amount of filler in a mix has an influence on heat capacity,[51] and the degree of hydration will also have an effect, as new hydration products are formed.[52] The presence of moisture also has a significant contribution.

Tarasov et al.[53] calculated volumetric heat capacity values for dry foam concrete with 300 kg/m^3 cementitious density and increasing amounts of silica sand fine aggregate. Mixes with dry densities of 350, 400, 800, and 1200 kg/m^3 were found to have volumetric heat capacities of 916, 967, 1479, and 1998 kJ/m^3·K, respectively. By comparison, normal density concrete may have a specific heat of between 0.79 and 0.92 kJ/kg·K, corresponding

47 Tada (1986) 24
48 Richard et al. (1975) 501
49 ACI 122R-02 Section 4.1.2
50 Tarasov et al. (2010) 903
51 Panesar (2013) 577
52 Tarasov et al. (2010) 903
53 Tarasov et al. (2010) 903

approximately to between 1900 and 2200 kJ/m^3·K.[54]

Heat capacity is important for the resistance of foam concrete to fire and elevated temperatures. Loss of concrete strength results from the decomposition of hydrate products, as heat energy drives off chemically combined water. If more heat energy can be absorbed by the solid mass, this phenomenon will be lessened.[55]

It is also conceivable that foam concrete could be used for thermal mass in passive solar design.[56] Tonyan and Gibson[57] suggested that foam concrete was attractive for structural sandwich panels, in part due to its high heat capacity.

As discussed in Section 6.2.2, heat capacity is an important parameter during curing to control temperature rise due to heat of hydration. The amount of mix water may have a dominant influence, due to the high heat capacity of water.[58]

6.3.4c *Thermal Diffusivity*

Thermal diffusivity is a measure of heat transport relative to energy storage, i.e., it is the ratio of a material's thermal conductivity to its volumetric heat capacity. Consequently, thermal diffusivity indicates how quickly a material will change in temperature.[59] In equation form, thermal diffusivity, $\propto$, may be expressed as

$$\propto = \frac{k}{\rho c_p}$$

where

k is thermal conductivity ($W/m \cdot K$),

ρ is density (kg/m^3), and

c_p is specific heat capacity ($J/kg \cdot K$)

Foam concrete has a relatively low thermal conductivity and a relatively high heat capacity. Consequently, the material changes temperature slowly. This property is especially important for the resistance extreme heat and fire, as discussed above in Section 6.3.4b and

54 ACI 122R-02 Section 5.1.4
55 Mydin and Wang (2012) 215, Metha (1986) 29, Zhang et al. (2014) 122
56 ACI 122R-02 Section 5.1.4
57 Tonyan and Gibson (1992a), Tonyan and Gibson (1992b)
58 Jones and McCarthy (2006) 1036, Tarasov et al. (2010) 901
59 ACI 122R-02 Section 4.1.1

in Section 6.3.5c. Li et al.[60] developed a numerical simulation based on thermal diffusivity to demonstrate the superior fire resistance of foamed concrete compared to normal density concrete.

Zhang et al.[61] empirically determined the thermal diffusivity of geopolymer foam concrete. Where dry density ranged from 583 to 1370 kg/m^3, thermal diffusivity increased with density from 0.27 to 0.34 mm^2/s. In comparison, the thermal diffusivity of fully hydrated, normal density, ordinary Portland cement concrete is approximately 1.1mm^2/s.[62]

[60] Li et al. (2013) 19
[61] Zhang et al. (2015) 100-101
[62] Schutter and Taerwe (1995). Cited in Zhang et al. (2015) 101

6.3.5 Durability Properties

6.3.5a Rate of Carbonation

The alkalinity of concrete is reduced over time due to the process of carbonation. This phenomenon has important implications for the corrosion of reinforcing steel. At relative humidities of approximately 50 to 70%, carbon dioxide from the atmosphere dissolves readily in water at the concrete surface, and produces mild carbonic acid. The acid reacts with calcium hydroxide, $Ca(OH)_2$, to produce calcium carbonate, $CaCO_3$.[1] As the pH of the concrete surrounding steel reinforcing decreases below 10, surface passivation of the steel dissolves, and corrosion begins.[2]

Compared to normal density concrete, foam concrete is relatively permeable to water vapour and carbon dioxide. (Refer to Section 6.3.3d.) Consequently, steel reinforcing is not typically recommended in foam concrete.[3] However, Kearsley and Booyens[4] reported that use of coarse fly ash filler as a complete replacement for sand filler significantly reduced permeability of foam concrete to levels appropriate for the use of carbon steel reinforcing bar.[5]

Jones and McCarthy[6] conducted accelerated carbonation testing on foam concrete samples. Use of coarse fly ash filler decreased carbonation penetration in mixes of 1400 kg/m^3 plastic density, but increased carbonation penetration in mixes of 1800 kg/m^3 plastic density. Regan and Arasteh[7] reported similar conclusions for lightweight aggregate foam concrete. For conventional foam concrete with Portland cement contents of between 270 and 355 kg/m^3, and densities between 1330 and 1750 kg/m^3, Brady[8] determined that the average rate of carbonation was approximately 5.7 mm/year$^{0.5}$, which is 50% higher than normal density concrete with similar cementitious density.

Typically, the rate of carbonation in foam concrete may be expected to decrease with increasing density, and with increasing cementitious density. The high cement

1 Neville (2006) 98
2 Kosmatka et al. (2002) 266
3 Brady et al. (2001) 10
4 Kearsley and Booyens (1998)
5 Kearsley and Booyens (1998)
6 Jones and McCarthy (2005b) 27
7 Regan and Arasteh (1990). Cited in Jones and McCarthy (2005b) 27
8 Brady (2000). Cited in Brady et al. (2001) C15

content in many foam concrete mixes helps to reduce the rate of carbonation.[9]

6.3.5b *Resistance to Sulfate Attack*

The presence of sulfates can cause destructive action in concrete. A distinction may be drawn between chemical attack and physical attack. In the first case, a chemical reaction between sulfates and the cement paste consumes calcium from calcium hydroxide and calcium silicate hydrate phases, undermining the strength of the paste. The production of gypsum and ettringite may also cause damage to a specimen through expansion. In the second case, the crystallization of sulfate salts in pores near the surface of a specimen produce internal pressures, which are relieved by spalling and disintegration. Many authors propose that the term 'sulfate attack' refers only to the former mechanism.[10]

Sulfates may be introduced within a fresh mix via the aggregate or mix water (due to contamination), via the cement (due to over sulfation), or via delayed ettringite formation (due to heat of hydration and temperature rise), discussed in Section 6.2.3.[11] In addition to these sources of internal sulfate attack, sulfates from the environment may also enter a hardened cement paste over time. Various parts of the world have soils with naturally high concentrations of sulfates. Sulfates concentrations may also be high at former industrial sites, known as 'brownfields',[12] and near seawater. Severity and nature of damage vary according sulfate type.[13]

The resistance of foam concrete to chemical attack is an important property, as the material is frequently used in foundations and fill applications where sulfates may be present.[14] Jones and McCarthy[15] tested Portland cement foam concrete specimens with plastic densities of 1000 and 1400 kg/m^3, utilizing sand or coarse fly ash filler. The specimens experienced minimal expansion over a period of 12 months, indicating good performance. Denser mixes provided slightly better resistance to attack, which was attributed to a less interconnected pore structure, slowing the ingress of the aqueous

9 Fabian et al. (2006) 189
10 Neville (2006) 117
11 Scrivener (2004)
12 Neville (2006) 121
13 Neville (2006) 122
14 Jones and McCarthy (2005c) 1405, Jones et al. (2012) 521
15 Jones and McCarthy (2005c) 1405

sulfate solution.

Jones et al.[16] has also conducted testing on foam concrete with recycled secondary aggregate fillers, including demolition fines, incinerator bottom ash, glass fines, foundry sand, and crumb rubber. At 200 days, expansion was low for samples with demolition fines, glass fines, and foundry sand in particular. X-ray diffraction analyses confirmed the presence of expansive reaction products such as ettringite; however, it is assumed that these formed within the available space of the air voids.

Mamun and Bindiganvile[17] studied the sulfate resistance of conventional and fibre reinforced foam concrete, with densities of 475, 750, and 1200 kg/m^3. The authors noted that the influence of sulfate attack on flexural response was more pronounced than on compressive strength. Heavier mixes were more susceptible to attack, while the flexural strength of the lightest mixes actually increased during the first thirty days of exposure. The authors concluded that the sulfate exposure produced a self-healing effect in light mixes, due to the production of expansive crystals that increased the density of the paste; the carbonation of calcium hydrates, which closed existing cracks; and the continued hydration of previously unhydrated cement grains.[18] Similarly, Mamun et al.[19] determined that fibre-reinforced foam concrete exposed to sulfate experienced an increase in thermal conductivity upon exposure to sulfates, due to densification.

6.3.5c *Freeze-Thaw Performance*

In order to understand and compare the potential for frost action in foam concrete materials, the mechanisms of freeze-thaw damage must be clearly understood.

Technical literature often indicates that freeze-thaw damage in concrete is due to the expansion of water as it freezes.[20] In this model, the expansion of water within a cavity is believed to produce a hydraulic pressure that may exceed the concrete's tensile strength, causing mechanical damage. Damage may be avoided if spaces are provided into which

16 Jones et al. (2012) 521
17 Mamun and Bindiganvile (2011)
18 Mamun and Bindiganvile (2011) 3429-3430
19 Mamun et al. (2014)
20 Portland Cement Association (2015a), Kosmatka et al. (2002) 12, Brady et al. (2001) C12

capillary water can escape and expand safely.[21] These spaces may be distributed through the cement paste through the use of chemically produced gases, air entrainers or preformed foam.

While the expansion of water may account for some freeze-thaw degradation in certain situations, it is now understood that it is not the only mechanism, nor is it the most significant. In fact, freeze-thaw damage occurs even when water is replaced with fluids that do not expand upon freezing.[22]

Capillary theory, described by Everett in 1961,[23] helps explain the phenomenon of freeze-thaw damage more completely. The three-dimensional network of pores of varying scales is significant. Essentially, water is held more rigidly in within smaller pores than within larger cavities. Restrictions in molecular movement influence the relative freezing points of liquids within the pores. Water in macroscopic air voids may freeze at around 0°C, depending on the presence of salts, etc.; conversely, water in extremely small gel pores may be unable to reorder itself as ice, unless cooled below −78°C.[24]

Consequently, in typical freezing service conditions, water in small pores exists as supercooled liquid, in a higher energy state than the frozen water in larger voids. Driven by the difference in entropy, water migrates from the smaller pores to the larger pores, where it freezes and accumulates. The volume of the larger pores will eventually be filled with ice. If migration of water from smaller pores continues towards these lower-energy sites, internal pressures will develop, dilating the ice-filled cavities and potentially damaging the specimen.

Water migrates from small pores to large pores; thus, from gel pores to capillaries, and from capillaries to air voids. In normal density cement paste, the proportion of air-voids is very low. Moisture contained within a sample is held mainly within capillaries, gel pores, and interlayer water. The migration of water from gel pores into capillary voids will be the main cause of freeze-thaw damage in normal density cement paste.[25]

The proportion of voids in cellular concrete is different from that of normal density

---

21 Powers and Willis (1950). More precisely, air voids serve as nucleation sites for the accumulation of ice, as described by Powers and Helmuth (1953).
22 Mehta (1986) 123, Everett (1961) 1541
23 Everett (1961)
24 Mehta (1986) 123
25 Mehta (1986) 123

concrete: or example, the volume of a low-density foam concrete sample may consist of 50% air void and 30% capillary pores. In a saturated sample, the majority of water is held in capillaries and air voids, and the greatest risk of freeze-thaw damage is due to the migration of water from capillaries to air voids.[26]

Thus, although normal density cement paste and foam concrete may both experience frost action due to capillary effects, the critical migration of water in foam concrete occurs between larger pores. This situation has a significant influence on freeze-thaw behaviour, as it is related to the volume of water available, the volume of void available to be filled with freezing water, the ease of migration of water between pores, and the freezing point or supercooling of pore water.

Much technical literature asserts that foam concrete has excellent freeze-thaw characteristics, as foam concrete performs well in many typical freeze-thaw tests.[27] The total large volume of air void typically provides ample space for the accumulation of water. However, two conditions should be noted in which foam concrete may perform poorly.

Firstly, it is important to observe that, due to its porous structure, an exceptionally large volume of water may be present in a foam concrete sample. Thus, a great volume of supercooled liquid water may exist in the capillary pores. If a large amount of water from the capillary pores is driven into already saturated larger voids, significant pressures and dilation may occur. The expansion could potentially be greater than in a sample of normal density cement paste, due to the greater volume of migrating water.

A second condition is in which foam concrete is particularly susceptible to freeze-thaw damage arises from a combination of foam concrete properties. In service, foam concrete may be placed such that one surface is vulnerable to moisture and freezing temperatures. Because of its permeability or capillary water uptake, it may be saturated to a significant depth. Due to the insulating effect of air voids, another zone may be kept warm. Differential strain in the saturated, frozen region and the dry, warm region can cause internal cracking. Senbu and Kamada[28] developed a test method to assess freeze-thaw performance of aerated autoclaved concrete for this condition. Tikalsky et al.[29]

---

[26] Senbu and Kamada (1990) 254
[27] Brady et al. (2001) 10, C12; Jones and McCarthy (2005a) 72
[28] Senbu and Kamada (1990)
[29] Tikalsky et al. (2004)

adapted this test for foam concrete. In a study of varying densities, cementitious contents, and proportions of sand and fly ash fillers, the authors determined that important factors for freeze-thaw resistance in this condition were mechanical strength, depth of initial penetration, and adsorption and absorption rates. Density did not appear to be a significant variable.

In order to limit liquid saturation, hydrophobing agents or external water repellents are used to avoid freeze-thaw damage in autoclaved aerated concrete.[30] Such agents may also provide enhanced durability for foam concrete. Additionally, Van Deijk[31] has suggested protein-based surfactants impart some level of water repellence to foam concrete, reducing the absorption of water. Neville[32] suggested that both gas and foam concretes should be protected from water by rendering when used on the exterior of a structure.

6.3.5d Resistance to Fire and Elevated Temperatures

Although concrete is incombustible, the strength of concrete can be compromised by exposure to extreme heat. At temperatures higher than 200°C, Portland cement hydration products decompose, releasing chemically bound water.[33] Porosity increases,[34] and thermal gradients or expansion of reaction products may induce bulk cracking.[35]

The issue of fire and extreme heat resistance is complex, as it involves heat transfer and structural capacity of a changing material.[36] Commonly, the thermal resistance of a material may be evaluated by measuring changes to strength or volume following high temperatures exposure.[37] Other tests may measure the time required for a given temperature rise across a panel of a certain thickness.[38]

In general, foam concrete offers excellent fire performance.[39] Air voids provide insulation to protect inner zones from extreme heat. At high temperatures, heat transfer

30 RILEM Technical Committees 78-MCA and 51-ALC (1993) 33
31 Van Deijk (1991) 49
32 Neville (1963) 441
33 Mydin and Wang (2012b) 214, Mehta (1986) 29
34 Zhang et al. (2014) 122
35 Zhang et al. (2015) 101
36 Jones and McCarthy (2005b) 29
37 Zhang et al. (2014) 122
38 Aldridge (2005) 9-10, Li et al. (2013)
39 Cf. ACI 523.1R-06, Section 3.9, Fouad (2006) 566, Amran et al. (2015) 1001.

through a porous medium is strongly influenced by radiation. The closed cell structure of foam concrete provides many interruptions to the movement of heat by radiation, at each air-solid interface.[40] Furthermore, foam concrete has a relatively high heat capacity. Heat energy is absorbed into the material, suppressing temperature change.[41]

Fire endurance may be enhanced with a reduction in density.[42] Jones and McCarthy[43] noted that there is proportionally less strength loss in foam concrete compared to normal density concrete when exposed to extreme heat, especially at lower densities.

The temperature resistance of foam concrete may be further enhanced with the use of geopolymers. Geopolymer gels typically have extremely high temperature stability, and may actually increase in strength with exposure to temperatures of between 400 and 800°C. Thermal conductivity is low, due to low amounts of chemically bound water.[44]

Consequently, foam concrete may be suitable for the construction of buildings and structures that require extreme fire resistance.[45] Kearsley and Mostert[46] promoted the use of foam concrete in firewalls and refractory applications, noting that foam concrete containing fly ash filler, and with densities between 550 and 1050 kg/m^3 could withstand temperatures of 800°C. Krivenko et al.[47] compared thermomechanical properties of geopolymer and Portland cement foam concrete. They noted that the mechanical properties of geopolymer foam concrete may improve during service in a high heat environment, and suggested that the material offered better performance for lower cost than other heat resistant ceramics. Krivenko et al.[48] also suggested that heat resistant foam concrete could be appropriate for underground constructions and towers. Li et al.[49] simulated the movement of heat energy through a foam concrete wall in a fire event, and concluded that walls composed of fly ash based foam concrete could significantly increasing emergency egress time, compared to normal density concrete walls.

Comparisons of foam concrete and vermiculite lightweight aggregate concrete

---

40 Valore (1954b) 834, Panesar (2013) 577
41 Mydin and Wang (2012b) 215, Zhang et al. (2014) 122
42 Ramamurthy et al. (2009) 394
43 Jones and McCarthy (2005b) 29
44 Zhang et al. (2015) 101
45 Zhang et al. (2014) 123
46 Kearsley and Mostert (2005c) 93
47 Krivenko et al. (2005)
48 Krivenko et al. (2005) 104
49 Li et al. (2013) 13

suggested that at lower densities of 500 kg/m^3, foam concrete had 30% better endurance, and 38% higher strength for the given testing parameters. Conversely, at higher densities of approximately 1250 kg/m^3, vermiculite lightweight aggregate concrete had somewhat better resistance to degradation under extreme heat.[50]

Sayadi et al.[51] tested the fire resistance of foam concrete with between 0 and 82% expanded polystyrene particles. Fire resistance decreased dramatically with an increasing volume of expanded polystyrene; additionally, the polystyrene beads were combustible and produced smoke.

In addition to its various construction uses, foam concrete has been used successfully as a fire extinguishing grout for coal mine fires.[52] Highly flowable and fire-resistant material fills surficial ventilation openings, blocking sources of oxygen. If the grout is exposed to high heat while in a plastic state, it will not flash set or explode with steam.

[50] Aldridge (2005) 9-10
[51] Sayadi et al. (2016b) 719-721
[52] Colaizzi (2004) 79

6.3.6 Acoustic Properties

6.3.6a Sound Insulation

Sound insulation is the capacity of a membrane or assembly to suppress the transmission of air-borne sound energy. It is typically measured as transmission loss, TL, in decibels (dB). For a solid wall, transmission loss may be determined according to the well-known mass law of sound insulation developed by London,[1] presented by Warnock[2] in an approximate equation:

$$TL \approx 20 \log_{10} m_s f - 48$$

where m_s is the mass per unit area, or 'surface density', and f is the frequency of the sound. Thus, transmission loss is approximately proportional to the mass of a wall:[3] doubling the density of a partition will increase transmission loss by approximately 6 dB.

According to mass law, low-density foam concrete will perform poorly relative to normal density concrete. However, Tada[4] noted that transmission loss is also dependent on the rigidity and internal resistance of the wall. Thus, the thickness of a cellular concrete wall may contribute somewhat to ensuring adequate transmission loss, as well. Short and Kinniburgh[5] also note that lightweight concrete may perform better than would be anticipated by mass law. However, air tightness is necessary to ensure that sound will not 'leak' through an assembly.[6]

6.3.6b Sound Absorption

Sound absorption is a distinct property from sound insulation. While sound insulating materials reduce the sound energy transmitted through a membrane or assembly, sound absorbing material reduce the amount of sound energy reflected from the barrier.[7]

While the ability of foam concrete to isolate sound may be poor in comparison to normal density concrete, its ability to absorb sound may be relatively good. Instead of

---

1 London (1949)
2 Warnock (1985)
3 Short and Kinniburgh (1978) 73
4 Tada (1986) 23
5 Short and Kinniburgh (1978) 73
6 Short and Kinniburgh (1978) 73, Leitch (1980). Cited in Narayanan and Ramamurthy (2000b) 328
7 Short and Kinniburgh (1978) 73

being reflected off of a stiff surface, sound energy is captured within small air voids at the surface of a wall and lost as heat.[8] Interconnectivity of bubbles allows for sound energy to travel deeper into the surface of a wall, improving absorption coefficients.[9] A greater pore size distribution may help attenuate sound at different frequencies. Aliabdo et al.[10] reported that the sound attenuation coefficient of cellular concrete made using crushed clay brick was better than when using natural sand. This trend was attributed in part to a more irregular and interconnected pore structure.

Laukaitis and Fiks[11] reported mean normal incidence absorption coefficients for foam concrete of different densities. Mixes with dry densities of 250, 300, 400, and 500 kg/m^2 had mean absorption coefficients of 0.24,0.22, 0.15, and 0.12, respectively. Absorption coefficients will decrease if exposed surfaces are sealed, for example, with paint.[12]

In a study of the acoustical properties of geopolymer foam concrete, Zhang et al.[13] noted that substituting slag for fly ash increases sound absorption in the higher frequency range, between 800 and 1600 Hz, due to a change in pore structure. Moreover, the researchers found that increasing foam dosage made foam concrete more absorptive in the 600 to 1000 Hz range, but less absorptive for lower frequencies. Increasing panel thickness increased the absorption of lower frequencies, in particular.

8 Neville (1963) 446
9 Laukaitis and Fiks (2015) 291
10 Aliabdo et al. (2014)
11 Laukaitis and Fiks (2015) 291
12 Cf. RILEM Technical Committees 78-MCA and 51-ALC (1993) 40
13 Zhang et al. (2015) 104

6.3.7 Energy Absorption

The capacity of cellular concrete to absorb impact has been recognized since 1933, when a patent proposed using finely shredded redwood bark reinforcement to produce a material whose "power to absorb sudden blows" purportedly made it "ideal as a protective shield over the roofs of houses adjacent rocky mountains or banks from which large rocks may become loosened, and also as a protection to arsenals and other buildings against deliberate attack."[1] Today, foam concrete is used for military purposes, and to absorb the impact of rock fall. It is also used to absorb the strain of differential settlement, the energy of mining explosions or earthquakes, and the impact of vehicles.

In addition to its uses in explosion prevention[2] and defensive structures,[3] foam concrete has an important military use as a bullet-trapping medium for small arms training. Shock-absorbing concrete, known as SACON, is reinforced with steel fibres for the fabrication of target structures. The material reduces ricochets, does not burn or rot, is not damaged by insects, and prevents metal debris from contaminating the soil. Fabian et al.[4] developed foam concrete with a density of 1440 kg/m^3 and a flexural strength of 3.4 MPa to absorb 3139 tons of bullets used annually in small arms military training ranges in the United States.

Foam concrete is used for padding and bedding utility systems. In mountainous areas, foam concrete may protect pipelines from rockfall. As a deformable bedding material for long pipelines, foam concrete crushes to relieve stress concentrations due to differential movement or settlement. Where it is used for trench reinstatement, foam concrete also absorbs the strain of differential settlement or surcharge loads, reducing risk of damage to utilities.[5] Foam concrete can also be placed in the annulus around vertical delivery lines, in order to absorb the vibration energy of materials as they descend through the conduit, reducing pipe cracking and consequent corrosion.

Foam concrete can reduce vibration due to blasting shock in airtight walls for

1 U.S. Patent 2023800 A
2 Jones and Zheng (2013) 209
3 Tian, Zhang and Niu (2016) 195
4 Fabian et al. (2006) 187
5 Dolton and Hannah (2006) 4

mining.[6] A wall assembly consisting of foam concrete, and foam concrete-filled steel piers, is capable of bearing mine ground pressures while also absorbing explosion surge pressures, maintaining an air tight seal and preventing collapse. Similarly, foam concrete tunnel linings can dampen seismic response.[7]

Foam concrete may also be used in crash barriers for ground vehicles[8] or aircraft arresting systems. Soft ground arrestor systems induce drag forces on the landing gear of an aircraft to reduce its stopping distance, in the event of an overrun during takeoff or during an aborted takeoff. They are invaluable where natural obstacles, local development, or environmental constraints preclude the possibility of building a long extension beyond the end of a runway. Plastic foam has been proposed as a crushing surface;[9] however, foam concrete provides additional advantages of being non-susceptible to degradation by hydrocarbons or organisms.[10] Heymsfield et al.[11] investigated twenty-six low-density concrete mixes for their capacity to decelerate an aircraft. Zhang et al.[12] produced a model to analyze the interaction of an aircraft landing gear and a foam concrete arresting system. They noted that differences among overrunning aircraft have significant effects on arresting efficiency. The first operational use of foam concrete as an aircraft soft ground arrestor bed was in May of 1999 at John F. Kennedy Airport in New York, one year after its installation.[13]

Energy absorption is related to several of mechanical and physical properties. Compressive strength, flexural strength, elasticity modulus, and Poisson's ratio are significant parameters, as is the geometry of the air void system, which collapses during crushing.[14]

The energy absorbed by the crushing of foam concrete may be quantified according to indentation volume or indentation depth produced by an impact of known kinetic

6 Tang et al. (2013) 345
7 Jiang and Zhang (2011) 691
8 Tom et al. (2003)
9 White and Agrawal (1993)
10 Aldridge (2005) 8
11 Heymsfield et al. (2008)
12 Zhang et al. (2013)
13 Anon. (1999)
14 Wee et al. (2011) 591

energy. Jones and Zheng[15] determined that impact absorption was related to w/c ratio, density, and compressive strength. For good energy absorption capacity, mixes required relatively strong bubble walls and sufficient void space into which crushed debris could be pushed, to avoid global fracturing of the specimen. 1000 kg/m^3 mixes appeared to perform better than other mixes of 500, 600, or 1400 kg/m^3 plastic density.

Fabian et al.[16] tested the capacity of SACON to absorb energy from bullets by repeatedly firing ammunition at the same point. In an appropriately proportioned mix, bullets collected in a dense mass within the specimen, or deflected upwards, rather than cracking the specimen or penetrating the rear surface.

Tang et al.[17] determined the capacity of foam concrete to dampen vibration from a shock through numerical analysis. Zhang et al.[18] analyzed arrestor bed capacity numerically, based on drag forces generated by the crushing, tearing, adhesive-resistant, and equivalent friction forces.

15 Jones and Zheng (2013) 215
16 Fabian et al. (1996)
17 Tang et al. (2013)
18 Zhang et al. (2013)

6.4 Sustainability Considerations

The environmental impact of a material is complex and multifaceted. Many factors must be considered in assessing sustainability, including the consumption of raw materials, the use of energy for transportation or processing, design life and durability, the capacity of the material resist heat transfer or other forms of energy loss, interactions and synergies within systems and assemblies, and whether viable alternatives exist for a given application. Some major considerations for the production of foam concrete are summarized in brief, below.

6.4.1 Constituent Materials

The production of cement is estimated to contribute no less than 5 to 7% of global carbon dioxide emissions.[1] Some cementitious materials, such as phosphate binders, are especially toxic.[2] Foam concrete typically has a high cementitious density; thus, a significant focus for improving the sustainability of foam concrete concerns the transition to binders with a relatively low ecological impact. Partially replacing cement binders with supplementary cementitious materials from industrial sources, such as fly ash, silica fume, and slag, helps to reduce CO_2 emissions and divert these byproducts from landfills,[3] and use of geopolymer binders can significantly reduce CO_2 production.[4]

Water demand is relatively high for foam concrete recipes. Purer water may be required for foam concrete than for normal density concrete, as contaminants may disturb the chemistry of the aerated surfactant.[5]

Aggregate use is typically low in foam concrete, while filler volume varies according to density. Recycled secondary aggregates may be used to reduce the need for natural aggregates.[6] Foam concrete may also encapsulate waste or hazardous solid materials as fillers.[7]

---

1 McLellan et al. (2011)
2 Krivenko et al. (2005) 98
3 She, Chen, Zhang and Jones (2013) 1278
4 Stengel et al. (2009), Weil et al. (2009), McLellan et al. (2011)
5 Brady et al. (2001) C3; Fouad (2006) 562
6 Jones et al. (2012)
7 Lee and Hung (2005) 16-19

6.4.2 *Transportation To or From Site*

Foam concrete can be very efficient to transport where wet mortar or dry mortar delivery systems are employed. By transporting a dense base mix and aerating it on-site, truck movements can be reduced by 80% or more for low density mixes,[8] reducing fuel consumption and road and vehicle wear. Likewise, material that can be crushed to reduce volume may be more efficient to remove from a site.

Lightweight precast products may require less energy and equipment to move and assemble. [9]

6.4.3 Disruption of Site

As a free flowing fill which hardens into a cohesive solid, foam concrete may reduce the amount of excavation required on certain ground works projects.[10] Its capacity to limit erosion may be especially ecologically beneficial in works adjacent to waterways.[11]

6.4.4 Embodied Energy for Curing

Whereas high temperatures require for manufacturer or curing other inorganic lightweight materials such as AAC or foam glass, foam concrete will stiffen and set at normal temperatures and pressures. Note, however, that significant embodied energy is required for the production of Portland cement.

6.4.5 Durability

As discussed in the previous Sections, foam concrete is reasonably resistant to degradation by hydrocarbons and micro-organisms;[12] fire and extreme temperatures;[13] sulfate attack;[14] freeze-thaw action; [15] explosive stresses; [16] seismic stresses and vibration.[17] This durability

8 Aldridge (2005) 6
9 Mydin and Wang (2011) 66
10 O'Reilly (2009) 16-17
11 Van Deijk (1991) 51
12 Aldridge (2005) 8
13 Jones and McCarthy (2005b) 29
14 Jones and McCarthy (2005c) 1405, Mamun and Bindiganvile (2011)
15 Brady et al. (2001) C12
16 Tang et al. (2013) 345

enhances the service life of foam concrete and the materials and structures that the foam concrete protects.

6.4.6 Environmentally Beneficial Applications

Foam concrete may contribute to sustainability through many existing or proposed applications.

Thermal insulation

Foam concrete resists the flow of heat in building,[18] refractory,[19] and utility[20] applications. As a highly flowable material, foam concrete may be capable of upgrading the thermal resistance of voids beneath floors[21] or in hollow walls[22], where other materials would be inadequate.

Enabling re-use or extended use of existing structures

Foam concrete may allow existing structures to be reused, where they would otherwise require demolition or more significant renovation. Grouting can provide structural support under existing floors[23], and foam concrete fill can stabilize structures on unstable soils at risk of collapse.[24] The service life of utilities may likewise be prolonged. For example, foam concrete fill has been placed under aging tank bottoms to relieve stresses in the metal.[25]

---

17 Jiang and Zhang (2011)
18 Kearsley and Mostert (2005b) 144
19 Krivenko et al. (2005) 102
20 Dolton and Hannah (2006) 1
21 Liew (2005) 50
22 Shi et al. (2012) 23
23 Dolton and Hannah (2006) 8
24 Basiurski and Wells (2001) 68
25 Van Deijk (1991) 51

Containment of hazardous waste

Foam concrete may be used to contain industrial[26] or nuclear waste,[27] reducing contamination of the environment. As a bullet-absorbing medium, foam concrete reduces soil contamination on small arms firing ranges.[28]

Water filtration

Specially formulated foam concrete may provide a cost effective medium for removing heavy metals from industrial wastewater.[29]

Carbon sequestering

The capacity for foam concrete to sequester carbon dioxide has been considered. U.S. Patents under the Wisconsin Electric Power Company describe a technique for producing cementitious foam capable of sequestering carbon dioxide emitted at gas flues.[30] The original patent suggested that the foam concrete be produced using fly ash; a subsequent patent proposed that cement-kiln dust, lime kiln dust, or slag cement may be used. The high surface area and permeability of the material enhances the rate of carbonation.

Stormwater management

Foam concrete may be used as a permeable material for stormwater runoff management, minimizing erosion, improving groundwater recharge, and reducing hydraulic loads on existing sewer systems.[31]

Material reuse

Foam concrete may be crushed and reused in the production of new concrete[32] as powder, and perhaps also in aggregate form.[33]

---

26 Lee and Hung (2005) 17
27 Ashworth et al. (2013) 58-66
28 Fabian et al. (1996) 118
29 Doniec (2008) 264
30 U.S. Patents 7390444 B2, 9028607 B2
31 Van Deijk (1991) 51, U.S. Patent 8172937 B2
32 Jones and Zheng (2013) 209
33 Refer to Appendix E.

A-7

Comparison of Lightweight, Mineral-Bound Materials

In researching competitive uses for foam concrete, comparison to the performance to other similar materials is invaluable. This chapter reviews properties and published data for various lightweight mineral-bound materials, including foam concrete, aerated autoclaved (gas) concrete, lightweight aggregate concrete, and no-fines concrete. Two other comparable inorganic porous materials, foamed glass and thermally insulating brick, have also been included for reference where pertinent.

7.1 General Considerations

7.1.1 Strategies for Introducing Void

Concrete products designed to be lightweight must incorporate void. Mechanical, chemical, or physical mechanisms may be used to introduce these voids into the concrete mix.

Foam concrete is created by mechanically producing voids in the form of fine bubbles. These voids may either be folded into the paste with a strong shearing action during mixing, or generated outside of the paste and blended into it. Gas concrete, including most aerated autoclaved concrete, is produced by evolving a gas through a chemical reaction in the paste.

In addition to these methods, voids may be introduced physically to reduce the weight of a concrete mass through lightweight aggregates, particle packing, or forming:

i) Lightweight aggregates are porous materials that may be placed in a mix to displace denser mortar.

ii) In no-fines concrete, fine aggregate is eliminated from a recipe. The resulting particle packing introduces interstitial voids between the aggregates, reducing the density of the mix.

iii) For many applications, use of normal density concrete cast in an efficient form may provide the best solution. Large-scale voids may be formed where solid material is not structurally required. Voided slab systems, hollow masonry blocks, and many other engineered forms are based on this strategy of reducing non-working dead load.

Thus, foam and gas concretes introduce voids in a mortar; lightweight aggregate concrete introduces voids in the aggregate; no-fines concrete introduces interstitial voids between the aggregate; and voided products introduce voids through the form of the product itself. These strategies are depicted schematically below. Note that these strategies may also be combined: for example, in the form of a lightweight aggregate foam concrete voided block unit.

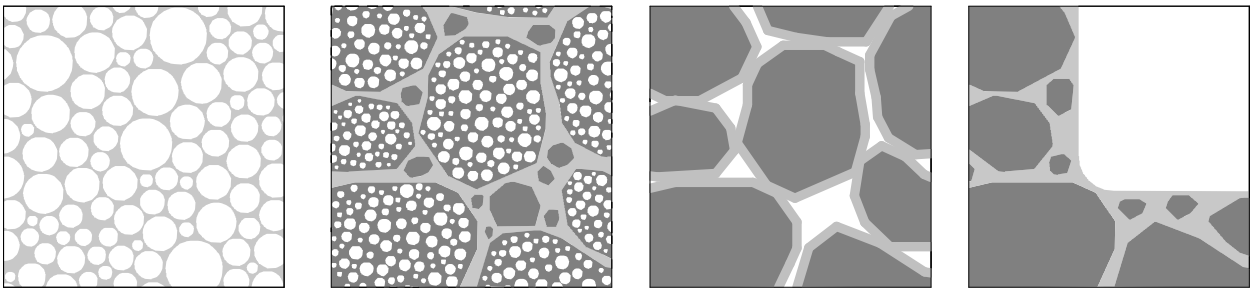

Figure A-7.1 Strategies for introducing void in concrete.

7.1.2 Production and Use

The production of foam concrete and gas concrete has been described in Chapter 3. Foam concrete is principally used as an in-situ geotechnical or insulating backfill material, although it may also be used for a variety of structural and semi-structural purposes.[1] Gas concrete is usually autoclaved and used for modular building components such as blocks or reinforced slabs.[2]

Lightweight aggregates (LWAs) may be created from a variety of natural or manufactured source materials. Several LWAs are described in Section 5.1.4. LWA concrete may be used in structural lightweight cast-in-place concrete, precast units including masonry blocks, and as geotechnical or insulating fill.

No-fines aggregate may be produced either from normal density aggregate, or from lightweight aggregates such as clinker or foamed slag.[3] Aggregates are graded to be very similar in size, often approximately 10 mm, to ensure an open and consistent geometry.[4] The large particles are held together with a thin layer of cement, up to approximately 1.2 mm thick. No-fines concrete is used in landscaping applications such as retaining walls and paved surfaces, to take advantage of the material's excellent permeability and lack of capillarity. It may cast as a durable exterior wall with some thermal resistance for building up to four storeys in height[5] or more.[6] No-fines exterior walls are protected from rain penetration with rendering.[7]

Foamed glass is produced by heating crushed glass and a chemical gassing agent: the molten glass forms a closed bubble structure, which remains stable as the glass is cooled.[8] Foamed glass is typically used for wall, roof, and below-ground thermal insulation, or for sound insulation.

Thermal brick may be prepared by incorporating sawdust or other industrial[9] or agricultural[10] wastes in the unfired clay. These pore forming agents may be either organic

1 Van Deijk (1991) 51
2 Short and Kinniburgh (1978) 292
3 Short and Kinniburgh (1978) 30
4 Short and Kinniburgh (1978) 91
5 Neville (1963) 454
6 Short and Kinniburgh (1978) 93
7 Short and Kinniburgh (1978) 91
8 Pittsburgh Corning (n.d.) 7
9 Eliche-Quesada (2012)

or mineral in nature. When the brick is fired, organic pore-forming agents are consumed, leaving small pores due to the breakdown of the organic solids and the evolution of carbon dioxide,[11] while pore-forming agents from mineral sources produce carbon dioxide due to the decomposition of calcium carbonate.[12] Thermal brick offers thermal and fire resistance as well as structure for exterior or partition walls.

7.1.3 Air-Void Systems

Foam concrete air voids produced by dry foam are between 0.1 and 1.5 mm in size, with coalescence sometimes producing larger voids.[13] Wet foam produces bubbles of 2 to 5 mm in size.[14] Total air void volume in foam concrete may vary from 10% to more than 90%. Air voids may be reasonably spherical and uniform in size,[15] and interconnectivity is typically low,[16] in well-proportioned mixes.

AAC air voids range from 0.1 to 1.5 mm in diameter, with the largest voids being approximately 3.0 mm.[17] Total void volume is typically around 80%,[18] and seldom less than 50%.[19] Voids may be somewhat elongated due to pressures on the bubble during gas evolution, causing inhomogeneity within specimens.[20] Interconnectivity of pores is higher in gas concrete than in foam concrete for a given density, as demonstrated by Laukaitis and Fiks.[21]

Pores in lightweight aggregates may be approximately 5 to 300 μm in diameter. Zones of porous aggregate are separated by dense mortar, reducing interconnectivity. Interior pores within the aggregate may also be non-interconnected.[22]

No-fines concrete has a highly open porosity, with irregular voids of approximately 2 to 7mm in size. [23]

---

10 Sutcu et al. (2016) 185-186
11 Bories et al. (2014) 191
12 Bories et al. (2014) 187
13 Brady et al. (2001) 2
14 Ramamurthy et al. (2009) 389
15 Nambiar and Ramamurthy (2007a) 229
16 Nambiar and Ramamurthy (2007b) 1347
17 Petrov and Schlegel (1994) 835
18 RILEM Technical Committees 78-MCA and 51-ALC (1993) 9
19 RILEM Technical Committees 78-MCA and 51-ALC (1993) 4
20 Valore (1954b) 819; Cabrillac et al. (2006). Cited in Ramamurthy et al. (2009) 391
21 Laukaitis and Fiks (2006) 291
22 Expanded Shale Clay and Slate Institute (2007) Section 3.4

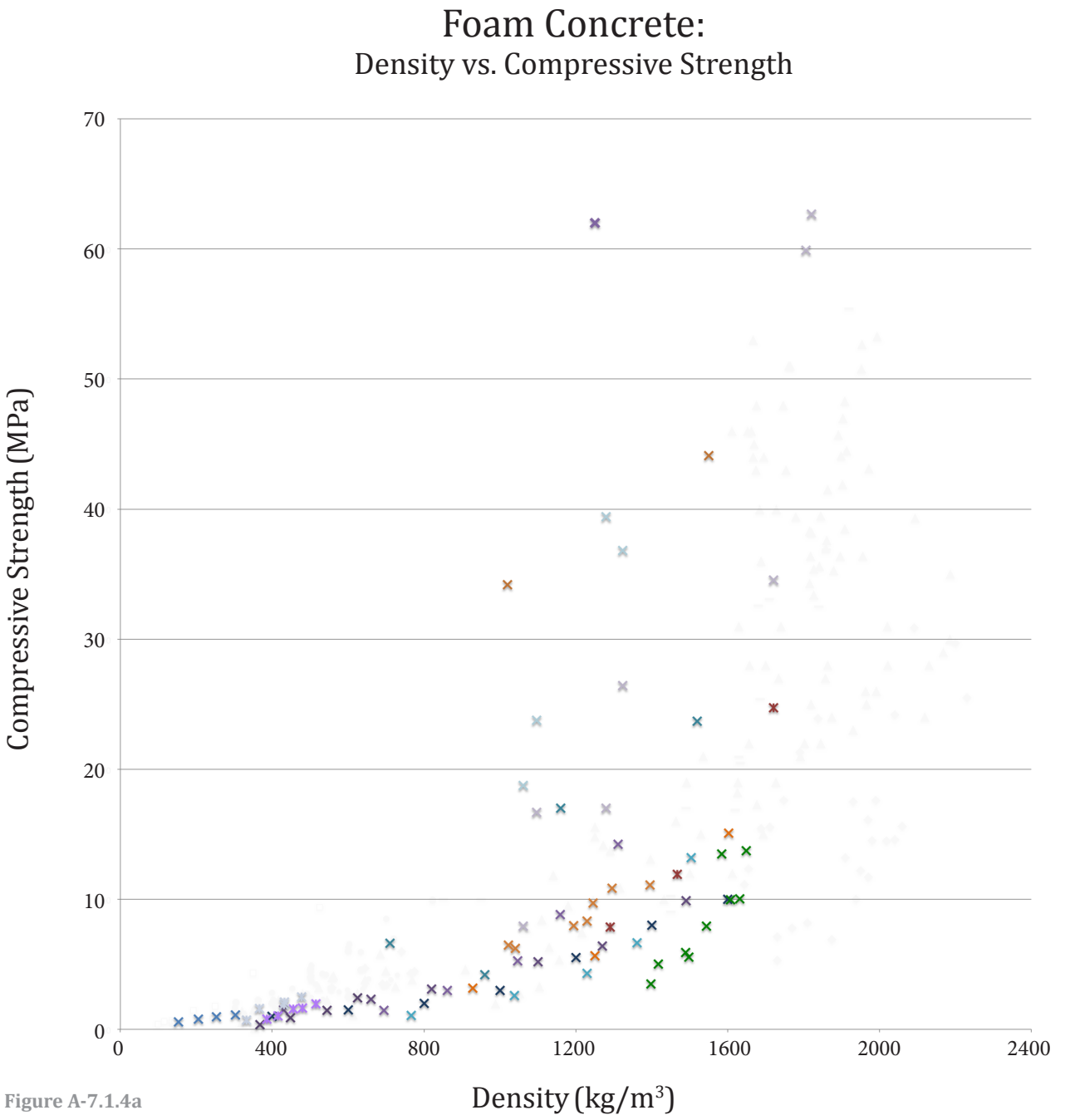

Figure A-7.1.4a

The volume fraction of air void in foam glass is typically greater than 85%. Normally, a significant fraction of pores are smaller than 0.5 mm, although pore sizes of 1 to 3 mm are possible depending on the manufacturing process.[24] Foam glass thermal insulation may be produced with a high degree of closed porosity,[25] while foam glass soundproofing may be designed to have a more open porosity.[26]

The porosity of thermal brick may be in the order to 25 to 50%.[27] Porosities of up to 65% are possible, but such materials may be too fragile for commercial use as masonry materials.[28] Pore size is dependent on the size of the pore-forming agent, which varies widely.[29] Interconnectivity of voids is often relatively high, with open porosities in the order of 70%.[30]

7.1.4 Compressive Strength and Density

Comparative plots of compressive strength and density for various lightweight, mineral-bonded materials are provided as Figures 7.1.4a to 7.1.4f on the following pages.

Foam concrete may be produced over a remarkably large range of densities. Most mixes are between 300 and 1600 kg/m^3.[31] Very lightweight mixes may be as low as 150 kg/m^3,[32] while dense mixes may be 1800 kg/m^3 [33] or more.[34]

Low-density foam concrete may have a compressive strength of less than 1.0 MPa.[35] In the medium density range, a wide range in compression strength is possible. Proportions of cement, mineral admixtures, fine aggregate, and foam volume may be varied to produce strengths from less than 3 MPa, to in excess of 30 MPa, for densities between 1000 and 1400 kg/m^3.[36] At higher densities of 1600 kg/m^3, typical mixes may offer

---

23 Sommerville et al. (2010) 24
24 König et al. (2016) 190
25 Pittsburgh Corning (2009) 4
26 König et al. (2016) 190
27 Sutcu et al. (2016) 188, Koronthalyova (2011) 880
28 Bories et al. (2014) 192
29 Bories et al. (2014) 187
30 Kazmi et al. (2016) 39, Bories et al. (2014) 192, Koronthalyova (2011) 881
31 Barnes (2009) 3
32 Pan et al. (2014) 256
33 Jones and McCarty (2005b) 25
34 Gunawan and Busra (2014), Cong and Bing (2015)
35 Barnes (2009) 7
36 Pan et al. (2007) 297

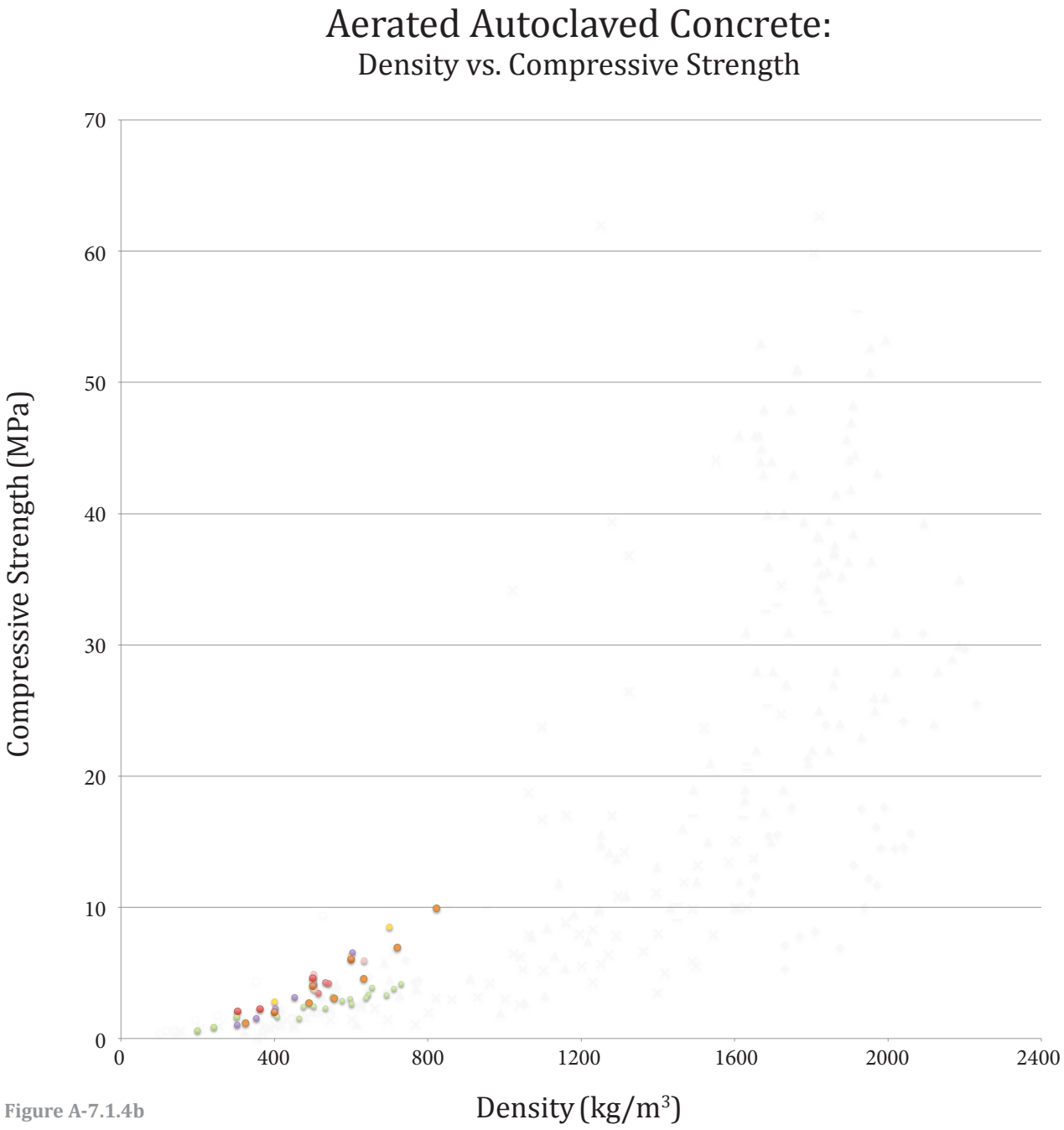

Figure A-7.1.4b

compression strength of 7.5 to 10 MPa,[37] although high strengths of 44 MPa,[38] 50 MPa[39] or 62 MPa[40] have been reported for mixes of less than 1620 kg/m^3 density. Such high strength mixes may require the inclusion of costly chemical and mineral admixtures.

Autoclaving is an effective process for strength gain of low-density cellular concrete. At higher densities, AAC blocks require increasingly more energy to cure, cut and transport relative to strength gained, and thermal insulation values diminish, so most AAC mixes are relatively light, between 480 and 960 kg/m^3. Densities as low as 240 kg/m^3 are possible.[41] Autoclaving produces excellent compressive strength to density performance, as lime and silica/ alumin ingredients are fused into a crystalline mass under the heat and pressure of steam.[42] Typical mixes with dry densities of 500 to 880 kg/m^3 may have compressive strengths of 2.8 to 6.0 MPa respectively;[43] stronger mixes, with densities of 820 kg/m^3, approach 10 MPa in compressive strength.[44]

Lightweight aggregate concretes may be produced at a considerable range of densities greater than 240 kg/m^3. Perlite, vermiculite, and expanded polystyrene aggregates are typically used in very low-density mixes for insulating applications. They may also be sometimes incorporated in moderate strength concrete. Natural aggregates such as pumice, scoria, or tuff are typical aggregates for moderate strength mixes, and expanded clay, slag, fly-ash, shale and slate may be used in moderate strength or structural low density concretes.[45]

Compressive strength increases with density. From Figure 7.**1.4c**, we may identify a concentration of low-strength, low-density mixes intended for insulating applications, a gradient from moderate strength mixes to structural lightweight concrete, and a concentration of structural lightweight concrete mixes designed for exceptional strength.

---

37 Barnes (2009) 7
38 Pan et al. (2007) 297
39 Fujiwara et al. (1995) Cited in Wee et al. (2011) 584
40 Kearsley (1999). Cited in Wee et al. (2011) 584
41 Tonyan and Gibson (1992b) 6371
42 Narayanan and Ramamurthy (2000b) 322
43 Short and Kinniburgh (1978) 302
44 Chen, Peng, Zhang and Liu (2013) 447
45 Barton et al. (1979) 4

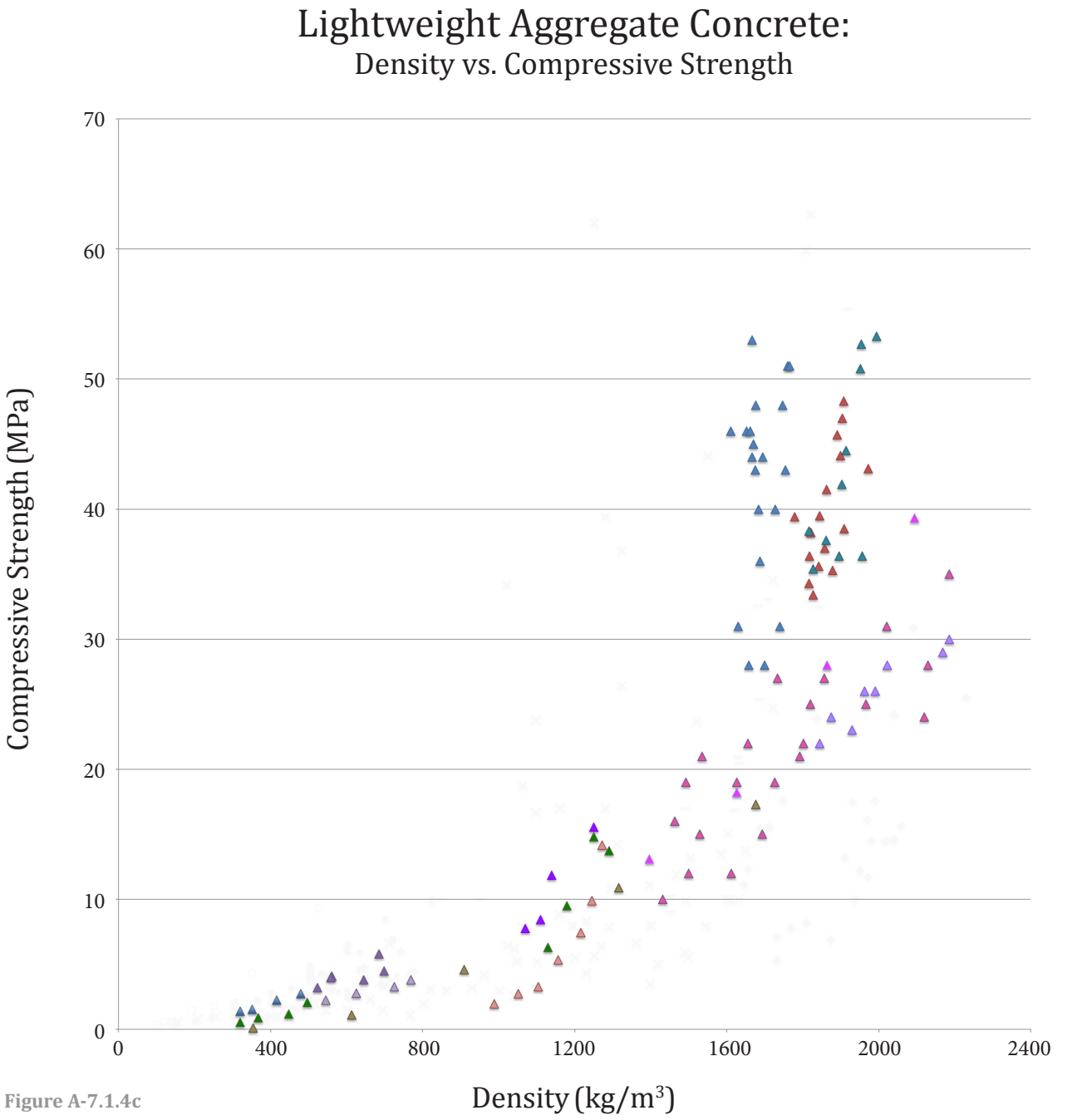

Figure A-7.1.4c

No-fines concrete with normal density aggregate is confined to a relatively narrow range of densities. Most mixes have a density between 1500 kg/m^3 to 1900 kg/m^3, due to the geometrical limitations of packing regularly sized aggregate and the desire for insulation performance.[46] Compressive strength may range from 5 to 13 MPa, respectively.[47] Relatively dense mixes of 2200 kg/m^3 have also been produced, which approach 30 MPa.[48] In multi-story structures, cement content may be varied at different storey heights to provide the strength required.[49]

Lightweight aggregate may be used in no-fines concrete recipes, to reduce density as low as 640 kg/m^3.[50] Additional cement is normally required, providing strength in the order of 2.8 to 3.5 MPa.[51]

Commercially produced thermal brick is commonly produced at densities of between 800 and 1000 kg/m^3, although denser products are possible. Most commercially produced foam glass compares to the lightest of foam concrete mixes, although impressive performance is possible from denser mixes, with strengths approaching 10 MPa.

In examining this performance data for various lightweight materials, it is possible to detect certain niches in which foam concrete may perform exceptionally well.

For example, foam concrete is relatively well suited to the production of extremely low-density mixes. A fine-grain mixture of water, foam, and cementitious particles allows for the production of highly porous concrete with a homogenous structure. Foam concrete may be better suited to extremely light-weight applications than either LWAC, which uses large aggregate particles, or autoclaved aerated concrete, which relies on the presence of sand particles for the production of calcium silicate hydrate crystal. Low-density foam glass offers similar performance to foam concrete, but has significant limitations of manufacture, discussed below. Ultra low-density foam concrete mixes have potential in

46 Short and Kinniburgh (1978) 100
47 Short and Kinniburgh (1978) 94
48 Tittarelli et al. (2014) 33
49 Short and Kinniburgh (1978) 29
50 Neville (1963) 455
51 Short and Kinniburgh (1978) 100

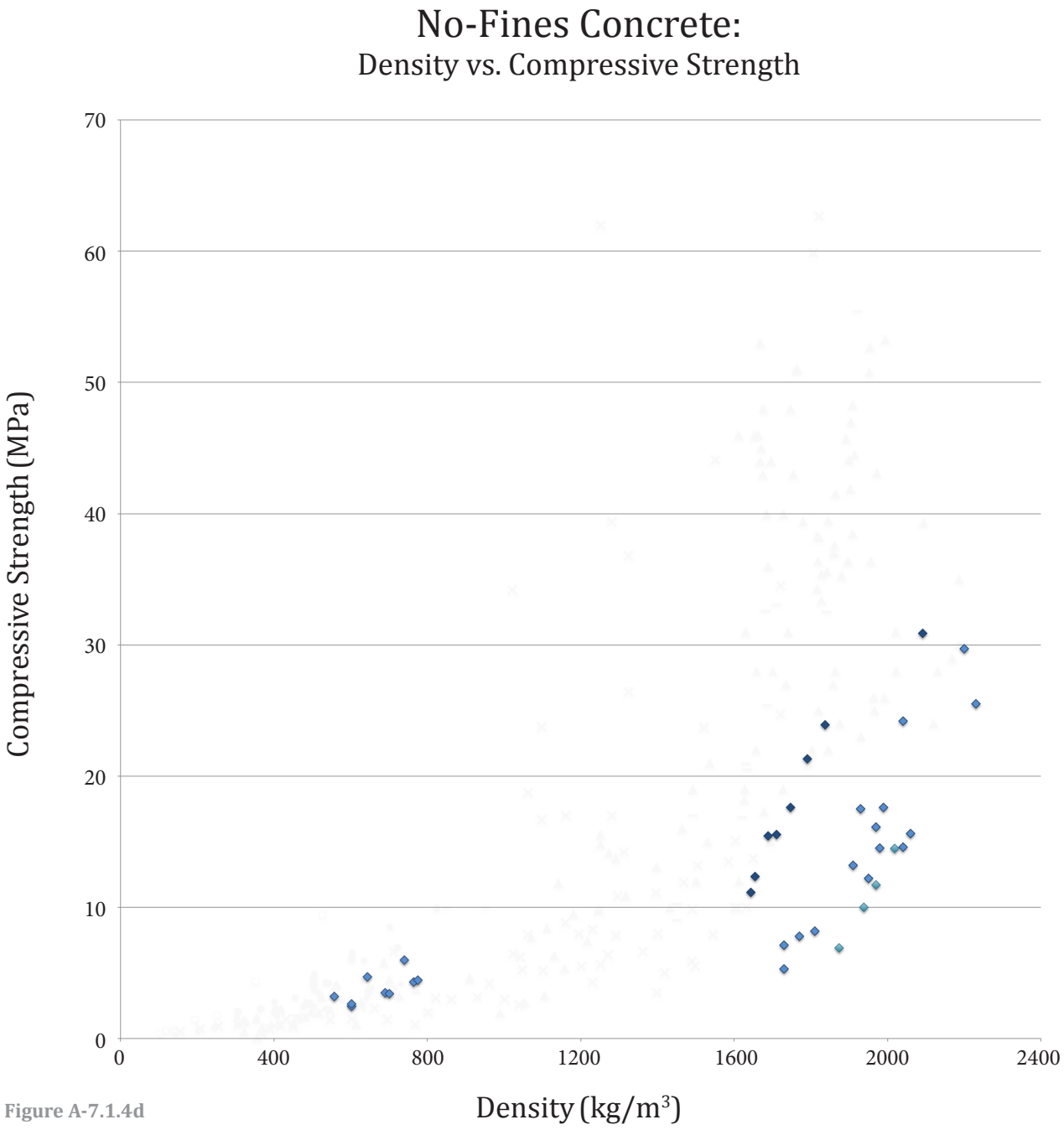

Figure A-7.1.4d

thermally insulating purposes.[52]

For mixes from 300 to 800 kg/m^3, autoclaved aerated concrete and insulating brick perform especially well. However, these materials cannot be cast *in situ*. Cement-bonded wood fibre products, such as Durisol block, may be considered a form of lightweight aggregate no-fines concrete, and also appear to perform well within this density range.

For mixes between 1000 kg/m^3 and 1400 kg/m^3, foam concrete mixes vary greatly in compressive strength. By contrast, LWAC is more constrained in mix design, both by efficient ratios of aggregate-to-mortar volume, and by available densities of aggregate. Substituting lightweight fine aggregate for normal density aggregates, [53] blending lightweight and normal density aggregates,[54] altering the aggregate size,[55] or increasing air entrainment in the mortar,[56] gives LWAC mix designers somewhat more latitude in varying compression strength and density characteristics; nevertheless, as a heterogeneous composite, LWAC is subject to certain limitations.[57] Consequently, foam concrete may be especially valuable outside of the normal strength-density parameters of LWAC design. Medium density, low-strength mixes with low cement content and low cost may be useful for some fill applications. Conversely, certain special niches may require the medium-density, high-strength properties that foam concrete with a high cementitious content can provide.

For higher density, high strength mixes, LWACs is likely to prove more cost effective than foam concrete in most situations. Many LWAC mixes between 1600 and 1900 kg/m^3 density are capable of achieving strength higher than 40 MPa,[58] while reports of foam concrete with strength greater than 40 MPa are relatively uncommon, and at present have only been achieved in laboratory conditions.

Foam concrete mixes are typically stronger than no-fines concrete of the same

---

52 Pan et al. (2014) 256
53 ACI 213-03 Section 2.3.6
54 ACI 213-03 Section 3.2.1.2
55 ACI 213-03 Section 2.3.4.1
56 ACI 213-03 Section 3.2.1.5
57 ACI 213-03 Section 3.4
58 Lotfy et al. (2015) 189

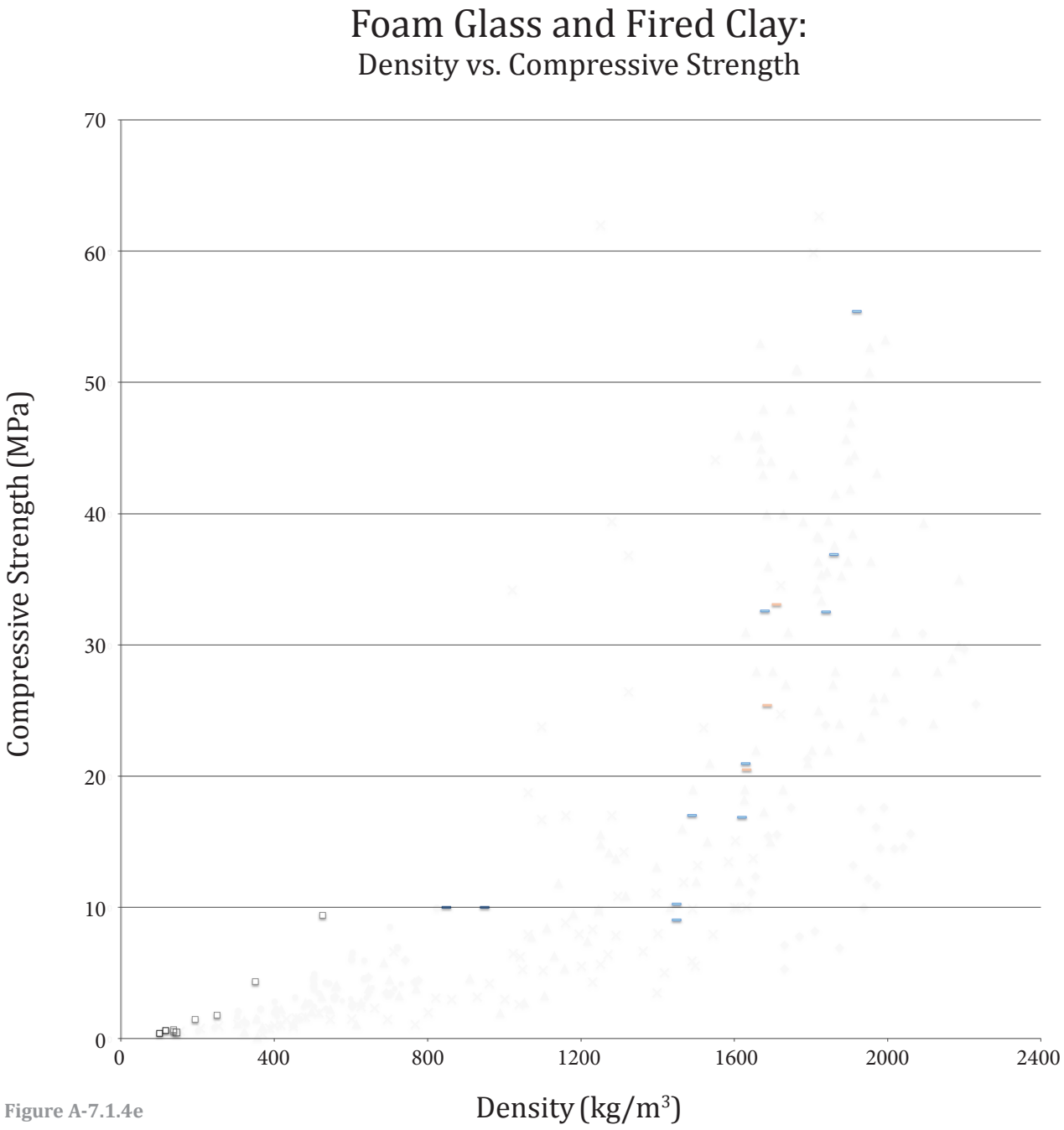

Figure A-7.1.4e

Extended Legend

- Foam Concrete (conventional): BCA (1994) [Theoretical]
- Foam Concrete (cement-fly ash, 56-day): Kearsley (1999) [Lab]
- Foam Concrete (cement-sand): Ramamurthy and Narayanan (2000) [Lab]
- Foam Concrete (cement-fly ash): Ramamurthy and Narayanan (2000) [Lab]
- Foam Concrete (cement-sand): Kostmatka et al. (2002) [Theoretical]
- Foam Concrete (neat cement): Kostmatka et al. (2002) [Theoretical]
- Foam Concrete (cement-fly ash): Kearsley and Mostert (2005) [Lab]
- Foam Concrete (cement-fly ash, hot water curing, 56-day): Kearsley and Mostert (2005) [Lab
- Foam Concrete (cement-mineral admixtures) Zhihua et al. (2007) [Lab]
- Foam Concrete (cement-sand-mineral admixtures) Zhihua et al. (2007) [Lab]
- Foam Concrete (cement-sand): Zhihua et al. (2007) [Lab]
- Foam Concrete (cement-sand-fly ash): Nambiar and Ramamurthy (2009) [Lab]
- Foam Concrete (cement-sand): Nambiar and Ramamurthy (2009) [Lab]
- Foam Concrete (geopolymer slag): Yang et al. (2014) [Lab]
- Foam Concrete (LWA, geopolymer): Liu et al. (2014) [Lab]
- Foam Concrete (cement-mineral admixtures, etc.): Zhihua et al. (2014) [Lab]
- AAC: Neville (1963) [Lab]
- AAC: Funke and Eliasson (1978) [Lab]
- AAC: CEB Manual (1977) [Theoretical]
- AAC: Hebel (1982) [Manufacturer]
- AAC: Ozawa (1983) [Lab]
- AAC: Tada (1986) [Lab]
- AAC: ASTM C1693 [Theoretical]
- AAC: Chen et al. (2013) [Manufacturer]
- AAC: Jerman et al. (2013) [Lab]
- LWA (expanded polystyrene): Kosmatka et al. (2002) [Theoretical]
- LWA (polystyrene): Schackow et al. (2014) [Lab]
- LWA (vermiculite): Kosmatka et al. (2002) [Theoretical]
- LWA (perlite): Sengul et al. (2011) [Lab]
- LWA (perlite): Kosmatka et al. (2002) [Theoretical]
- LWA (pumice): Hossain et al. (2011) [Lab]
- LWA (Pumice): Gündüz (2008) [Lab]
- LWA (volcanic scoria): Hossain (2004) [Lab]
- LWA (expanded glass): Bumanis et al. (2013) [Lab]
- LWA (expanded clay): Floyd et al. (2015) [Lab}
- LWA (expanded shale): Floyd et al. (2015) [Lab]
- LWA (expanded shale): Lotfy et al. (2015) [Lab]
- LWA (expanded polystyrene): Tang and Nadeem (2008) [Lab]
- No-fines concrete (normal aggregate): Neville (1963) [Theoretical]
- No-fines concrete (nomal aggregate): Ghafoori and Dutta (1995) [Lab]
- No-fines concrete (lightweight aggregate): Zaetang et al. (2013) [Lab]
- No-fines concrete (normal aggregate): Tittarelli et al. (2013) [Lab]
- No-fines concrete (cement-bonded wood aggregate): Durisol (n.d.) [Manufacturer]
- Fired clay brick (sawdust): Wienerberger (2014) [Manufacturer]
- Fired Clay Brick (olive mill waste): Sutcu et al. (2016) [Lab]
- Fired clay brick (various): Zhang et al. (2016) [Lab]
- Foam glass: Giavan and Adams (1979) [Manufacturer]
- Foam glass: König et al. (2016) [Lab]
- Foam glass: Foamglas (2013) [Manufacturer]

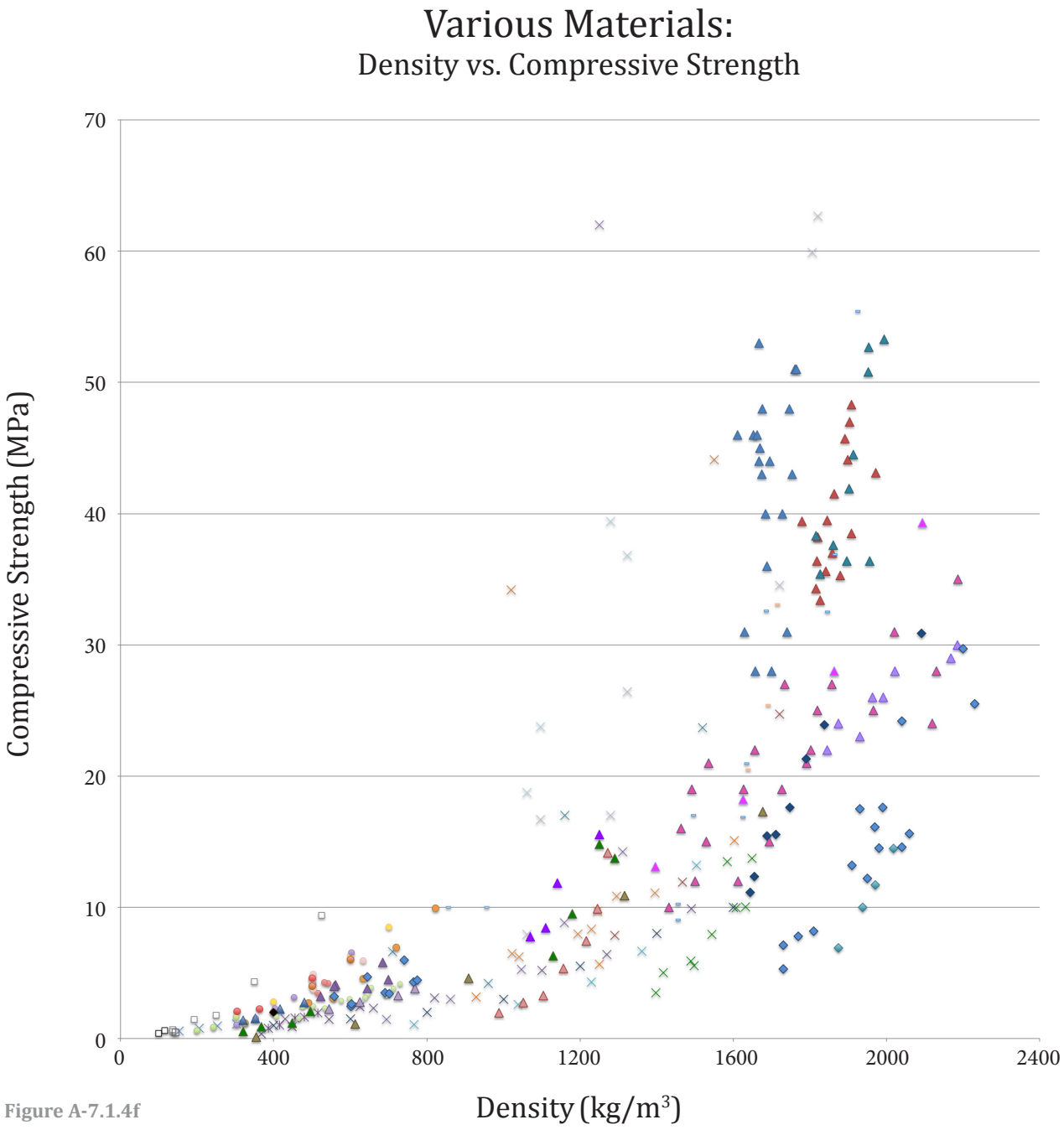

Figure A-7.1.4f

Legend

- Foam Concrete
- Areated Autoclaved Concrete
- Lightweight Aggregate Concrete
- No-Fines Concrete
- Foam Glass
- Fired Clay

For more detail, refer to extended legend on facing page.

density; however foam concrete will also normally have a higher cost due to its greater cementitious density.

7.1.5 Cementitious Density

Since cementitious content is strongly related to strength, and to cost, a plot of density vs. cementitious density is included as Figure 7.**1.5**. Reported total cementitious densities include supplementary cementitious materials such as fly ash, ground granulated blast furnace slag, and silica fume.

It is evident that high strength foam concrete mixes develop strength from exceptionally high cementitious densities. In Figure 7.**1.5**, some dense mixes of 1800 kg/m^3 have total cementitious densities of approximately 1400 kg/m^3, helping to explain the compressive strengths observed in Figure 7.**1.4a**.

Most lightweight aggregate concrete mixes use between 300 and 500 kg/m^3. No-fines mixes typically incorporate between 200 and 400 kg/m^3 of binder.

7.2 Issues of Production

Issues of production are compared below, including workability, sensitivity to water content and timing of hydration for cement-bonded products; as well as rate of curing, drying shrinkage or dimensional tolerances, and limitations of shape and scale.

7.2.1 Workability

For materials that may be placed *in situ*, workability is an important consideration.

Foam concrete is extremely fluid, with consistency similar to yogurt. Its workability is measured in flow rate or spread rate, rather than slump, and it is well suited to filling inaccessible spaces and constricted voids.[59]

LWAC mixes usually have a low slump, with maximums as low as 75 or 125 mm for some applications. .[60] The buoyant force of coarse LWAs must be resisted by the stiffness of the mix to avoid segregation and bleeding. Air entraining agents are used not only to improve durability, but also to improve workability in LWACs, as the mixes tend to be harsh due to the roughness of the aggregate.[61] Lightweight fines may also be replaced by normalweight fines to improve workability; however, density and thermal conductivity will increase.[62]

No-fines concrete exhibits almost no slump. The aggregate packs tightly with minimal cementitious mortar. Subsequently, no-fines concrete exerts very little hydrostatic pressure when it is placed, allowing for the use of lightweight forms.

7.2.2 Sensitivity to Water Content

Foam concrete is reasonably tolerant to variations in water-cement content. Water content should be adjusted to provide good consistency: if the mix is too stiff, bubbles may rupture, and if the mix is too fluid, bubbles may migrate, leading to segregation. Superplasticizer and water reducing admixtures are often unsuitable for foam concrete.

---

59 Van Deijk (1991) 49

60 Because LWAC mixes have less self-weight than NWAC, the reported slump of LWAC is usually less than NWAC for the same effective workability (i.e., yield stress). Furthermore, lighter LWAC mixes will report a lower slump than denser LWAC mixes. Cf. Seng (2006) 102

61 Neville (1963) 444

62 Neville (1963) 444

Extended Legend

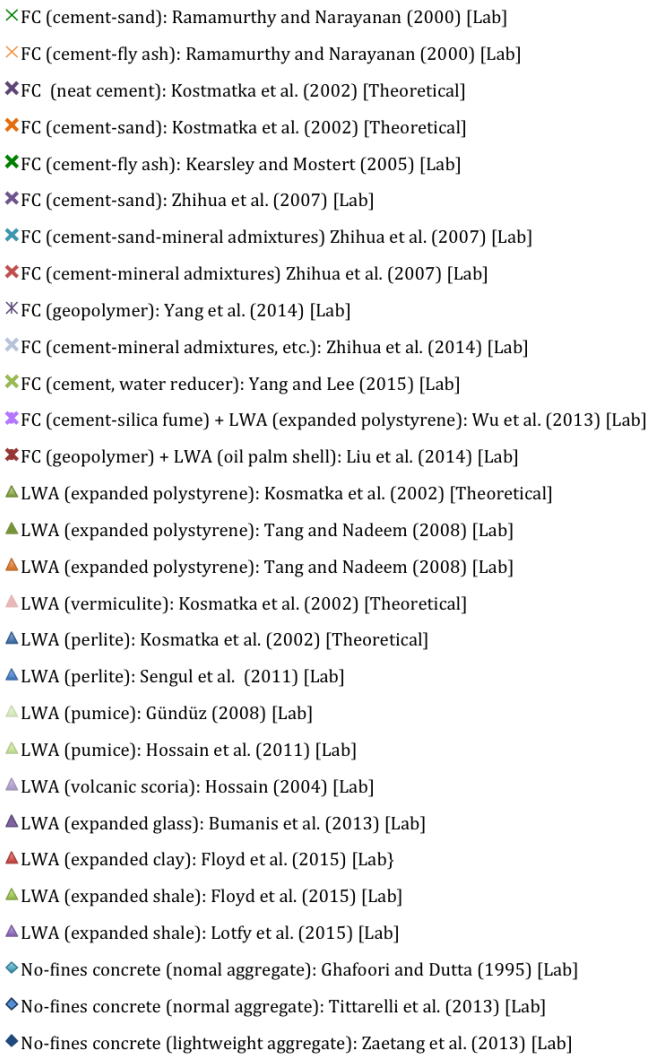

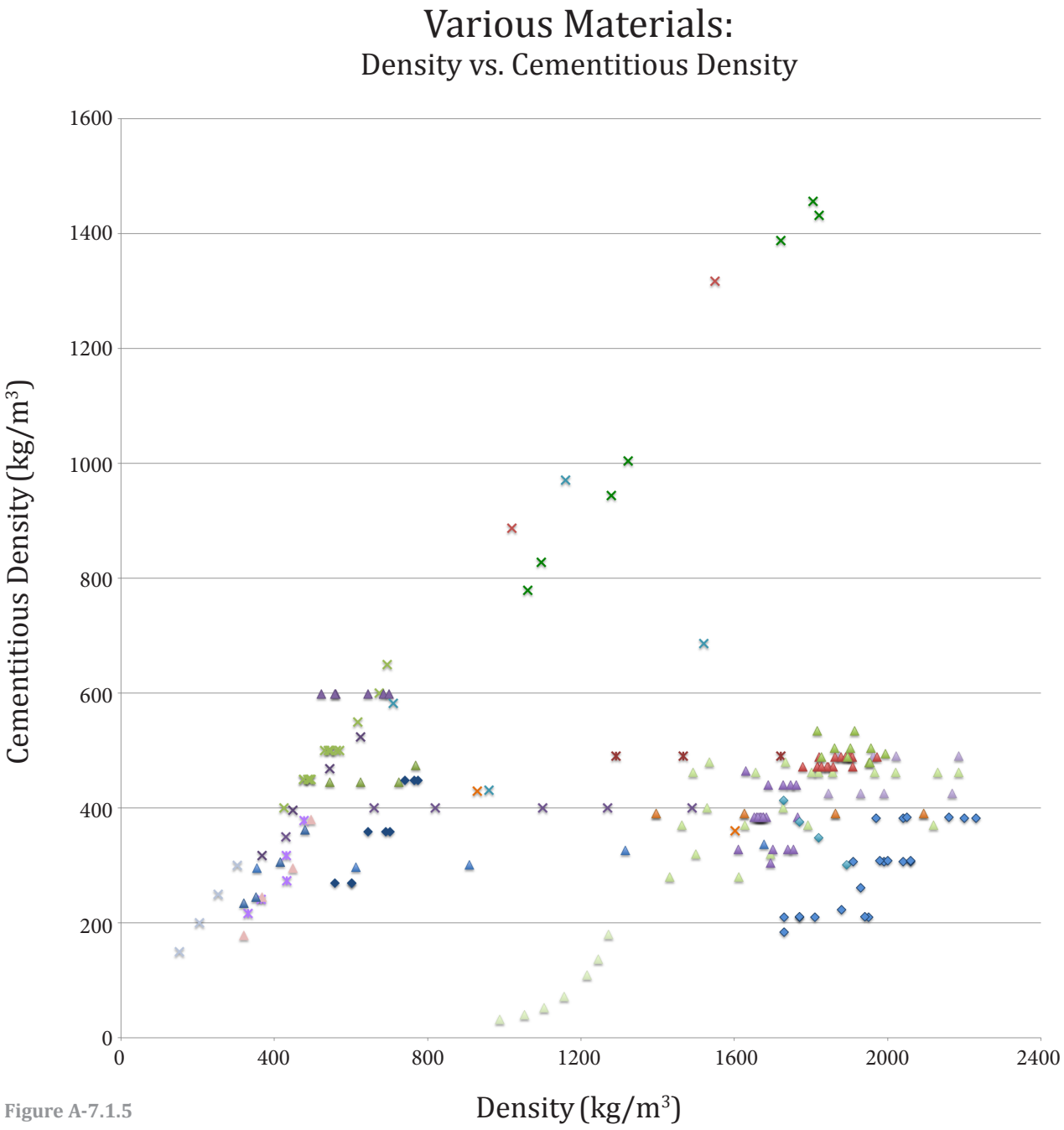

Figure A-7.1.5

Legend

- Foam Concrete
- Lightweight Aggregate Concrete
- No-Fines Concrete

For more detail, refer to extended legend on facing page.

Lightweight aggregates should be prewetted, or else they may absorb mixing water and interfere with workability or cement hydration.[63] Interestingly, the capacity of lightweight aggregate to absorb water permits hygrol equilibrium between aggregates and mortar paste. This equilibrium assists in the production of a continuous, high quality matrix in lightweight aggregate concrete, whereas in normal density concrete, water accumulates around the non-absorbent coarse aggregate, resulting in a 'transition zone' of weak, pervious mortar.[64] Furthermore, lightweight aggregates can store water and release it slowing into a mix from within during curing, improving concrete quality.[65] As with normal density concrete, the strength of the mortar may be further enhanced with the use of superplasticizers and water reducing admixtures.[66]

No-fines concrete is highly sensitive to w/c ratio. Insufficient water will result in lack of hydration and cohesion between the cement particles, while too much water will wash the cement film off of the larger aggregate, weakening the cast.[67] Water reducing agents may be used.[68]

7.2.3 Sensitivity to Timing

Foam concrete stiffens and sets slowly, relative to normal density concrete, due to retarding properties of the surfactant.[69] The slow set up and fluidity of the mix have significant implications for demoulding times. Modern surfactants are designed to produce foam that remains stable and resilient, even during long periods of mixing and travel.

Similar considerations of timing for mixing and placing apply to lightweight aggregate concrete as to normal density concrete. Placing and finishing is often easier and faster for the former. Overworking must be avoided, to prevent segregation of the buoyant aggregate.[70] Lightweight aggregate concrete may be produced as a stiff, dry mix, allowing for rapid manufacture and demoulding of lightweight concrete blocks and other precast forms.

---

63 ACI 213-03 Section 3.7.1
64 ACI 213-03 Section 4.14.3
65 ACI 213-03 Section 3.6.2
66 ACI 213-03 Section 2.3.6
67 Short and Kinniburgh (1978) 30
68 Shu et al. (2011) 3188
69 Brady et al. (2001) C8
70 ACI 213-03 Section 10

No-fines concrete must be placed relatively soon after hydration has occurred, within as few as 20 minutes.[71] Water cannot be added to the mix to increase its working time, as the cement mortar may be washed off of the aggregate. No-fines concrete cures rapidly. It shrinks to its final volume within a relatively short period of time, which allows it to be rendered promptly, but which may have implications for its compatibility with other types of concrete in construction.

AAC, foam glass, and thermal brick are manufactured relatively quickly through autoclaving, annealing, or firing processes, respectively.

7.2.4 Format: Shape of Cast

The plastic nature of concrete, and its ability to fill an irregular void, is an important attribute for many engineering applications. Foam concrete can conform readily to the volume of a container, whether prismatic or irregular. Foam concrete is especially suited to filling constricted voids due to its flowability.

Lightweight aggregate concrete mixes will also conform readily to most forms, although the coarseness of the aggregate and the stiffness of the mix may preclude use in some highly constricted spaces.

No-fines concrete is not suitable for void-filling applications, due to its extremely low slump. It may be cast *in situ* as a surface for landscaping applications, however; or it may be used for loadbearing walls with a relatively thick slenderness ratio.[72] It is not typically used in horizontal slabs or beams due to its penetrability and issues of reinforcing.[73]

Conversely, AAC, foamed glass, and thermal brick cannot be cast irregular *in situ* forms, but are typically prepared as prefabricated blocks or panels. AAC products are typically prismatic; foam glass is also produced in shapes to cover standard pipes, valves, fittings, and curved segments;[74] and thermal brick may be produced in hollow extruded forms for blocks or brick ceilings.[75]

---

71 The Aberdeen Group (1961) 2
72 Short and Kinniburgh (1978) 104
73 Tittarelli et al. (2013) 119, Short and Kinniburgh (1978) 103
74 Pittsburgh Corning (2009) 20
75 Wienerberger (2016)

7.2.5 Format: Scale of Pour

Concrete cast *in-situ* may be placed at considerable scales.

Valore suggested that foam concrete could be placed in cavity walls up to 6 or 9m in height in a single pour without collapse of the preformed foam.[76] However, for mass pours, Brady et al. recommended that the maximum pour depth of foam concrete should not be greater than 1.5 m within a 16 hour period, to avoid settlement or collapse of the bubble structure.[77] Foam concrete may be built up in large pours. For example, 150 m^3 of foam concrete was laid per day as backfill for a project at the Caranary Wharf in London in layers of 0.5 to 1.0 m thick, building a road foundation with a total volume of 27,000 m^3 and a maximum height of 10 m.[78]

Among cast *in situ* concretes, foam concrete is especially well suited to filling small spaces, due to the fineness of its ingredients and its high workability. Furthermore, the heat of hydration causes the air bubbles to expand slightly, ensuring good contact and void filling of tight spaces.[79]

Lightweight aggregate concrete may be used in massive pours,[80] subject to many of the same considerations as normal density concrete, such as thermal gradient cracking due to heat of hydration, or drying shrinkage.[81] Use in constricted spaces is limited, as described above.

No-fines concrete walls may be cast at heights of over 7 m and in lengths of up to 18m, as the low slump concrete exerts minimal hydrostatic force on its tall formwork.[82] Use in constricted spaces is not recommended due to low workability.

Autoclaved aerated concrete panels and blocks are products are limited to the scales allowed by factory autoclaving, was well as the limitations of transport.[83] The sizes of foam glass[84] and clay brick blocks, panels, and other products are designed for easy handling and modular construction with minimal wastage.

---

76 Werkema et al. (1961) 36
77 Brady et al. (2001) 7
78 Van Deijk (1991)
79 Barnes (2009) 7
80 ACI 213-03 Section 1.2
81 ACI 213-03 Section 4.9
82 The Aberdeen Group (1961) 1
83 Jones and McCarthy (2005b) 21
84 Pittsburgh Corning (2009) 17

7.2.6 Drying Shrinkage and Dimensional Tolerances

Drying shrinkage of neat cement foam concrete is exceptionally high. Shrinkage is moderately better in mixes that include fine aggregate restraint. Values of 0.33 to 0.44% for neat mixes,[85] or 0.07 to 0.12% for sanded mixes,[86] are typical. The expansion of air bubbles due to heat of hydration helps ensure good contact in void filling applications.[87]

Lightweight concretes may exhibit greater initial shrinkage than normal density concrete, by approximately 5 to 40 percent.[88]

Drying shrinkage of no-fines concrete is extremely low, as the aggregates bear directly upon each other with little to no mortar separating them. The total shrinkage of no-fines concrete may be half as great as that of normal density concrete, with 50 to 80 percent of the total shrinkage occurring in the first ten days.[89]

Autoclaving significantly reduces drying shrinkage in cellular concrete[90] by reducing the number of very fine pores subject to capillary tension,[91] and improving the mineralogical composition of calcium silica hydrates within the mix.[92] Thermal brick undergoes high shrinkage during firing, exceeding that of any of the other materials described here.[93] AAC,[94] foam glass, and thermal brick[95] are typically factory fabricated to precise geometric tolerances. Published data on the drying shrinkage of various materials is given in Figure 7.**2.6**.

7.2.7 Ease of On-Site Modification

Foam concrete, AAC, foam glass,[96] and porous brick[97] can usually be modified easily on-site with ordinary hand or power tools. Lightweight aggregate concrete may be more resistant to cutting or drilling due to the denser paste phase.

---

85 Neville (1963) 448
86 Nambiar and Ramamurthy (2009) 632
87 Barnes (2009) 7
88 Neville (1963) 445
89 The Aberdeen Group (1961) 1
90 Neville (1963) 454
91 RILEM Technical Committees 78-MCA and 51-ALC (1993) 28
92 Alawad et al. (2015) 382, Winter (2016)
93 Cf. Zhang et al. (2016) 157
94 Neufeld et al. (1994) 36
95 Wienerberger (2014) 27
96 Pittsburgh Corning (2009) 20
97 Wienerberger (n.d.) 15

7.3 Issues of Durability

7.3.1 Capillary Water Uptake

Capillary water uptake in foam concrete occurs mainly via the capillary pores of the matrix, and not via closed air voids. Subsequently, mixes with a greater volume of air voids will offer less cross sectional area for the conveyance of water, and mixes with finer bubbles will produce a more tortuous path for the water to travel along. In general, sorptivity will be greater than in normal density concrete, since the higher water cement ratios required will result in a greater volume of capillary voids in the paste.[98] Cracking due to drying shrinkage or thermal gradients may significantly increase water uptake.

Water uptake through a sample of lightweight aggregate concrete may be low, as the porous aggregates can be isolated within a dense, impervious paste. Moreover, the strong adhesion between the porous lightweight aggregate and a matrix reduces microcracking, eliminating or suppressing this path for water penetration.[99] Aggregate may be coated with a hydrophobing agent to reduce the ingress of water.[100]

No-fines concrete also has low capillary water uptake, despite its interconnected void structure. The interstitial voids between the coarse aggregates are sufficiently large that they will not draw water by capillarity.[101]

In contrast, the air voids of AAC are fine enough to fill by suction, and AAC typically has a higher sorptivity than foam concrete, lightweight aggregate, or no-fines concrete.[102] Typically, capillary water uptake may be between 4 and 8 $kg/m^2h^{½}$,[103] which is equivalent to 0.067 and 0.133 $kg/m^2s^{½}$.

Capillary action is negligible in closed cell foam glass, as water can travel neither via the closed cells, nor via the solid glass matrix.[104] Conversely, water travels readily via porous brick.[105]

---

98 Nambiar and Ramamurthy (2007b)
99 ACI 213-03 Sections 4.14.2, 4.14.3, 4.15
100 Neville (1963) 444
101 Neville (1963) 454
102 Yang and Lee (2015), Ramamurthy et al. (2009) 391, Laukaitis and Fiks (2006) 291
103 RILEM Technical Committees 78-MCA and 51-ALC (1993) 26
104 Pittsburgh Corning (2009) 4
105 Bories et al. (2014) 192

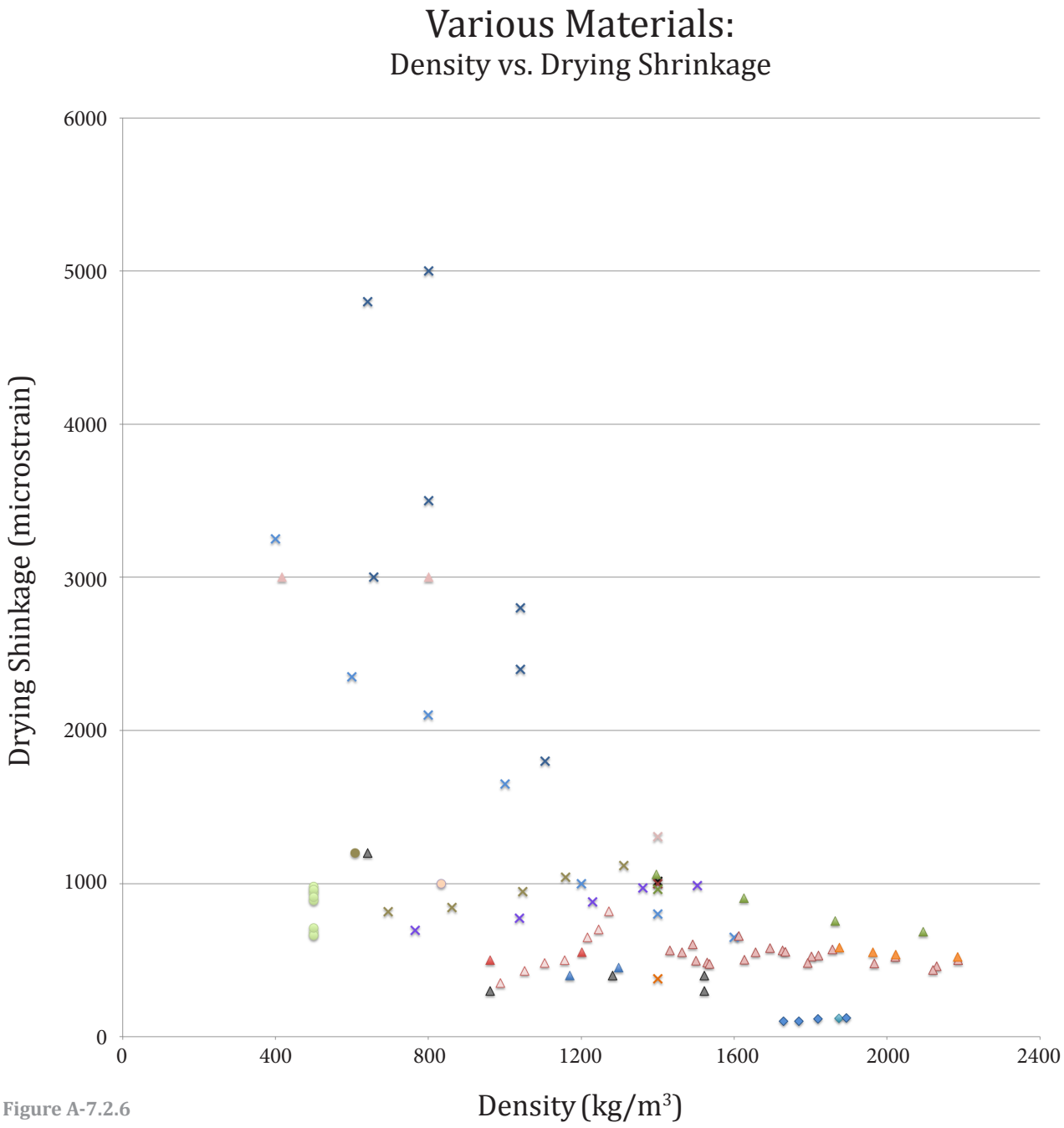
Various Materials:
Density vs. Drying Shrinkage
Drying Shinkage (microstrain)
6000
5000
4000
3000
2000
1000
0
0
400
800
1200
1600
2000
2400
Density (kg/m3)

Figure A-7.2.6

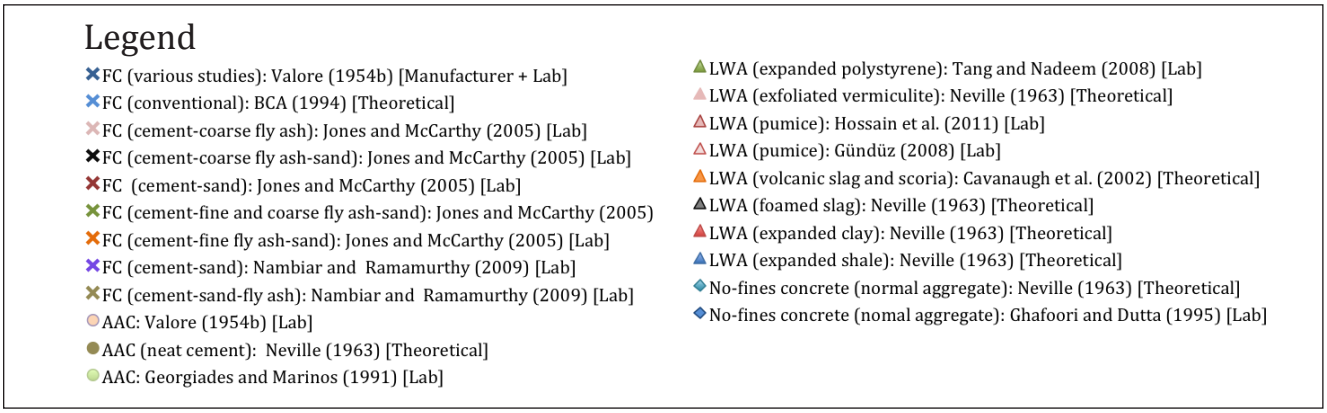
Legend
FC (various studies): Valore (1954b) [Manufacturer + Lab]
FC (conventional): BCA (1994) [Theoretical]
FC (cement-coarse fly ash): Jones and McCarthy (2005) [Lab]
FC (cement-coarse fly ash-sand): Jones and McCarthy (2005) [Lab]
FC (cement-sand): Jones and McCarthy (2005) [Lab]
FC (cement-fine and coarse fly ash-sand): Jones and McCarthy (2005)
FC (cement-fine fly ash-sand): Jones and McCarthy (2005) [Lab]
FC (cement-sand): Nambiar and Ramamurthy (2009) [Lab]
FC (cement-sand-fly ash): Nambiar and Ramamurthy (2009) [Lab]
AAC: Valore (1954b) [Lab]
AAC (neat cement): Neville (1963) [Theoretical]
AAC: Georgiades and Marinos (1991) [Lab]
LWA (expanded polystyrene): Tang and Nadeem (2008) [Lab]
LWA (exfoliated vermiculite): Neville (1963) [Theoretical]
LWA (pumice): Hossain et al. (2011) [Lab]
LWA (pumice): Gündüz (2008) [Lab]
LWA (volcanic slag and scoria): Cavanaugh et al. (2002) [Theoretical]
LWA (foamed slag): Neville (1963) [Theoretical]
LWA (expanded clay): Neville (1963) [Theoretical]
LWA (expanded shale): Neville (1963) [Theoretical]
No-fines concrete (normal aggregate): Neville (1963) [Theoretical]
No-fines concrete (nomal aggregate): Ghafoori and Dutta (1995) [Lab]

7.3.2 Permeability to Gases

Foam concrete is fairly permeable to water vapour and carbon dioxide, thus use of steel reinforcing can be problematic.[106]

Lightweight aggregate concretes may be less permeable that normal density concrete due to the strong adhesion between the porous aggregate and the paste, and the elastic compatibility of these two phases, which generates a dense interfacial zone and reduces microcracking, respectively.[107] The mortar of high quality lightweight aggregate concrete can be sufficiently dense to resist the ingress of chlorides and carbonation, and can offer adequate protection against reinforcing corrosion.[108] If concerns about steel corrosion remain, reinforcing may be coated in a rich, protective mortar.[109]

No-fines concrete is highly permeable, and highly susceptible to carbonation.[110] Air tightness is improved by rendering.[111] Protected or corrosion-resistant materials should be considered where reinforcement is necessary. [112]

Aerated autoclaved concrete has a highly open porosity[113] and is more permeable than foam concrete.[114] Steel reinforcing may be coated in a denser mortar before it is embedded in AAC to help to protect it from corrosion. [115]

Foam glass may be composed of hermetically sealed glass cells that are impermeable to liquid, vapour, and radon.[116] Thermal brick may be parged to achieve typical wall air tightness values of less than 1.2 $m^3/h \cdot m^2$.[117]

7.3.3 Thermal Performance

Thermal conductivity is usually dominated by density; however, the microstructural characteristics of various materials will also influence performance. Figures 7.**3.3a** to

[106] Brady et al. (2001) 10
[107] ACI 213-03 Section 4.14.2
[108] ACI 213-03 Section 4.14.1.2
[109] Neville (1963) 444
[110] Tittarelli et al. (2014) 36
[111] Neville (1963) 457
[112] Tittarelli et al. (2013) 119
[113] Koronthalyova (2011) 880, Laukaitis and Fiks (2006) 291
[114] Ramamurthy et al. (2009) 391 classification
[115] Valore (1954b) 826
[116] Pittsburgh Corning (n.d.) 13
[117] Wienerberger (2014) 113

7.**3.3e** plot thermal resistance against density for a variety of lightweight mineral-bonded materials.

Neat cement foam concrete performs relatively well due to its homogenous structure of fine closed-cell bubbles with thin cell walls, which interrupt heat transfer by convection and radiation, and create a tortuous path for conduction. Foam concrete with sand filler is somewhat more conductive due to its thicker cell walls.[118] The thermal performance of aerated autoclaved concrete may be similar to that of foam concrete with a high filler-cement ratio.

The thermal performance of lightweight aggregate concrete depends largely on the properties of the aggregate. Perlite, vermiculite, and expanded polystyrene aggregates, in particular, are commonly used for insulating purposes.[119] The thick mortar paste surrounding the aggregate allows a relatively easier path for heat transfer by conduction, compared to the thin cell walls of foam concrete.

No-fines concrete is generally a poor insulator, as its open structure permits convection, and as the heavy aggregate provides paths for conduction.[120]

Foam glass has good thermal performance due to its closed porosity and thin cell walls.[121]

The thermal resistance of thermal brick is dependent on the type of pore-forming agent used. Sawdust, glycerin, and olive mill solid residue appear to produce porous brick with low thermal conductivity values.[122]

Other factors may also influence actual thermal performance, such as moisture content or pressure differentials on either side of an assembly. For example, Yang and Lee[123] noted that the interconnected void structure of AAC encourages capillary suction and water absorption, undermining its thermal resistance. Windwashing effects may be more pronounced on materials with an interconnected void structure, such as AAC or no-fines concrete, than on highly closed cell materials like foam concrete, foam glass, or porous clay.

---

[118] Brady et al. (2001) C16
[119] Kosmatka et al. (2002) 316
[120] Sommerville et al. (2010) 11
[121] Pittsburgh Corning (2009) 4
[122] Bories et al. (2014) 194
[123] Yang and Lee (2015) 110

7.3.4 Freeze-Thaw Performance

Freeze thaw performance of foam concrete is generally good, as air voids provide space for the accumulation of frozen moisture. However, the material may be subject to significant damage when it is highly saturated; or the material may spall due to differential strain between saturated, frozen zones and dry, non-frozen zones.[124] AAC is subject to these same failure mechanisms.[125]

ACI Committee 213[126] concluded that properly proportioned, air-entrained lightweight aggregate concrete with a high quality binder provides satisfactory freeze-thaw durability in usual laboratory testing programs.

In no-fines concrete, the thin layer of cement paste surrounding aggregates may be quickly saturated in the presence of water, which may lead to debonding during freezing. Freeze-thaw deterioration may also be strongly related aggregate type.[127] Using air entrainment has been shown to improve freeze-thaw performance.[128]

Foam glass with closed pores exhibits good resistance to freeze-thaw cycles, as moisture does not penetrate the material.[129] However, foam glass with a more open porosity will be vulnerable to freeze-thaw action.[130]

Thermal brick may perform satisfactorily in freeze thaw tests.[131] This success may be attributed to the network of interconnected pores of varying scales, which permit migration of water, and provide space for the accumulation of water, during freezing.[132]

7.3.5 Thermal and Hygroscopic Movement

Foam concrete typically has high thermal and hygroscopic movement, due to the lack of restraining aggregate. Conversely, the thermal and moisture movement of AAC is significantly improved due to the autoclaving process.[133] The coefficient of linear

[124] Tikalsky et al. (2004) 890
[125] Senbu and Kamada (1990)
[126] ACI 213-03 Section 4.14
[127] Kevern et al. (2010) 469-470
[128] Ghafoori and Dutta (1995) 190
[129] Frickland et al. (1981)
[130] König (2016) 196
[131] Lucideon (2014) 17
[132] Everett (1961)
[133] Neville (1963) 454

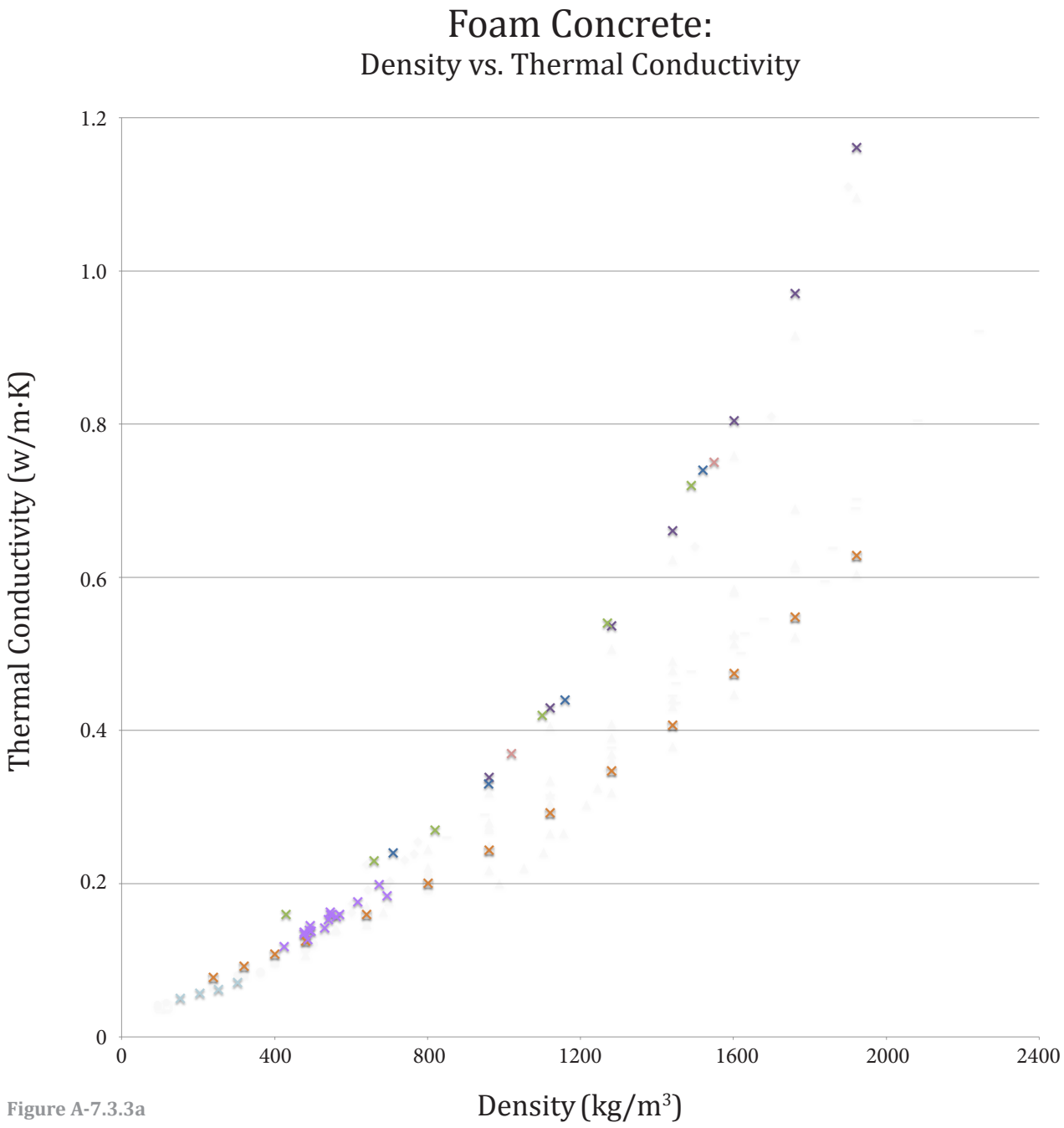

Figure A-7.3.3a

expansion of AAC is typically between 8 and $10 \cdot 10^{-6}$ mm/mm/°C.[134]

The thermal expansion coefficient of lightweight aggregate concrete is typically between 7 and $11 \cdot 10^{-6}$ mm/mm/°C,[135] slightly lower than that of normal density concrete.[136] Thermal movement of no-fines concrete is dependent on the aggregate type, but it may be in the order of 60 to 80% that of normal density concrete, due to the reduction of paste volume between the aggregates.[137] Commercially produced thermal brick exhibits low thermal movement relative to normal brick or concrete unit masonry, allowing control joints spacing of up to 20 m.[138] Foam glass typically has coefficient of thermal expansion in the order of $8 \cdot 10^{-6}$ mm/mm/°C, although for specially formulated foam glass the coefficient may be as low as $2.9 \cdot 10^{-6}$ mm/mm/°C.[139]

7.3.6 Fire Performance

Fire resistance is a complex issue. Issues of heat transfer, thermal movement,[140] permeability, tensile strength, resistance to spalling,[141] etc. will affect a material's ability to remain intact and support load during a fire event.

Foam concrete generally performs well as a fire resistant material. The thermal resistance of the material protects the inner core of a wall from extreme temperatures, while its permeability to air and water vapour allows the pressures of expansive gases to be relieved. The relatively high elasticity of the material allows differential temperature strains to be accommodated. However, at high temperatures, the foam concrete experiences significant shrinkage, which can induce spalling between exposed heated layers and a protected inner zone.[142] Nevertheless, foam concrete exhibits proportionally less strength loss than normal density concrete, particularly at lower densities.[143] Similarly, the flame spread rating of foam concrete may be expected to be better than that

134 Short and Kinniburgh (1978) 307
135 ACI 213-03 Section 4.17
136 Neville (1963) 373
137 Neville (1963) 457
138 Wienerberger (2014) 9
139 Frickland et al. (1981) Table 1
140 Zhang et al. (2014) 123
141 ACI 213-03 Section 4.19
142 Brady et al. (2001) C16
143 Jones and McCarthy (2005b) 29

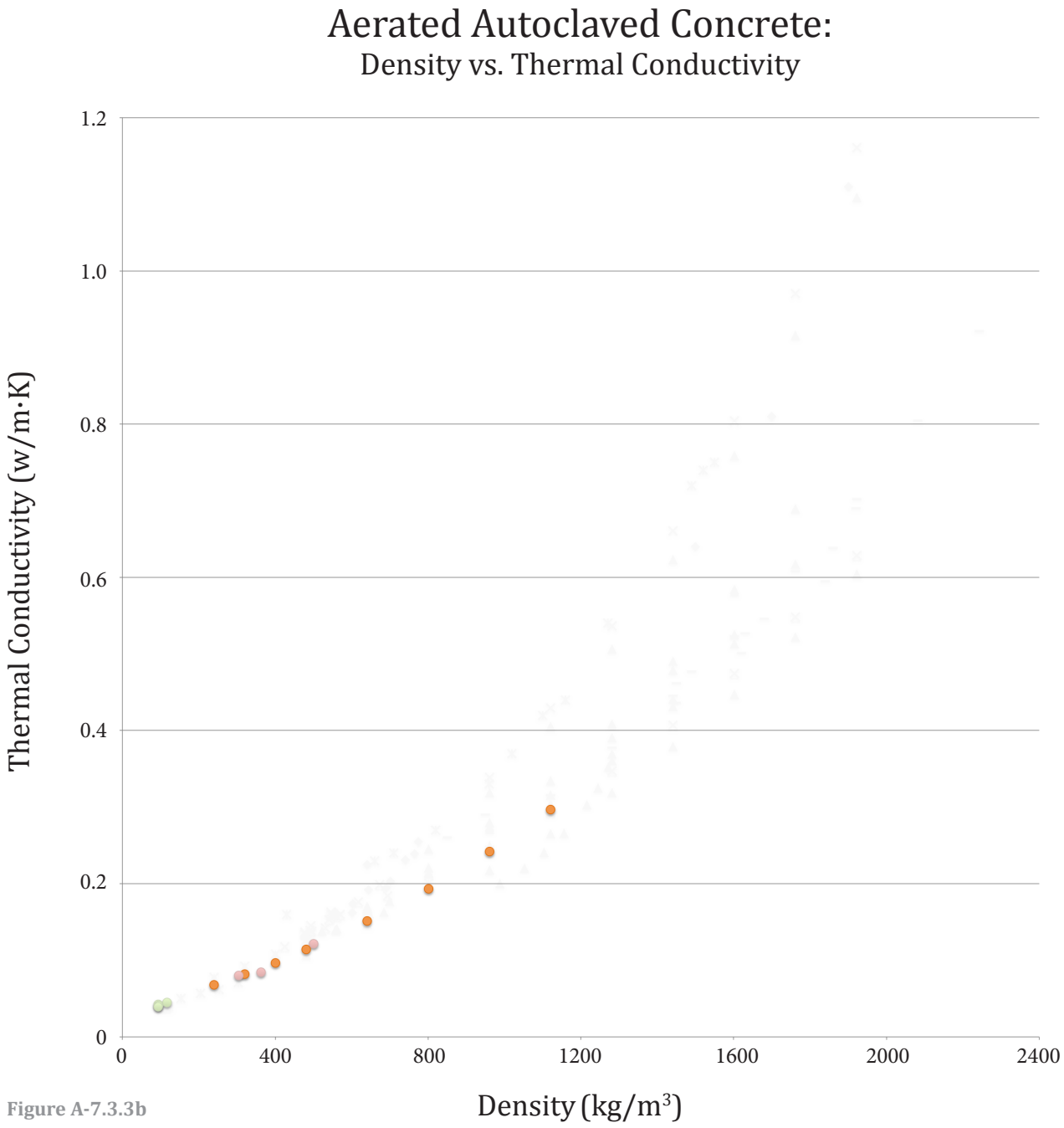

Figure A-7.3.3b

of normal density concrete.[144] Jones and McCarthy commented that 100 mm thick foamed concrete slabs with oven dry densities of 930 and 1250 kg/m^3 have achieved fire resistance of 3.75 and 2.5 h, respectively.[145] Geopolymer foam concrete provides even greater fire resistance.[146]

Like foam concrete, aerated autoclaved concrete is resist resists the flow of heat, and allows water held in crystalline form to escape the porous material without causing surface spalling. AAC may be used as a structural material, or as a cladding to protect vulnerable materials from extreme temperatures.[147] No toxic gases or vapours are released.[148]

Lightweight aggregate concrete is resistant to fire and elevated temperatures due to its low thermal conductivity and a low coefficient of thermal expansion. Pyroprocessed lightweight aggregates are produced in extreme temperatures, and are consequently also heat resistant.[149] Concrete cover requirements for fire protection can often be reduced slightly when using lightweight aggregate concrete instead of normal density concrete.[150] However, high moisture contents absorbed within lightweight aggregates can increase the risk of spalling.[151]

No-fines concrete is non-combustible, and its fire-resistance is reasonably good. However, in service, if the rendering over a wall fails, flames may pass through the highly permeable material into an adjacent space.[152]

Foam glass is incombustible, and foam glass with a highly closed porosity will not wick organic combustible fluids.[153] Thermal brick is fired in its production process and is inherently resistant to extreme heat.[154]

---

144 Brady et al. (2001) C16
145 Jones and McCarthy (2005b) 29
146 Zhang et al. (2014) 113
147 RILEM Technical Committees 78-MCA and 51-ALC (1993) 188
148 Xella (2010) 20
149 ACI 213-03 Section 4.19
150 ACI 213-03 Section 4.19.2
151 ACI 213-03 Section 4.19.3
152 Ashton and Bigmore (1954) 7
153 Pittsburgh Corning (2009) 9
154 Wienerberger (2014) 9

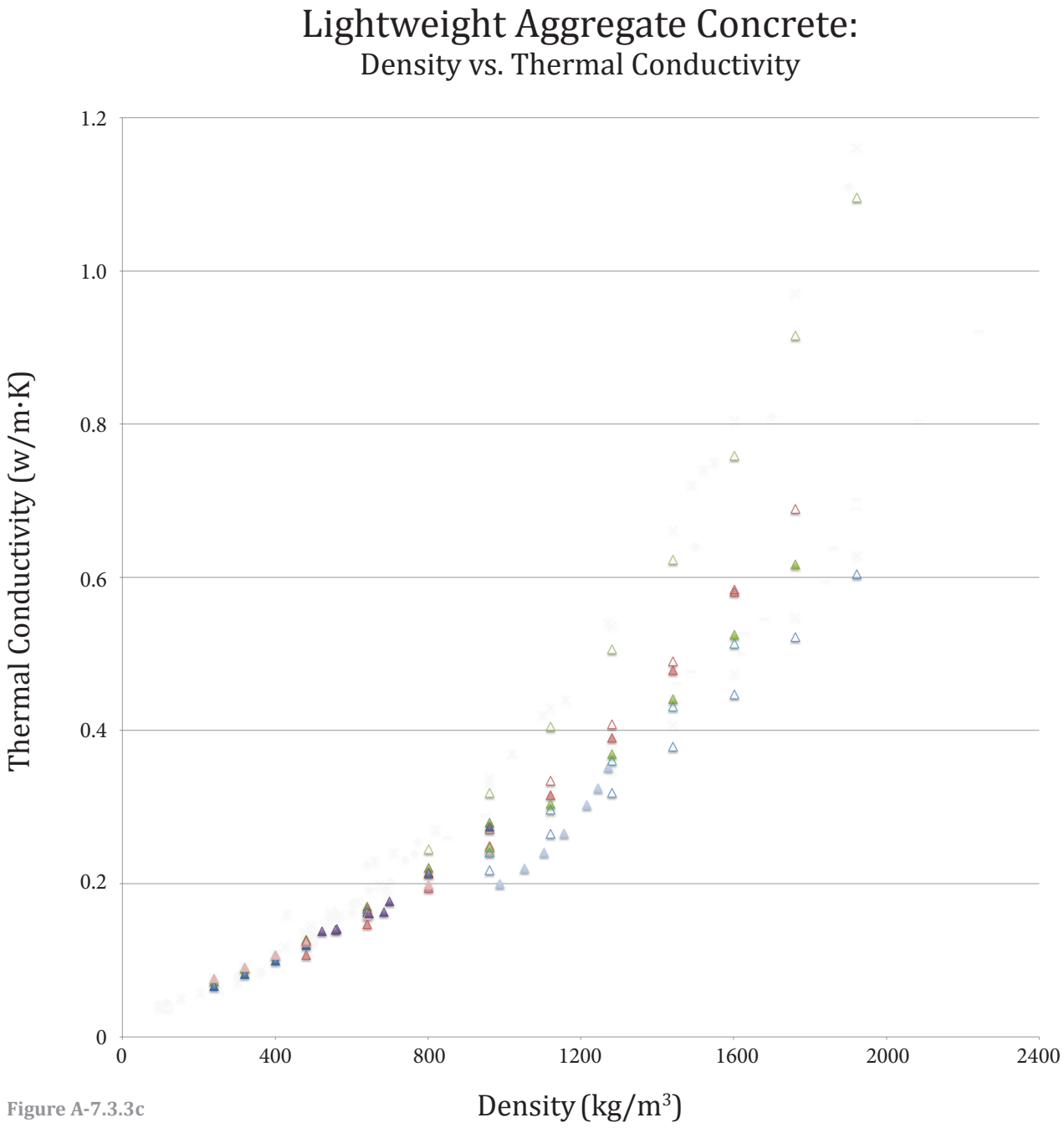

Figure A-7.3.3c

Legend

- LWA (expanded polystyrene): Cavanaugh et al. (2002) [Theoretical]
- LWA (natural pumice): Cavanaugh et al. (2002) [Theoretical]
- LWA (pumice): Gündüz (2008) [Lab]
- LWA (Expanded perlite): Cavanaugh et al. (2002) [Theoretical]
- LWA (exfoliated vermiculite: Cavanaugh et al. (2002) [Theoretical]
- LWA (expanded glass): Bumanis et al. (2013) [Lab]
- LWA (sintered fly ash and coal cinders): Cavanaugh et al. (2002) [Theoretical]
- LWA (volcanic slag and scoria): Cavanaugh et al. (2002) [Theoretical]
- LWA (expanded slag): Cavanaugh et al. (2002) [Theoretical]
- LWA (expanded and sintered clay, shale, and slate): Cavanaugh et al. (2002) [Theoretical]
- LWA (sanded expanded clay, shale, and slate): Cavanaugh et al. (2002) [Theoretical]

7.3.7 Resistance to Pests and Mould

Each of the inorganic materials under investigation are relatively resistant to pests. The air void system of no-fines concrete is the most open and interconnected, making it potentially more susceptible to insect infestation than other closed cell materials. Brady et al.[155] noted that there may be a minor risk of rodent attack where foam concrete is used to embed sewer pipe, due to the low strength of the material.

The mineral-bound materials under review usually have a low organic content, reducing the risk of mould growth. However, in conditions of high relative humidity, with pH between 4.5 and 8, mould growth is possible, especially if organic contaminants from the environment enter pores in the material.[156] Foam glass, with a highly closed porosity, may be especially resistant to the spread of mould.[157]

7.3.8 Resistance to Abrasion

Foam concrete is a relatively weak material, which may be easily abraded. The porous structure consists of unsupported cell walls. Additional cover may be necessary where abrasion will be a concern, such as on floors.[158]

AAC is subject to similar considerations. Care must be taken to avoid chipping and cracking of precast cellular concrete element during transport.[159] Abrasion resistance of cellular concretes may, however, be enhanced with coatings. For example, initial studies suggest that coatings may allow specialized cellular concrete to be used as a paving surface, capable of absorb air pollution in urban environments.[160]

The solid paste phase of lightweight aggregate is resistant to abrasion, while the porous particles are more vulnerable. Nevertheless, lightweight aggregate concrete has been used such successfully on bridge decks, exhibiting similar wear performance to

[155] Brady et al. (2001) C16
[156] Xella (2010) 19
[157] Pittsburg Corning (2009) 3
[158] Basiurski and Wells (2001) 67
[159] Valore (1961) 6
[160] Maury-Ramirez et al. (2012) 218

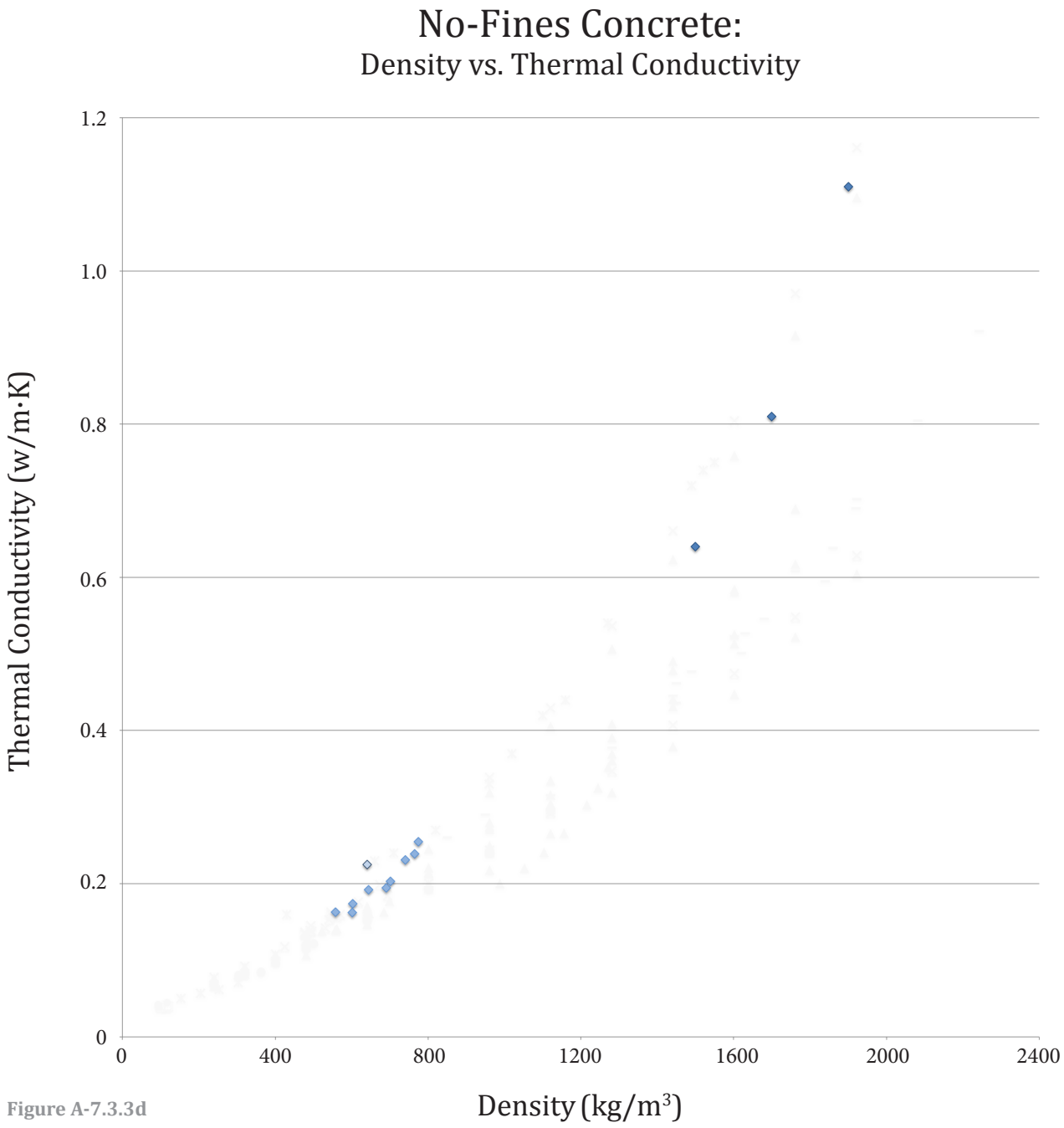

Figure A-7.3.3d

conventional normal density concrete. Surface treatments may also be applied for certain industrial applications.[161]

No-fines concrete exhibits reasonably good abrasion resistance, which is especially important in pervious paving applications. Wear rates decrease with increasing cementitious content, and increasing compaction during placing.[162] Decreasing aggregate size, and incorporating silica fume or superplasticizer, can also increase abrasion resistance. [163]

7.3.9 Acoustic Properties

In general, sound attenuation increases with mass, according to mass law; thus, sound transmission through a partition is proportional to the density and thickness of the partition.[164] However, the stiffness of materials also contributes to sound loss, and low-density materials such as foam concrete and AAC may perform better than anticipated by mass law.[165]

Sound may penetrate through unsealed joints in an assembly, or through materials with a highly interconnected porosity, such as unrendered no-fines concrete.

Sound absorption increases with surface texture and interconnectivity of pores, as sound energy penetrates further into the material and is lost as heat. The texture of uncoated foam concrete and AAC make it suitable for absorbing high frequency industrial noise, in particular.[166] AAC is somewhat better that foam concrete in terms of sound absorption due to its more open porosity.[167]

[161] ACI 213-03 Section 4.20
[162] Ghafoori and Dutta (1995b) 189
[163] Yang and Jiang (2003) 381
[164] London (1949)
[165] RILEM Technical Committees 78-MCA and 51-ALC (1993) 38-39
[166] RILEM Technical Committees 78-MCA and 51-ALC (1993) 40, Brady et al. (2001) 4
[167] Laukaitis and Fiks (2006) 295

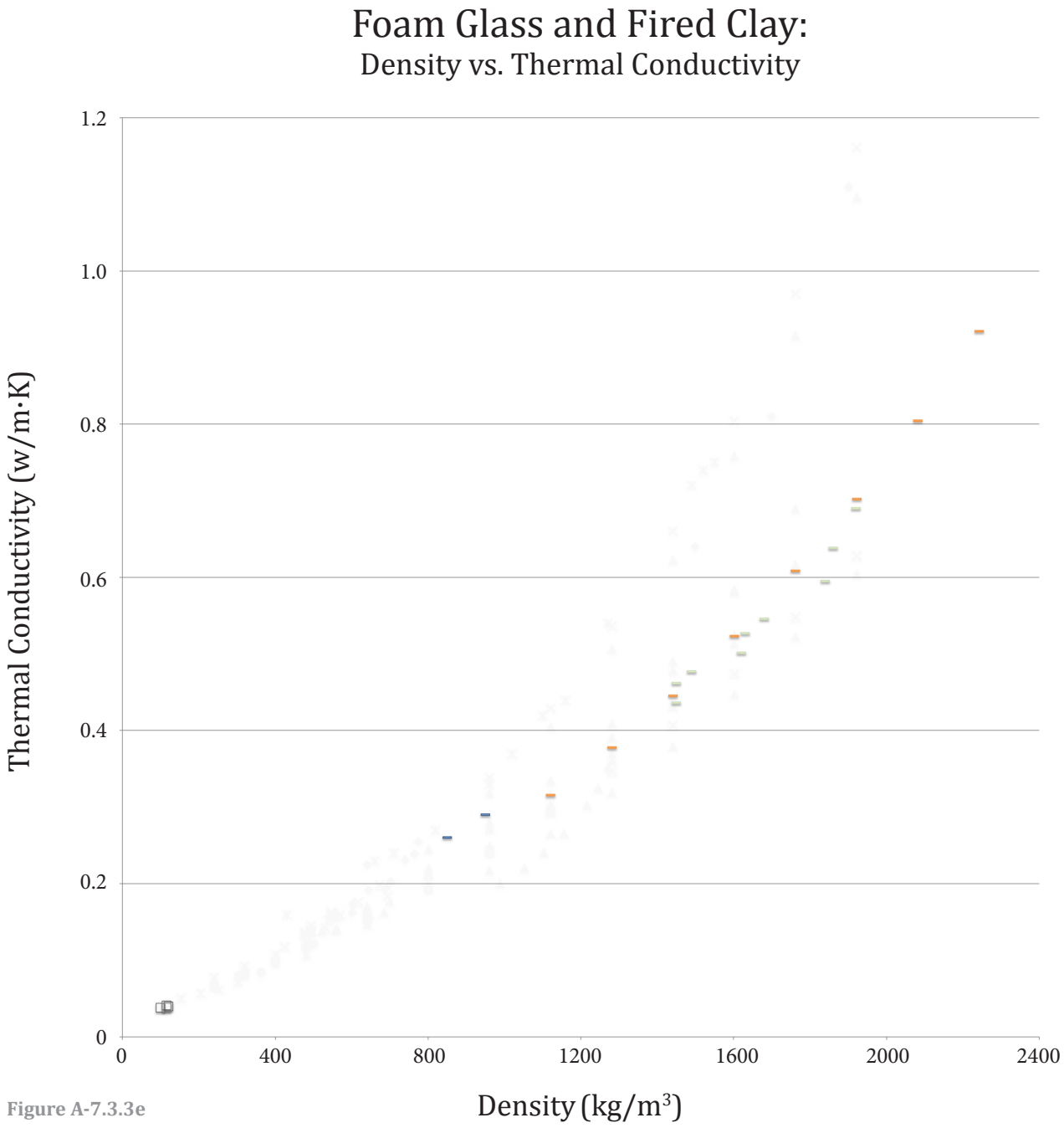

Figure A-7.3.3e

7.3 Issues of Sustainability

Reduced shipping costs, and reduced structural requirements, are common advantages cited for the use of lightweight materials.[168] Furthermore, lightweight materials can improve thermal performance, saving energy over the course of a structure's design life,[169] and lightweight structures are resistant to damage from earthquakes.[170] These aspects of transportation, efficient material use, thermal control, durability and resilience contribute to the overall sustainability of lightweight mineral-bound materials. Additionally, the porous structure of cellular concretes also presents opportunities for use in water filtration,[171] carbon sequestering,[172] stormwater management,[173] and absorption of air pollution in urban environments.[174]

However, the embodied energy of lightweight materials may be high due to use of earth materials and production processes. For example, foam concrete typically requires large proportions of binders and potable water.[175] Use of cement is a major contributor to the production of carbon dioxide. Much research has been done to minimize the use of cement, and to incorporate industrial waste products into foam concrete mixes as binders or fillers.

Aerated autoclaved concrete is consumes large amount of energy during autoclaving, in the order of 1005 MJ/m^3 at a density of 500 kg/m^3. Nevertheless, this energy usage is still significantly lower than that of other building materials such as fired brick.[176] Lifecycle analyses have suggested that AAC may provide a net reduction of greenhouse gas emissions, due to the benefits of its thermal insulation.[177]

Lightweight aggregate mixes typically have similar cementitious density to normal density concrete. The embodied energy of aggregates materials such as slate, shale, clay, and vermiculite is high on account of the temperatures required for pyroprocessing.

---

168 Short and Kinniburgh (1978) 2-3
169 Yang and Lee (2015) 110
170 RILEM Technical Committees 78-MCA and 51-ALC (1993) 112
171 Doniec (2008) 264
172 U.S. Patents 7390444 B2, 9028607 B2
173 Van Deijk (1991) 51, U.S. Patent 8172937 B2
174 Maury-Ramirez et al. (2012) 218
175 Brady et al. (2001) C1, C3
176 RILEM Technical Committees 78-MCA and 51-ALC (1993) 9
177 Yang and Lee (2015) 110

Lightweight aggregates may also be produced from industrial waste materials such as fly ash and slag.

No-fines concrete performs relatively well from an environmental perspective. Required cementitious densities and water usage are relatively low, and the mix will cure at normal temperatures. When used as a permeable paving, no-fines concrete can reduce groundwater run-off.

Significant amounts of recycled glass are incorporated in the production of foam glass, in the order of 60% or more.[178] Embodied energy is high, however, due to the temperatures required for annealing. The product does not contain ozone-depleting propellants, flame retardents, or binding agents.[179] After demolition, foam glass can be repurposed as landscaping filler or as thermally insulating aggregate.[180]

Insulating brick uses up to 30% of materials from alternative, recycled, or secondary sources in its manufacture.[181] Manufacturers attempt to minimize embodied energy with lower firing temperatures.[182] 95% less water may be used during wall construction than with conventional concrete block, due in part to finer mortar joints, and wastage is advertised to be in the order of 2%.[183]

[178] Pittsburgh Corning (n.d.) 7
[179] Pittsburgh Corning (n.d.) 9
[180] Pittsburgh Corning (n.d.) 13
[181] Wienerberger (2014) 5
[182] Wienerberger (2014) 10
[183] Wienerberger (2014) 11

A-8

Use of Foam Concrete

8.1 Existing and Proposed Applications

The following list summarizes actual and potential applications for foam concrete. Applications for which foam concrete has merely been proposed, but for which there are no built examples, are noted as (proposed).

Buildings

Roof

- Profiling flat roof screed for positive drainage[1]
- Insulating fill for roof[2]
- Sprayed insulating material for concrete domes[3]
- Fire resistance rated cover for roof deck[4]

Walls

- Structural enclosure for cold climates[5]

[1] Barnes (2009) 4
[2] Van Deijk (1991) 51
[3] Brady et al. (2001) C20
[4] Nandi et al. (2016) 41

- Structural enclosure for hot climates[6]
- Earthquake resistant structural enclosures[7]
- Precast non-structural blocks for apartment blocks, offices, and hotels[8]
- Precast structural blocks (proposed) [9]
- Precast in-fill blocks for multi-ribbed composite wall structure (proposed)[10]
- Sandwich panel fill for rapid tilt-up low-rise residential construction without need for heavy machinery (proposed)[11]
- Sandwich panels fill for emergency shelter (proposed)[12]
- Firewalls[13]
- Firebreaks[14]
- Thermal fill for new cavity walls[15]
- Thermal upgrade for traditional cavity walls, to avoid disrupting heritage aesthetic (proposed)[16]
- Acoustic surfaces[17]
- Decorative panels[18]

Floor

- Acoustically insulating fill beneath existing floors[19]
- Thermally insulating layer for installation of in-floor heating[20]
- Thermally insulating fill beneath existing floors (proposed) [21]
- Self consolidating concrete fill for leveling floors[22]
- Grouting to provide structural support beneath existing floors[23]

---

5 Proshin et al. (2005) 113-120
6 Kearsley and Mostert (2005b) 144, Kearsley (1999b) 4
7 Bindiganavile and Hoseini (2008) 251
8 Basiurski and Wells (2010) 151
9 Narayanan and Ramamurthy (2012) 144
10 Sun (2013)
11 Mydin and Wang 2011 66
12 Panesar (2013) 576
13 Kearsley and Mostert (2005c) 89
14 Basiurski and Wells (2001) 67
15 Werkema et al. (1961) 36
16 Shi et al. (2012) 23
17 Zhang et al. (2015) 104
18 Basiurski and Wells (2001) 67
19 Van Deijk (1991) 51
20 Yang et al. (2014) 226-227
21 Liew (2005) 50
22 Barnes (2009) 4

Foundations

- Insulating foundation walls[24]
- Insulation for existing crawlspaces[25]
- Insulating or non-insulating mud slab for new construction[26]
- Raft foundation, for thermal insulation and load-spreading[27]
- Cast-in-place foam concrete piles, for improving bearing capacity in soft soils through development of skin friction[28]
- Lightweight fill to provide direct load path from existing slab to ground[29]
- Thermal isolation of structures built on permafrost[30]
- Frost protection for existing foundations[31]
- Frost protection for pile caps[32]
- Stabilization of structure built on unsound soils[33]
- Pontoons for floating dwellings[34]
- Pontoon bridges and floating docks[35]

Backfill

- Backfill for disused crawlspaces and basements[36]

Miscellaneous

- Precast glass fibre-reinforced products, including fence posts, poles, lintels, window and door frames (proposed)[37]

Geotechnical

- Non-settling fill as replacement for existing inadequate/unsuitable soils[38]

---

23 Dolton and Hannah (2006) 8
24 Jones and Giannakou (2004)
25 Van Diejk (1991) 52
26 Van Deijk (1991) 51
27 Van Deijk (1991) 51
28 Van Deijk (1991) 51
29 Dolton and Hannah (2006) 8
30 Dolton and Hannah (2006) 7
31 Amran et al. (2015) 1002
32 Amran et al. (2015) 1002
33 Basiurski and Wells (2001) 68
34 Barnes (2009) 4
35 Wahlman (1991) 6
36 Amran et al. (2015) 1001
37 Brady et al. (2001) C20

- Cohesive fill for elevating sites with weak soils[39]
- Stabilizing cover over soils on slopes[40]
- Emergency void-filling[41]

Landscape

- Permeable pavement underlayment and recharge beds[42]
- Permeable subbase for sports fields and athletic tracks[43]
- Stormwater runoff detention management[44]

Utilities

- Insulating backfill for utility trenches, which does not require compaction, and may be easily re-excavated[45]
- Annular grouting around pipe casings[46]
- Backfill of redundant sewers[47]
- Backfill of redundant storage tanks[48]
- Thermal insulation or fire protection around storage tanks (proposed)[49]
- Insulation and support for hot oil or gas pipelines installed over permafrost[50]
- Protection for pipelines from impact of rockfall[51]
- Protection for pipelines from damage due to backfilling[52]
- Bedding material for pipelines to absorb stresses of differential movement/settlement[53]

---

38 Van Deijk (1991) 51
39 Hooimeijer (2011) 229, Basiurski and Wells (2001) 69
40 Van Diejk (1991) 51
41 Basiurski and Wells (2001) 68
42 Nandi et al. (2016) 41
43 Van Deijk (1991) 51
44 U.S. Patent 8172937 B2, cf. Alobaidi et al. (2000) 151
45 Dolton and Hannah (2006) 10
46 Dolton and Hannah (2006) 8
47 Brady et al. (1991) 3
48 Amran et al. (2015) 1001
49 Cellular Concrete Solutions (n.d.) 8
50 Dolton and Hannah (2006) 4
51 Dolton and Hannah (2006) 4
52 Dolton and Hannah (2006) 4
53 Dolton and Hannah (2006) 4

- Support of existing tanks to relieve stresses on welded joints[54]
- Support of new tanks to allow the use of thinner steel walls[55]

Transportation

- Backfill of voids beneath existing roads[56]
- Replacement of unstable soils for new roads[57]
- Cohesive subbase for new roads over unstable soils[58]
- Elevating fill for new roads[59]
- Insulating subbase to prevent frost heave of new roads[60]
- Bulk filling of redundant tunnels and subways[61]
- Lightweight backfill for spandrels of masonry arch bridges[62]
- Repair of existing bridge decks[63]
- Lightweight, cohesive fill for bridge abutments[64]
- Permeable fill for drainage in long tunnels[65]
- Backfill for voids around tunnel lining[66]
- Finished interior surfaces of tunnels for dampening seismic response[67] or impact absorption[68]
- Train platform in-filling/re-profiling[69]
- Crash barriers for ground vehicles (proposed)[70]
- Runway stopping pad for airplanes[71]

---

54 Van Deijk (1991) 51
55 Van Deijk (1991) 51
56 Amran et al. (2015) 1001, Alobaidi et al. (2000) 152
57 Basiurski and Wells (2001) 71
58 O'Reilly (2009) 16-17
59 Cox (2005) 111, Van Deijk (1991)
60 Amran et al. (2015) 1001
61 Brady et al. (2001) 3
62 Brady et al. (2001) 2
63 The Concrete Society (2016)
64 Basiurski and Wells (2001) 68
65 Choi and Ma (2015) 93
66 Jones and McCarthy (2005a) 66
67 Jiang and Zhang (2011)
68 Jones and McCarthy (2005a) 66
69 Liew (2005) 46
70 Tom et al. (2003)
71 Zhang et al. (2013)

Industrial

- High frequency sound insulation[72]
- Precast sandwich panels as foundation for gantry crane in areas of weak soil[73]
- Lightweight, cohesive backfill for harbor quays to reduce lateral loads on retaining walls[74]
- Thermal insulation in refractory applications[75]
- Filtering system for wastewater from electroplating process (proposed)[76]

Mining

- Backfill for disused mines to minimize subsidence or collapse,[77] or to prevent entry of animals or humans[78]
- Air tight walls to prevent the spread of fire in coal mines[79]
- Air tight grout to seal air leakages in coal mines, helping to prevent spontaneous combustion[80]
- Fire extinguishing grout to be injected into all surficial ventilation openings during a coal seam fire[81]
- Impact absorbing blast walls for explosion prevention [82]
- Precast modular support systems (cribbing) designed for deep level, seismically active mining[83]

Nuclear

- Containment of hazardous waste[84]

---

72 Brady et al. (2001) 4
73 Van Deijk (1991) 51
74 Van Deijk (1991) 51, Dolton and Hannah (2006) 9
75 Kearsley and Mostert (2005c) 89-96, Krivenko et al. (2005) 97-104
76 Doniec (2008) 264
77 Boughrarou and Cale (2005) 133-142
78 Dolton and Hannah (2006) 10
79 Tang et al. (2013) 345
80 Lu and Qin (2015)
81 Colaizzi (2004) 79
82 Tang et al. (2013) 345, Jones and Zheng (2013) 209
83 Erasmus and Smit (2005) 121-131
84 Ashworth et al. (2013)

Military

- Defensive structures[85]
- Bullet-absorbing walls[86]
- Bullet traps on shooting ranges, to prevent metal debris from being mixed into the soil[87]
- Explosion prevention[88]

[85] Tian, Zhang and Niu (2016) 195
[86] Brady et al (2001) C20
[87] Fabian et al. (1996) 118
[88] Jones and Zheng (2013) 209

8.2 Significant Foam Concrete Projects

The selection of projects in the table below indicates the development and advancement for foam concrete use worldwide, over the past thirty years.

Year(s)	Project	Location	Type	Foam Concrete Volume (m^3)
1986	Fill for Harbour	Netherlands	Lightweight fill for large scale harbor fill [89]	19,500 [90]
1989	Cypress Avenue	Oakland, California	Road reconstruction following earthquake to minimize future seismic shock	73,400 [91]
1989-1990; 1996-2002	Canary Wharf	London, UK	Foundations for access road and associated work	33,000 [92] + 20,000 [93]
1990	Blidögatan, Malmö harbour	Malmö, Sweden	Rebuilding a street subject to heavy traffic	700 [94]
1992	Durapak ®	South Africa	Precast foam concrete supports for use in gold mines	Unknown [95]
1994	Heathrow railway	London, UK	Tunnel stabilization	12,000 [96]
1993	Nagano Expressway	Nagano Prefecture, Japan	Repair of embankment after landslide	Unknown [97]
1995	University of Singapore	Singapore	Trench reinstatement for telecommunication utilities	Unknown [98]
1996	Colchester railway bridge	Colchester, UK	Backfill for bridge abutments	4,000 [99]
1996	Shock Absorbing	USA	Shock Absorbing Concrete	Unknown [100]

89 Jones and McCarthy (2005a) 64
90 Brady (2001) C21
91 Jones and McCarthy (2005a) 64
92 Van Deijk (1991) 54
93 Cox (2005) 107
94 Wahlman (1991) 6
95 Erasmus and Smit (2005) 121-131
96 Basiurski and Wells (2001) 68
97 Basiurski and Wells (2001) 71
98 Basiurski and Wells (2001) 72
99 Brady et al. (2001) C20
100 Fabian et al. (1996)

	Concrete (SACON)		developed for US Military applications	
1996	Royal Gniezno Cathedral	Gniezno, Poland	Stabilization of cathedral on hill	4,500 [101]
1997	Purmerend Road Junction	Purmerend, Netherlands	Raising road junction 2.5m	23,000 [102]
2001-2002	I-90/Route 1A Interchange	Boston, Massachusetts	Soil replacement for bearing overpass abutments	70,000 [103] (estimated)
2001-2009[104]	Combe Down Stone Mines	Near Bath, UK[105]	Abandoned mine stabilization	576,691[106]
2003-2004	Woodrow Wilson Bridge	Washington, DC	Fill for abutments	53,500 [107]
2013	Sellafield reprocessing complex	Cumbria, UK	Decommissioning of Nuclear Plant	1,300 [108]

Table A-8.2 Significant foam concrete projects worldwide.

[101] Basiurski and Wells (2001) 68
[102] Cox (2005) 111
[103] Cox (2005) 112
[104] Bath & North East Somerset Council (2010b)
[105] Boughrarou and Cale (2005) 133-142
[106] Bath & North East Somerset Council (2010a)
[107] Cox (2005) 111
[108] Ashworth et al. (2013)

8.3 Annual Use of Foam Concrete by Region

The table below suggests the typical annual market size of foam concrete in various regions of the world.

Date of Statistic	Use	Region	Estimated Annual Foam Concrete Volume (m^3/yr)
2005	All Uses	UK	250,000-300,000 [109]
2008	All Uses	Western Canada	50,000 [110]
2014	In-floor heating systems	Republic of Korea	250,000 [111]

Table A-8.3 Annual use of foam concrete by region.

[109] Jones and McCarthy (2005a) 64
[110] Bindiganavile and Hoseini (2008) 251
[111] Yang et al. (2014) 226

B

Studies on the Use of Fly Ash, Slag, and Silica Fume in Foam Concrete

Reference	Fly ash*	Slag	Silica Fume
Fujiwara et al. (1995)			X
Kearsley (1996)	X		X
Pickford and Crompton (1996)		X	
Kearsley (1999b)	X		
Byun et al. (1998)	X		X
Kearsley and Wainwright (2001b)	X		
Lee et al. (2001)	X		
Kearsley and Wainwright (2001a)	X		
Kearsley and Wainwright (2001b)	X		
Kearsley and Wainwright (2002)	X		
Tasdemir (2003)	X		X
Jones and Giannakou (2004)	X		
Colaizzi (2004)	X		
Tikalsky et al. (2004)	X		
Kearsley and Mostert (2005a)	X		
Kearsley and Mostert (2005b)	X		
Kearsley and Mostert (2005c)	X		
Jones and McCarthy (2005a)	X		
Jones and McCarthy (2005b)	X		
Jones and McCarthy (2005c)	X		
Tarasov et al. (2005)	X		

Papayianni and Milud (2005)	X		
Nambiar and Ramamurthy (2006a)	X		
Nambiar and Ramamurthy (2006b)	X		
Jones and McCarthy 2006	X	X	
Wee et al. (2006)		X	
Nambiar and Ramamurthy (2007a)	X		
Nambiar and Ramamurthy (2007b)	X		
Pan et al. (2007)	X	X	X
Nambiar and Ramamurthy (2008)	X		
Tarasov et al. (2010)	X		
Zhang et al. (2011)	Geopolymer		
Wee et al. (2011)		X	
Jitchaiyaphum et al. (2011)	X		
Zulkarnain and Ramli (2011)			X
Al Bakri Abdullah et al. (2012)	Geopolymer		
Narayanan and Ramamurthy (2012)	X		
Jones et al. (2012)	X		
Shi et al. (2012)	X		
Tapia (2013)	X		
Li et al. (2013)	X		
She, Chen, Zhang and Jones (2013)	X		
She, Zhang, Jones and Guo (2013)	X		
Wu et al. (2013)			X
Roslan et al. (2013)	X		
Awang and Ahmad (2014)	X		
Pan et al. (2014)		X	
Cong and Bing (2014)			X
Hilal et al. (2014b)	X		X
Yang et al. (2014)		Geopolymer	
She et al. (2014b)	X		
Chen et al. (2014)	X		
Liu et al. (2014)	Geopolymer		
Mamun et al. (2014)	X		
Khan (2014)	X		X
Abdollahnejad et al. (2015)	Geopolymer		
Hilal et al. (2015b)	X		X
Hilal et al. (2015c)	X		X
Huang et al. (2015)	X		
Lu and Qin (2015)	X		
Zhang et al. (2015)	Geopolymer	Geopolymer	
Yue and Bing (2015)	X		
Sayadi et al. (2016a)	X		
Sayadi et al. (2016b)	X		

Sayadi et al. (2016c)	X		
Tian, Zhang and Niu (2016)		X	
Tian, Yan, Hu, Xu, Chen, and Shi (2016)	X		

Total Number of Studies	57	9	12

Table B.1 Studies on the use of fly ash, slag, and silica fume in foam concrete.

*No differentiation has been made between studies which treat fly-ash as binder and those which treat fly-ash as a filler. Fine fly ash is often considered a binder, and coarse fly ash a filler; both are pozzolanic, although the former is typically less so. Cf. Jones and McCarthy (2005c) 1398, 1404

C

Maps of Cementitious Material Sources in Canada and the United States

Sources of Portland cement, slag, silica fume, and fly ash are charted in maps on the following pages, based on data from the references cited in the table below.

	Canada	United States
Sources of Portland Cement	Cement Association of Canada (2016) Smith (2014)	Hanle et al. (2004)
Sources of Fly Ash	Sas (2015)	US Energy Information Administration (2016)
Sources of Silica Fume	Minerals and Metals Sector NRCAN, National Energy Board (2012)	Kramer et al. (1998)
Sources of Blast Furnace Slag	Environment and Climate Change Canada (2013) Environment and Climate Change Canada (2015)	van Oss (2004)

Table C.1 Data references for maps of cementitious material sources in Canada and the United States.

Map of Portland Cement Plants (Sources of Portland Cement) in Canada and the United States

Map of Coal-Fired Power Plants (Sources of Fly-Ash) in Canada and the United States

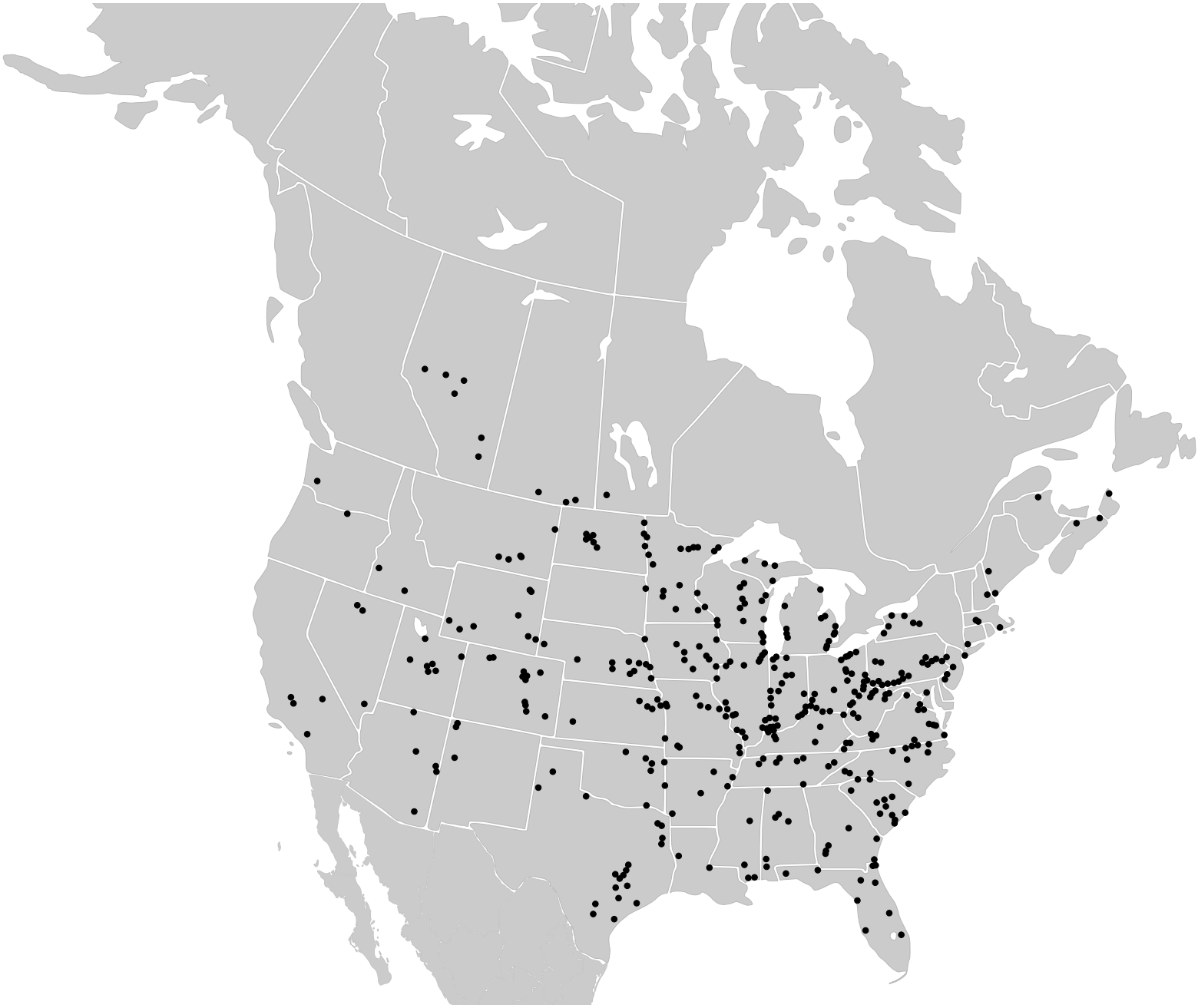

Map of Ferrosilicone Smelting Plants (Sources of Silica Fume) in Canada and the United States

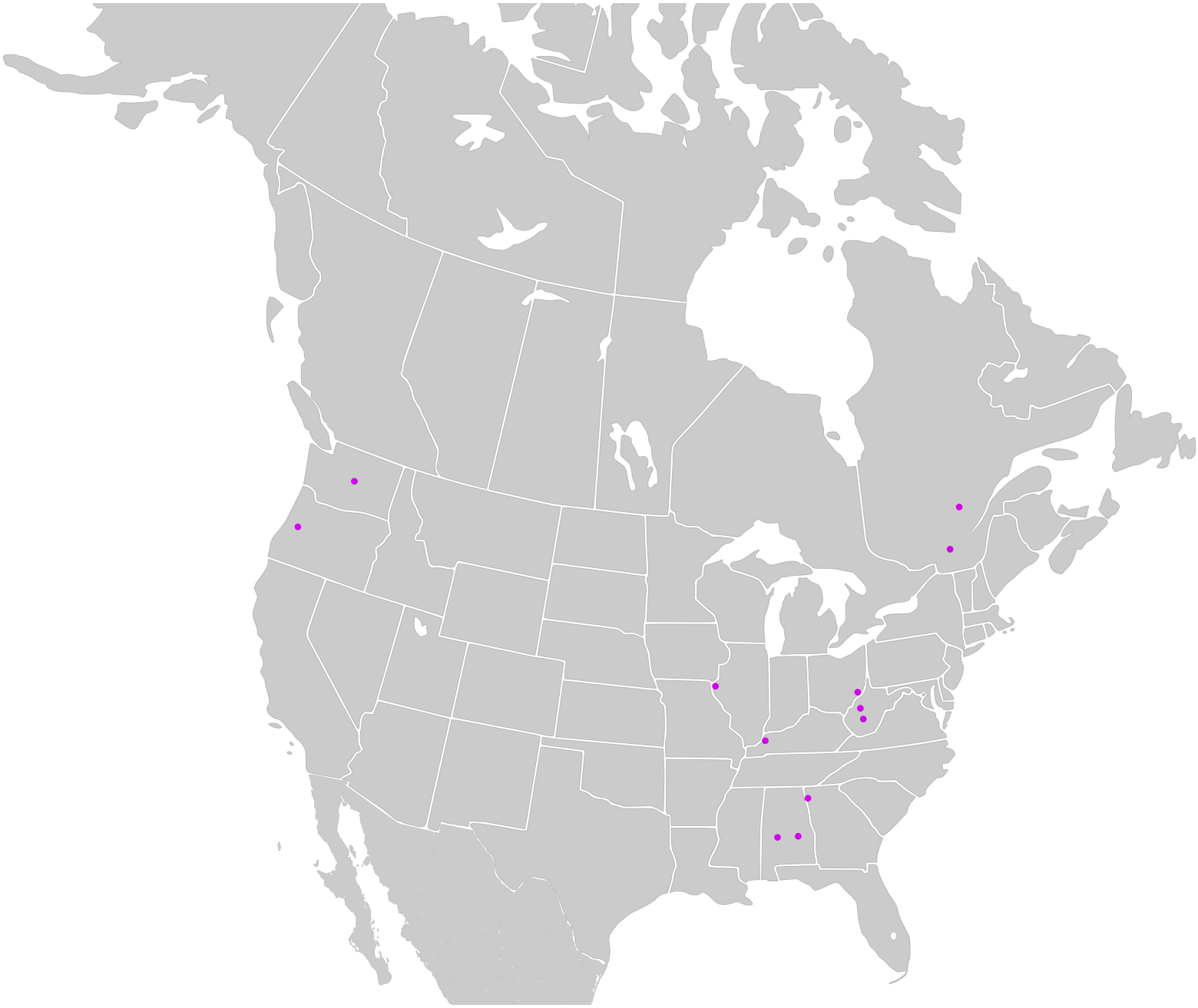

Map of Ironmaking Plants (Sources of Blast Furnace Slag) in Canada and the United States

Composite Map of Cementitious Material Sources in Canada and the United States

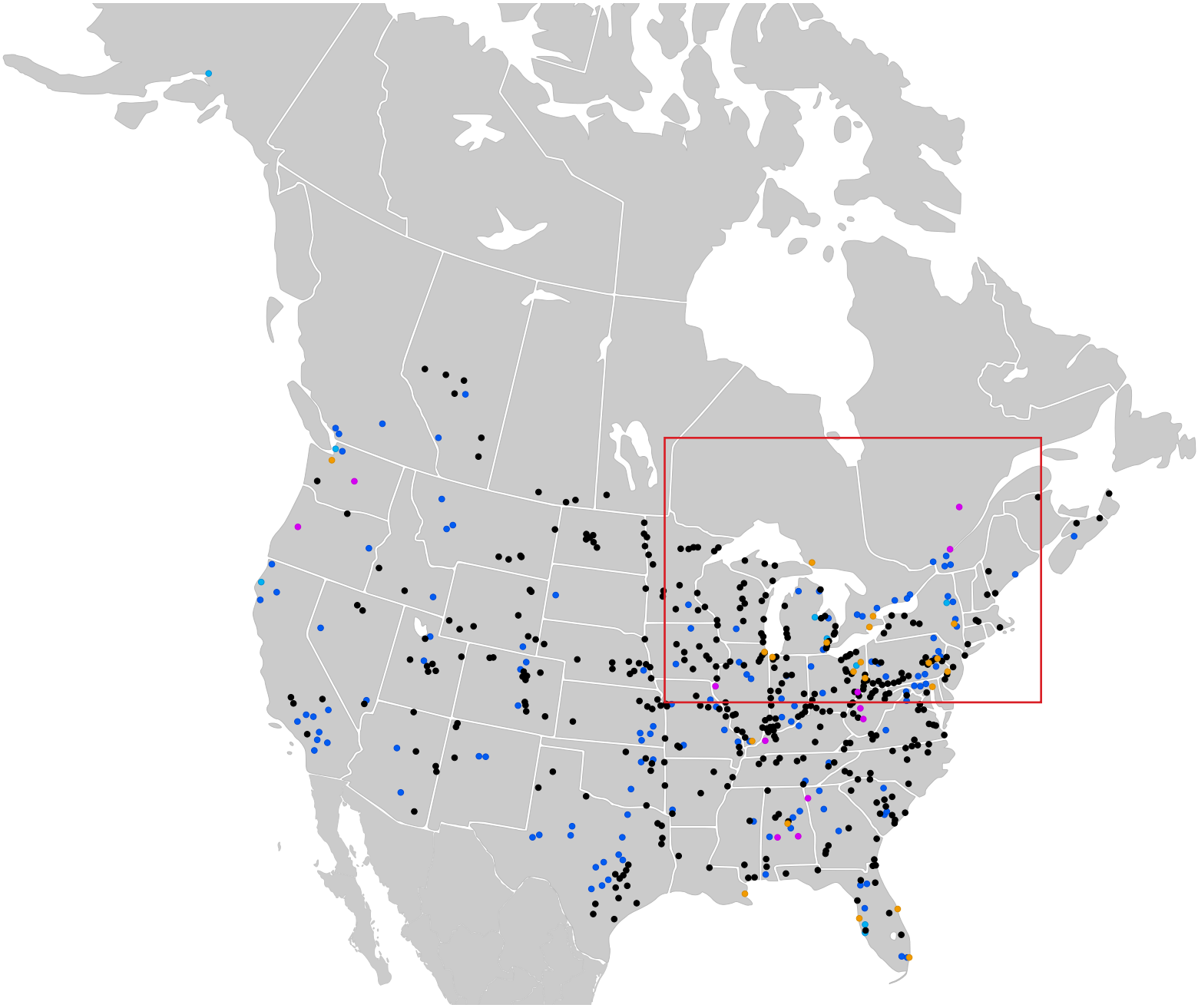

Detail of Composite Map of Cementitious Material Sources in Canada and the United States, Relative to Testing Location

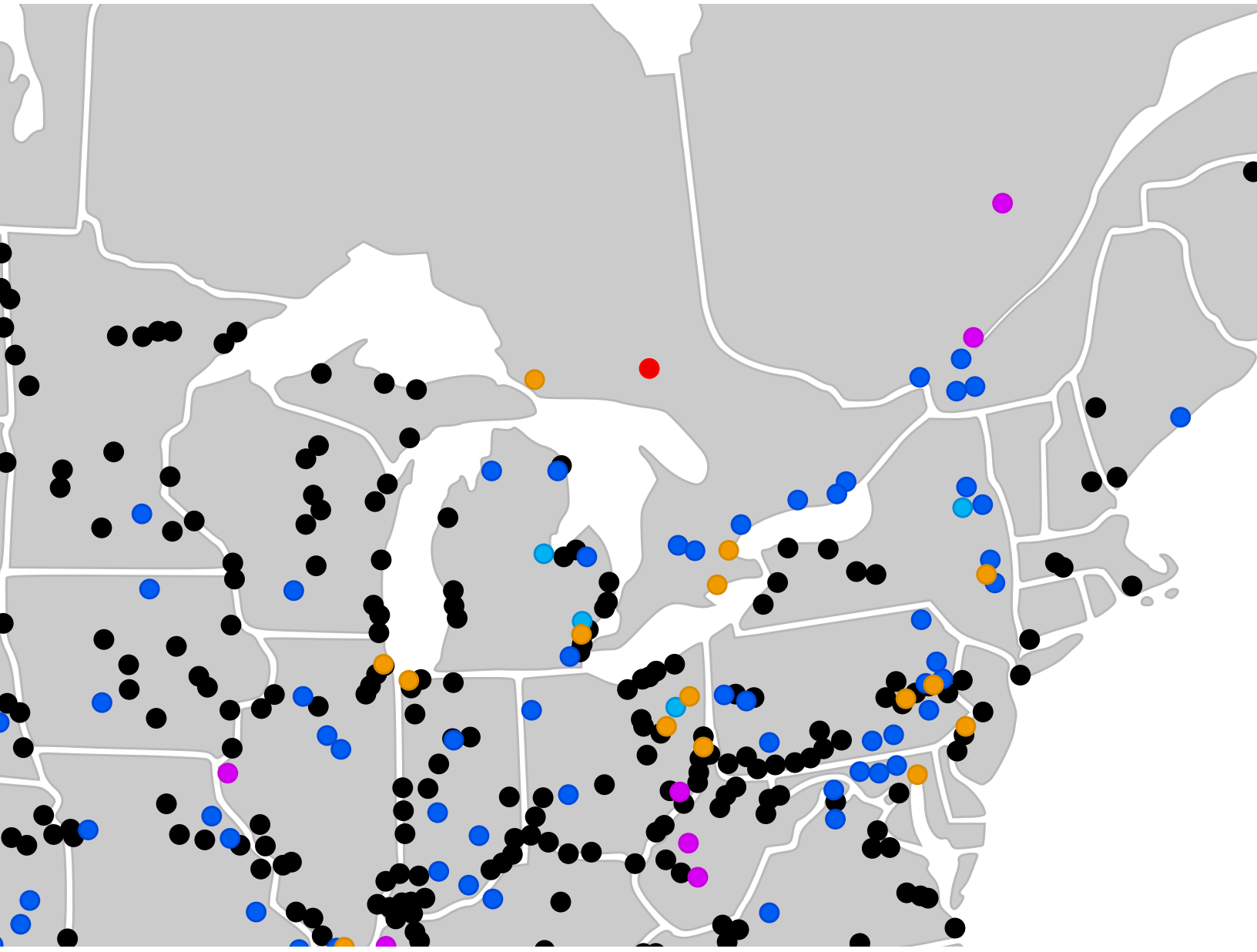

D

Detailed Methodology for Mix Proportioning

The mix proportioning method used for producing foam concrete samples is based on the method developed at the University of Dundee,[1] as described in D.1. The moisture content of the sand was also taken into account, as explained in D.2.

D.1 Mix Proportioning

To enable ease of proportioning, a simple computer program was developed to ensure accurate batching. The process for proportioning mixes is as follows:

1) Set the desired total cementitious content. Cementitious content is 410 kg/m^3 for the main recipes tested, unless noted otherwise. Cementing materials are significantly more expensive than other ingredients. Maintaining a constant cementitious density allows for ready comparison of recipes for both relative strength and cost.
2) Set the proportion of cementitious content to be composed of ground-granulated blast furnace slag or silica fume, if desired. The remainder of cementitious content will be Portland cement.

[1] Giannakou and Jones (2002). Cited in Jones et al. (2012) 516

3) Set the desired water-binder ratio.[2]
4) Set the desired cement-filler ratio.
5) The required volume of foam is updated automatically.[3]

The program takes into account the density[4] of each ingredient. The target plastic density of the mix, D, may thus be taken as the sum of the mass per cubic meter of fresh concrete contributed by each ingredient. Thus,

$$D = w + b + s + f$$

where

w is the mass of water per cubic meter of fresh concrete;

b is the mass of cementitious content per cubic meter of fresh concrete;

s is the mass of sand per cubic meter of fresh concrete; and

f is the mass of foam per cubic meter of fresh concrete.

The mass of cementitious content per cubic meter of wet concrete, b, is given by

$$b = b_{pc} + b_{sf} + b_{gs}$$

where

b_{pc} is the mass of Portland cement per cubic meter of fresh concrete;

b_{sf} is the mass of silica fume per cubic meter of fresh concrete; and

b_{gs} is the mass of slag per cubic meter of fresh concrete.

The mass of foam per cubic meter of fresh concrete, f, may be found by multiplying the volume of foam per cubic meter of fresh concrete by its density.

$$f = V_{foam} \cdot \rho_{foam}$$

---

2 Refer to the discussion on equivalent water-binder ratios in Appendix I.

3 This method assumes that the total volume of a cement-water mixture remains constant during hydration. Cf. Metha (1986) 27

4 That is, the particle density in the case of sand and cementitious ingredients; liquid density in the case of water; and total density in the case of the foam. The binder, filler and water are assumed to generate a slurry with no air voids. When the foam is added, bubbles are assumed to remain whole and entirely surrounded by paste.

The volume of foam per cubic meter of fresh concrete is determined by subtracting the volumes of the other materials from a one cubic meter volume,

$$V_{foam} = 1 - \left[\left(\frac{w}{\rho_w}\right) + \left\{\left(\frac{b_{pc}}{\rho_{b_{pc}}}\right) + \left(\frac{b_{sf}}{\rho_{sf}}\right) + \left(\frac{b_{gs}}{\rho_{b_{gs}}}\right)\right\} + \left(\frac{s}{\rho_s}\right)\right]$$

where ρ_w, $\rho_{b_{pc}}$, ρ_{sf}, $\rho_{b_{gs}}$, and ρ_s are the specific densities of water, Portland cement, silica fume, slag, and sand, respectively.

Upper and lower plastic density limits were established as ±50 kg/m^3 from the target density, as recommended by ASTM C796, Section 7.3.1, and Brady et al.[5] Thus,

$D_{max} = D + 50kg/m^3$ and $D_{min} = D - 50kg/m^3$

By inputting the mass and volume of an empty container, the program reveals a target mass, as well as upper and lower limits, for the container when filled with the plastic mix. This protocol aids in rapidly confirming that an appropriate plastic density has been attained during batch testing.

[5] Brady et al. (2001) 8

D.2 Accounting for Sand Moisture Content

Large amounts of sand fine aggregate may be used in denser foam concrete recipes. Moisture content in the sand can have a significant effect on the actual water-binder ratio of a mix. The following process was employed to correct for the moisture content of the sand:

1) Each day, a representative sample of sand, approximately 0.5 kg in mass, was removed from the source and placed in a pan of known mass. The mass of the moist sand was determined and recorded.
2) The sand and pan were placed on a heating element to remove moisture, until constant mass.
3) Moisture content of the sand, MC_{sand}, was calculated as the absolute change in mass, divided by the original mass of moist sand.
4) The actual mass of moist sand required, s', was calculated according to the following formula:

$$s' = s/(1 - MC_{sand})$$

where s is the nominal mass of sand required.

5) The actual mass of water required, w', was calculated according to the following formula, to account for the contribution of the wet sand to the mixing water:

$$w' = w - (s \cdot MC_{sand})$$

where w is the nominal mass of water required.

Figure D.2.1 Sample of sand dried on hot plate to determine moisture content.

E

Notes on the Production of Foam Concrete Aggregate

The use of crushed and graded foam concrete as a lightweight aggregate was explored. This material was termed 'foam concrete aggregate' (FCA), and is shown in Figure E.**1.1**.

This appendix includes a list of possible benefits of foam concrete aggregate (E.1), notes on design parameters to be explored (E.2), early observations regarding the production of FCA (E.3), and formulae for calculating the total cementitious density of concrete mixes which incorporate foam concrete aggregate, which is helpful for preliminary costing (E.4).

Test results for mixes that include FCA may be found in Sections 6.4, 6.4, 6.9, and 6.11. Additional results for more than fifty FCA mixes will be published at a later time, as part of ongoing research activities.

E.1 Motivation for Investigating Foam Concrete Aggregate

Foam concrete aggregate may offer the following advantages:

1) May be Produced On-Demand with Ordinary Batching Equipment

FCA may be manufactured on-demand, without the need for specialized pyroprocessing equipment, or access to naturally-occurring porous stone from which many other lightweight aggregates are derived.[1]

2) May Allow Foam Concrete to be Incorporated in Dry-cast Processes

Foam concrete aggregate may allow foam concrete to be incorporated in the production of drycast products, such as lightweight block or other precast products. Lightweight concrete block appears to be an attractive application for foam concrete, as typical strength and density requirements may be readily met by conventional foam concrete mixes. However, foam concrete is highly flowable, and takes a long time to stiffen and set. Various researchers[2] have attempted to accelerate the curing of foam concrete, so that block moulds may be re-used within a matter of hours. However, this production rate does not compare to the efficiency of a drycasting process, where moulding and demoulding may be completed within a matter of seconds.

3) May Help Control Drying Shrinkage, Compared to Conventional Foam Concrete

Drying shrinkage is a major concern for foam concrete. Cure foam concrete fragments may be sufficiently inert to resist some early drying shrinkage.

4) Permits Recycling of Excavated Foam Concrete

Foam concrete is often desired for applications where future excavation may be necessary (trench reinstatement, fill projects, etc.). Finding a use for excavated foam concrete would be economically and environmentally beneficial.

5) Permits Re-use of Excess Batched Foam Concrete

Foam concrete is often used in applications where the total required volume is not certain, for example, in the annular grouting of pipes, delivery lines, and culverts, or in fill projects.

---

1 Fouad (2006) 562

2 Narayanan and Ramamurthy (2012) 144

Figure E.1.1 FCA crushed to varying particle sizes.

Developing a process for casting and grading mixed material provides an opportunity for excess cement-rich material to be reused efficiently.

E.2 Design Parameters for Foam Concrete Aggregate

The following design parameters may be considered and optimized in the production of foam concrete lightweight aggregate (listed chronologically in the process of producing FCA concrete):

- mix design of the lightweight aggregate;
- curing environment of the lightweight aggregate material;
- duration of curing time;
- particle size;
- stockpiling environment; and
- mix design of matrix.

Among these parameters, the mix design of the lightweight aggregate, particle size, and the mix design of the matrix are anticipated to be most significant.

Testing of conventional foam concrete gives insight into some of the properties of foam concrete aggregate, including density, mechanical properties, and freeze-thaw resistance.

Measurements of density, water reference content, and capillary water uptake may be reviewed in order to estimate appropriate moisture conditions for foam concrete aggregate included in wet or dry-cast mixes, to minimize segregation (refer to Section 6.3) or collapse of foam bubbles in contact with dry solids (refer to Section 7.1).

The interstitial void content between packed aggregate particles has important implications for mix design, as it indicates the volume proportion that must be filled by finer aggregate and cement paste. Evaluation of aggregate bulk density may be conducted in conformance with ASTM C29.[3]

[3] ASTM C29/C29M-17

Figure E.2.1 FCA in wet-cast mix.

Figure E.2.2 FCA in foam concrete matrix.

Figure E.2.3 FCA in no-fines mix.

Particle shape, angularity, and surface textures will affect the workability of FCA mixes. FCA mixes tend to be very harsh, due to interlocking of the porous aggregate surfaces.

FCA may be incorporated into drycast, wet-cast, or no-fines mixes. FCA may also be reconstituted within a foam concrete matrix. (Figures E.**2.1** to E.**2.3**.)

E.3 Production of Foam Concrete

Large quantities of foam concrete aggregate were produced for testing, as shown in Figure E.3.1. The manufacturing process was as follows:

1) A large volume of foam concrete is proportioned, mixed, and cast.
2) The foam concrete is permitted to harden
3) The foam concrete is 'excavated', crushed, and graded as a lightweight aggregate.

It is desirable to minimize the curing time of foam concrete aggregate, in order to speed production scheduling, minimize the area required for stockpiling, and to reduce the amount of energy required for crushing. It is also important to recover a large proportion of useful particle sizes during crushing.

Figures E.**3.1** to E.**3.3** show the aggregate particle size distribution of foam concrete samples broken at 1 day, 3 days, and 7 days. For these tests, twelve cylinders of 100x200mm were cast from the same batch, and seal-cured at 23±2°C. Four specimens were tested for compressive strength at each time interval. Immediately after failure, the broken pieces of each cylinder were forced through a 20 x 20mm square metal lattice, producing foam concrete aggregates with a particle size of 20mm or less. The particles were sieved in accordance with ASTM C136,[4] in order to evaluate their particle size distribution.

Variability in particle size distribution was greatest for samples crushed at Day 1. Furthermore, a large proportion of particles were smaller than 2.5mm. These small particles may be too small to contain closed air voids, and were deemed less desirable than

[4] ASTM C136/C136M-14. Cf. ASTM C330/C330M-14, Table 1

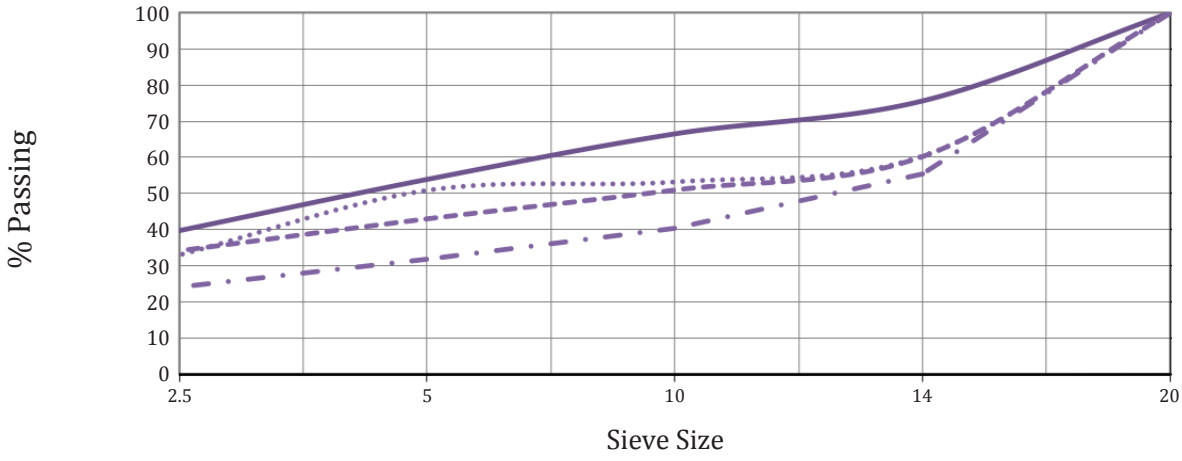

Figure E.3.1 Particle size distribution of FCA crushed after 1 day of curing.

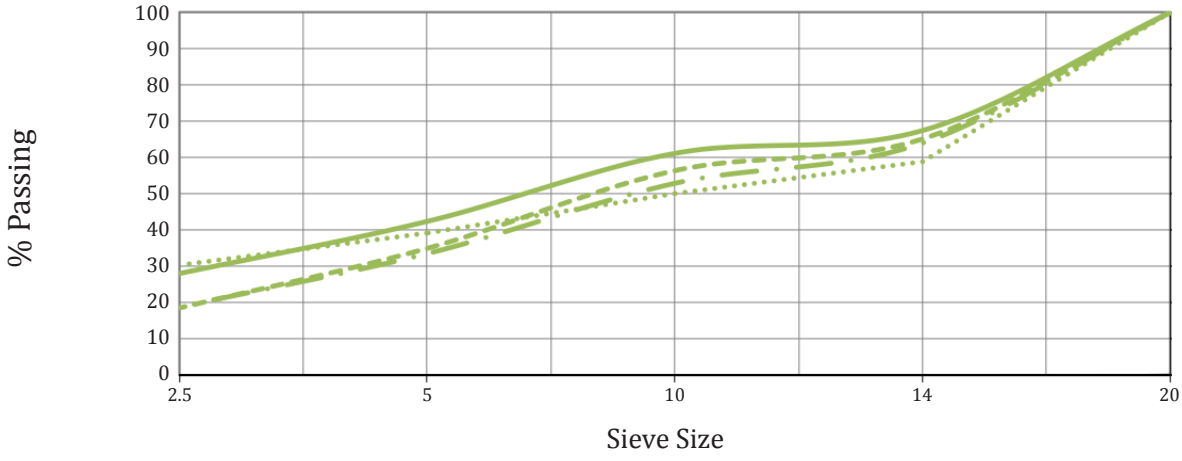

Figure E.3.2 Particle size distribution of FCA crushed after 3 days of curing.

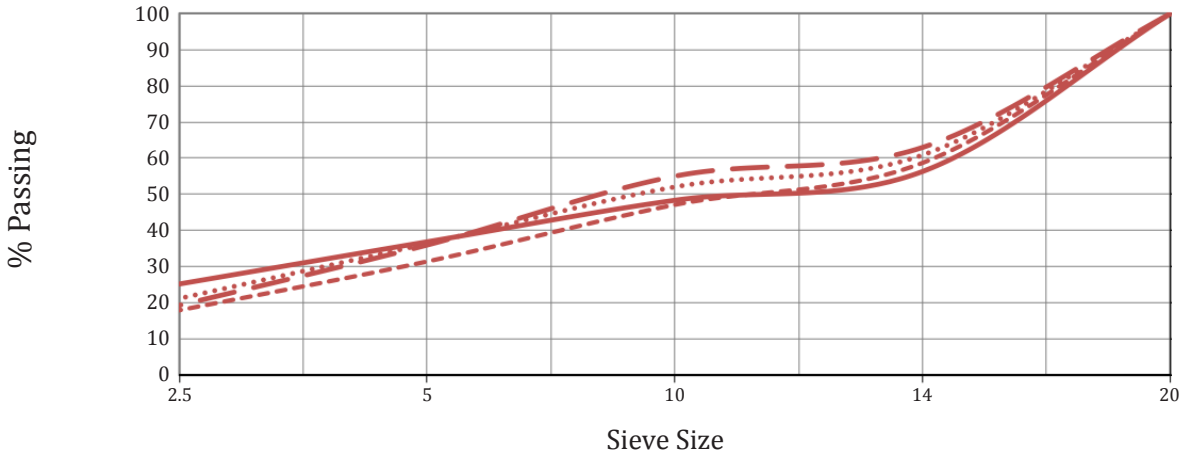

Figure E.3.3 Particle size distribution of FCA crushed after 7 days of curing.

larger particles. The Day 3 tests produced almost the same particle size distribution as the Day 7 tests, with similar variability in results. Presumably, a mix cured for three days will require less energy to crush, due to its slightly lower compressive strength; stockpiling time is also reduced.

Based on these preliminary results, crushing foam concrete after 3 days of curing may be favourable timing.

A large portion of fine material is evident in the Figures, which may limit the commercial viability of FCA. A large-scale jaw crusher was used for subsequent production.

E.4 Cementitious Density Calculations

For mixes that incorporate foam concrete lightweight aggregate, binder is present in both the aggregate and in the matrix. The total cementitious density, b_{total}, may be found according to the following equation:

$$b_{total} = b_{LWA}V_{LWA} + b_{matrix}V_{matrix}$$

where

b_{LWA} and b_{matrix} are the cementitious densities of the lightweight aggregate and matrix, respectively, and

V_{LWA} and $V_{matrix}$are the volume fractions of the lightweight aggregate and matrix, respectively.

In mix design, aggregate and matrix are often proportioned by mass, rather than by volume. Volume fractions of lightweight aggregate and matrix my be found according to the following equations:

$$V_{LWA} = \frac{\frac{M_{LWA}}{\rho_{LWA}}}{\frac{M_{LWA}}{\rho_{LWA}} + \frac{M_{matrix}}{\rho_{matrix}}} \qquad V_{matrix} = \frac{\frac{M_{matrix}}{\rho_{matrix}}}{\frac{M_{matrix}}{\rho_{matrix}} + \frac{M_{LWA}}{\rho_{LWA}}} = 1 - V_{LWA}$$

where

M_{LWA} and M_{matrix} are the mass proportions of the lightweight aggregate and matrix, respectively, and

ρ_{LWA} and ρ_{matrix} are the dry densities of the lightweight aggregate and matrix, respectively.

Particle sizes were kept sorted in separate containers, and air-cured until 28 days after creation, before being incorporated into lightweight mixes.

F

Fine Aggregate Grading Data

Fine aggregate used throughout the experimental program was natural sand, conforming to ASTM C33, Table 1, as well as the more stringent requirements of Ontario Provincial Standard Specification 1002, Table 1, Grading Requirements (LS-602) for Fine Aggregate. A typical sample is shown below.

Concrete Sand Sieve Analysis				Gradation Limits per OPSS 1002, Table 1[1]	
Sieve Size (mm)	Retained Weight	Cum. % Retained	% Passing	% Passing	
				Coarse	Fine
9.5	0.0	0.0%	100.0%	100%	100%
4.75	10.3	0.9%	99.1%	95%	100%
2.36	137.9	12.1%	87.9%	80%	100%
1.18	400.0	35.2%	64.8%	50%	85%
0.6	707.6	62.2%	37.8%	25%	60%
0.3	966.2	85.0%	15.0%	10%[2]	30%
0.15	1062.2	93.4%	6.6%	0%	10%
0.075	1114.1	98.0%	2.0%	0%	3%
PAN	1136.3	99.9%	0.1%	n/a	n/a
Fineness Modulus =		2.89		3.1	2.3

Table F.1 Typical sieve analysis of natural sand used in experimental program.

[1] Note: Fine aggregate shall have no more than 45% passing and sieve and retained on the next consecutive sieve.

[2] ASTM C33/C33M-14, Table 1 allows 5-30% passing through the 0.3mm sieve.

G

Surfactant Specifications

Specifications for the surfactant used throughout the experimental program are given in the table below.

Identification

Supplier	Cellular Concrete Technologies LLC
Product name[1]	Stable Air® Class A Foam Concentrate
Synonyms[2]	Protein foam concentrate
Certifications[3]	ASTM C260/260M AASHTO M 154

Physical Characteristics[4]

Appearance	Golden brown liquid
Odor	Similar to orange blossoms
Specific gravity	1.10 @ 15°C

1 Cellular Concrete Technologies (2013b) 1
2 Cellular Concrete Technologies (2013b) 1
3 TEC Services Inc. (2011).
4 Cellular Concrete Technologies (2013a) 3

Chemical Characteristics[5]

Solubility in water	100%, forms foam
pH	8.0
Evaporation rate	<1 (Butyl Acetate = 1.0)
Environmental fate	Readily biodegradable

Composition[6]

Component	*% by weight*
Alpha-olefin Sulfonate Solution	60 – 80
2,4-pentanediol, 2-methyl-	10 – 30
Water	<6
Lauryl alcohol	1 – 5
d-liomonene	0.5 – 5

Table G.1 Specifications for surfactant used in experimental program.

[5] Cellular Concrete Technologies (2013a) 3-4, Cellular Concrete Technologies (2013b) 4
[6] Cellular Concrete Technologies (2013a) 1

H

Foam Generator Specifications

Details for the foam generator used throughout the experimental program are given below.

Identification

Supplier	Cellular Concrete Technologies, LLC
Model number	M100

Inputs

Electricity	Single Phase, 120V, 15 Amps, Grounded NEMA 5-15
Water	5 gal/min @ 40-60 psi (19 L/min @ 280-410 kPa) Garden Hose Thread: ¾" Dia. w/ 11.5 TPI
Air	10 cfm @ 120 psi (280 L/min @ 830 kPa) Standard ¼" Air Hose Coupler (Military specification MIL-C-4109)
Surfactant dilution rate[1]	1 : 120

Foam Output

Foam specific density[2]	0.068 – 0.070 (68-70 g/L)
Stated flow rate[3]	7.43 ft^3/min (3.51 L/s)

Table H.1 Details for foam generator used in experimental program.

1 Cellular Concrete Technologies (2011) 2
2 The intended foam density is engraved on foam generator.
3 Cellular Concrete Technologies (2012)

I

Equivalent Water-Binder Ratios Including Foam Dilution Water

As explained in Section 6.1.1.6, water-binder ratios cited throughout the experimental program do not include the contribution of the dilution water from the foam. Dilution water is assumed to be necessary for the stability of the foam, and thus does not contribute directly to the wetting and workability of the mix, and does not contribute immediately to the hydration water available to the cement particles.

Defining water-binder ratios in terms of the total cementitious content of a mix is expedient in a commercial setting. However, some studies may choose to include the dilution water when reporting water-binder ratios. For example, ASTM Standard C796[1] proposes that a water-cement ratio of 0.58 may be used as a starting point for mixes with Type I cement, and includes the weight of the foam in this value.

For comparative purposes, the water-binder ratio including the contribution of dilution water from the foam, w/b', may be calculated as

$$w/b' = \frac{w + f \cdot \left(1 - \frac{s}{d}\right)}{b}$$

[1] Cf. ASTM C796/C796M-12, Section 8.4.3.1

where

w is the mass of mix water per cubic meter of wet concrete;

f is the mass of foam per cubic meter of wet concrete;

$\frac{s}{d}$ is the ratio of surfactant to dilution water; and

b is the mass of cementitious content per cubic meter of wet concrete.

Typically, the ratio of surfactant to dilution water is small enough that the multiplier $\left(1 - \frac{s}{d}\right)$ may be neglected in the calculation.

A comparison of water-binder ratios, including and excluding the contribution of dilutions water from the foam, is shown in the table below for reference, for mixes with cementitious density of 410kg/m^3. Equivalent water-binder ratios closest to the ASTM Standard C796 value of 0.58 are shown in bold.

Water-binder ratio, excluding contribution of dilution water (as specified throughout thesis document)	Water-binder ratio, including contribution of dilution water			
	Filler-binder ratio			
	0:1	**1:1**	**2:1**	**3:1**
0.45	**0.56**	0.54	0.51	0.49
0.50	0.61	**0.58**	**0.56**	0.53
0.55	0.66	0.63	0.61	**0.58**
0.60	0.70	0.68	0.65	0.63
0.65	0.75	0.72	0.70	0.67
0.70	0.80	0.77	0.74	0.72
0.75	0.84	0.82	0.79	0.77

Table I.1 Comparison of nominal water-binder ratios, and equivalent water-binder ratios that include contribution of dilution water.

J

Method for Calculating Specimen Volume Gravimetrically

Precise volumetric measurements were required for numerous aspects of the experimental program, including measurements of porosity and dry density (refer to Section 5.2.1), segregation (Section 5.3.2), drying rates (Section 5.5.1), moisture storage (Section 5.5.2), and degree of saturation for freeze-thaw testing (Section 5.7.1). For these tests, specimen volumes were determined gravimetrically, through the displacement of water. This approach was found to be precise and consistent. The methodology is described below, and the experimental setup is shown in Figure J.**1**.

Step 1 A foam concrete specimen is saturated, so that water will not be absorbed into the specimen during measurement. Vacuum saturation is ideal (refer to Section 5.2.1), but long-term immersion is acceptable for saturation of voids near the specimen surface. The specimen is stored in a water-filled vessel.

Step 2 A second, empty vessel is placed on a weigh scale, accurate to within 0.1% of the specimen mass. A third vessel with a spigot is placed on a stable surface and directed such that water from the spigot will flow into the second vessel without splashing.

Step 3 The third vessel is filled above the spigot opening, with distilled water that has been conditioned to the ambient temperature of the lab. Water drains into the second vessel, until the third vessel is full to the brim of the spigot. The weigh scale is tared.

Step 4 The specimen is rapidly removed from underwater using tongs. Tongs with minimal wetted surface area are preferred.

Step 5 The specimen is permitted to drip, briefly, eliminating excess water from the specimen surface. (Wiping the specimen with a moist cloth was also evaluated as an alternative methodology; however, allowing excess water to drip produced more consistent results.)

Step 6 The specimen is totally immersed in the third, water-filled vessel. Displaced water flows through the spigot into the second vessel. Since the tongs are wetted during immersion of the specimen, they are hung above the third vessel to capture any water that drips from their surface. The mass of the water displaced by the specimen is recorded.

Step 7 The mass of the displaced water is converted into a volume measurement, based on the density of distilled water at the ambient lab temperature.

Step 8 The process is repeated three times.

Results for the same specimen should be within 0.5%. With practice, coefficients of variation of better than 0.3% are consistently achievable (refer to Figure J.**2**). Specimen volume is taken as the average of three results.

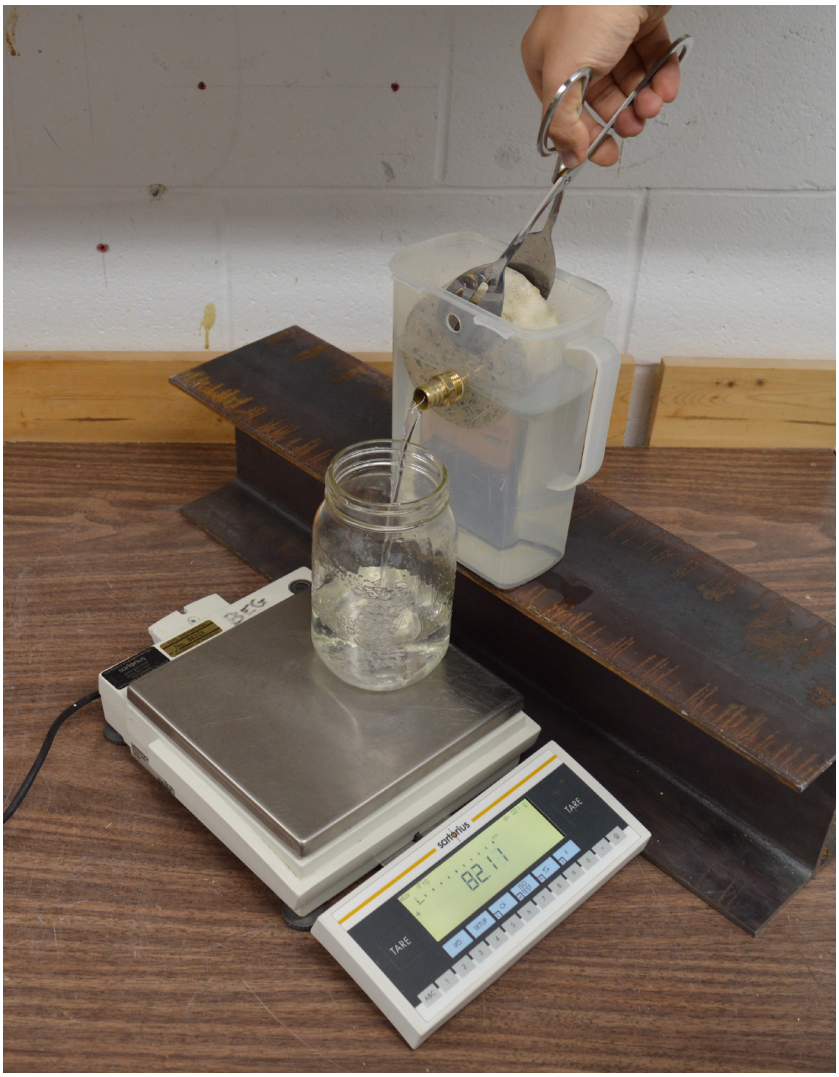

Figure J.1 Determination of volume by displacement.

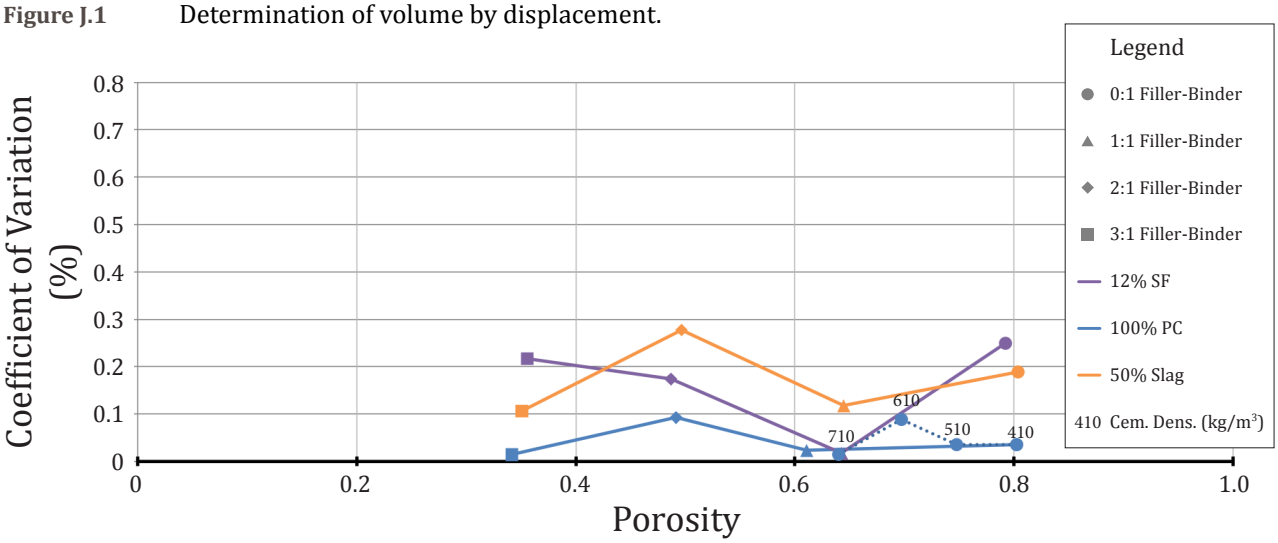

Figure J.2 Coefficient of variation among volume measurements for a variety of specimens. Results are typical.

K

Method for Calculating Theoretical Porosity Values

Theoretical porosity, P, may be estimated as the sum of the proportion of air void, A, and the proportion of capillary voids, C, in a mix. Voids due to shrinkage cracking were not considered for the purposes of estimating porosity.

$$P = A + C$$

The proportion of air void, A, may be derived from the volume of foam in liters per cubic meter of mix, V_{foam}, calculated as described Appendix D.

$$A = \frac{V_{foam}}{1000\ L/m^3}$$

The volume of capillary voids in the mix, C, may be taken as the volume of water in a sample that is not chemically bound within the reaction products.

The mass of uncombined water in a mix is equal to the mass of mix water, w, less the amount of chemically bound water, w_{comb}:

$$w_{uncomb} = w - w_{comb}$$

Assuming that the mass of hydrated binder reaction products will be 1.2 times the mass of the unhydrated binder, in accordance with ASTM C567,[1] the mass of chemically bound

[1] ASTM C567/C567M-14, Section 9.1

water in the mix at 28 days is proposed to be 0.2 times the mass of the binder, b. For Portland cement, this value is equivalent to a degree of hydration of between 75 and 80%, since complete hydration would require an amount of water equal to 0.26 times the mass of the binder.[2]

$$w_{comb} = b \cdot 0.2$$

Thus, the mass of uncombined water may be taken as

$$w_{uncomb} = \left(\frac{w}{b}\right) \cdot b - (b \cdot 0.2)$$

$$= \left(\frac{w}{b} - 0.2\right) \cdot b$$

Subsequently, the volume of capillary voids, which is the volume of chemically unbound water, may be determined in relation to the total cementitious density, b', and the density of water, ρ_{water}.

$$C = \frac{\left(\frac{w}{b} - 0.2\right) \cdot b'}{\rho_{water}}$$

Thus, theoretical porosity, P, may be calculated via the following equation:

$$P = \frac{V_{foam}}{1000\ L/m^3} + \frac{\left(\frac{w}{b} - 0.2\right) \cdot b'}{\rho_{water}}$$

where

V_{foam} is the volume of air void per cubic meter of mix,

$\frac{w}{b}$ is the water-binder ratio,

b' is the total cementitious density, in kg/m^3, and

ρ_{water} is the density of water, in kg/m^3.

[2] Powers (1949). Cf. Young et al. (1998) 221

L

Method for Calculating Theoretical Oven-Dry and Dry Densities

Oven-Dry Density

Oven-dry density for structural lightweight concrete is defined in ASTM C567[1] as the density of a specimen after being placed in a drying oven at 110 ± 5 °C, until constant mass. The following sections consider the contribution of solid materials, degree of hydration, and volume of surfactant to the oven-dry density of a hardened foam concrete sample.

Contribution of Solid Materials, and Degree of Hydration

Where the material composition of a structural lightweight concrete mix is known, ASTM C567[2] proposes the following equation for determining the oven dry density of the mix, O_c:

$$O_c = (M_{df} + M_{dc} + 1.2M_{ct})/V$$

where

M_{df} is the mass of dry fine aggregate,

M_{dc} is the mass of dry coarse aggregate,

---

1 ASTM C567/C567M-11, Section 3.2.2.

2 ASTM C567/C567M-11, Section 9.1, Equation 5.

M_{ct} is the mass of cement, and

V is the volume of concrete produced.

The factor 1.2 helps to approximate the mass of cement plus chemically combined water, at 28 days. Thus, the mass of the chemically combined water is assumed to be 0.2 times the mass of the binder. According to Powers,[3] in a fully hydrated Portland cement mix, the mass of chemically combined water will be 0.26 times the binder. By implication, ASTM C567 assumes that the degree of hydration of a Portland cement mix at 28 days, α_{28}, will be between approximately 77%:

$$\alpha_{28} = \frac{0.2}{0.26} = 76.9\%$$

Thus, the oven-dry density equation may be expressed as

$$O_c = (M_{df} + M_{dc} + (1 + 0.26\alpha) \cdot M_{ct})/V$$

where α is the degree of hydration.

Note that any moisture content in solid materials must be taken into account, in order to accurately predict oven-dry mass. Refer to the Section, "Mix proportioning: Sand Moisture Content" in Appendix D.

Contribution of Foam Surfactant

The mass of surfactant in a cubic meter of foam, M_{surf}, may be calculated as follows:

$$M_{surf} = (\rho_{foam}) \cdot \frac{V_{surf} \cdot SG_{surf}}{(V_{water} \cdot SG_{water}) + (V_{surf} \cdot SG_{surf})}$$

where

ρ_{foam} is the density of the foam,

V_{surf} and V_{water} are the volumes of surfactant and water, respectively, and

SG_{surf} and SG_{water} are the specific gravity of surfactant and water, respectively.

Since the volume of surfactant is small,

$$M_{surf} \approx (\rho_{foam}) \cdot \frac{V_{surf} \cdot SG_{surf}}{V_{water} \cdot SG_{water}}$$

$$\approx (\rho_{foam}) \cdot DR \cdot SG_{surf}$$

[3] Powers (1949). Cf. Young et al. (1998) 221

where DR is the dilution rate of the surfactant.

The foam generator used in the experimental program produces foam with a density of 70 kg/m^3,[4] for a dilution rate of 1:120.[5] The specific gravity of the unfoamed surfactant is 1.10 at 15°C.[6] Thus,

$$M_{surf} \approx 70\frac{kg}{m^3} \cdot \left(\frac{1}{120}\right) \cdot 1.1$$

$$\approx 0.64\frac{kg}{m^3}$$

Evidently, the contribution of the surfactant to the mass of a hardened sample is negligible, even when a large proportion of the volume of a mix is foam.

Dry Density ('Equilibrium Density')

Equilibrium density for structural lightweight concrete is defined in ASTM C567[7] as the density of a specimen after exposure to a relative humidity of 50 ± 5% and a temperature of 23 ± 2°C, until constant mass. According to Note 1 of Section 5, extensive testing of lightweight aggregate mixes has shown that equilibrium density may be estimated by adding 50 kg/m^3 to the oven dry density of a sample. Apparently, the initial moisture content of the mix is not a significant factor in the final equilibrium density for lightweight aggregate concrete mixes.[8]

Based on the experimental program, the equilibrium moisture content of foam concrete at 50% RH appears to be somewhat less. EMC at 50% RH was a low as 21 kg/m^3 for neat cement mixes, increasing to as high as 43 kg/m^3 for denser mixes with a filler-binder ratio of 3:1 (refer to Figure 6.**12f**). .

Tests in Section 6.12 have shown that, for a given storage environment, moisture content appears to increase with an increase in volume of sorbing paste (refer to Figure 6.**12h**). Mixes with a higher water-binder ratio will have a lower air-void volume, resulting

4 The intended foam density is engraved on foam generator. Cf. Appendix H.
5 Cellular Concrete Technologies (2011) 2. Cf. Appendix H.
6 Cellular Concrete Technologies (2013a) 3. Cf. Appendix G.
7 ASTM C567/C567M-11, Section 3.2.1.
8 Cf. ACI 213R-12, Section 4.4.2.

in a higher volume of sorbing paste with a greater volume of capillary voids, for the same dry density. Thus, for a given environment, the moisture content in a hardened specimen may be expected to increase with a higher initial water-binder ratio.

To account for this effect, equilibrium density may be estimated by assuming that a certain proportion of free water in a mix is retained in the hardened sample at equilibrium conditions. In Figure **L.1**, known equilibrium densities at storage in 50 and 80% RH are expressed as a percentage of mix free water, and plotted against porosity. From the plot, it appears that approximately 20% of free water is retained at 50% RH, and between approximately 50 and 70% of free water is retained at 80% RH. (Further discussion of sorption patterns is available in Section 6.12.)

The calculated 'dry density' values used in Figure 6.**6.1.2a** assumes that 40% of free water is retained in each hardened specimen, which provides a reasonable preliminary estimate of density for in-service conditions.

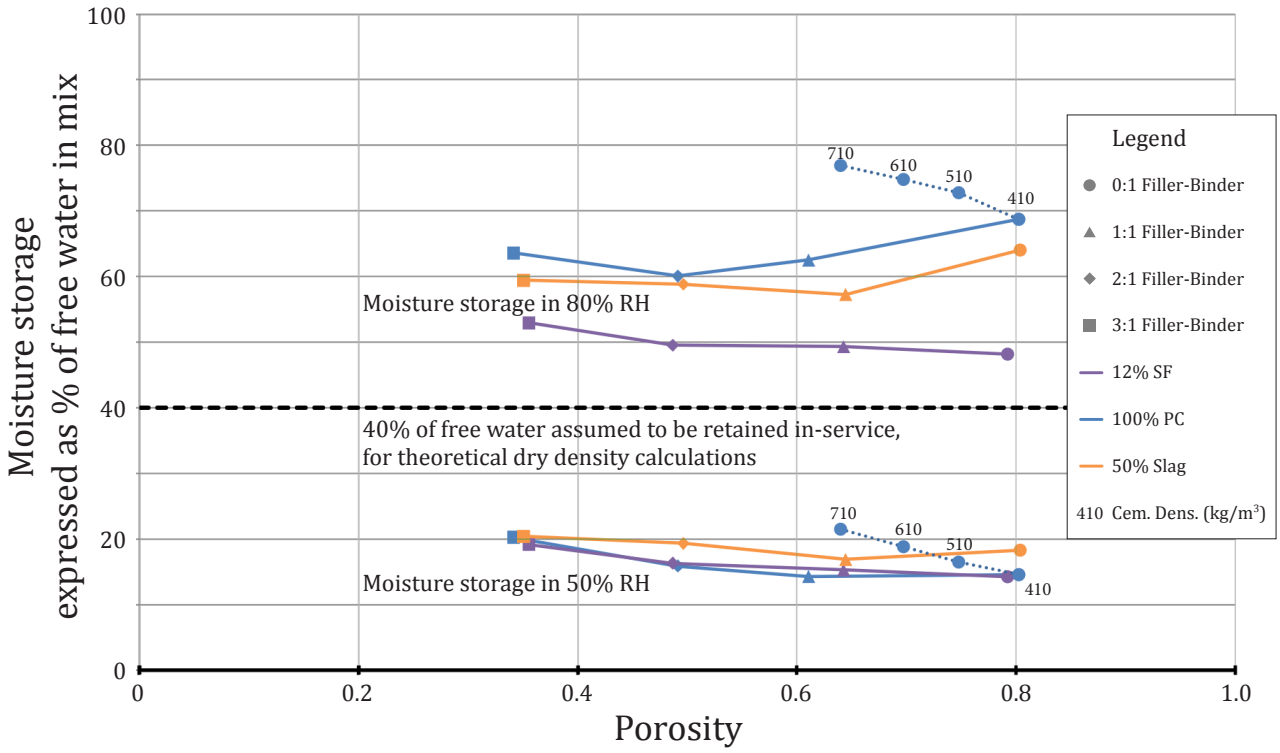

Figure L.1 Moisture storage of specimens in 50% and 80% RH, expressed as a percentage of mix free water. A degree of hydration of 80% has been assumed.

M

Record of Alternative Testing Methodologies

A number of testing methodologies were developed or considered during the course of this research, which were ultimately not used for the results presented in Chapter 6. These alternative methodologies are documented here as a reference.

Specifically, this Appendix records contemplated methodologies for conducting creep testing (M.1), for calculating rates of capillary water uptake (M.2), for conditioning freeze-thaw specimens (M.3), for preparing salt scaling tests (M.4), and for measuring the abrasion of fresh foam concrete in a delivery line (M.5).

M.1 Creep Testing

Creep testing in the experimental program was conducted using a steel loading frame, as described in Section 5.4.5 and as shown in Figures 5.**4.5a** and 5.**4.5b**. Compressive force was applied to the specimens by tightening nuts against stacks of disc springs, designed for the intended loads. The nuts were tightened at regular intervals to accommodate creep deformation of the specimens.

An alternative creep apparatus was also considered. The apparatus used a lever arm and a mass to apply a constant gravity load, as shown in Figure M.**1.1**. Cylinders, prepared as per Section 5.4.5, were intended to be installed in the device as follows:

> Place the cylinder stack in the apparatus shown in Figure M.**1.1**. Temporarily support the steel lever arm shall be with a hydraulic jack, to permit alignment of the composite cylinder within the apparatus. Measure the gauge length of each cylinder with a DEMEC strain gauge. Then, place the concrete mass on the end of the lever arm, and lower the hydraulic jack in a controlled manner, increasing the load on the cylinder stack over a period of 5 ± 1 seconds. The applied load shall not be greater than 40% of the compressive strength of weakest sample.
>
> The creep testing shall occur inside an environment maintained at a temperature of 23 ± 2 °C, and relative humidity of 50 ± 4%. The two remaining cylinders for each mix shall be used as control samples and placed in the same environment as the loaded samples, to observe the length change due to drying shrinkage. Each control sample and loaded sample will be measured using a DEMEC strain gauge according to the following schedule, following loading of the samples:
>
> - immediately
> - daily until the end of the first week
> - weekly until the end of the first month
> - monthly until the end of the sixth month

The lever-arm creep apparatus has an advantage in maintaining constant loading without requiring routine adjustment. However, the smaller scale of the disc spring creep apparatus proved to be more convenient during the experimental program. The smaller testing apparatus allowed testing to be conducted in a climate control chamber with more tightly controlled conditions.

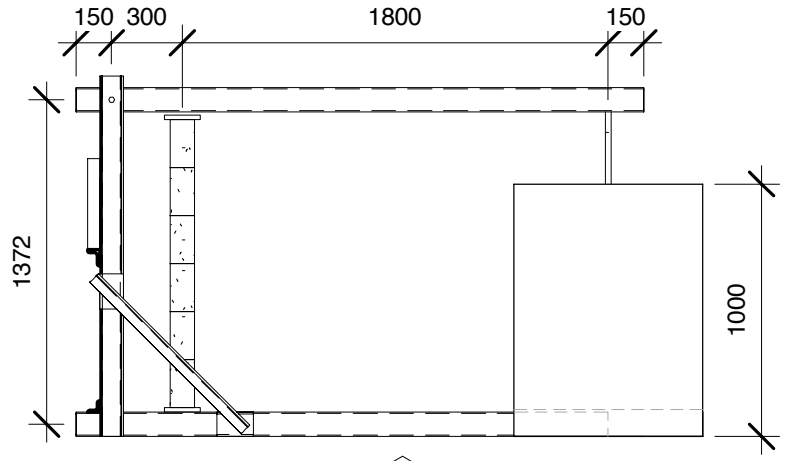

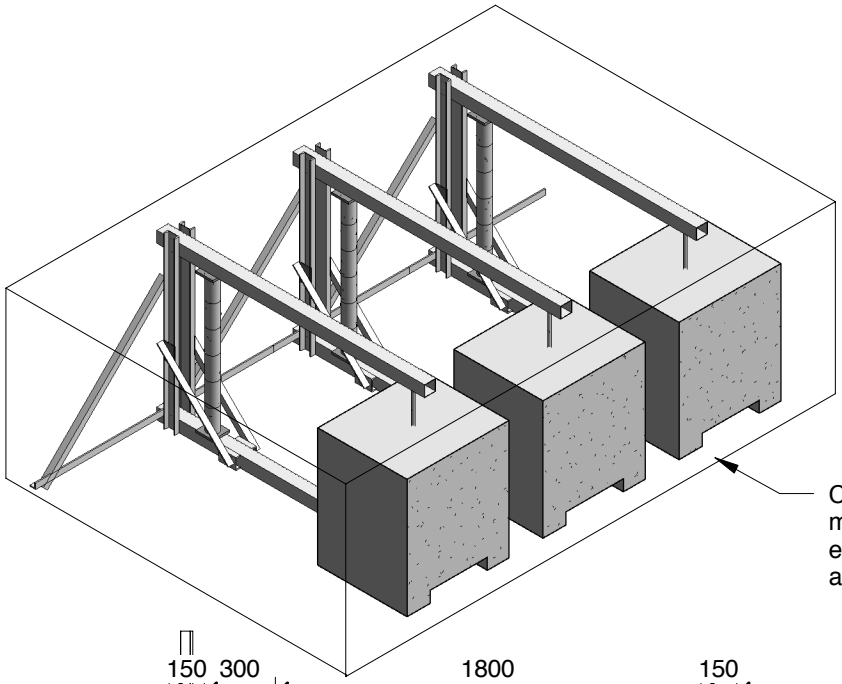

Creep apparatus to be maintained in conditioned environment of 23 ± 2 °C, and 50 ± 4% RH

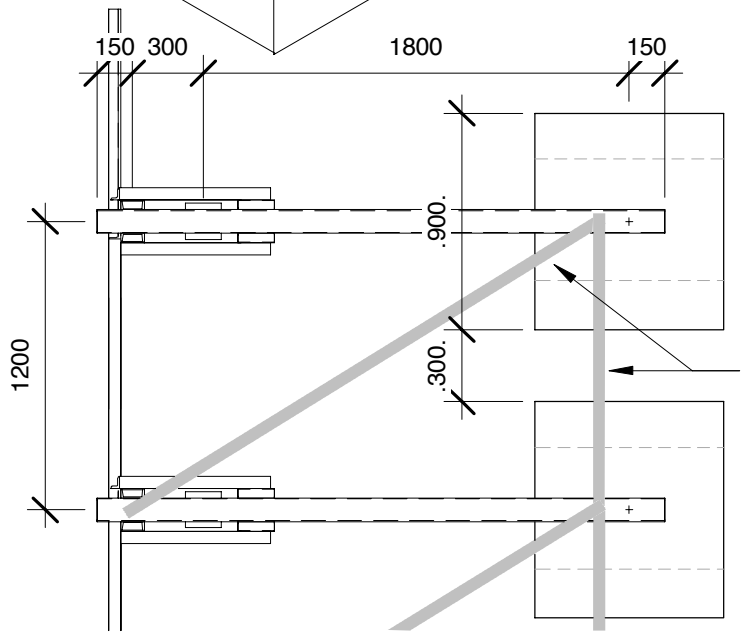

Additional steel straps for resisting torsion about steel column

M.2 Capillary Water Uptake Rates

Capillary water uptake is normally plotted as the accumulation of water mass in a specimen per unit area of the immersed surface, against the square root of time. Such plots are shown throughout Section 6.14. Testing standards describe diverse approaches to expressing water absorption as a coefficient.

The accumulated mass of water per unit area, Δm_t, is generally calculated as

$$\Delta m_t = \frac{m_t - m_i}{A}$$

where

Δm_t is the accumulated moisture from the start of the test until time 't',

m_t is the mass of the sample at time 't',

m_i is the mass of the sample at the start of the test, and

A is the area of the immersed surface.

Where plotted points describe a line, ISO 15148[1] proposes that the water absorption coefficient, A_w, may be given as

$$A_w = \frac{\Delta m'_{tf} - \Delta m'_0}{\sqrt{t_f}}$$

where

$\Delta m'_0$ is the value of Δm where a line of best fit cuts the vertical axis,

$\Delta m'_{tf}$ is the value of Δm on the line of best fit at time t_f, and

t_f is a time at or before a 'nick-point time.' The nick-point time is taken to be the time at which the rate of water uptake per root time decreases due to initial saturation of the entire volume of the sample.

According to ASTM C1585,[2] rates of absorption should be determined both before and after this clear change in slope.

If the plotted points described a curve, ISO 15148[3] recommends calculating a water absorption coefficient, $A_{w,24}$, as the accumulated water mass per unit area at 24 hours,

---

1 Refer to ISO 15148 (2002), Section 8.

2 ASTM C1585-13

3 Refer to ISO 15148 (2002), Section 8.

$\Delta m_{t,24}$, divided by the square root of 24 hours (or 86400 seconds):

$$A_{w,24} = \frac{\Delta m_{t,24}}{\sqrt{86400\ \text{s}}}$$

Conversely, ASTM C1794,[4] *Standard Test Methods for Determination of the Water Absorption Coefficient by Partial Immersion*, intended for evaluation of "the rate of absorption of water due to capillary forces for building materials in contact with normal or driving rain above grade," recommends calculating a water absorption coefficient for non-linear graphs at 4 hours, rather than 24 hours.

Finally, ASTM C1585,[5] *Standard Test Method for Measurement of Rate of Absorption of Water by Hydraulic-Cement Concretes*, suggest that "if the data [...] do not follow a linear relationship (a correlation coefficient of less than 0.98) and show a systematic curvature, the [...] rate of water absorption cannot be determined."

Low-density foam concrete specimens exhibited non-linear patterns of capillary water uptake (refer to Section 6.14). The calculation methodology strongly influences the reported water absorption coefficient, as shown in Figure M.**2.1**.

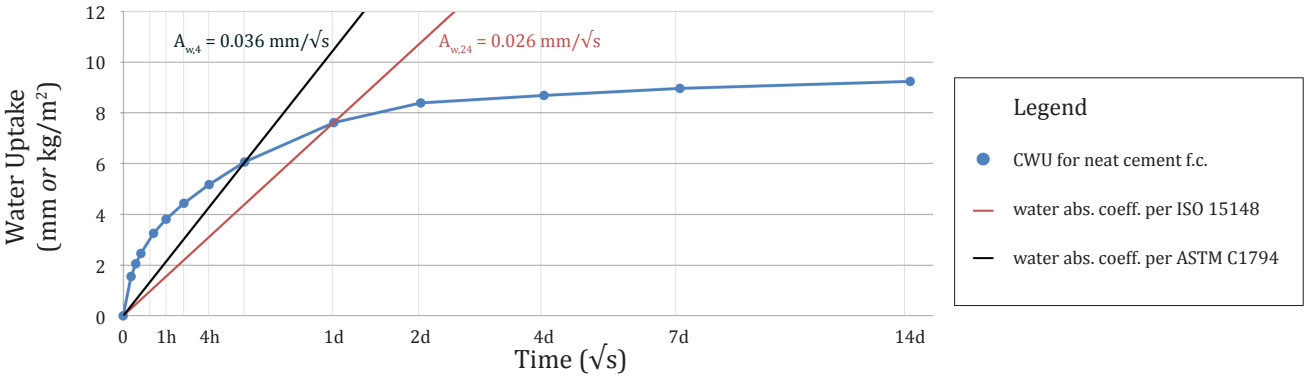

Figure M.2.1 Non-linear CWU of neat Portland cement specimen, after conditioning at 50°C for three days. The reported coefficient varies according to the convention of the testing methodology.

To facilitate convenient comparison with other data, test results in Section 6.14 were reported in several ways: as an uptake coefficient during initial stabilization (Figure 6.**14g**); as an early uptake coefficient after stabilization (Figure 6.**14h**); as an accumulation of moisture in 50mm thick specimens after 24 hours (Figure 6.**14i**); and as an accumulation of moisture after 14 days (Figure 6.**14j**).

4 ASTM C1794-15, Section 9.5
5 ASTM C1585-13,

M.3 Conditioning Freeze-Thaw Specimens

Freeze-thaw specimens in Section 6.16.1 were conditioned by immersion in liquid water, prior to placement in a freeze-thaw bath. This process is described in Section 5.7.1.

Wetting specimens by means of vacuum saturation was considered as an alternative, but was rejected since this process would likely distribute moisture throughout the pore structure of the foam concrete in a way that was not representative of normal moisture ingress in foam concrete in the field (refer to Figures 6.**16.1k** to 6.**16.1m**). Note as well that oven drying, which is normally completed prior to vacuum saturation,[6] could cause meaningful changes to the microstructure of the foam concrete, affecting subsequent moisture distribution (refer to Figures 6.**13c**, 6.**14l**, 6.**14m**, and 6.**14n**).

Refer to the discussion at the end of Section 6.16.1 for additional considerations.

M.4 Salt Scaling Testing

Test Method LS-412 from the Ministry of Transportation, Ontario[7] is used for measuring the saline freeze-thaw scaling of normal density concrete exposed to de-icing salts. This test method was attempted on foam concrete panels, but was found to be unsuitable. The attempted procedure is summarized below:

> After the foam concrete panels are cured, prepare a softwood dyke for each panel, painted with a latex paint to limit water absorption. Glue the dyke to the sides of each panel, as shown in Figure M.**4.1**. The dykes shall extend 25mm above the top surface of each panel. Apply sealant around the perimeter of the panel to prevent surface water from leaking at the joint between the panel and the dyke, per Figure M.**4.2**.
>
> Pour a solution of 3% sodium chloride over the surface of each panel to a depth of approximately 6mm. Store the panels in a freezing environment of −18 ± 2°C, supported on wooden strips to permit free circulation of cold air, for between 16 and 18 hours. After this time, permitted the panels to thaw for 6 to 8 hours in a

[6] Fagerlund (1977)
[7] MTO LS-412 (1997). Cf. OPSS 1352 (1989).

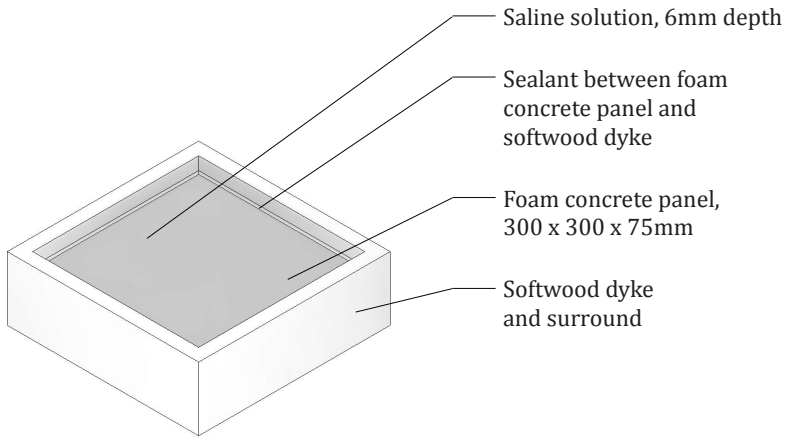

Figure M.4.1 Isometric drawing of foam concrete panel with softwood dyke and surround.

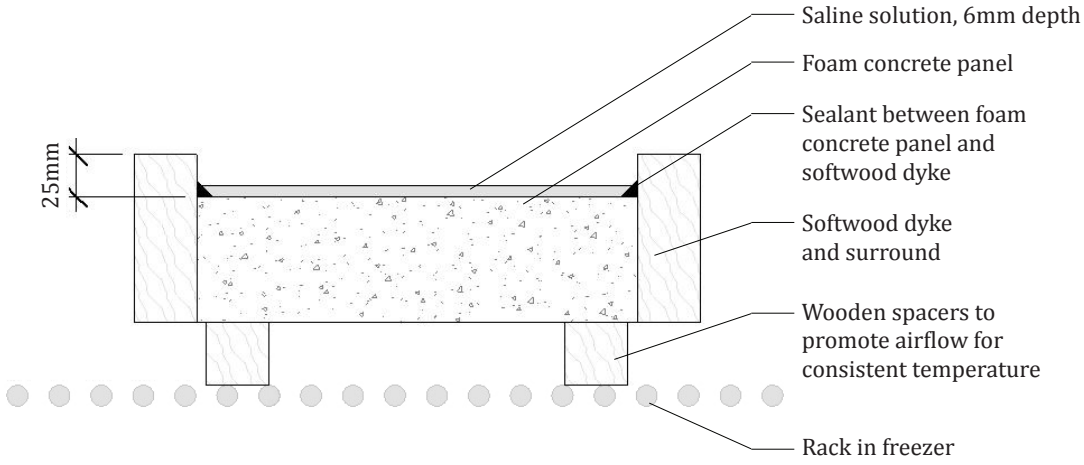

Figure M.4.2 Section through foam concrete panel with softwood dyke and surround, based on MTO Test Method LS-412.

condition of 23 ± 2°C and a relative humidity between 45 and 65%. Add aqueous solution as required to maintain a 6mm depth, before returning the samples to the freezing environment for the next cycle.

After five freeze-thaw cycles, wash any loose flakes and particles of concrete from the surface of each panel. Collect the particles in a funnel of filter paper. Oven-dry the particles at 105°C until constant mass, and record this value as the loss of mass from the panel.

Reapply a solution of 3% sodium chloride to the washed panels, before recommencing the next series of freeze-thaw cycles. Specimens are to be kept frozen in the event of any interruption to the daily cycling.

Results of the test are shown in Figures M.**4.3** and M.**4.4**, alongside test results reported from Chapter 6. After 15 cycles, the high capillarity of the foam concrete, combined with freeze-thaw deterioration at the edges of the panels, made it difficult to retain water on the surface of the panels. Testing was terminated, and a new test strategy devised, as described in Section 5.7.2.

The rate of loss of mass and depth was lower for the dyked panel testing, than for the tests from Section 5.7.2. This trend may be a consequence of the difficulty of maintaining a 6mm deep layer of water on the dyked panels; or may indicate that the testing conditions of Section 5.7.2 are especially harsh.

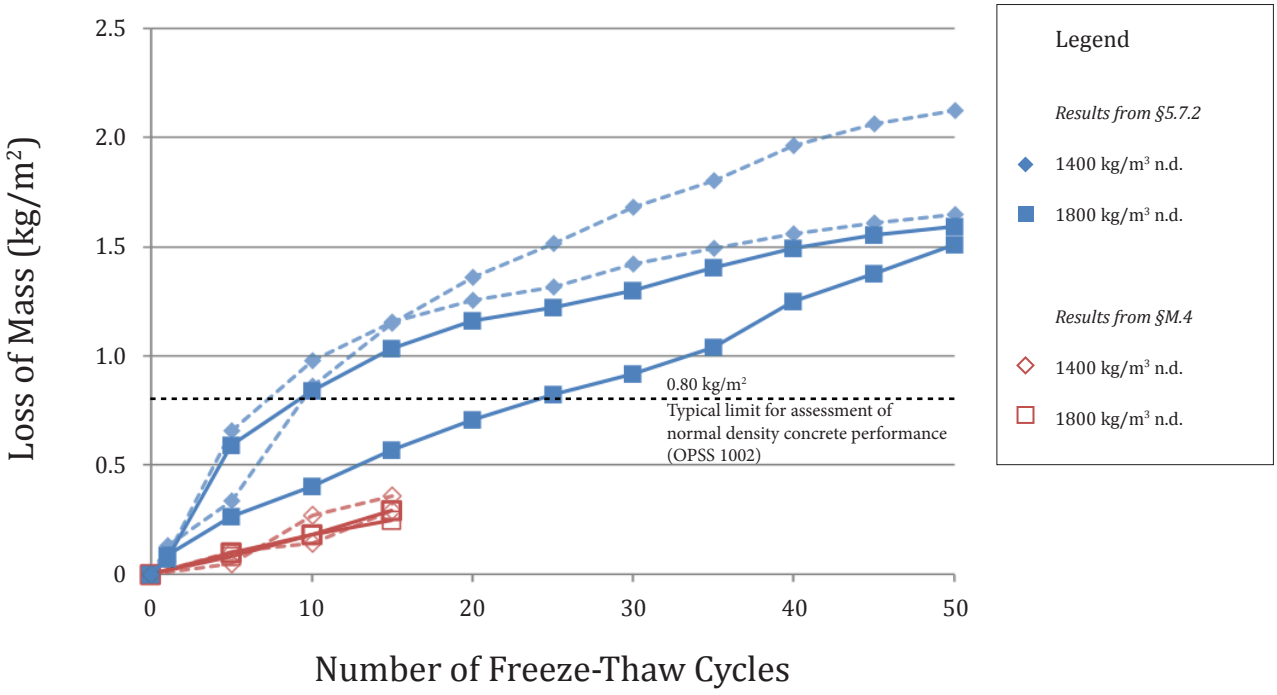

Figure M.4.3 Loss of mass due to saline freeze-thaw scaling. Refer also to Figure 6.**16.2a**.

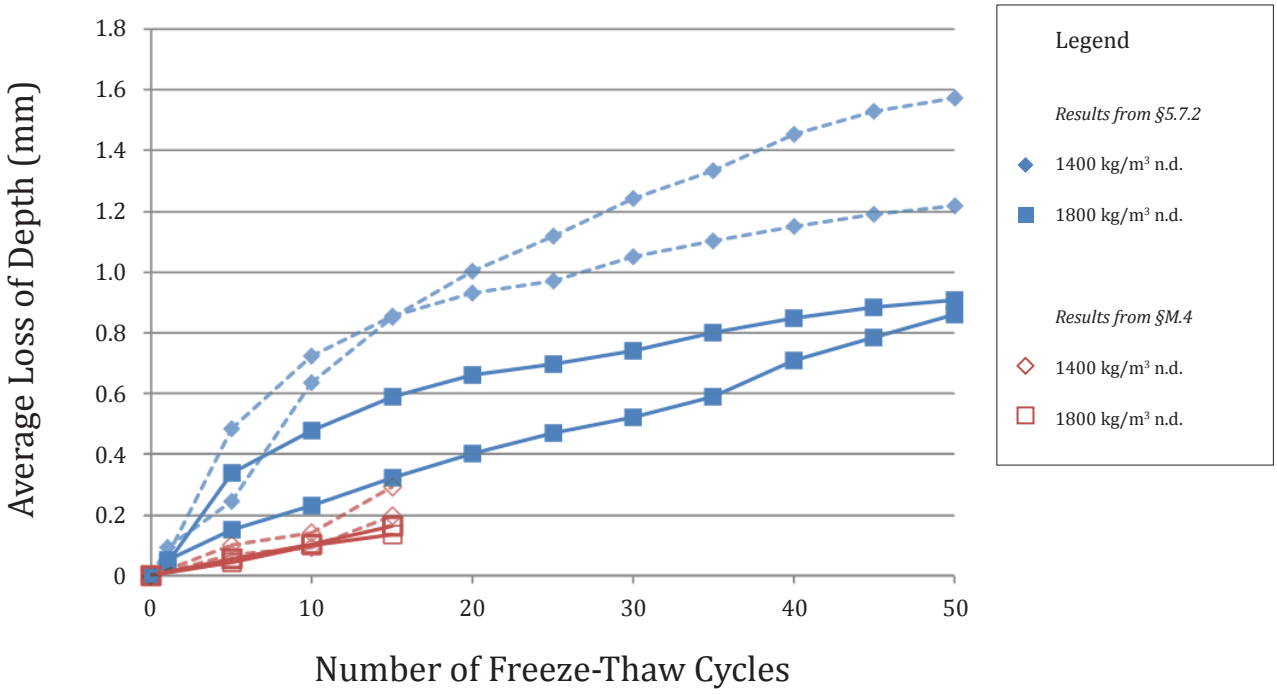

Figure M.4.4 Average loss of depth due to saline freeze-thaw scaling. Refer also to Figure 6.**16.2b**.

M.5 Measuring Abrasion of Foam Concrete in Delivery Pipe

During the course of the research, a mining client wished to know the rate of pipe wear that could be anticipated for fresh foam concrete in vertical delivery lines. A double toroid wheel was designed, as shown in Figures M.**5.1** to M.**5.3**. Proposed operation was as per Figure M.**5.4**. The apparatus was not built.

Calculations for the structure, mechanics, power, and operation of the toroid wheel are available from the author upon request.

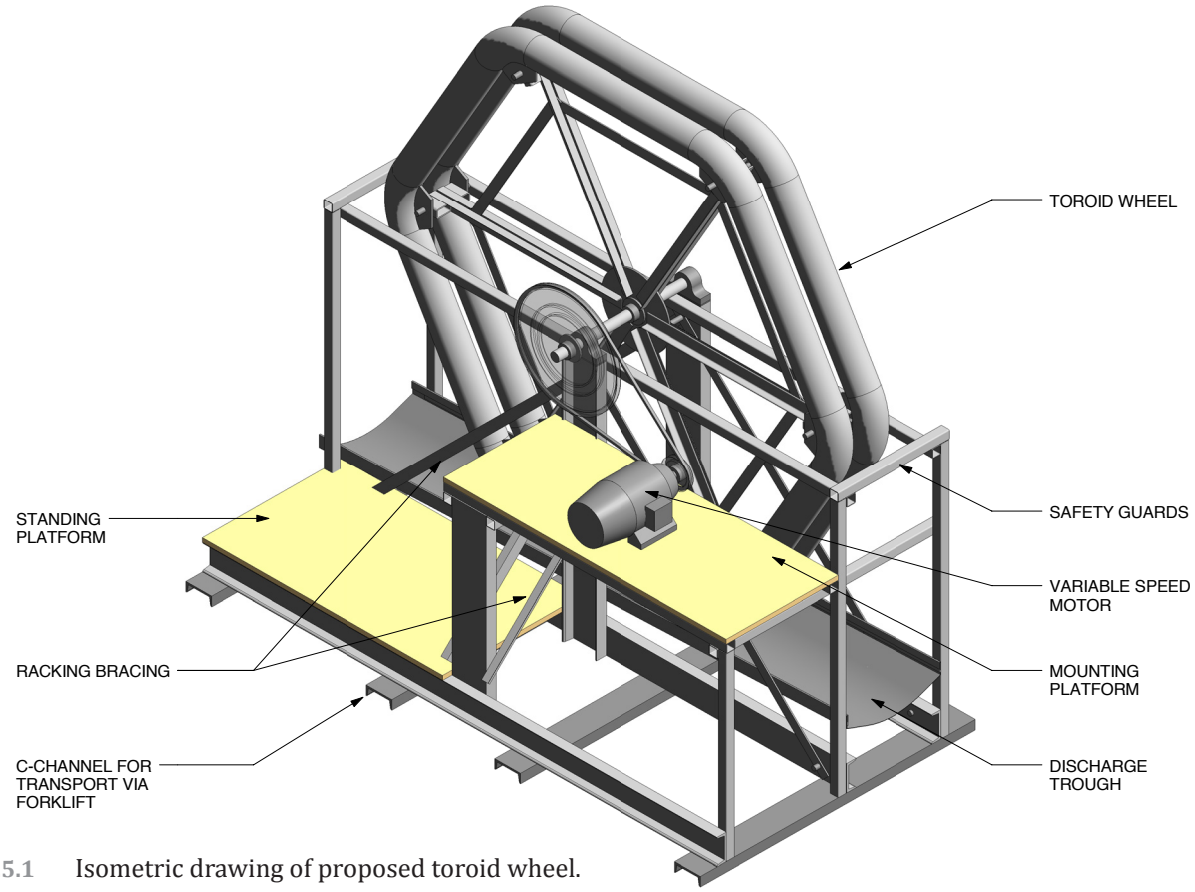

Figure M.5.1 Isometric drawing of proposed toroid wheel.

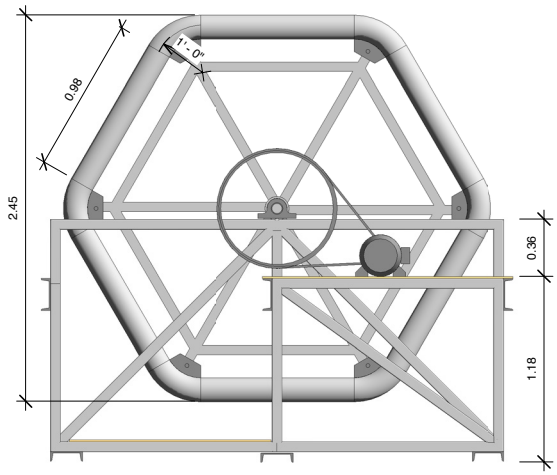

Figure M.5.2 Elevation of proposed toroid wheel.

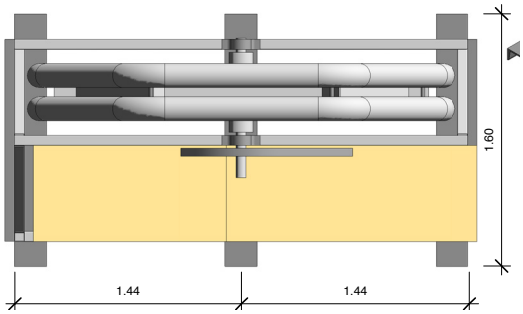

Figure M.5.3 Plan of proposed toroid wheel.

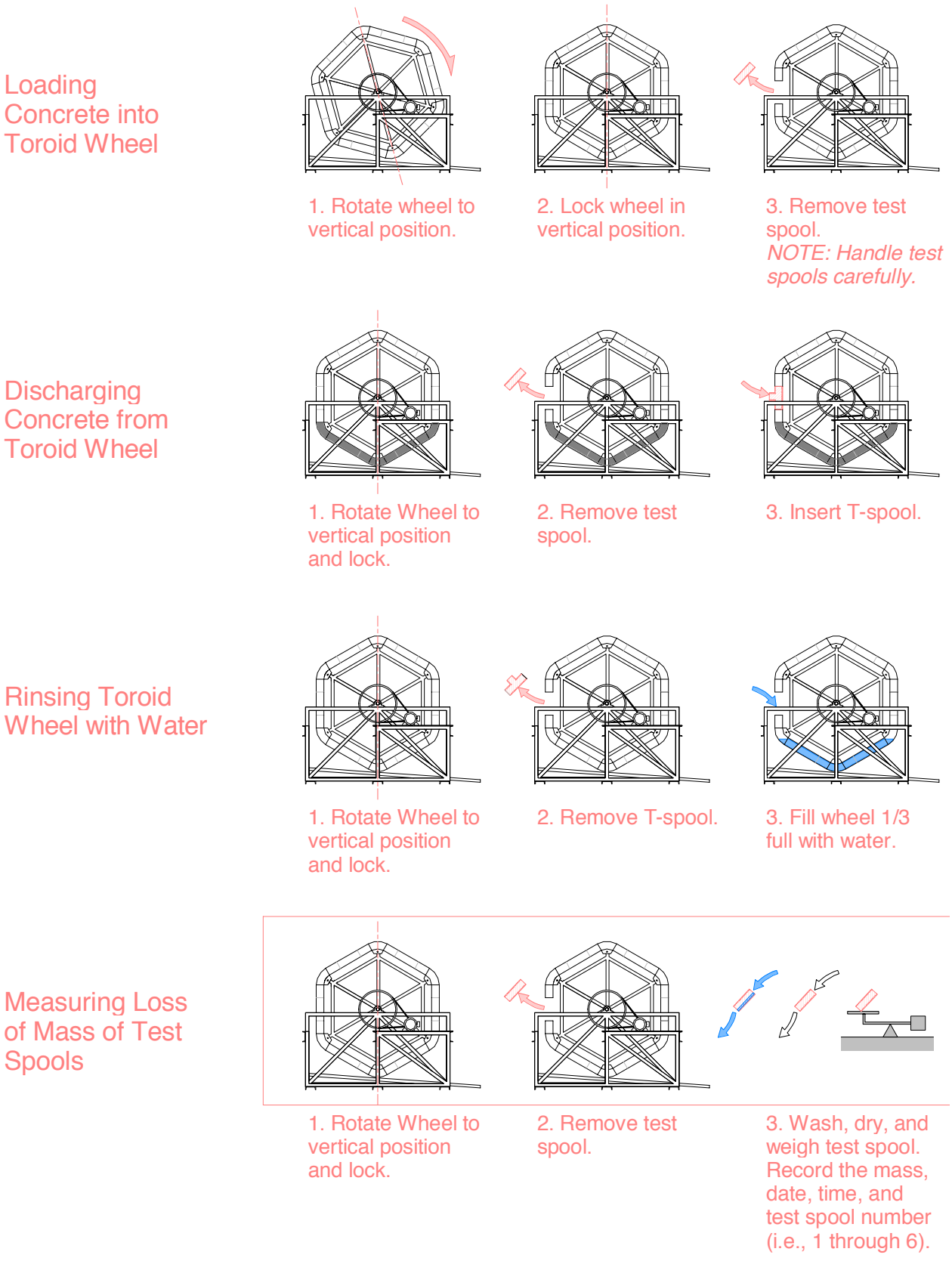

Figure M.5.4 Proposed method for testing abrasion of foam concrete slurry on delivery lines.

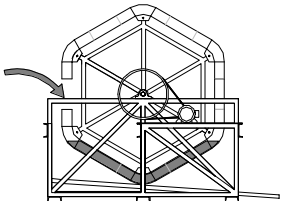

4. Place fresh concrete in wheel.

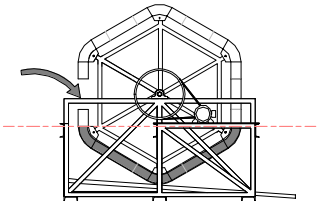

5. Wheel shall be 1/3 full of concrete per marker guides.

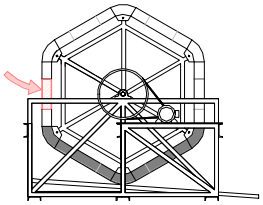

6. Replace test spool.

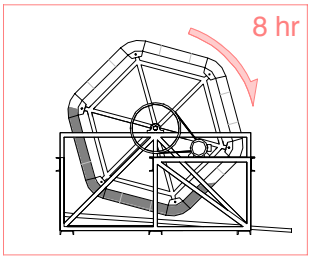

7. Rotate wheel for 8 hour duration.

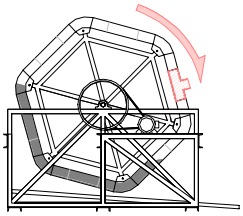

4. Rotate wheel slowly.

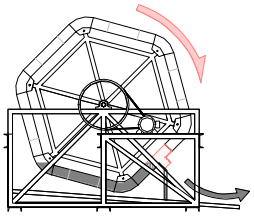

5. Discharge concrete from wheel via T-spool.

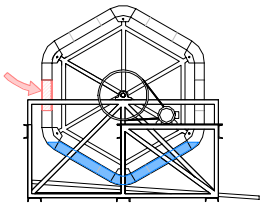

4. Insert test spool.

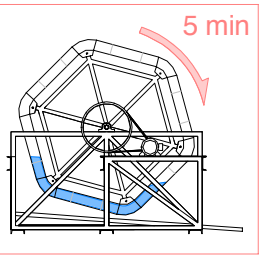

5. Rotate wheel for 5 minute duration to rinse wheel.

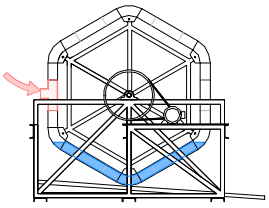

6. Insert T-spool.

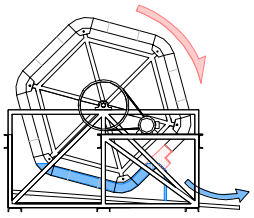

7. Discharge water from wheel via T-spool.

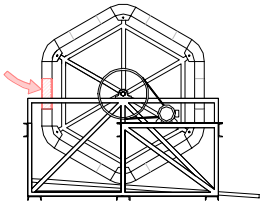

4. Replace test spool.

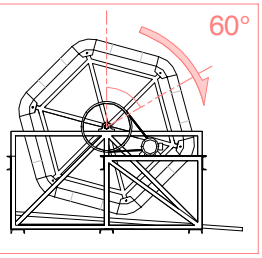

5. Rotate wheel 60°, lock, and repeat measuring process for each of the six test spools.

N

Calculations for Thermal Conductivity Testing

Data from the guarded hot plate apparatus described in Section 5.6.1 was analyzed using software to determine an average thermal conductivity value for the assembly, k_{avg}, in accordance with Fourier's Law,

$$k = \frac{q \cdot l}{A \cdot \Delta T}$$

where

k is the thermal conductivity (W/mK),

q is the heat flow (W),

l is the thickness (m),

A is the area through which heat is flowing (m^2), and

ΔT is the temperature gradient (K).

This average thermal conductivity value was converted to a resistance value for the assembly, R_{total}, by dividing it by the total thickness of the assembly, l_{total}.

$$R_{total} = \frac{k_{avg}}{l_{total}}$$

In order to parse out the contribution of the plastic facer to the thermal resistance of the assembly, a gypsum board was measured in the guarded hot plate apparatus at the same operating conditions as the foam concrete panels, with and without top and bottom facers.

The thermal resistance of the gypsum board, R_{gwb}, was determined by dividing the thickness of the sample, l_{gwb}, by it conductivity, k_{gwb}. Similarly, the thermal resistance of the gypsum board and facer assembly, R_{gwb+2f}, was determined by dividing the thickness of the assembly, l_{gwb+2f}, by it average conductivity, k_{gwb+2f}. The thermal resistance of each facer, R_f, was calculated as

$$R_f = \frac{R_{gwb+2f} - R_{gwb}}{2}$$

The thermal conductivity of each facer, k_f, was therefore taken to be

$$k_f = \frac{l_f}{R_f}$$

where l_f is the thickness of each facer.

For the foam concrete panel and facer assemblies,

$$R_{tot} = R_{f,top} + R_c + R_{f,bot}$$

where R_{tot}, $R_{f,top}$, R_c, and $R_{f,bot}$ are the thermal resistance values of the total assembly, the top facer, the foam concrete panel, and the bottom facer, respectively. By substitution,

$$R_{tot} = \frac{l_c}{k_c} + \frac{2l_f}{k_f}$$

Thus, the conductivity of the foam concrete panel, k_c, may be calculated as

$$k_c = \frac{l_c}{\left(R_{tot} - \frac{2l_f}{k_f}\right)}$$

O

Notes on Segregation in Large Scale Batching

Issues of segregation are discussed in Sections 6.1.3 and 6.3. In general, large scale batching tends to increase the risk of segregation in foam concrete mixes, compared to laboratory produced specimens, since the acceleration caused by large rotating drums increases the mobility of dense sand particles. Mix designs that produce satisfactory specimens in a laboratory setting may need to be modified for commercial use (refer to Section 6.1.3).

Sensitivity of segregation to the scale of production is most apparent in low-density sanded mixes. As a demonstration, the following photographs depict specimens from identical mixes, produced in the lab and at a batching plant. The mix specifications were as indicated in the table below.

Cementitious density	410 kg/m^3
Filler-binder ratio	0.5:1
Water-binder ratio	0.55
Nominal density	800 kg/m^3
Maximum aggregate particle size	4.75mm

Table O.1 Specifications for demonstration mix produced in the lab and at batching plant.

A cut cross-section of the laboratory-produced specimen is shown in Figure O.**1**. The image is at 2x magnification. The structure and air void system of the casting appears to be fairly homogenous. Small grains of sand are visible within the mix. Large grains of sand have been pushed along the surface of the porous matrix during the cutting process, leaving grooves, but the specimen is sound.

In contrast, Figures O.**2** to O.**4** show a 300mm diameter, 1800mm high cast poured from foam concrete mixed in a truck. Significant segregation was evident throughout the specimen. The casting broke into three segments during demoulding. The top portion of the casting was extremely light, with white veins of foam visible where cement and aggregate particles had dropped from the mix. This portion of the casting could be easily compressed by hand, with minimal resistance. The middle segment was more dense; however, white veins were evident in the hardened paste, and the surface of the segment was spalled. At some locations, the casting could be compressed by hand with minimal resistance; other regions consisted of reasonably stiff foam concrete. The lowest segment of the casting appeared to be of reasonable quality foam concrete, although it was noticeably more dense than the laboratory specimen shown in Figure O.**1**. A base of very dense paste, approximately 40mm thick, was visible at the bottom of the specimen, where the plastic mix was in contact with a sandy surface at the ground level. Destructive analysis of this base revealed that it did not contain air voids.

This comparison demonstrates that producing foam concrete on a large scale can amplify effects that are obscured or unimportant in a laboratory context. The performance attained by carefully prepared laboratory mixes may be difficult to replicate during large-scale batching. In order to ensure the quality of sanded low-density foam concrete, it may be necessary use a lower water-binder ratio than indicated by laboratory test results, to increase the stiffness of the mix and resist segregation. It may also be necessary to reduce the maximum aggregate particle size, as these dense particles tend to drop from the mix.

Figure 0.1 Cross-section of low-density sanded foam concrete prepared in laboratory setting, with good homogeneity.

Figure 0.2 Top of low-density sanded foam concrete prepared in a batching plant. Significant segregation is evident.

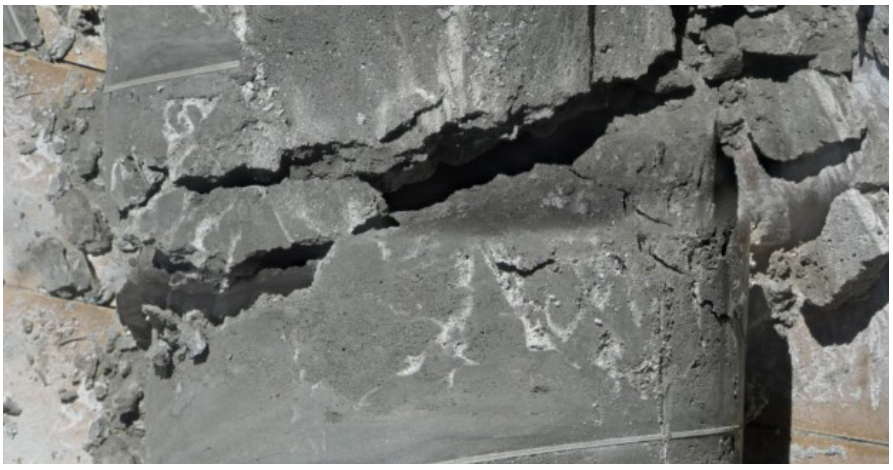

Figure 0.3 Detail at fracture.

Figure 0.4 Elevation.

P

Notes on the Use of Superplasticizer in Foam Concrete

Foam concrete typically has high water-binder ratios, resulting in high capillary porosity. It may be desirable to reduce water demand for reasons of conservation or reduction of plastic self-weight. Reducing capillary porosity may also aid in controlling properties such as gaseous or liquid permeability, drying shrinkage, or creep.

Superplasticizer is occasionally suggested as a possible means to reduce foam concrete water demand. However, water-reducing admixtures and superplasticizers can be incompatible with foam concrete surfactants (refer to Section 7.1; Appendix A, Sections 5.1.2 and 5.1.6). A demonstration of the effects of a superplasticizer on the appearance and compressive strength of foam concrete is included below.

The workability of several mixes, with and without superplasticizer, is recorded in Figure P.**2**. First, slump was determined for neat cement mixes with cementitious densities of 410 and 510 kg/m^3 and water-binder ratios of 0.55 and 0.5, respectively.

Slump was then measured for neat cement mixes with cementitious densities of 410 and 510 kg/m^3, and a water-binder ratios of 0.45. This water-binder ratios was lower than optimal (refer to Figure 6.**1.2.1a**), but was deemed sufficient to avoid extracting dilution water from the foam, which would cause instability.

Finally, superplasticizer was added incrementally to enhance the workability of mixes with water-binder ratios of 0.45, until the slump flow was similar to that of the original mixes with appropriate water-binder ratios.

Break results of mixes with varying water-binder ratios are shown in Figure P.**3**. Results from mixes with superplasticizer are marked with hollow squares. Despite their workability, the superplasticizer mixes did not perform as well as conventional mixes with optimal water-binder ratios. Superplasticizer mixes did appear to perform slightly better than conventional mixes with water-binder ratios of 0.45.

Comparisons of cast conventional and superplasticizer mixes are shown in the image below. Large air-voids are visible in surface of the specimens that included superplasticizer. Superplasticizer acted as a defoaming agent, promoting bubble rupture and coalescence.

Figure P.1 Comparison of the cast surfaces of conventional (left) and superplasticizer (right) mixes. Note the coallescence in the superplasticzer mix. The closest portions of cylinders are at 1.5x magnification.

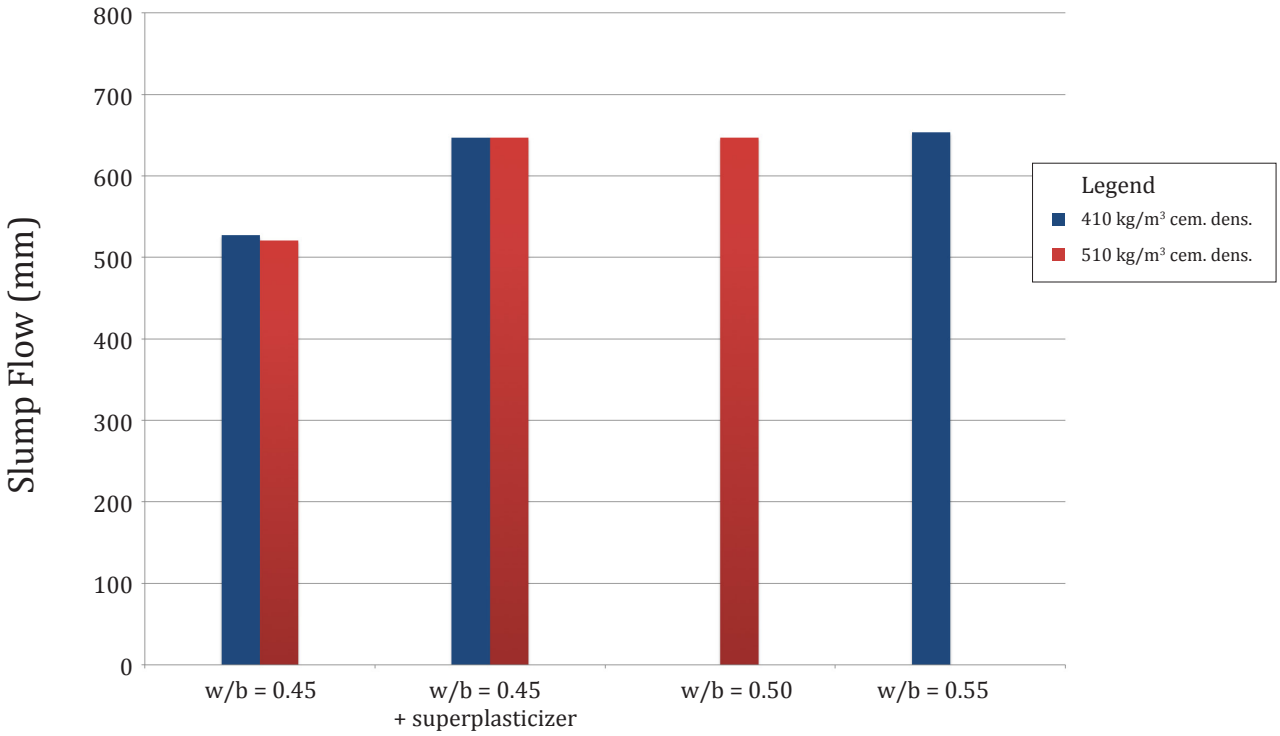

Figure P.2 Slump flow of neat cement mixes, with water-binder ratios and superplasticizer as indicated.

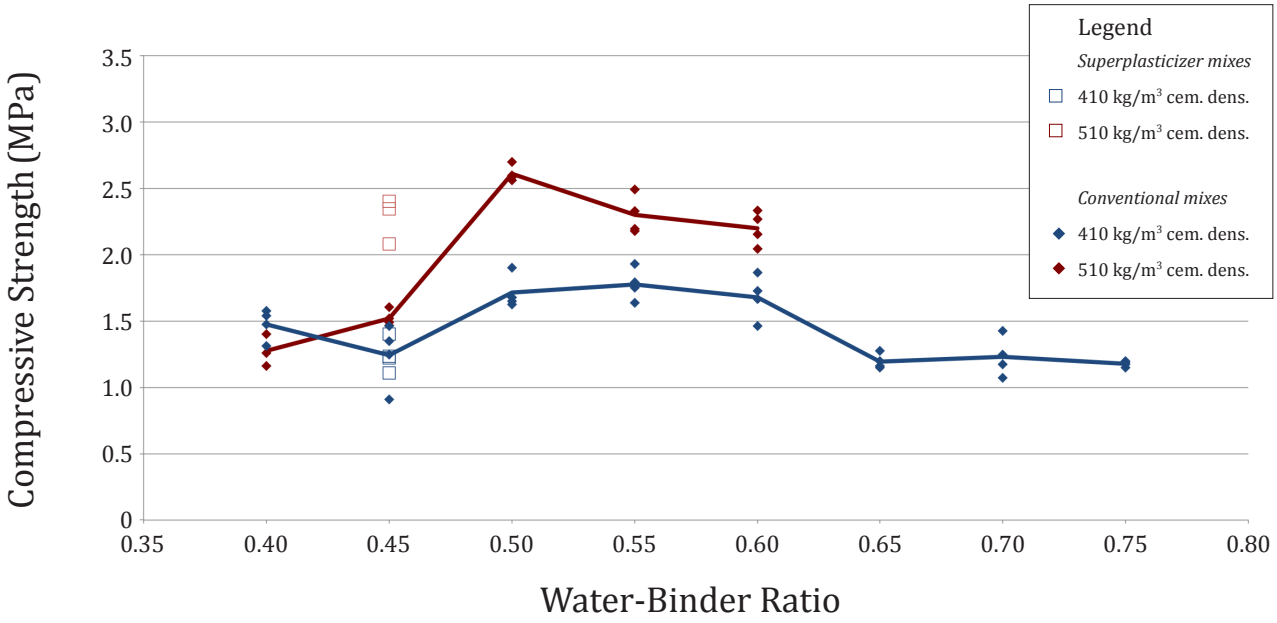

Figure P.3 Compressive strength vs. water-binder ratio.

Q

List of Recommended Mix Designs

This data is redacted. Please contact the author or industry sponsor of this research for further information.

R

Tabulated Data from Experimental Program Results

Tabulated data are available from the author upon request.

Please contact Justin Breg at jfbreg@uwaterloo.ca.

S

Supporting Analysis for Recommended Mix Tolerances

Very tight tolerances were found to be practicable when producing small-scale batches in a laboratory setting. Such stringent standards are important for establishing trends, since small variations in physical characteristics such as density can have significant effects on mechanical or other properties. For commercially produced foam concrete, it is helpful to provide more relaxed standards, in keeping with concrete industry norms.

Proposed tolerances for foam concrete mix proportions were given in Section 8.5. Tolerances were provided for 'critical applications', defined as targeting compressive strength within 10% of predicted values; or 'non-critical applications' defined as targeting compressive strength within 15% of predicted values.

Justification for the proposed tolerances is provided in the sections below, for quantity of binder (S.1), quantity of filler (S.2), plastic density, i.e. quantity of foam (S.3), water-binder ratios (S.4), and sand moisture content (S.5). The cumulative effect of parameter variance is discussed in S.6. Data is drawn from throughout the experimental program, as noted. Calculation methods are heuristic and conservative.

S.1 Quantity of Binder

Proposed tolerances for quantity of binder are reproduced in the table below.

Mix parameter	Tolerance for research	Tolerance for industry		Notes
		Critical	Non-Critical	
Quantity of binder	±0.5%	±5 kg/m^3	±10 kg/m^3	If variance is suspected, consult figures in Appendix S to estimate impact on mix properties.

Table S.1.1 Proposed tolerances for quantity of binder in mix proportioning, from Section 8.5.

In Figures S.1.1 and S.1.2, the compressive strengths of sanded Portland cement specimens are plotted against cementitious density, with nominal dry density of the mixes held constant. (Data are for 28 day specimens, from Figures 6.**1.2.2a** and 6.**1.2.2b**).

The slope of the line-of-best-fit represents the average change in compressive strength (MPa) per unit change in cementitious density (kg/m^3). The maximum influence of the proposed tolerances is expressed as a percentage in the table below, based on the minimum compressive strength of specimens in each data series (i.e. worst case).

Nominal density (kg/m^3)	Slope (MPa/ kg/m^3 of cem.)	Permissible tolerance	Influence on strength (MPa)	Min. f'c in series (MPa)	Max. influence on strength, %
1400	0.024	±5 kg/m^3	±0.12	5.2	**±2.3%**
		±10 kg/m^3	±0.24		**±4.6%**
1800	0.038	±5 kg/m^3	±0.19	14.1	±1.3%
		±10 kg/m^3	±0.38		±2.7%

Table S.1.2 Table for calculating influence of proposed binder tolerances on strength. Worst case in bold.

Results demonstrate that modest variations in the quantity of binder in a foam concrete mix have a meaningful influence on compressive strength.

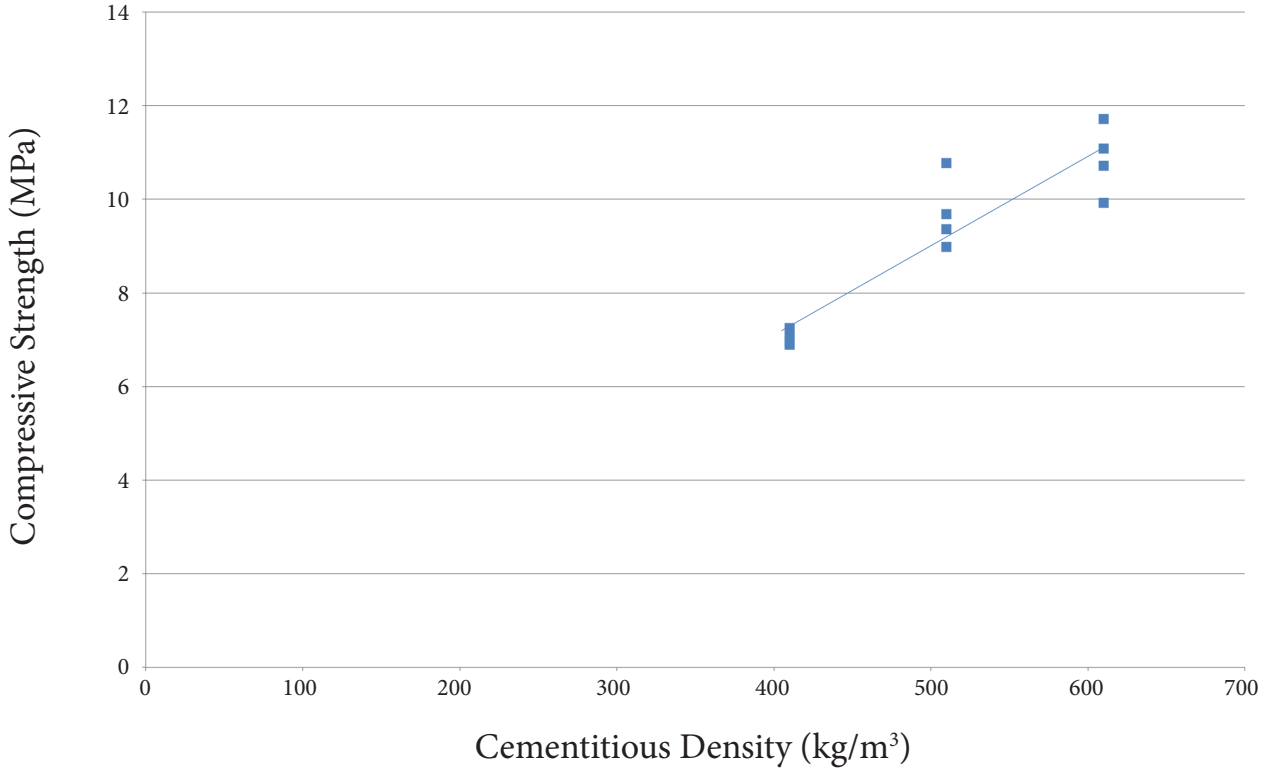

Figure S.2.1 Compressive strength vs. cementitious density, PC mixes, 1400 kg/m³ nominal density, 28 days.

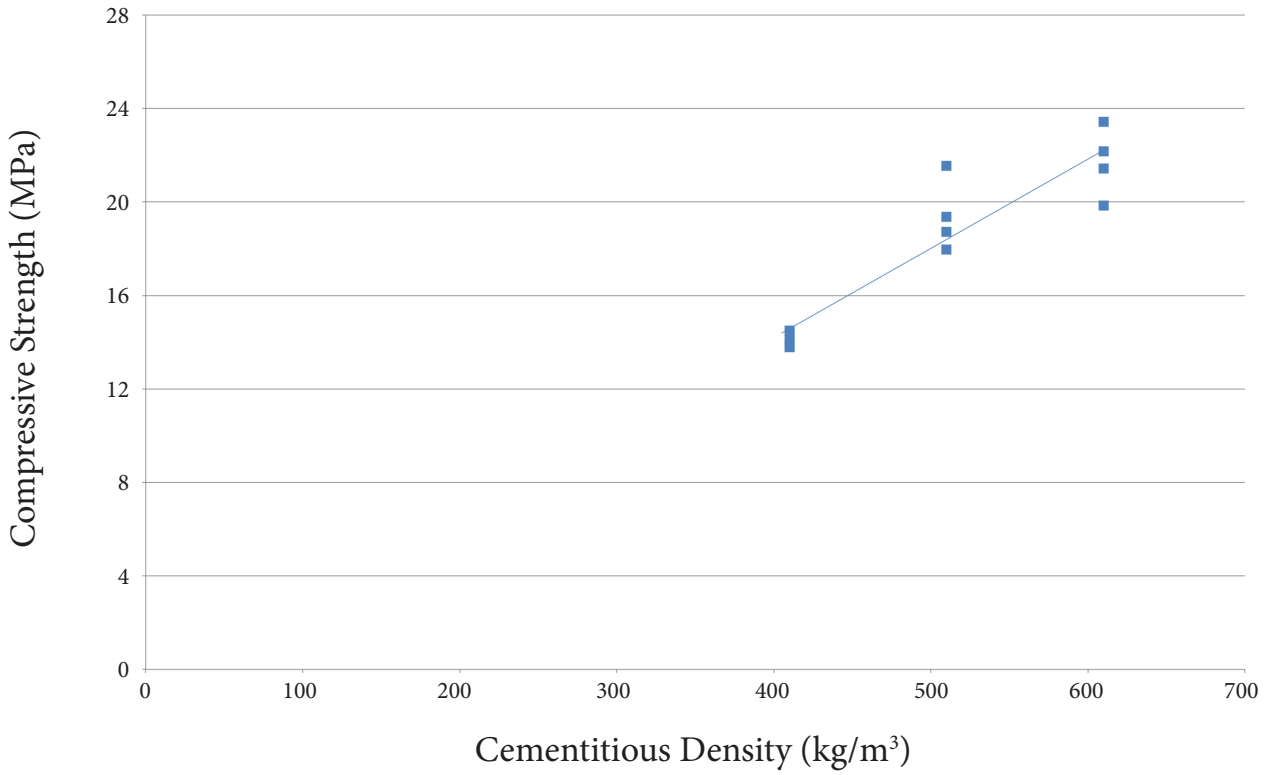

Figure S.2.2 Compressive strength vs. cementitious density, PC mixes, 1800 kg/m³ nominal density, 28 days.

S.2 Quantity of Filler

Proposed tolerances for quantity of filler are reproduced in the table below.

Mix parameter	Tolerance for research	Tolerance for industry		Notes
		Critical	Non-Critical	
Quantity of filler	±0.5%	±10 kg/m³	±20 kg/m³	If variance is suspected, consult figures in Appendix S to estimate impact on mix properties.

Table S.2.1 Proposed tolerances for quantity of filler in mix proportioning, from Section 8.5.

Figure S.2.1 plots compressive strength against quantity of sand aggregate, with cementitious density held constant. (Data are for 56-day specimens, from Figure 6.**6.4g**).

The maximum influence of the proposed tolerances is expressed as a percentage in the tables below, based on the slopes of upper and lower line segments, and the minimum compressive strength along each line segment (i.e. worst case).

Cem. dens. (kg/m³)	Cem. blend	Slope (MPa/ kg/m³ of filler)	Permissible tolerance	Influence on strength (MPa)	Min. f'c along segment (MPa)	Max. influence on strength, %
410	PC	0.0104	±10 kg/m³	±0.10	3.3	**±3.1%**
			±20 kg/m³	±0.21		**±6.2%**
	SF	0.0149	±10 kg/m³	±0.15	5.8	±2.6%
			±20 kg/m³	±0.30		±5.2%
	Slag	0.0119	±10 kg/m³	±0.12	4.3	±2.8%
			±20 kg/m³	±0.24		±5.6%
510	PC	0.0104	±10 kg/m³	±0.10	5.0	±2.1%
			±20 kg/m³	±0.21		±4.1%
	SF	0.0116	±10 kg/m³	±0.12	9.2	±1.3%
			±20 kg/m³	±0.23		±2.5%

Table S.1.2 Table for calculating influence of proposed filler tolerances on strength. Based on lower line segments from Figure S.**1.1**. Worst case in bold.

Cem. dens. (kg/m³)	Cem. blend	Slope (MPa/ kg/m³ of filler)	Permissible tolerance	Influence on strength (MPa)	Min. f'c along segment (MPa)	Max. influence on strength, %
410	PC	0.0222	±10 kg/m³	±0.22	7.6	±2.9%
			±20 kg/m³	±0.44		±5.8%
	SF	0.0318	±10 kg/m³	±0.32	11.9	±2.7%
			±20 kg/m³	±0.64		±5.3%
	Slag	0.0276	±10 kg/m³	±0.28	9.2	±3.0%
			±20 kg/m³	±0.55		±6.0%
510	PC	0.0261	±10 kg/m³	±0.26	7.7	**±3.4%**
			±20 kg/m³	±0.52		**±6.8%**
	SF	0.0271	±10 kg/m³	±0.27	12.2	±2.2%
			±20 kg/m³	±0.54		±4.4%

Table S.1.2 Table for calculating influence of proposed filler tolerances on strength. Based on upper line segments from Figure S.**1.1**. Worst case in bold.

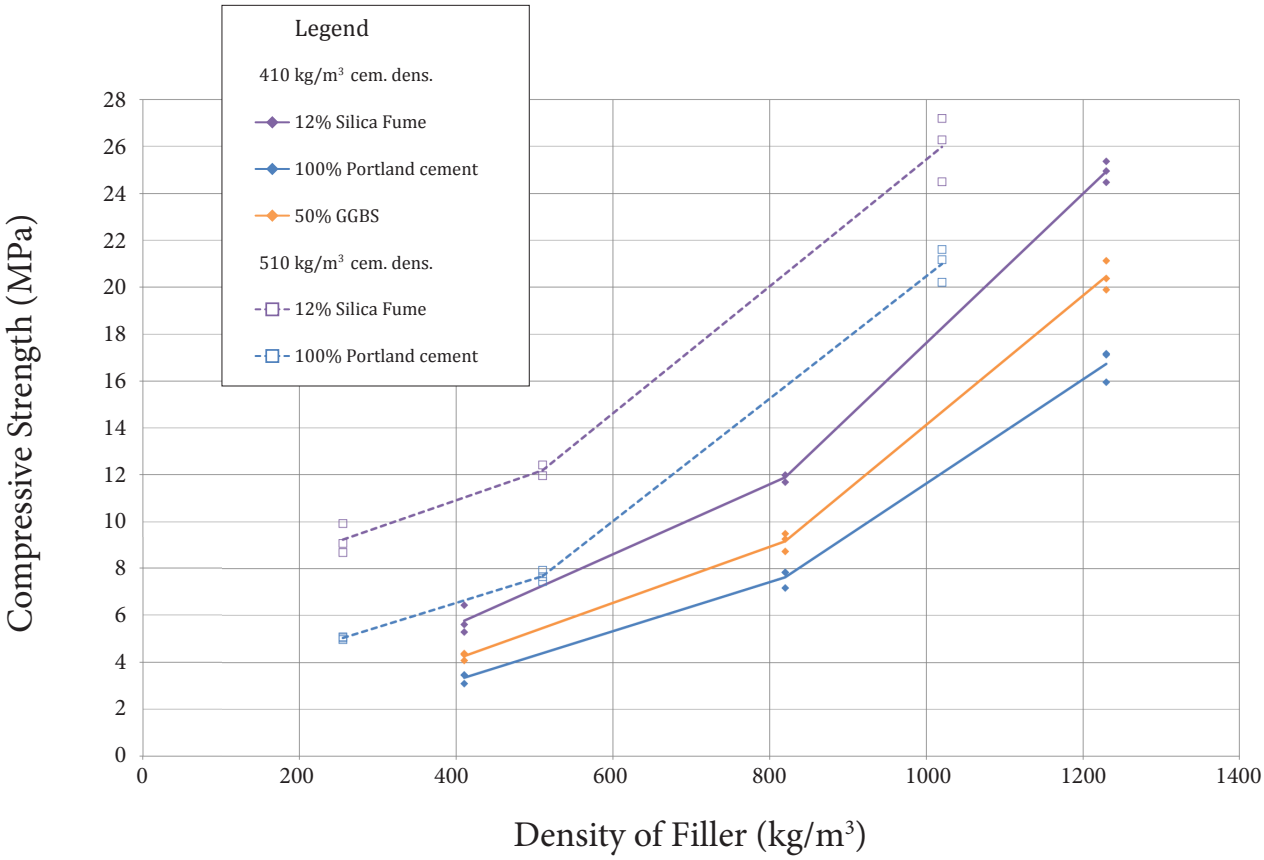

Figure S.2.1 Compressive strength vs. filler density, 56 days moist-cured.

S.3 Plastic Density (Quantity of Foam)

Proposed tolerances for plastic densities are reproduced in the table below.

Mix parameter	Tolerance for research	Tolerance for industry		Notes
		Critical	Non-Critical	
Plastic Density	±10 kg/m³ preferred	±25 kg/m³	±50 kg/m³	Deviations of ±50kg/m³ from target density are permitted per ASTM C796, Section 7.3.1. Closer tolerances req'd for low density mixes. Refer to Appendix S.

Table S.5.1 Proposed tolerances for plastic density in mix proportioning, from Section 8.5.

In Figure S.**3.1**, compressive strength is plotted against plastic density (controlled by foam volume), with all other mix proportions held constant (cement, filler, water). Data are for 56-day specimens, from Figure 6.**6.114b**. The maximum influence of the proposed tolerances is expressed as a percentage in the table below.

F/b ratio	Cem. blend	Slope (MPa/ kg/m³ plastic density)	Permissible tolerance	Influence on strength (MPa)	Min. f'c along segment (MPa)	Max. influence on strength, %
0:1	PC	0.0125	±25 kg/m³	±0.37	1.42	**±22.1%**
			±50 kg/m³	±0.75		**±44.1%**
	SF	0.0163	±10 kg/m³	±0.41	2.67	±15.3%
			±20 kg/m³	±0.82		±30.5%
2:1	PC	0.0398	±10 kg/m³	±1.00	7.62	±13.1%
			±20 kg/m³	±1.99		±26.1%
	SF	0.0389	±10 kg/m³	±0.97	11.89	±8.2%
			±20 kg/m³	±1.97		±16.4%

Table S.5.2 Table for calculating influence of proposed plastic density tolerances on strength.

Variations in density have a significant influence on strength, especially for low density mixes (high foam volume). Fortunately, the densities of low density mixes are relatively easy to control in practice: there is already a large volume of foam present in the mix, so incremental additions of foam have less effect, proportionally.

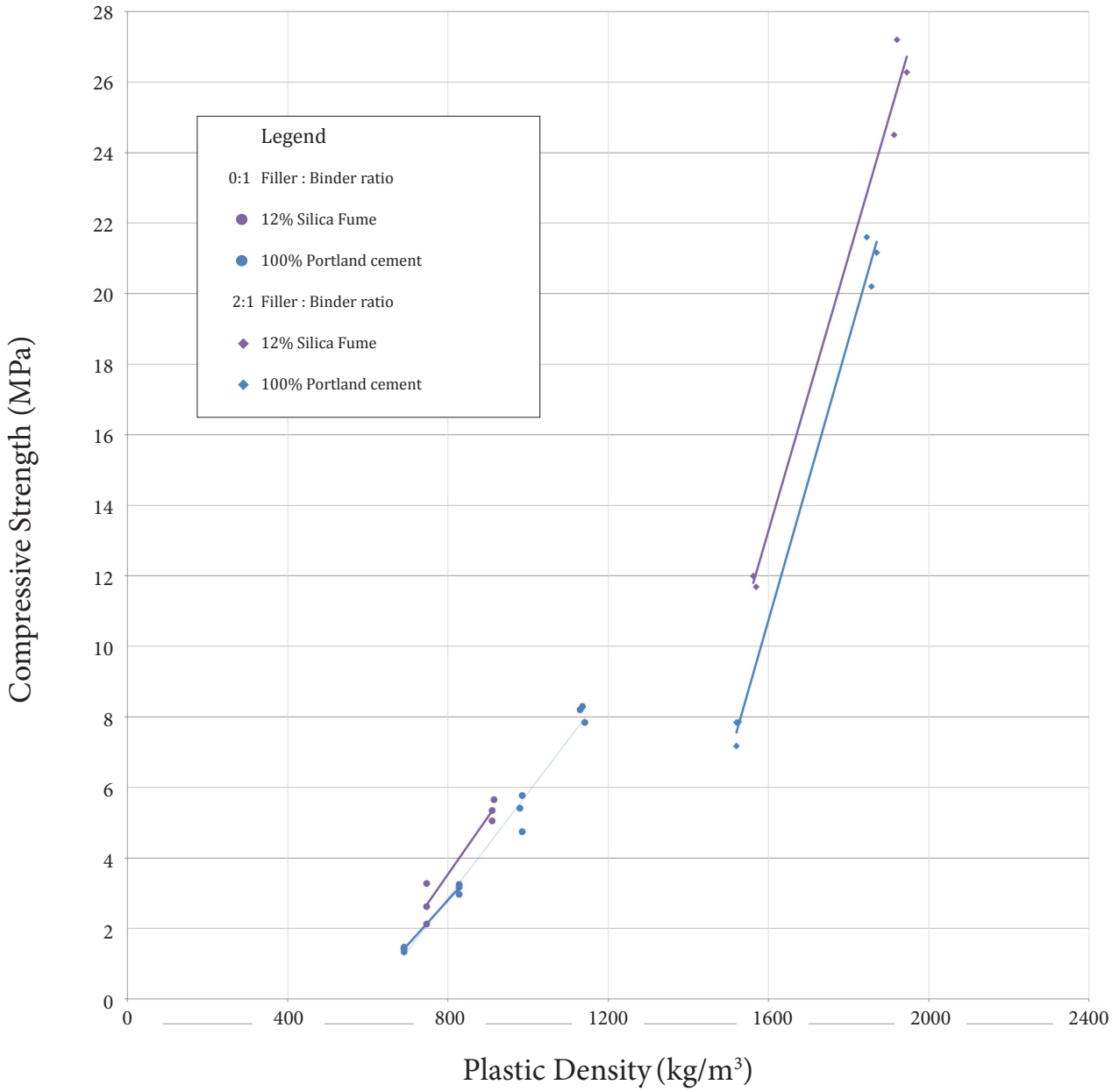

Figure S.3.1 Compressive strength vs. plastic density, 56 days moist-cured.
Linear trendlines are given for mix series with ratios of filler:cement:water held constant.
Slopes of trendlines are reported in Table S.5.2.

S.4 Water-Binder Ratio

Proposed tolerances for water-binder ratios are reproduced in the table below.

Mix parameter		Tolerance for research	Tolerance for industry		Notes
			Critical	Non-Critical	
Water-Binder Ratio	PC	±0.01	±0.05	±0.05	Tolerance to hydration varies with the use of SCMs. Tighter tolerances are recommended with increased cementitious density.
	Slag	±0.01	±0.02	±0.02	
	SF	±0.01	±0.02	±0.02	

Table S.3.1 Proposed tolerances for water-binder ratios in mix proportioning, from Section 8.5.

These recommendations are based on the results presented in Figures 6.**1.1.1a** to 6.**1.1.4f**, 6.**1.2.1a**, and 6.**1.2.2a**, several of which are replicated here. Commentary on these data are available for review in Section 6.1. Generally, the following trends are evident:

- use of SCMs necessitates tighter tolerances;
- increasing cementitious density necessitates tighter tolerances; and
- tolerance to variation in water-binder ratio increases with increasing filler.

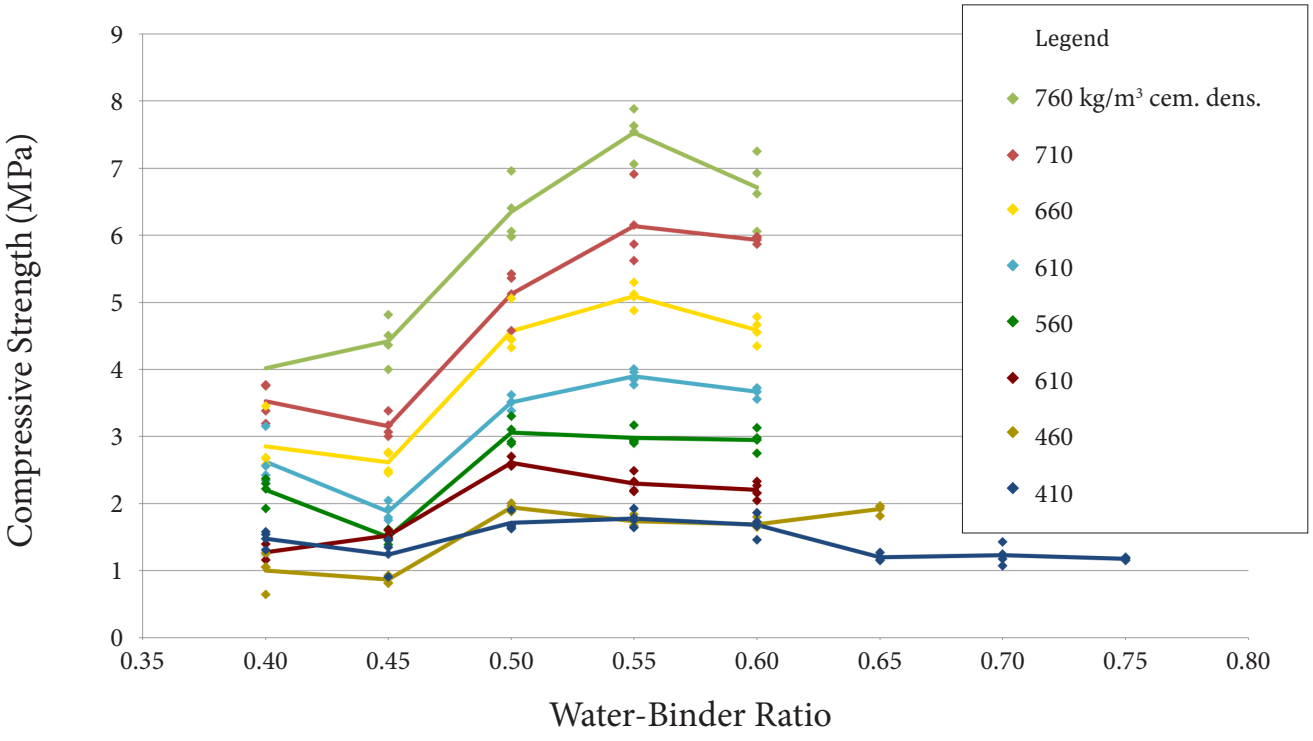

Figure S.4.1 Water demand for low density mixes, varying cementitious density. From Figure 6 **1.2.1a**

0:1 Filler-Binder Ratio

Compressive Strength vs. w/b Ratio

Portland Cement

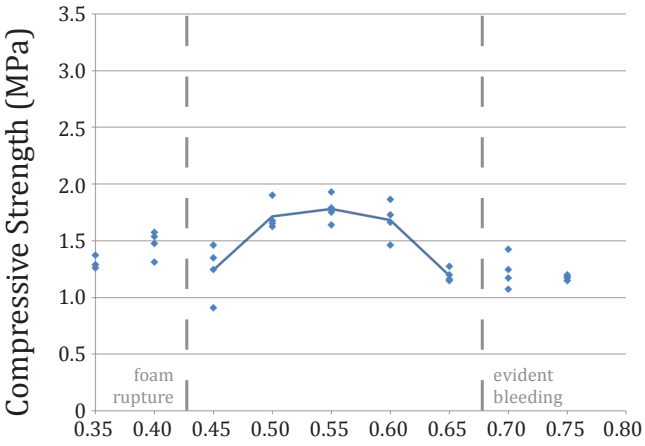

Figure S.4.2

Composite Plot

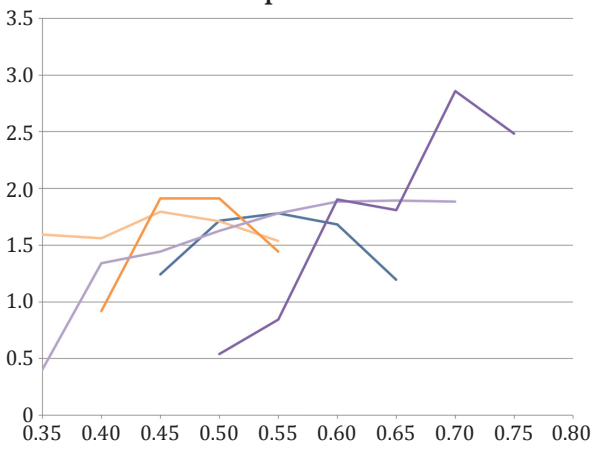

Figure S.4.3

30% Slag Replacement

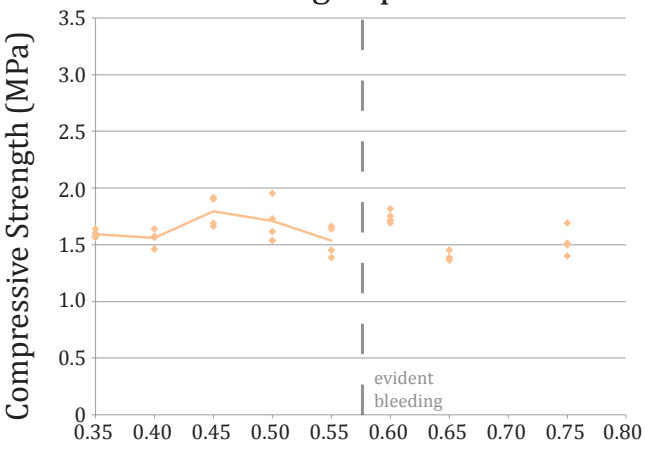

Figure S.4.4

6% Silica Fume Replacement

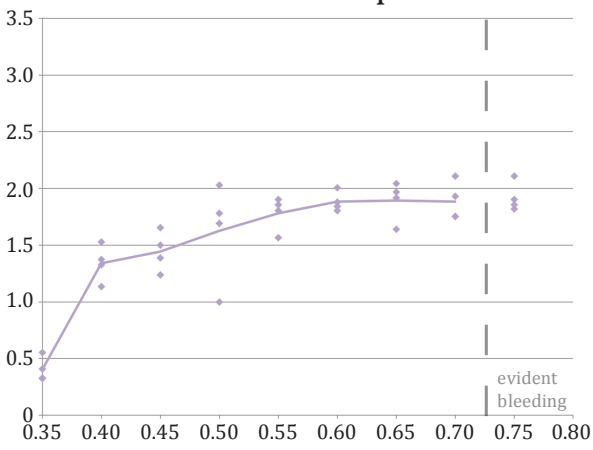

Figure S.4.5

50% Slag Replacement

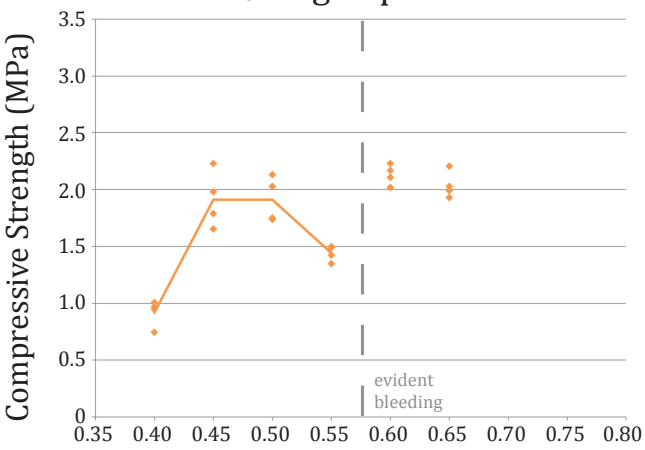

Figure S.4.6

12% Silica Fume Replacement

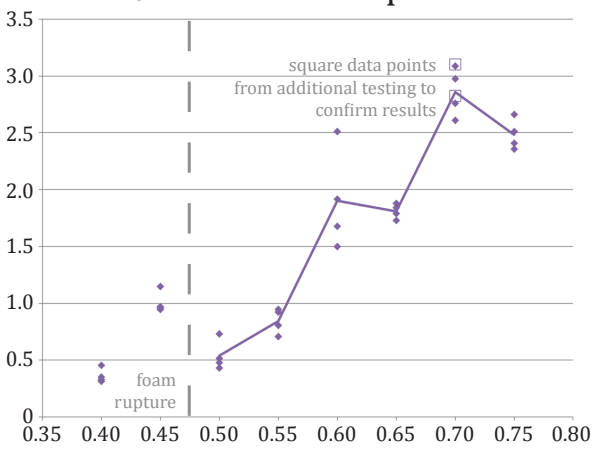

Figure S.4.7

S.5 Sand Moisture Content

Proposed tolerances for water-binder ratios are reproduced in the table below.

Mix parameter	Tolerance for research	Tolerance for industry		Notes
		Critical	Non-Critical	
Sand, moisture content	±0.2%	±0.5%	±1.0%	It is critical to account for MC in dense (sanded) mixes.

Table S.5.1 Proposed tolerances for sand moisture contents, from Section 8.5.

Sanded foam concrete mixes may include large proportions of fine aggregate. Moist sand can contribute a large amount of water to a mix, affecting the effective water-binder ratio and influencing consistency, stability, segregation, and porosity. Mix designs should be adjusted for the moisture content of the sand, as described in Appendix D.

The influence of the proposed tolerances for sand moisture content on the effective water-binder ratio is given in the table below, for a range of cementitious densities and filler-binder ratios.

Cem. dens. (kg/m^3)	Filler-binder ratio	Permissible tolerance	Influence on w/b ratio
410	1:1	±0.5%	±0.005
		±1.0%	±0.010
	2:1	±0.5%	±0.010
		±1.0%	±0.020
	3:1	±0.5%	**±0.015**
		±1.0%	**±0.030**
510	0.5:1	±0.5%	±0.003
		±1.0%	±0.005
	1:1	±0.5%	±0.005
		±1.0%	±0.010
	2:1	±0.5%	±0.010
		±1.0%	±0.020

Table S.5.2 Proposed tolerances for sand moisture contents, from Section 8.5.

Resulting variation in w/b ratios is consistent with permissible limits given in S.4.

S.6 Cumulative Effect of Parameter Variance

Maximum total anticipated effects on compressive strength are given in bold in the table below for Portland cement mixes with 410kg/m^3 cementitious density, and filler-binder ratio of 0:1. An appropriate water-binder ratio is assumed. Note that variability related to the use of fillers does not apply for neat cement mixes.

Mix parameter	Research	Industry Applications	
		Critical	Non-Critical
	Tolerance	Tolerance	Tolerance
	Deviation (max.)	**Deviation**	**Deviation**
Plastic Density	±10 kg/m^3	±25 kg/m^3	±50 kg/m^3
	±8.8%	**±22.1%**	**±44.1%**
Cumulative dev.	**±8.8%**	**±22.1%**	**±44.1%**
Desired limits	**(low as possible)**	**±10.0%**	**±18.0%**

Table S.6.1 Cumulative effect of variations on strength for 0:1 Portland cement mix.

Variations in the foam volume alone can have a significant effect on the strength of low density, neat cement mixes, exceeding desired limits. In practice, during the course of this research, mixes produced with care in a commercial batching plant according to recommended tolerances were within desired limits of laboratory results.

Figure S.6.1 Batching of low density foam concrete in the field. Producing good quality, neat cement foam concrete to a specificiation is relatively uncomplicated: the material is highly homogenous (no aggregate), and foam volumes are high, permitting a large margin of error in adding foam volume to achieve a particular density.

Table S.6.2 indicates the maximum anticipated effects on compressive strength for Portland cement mixes with 410kg/m^3 cementitious density, and filler-binder ratio of 2:1. An appropriate water-binder ratio is assumed.

Mix parameter	Research	Industry Applications	
		Critical	Non-Critical
	Tolerance	Tolerance	Tolerance
	Deviation	**Deviation**	**Deviation**
Quantity of binder	±0.5%	±5 kg/m^3	±10 kg/m^3
	±1.0%	**±2.3%**	**±4.6%**
Quantity of filler	±0.5%	±10 kg/m^3	±20 kg/m^3
	±1.2%	**±2.9%**	**±5.8%**
Plastic Density	±10 kg/m^3	±25 kg/m^3	±50 kg/m^3
	±5.2%	**±13.1%**	**±26.1%**
Cumulative dev.	**±7.5%**	**±19.1%**	**±39.6%**
Desired limits	**(low as possible)**	**±10.0%**	**±18.0%**

Table S.6.2 Cumulative effect of variations on strength for 2:1 Portland cement mix.

Cumulative variations in mix parameters can have a significant effect on strength, which may exceed desired limits. The cumulative deviation noted in the table above represents a worst case. This result, however, is statistically unlikely.

Anticipated probability distributions for research and industry applications are indicated in Figure S.**6a**, based on values from Table S.6.2. Each plot was produced from 10^5 trials in a Monte Carlo simulation. For each trial, a random, uniformly distributed value was chosen from within the bounds defined for each parameter. The product of the three deviation values was taken as the cumulative deviation, which is plotted on the x-axis as a percentage of target compressive strength.

The plots are plateau-shaped. The plateaus account for approximately half of the

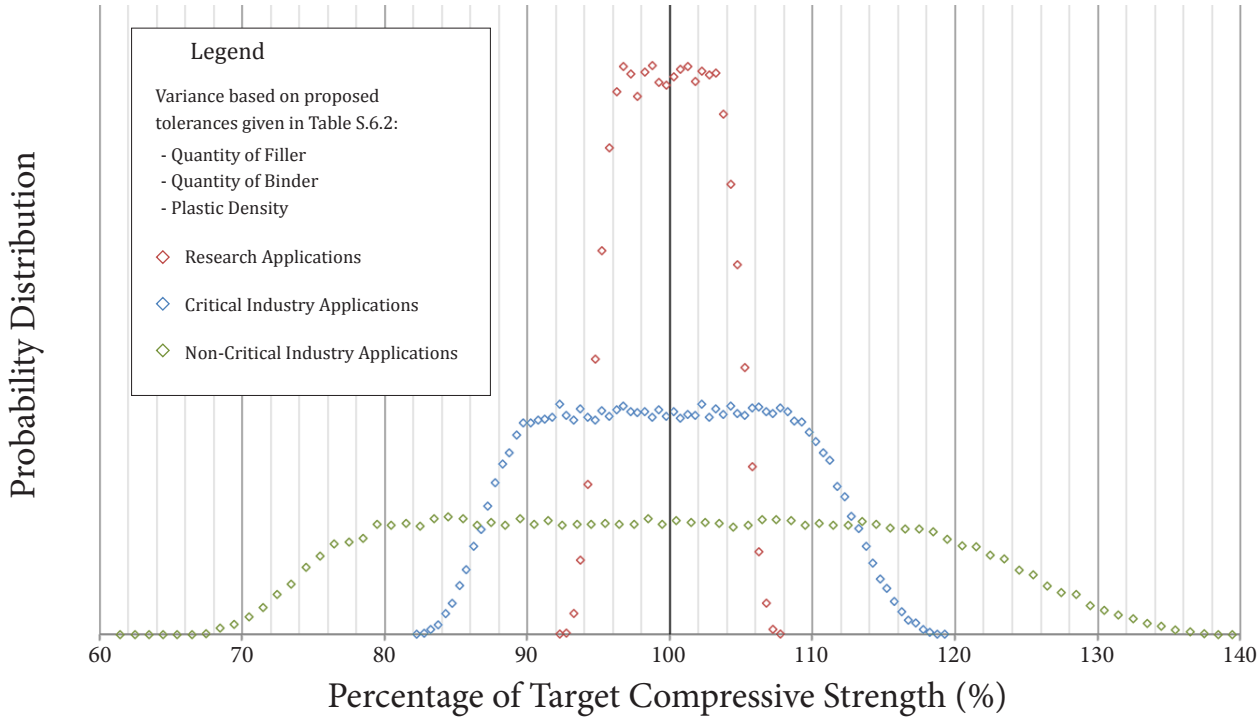

Figure S.6a Probability distribution. Deviation from target compressive strength is due to cumulative variability in quantity of binder, quantity of filler, and plastic density. (Parameter variations are randomly, uniformly distributed per limits given in Table S.6.2.)

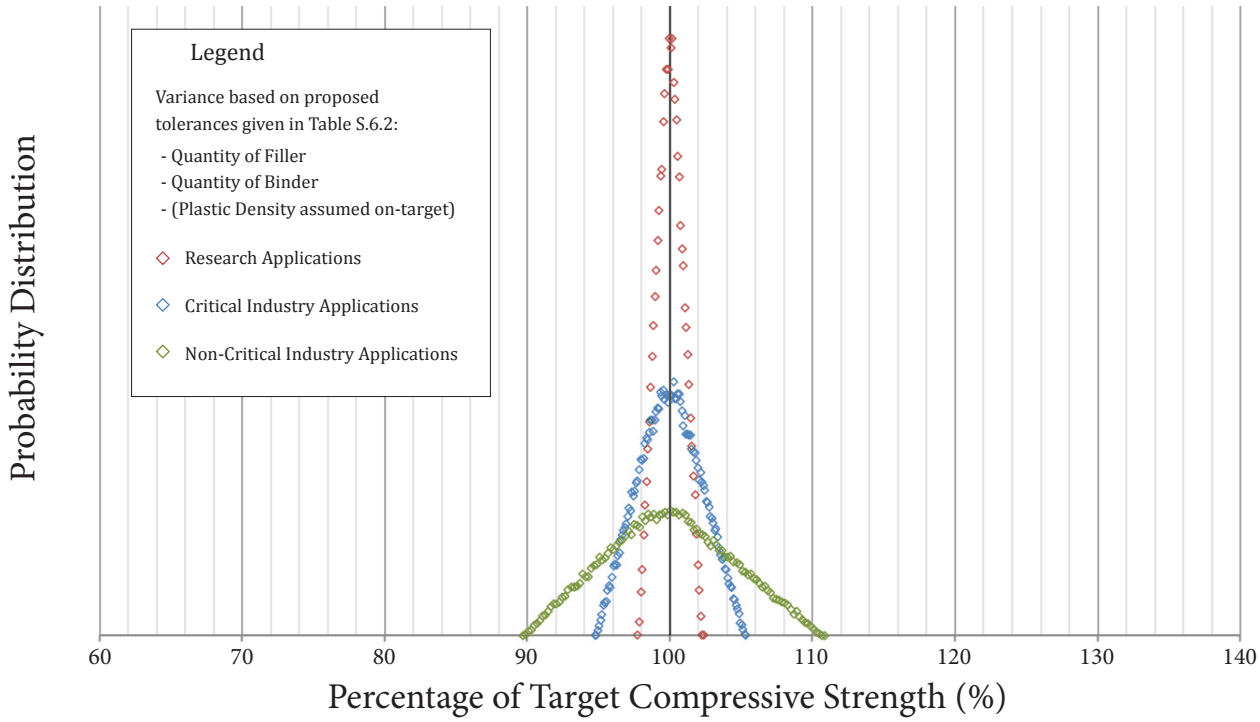

Figure S.6b Probability distribution. In this Figure, deviation from target compressive strength is due only to cumulative variability in quantity of binder and quantity of filler. Plastic density is assumed to be on-target. Cumulative deviation is low, highlighting the importance of tight tolerances on plastic density. (Parameter variations are randomly, uniformly distributed per Table S.6.2.)

domain of the distribution.

It is important to recognize that most of the cumulative deviation in compressive strength is due to variability in plastic density. As a demonstration, in Figure S.**6b**, plastic density is assumed to be on-target in all trials. In this scenario, the maximum anticipated cumulative deviation in compressive strength is only approximately ±2% for research tolerances, and ±5 and ±11% for critical and non-critical industry applications, respectively. Plastic densities should be controlled as tightly as is reasonable possible, to help achieve desired mechanical properties.

The plots above assume random, uniformly distributed parameter deviation, within specified bounds. However, it is reasonable to suggest that batchers will frequently be close to the desired target, and will seldom be at the extreme allowable limits. In Figure S.**6c**, Monte Carlo simulations were conducted using parameter values with a normal distribution. Upper and lower parameter bounds given in Table S.6.2 were taken to represent three standard deviations, so that 99.7% of the randomly generated deviation values fell between these bounds.

The resulting probability distribution plots follow quasi-normal distributions. Cumulative deviation is indicated in the table below at 1, 2, and 3 standard deviations, representing approximately 68, 95, and 99.7% confidence, respectively.

Mix parameter	Research	Industry Applications	
		Critical	Non-Critical
Dev. at 1σ (68%)	**±1.8%**	**±4.6%**	**±9.0%**
Dev. at 2σ (95%)	**±3.7%**	**±9.2%**	**±17.9%**
Dev. at 3σ (99.7%)	**±5.5%**	**±13.8%**	**±26.9%**
Desired limits	**(low as possible)**	**±10.0%**	**±18.0%**

Table S.6.3 Cumulative deviation at 1σ, 2σ, and 3σ for the probability distributions in Figure S.**6c**.

According to the assumptions described above, approximately 95% of trials (two standard deviations) will lie within desired limits for compressive strength. Correspondingly, more than 97.5% of trials will meet or exceed the minimum desired compressive strength.

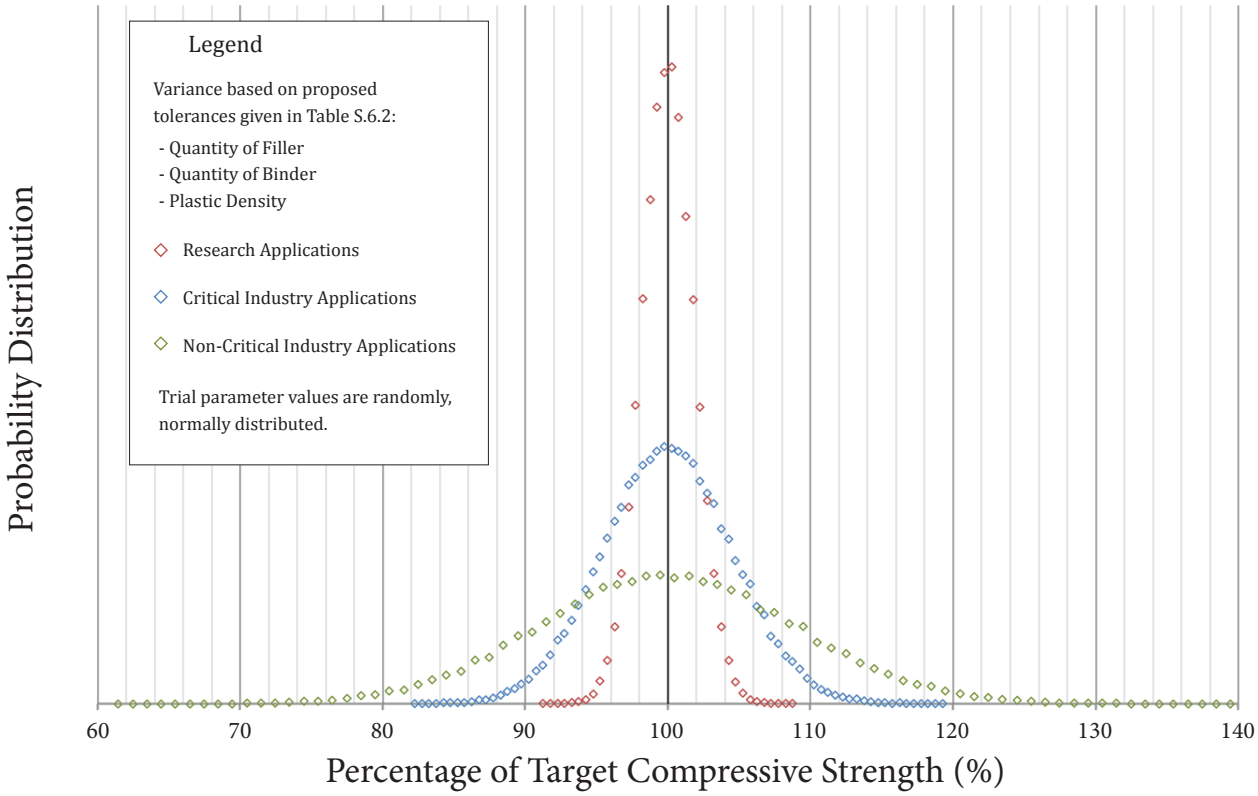

Figure S.6c Probability distribution. Deviation from target compressive strength is due to cumulative variability in quantity of binder, quantity of filler, and plastic density. (Parameter variations are randomly, normally distributed per limits given in Table S.6.2.)

T

Supplementary List of Topics for Future Research

Two research areas were identified in Section 9.6 as being especially critical for the continued expansion and refinement of a comprehensive mix design framework for foam concrete; namely: a large-scale study of reinforcing for foam concrete (specifically fibre reinforcing), and further investigation into foam concrete aging.

Other possible areas of foam concrete testing have been raised throughout the research program. These topics are documented in the following lists.

New types or combinations of ingredients:

- use surfactant from a different manufacturer[1]
- use silica flour, to accelerate curing
- use filler with a fine particle size, to reduce issues of segregation in low density mixes. Attempt to establish a relationship between mix density and maximum allowable filler particle size. (Water content will be a relevant variable, to account for the increased surface-area to volume ratio for wetting fine particle sizes)
- use ternary cementitious blends

[1] Cf. Panesar (2013)

- use other types of binders

Water demand:

- floawability of mixes with appropriate water-binder ratios may be evaluated for a variety of cementitious blends and plastic densities, in order to observe whether there is a correlation between optimal water-binder ratio and consistency
- self-weight of foam concrete varies significantly, and has a strong influence on the results of gravity-dependent flow test (refer to Section 7.1). Other methods of evaluating consistency should be considered and analyzed for patterns (e.g. marsh cone)
- intermediate steps in water content should be tested, for more precise optimization of water-binder ratios, especially for mixes that appeared to be less tolerant to variations in water content such as low-density slag or 12% silica fume mixes

Mechanical properties:

- benchmark tensile strengths of mixes, with and without reinforcing
- mechanical properties should be tested on specimens conditioned to high and low internal relative humidities, to confirm whether contribution of loadbearing water has a meaningful influence.
- cracking in the bulk may affect mechanical properties. Given the high drying shrinkage of foam concrete, mechanical properties should be evaluated for specimens subjecting to varying curing and drying regimes which correspond to actual field conditions.
- quantify capacity for impact absorption
- measure Poisson's ratio using circumferential extensometer, rather than the diametral extensometer used in Section 5.4.3. Measuring dilation circumferentially may yield more representative values for Poisson's ratios by flattening local effects and reducing scatter
- determine dynamic moduli of elasticity

- mechanical properties of dense mixes with cementitious densities lower than 410 kg/m^3 should be tested, as less expensive mixes which may be suitable for certain applications

Creep:

- study effect of variations in water-binder ratio on creep
- study effect of variations in water-binder ratio on drying shrinkage
- study effect of drying environment RH on creep

Drying shrinkage:

- study effect of variations in water-binder ratio on drying shrinkage
- study effect of drying environment RH on drying shrinkage
- study effects of size on drying shrinkage
- study effect of fine, inert filler on drying shrinkage (refer to Figure 8.**2b**)

Moisture storage:

- determine moisture storage of foam concrete at 90% RH
- determine moisture storage of foam concrete from 95 to ~99% RH, using pressure plate apparatus

Moisture movement:

- determine actual strain induced by wetting, rather than calculating pressure based on strain (refer to Figure 6.**13b**)
- study effect of variations in high RH curing time on moisture movement
- study effect of drying environment RH on drying shrinkage

Transport properties:

- consider the capacity of non-structural coatings to suppress capillary water uptake. Water repellent additives may also be tested
- rates of moisture ingress given in Section 6.12 for dry specimens in 80 and 90% RH environments indicate that water vapour decreases with increasing moisture

content of the paste, possibly due to a sealing effect. This effect may not be apparent when conducting typical dry-cup or wet-cup water vapour permeance testing.[2] Water vapour permeance may be undertaken to test or refine the transport model proposed in Section 7.3.7

Thermal conductivity:

- study influence of moisture content on thermal conductivity

Freeze-thaw resistance:

- test mixes with nominal densities of 1000 and 1800 kg/m^3
- study influence of cementitious density on freeze-thaw resistance
- study influence of fibre reinforcing on freeze-thaw resistance

Freeze-thaw salt scaling:

- saline freeze-thaw susceptibility of mixes with SCMs may be tested. Silica fume mixes are of particular interest due to reduced permeability and high strength.
- patterns of saline freeze-thaw susceptibility in low-density mixes should be studied, to assess the durability of low density foam concrete fill exposed to de-icing salts
- correlations between permeability, or compressive or tensile strength, and spalling, may be sought, to help anticipate saline freeze-thaw performance from mechanical properties

Microstructural analysis:

- calibrate results from Section 6.17.2 with known test method (for example, the RapidAir 457 automated air void analysis system manufactured by Concrete Experts International)
- specimens may be resin-impregnated; then cut and studied, in order to avoid problems of sand particles falling out or eroding the surface of the specimen during cutting of the samples (refer to Section 6.17.2)

[2] Cf. ASTM E96/E96M–16

- interconnectivity of air voids may be quantified with in-plane permeability tests, such as ASTM D4716.[3]
- air-void systems may be more thoroughly characterized with the help of X-ray computerized tomography (X-CT), coupled with three-dimensional image processing, to gain precise information on air-void size and air void size distribution, as permitted by the voxel resolution of the equipment.[4]
- a scanning electron microscope may be used to study patterns of foam collapse during curing or drying[5]
- X-ray diffraction (XRD) may be used to evaluate the mineral phases of reaction products of various foam concrete mixes, and may also evaluate whether C-S-H phases have deteriorated due to carbonation during curing[6]
- note that total vacuum saturation methods are reported to provide more accurate measurements of porosity than apparent or mercury intrusion porosimetry (MIP) methods,[7] and should continue to be used to calculate total porosity for foam concrete.

Other properties:

- evaluate resistance to fire and elevated temperatures
- evaluate abrasion of fresh foam concrete (refer to Appendix M)
- evaluate resistance to sulphate attack
- evaluate resistance to carbonation

Foam concrete aggregate (FCA) concrete:

- six variables are identified as significant in the production of FCA concrete, as discussed in Appendix E. All variables should be considered in a more thorough investigation, in order to determine in which situations FCA may be especially competitive with conventional lightweight aggregates. The mix design of the matrix surrounding the FCA, in particular, should be studied.

---

3 ASTM D4716/D4716M-14
4 She, Chen, Zhang, and Jones (2013)
5 Akthar and Evans (2010)
6 Jiang et al. (2016b) 958
7 Hilal et al. (2014a) and Hilal et al. (2015c). Cited in Amran et al. (2015) 998

- test permeable 'no-fines' FCA mixes, to avoid buoyancy effects in mass pours
- prewet FCA to avoid minimize of segregation and densification observed in Section 6.3 and 6.4, and to avoid foam collapse caused by bubbles coming in contact with dry ingredients

Predictive modeling:

- results from the database developed in through this study may be translated into predictive models, such as those using artificial neural networks, as proposed by Bayuaji and Nuruddin[8] and Nehdi et al.[9]

Geometric modeling and fabrication of new foam concrete products:

- research must account not only for material properties, but also geometric properties that capitalize on foam concrete's advantages. Developments may include the fabrication of full-scale mock-ups of possible products, to refine products in light of issues of manufacture, logistics, and assembly.

[8] Bayuaji and Nuruddin (2008)
[9] Nehdi et al. (2001)